Methods in Molecular Biology 1208

Springer Protocols

Donald Armstrong *Editor*

Advanced Protocols in Oxidative Stress III

Humana Press

METHODS IN MOLECULAR BIOLOGY

Series Editor
John M. Walker
School of Life Sciences
University of Hertfordshire
Hatfield, Hertfordshire, AL10 9AB, UK

For further volumes:
http://www.springer.com/series/7651

Advanced Protocols in Oxidative Stress III

Edited by

Donald Armstrong

University of Florida, Gainsville, FL, USA

Humana Press

Editor
Donald Armstrong
University of Florida
Gainsville, FL, USA

ISSN 1064-3745 ISSN 1940-6029 (electronic)
ISBN 978-1-4939-1440-1 ISBN 978-1-4939-1441-8 (eBook)
DOI 10.1007/978-1-4939-1441-8
Springer New York Heidelberg Dordrecht London

Library of Congress Control Number: 2014945207

Cover Illustration: Color map representing the dissimilarity of chromatographic profiles, obtained for 13 different validation samples containing *Passiflora incarnata* in pharmaceutical preparations. Each preparation consists of a mixture of pharmaceutical and/or herbal ingredients. A low dissimilarity (high similarity) is represented by a blue color, while a high dissimilarity (low similarity) is represented by a red color.

Printed on acid-free paper

Humana Press is a brand of Springer
Springer is part of Springer Science+Business Media (www.springer.com)

Preface

I started as an editor in 1996 to publish books for Humana Press that emphasized methods and protocols related to free radicals pathology and antioxidants protection that was launched in the first featured volume (number 108) that appeared in 1998. This was followed by volumes 186 and 196 in 2002, which, at that time, completed the first three books on oxidative stress. In 2007, I was guest editor for a special issue, volume 37, on a Free Radicals in Biosystems symposium also published by Humana Press in the journal of *Molecular Biotechnology*. In 2009, I edited volumes 579 and 580 on *Lipidomics: Methods and Protocols* and coauthored volume 1028 in 2013 on *Oxidative Stress and Nanotechnology*. More books are under consideration. Our expectation is to publish additional high-quality and useful protocols. I hope those will be available by 2015/2016 to complete the basic scientific desk reference.

In 2008, a new collection of volumes was approved; the first being called *Advanced Protocols in Oxidative Stress I* (volume 477) and 2 years later in 2010 was *Advanced Protocols in Oxidative Stress II*, volume 594. The proliferation of information in search engines make it possible to review meaningful information relative to methods approximately every 2–3 years. Data currently shows no change since 2000 in the antioxidant-to-oxidative stress ratio as a percentage of total citations and has remained constant in this subheading category:

Total citations	AOX–OS/ratio
2000—Oxidative stress and free radicals = 2,873 Antioxidants = 903	24 %
2008—Oxidative stress and free radicals = 15,938 Antioxidants = 5,109	24 %
2010—Oxidative stress and free radicals = 25,975 Antioxidants = 7,283	22 %
2013—Oxidative stress and free radicals = 29,076 Antioxidants = 8,001	22 %

This analysis indicates that, even though the free radical biomarkers showed a substantial increase over the last 3 years, the antioxidant number has remained relatively constant since 2000, which is our reference point, meaning that antioxidant capacity biomarkers should be the next target for new research to keep pace and balance.

The present book is the latest venture under the advanced heading. It has 31 chapters and covers technology ranging from a portable hand-held detector for remote analysis of antioxidant capacity to sophisticated technology such as shotgun lipidomics, mitochondrial imaging, nanosensors, fluorescent probes, chromatographic fingerprints, computational models, and biostatistical applications. Several chapters have shown the effect of

pro-oxidation and antioxidants as inflammatory mediators in signaling pathways leading from the initial stimulus to termination through redox cycles. Such books save the investigator significant time and effort allowing them to focus on their topic of interest. The overall series has 266 cutting-edge technologies to select from at the present time.

I acknowledge Dennis Armstrong who assisted me with organization, computerization, and updated technology, the in-house editors, and numerous colleagues who encouraged me to develop and expand the series.

Gainsville, FL, USA ***Donald Armstrong***

Contents

Part II Antioxidant Technology and Application

Contributors

H.A. Abu-Rizq • *Aridland Agricultural Production Program (AAPP), Environment and Life Sciences Centre, Kuwait Institute for Scientific Research (KISR), Safat, Kuwait*

Mohammad Afzal • *Department of Biological Sciences, Faculty of Science, Kuwait University, Safat, Kuwait*

Silvana Andreescu • *Department of Chemistry and Biomolecular Science, Clarkson University, Potsdam, NY, USA*

Cristina Bischin • *Department of Chemistry and Chemical Engineering, Babes-Bolyai University, Cluj-Napoca, Romania*

Nathan S. Bryan • *Department of Integrative Biology and Pharmacology, Texas Therapeutics Institute, Brown Foundation Institute of Molecular Medicine, The University of Texas Graduate School of Biomedical Sciences at Houston, The University of Texas Health Science Center at Houston, Houston, TX, USA*

Juan M. Casas-Solvas • *Department of Chemistry and Physics, University of Almería, Almería, Spain*

Casey D. Charvet • *Department of Ophthalmology and Visual Sciences, Case Western Reserve University, Cleveland, OH, USA*

Xiwei Chen • *Department of Biostatistics, New York State University at Buffalo, Buffalo, NY, USA*

Steven A. Cohen • *Department of Chemistry, University of British Columbia, Kelowna, BC, Canada*

Mario Contin • *Department of Analytical Chemistry, Faculty of Pharmacy and Biochemistry, Universidad de Buenos Aires, Buenos Aires, Argentina*

Deborah Custers • *Division of Food, Medicines, and Consumer Safety, Section Medicinal Products, Scientific Institute of Public Health (WIV-ISP), Brussels, Belgium*

Valentina D'Oria • *Research Laboratories, Bambino Gesu' Pediatric Hospital IRCCS, Rome, Italy*

Grigore Damian • *Department of Physics, Babes-Bolyai University, Cluj-Napoca, Romania*

Eric Deconinck • *Division of Food, Medicines, and Consumer Safety, Section Medicinal Products, Scientific Institute of Public Health (WIV-ISP), Brussels, Belgium*

Laura Estévez • *Department of Physical Chemistry, University of Vigo, Vigo, Spain*

Maria Fedorova • *Institute of Bioanalytical Chemistry, Faculty of Chemistry and Mineralogy and Center for Biotechnology and Biomedicine, Universität Leipzig, Leipzig, Germany*

Sabrina Flor • *Department of Analytical Chemistry, Faculty of Pharmacy and Biochemistry, Universidad de Buenos Aires, Buenos Aires, Argentina*

Detao Gao • *Department of Molecular Cardiology, Lerner Research Institute, Cleveland Clinic, Cleveland, OH, USA*

Mercedes García-Bugarín • *Department of Inorganic Chemistry, University of Vigo, Vigo, Spain*

Luis García-Fuentes • *Department of Chemistry and Physics, University of Almería, Almería, Spain*

Behrouz Gharesi-Fard • *Immunology Department, Shiraz University of Medical Sciences, Shiraz, Fars, Iran*
Albert W. Girotti • *Department of Biochemistry, Medical College of Wisconsin, Milwaukee, WI, USA*
W. Broc Glover • *Department of Chemistry, University of British Columbia, Kelowna, BC, Canada*
İlhami Gülçin • *Department of Chemistry, Faculty of Science, Atatürk University, Erzurum, Turkey; Department Zoology, College of Science, King Saud University, Riyadh, Saudi Arabia*
Dimitra Hadjipavlou-Litina • *Department of Pharmaceutical Chemistry, School of Pharmacy, Aristotle University of Thessaloniki, Thessaloniki, Greece*
Ingrit Hamann • *Faculty of Pharmacy and Pharmaceutical Sciences, University of Alberta, Edmonton, AB, Canada*
Keli Han • *Dalian Institute of Chemical Physics, Chinese Academy of Sciences, Dalian, Liaoning, China*
Andrea Hartwig • *Institute of Applied Biosciences, Food Chemistry and Toxicology, Karlsruhe Institute of Technology (KIT), Karlsruhe, Germany*
Yuning Hong • *Department of Chemistry and Institute for Advanced Study, The Hong Kong University of Science and Technology, Clear Water Bay, Kowloon, Hong Kong, China*
Zafar Iqbal • *Department of Pharmacy, University of Peshawar, Peshawar, Pakistan*
Abad Khan • *Department of Pharmacy, University of Peshawar, Peshawar, Pakistan; Department of Pharmacy, University of Swabi, Swabi, Pakistan*
Muhammad Imran Khan • *Department of Pharmacy, University of Peshawar, Peshawar, Pakistan; Department of Pharmacy, Women Institute of Learning, Abbottabad, Pakistan*
Lucia Kovacikova • *Institute of Experimental Pharmacology and Toxicology, Slovak Academy of Sciences, Bratislava, Slovakia*
Tamas Kriska • *Department of Pharmacology and Toxicology, Medical College of Wisconsin, Milwaukee, WI, USA*
Chris W.T. Leung • *Department of Chemistry, The Hong Kong University of Science and Technology, Clear Water Bay, Kowloon, Hong Kong, China*
Peng Li • *Dalian Institute of Chemical Physics, Chinese Academy of Sciences, Dalian, Liaoning, China*
Ran Liang • *Department of Chemistry, Renmin University of China, Beijing, China*
Dov Lichtenberg • *Department of Physiology and Pharmacology, Sackler School of Medicine, Tel Aviv University, Tel-Aviv, Israel*
Zhangrong Lou • *Dalian Institute of Chemical Physics, Chinese Academy of Sciences, Dalian, Liaoning, China*
Silvia Lucangioli • *Department of Pharmaceutical Technology, Faculty of Pharmacy and Biochemistry, Universidad de Buenos Aires, Consejo Nacional de Investigaciones Cientificas y Tecnológicas, CONICET, Buenos Aires, Argentina*
Luís M. Magalhães • *REQUIMTE, Department of Chemical Sciences, Faculty of Pharmacy, University of Porto, Porto, Portugal*
Magdalena Majekova • *Institute of Experimental Pharmacology and Toxicology, Slovak Academy of Sciences, Bratislava, Slovakia*
Tadeusz Malinski • *Department of Chemistry & Nanomedical Research Laboratories, Ohio University, Athens, OH, USA*

Mohamed H. Mansour • *Department of Biological Sciences, Faculty of Science, Kuwait University, Safat, Kuwait*
Manuela Martinefski • *Department of Analytical Chemistry, Faculty of Pharmacy and Biochemistry, Universidad de Buenos Aires, Buenos Aires, Argentina*
Manuel C. Martos-Maldonado • *Department of Chemistry and Physics, University of Almería, Almería, Spain*
Ivana Milic • *Institute of Bioanalytical Chemistry, Faculty of Chemistry and Mineralogy and Center for Biotechnology and Biomedicine, Universität Leipzig, Leipzig, Germany*
Ricardo A. Mosquera • *Department of Physical Chemistry, University of Vigo, Vigo, Spain*
Augustin C. Mot • *Department of Chemistry and Chemical Engineering, Babes-Bolyai University, Cluj-Napoca, Romania*
Susan J. Murch • *Department of Chemistry, University of British Columbia, Kelowna, BC, Canada*
Ernst H. Oliw • *Division of Biochemical Pharmacology, Department of Pharmaceutical Biosciences, Uppsala Biomedical Center, Uppsala University, Uppsala, Sweden*
Jacques Omer De Beer • *Division of Food, Medicines, and Consumer Safety, Section Medicinal Products, Scientific Institute of Public Health (WIV-ISP), Brussels, Belgium*
Stella A. Ordoudi • *Laboratory of Food Chemistry and Technology, School of Chemistry, Aristotle University of Thessaloniki, Thessaloniki, Greece*
Stefania Petrini • *Research Laboratories, Bambino Gesu' Pediatric Hospital IRCCS, Rome, Italy*
Fiorella Piemonte • *Research Laboratories, Bambino Gesu' Pediatric Hospital IRCCS, Rome, Italy*
Dan Pierini • *Department of Integrative Biology and Pharmacology, Texas Therapeutics Institute, Brown Foundation Institute of Molecular Medicine, The University of Texas Graduate School of Biomedical Sciences at Houston, The University of Texas Health Science Center at Houston, Houston, TX, USA*
Irina A. Pikuleva • *Department of Ophthalmology and Visual Sciences, Case Western Reserve University, Cleveland, OH, USA*
Ilya Pinchuk • *Department of Physiology and Pharmacology, Sackler School of Medicine, Tel Aviv University, Tel-Aviv, Israel*
Eugene A. Podrez • *Department of Molecular Cardiology, Lerner Research Institute, Cleveland Clinic, Cleveland, OH, USA*
Eleni Pontiki • *Department of Pharmaceutical Chemistry, School of Pharmacy, Aristotle University of Thessaloniki, Thessaloniki, Greece*
Salette Reis • *REQUIMTE, Department of Chemical Sciences, Faculty of Pharmacy, University of Porto, Porto, Portugal*
Lawrence M. Sayre • *Department of Chemistry, Case Western Reserve University, Cleveland, OH, USA*
Marcela A. Segundo • *REQUIMTE, Department of Chemical Sciences, Faculty of Pharmacy, University of Porto, Porto, Portugal*
Erica Sharpe • *Department of Chemistry and Biomolecular Science, Clarkson University, Potsdam, NY, USA*
Takayuki Shibamoto • *Department of Environmental Toxicology, University of California, Davis, CA, USA*
Radu Silaghi-Dumitrescu • *Department of Chemistry and Chemical Engineering, Babes-Bolyai University, Cluj-Napoca, Romania*

Leif H. Skibsted • *Food Chemistry, Department of Food Science, University of Copenhagen, Frederiksberg C, Denmark*
Milan Stefek • *Institute of Experimental Pharmacology and Toxicology, Slovak Academy of Sciences, Bratislava, Slovakia*
Ge Tao • *Department of Biostatistics, New York State University at Buffalo, Buffalo, NY, USA*
Ildikó V. Tóth • *REQUIMTE, Department of Chemical Sciences, Faculty of Pharmacy, University of Porto, Porto, Portugal*
Valeria Tripodi • *Department of Pharmaceutical Technology, Faculty of Pharmacy and Biochemistry, Universidad de Buenos Aires, Consejo Nacional de Investigaciones Cientificas y Tecnológicas, CONICET, Buenos Aires, Argentina*
Maria Z. Tsimidou • *Laboratory of Food Chemistry and Technology, School of Chemistry, Aristotle University of Thessaloniki, Thessaloniki, Greece*
Antonio Vargas-Berenguel • *Department of Chemistry and Physics, University of Almería, Almería, Spain*
Albert Vexler • *Department of Biostatistics, New York State University at Buffalo, Buffalo, NY, USA*
Anneli Wennman • *Division of Biochemical Pharmacology, Department of Pharmaceutical Biosciences, Uppsala Biomedical Center, Uppsala University, Uppsala, Sweden*
Jian-Ping Zhang • *Department of Chemistry, Renmin University of China, Beijing, China*
Ben Zhong Tang • *Department of Chemistry, The Hong Kong University of Science and Technology, Clear Water Bay, Kowloon, Hong Kong, China; Institute for Advanced Study, The Hong Kong University of Science and Technology, Clear Water Bay, Kowloon, Hong Kong, China; Division of Biomedical Engineering, The Hong Kong University of Science and Technology, Clear Water Bay, Kowloon, Hong Kong, China; State Key Laboratory of Molecular Neuroscience, The Hong Kong University of Science and Technology, Clear Water Bay, Kowloon, Hong Kong, China; Institute of Molecular Functional Materials, The Hong Kong University of Science and Technology, Clear Water Bay, Kowloon, Hong Kong, China*

Part I

Reactive Oxygen and Nitrogen Techniques

Chapter 1

Derivatization and Detection of Small Aliphatic and Lipid-Bound Carbonylated Lipid Peroxidation Products by ESI-MS

Ivana Milic and Maria Fedorova

Abstract

Double bonds in polyunsaturated fatty acids (PUFA) and lipids are one of the major targets of reactive oxygen species (ROS). The resulting lipid peroxidation products (LPP) represent a group of chemically diverse compounds formed by several consecutive oxidative reactions. Oxidative cleavage leads to the formation of small aliphatic and lipid-bound aldehydes and ketones (oxoLPPs). These strong electrophiles can readily react with nucleophilic substrates, for example, side chains in proteins which can alter structure, function, and cellular distribution of the modified proteins. Despite growing interest in the field of oxidative lipidomics, only a few dominantly formed oxoLPP were identified. Due to the chemical and physical properties, aliphatic oxoLPPs are usually analyzed using gas chromatography-mass spectrometry (GC- MS), while nonvolatile lipid-bound oxoLPPs require liquid chromatography-mass spectrometry (LC-MS). To overcome the need for the two analyses, we have developed a new derivatization strategy to capture all oxoLPP independent to their properties with electrospray ionization (ESI) MS allowing simultaneous detection of aliphatic and lipid-bound oxoLPPs. Thus, the 7-(diethylamino)coumarin-3-carbohydrazide (CHH) derivatization reagent allowed us to identify 122 carbonyl compounds in a mixture of four PUFA and phosphatidylcholines (PC) oxidized in vitro.

Key words Derivatization, ESI-MS, Lipid peroxidation, Reactive carbonyls

1 Introduction

Oxidative stress is generally characterized by overproduction of reactive oxygen species (ROS), which can damage virtually all components of the cell, including proteins, lipids, and DNA. In that respect, oxidized lipids, proteins, and DNA are often used to characterize the extent of oxidative damages [1]. Polyunsaturated fatty acids (PUFA) and lipids are particularly vulnerable to oxidation due to the high reactivity of allylic carbons toward ROS. Lipid hydroperoxides are formed through several consecutive reactions initiated by the hydroperoxyl radical attack at double bond of free PUFA or as a part of phospholipids, which are considered as early

Donald Armstrong (ed.), *Advanced Protocols in Oxidative Stress III*, Methods in Molecular Biology, vol. 1208,
DOI 10.1007/978-1-4939-1441-8_1,

lipid peroxidation products. Further oxidation of lipid hydroperoxydes can cleave the alkyl chain, thus generating a wide variety of small aliphatic oxoLPPs and lipid-bound carbonyls, usually termed lipid peroxidation end products [2]. Altogether, these reactive electrophiles can readily react with nucleophilic substrates such as amino acid side chains (cysteine, histidine, and lysine), forming stabile adducts. Thus ε-amino group in lysine can yield both Michael and Schiff base adducts, while the thiol group in cysteine and the secondary amine in histidine are modified via Michael addition. Once modified by reactive aldehydes, proteins can lose their biological activity or initiate a wide variety of inflammatory and immunogenic responses [3, 4].

Since hydroxy-alkenals were discovered in 1975, and soft ionization techniques introduced into mass spectrometry in the late 1980s, oxoLPP modification of proteins has been intensively studied. 4-Hydroxy-2-nonenal, malondialdehyde and acrolein, the most studied oxoLPPs, are considered as good biomarkers of oxidative stress [5–7]. Various studies linked these oxoLPPs to the onset of several cardiovascular and neurodegenerative diseases, such as atherosclerosis, diabetes mellitus, and Parkinson's, Huntington's, and Alzheimer's disease as well as aging [8, 9]. Moreover, since biological membranes consist mostly of phospholipids (70–80 %), lipid peroxidation can influence the membrane properties, such as fluidity, permeability, and ion transport. Additionally, the glycerophosphatidylethanolamines are reactive toward aldehydes predominantly forming Schiff bases. Depending upon the oxoLPP structure, these modifications can introduce positive or negative membrane curvatures or induce inflammation [10, 11].

Owing to growing evidences of the biological significance of oxoLPPs, the interest in oxo-lipidomics research has rapidly increased. So far, relatively low numbers of oxoLPPs have been indentified relative to the predicted chemical structures, most likely due to analytical limitations. The thiobarbituric acid assay, commonly employed for the quantification of malondialdehyde, shows low specificity and sensitivity [12]. These limitations can be overcome by HPLC separation but still do not provide structural information about the detected aldehydes [13]. Nowadays, HPLC techniques coupled to mass spectrometry seem to be best suited for detection and identification of oxoLPPs. However, low ionization efficiency of carbonyl group challenges mass spectrometry analysis. Therefore, the analytical strategy usually employs chemical derivatization of carbonyls prior to LC-MS. While aliphatic aldehydes have low ionization efficiencies, phospholipid-bound (PL-bound) aldehydes can be analyzed directly. Nevertheless, due to the different ionization efficiencies of phospholipids, the direct analysis of PL-bound aldehydes in complex mixtures can suppress phospholipid classes with lower ionization efficiencies or even completely discriminate those that are not ionizable in the

selected ion mode. Therefore, adequately designed carbonyl specific derivatization tags would allow the same conditions for the analysis of all PL-bound aldehydes, but additionally discriminate the PL-bound LPPs with the carboxyl moiety.

Using LC-MS with electrospray ionization (ESI) in the positive ion mode and no derivatization step, Domingues's group recently reported only PL-bound aldehydes after oxidation of phosphatidylcholines [14, 15], which was confirmed by dinitrophenylhydrazine (DNPH) derivatization of in vitro oxidized phosphatidylcholines. Since aliphatic alkenals and hydroxyalkenals are discriminated in the positive ion mode ESI-MS [16], they are usually analyzed by GC-MS after derivatization with O-(2,3,4,5,6-pentafluorobenzyl)hydroxylamine, while PL-bound aldehydes are not detected or at least have not been reported by now [17]. To the best of our knowledge, no derivatization reagent has been reported for the simultaneous detection of both aliphatic and PL-bound oxoLPPs in positive ion mode ESI-MS.

To overcome the aforementioned limitations, we have used 7-(diethylamino)coumarin-3-carbohydrazide (CHH) as a carbonyl derivatization reagent [18]. Its tertiary amino group significantly improved ionization efficiencies of oxoLPPs. Moreover, derivatized polar short chain alkenals, hydroxy-alkenals, and oxo-carboxylic acids can be simultaneously extracted with PL-bound derivatives using organic solvents and separated by reversed-phase chromatography (RPC). Here, we describe derivatization of aldehyde standards, in vitro oxidized PUFA and PL, and complex biological samples as cell pellets and blood plasma. We have also designed ESI-MS acquisition methods combining gas phase fractionation with data-dependent acquisition (DDA), without requirements for chromatographic separation of derivatized oxoLPPs prior to the analysis. We describe in detail how to combine high mass accuracy of FT-MS scans with the information obtained from tandem mass spectra to reveal the structures of different oxoLPP classes, present even in complex sample mixtures.

2 Materials

2.1 Chemicals and Solutions

1. Methanol and dimethylformamide were purchased from Biosolve (Valkenswaard, Netherlands), chloroform from Merck KGaA (Darmstadt, Germany), ethanol from Carl Roth GmbH & Co. KG (Karlsruhe, Germany).
2. Copper(II) sulfate and ascorbic acid were obtained from Fluka Chemie GmBH (Buchs, Switzerland). Stock solutions (5 mmol/L and 20 mmol/L) were prepared by dissolving $CuSO_4$ (1.6 mg) or ascorbic acid (7 mg) in deionized water (2 mL), respectively (*see* **Note 1**).

3. A stock solution of 7-(diethylamino)coumarin-3-carbohydrazide (CHH, 0.1 mol/L, Sigma-Aldrich GmbH, Taufkirchen, Germany) was prepared in dimethylformamide and stored in an amber polypropylene tube (Eppendorf, 1.5 mL) at 4 °C.
4. Ammonium formate was from Sigma-Aldrich GmbH (Taufkirchen, Germany). The ESI-solution was prepared by dissolving 0.0315 g of NH_4HCO_2 in a mixture of 66 mL of methanol and 33 mL of chloroform. This solution was degassed for 15 min in the ultrasonic bath.

2.2 Lipid Standards

1. Hexanal was from Sigma-Aldrich GmbH (Taufkirchen, Germany). Stock solution of 25 mM was prepared in methanol and stored at −20 °C.
2. 2-Hydroxy-2-nonenal (HNE) was from Enzo Life Sciences (Lausen, Switzerland). Aliquots of 25 mM HNE in ethanol (Carl Roth GmbH & Co. KG) were stored at −80 °C.
3. Oleic, linoleic, arachidonic, and docosahexaenoic acid were purchased from Sigma-Aldrich GmbH (Taufkirchen, Germany) and stored at −20 °C.
4. 1-Palmitoyl-2-(9-oxononanoyl)-*sn*-glycerophosphatidylcholine (PNPC) was purchased from Avanti Polar Lipids, Inc. (Alabaster, Alabama), dissolved in chloroform, and aliquoted in borosilicate glass. Aliquots were dried and stored under nitrogen at −80 °C.
5. 1-Palmitoyl-2-oleoyl-*sn*-glycerolphosphatidylcholine (POPC), 1-palmitoyl-2-linoleoyl-*sn*-glycerolphosphatidylcholine (PLPC), 1-stearoyl-2-arachidonyl-sn-glycerolphosphatidylcholine (SAPC), and 1-palmitoyl-2-docosahexanoyl-*sn*-glycerolphosphatidylcholine (PDPC) were purchased from Avanti Polar Lipids, Inc. (Alabaster, Alabama) as 25 mg (10 mg/mL) chloroform solutions. These solutions were aliquoted and stored in borosilicate glass vials at −80 °C.

3 Methods

3.1 Derivatization of Lipid Peroxidation-Derived Carbonyls

3.1.1 Classical Methods

1. Dinitrophenylhydrazine (DNPH) is widely used for chemical derivatization of protein carbonylation sites. It is known to derivatize PL-bound carbonyl compounds and allows their identification in positive ion mode ESI-MS [19]. Due to the instability of the formed Schiff base, it is usually reduced to amines with cyanoborohydride. This protocol is published in [20].
2. 4-(2-(Trimethylammonio)ethoxy)benzenaminium halide (4-APC) was recently shown to selectively derivatize carbonyl groups of small aliphatic aldehydes. It can be used for their identification and

quantification using positive ion mode MS [21]. Although it appears promising, the reagent is still not commercially available.

3. O-(2,3,4,5,6-Pentafluorobenzyl)hydroxylamine (PFBHA) is a derivatizing reagent widely used for the derivatization of aliphatic aldehydes prior to gas chromatography-mass spectrometry (GS-MS) in positive ion mode. The derivatization protocol was reported earlier [22].

3.1.2 Derivatization of Hexanal, HNE, and PNPC

This section describes a strategy for derivatization of standard carbonyl compounds. Hexanal, HNE, and PNPC, three structurally different and biologically relevant aldehydes, derived from peroxidation of linoleic acid and PLPC, were derivatized with CHH.

1. Stock solutions of hexanal (2 μL, 25 mmol/L) and HNE (2 μL, 25 mmol/L) were separately diluted with deionized water (3 μL) to obtain 10 mmol/L solutions.
2. Dried PNPC (25 μg) was reconstituted in 5 μL of 50 % aqueous methanol to obtain a 7.7 mmol/L PNPC solution.
3. Carbonyl groups were derivatized with CHH by mixing equally concentrated sample and CHH in a ratio 1:10 (v/v). Briefly, hexanal (5 μL, 10 mmol/L) and HNE (5 μL, 10 mmol/L) were separately derivatized with CHH (50 μL, 10 mmol/L in 50 % aqueous acetonitrile). Derivatization of PNPC (5 μL, 7.7 mmol/L in 50 % aqueous acetonitrile) was done using CHH (50 μL of 7.7 mmol/L in 50 % aqueous acetonitrile). Mixtures were incubated at 37 °C for 1 h and used directly for measurement or stored at −20 °C (*see* **Note 2**).

3.1.3 Derivatization of Carbonyl Compounds Derived from In Vitro PUFA Oxidation

This section demonstrates strategies for in vitro oxidation of PUFA and derivatization of carbonyl compounds with CHH.

1. Pure oleic (0.95 μL), linoleic (0.94 μL), arachidonic (0.84 μL), and docosahexaenoic acid (1.05 μL) were separately dissolved in 30 μL of ethanol. To each solution was added deionized water (225 μL), $CuSO_4$ (30 μL, 5 mmol/L), and ascorbic acid (15 μL, 20 mmol/L), and samples were rigorously vortexed (*see* **Note 3**). Final oxidation reaction mixture consisted of 10 mmol/L PUFA, 0.5 mmol/L $CuSO_4$, and 1 mmol/L ascorbic acid in 10 % aqueous ethanol (*see* **Note 4**). Reaction mixtures were incubated for 72 h at 37 °C. Samples were aliquoted and stored at −20 °C for further analysis (*see* **Note 5**).
2. Derivatization of carbonyl groups with CHH was done by mixing equally concentrated sample and CHH in a ratio of 1:10 (v/v). Each oxidized PUFA solution (5 μL, 10 mmol/L) was mixed with CHH (50 μL, 10 mmol/L in 50 % aqueous acetonitrile) and incubated for 1 h at 37 °C. Samples can be analyzed immediately or stored at −20 °C for up to 3 months.

3.1.4 Derivatization of Carbonyl Groups Derived from In Vitro Oxidation of PC Vesicles

This section illustrates strategies for the formation and in vitro oxidation of lipid vesicles, as well as derivatization of formed low and PC-bound LPP with CHH.

1. Stock solutions of POPC, PLPC, SAPC, and PDPC (16.25 μL, 10 mg/mL) were mixed in flat-bottom borosilicate glass vial with 365 μL of chloroform. PC mixtures were slowly dried under a steam of nitrogen and rehydrated in ammonium-bicarbonate buffer (143 μL, 3 mM, pH 7.6). Solution was sonicated in ultrasonic bath for 15 min to produce 1.5 mmol/L PC vesicles (*see* **Note 6**).
2. PC vesicles (125 μL, 1.5 mmol/L) were mixed with water (363.75 μL), $CuSO_4$ (7.5 μL, 5 mmol/L), and ascorbic acid (3.75 μL, 20 mmol/L). The final oxidation mixture consisted of 1.5 mmol/L PC vesicles, 75 μmol/L $CuSO_4$, and 150 μmol/L ascorbic acid in 0.75 mmol/L ammonium-bicarbonate buffer.
3. PC vesicles were oxidized for 72 h at 37 °C. Samples were aliquoted and stored at −20 °C prior to further analysis (*see* **Note 5**).
4. Derivatization of carbonyl groups with CHH was done by mixing equally concentrated sample and CHH in the ratio 1:10 (v/v). Each oxidized PUFA solution (5 μL, 10 mmol/L) was incubated with CHH (50 μL, 10 mmol/L in 50 % aqueous acetonitrile) for 1 h at 37 °C. Samples can be analyzed immediately or stored at −20 °C for up to 3 months.

3.1.5 Derivatization of Low Molecular Weight and PC-Bound Carbonyls Derived from Primary Fibroblasts and Pooled Blood Plasma

This section explains in details the derivatization of lipid-derived carbonyl compounds extracted from primary fibroblasts or human blood plasma.

1. Primary fibroblasts were grown in T75 culture flasks until 75 % confluence. Cells were detached with trypsin. The cell pellet was washed three times with cold PBS, resuspended in 50 μL of ice cold 0.1 % aqueous ammonium-acetate, followed by centrifugation at $500 \times g$. Aqueous phase was discarded. It is recommended to immediately perform lipid extraction (*see* **Note 7**).
2. Carbonylated oxoLPPs were analyzed in 5 μL of pooled human male serum (Sigma-Aldrich GmbH, Taufkirchen, Germany) per assay.
3. Derivatization of lipid-derived carbonyls present in cells or blood plasma should be done prior to the lipid extraction due to the volatile nature of aliphatic aldehydes. We have observed a significantly lower number of detected carbonyls when the derivatization step followed lipid extraction due to the loss of volatile aliphatic aldehydes most probably during the drying of lipid extracts. CHH-derivatization of lipid-derived carbonyls

prior to the lipid extraction minimizes their volatility and prevents their loss during lipid extraction.

4. For the derivatization of lipid-bound carbonyls, cell pellets and 5 μL of pooled blood plasma were mixed with 50 and 45 μL of 0.1 % aqueous ammonium-acetate, respectively. In both cases derivatization of carbonyls was performed by adding 3.5 μL of 100 mmol/L CHH stock solution, that is, 7 mmol/L CHH in the final derivatization mixture. Incubation was done for 1 h at 37 °C.
5. Following CHH-derivatization, 25 μL of deionized water was added to each sample to increase the water content prior to liquid-liquid extraction. Lipids were extracted using methyl-tert-butyl ether (MTBE) as described previously [23]. Briefly, 350 μL of methanol (*see* **Note 8**) and 1,250 μL of MTBE were added stepwise to CHH-derivatized cell pellets or plasma samples, followed by 10 s vortexing after each step. The mixture was left on rotating shaker for 1 h at 4 °C.
6. To induce phase separation, 313 μL of deionized water was added. Samples were left on a rotary shaker for additional 10 min and centrifuged for 10 min at 1,000 × *g*. Upper phase was collected in the separate polypropylene tube (Eppendorf, 2 mL).
7. The lipid-containing organic phase forms the upper layer due to the lower density of MTBE compared to water. Thus, contamination of organic phase during its recovery is minimized. Additionally, extraction with MTBE shows higher recoveries for polar compounds than standard extraction protocols used in lipidomics, e.g., Folch or Bligh and Dyer methods.
8. Remaining aqueous phase was diluted with 500 μL of a mixture consisting of MTBE, methanol, and water in a ratio of 4:1.2:1 (v/v/v), vortexed and centrifuged for 10 min at 1,000 × *g*. The upper phase was combined with the first one and dried under vacuum.
9. Dried lipid extracts were reconstituted in 50 μL of ESI-solution directly prior to analysis or stored at −20 °C under nitrogen for up to 6 weeks.

3.2 Detection of LPPs

3.2.1 Classical Methods

Measurement of lipid peroxidation-derived carbonyls by mass spectrometry represents a challenging task due to the low ionization efficiencies of aldehyde and keto groups by ESI and MALDI. Chemical derivatization of carbonyl groups with a reagent that provides high proton affinities is a usual approach for carbonyl measurement by MS.

1. DNPH-derivatized PC-bound aldehydes and ketones can be analyzed in positive ion mode ESI-MS with a mass shift of 180 u corresponding to the hydrazones, while small LPPs are

discriminated. DNPH-derivatized PC-bound LPP exhibit specific fragmentation patterns under CID conditions that can be used as an additional confirmation of the carbonyl group. This protocol for the measurement and data interpretation was reported recently [16]. DNPH derivatives of small aliphatic aldehydes and ketones can be analyzed in negative ion mode using atmospheric pressure photoionization-mass spectrometry (APPI-MS), as it was shown in [24].

2. PFBHA-derivatization followed by GC-MS is still the most popular method for analyzing aldehydes and ketones. Derivatized carbonyls show fragment ions corresponding to the signals with *m/z* 181 characteristic of PFB-oximes. Additionally, depending upon a structure of derivatized aldehyde or ketone, several other fragment reporter ions are observed. Detailed protocols for spectra analyses are available at [22].

3.2.2 ESI-MS/MS Analysis as a Tool for Identification of CHH-Derivatized Carbonyls

CHH-derivation of carbonyl groups allowed the simultaneous extraction and detection of both low and high molecular weight oxoLPPs. The high hydrophobicity of CHH enables simultaneous extraction of water soluble, lipid-bound, and highly hydrophobic aldehydes. The tertiary amine group present in CHH allows a superior ionization of derivatives in the positive ion mode. Specific neutral loss and fragment ions generated during CID fragmentation of derivatized compounds can be used for unequivocal identification of carbonyl compounds.

1. Samples were diluted to 10 pmol/μL in ESI-solution (*see* Subheading 2.1, **item 4**) and analyzed by direct infusion (15 μL) using robotic nanoflow ion source TriVersa NanoMate (Advion BioSciences, Ithaca, NY) and nanoelectrospray chips (1.4 kV ionization voltage, 0.4 psi nitrogen backpressure) coupled to an LTQ Orbitrap XL ETD mass spectrometer (Thermo Fisher Scientific GmbH, Bremen, Germany) operated in positive ion mode. Transfer capillary temperature was 200 °C and the tube lens voltage was set to 120 V. Mass spectra were acquired with a target mass resolution of 100,000 at *m/z* 400 in the Orbitrap mass analyzer.
2. Tandem mass spectra (MS/MS) were acquired in the linear ion trap (LTQ) using an isolation width of 1.5 Da and previously optimized collision-induced dissociation (CID) normalized collision energy (nCE) of 35 %. Helium was used as collision gas.
3. CHH-derivatized oxoLPPs derived from PUFA oxidations were measured for 15 min using data-dependent acquisition (DDA from *m/z* 300–800). Five most intense ions from each MS survey scan acquired in Orbitrap were selected for CID fragmentation in the LTQ. *M/z* values corresponding to the fragmented ions were excluded from DDA for a period of 300 s with the maximal exclusion list size of 500 *m/z* values.

4. Due to the presence of high amounts of unmodified lipids derived from in vitro oxidized PC vesicles, cell and plasma extracts, detection of oxoLPPs required optimization of MS acquisition conditions to get MS/MS information for low abundant ions of carbonylated LPP. Therefore, gas phase fractionation (GPF) was used. DDA (top 5) spectra were acquired for several consecutive narrow m/z ranges (280–450, 450–600, 600–750, 750–900, 900–1,100 m/z) for 3 min. The isolation width was set to 1 u in the first two segments and 1.5 u in the following three segments. Analyzed m/z values were excluded from DDA for only 45 s allowing the collection of at least four tandem spectra for each compound. The total analysis time was 15 min. As the ion trap requires a certain offset to isolate the highest number of precursor ions, one representative signal was selected for each m/z range in GPF mode to optimize the isolation offset. Interestingly, the isolation offset depended on the m/z value. In the lowest m/z range (280–450), the highest signal intensity was obtained for an offset of zero. The optimum isolation offset increased stepwise by 0.1 u for each of the subsequent GPF segments, reaching 0.4 u for the upper mass range (m/z 900–1,100). For each segment, a specific offset of the precursor ion isolation in the LTQ was used (0, 0.1, 0.2, 0.3, and 0.4 Da). Recorded spectra were analyzed with Xcalibur (version 2.0.7, Thermo Fisher).
5. All tandem mass spectra of derivatized oxoLPPs were interpreted manually.

3.3 Data Interpretation

This section describes the general strategy to interpret CID tandem mass spectra, including reporter and neutral loss ions specific for CHH-derivatized saturated, unsaturated, and hydroxylated oxoLPP.

3.3.1 Assignment of CHH Specific Fragment Ions

CID fragmentation of pure CHH standard (m/z 276.13) yielded a base peak at m/z 244 corresponding to the loss of the hydrazine moiety (cleavage of amide bound; -N_2H_4, –32 u) and two weaker signals at m/z 262 and 218 (Fig. 1a). These ions were used for specific identification of CHH-oxoLPP derivatives and further to referred as reporter ions.

3.3.2 Interpretation of CID Spectra of Derivatized Alkenals, Alkanals, and Dicarbonyls

1. CHH-hexanal adduct (m/z 358.21) was fragmented using CID. The base peak of the tandem mass spectrum corresponded to the CHH-reporter ion at m/z 244 (Fig. 1b). CID spectra of hexanal and of all other alkanals do not contain any aldehyde specific ions due to the absence of preferential fragmentation sites, such as double bounds or functional groups along the aliphatic chain.
2. Fragmentation of CHH-4-octenal adduct (m/z 384.23; Fig. 1c) detected after oxidation and derivatization of linoleic

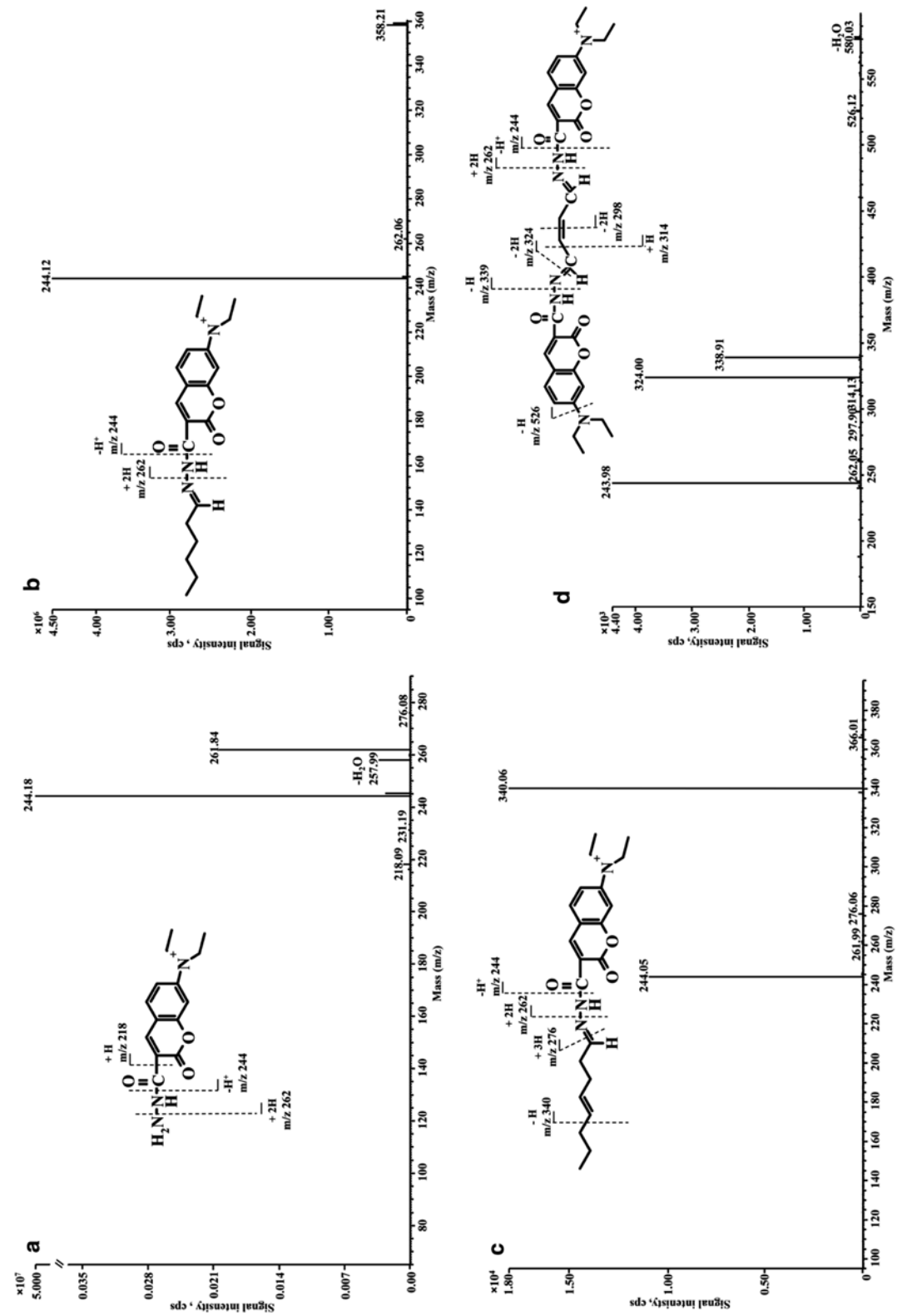

Fig. 1 CID spectra of CHH (**a**) and CHH-derivatives of hexanal (**b**), 4-hexenal (**c**), and 4-oxo-2-butenal (**d**)

acid and PC vesicles also resulted in intense CHH-reporter ions visible as signal at m/z 244. However, the base peak at m/z 340 corresponded to propane neutral loss ($-C_3H_8$, −44 Da) formed by cleavage next to the double bound.

3. Dicarbonyl compounds were doubly derivatized. For instance, 4-oxo-2-butenal was detected in the oxidized PUFA mixtures and PC vesicles as a double CHH-derivative (m/z 599.26; Fig. 1d). Peaks corresponding to the neutral loss of CHH ($-C_{14}H_{17}N_3O_3$, −275 Da) and CHH-reporter ions were present in all tandem mass spectra of doubly derivatized oxoLPPs. The CID spectrum of CHH-4-oxo-2-butenal additionally showed peaks due to the neutral losses of diethylamine ($-C_4H_{11}N$, −73 Da) and 7-(diethylamino)-2-oxo-coumarin ($-C_{14}H_{16}N_2O_3$, −260 Da). Structure-specific signals at m/z 298 and 314 resulted from neutral loss of CHH-ethanal ($-C_{16}H_{19}N_3O_3$; −301 Da) and fragmentation adjacent to the double bond of aldehyde.

3.3.3 Interpretation of CID Spectra of Derivatized Hydroxy- and Dihydroxy-Alkanals

Hydroxy-alkenals are well-known biomarkers of lipid peroxidation and oxidative stress in general. Some of them like HNE and 4-hydroxy-2-hexenal (HHE) are specific for the peroxidation of ω-6 and ω-3 fatty acids. Their elevated concentrations were detected in blood plasma of patients with atherosclerosis and diabetes. Derivatization reagents providing superior ionization efficiencies could improve the detection of hydroxy-alkenals in other biological materials as well. Moreover, profiling of hydroxy-alkenals in mixtures of oxidized abundant PUFA in humans could reveal other hydroxy-alkenals as candidates for lipid oxidative damage. Due to the presence of double bond(s) and hydroxyl groups, CID fragmentation of hydroxy-alkenals displays rich tandem mass spectra with relatively intense peaks corresponding to the ions formed by the loss of the hydroxyl group, which represents the main characteristic of this class of alkanals.

1. The base peak in CID spectrum of CHH-4-hydroxy-2-nonenal (m/z 414.24) corresponded to the CHH-reporter ion at m/z 244. Other signals represented aldehyde specific fragments. Elimination of water from the C-4 atom of 4-hydroxy-2-nonenal most likely generates a new double bond between C-4 and C-5 atoms (Fig. 2a). Similarly, fragmentation between C-4 and C-5 atoms is followed by a water loss generating a fragment ion observable as peak at m/z 326. In the same way, peaks at m/z 340 and 354 can be explained by fragmentation between C-5/C-6 and C-6/C-7 atoms followed by the loss of water. Fragmentation along the alkyl chain adjacent to the double bond at C-2 generates a signal at m/z 314, while peak at m/z 340 can be explained as alkyl chain cleavage between C-5 and C-6 followed by the water elimination. Two other

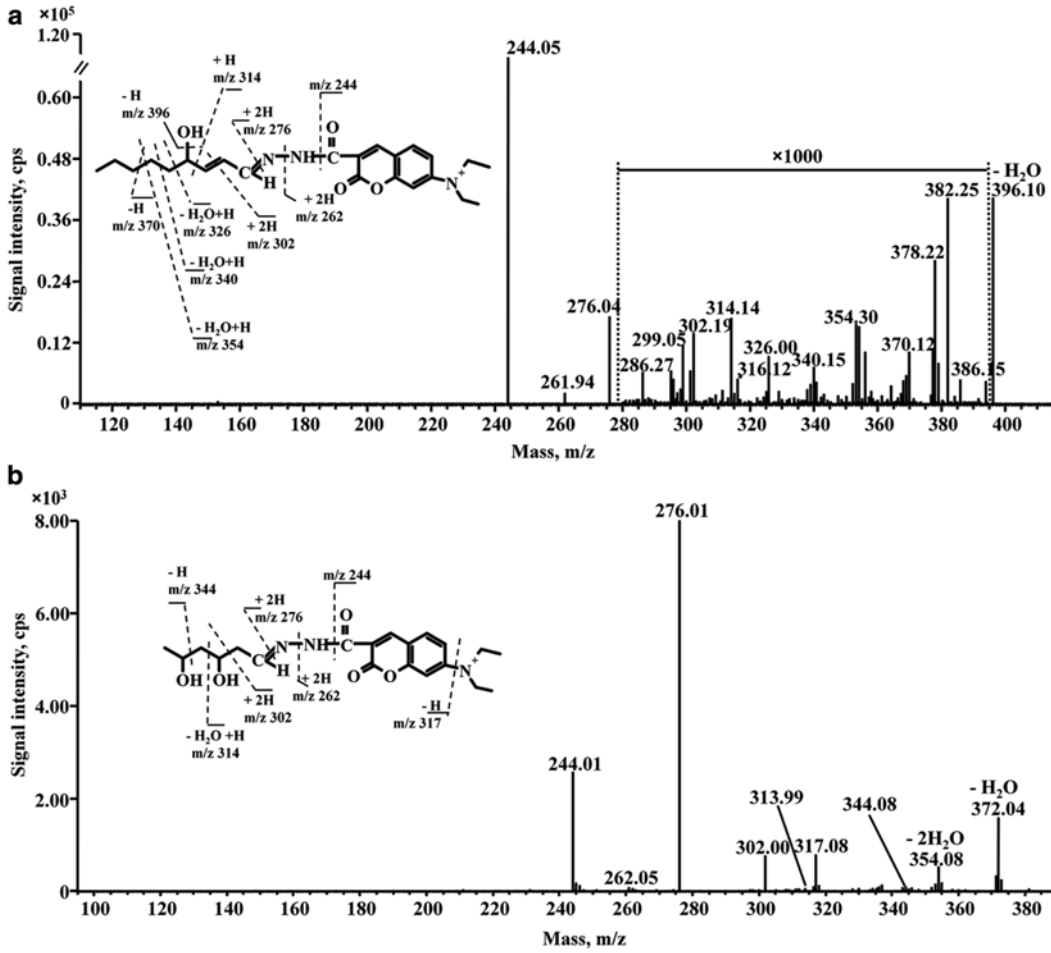

Fig. 2 CID spectra of CHH-derivatized 4-hydroxy-2-nonenal (**a**) and 3,5-dihydroxy-hexanal (**b**)

types of fragment ions are formed due to the alkyl chain cleavage at and next to the double bond, as indicated by signals at *m/z* 302 and 314.

2. CHH-3,5-dihydroxy-hexanal derivative (*m/z* 390.20) was detected after oxidation of docosahexaenoic acid and PC vesicles. Beside the CHH-reporter at *m/z* 244, peak at *m/z* 317 was formed by the neutral loss of diethylamine from the CHH moiety (Fig. 2b). Two successive water losses were main characteristic for the CID spectra of dihydroxy-alkanals. Cleavage of hydroxyl groups (*m/z* 372 and 354) generated of two double bonds between C-2 and C-3 atoms. The neutral loss of ethanol (-C_2H_5OH, –46 Da) allowed to assign of one hydroxyl group to the C-5 atom. Fragment ions at *m/z* 302 and 314, characteristic for the double bond at C-2 carbon, confirmed the second hydroxyl group at C-3 atom.

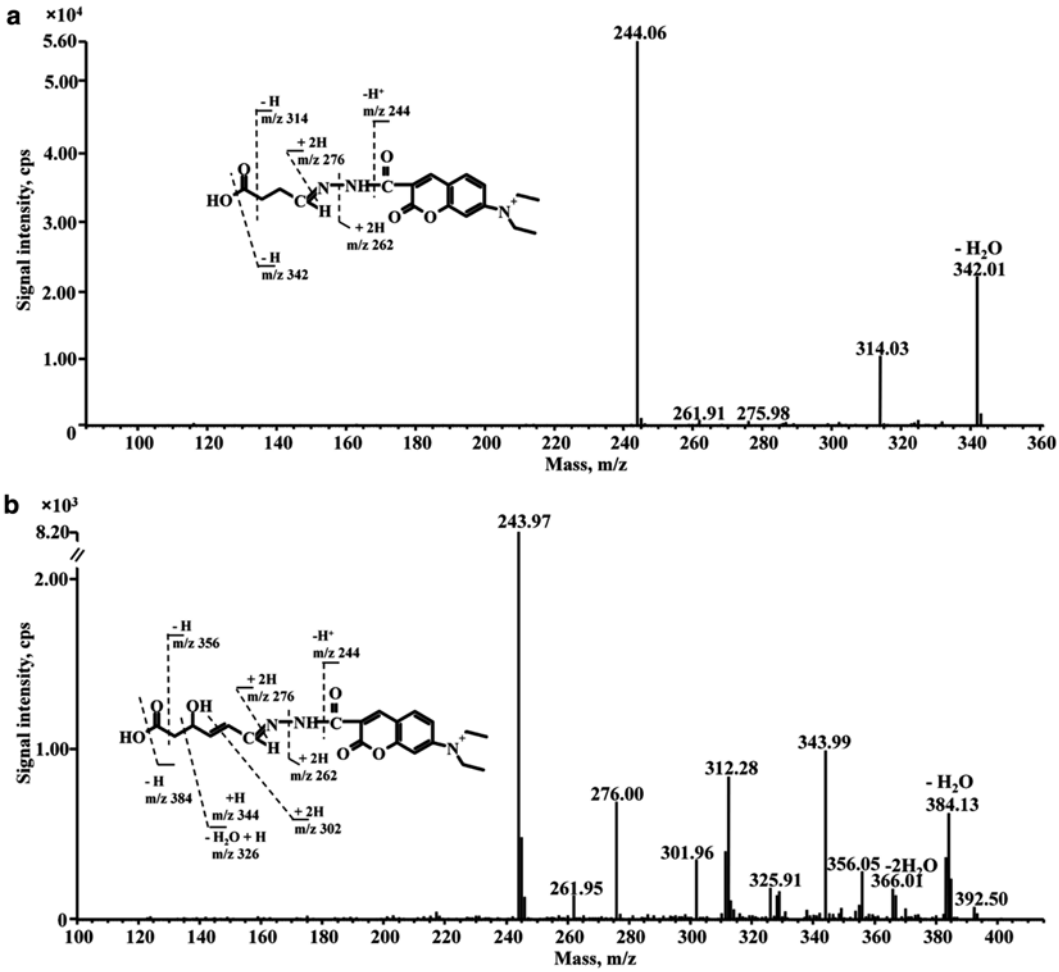

Fig. 3 CID spectra of CHH-derivatized 4-oxo-butanoic acid (**a**) and 4-hydroxy-6-oxo-2-hexenoic acid (**b**)

3.3.4 Interpretation of CID Spectra of Derivatized Oxo-Carboxylic Acids and Hydroxyl-Oxo-Carboxylic Acids

Oxo-carboxylic acids are oxoLPPs derived from oxidative cleavage of free PUFA or during deesterification of PL-bound aldehydes. The carboxyl moiety is usually retained at the methyl end of the truncated carboxylic acid. Additional oxidation of oxo-carboxylic acids can introduce hydroxyl groups along the alkyl chain. CHH-derivatives of unsaturated oxo-carboxylic acid display rather simple CID spectra. Besides the CHH-reporter ions at *m/z* 244, 261, and 276, all oxo-carboxylic acids show relatively intense characteristic neutral losses of water and formic acid (-CH_2O_2, –46 Da).

1. The CID spectrum of CHH-4-oxo-butanoic acid derivative (*m/z* 382.14) obtained by oxidation of docosahexaenoic acid displayed these losses at *m/z* 342 and 314 (Fig. 3a).
2. A more complex tandem mass spectrum was recorded for CHH-4-hydroxy-6-oxo-2-hexenoic acid (*m/z* 402.16; Fig. 3b)

resulting from oxidation of docosahexaenoic acid. Besides CHH-reporters (*m/z* 244, 261, and 276) and signals corresponding to carboxylic acid-specific neutral losses (*m/z* 384 and 356), the presence of a hydroxyl group was confirmed by a signal at *m/z* 366 formed due to the second water loss. Peaks at *m/z* 344 and 326 can be explained by fragmentation between C-2 and C-3 atoms followed by a water loss. The newly formed fragment ion visible at *m/z* 326 most likely contains sp-hybridized carbons.

3.3.5 Interpretation of CID Spectra of Derivatized Phospholipid(PL)-Bound Aldehydes

The analytical approach applied to oxoLPPs obtained by PUFA oxidation can be applied to phospholipid-bound carbonyls as well. CID spectra of PC-bound carbonyls displayed characteristic mass losses specific for the CHH-derivatization rather than the CHH-derivatization reporter at *m/z* 244 which was not detected due to the low mass cutoff of the ion trap mass analyzer used in this study. Neutral losses of CHH (-$C_{14}H_{17}O_3N_3$, –275 Da) and phosphorylcholine and CHH (-$HPO_4(CH_2)_2N(CH_3)_3$-$C_{14}H_{17}O_3N_3$, –458 Da) were present in all tandem mass spectra of PC-bound aldehydes. Additionally, PC-bound aldehydes retain all the fragments characteristic to phosphatidylcholine species.

1. The tandem mass spectrum of CHH-PNPC (*m/z* 907.56; Fig. 4a) showed peaks at *m/z* 848 and 724 resulting from the neutral losses of trimethylamine (-$N(CH_3)_3$, –59 Da) and phosphorylcholine (-$HPO_4(CH_2)_2N(CH_3)_3$, –183 Da) from the precursor, indicating that the derivatized PL-carbonyl belonged to the phosphatidylcholine subclass. Fragment ions at *m/z* 651 and 639 corresponded to deesterification of palmitic acid (-$R_{pal}COOH/R_{pal}$=C=O, –256/238 u) and additionally confirmed that the CHH-tag was present at the *sn*-2 position. Under CID conditions CHH-derivatized 9-oxononanoic acid was cleaved from the *sn*-2 position (-CHH=$R_{ox}COOH$/CHH=R_{ox}=O=H, –411/393), resulting in signals at *m/z* 496 and 478. Since oxoLPP esterified at *sn*-2 is saturated, there was no signal corresponding to the oxoLPP alkyl chain.
2. The hydroxylated form of PNPC, CHH-derivatized 1-palmitoyl-2-(3-hydroxy-9-oxononanoyl)-*sn*-glycerophosphatidylcholine (*m/z* 923.55; Fig. 4b), showed very intense signal corresponding to a water loss, most likely from the hydroxy group. Besides the aforementioned CHH- (*m/z* 663, 648, and 465), phosphatidylcholine-specific neutral losses (*m/z* 869 and 740), and fragments formed due to the deesterification of oxoLPP with CHH-tag (*m/z* 478 and 496), additional signals at *m/z* 566, 580, and 594 were observed. The ions correspond to the fragmentation of the oxoLPP alkyl

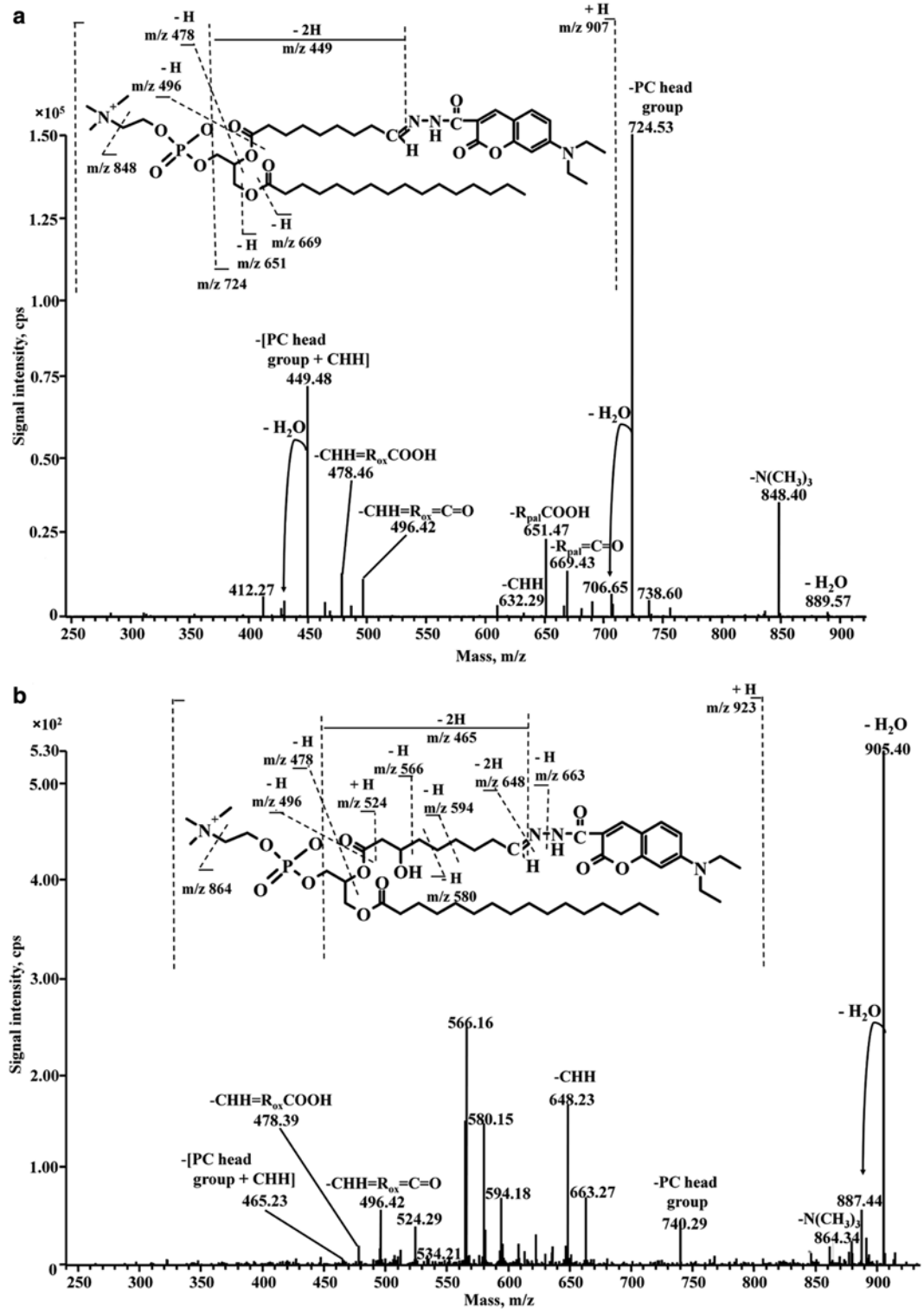

Fig. 4 CID spectrum of 1-palmitoyl-2-(9-oxononanoyl)-*sn*-glycerophosphatidylcholine (**a**) and 1-palmitoyl-2-(3-hydroxy-9-oxononanoyl)-sn-glycerophosphatidylcholine (**b**) derivatized with CHH

chain. Considering that most probable fragmentation site next to the sp^2-hybridized or hydroxylated C-atoms carbon atoms with hydroxyl group, and comparing relative intensities of observed fragment ions, it was concluded that the hydroxyl group was localized at the C-7 atom.

4 Notes

1. Samples should be analyzed within a period of 3 months after freezing. Longer sample storage is not recommended.
2. Aqueous solutions of $CuSO_4$ and ascorbic acid were freshly prepared every time prior to the oxidation of PUFA and PC vesicles.
3. Ethanol was used to dissolve PUFA and to improve their solubility in the aqueous solutions. The solutions should be transparent.
4. Oxidation in the system with transition metal ions and ascorbic acid requires at least twofold molar excess of ascorbic acid over the metal ions.
5. Oxidation mixtures of PUFA and PC vesicles can be stored at −20 °C for at least 3 months prior to the analysis. Multiple thawing and freezing of the sample should be prevented, as it can influence further oxidation and degradation. Therefore, aliquoting the oxidation mixture prior freezing is recommended.
6. After sonication, solution should be transparent. If the solution is turbid, sonication should be repeated up to four times. Longer sonication times should be avoided as they can cause lipid oxidation due to the aqueous environment and heat produced in the ultrasonic bath. PC vesicle solution can be stored at −20 °C for 3 months without sample oxidation.
7. Small aliphatic aldehydes are produced in cultivated cells or formed in vivo at very low amounts. Taking into account their volatility, it is recommended to perform lipid extraction and carbonyl derivatization directly after collecting the cells.
8. Special caution should be taken here. If too much methanol is added, the phases will not separate after addition of water.

Acknowledgments

Financial support from the European Regional Development Fund (ERDF, European Union and Free State Saxony) and the “Bundesministerium für Bildung und Forschung” (BMBF) are gratefully acknowledged.

References

1. Dalle-Donne I, Aldini G, Carini M, Colombo R, Rossi R, Milzani A (2006) Protein carbonylation, cellular dysfunction, and disease progression. J Cell Mol Med 10:389–406
2. Spiteller G (1998) Linoleic acid peroxidation—the dominant lipid peroxidation process in low density lipoprotein—and its relationship to chronic diseases. Chem Phys Lipids 95:105–162
3. Domingues RM, Domingues P, Melo T, Perez-Sala D, Reis A, Spickett CM (2013) Lipoxidation adducts with peptides and proteins: deleterious modifications or signaling mechanisms? J Proteomics 92:110–131
4. Fedorova M, Bollineni RC, Hoffmann R (2013) Protein carbonylation as a major hallmark of oxidative damage: update of analytical strategies. Mass Spectrom Rev 33:79–97
5. Spickett CM (2013) The lipid peroxidation product 4-hydroxy-2-nonenal: advances in chemistry and analysis. Redox Biol 1:145–152
6. Negre-Salvayre A, Coatrieux C, Ingueneau C, Salvayre R (2008) Advanced lipid peroxidation end products in oxidative damage to proteins. Potential role in diseases and therapeutic prospects for the inhibitors. Br J Pharmacol 153:6–20
7. Uchida K (1999) Current status of acrolein as a lipid peroxidation product. Trends Cardiovasc Med 9:109–113
8. Perluigi M, Coccia R, Butterfield DA (2012) 4-Hydroxy-2-nonenal, a reactive product of lipid peroxidation, and neurodegenerative diseases: a toxic combination illuminated by redox proteomics studies. Antioxid Redox Signal 17:1590–1609
9. Mattson MP (2009) Roles of the lipid peroxidation product 4-hydroxynonenal in obesity, the metabolic syndrome, and associated vascular and neurodegenerative disorders. Exp Gerontol 44:625–633
10. Guo L, Chen Z, Cox BE, Amarnath V, Epand RF, Epand RM, Davies SS (2011) Phosphatidylethanolamines modified by gamma-ketoaldehyde (gammaKA) induce endoplasmic reticulum stress and endothelial activation. J Biol Chem 286:18170–18180
11. Antonny B (2011) Mechanisms of membrane curvature sensing. Annu Rev Biochem 80:101–123
12. Rael LT, Thomas GW, Craun ML, Curtis CG, Bar-Or R, Bar-Or D (2004) Lipid peroxidation and the thiobarbituric acid assay: standardization of the assay when using saturated and unsaturated fatty acids. J Biochem Mol Biol 37:749–752
13. Chirico S, Smith C, Marchant C, Mitchinson MJ, Halliwell B (1993) Lipid peroxidation in hyperlipidaemic patients. A study of plasma using an HPLC-based thiobarbituric acid test. Free Radic Res Commun 19:51–57
14. Reis A, Domingues MR, Amado FM, Ferrer-Correia AJ, Domingues P (2007) Radical peroxidation of palmitoyl-lineloyl-glycerophosphocholine liposomes: identification of long-chain oxidised products by liquid chromatography-tandem mass spectrometry. J Chromatogr B Analyt Technol Biomed Life Sci 855:186–199
15. Reis A, Domingues P, Ferrer-Correia AJ, Domingues MR (2007) Identification of free radicals of glycerophosphatidylcholines containing omega-6 fatty acids using spin trapping coupled with tandem mass spectrometry. Free Radic Res 41:432–443
16. Milic I, Fedorova M, Teuber K, Schiller J, Hoffmann R (2012) Characterization of oxidation products from 1-palmitoyl-2-linoleoyl-sn-glycerophosphatidylcholine in aqueous solutions and their reactions with cysteine, histidine and lysine residues. Chem Phys Lipids 165:186–196
17. Li Z, Jacobus LK, Wuelfing WP, Golden M, Martin GP, Reed RA (2006) Detection and quantification of low-molecular-weight aldehydes in pharmaceutical excipients by headspace gas chromatography. J Chromatogr A 1104:1–10
18. Milic I, Hoffmann R, Fedorova M (2013) Simultaneous detection of low and high molecular weight carbonylated compounds derived from lipid peroxidation by electrospray ionization-tandem mass spectrometry. Anal Chem 85:156–162
19. Bollineni R, Hoffmann R, Fedorova M (2011) Identification of protein carbonylation sites by two-dimensional liquid chromatography in combination with MALDI- and ESI-MS. J Proteomics 74:2338–2350
20. Yuan Q, Zhu X, Sayre LM (2007) Chemical nature of stochastic generation of protein-based carbonyls: metal-catalyzed oxidation versus modification by products of lipid oxidation. Chem Res Toxicol 20:129–139
21. Eggink M, Wijtmans M, Ekkebus R, Lingeman H, de Esch IJ, Kool J, Niessen WM, Irth H (2008) Development of a selective ESI-MS derivatization reagent: synthesis and optimization for the analysis of aldehydes in biological mixtures. Anal Chem 80:9042–9051
22. Long EK, Smoliakova I, Honzatko A, Picklo MJ Sr (2008) Structural characterization of alpha, beta-unsaturated aldehydes by GC/MS

is dependent upon ionization method. Lipids 43:765–774

23. Matyash V, Liebisch G, Kurzchalia TV, Shevchenko A, Schwudke D (2008) Lipid extraction by methyl-tert-butyl ether for high-throughput lipidomics. J Lipid Res 49:1137–1146

24. van Leeuwen SM, Hendriksen L, Karst U (2004) Determination of aldehydes and ketones using derivatization with 2,4-dinitrophenylhydrazine and liquid chromatography-atmospheric pressure photoionization-mass spectrometry. J Chromatogr A 1058:107–112

Chapter 2

Specific Imaging and Tracking of Mitochondria in Live Cells by a Photostable AIE Luminogen

Chris W.T. Leung, Yuning Hong, and Ben Zhong Tang

Abstract

Tracking the dynamics of mitochondrial morphology has attracted much research interest because of its involvement in early stage apoptosis and degenerative conditions. To follow this process, highly specific and photostable fluorescent probes are in demand. Commercially available mitochondria trackers, however, suffer from poor photostability. To overcome this limitation, we have designed and synthesized a fluorescent agent, tetraphenylethene-triphenylphosphonium (TPE-TPP), for mitochondrial imaging. Inherent from the mitochondrial-targeting ability of TPP groups and the aggregation-induced emission (AIE) characteristics of the TPE core, TPE-TPP possesses high specificity to mitochondria, superior photostability, and appreciable tolerance to environmental change, allowing imaging and tracking of the mitochondrial morphological changes in a long period of time.

Key words Aggregation-induced emission, Photostable, Morphological change, Triphenylphosphonium

1 Introduction

Mitochondria, the organelle found in almost all eukaryotic cells, play a vital role in the life and death of cells. The most prominent function of mitochondria is to produce ATP, the energy currency of the cell. The production of ATP involves a series of electron transport systems in the oxidation phosphorylation pathway, which is also found to be associated with the generation of reactive oxygen species (ROS) [1, 2]. The production of ROS in mitochondria leads to propagation of free radicals, damaging of cells, and contribution to cell death, which is known as mitochondria-mediated apoptosis [3, 4]. The morphology of mitochondria, though varies upon cell type, cell-cycle stage, and intracellular metabolic state, is affected by and thus reflects cell functioning [5]. The morphology is controlled by a set of proteins, mutations of which will cause

Donald Armstrong (ed.), *Advanced Protocols in Oxidative Stress III*, Methods in Molecular Biology, vol. 1208,
DOI 10.1007/978-1-4939-1441-8_2,

several human diseases including degenerative diseases such as Parkinson's and Alzheimer's diseases [6]. Recent reports also show that proteins participating in apoptosis can affect the morphology of mitochondria [5, 7]. Tracking the mitochondrial morphological change may give insight for studying apoptosis and degenerative conditions.

Fluorescent probes that can selectively illuminate cellular mitochondria are powerful tools for monitoring the morphological changes and studying these processes. For observing the dynamic changes in certain period of time, the probe must be photostable under the continual irradiation of light from fluorescent microscopes. Conventional fluorescent dyes for mitochondria staining have been developed [8, 9]. Their photostability, however, leaves much to be desired. Very diluted solutions of these dyes are used in the imaging process and such small numbers of the dye molecules can be quickly photobleached when a harsh laser beam is used as the excitation light source. The photostability cannot be improved by using higher fluorophore concentration due to the accompanying concentration-quenching effect.

Triphenylphosphonium-functionalized aggregation-induced emission (AIE) luminogens are tackling those problems with high tolerance to changing microenvironment, photostability, and its AIE features. Their characteristics exhibit opposite phenomena: they are almost nonfluorescent when molecularly dissolved but become highly emissive in the aggregate state with fluorescence increasing along with the increase of fluorophore concentration [10]. Restriction of intramolecular motions (RIM) is proposed as the main cause of the AIE effect [11]. Lipophilic AIE molecules form nanoaggregates in aqueous solution spontaneously because of their hydrophobic nature [12]. These nanoaggregates have been successfully applied for long-term cell tracking in our previous work [13]. It is envisaged that the nanoaggregates of the AIE molecules would possess better photostability than single fluorescent molecule in dilute solutions.

In this chapter, AIE luminogens are decorated with mitochondria-targeting moieties to achieve higher specificity to mitochondria. Tetraphenylethene (TPE), an archetypal AIE luminogen, was synthesized and functionalized with triphenylphosphonium (TPP) groups (TPE-TPP, Fig. 1). TPP is a well-known functional group that facilitates the entrance of molecular probes into mitochondria by its lipophilicity and electrophoretic force [2]. We here demonstrate that TPE-TPP can light up mitochondria specifically in live cells (*see* Fig. 2) with superior photostability that enables the observation of mitochondrial morphological changes (*see* Fig. 3).

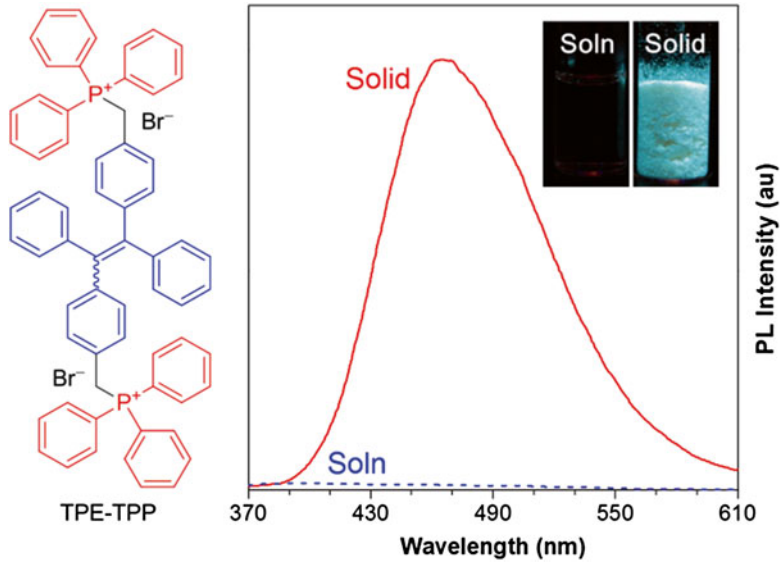

Fig. 1 Chemical structure of TPE-TPP; PL spectra of TPE-TPP in solid and solution (soln) states. *Inset*: Photographs of DMF solution (*left*) and solid powder (*right*) of TPE-TPP taken under UV irradiation. Concentration of TPE-TPP, 10 μM; excitation wavelength, 321 nm

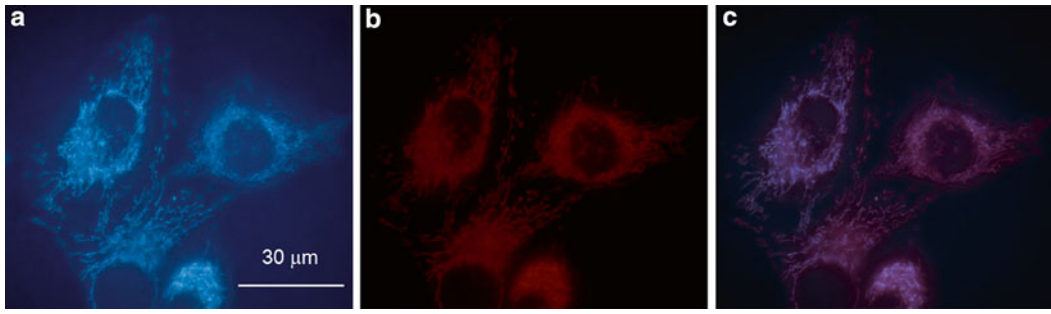

Fig. 2 Fluorescent images of HeLa cells stained with (**a**) TPE-TPP (5 μM) for 1 h and (**b**) MitoTracker® Red FM (MT, 50 nM) for 15 min. (**c**) Merged images of panels (**a**) and (**b**). Excitation wavelength: 330–385 nm (for TPE-TPP) and 540–580 nm (for MT)

2 Materials

2.1 Equipment

1. NMR analysis was conducted on a Bruker ARX 400 spectrometer with tetramethylsilane (TMS; $\delta = 0$) as internal standard.
2. Mass spectroscopy was carried out on a Finnigan TSQ 7000 triple quadrupole spectrometer operating in fast-atom bombardment (FAB) mode and API QSTAR XL System mode.
3. Fluorescence spectra were taken on a PerkinElmer LS 55 spectrofluorometer with a Xenon discharge lamp excitation.

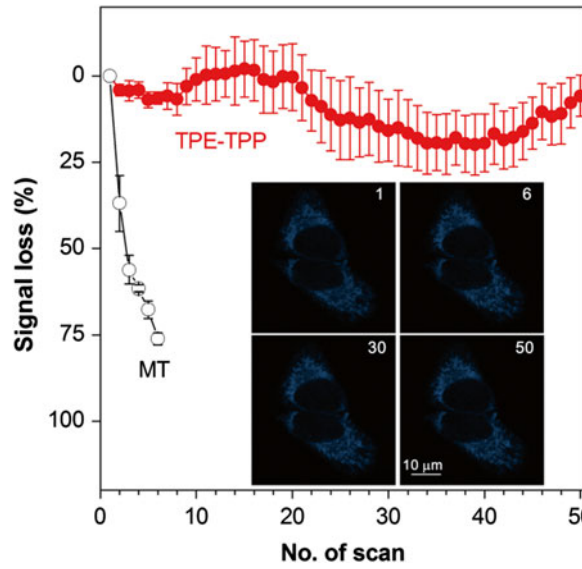

Fig. 3 Signal loss (%) of fluorescent emission of TPE-TPP (*solid circle*) and MT (*open circle*) with increasing number of scans. *Inset*: example of fluorescent images of living HeLa cells stained with TPE-TPP (5 μM) with increasing number of scans (1–50 scans; the number of scan shown in the *upper right corner* of the panel). Excitation wavelength, 405 nm; emission filter, 449–520 nm; irradiation time, 7.75 s/scan

4. The HeLa cells were imaged under a fluorescence microscope (BX41 microscope; for TPE-TPP, $\lambda_{ex} = 330–385$ nm, diachronic mirror = 400 nm and emission filter = 420 nm long pass; for MT, $\lambda_{ex} = 540–580$ nm, diachronic mirror = 600 nm and emission filter = 610 nm long pass).
5. The photostability test was investigated by confocal microscope (Zeiss laser scanning confocal microscope; LSM7 DUO). TPE-TPP was excited at 405 nm (6 % laser power) and the fluorescence was collected at 449–520 nm. MT was excited at 560 nm (18 % laser power) and fluorescence was collected at 581–688 nm.

2.2 Reagents and Chemicals

THF (Labscan) was purified by simple distillation from sodium benzophenone ketyl under nitrogen immediately before use. Zinc dust, titanium(IV) chloride, *N*-bromosuccinimide (NBS), benzoyl peroxide (BPO), triphenylphosphine (PPh_3), benzaldehyde, 4-cyanobenzaldehyde, carbon tetrachloride, 4-nitrobenzaldehyde, triphenylamine, *N*,*N*-dimethylformamide (DMF), dichloromethane (DCM), dimethylsulfoxide (DMSO), and other reagents were all purchased from Aldrich and used as received.

2.3 Cell Culture

The following materials are used for culturing the HeLa cells.

1. Minimum essential medium, FBS, penicillin, and streptomycin were purchased from Gibco, Invitrogen.
2. 4-(2-hydroxyethyl)-1-piperazineethanesulfonic acid (HEPES) was purchased from Sigma.
3. 35 mm culture dishes were purchased from Corning.
4. Phosphate-buffered saline (PBS).
5. Cover slides.
6. Cell culture CO_2 incubator.

3 Methods

3.1 Synthesis (Scheme 1)

3.1.1 Synthesis of 1,2-bis (4-methylphenyl)-1,2-diphenylethene (2)

1. A suspension of 4-methylbenzophenone (1, 3.6 g, 10.0 mmol), $TiCl_4$ (1.9 g, 10.0 mmol), and Zn dust (1.3 g, 20.0 mmol) in dry THF (100 mL) was refluxed for 20 h.
2. Afterward, the reaction mixture was cooled to room temperature and filtered. The filtrate was evaporated and the crude product was purified on a silica-gel column using DCM as eluent.

3.1.2 Synthesis of 1,2-bis[4-(bromomethyl) phenyl]-1,2-diphenylethene (3)

1. To a mixture of 2 (1.8 g, 5.0 mmol) and NBS (1.7 g, 10.0 mmol) in CCl_4 was added catalytic amount of BPO at room temperature. The mixture was stirred and heated to reflux for 8 h.
2. After filtration and solvent evaporation, the product was purified by silica-gel chromatography using DCM/hexane (1:4 v/v) as eluent.

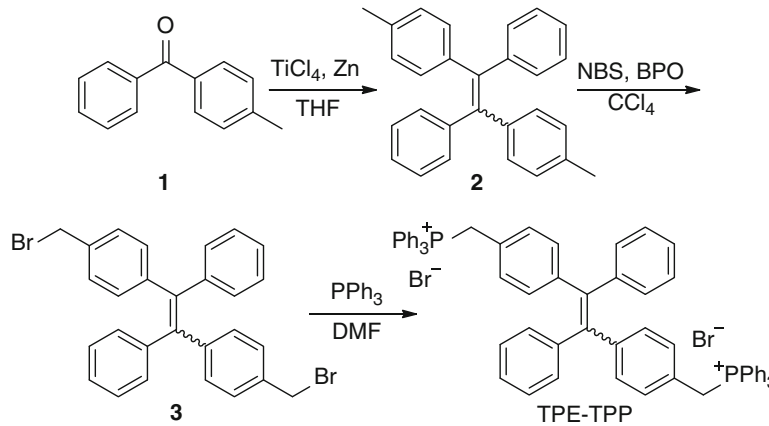

Scheme 1 Synthetic route to TPE-TPP

3.1.3 Synthesis of bis (triphenylphosphonium) tetraphenylethene (TPE-TPP)

1. Triphenylphosphonium salt, TPE-TPP, was prepared from 3 (0.5 g, 1.0 mmol) and triphenylphosphine (1.0 g, 4.0 mmol) in DMF at 100 °C.
2. After stirring for 24 h, the solution was poured into large amount of toluene.

3.2 Cell Imaging by TPE-TPP

3.2.1 Cell Culture

The HeLa cells were cultured in minimum essential medium containing 10 % fetal bovine serum and antibiotics (100 units/mL penicillin and 100 μg/mL streptomycin) in a 5 % CO_2 humidity incubator at 37 °C.

3.2.2 Cell Imaging

1. HeLa cells were grown overnight on a 35 mm petri dish with a coverslip.
2. The live cells were stained with 5 μM of TPE-TPP for 15 min, 30 min, or 2 h (by adding 2 μL of a 5 mM stock solution of TPE-TPP in DMSO to 2 mL culture medium) or 50 nM MitoTracker® Red FM (MT) for 15 min (by adding 0.5 μL of a 200 μM stock solution of MT in DMSO to 2 mL culture medium).
3. The live cells were washed with PBS three times after incubation with dyes.
4. Imaging medium (10 mM HEPES in MEM) was added to the dish.
5. The cells were observed under a fluorescent microscope through the observation window.

3.2.3 Mitochondrial Morphological Change (Photostability Test)

1. HeLa cells were grown overnight on a plasma-treated 25 mm round coverslip mounted to the bottom of a 35 mm petri dish with an observation window.
2. The live cells were stained with 5 μM of TPE-TPP for 30 min (by adding 2 μL of a 5 mM stock solution of TPE-TPP in DMSO to 2 mL culture medium) or 50 nM MitoTracker® Red FM (MT) for 15 min (by adding 0.5 μL of a 200 μM stock solution of MT in DMSO to 2 mL culture medium).
3. The live cells were washed with PBS three times after incubation with dyes.
4. 2 mL of imaging medium (10 mM HEPES in MEM) was added to the dish.
5. HeLa cells were then imaged by confocal microscope.
6. 10 μM CCCP (by adding 1 μL of a 200 mM stock solution of CCCP in DMSO to 2 mL culture medium) after the HeLa cells were imaged.
7. TPE-TPP-stained living HeLa cells were scanned for 50 times with 7.75 s/scan irradiation time.
8. MT-stained living HeLa cells were scanned for 7 times with 7.75 s/scan irradiation time.

4 Notes

1. Drill a hole of around 10 mm diameter in the middle of the dish. Place cover slide over the dish using paraffin.
2. When comparing the specificity of TPE-TPP and MT to mitochondria, MT should be excited before TPE-TPP as it is easily quenched by excitation wavelength.
3. Add the CCCP carefully into the dish after imaging by confocal microscope as the disturbance to the cells should be minimized for comparing the morphological change.
4. The power used for test photostability of TPE-TPP and MT should be unified for fair measurement.

Acknowledgments

This work was partially supported by the Research Grants Council of Hong Kong (604711, 602212, HKUST2/CRF/10, and N_HKUST620/11), the University Grants Committee of Hong Kong (AoE/P-03/08), HKUST (RPC10SC13, RPC11SC09, and SRFI11SC03PG), the Innovation and Technology Commission (ITCPD/17-9), and the National Science Foundation of China (20974028). B.Z.T. thanks the support from Guangdong Innovative Research Team Program of China (201101C0105067115).

References

1. Ow Y, Green D, Hao Z, Mak T (2008) Cytochrome c: functions beyond respiration. Nat Rev Mol Cell Biol 9:532–542
2. Hoye A, Davoren J, Wipf P (2008) Targeting mitochondria. Acc Chem Res 41:87–97
3. Dickinson B, Srikun D, Chang C (2010) Mitochondrial-targeted fluorescent probes for reactive oxygen species. Curr Opin Chem Biol 14:50–56
4. Dickinson B, Chang C (2008) A targetable fluorescent probe for imaging hydrogen peroxide in the mitochondria of living cells. J Am Chem Soc 130:9638–9639
5. Karbowski M, Youle R (2003) Dynamics of mitochondrial morphology in healthy cells and during apoptosis. Cell Death Differ 10: 870–880
6. Masanta G, Heo C, Lim C (2012) A mitochondria-localized two-photon fluorescent probe for ratiometric imaging of hydrogen peroxide in live tissue. Chem Commun 48:3518–3520
7. Gandre-Babbe S, van der Bliek AM (2008) The novel tail-anchored membrane protein Mff controls mitochondrial and peroxisomal fission in mammalian cells. Mol Biol Cell 19:2402–2412
8. Miyake T, McDermott J, Gramolini A (2011) A method for the direct identification of differentiating muscle cells by a fluorescent mitochondrial dye. PLoS One 6:e28628
9. Neto B, Carvalho P, Santos D (2012) Synthesis, properties and highly selective mitochondria staining with novel, stable and superior benzothiadiazole fluorescent probes Gatto. RSC Adv 2:1524–1532
10. Hong Y, Lam J, Tang B (2009) Aggregation-induced emission: phenomenon, mechanism and applications. Chem Commun 29:4332–4353
11. Hong Y, Lam J, Tang B (2011) Aggregation-induced emission. Chem Soc Rev 40: 5361–5388
12. Chen S, Tang B, Wong S (2012) An AIE-active hemicyanine fluorogen with stimuli-responsive red/blue emission: extending the pH sensing range by "switch + knob" effect. Chem Sci 3:1804–1809
13. Yong Y, Luo K, Tang B (2011) Cytophilic fluorescent bioprobes for long-term cell tracking. Adv Mater 23:3298–3302

Chapter 3

Analysis of Relationship Between Oxidized Phospholipid Structure and Interaction with the Class B Scavenger Receptors

Detao Gao, Lawrence M. Sayre, and Eugene A. Podrez

Abstract

Recognition of specific oxidized phospholipids $oxPC_{CD36}$ by scavenger receptors CD36 and SR-BI plays a critical role in several pathophysiological processes. The structural basis for the recognition of $oxPC_{CD36}$ by CD36 and SR-BI is poorly understood. We describe here the design and synthesis of a series of model oxidized phospholipids having various functional groups at *sn*-1, *sn*-2, and *sn*-3 positions. Synthetic methodologies and experimental details for the preparation of specific examples of model oxidized phospholipids are presented. The correlation between their structure and their ability to serve as ligands for CD36 and SR-BI was determined using competitive binding assay on cells overexpressing scavenger receptors, direct binding assay to scavenger receptors expressed as GST-fusion proteins, and cholesterol ester synthesis assay using mouse peritoneal macrophages.

Key words Atherosclerosis, Cardiovascular pathology, Oxidized phospholipids, Oxidized low-density lipoprotein (oxLDL), Scavenger receptors class B, CD36, SR-BI

1 Introduction

Specific oxidized phospholipids ($oxPC_{CD36}$) accumulate at sites of oxidative stress in vivo including atherosclerotic lesions and plasma in dyslipidemia [1, 2]. They serve as high-affinity ligands for scavenger receptors class B—CD36 and SR-BI [3, 4]. Recognition of $oxPC_{CD36}$ on the surface of cell membranes and lipoprotein particles by scavenger receptors class B plays an important role in several pathophysiological processes including atherosclerosis and thrombosis. $oxPC_{CD36}$ mediate uptake of oxidized low-density lipoprotein (oxLDL) by macrophages via CD36 and promote a prothrombotic state via platelet scavenger receptor CD36 [1, 2]. $oxPC_{CD36}$ also prevent binding of high-density lipoprotein (HDL) by SR-BI because of the close proximity of the binding sites for these two ligands on SR-BI. Furthermore, $oxPC_{CD36}$ interfere with SR-BI-mediated selective uptake of cholesteryl esters in

Donald Armstrong (ed.), *Advanced Protocols in Oxidative Stress III*, Methods in Molecular Biology, vol. 1208,
DOI 10.1007/978-1-4939-1441-8_3,

hepatocytes [4]. These data demonstrate that specific oxidized phospholipids may have a detrimental effect due to specific interaction with scavenger receptors class B and indicate the importance of understanding the precise molecular mechanism of the recognition of $oxPC_{CD36}$ by scavenger receptors class B.

Initial studies have demonstrated that *sn*-2 acyl group of $oxPC_{CD36}$ that incorporates a terminal γ-hydroxy (or oxo)-α,β-unsaturated carbonyl is essential for high-affinity binding to CD36 [3]. Truncated oxidized *sn*-2 fatty acid moiety has been shown to protrude into the aqueous phase rendering it accessible for recognition by scavenger receptors [5]. It has been shown that electrophilic reactivity is not a prerequisite for high-affinity CD36 binding since the relatively unreactive $oxPC_{CD36}$ with γ-hydroxy-α,β-unsaturated-enoic acid groups at *sn*-2 position is an excellent ligand [3]. We have recently demonstrated that two lysine groups in CD36 (Lys164/166) are indispensable for the binding of $oxPC_{CD36}$ to CD36 [6]. These studies suggested an electrostatic interaction mechanism of the binding, where the negative charges in the oxidized phospholipids form salt bridges with the positive lysine groups in the binding domain of CD36.

To further elucidate the structural basis for the recognition of oxidized phospholipids by scavenger receptors class B, a series of model phospholipids having various functional groups at *sn*-1, *sn*-2, and *sn*-3 positions were designed and synthesized. Their ability to serve as ligands for CD36 and SR-BI was tested in competitive binding assay using cells overexpressing corresponding receptor and ^{125}I-oxidized LDL as a ligand and phospholipid vesicles containing oxidized phospholipids as a competitor. As a parallel approach, we assessed inhibition of cholesterol synthesis in murine peritoneal macrophages by model oxidized phospholipids as a measure of inhibition of oxidized lipoprotein uptake. Finally, we employed direct binding assay using phospholipid vesicles containing model oxidized phospholipids and ^{3}H-phospholipid tracer as a ligand and CD36 and SR-BI GST-fusion proteins.

2 Materials

2.1 Equipments (Major)

1. The described synthesis and purification protocols were carried out using standard equipment for organic synthesis laboratories.
2. Avanti Mini-Extruder Set, Avanti Polar Lipids Inc. (competitive binding assay, direct binding assay).
3. Vortex mixer, Argos Technologies FlexiFuge (for all assays).
4. Sonicator, Fisher Scientific FS30 (competitive binding assay, direct binding assay).

5. Cell culture incubator, NUAIRE IR AutoFlow NU-8500 (competitive binding assay, cholesteryl ester synthesis assay).
6. Orbital shaker, Barnstead/Lab-Line Lab Rotators (for all assays).
7. Beckman Coulter Beta/Gamma Counter LS5000TD (for all assays).
8. Centrifuge, Eppendorf 5417R (direct binding assay).
9. Reacti-Vap Evaporators, Thermo Scientific (cholesteryl ester synthesis assay).

2.2 Reagents and Supplies

1. For phospholipid synthesis, the solvents and reagents were of commercially available analytical grade quality. All chemicals were obtained from Sigma-Aldrich, Fisher Scientific, or Acros Organics.
2. Tissue culture media and additives were purchased from Invitrogen.
3. Low-density lipoprotein (LDL) was isolated and quantified as described [7] (competitive binding assay).
4. ^{125}I-LDL oxidized by MPO-H_2O_2-NO_2^- system (^{125}I-NO_2-LDL) were prepared as described [3] (competitive binding assay).
5. CD36 expressing HEK-293 cells were a generous gift from Dr. W. Frazier (Washington University, St. Louis, MO) (competitive binding assay).
6. SR-BI expressing HEK-293 cells were generated previously by Dr. Niladri S. Kar in our lab as described [4, 8] (competitive binding assay).
7. Diethylene triamine pentaacetic acid (DTPA), Sigma (competitive binding assay).
8. [^{3}H]dipalmitoylphosphatidylcholine ([^{3}H]DPPC), American Radiolabeled Chemicals (direct binding assay).
9. [^{14}C]oleate, ICN Pharmaceutical, Inc. (cholesteryl ester synthesis assay).
10. 1-palmitoyl-2-arachidonoyl-sn-glycero-3-phosphocholine (PAPC) and 1-palmitoyl-2-oleoyl-sn-glycero-3-phosphocholine (POPC), Avanti Polar Lipids (competitive binding assay, direct binding assay).
11. Scintillation cocktail, MP Biomedicals (for all assays).
12. Thioglycollate medium, Difco Laboratories (cholesteryl ester synthesis assay).
13. Cholesteryl oleate, Sigma (cholesteryl ester synthesis assay).
14. Cell culture plate, Corning Costar (competitive binding assay, cholesteryl ester synthesis assay).
15. Scintillation vials, Kimble chase (for all assays).

16. Whatman flexible plates for TLC (20 × 20 cm) (cholesteryl ester synthesis assay).
17. TLC developing tanks (Aldrich, L × H × W 27.0 cm × 26.5 cm × 7.0 cm) (cholesteryl ester synthesis assay).

3 Methods

3.1 Synthesis of Model Oxidized Phospholipids

3.1.1 The Preparation of Phospholipids (1a-g) (Scheme 3.1)

Phospholipids **1a** (1-palmitoyl-2-maleoyl-sn-glycero-3-phosphocholine, **PMPC**), **1b** (1-palmitoyl-2-phthalyl-sn-glycero-3-phosphocholine, **PPPC**), **1c** (1-palmitoyl-2-succinyl-sn-glycero-3-phosphocholine, **PSuPC**), **1d** (1-palmitoyl-2-glutaroyl-sn-glycero-3-phosphocholine,**PGPC**),and**1e**(1-palmitoyl-2-acetyl-sn-glycero-3-phosphocholine, **PAcPC**) were prepared by esterification of lysoPC with the corresponding acid anhydride under the catalysis of 4-dimethylaminopyridine (DMAP), following a literature procedure [9]. Phospholipid **1f** (1-palmitoyl-2-(9′-methoxyl-9′-oxo-nonanoyl)-sn-glycero-3-phosphocholine, **P9MNPC**) was synthesized by esterification of lysoPC with the methyl monoester of nonanedioic acid in the presence of *N,N′*-dicyclohexylcarbodiimide (DCC) and DMAP, as described elsewhere [9].

For the synthesis of phospholipids **1g** (1-palmitoyl-2-(8′-amino-8′-oxo)-octanoyl-sn-glycero-3-phosphocholine, **P8AOPC**) (*see* **Note 1**), octanedioyl dichloride (105 mg, 0.5 mmol) was dissolved in 15 ml anhydrous chloroform. To the mixture, 184 mg of DMAP (1.5 mmol) was added with stirring at room temperature. Ten minutes later, lysoPC (25 mg, 0.05 mmol, in 1 ml anhydrous chloroform) was added dropwise. After 1 h of reaction with

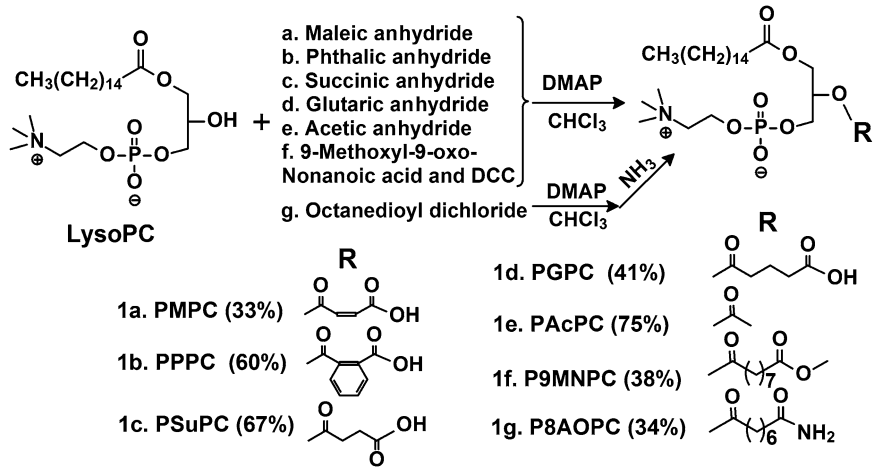

Scheme 1 Synthesis of PMPC, PPPC, PSuPC, PGPC, PAcPC, P9MNPC, and P8AOPC. *Reproduced from [JBC, 2010, 285*(7)*, 4447–54] with permission from [The American Society for Biochemistry and Molecular Biology]*

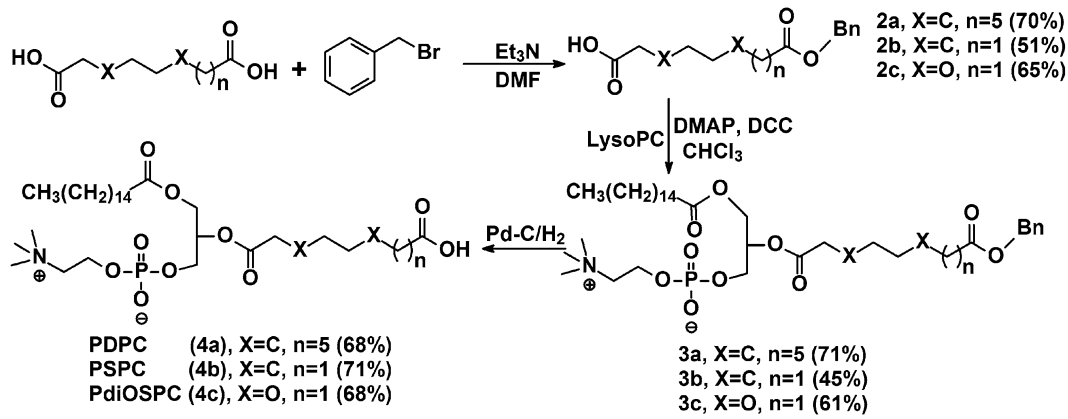

Scheme 2 Synthesis of PDPC, PSPC, and PdiOSPC. *Reproduced from [JBC, 2010, 285*(7)*, 4447–54] with permission from [The American Society for Biochemistry and Molecular Biology]*

stirring, ammonia gas was bubbled into the solution. Twenty-five minutes later, the mixture was concentrated to remove the solvent. The obtained residue was purified by 0.5 mm preparative silica gel TLC plate with $CHCl_3/CH_3OH/NH_3{\cdot}H_2O$ (29 %) (65/35/8, TLC: $R_f = 0.28$) to give a white solid (10.8 mg, 34 %).

3.1.2 The Preparation of Phospholipids (4a-c)

Phospholipid **4a** (1-palmitoyl-2-dodecanedioyl-sn-glycero-3-phosphocholine, **PDPC**), **4b** (1-palmitoyl-2-suberoyl-sn-glycero-3-phosphocholine, **PSPC**), and **4c** (1-palmitoyl-2-(3′,6′-dioxo)-suberoyl-sn-glycero-3-phosphocholine, **PdiOSPC**) were prepared using similar method, as shown in Scheme 3.2.

In the first step, the dicarboxylic acids were protected at one end with a benzyl group to yield the dicarboxylic monobenzyl esters, as previously described (*see* **Note 2**) [10]. In the second step, the dicarboxylic monobenzyl esters were first activated by DCC, then coupled with lysoPC with catalysis by DMAP to form the corresponding synthetic PCs (**3a**-**c**) [9]. In the third step, the benzyl groups of synthetic PCs (**3a**-**c**) were removed by hydrogenolysis with catalysis by palladium on carbon (Pd/C) to give the synthetic PCs (**4a**-**c**), as previously reported [10].

Experimental details for the preparation of **4a** were described as an example. Dodecanedioic acid (1.0 g, 4.3 mmol) and triethylamine (Et_3N) (1.24 ml, 8.6 mmol) were dissolved in DMF (50 ml) and cooled to 0 °C. To this solution, benzyl bromide (0.34 g, 2 mmol) dissolved in 50 ml DMF was added dropwise over a 1 h period. The reaction was stirred for an additional 4 h at 0 °C and allowed to slowly warm to room temperature overnight. The solvent was removed under reduced pressure. The resulting oily residue was dissolved in aqueous 1 N HCl saturated with NaCl (80 ml) and extracted with ethyl acetate (3 × 50 ml). The extracts were

combined and concentrated under reduced pressure. The residue was purified by flash chromatography on a silica gel column, which was eluted with hexane/ethyl acetate (2/1) to afford the monoester as white solid (12-(benzyloxy)-12-oxododecanoic acid (**2a**), 980 mg, 70 %).

The obtained monoester **2a** (64 mg, 0.2 mmol), lysoPC (26 mg, 0.053 mmol), and DMAP (5.5 mg, 0.045 mmol) in dry CH_2Cl_2 (4 ml) were stirred at room temperature. Then DCC (28 mg, 0.14 mmol) in CH_2Cl_2 (0.4 ml) was added to the solution. The resulting mixture was stirred at room temperature for 24 h. The solution was then filtered, and solvent was removed with a rotary evaporator. The obtained residue was applied to a 0.5 mm silica gel TLC plate, which was eluted with $CHCl_3$/MeOH/NH_4OH (28 %) (38/20/2). The major band (R_f = 0.2) was extracted with $CHCl_3$/MeOH/H_2O (1/2/0.8). The extract was filtered and then washed by Bligh/Dyer method, dried with anhydrous Na_2SO_4, and solvents were evaporated producing a white solid (1-palmitoyl-2-(12′-benzyloxy-12′-oxododecanoyl)-sn-glycero-3-phosphocholine (**3a**), 30 mg, 71 %).

The precursor **3a** (30 mg, 0.031 mmol) in 5 ml of $CHCl_3$/MeOH/H_2O (1/2/0.8) was hydrogenated over 10 % Pd/C (10 mg) at atmospheric pressure for 3 h. The catalyst was removed by filtration, and the filtrate was concentrated. The obtained residue was applied to a 0.5 mm silica gel TLC plate, which was eluted with $CHCl_3$/MeOH/H_2O/CH_3COOH (90/26/4/1). The major band (R_f = 0.16) was extracted with $CHCl_3$/MeOH/H_2O (1/2/0.8). The extract was filtered and then washed by Bligh/Dyer method, dried with anhydrous Na_2SO_4, and solvents were evaporated producing a white solid (1-palmitoyl-2-dodecanedioyl-sn-glycero-3-phosphocholine, **PDPC** (**4a**), 14.9 mg, 68 %).

3.1.3 The Preparation of Phospholipids (7a, 7b)

Phospholipid **7a** (1-palmitoyl-2-(6′-hydroxy)-hexanoyl-s*n*-glycero-3-phosphocholine, **P6HHPC**) and **7b** (1-palmitoyl-2-(8′-hydroxy)-octanoyl-sn-glycero-3-phosphocholine, **P8HOPC**) were prepared with similar method, as shown in Scheme 3.3. As reported earlier [11], the hydroxyl group of 6-hydroxyhexanoic acid and 8-hydroxyoctanoic acid were protected by treatment with *tert*-butyldimethylsilyl chloride (TBDMSCl) in the presence of imidazole, which neutralized the hydrochloric acid generated during the reaction. In the second step, TBDMS ether intermediates (**5a**, **b**) with a carboxylate group at the other end were first activated by DCC, then coupled with lysoPC under the catalysis of DMAP to form the corresponding synthetic PCs (**6a**, **b**) [9]. In the third step, the desilylation was achieved by treatment with *tetra*-n-butylammonium fluoride (TBAF) to give the synthetic PCs with a hydroxyl group at the terminal of *sn*-2 position (**7a**, **b**) [11].

Experimental details for the preparation of **7a** were described as an example. 6-hydroxyhexanoic acid (528 mg, 4 mmol) and

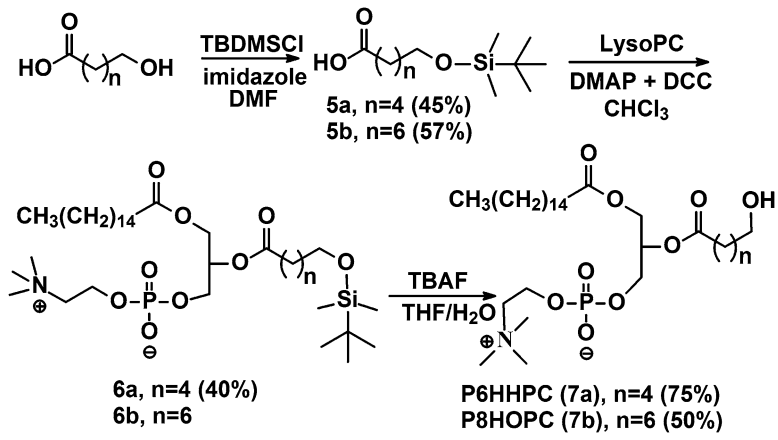

Scheme 3 The synthetic route for P6HHPC and P8HOPC. *Reproduced from [JBC, 2010, 285(7), 4447–54] with permission from [The American Society for Biochemistry and Molecular Biology]*

imidazole (653 mg, 9.6 mmol) were dissolved in 10 ml DMF to which was added TBDMSCl (660 mg, 4.4 mmol) at 0 °C. After 30 min, the reaction temperature rose to room temperature. After overnight reaction at room temperature, 20 ml ethyl ether and 20 ml saturated NaCl solution were added. The resulting solution was acidified with H_3PO_4 to pH 3. The ethyl ether layer was separated and concentrated under reduced pressure. The obtained pale yellow oil was purified by flash chromatography on silica gel (acetone/hexanes, 1/4, TLC: $R_f = 0.3$) to afford the 6-(*tert*-butyldimethylsilyloxy)-hexanoic acid (**5a**) (440 mg, 45 %). A procedure analogous to that described above for **3a** was used to prepare 1-palmitoyl-2-(6′-(*tert*-butyldimethylsilyloxy)-hexanoyl)-*sn*-glycero-3-phosphocholine (**6a**) (17.4 mg, 40 %).

The obtained compound **6a** in 2 ml THF was mixed with 100µl of tetra-n-butylammonium fluoride (TBAF) (1 M in THF). The resulting solution was stirred at room temperature for 5 h before removing the solvent with a rotary evaporator. The obtained residue was applied to a 0.5 mm silica gel TLC plate, which was eluted with $CHCl_3$/MeOH/CH_3COOH/H_2O (50/15/14/3). The product band ($R_f = 0.4$) was extracted with $CHCl_3$/MeOH/H_2O (1/2/0.8). The extract was filtered and then washed by Bligh/Dyer method, dried with anhydrous Na_2SO_4. Finally, the solvent was evaporated producing a white solid (1-palmitoyl-2-(6′-hydroxyhexanoyl)-*sn*-glycero-3-phosphocholine, **P6HHPC** (**7a**), 10.9 mg, 75 %).

3.1.4 The Preparation of Phospholipids (13, 15a-c, 17)

Lipid **13** (1-palmitoyl-2-suberoyl-sn-glycerol, **PSG**), phospholipid **15a** (1-acetyl-2-suberoyl-sn-3-phosphocholine, **AcSPC**), **15b** (1-palmitoyl-2-suberoyl-sn-glycero-3-phosphatidyl(N,N,N-

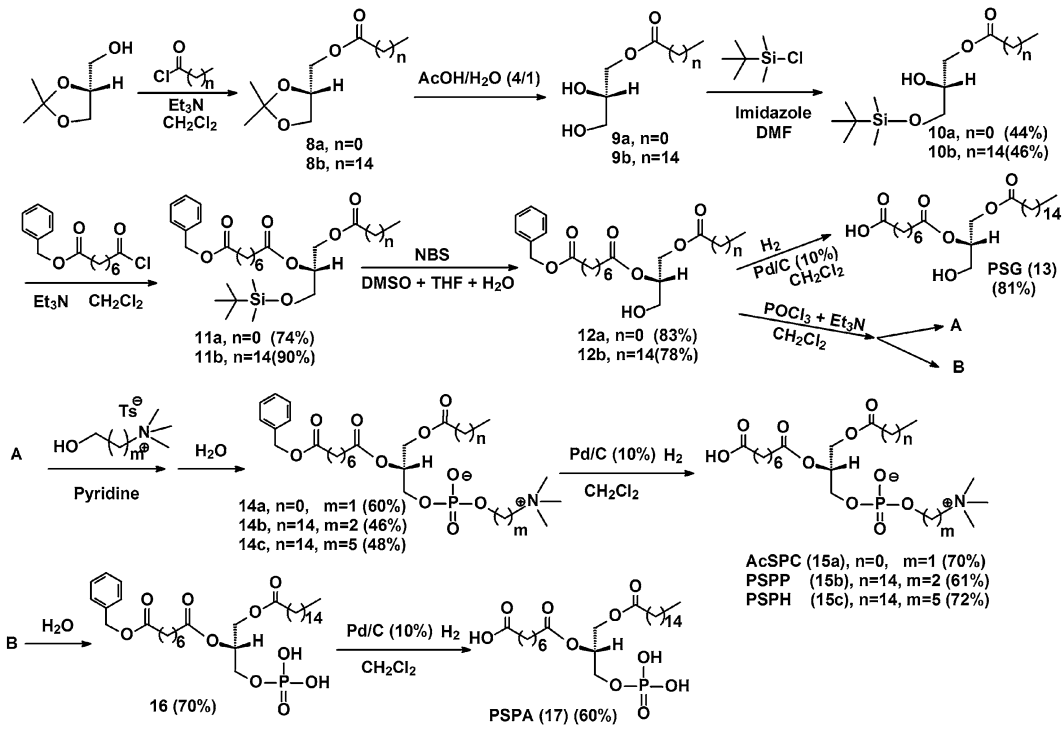

Scheme 4 The synthetic route for PSG, AcSPC, PSPP, PSPH, and PSPA. *Reproduced from [JBC, 2010, 285*(7), *4447–54] with permission from [The American Society for Biochemistry and Molecular Biology]*

trimethylamino)-propanol, **PSPP**), **15c** (1-palmitoyl-2-suberoyl-sn-glycero-3-phosphatidyl-(N,N,N-trimethylamino)-hexanol, **PSPH**), and **17** (1-palmitoyl-2-suberoyl-sn-glycero-3-phosphatidic acid, **PSPA**) were prepared with similar method, as shown in Scheme 3.4. In the first step, 1,2-O-isopropylideneglycerol was treated with acyl chlorides in methylene chloride in the presence of triethylamine to give monoester intermediates **8a**,**b**. Subsequent removal of the isopropylidene protecting group in 80 % acetic acid [12] delivered 1-O-acyl glycerol intermediates **9a**,**b**. These intermediates were then treated with TBDMSCl in DMF in the presence of imidazole to selectively protect the hydroxyl group at the sn-3 position, leading to the formation of 1-acyl-3-(*tert*-butyldimethylsilyl)-glycerol **10a**, **b** [11]. In the next step, **10a** and **10b** were treated with 7-benzyloxycarbonylheptanoyl chloride in the presence of excess triethylamine which was used to neutralize the newly formed HCl during the reaction. The resulting 1,2-O-acyl-3-O-TBDMS ether intermediates **11a** and **11b** were deprotected by *N*-bromosuccinimide (NBS) in DMSO/THF/H_2O solution to give the 1,2-di-O-acyl-*sn*-glycerols **12a** and **12b** (*see* **Note 3**) [13]. **12a** and **12b** were treated with phosphorus oxychloride in the presence of triethylamine, followed by addition of

N,N,N-trimethylamino-alkanol and subsequent hydrolysis in water to give the synthetic phospholipid precursors **14a**-**c** [14]. Debenzylation of **14a**-**c** by hydrogen provided the synthetic phospholipids **15a**-**c**. The hydrogenolysis of **12b** with catalysis by palladium on carbon removed the benzyl group at the *sn*-2 position and produced **PSG** [10, 13]. In addition, **12b** was treated with phosphorus oxychloride in the presence of triethylamine, followed by the hydrolysis in water to give the synthetic phospholipid precursor **16**. Debenzylation of the precursor **16** by hydrogen provided the synthetic phospholipid **17**.

Experimental details for the preparation of **15a** were described as an example. 1,2-O-isopropylideneglycerol (3.0 g, 23 mmol) and triethylamine (3.0 g, 30 mmol) were dissolved in 20 ml methylene chloride. Acetyl chloride (2.4 g, 30 mmol, in 10 ml methylene chloride) was added dropwise at room temperature in 30 min. The mixture was stirred at room temperature for 5 h and then filtered to remove the precipitate. The filtrate was washed with water 3 times and concentrated under reduced pressure to give colorless oil (1, 2-O-isopropylideneglycerol acetate (**8a**), 3.5 g, 87 %). The crude product was used directly in the next step without further purification.

Compound **8a** (3.3 g, 19 mmol) was dissolved in 15 ml 80 % acetic acid solution. The mixture was stirred at room temperature for 16 h and then concentrated under reduced pressure to give pale yellow oil (1-O-acetylglycerol (**9a**), 2.4 g, 89 %). The crude product was used directly in the next step without further purification.

Compound **9a** (2.0 g, 14.9 mmol) and triethylamine (1.8 g, 17.9 mmol) was dissolved in 7 ml DMF. To the mixture, *tert*-butyldimethylsilyl chloride (2.7 g, 17.9 mmol, in 10 ml DMF) was added dropwise in 30 min at room temperature. The mixture was stirred at room temperature for 1 day and then filtered to remove the precipitate. The filtrate was concentrated under reduced pressure to remove the solvent. The obtained residue was purified by flash chromatography on silica gel with hexanes/ethyl acetate (6/1, TLC: R_f = 0.2) to give pale yellow oil (1-acetoxy-3-(*tert*-butyldimethylsilyl)-oxypropan-2-ol (**10a**), 1.6 g, 44 %).

Compound **10a** (0.6 g, 2.4 mmol) and 0.23 g pyridine were dissolved in 6 ml methylene chloride. To the mixture, 7-benzyloxycarbonylheptanoyl chloride (0.82 g, 2.9 mmol, in 6 ml methylene chloride) was added dropwise at room temperature. The resulted mixture was stirred at room temperature for 6 h and then filtered to remove the precipitate. The filtrate was concentrated under reduced pressure to remove the solvent. The obtained residue was purified by flash chromatography on silica gel with hexanes/ethyl acetate (5/1, TLC: R_f = 0.5) to give pale yellow oil (1-(1-acetoxy-3-(*tert*-butyldimethylsilyloxy)-propan-2-yl)-8-benzyl octanedioate (**11a**), 1.0 g, 83 %).

Compound **11a** (0.9 g, 1.8 mmol) was mixed with 22 ml DMSO, 2.3 ml THF, 2.3 ml H_2O in 50 ml flask covered with aluminum foil to protect the reaction from light. Then *N*-bromosuccinimide (NBS) (1.5 g, 8.4 mmol) was added to the mixture at room temperature. One hour later, 50 ml 1 % sodium thiosulfate solution was added to quench the reaction. The mixture was extracted with ethyl acetate and the obtained crude product was purified by flash chromatography on silica gel with hexanes/ethyl acetate (1/1, TLC: $R_f = 0.4$) to give colorless oil (1-(1-acetoxy-3-hydroxypropan-2-yl)-8-benzyl octanedioate (**12a**), 0.51 g, 74 %).

Phosphorus chloride oxide (136 mg, 0.89 mmol) and triethylamine (98 mg, 0.97 mmol) were dissolved in 2.8 ml anhydrous methylene chloride. To the mixture, compound **12a** (269 mg, 0.71 mmol, in 2.6 ml methylene chloride) was added dropwise in 10 min at room temperature. 1.5 h later, choline tosylate (311 mg, 1.13 mmol) and 0.9 ml pyridine were added. The mixture was stirred at room temperature for 1 day before addition of 0.6 ml of water. One hour later, the reaction mixture was concentrated under reduced pressure to remove the solvent. The resulting residue was dissolved in THF/H_2O (3/1) and passed through an IWT TMD-8 (H^+, OH^-) ion exchange resin column. The obtained crude product was purified further by flash chromatography on silica gel with CH_3CN/H_2O (2/1, TLC: $R_f = 0.3$) to give colorless oil (1-acetyl-2-(8′-benzyloxy-8′-oxooctanoyl)-sn-3-phosphocholine (**14a**), 230 mg, 60 %).

Compound **14a** (73 mg, 0.13 mmol) in 7 ml of methylene chloride was hydrogenated over 10 % Pd/C (10 mg) at atmospheric pressure for 1 h. The catalyst was removed by filtration, and the filtrate was concentrated. The crude product was purified by 0.5 mm preparative silica gel TLC plate with CH_3OH/H_2O (3/1, TLC: $R_f = 0.3$) to give white solid (1-acetyl-2-suberoyl-sn-3-phosphocholine (**AcSPC**, **15a**), 43 mg, 70 %).

3.2 Competitive Binding Assay

1. Preparation of phospholipid vesicles: model oxidized phospholipid was dissolved by chloroform and mixed at 0.5–50 % ratio with PAPC or POPC in a glass vial. The chloroform was then evaporated under the nitrogen stream. The resulting residue was resuspended in 1× PBS, sonicated for 5 min at room temperature, and then passed through a 0.1 μm polycarbonate filter 11 times using an Avanti Mini-Extruder Set. The obtained unilamellar vesicles have a size close to 100 nm (*see* **Note 4**).
2. Preparation of solution A: 1.4 ml of LDL (3.5 mg/ml), 1.25 ml of ^{125}I-NO_2-LDL (0.2 mg/ml), 500 μl of DTPA (10 mM), and 500 μl of catalase (30 μM) were added to Dulbecco's modified Eagle's medium (DMEM) containing 5 % fetal bovine serum (FBS) to a final volume of 25 ml and mixed.

3. Preparation of solution B: 20 ml of solution A was mixed with 20 ml of DMEM/5 % FBS.
4. Preparation of solution of model oxidized phospholipids (final concentrations: 120, 60, 30, 15, 7.5, 3.75, and 1.87 μM): 100 μl of synthetic phospholipid vesicle solution (2.4 mM in 1× PBS) was mixed with 900 μl of DMEM/5 % FBS. The resulting solution was mixed with 1 ml of solution A, providing solution C containing 120 μM of model oxidized phospholipids. Then, 1 ml of solution C was diluted serially using equal volume of solution B, giving phospholipid solution D with half concentration (60 μM). The dilution process was repeated to make other phospholipid solutions mentioned above.
5. CD36-overexpressing and SR-BI-overexpressing HEK-293 cells were grown in 24-well cell culture plate containing DMEM (10 % FBS, 1 % P/S) until confluent. Then DMEM medium was removed, and 330 μl of the media containing ^{125}I-NO_2-LDL and various concentrations of phospholipid vesicles were added and incubated for 3 h on ice. Then the cells were washed with ice-cold DMEM (300 μl for each well) 3 times to remove unbound ^{125}I-NO_2-LDL. The cells were lysed by adding 750 μl of 0.1 M NaOH and shaking for 5 min. Lysates were transferred to scintillation vials. The vials were then filled with 5 ml scintillation cocktail. The cell-associated radioactivity was quantified with Beckman Coulter Beta/Gamma Counter (LS5000TD).
6. Each experiment was performed in triplicate, and results are expressed as the percentage of control binding and calculated as $100 \times (r/c)$, where c is the radioactivity count in control samples incubated without synthetic phospholipid competitor and r is the radioactivity count in samples incubated with phospholipid competitor. The percentage of control binding versus log [synthetic phospholipid] data was plotted using Prism software (GraphPad Inc., San Diego, CA) and the IC_{50} was calculated using the nonlinear regression curve fit with one-site competition. Values are expressed as means ± SEM. Statistical significance was evaluated using a two-tailed unpaired Student's *t*-test. Results were considered statistically significant with *P* values less than 0.05.

3.3 Direct Binding Assay

1. An array of GST-fusion proteins (GST-$CD36_{118\text{-}182}$, GST-$CD36_{164A166A}$, and GST-$SR\text{-}BI_{183\text{-}205}$) were made in a Rosetta^{TM}(DE3)pLacI strain of *Escherichia coli* as described previously [6]. GST-$CD36_{118\text{-}182}$ contains the region spanning CD36 amino acids 118–182, a binding domain for oxidized low-density lipoproteins and oxidized phospholipids [6]. We have previously found that lysine 164/166 in this region is critical for the binding activity. Site-directed mutagenesis of

lysine 164/166 to alanine (GST-$CD36_{164A166A}$) abolished binding [6]. GST-$SR\text{-}BI_{183\text{-}205}$ contains the region spanning SR-BI amino acids 183–205, a binding domain for high-density lipoproteins and oxidized phospholipids [4].

2. Stock solutions of small unilamellar vesicles comprised of POPC, model oxidized phospholipid, and [^{3}H]DPPC at indicated molar ratio were prepared as described above in the competitive binding assay.
3. To a 1.5 ml conical tube, 10 μl of glutathione-sepharose-bound proteins (250 μg/ml in 1× PBS), 3 μl of [^{3}H]DPPC-labeled phospholipid vesicles (100 μM), and 17 μl 1× PBS were added and mixed, followed by 3 h incubation at 4 °C with gentle rocking.
4. Then 950 μl of 1× PBS was added to each tube and the resulting mixture was centrifuged at 500 × *g* for 3 min to pellet the glutathione-sepharose beads. Supernatant was removed and the washing process was repeated two more times to remove the unbound synthetic phospholipid vesicles.
5. Next, 0.5 ml of 0.1 N NaOH was added to each tube, followed by 5 min gentle shaking on an orbital shaker. The resulting mixture was transferred to scintillation vials. The vials were filled with 5 ml scintillation cocktail. Then the associated radioactivity was quantified with Beckman Coulter Beta/Gamma Counter (LS5000TD).

3.4 Cholesteryl Ester Synthesis Assay

1. Thioglycollate-elicited mouse peritoneal macrophages (MPM) were isolated from wild type, CD36 knockout and SR-BI knockout mice according to the protocol described previously [15] and cultured for 48 h in RPMI-1640/10 % FBS medium in 12-well cell culture clusters (approximately 2×10^6 cells/well).
2. Confluent MPM was incubated with synthetic phospholipids (30 μM), [1-^{14}C]oleate (1.5 μCi/ml), and NO_2-LDL (25 μg/ml) in RPMI-1640/10 % FBS medium at 37 °C for 24 h. Then the supernatant was removed, and the cells were washed with 1 ml of 1× PBS for three times.
3. Then 1 ml of hexanes/isopropanol (3/2, v/v) solution was added to each well, and the plate was shaken vigorously for 30 min. The resulting extracts were transferred to glass tubes. Then another 0.6 ml of hexanes/isopropanol (3/2, v/v) solution was added to each well, and the process was repeated. The extracts were combined and dried using Reacti-Vap Evaporators at room temperature.
4. To the glass tube containing the dried residues, 140 μg of cholesteryl oleate in 100 μl of chloroform was added (*see* **Note 5**). After thorough mixing by vortex mixer, 50 μl of the resulting solution was applied to a TLC plate which was then developed

with hexanes/ethers/acetic acid (70/30/1, v/v/v). Next, the TLC plate was dried and stained with iodine vapor.

5. The cholesteryl oleate bands were cut and transferred into scintillation vials. The vials were filled with 5 ml scintillation cocktail. Incorporation of [^{14}C]oleate in cholesteryl esters was quantified with Beckman Coulter Beta/Gamma Counter (LS5000TD).

3.5 Results

3.5.1 Competitive Binding Assay

^{125}I-NO_2-LDL binds specifically to scavenger receptors CD36 and SR-BI via $oxPC_{CD36}$ [3, 4]; therefore, we assessed the binding activity of synthetic phospholipids by their ability to block the binding of ^{125}I-NO_2-LDL to cells overexpressing CD36 or SR-BI. Our recent observations indicated that the negative charge on the phospholipid is crucial for the binding activity to CD36 [6]. In order to see if the terminal carboxylate group alone is sufficient to generate high binding affinity to class B scavenger receptors, we designed and synthesized PSPC and PDPC (Fig. 1a). These phospholipids lack the γ-oxo-α,β-double bond present in the original $oxPC_{CD36}$ lipids. PSPC and PDPC were incorporated into inert PAPC vesicles (models of oxLDL phospholipid shell) and their activity was compared to their $oxPC_{CD36}$ analogs 5-keto-6-octendioic acid ester of lysoPC (KOdiA-PC) and 9-keto-10-dodecendioic acid ester of lysoPC (KDdiA-PC) (Fig. 1a) [1, 3]. Vesicles made of PAPC served as a negative control. We found that PSPC and PDPC have IC_{50} comparable to their $oxPC_{CD36}$ analogs for both CD36 and SR-BI (Fig. 1a), while vesicles made of native unoxidized phospholipids had low binding activity (Fig. 1a, data for PAPC are shown). This indicates that the negative carboxylate group in the *sn*-2 position of oxPC suffices to generate high binding affinity to class B scavenger receptors.

In order to see the effects of neutral polar functional groups in the distal end of the *sn*-2 position on receptor binding activity, we designed and synthesized a series of phospholipids that are similar to PSPC but possess different functional groups at the *sn*-2 position (Fig. 1b). P6HHPC, P8HOPC, P8AOPC, and P9MNPC have hydroxyl, amide, and methyl ester neutral polar groups at the terminus of *sn*-2 position (Fig. 1b). While the negatively charged carboxylate group that can form hydrogen bonds and salt bridges with the amino group of lysines in the binding domain of the receptor [6], these neutral groups can only form weak hydrogen bonds with the amino group of lysines. In addition, we synthesized PdiOSPC (Fig. 1b) with two oxygen atoms incorporated into the carbon chain at the *sn*-2 position which, theoretically, could make the chain more polar, serve as additional hydrogen bond acceptors, and thus increase the binding. The IC_{50} values (Fig. 1b) showed that the phospholipids with terminal neutral polar groups have noticeable binding activity to both receptors; however, the activity was much weaker compared to phospholipids with negative

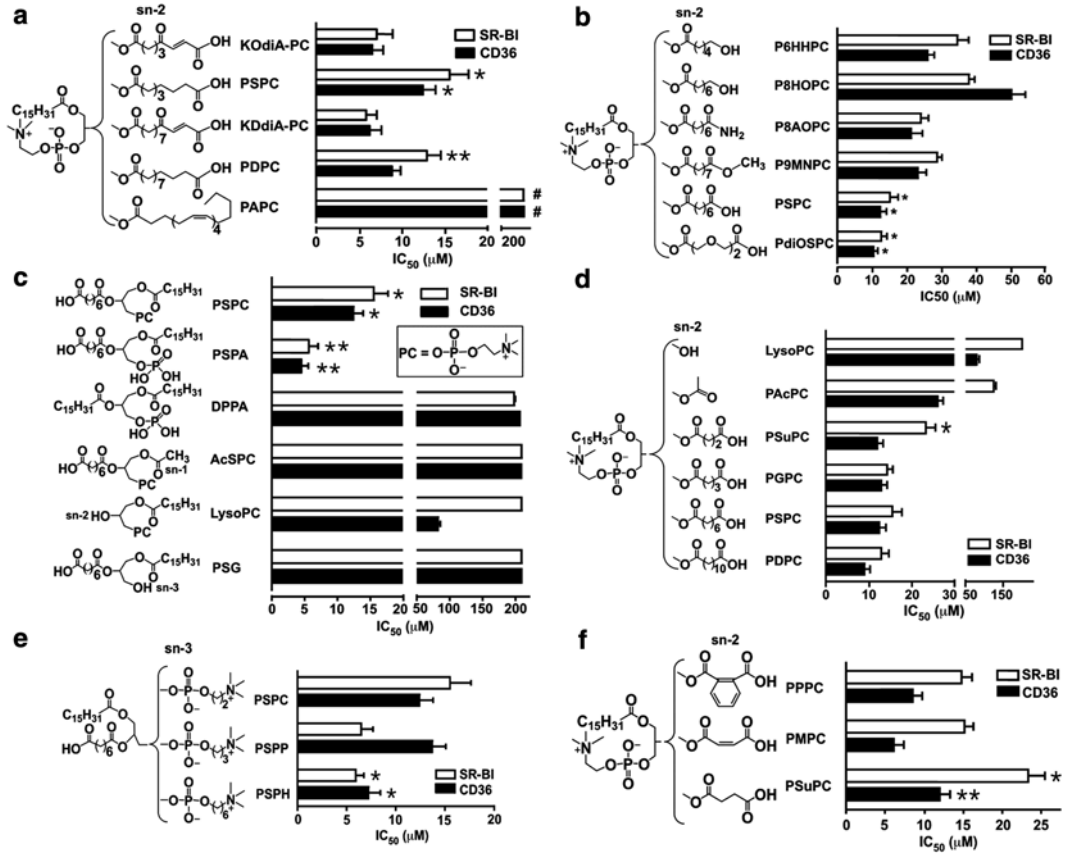

Fig. 1 Competitive binding activity of synthetic phospholipids. The synthetic phospholipids were analyzed for their ability to compete for the binding of ^{125}I-NO_2-LDL (5 μg/ml) to CD36 and SR-BI transfected 293 cells as described in the protocol. Binding abilities of the synthetic phospholipids to both receptors were determined by assessing the concentrations of synthetic phospholipids (presented as an equimolar mixture of synthetic phospholipids and PAPC) required to block 50 % of ^{125}I-NO_2-LDL binding (IC_{50}). Results represent the mean ± SEM of three independent experiments. (**a**) #$P < 0.0001$ for comparison versus KOdiA-PC, PSPC, KDdiA-PC and PDPC; *$P < 0.05$ for comparison versus KOdiA-PC; and **$P < 0.05$ for comparison versus KDdiA-PC. (**b**) *$P < 0.05$ for comparison versus P6HHPC, P8HOPC, P8AOPC, and P9MNPC. (**c**) *$P < 0.001$ for comparison versus DPPA, AcSPC, LysoPC, and PSG, and **$P < 0.05$ for comparison versus PSPC. (**d**) *$P < 0.05$ for comparison versus PGPC, PSPC, and PDPC. (**e**) *$P < 0.05$ for comparison versus PPPC and PMPC, **$P < 0.05$ for comparison versus PMPC. (**f**) *$P < 0.05$ for comparison versus PSPC. *Reproduced from [JBC, 2010, 285*(7)*, 4447–54] with permission from [The American Society for Biochemistry and Molecular Biology]*

carboxylate at the distal end of the *sn*-2 position (PSPC and PdiOSPC). Activity of PdiOSPC was similar to that of PSPC, suggesting that in the presence of a negative carboxylate, additional oxygen atoms in the *sn*-2 chain do not play significant role in binding activity (Fig. 1b).

Previous experiments demonstrated that a negative group at the *sn*-2 position of the phospholipid is required for high binding affinity to CD36 and SR-BI. To test whether additional negative

charge at the *sn*-3 position could further increase binding activity, we designed PSPA (Fig. 1c). PSPA has a negatively charged phosphate group at the *sn*-3 position instead of neutral phosphocholine group in PSPC. PSPA was found to have a higher activity than PSPC (Fig. 1c), further demonstrating the critical importance of a negative charge for high-affinity binding to scavenger receptors class B. To test whether a negative group at *sn*-3 alone is sufficient for the high-affinity binding, we designed 1, 2-dipalmitoyl-sn-glycero-3-phosphatidic acid sodium salt (DPPA) possessing a negative phosphate group at the *sn*-3 position and two long hydrophobic chains at *sn*-1 and *sn*-2 positions (Fig. 1c). DPPA was found to have very poor binding affinity (Fig. 1c), demonstrating that a negative group alone at *sn*-3 is not sufficient to induce the high-affinity binding. These data suggest that the cooperation of all three parts of the oxidized phospholipids may be important for the binding to CD36 and SR-BI. To test this hypothesis, we designed three phospholipids similar to PSPC in which one functional group either at the *sn*-1, *sn*-2, or *sn*-3 positions was significantly shortened or removed, as shown in Fig. 1c. AcSPC has an acetyl group at the *sn*-1 position instead of long hydrophobic chain. LysoPC and PSG contain only a hydroxyl group at *sn*-2 or *sn*-3 position, respectively. All three phospholipids (AcSPC, lysoPC, and PSG) exhibit a near complete lack of binding activity to both CD36 and SR-BI (Fig. 1c). These results strongly suggest that an optimal structure of the *sn*-1, *sn*-2, and *sn*-3 positions of the oxidized phospholipids is important for the recognition by CD36 and SR-BI.

To assess whether the chain length in *sn*-2 and *sn*-3 positions is important for optimal binding, we designed, synthesized, and tested a series of phospholipids with varying chain lengths at these positions, as shown in Fig. 1d, e. The IC_{50} data suggest that the chain length at the *sn*-3 position moderately affects the binding activity. Elongation of the carbon chain from 2 to 6 resulted in a 20–40 % reduction in IC_{50} for the phospholipids (Fig. 1e) on both CD36 and SR-BI. A comparison between PSuPC, PGPC, PSPC, and PDPC (Fig. 1d) shows that a chain length of four carbons at the *sn*-2 position of the phospholipids is sufficient for high-affinity binding, with only moderate changes following further elongation.

To test whether it is the electrophilic reactivity of the **γ**-oxo-α, β-double bond or other properties which contribute to increased activity of $oxPC_{CD36}$ such as KOdiA-PC and KDdiA-PC compared to PSPC and PDPC, we designed PMPC and PPPC and compared their activity to the activity of PSuPC. PMPC and PPPC contain the structural moieties at the *sn*-2 position, which are similar to γ-oxo-α, β-unsaturation of $oxPC_{CD36}$, but are not electrophilically reactive towards the lysine amino groups. The PSuPC used for comparison has an identical chain length but lacks the *sn*-2 α,

β-double bond (Fig. 1f). The competition assay showed that PPPC and PMPC have higher binding affinity to both receptors compared to PSuPC. This result suggests that electrophilic reactivity is not critical for the binding activity of phospholipids with carboxylate group in the *sn*-2 position and suggests that other properties are responsible for the binding.

3.5.2 Direct Binding Assays

To directly demonstrate the binding activity of the model synthetic phospholipids to scavenger receptors class B, we performed a parallel series of studies using direct binding assays. Each of a selected number of model synthetic phospholipid species covering a wide range of IC_{50} was incorporated into small unilamellar vesicles composed of unoxidized parent lipid as a carrier and a tracer level of [^{3}H]DPPC. Vesicles were then tested for their capacity to specifically bind to $CD36_{118\text{-}182}$ or $SR\text{-}BI_{183\text{-}205}$ GST-fusion proteins that are shown to contain the binding domain for oxidized lipoproteins and oxidized phospholipids [4, 6]. Although vesicles composed of POPC alone failed to demonstrate specific binding, vesicles containing PSPC, PDPC, PSPH, or PSPA bound to $GST\text{-}CD36_{118\text{-}182}$ or $GST\text{-}SR\text{-}BI_{183\text{-}205}$ at significantly greater levels than POPC alone (Fig. 2). At the same time, PSG or P8HOPC, which had weak competing activity, showed weak but detectable specific direct binding. In general, the ranking order of direct binding activity among the synthetic oxidized PC species was consistent with their inhibitory capacity noted in competition assays. These experiments demonstrate that model oxidized phospholipids directly interact with scavenger receptors. They also strongly suggest that the inhibitory effect of model synthetic phospholipids on the binding of NO_2-LDL is not due to indirect interaction with NO_2-LDL.

In order to show the role of the interaction between the negative carboxylate group of the phospholipids and the positive lysine amino group in the scavenger receptor binding domain, two lysine groups (164K, 166K) in $GST\text{-}CD36_{118\text{-}182}$ were replaced by alanine groups (164A, 166A) and the mutated $GST\text{-}CD36_{164A166A}$ was used in a direct binding assay. The test result demonstrated that replacing the two positive lysine groups with two neutral alanine groups led to the remarkable decrease in the direct binding capacity of model phospholipids with high binding activity and a negative carboxylate group at the *sn*-2 position (Fig. 2).

3.5.3 Cholesteryl Ester Synthesis Assay

Our data suggest that synthetic oxidized phospholipids may be able to interfere with foam cell formation by inhibiting the binding and subsequent uptake of oxidized lipoproteins mediated by scavenger receptors class B. Thus, we examined the effects of a select number of model synthetic phospholipids, covering a wide range of IC_{50} (AcSPC, P8HOPC, PSPA, PGPC, PDPC, PSPH, and PMPC) on macrophage foam cell formation. Murine peritoneal macrophages were incubated with indicated oxidized

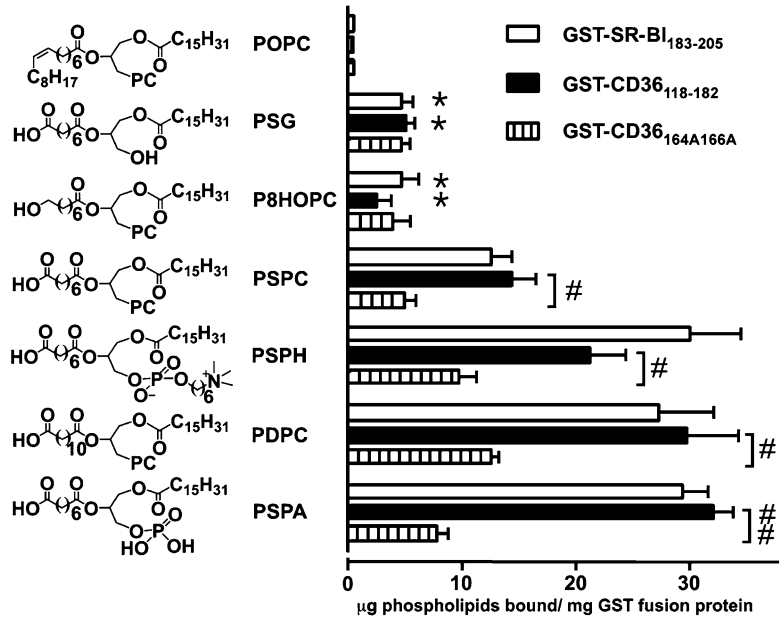

Fig. 2 Model synthetic phospholipids bind directly to CD36 and SR-BI peptides containing binding site for oxidized LDL. Binding of POPC vesicles containing 20 mol% of synthetic phospholipids and tracer amount of [^{3}H]DPPC to the indicated glutathione-sepharose-bound GST-fusion proteins (GST-CD36$_{118-182}$, GST-CD36164A166A, or GST-SR-BI$_{183-205}$) was assessed as described in the protocol. Results represent the mean ± SEM of three independent experiments. *$P < 0.01$ for comparison versus PSPC, PSPH, PDPC, and PSPA, and #$P < 0.05$ and ##$P < 0.01$. *Reproduced from [JBC, 2010, 285(7), 4447–54] with permission from [The American Society for Biochemistry and Molecular Biology]*

phospholipids, [^{14}C]oleate and LDL modified by the MPO-H_2O_2-NO_2^- system (NO_2-LDL)—which is a specific high-affinity ligand for class B scavenger receptors, but not for class A scavenger receptors [16]. Macrophage cholesteryl ester formation was monitored by measuring the [^{14}C]oleate incorporation into cholesteryl ester fraction of macrophage lipids. NO_2-LDL induced a significant [^{14}C]oleate incorporation into cellular cholesteryl ester pools in macrophages, as anticipated (Fig. 3). In contrast, cells incubated with NO_2-LDL in the presence of phospholipids with high binding activity (PSPA, PSPH, and PMPC) had significantly reduced [^{14}C]oleate incorporation into cellular cholesteryl ester pools (Fig. 3a). In agreement with binding studies, AcSPC had no effect and P8HOPC had a modest effect on cholesteryl ester accumulation in macrophages exposed to NO_2-LDL (Fig. 3). Similar results were obtained in CD36-deficient macrophages where uptake of NO_2-LDL was mediated by SR-BI (Fig. 3b). IC_{50} values of model oxidized phospholipids correlated strongly with the capacity to inhibit cholesteryl ester accumulation (Fig. 3c, d).

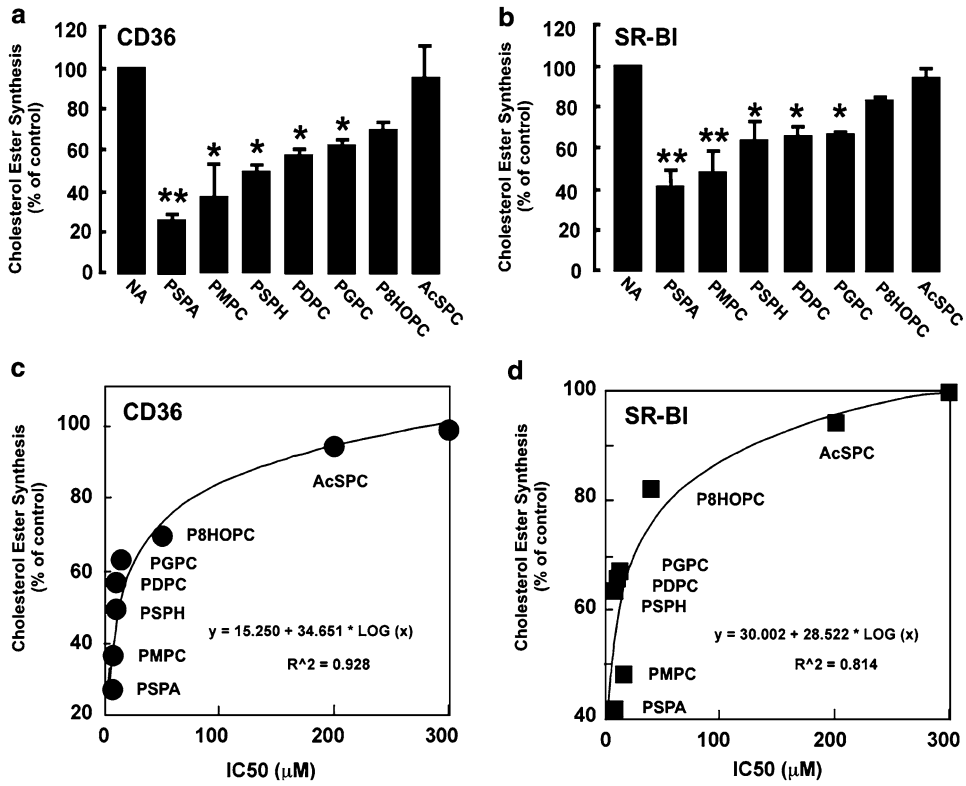

Fig. 3 Model synthetic phospholipids interfere with foam cell formation. Murine thioglycollate-elicited peritoneal macrophages were isolated from mice of indicated phenotype, cultured and incubated with NO_2-LDL (25 μg/ml) and [^{14}C] oleate (1.5 μCi/ml) in the presence or absence of indicated synthetic phospholipids (30 μM). (**a**, **b**) [^{14}C] cholesteryl ester synthesis assay was carried out as described in the protocol. (**c**, **d**) IC_{50} of synthetic phospholipids correlate with the capacity to inhibit cholesteryl ester accumulation in macrophages. *$P < 0.05$, **$P < 0.01$ versus NA (no addition). *Reproduced from [JBC, 2010, 285*(7)*, 4447–54] with permission from [The American Society for Biochemistry and Molecular Biology]*

4 Notes

1. In the synthesis of P8AOPC, DMAP was used in excess (threefold) over the suberyl chloride to ensure that all suberyl chloride molecules were converted to acylpyridinium. In comparison to suberyl chloride, much fewer lysoPC was added dropwise to ensure that suberyl chloride was in great excess during the reaction with lysoPC and that only one acyl chloride group in each suberyl chloride was esterified with lysoPC.
2. In this esterification reaction, benzyl bromide dissolved in dimethylformamide (DMF) was added dropwise to the dicarboxylic acids, which were used in excess to ensure that the monoester was the major product. Triethylamine was used to neutralize the hydrobromic acid generated in the reaction.

3. Standard reaction conditions (e.g., tetra-n-butylammonium fluoride treatment) for the desilylation of **11a** and **11b** facilitate the migration of acyl group from *sn*-2 position to *sn*-3 position. Desilylation using *N*-bromosuccinimide in DMSO/THF/H_2O solution could reduce the acyl migration dramatically.
4. To prevent the formation of larger destabilized aggregates, the newly prepared 100 nm unilamellar vesicles should be stored at 4 °C before use [17].
5. High concentration of unlabelled cholesteryl oleate was added as an internal standard. It can be easily visualized by iodine vapor and thus help locate the trace amount of radiolabeled cholesteryl oleate on the TLC plate.

Acknowledgement

This research was originally published in Journal of Biological Chemistry. Gao D. et al. Structural Basis for the Recognition of Oxidized Phospholipids in Oxidized Low Density Lipoproteins by Class B Scavenger Receptors CD36 and SR-BI. Journal of Biological Chemistry 2010, 285(7), 4447–4454. © The American Society for Biochemistry and Molecular Biology.

References

1. Podrez EA (2002) A novel family of atherogenic oxidized phospholipids promotes macrophage foam cell formation via the scavenger receptor CD36 and is enriched in atherosclerotic lesions. J Biol Chem 277:38517–38523
2. Podrez EA, Byzova TV, Febbraio M, Salomon RG, Ma Y, Valiyaveettil M, Poliakov E, Sun M, Finton PJ, Curtis BR, Chen J, Zhang R, Silverstein RL, Hazen SL (2007) Platelet CD36 links hyperlipidemia, oxidant stress and a prothrombotic phenotype. Nat Med 13:1086–1095
3. Podrez EA (2002) Identification of a novel family of oxidized phospholipids that serve as ligands for the macrophage scavenger receptor CD36. J Biol Chem 277:38503–38516
4. Ashraf MZ, Kar NS, Chen X, Choi J, Salomon RG, Febbraio M, Podrez EA (2008) Specific oxidized phospholipids inhibit scavenger receptor bi-mediated selective uptake of cholesteryl esters. J Biol Chem 283: 10408–10414
5. Greenberg ME, Li X-M, Gugiu BG, Gu X, Qin J, Salomon RG, Hazen SL (2008) The lipid whisker model of the structure of oxidized cell membranes. J Biol Chem 283:2385–2396
6. Kar NS, Ashraf MZ, Valiyaveettil M, Podrez EA (2008) Mapping and characterization of the binding site for specific oxidized phospholipids and oxidized low density lipoprotein of scavenger receptor CD36. J Biol Chem 283:8765–8771
7. Podrez EA, Schmitt D, Hoff HF, Hazen SL (1999) Myeloperoxidase-generated reactive nitrogen species convert LDL into an atherogenic form in vitro. J Clin Investig 103: 1547–1560
8. Podrez EA, Febbraio M, Sheibani N, Schmitt D, Silverstein RL, Hajjar DP, Cohen PA, Frazier WA, Hoff HF, Hazen SL (2000) Macrophage scavenger receptor CD36 is the major receptor for LDL modified by monocyte-generated reactive nitrogen species. J Clin Investig 105:1095–1108
9. Sun M, Deng Y, Batyreva E, Sha W, Salomon RG (2002) Novel bioactive phospholipids: practical total syntheses of products from the oxidation of arachidonic and linoleic esters of 2-lysophosphatidylcholine. J Org Chem 67:3575–3584
10. Owen RM, Gestwicki JE, Young T, Kiessling LL (2002) Synthesis and applications of end-labeled neoglycopolymers. Org Lett 4:2293–2296

11. Jha V, Kondekar NB, Kumar P (2010) Enantioselective synthesis of syn/anti-1, 3-amino alcohols via proline-catalyzed sequential alpha-aminoxylation/alpha-amination and Horner-Wadsworth-Emmons olefination of aldehydes. Org Lett 12:2762–2765
12. Bordoni A, de Lederkremer RM, Marino C (2006) Photoinduced electron-transfer alpha-deoxygenation of aldonolactones. Efficient synthesis of 2-deoxy-D-arabino-hexono-1,4-lactone. Carbohydr Res 341:1788–1795
13. Burgos CE, Ayer DE, Johnson RA (1987) A new, asymmetric synthesis of lipids and phospholipids. J Org Chem 52:4973–4977
14. Tsuboi S, Takeda S, Yamasaki Y, Sakai T, Utaka M, Ishida S, Yamada E, Hirano J (1992) A convenient synthesis of platelet-activating factors and their analogs from chiral epichlorohydrin. Chem Lett 21(8): 1417–1420
15. Zhang X, Goncalves R, Mosser DM (2008) The isolation and characterization of murine macrophages. Curr Protoc Immunol. doi: 10.1002/0471142735.im1401s83
16. Markwell MAK, Haas SM, Bieber LL, Tolbert NE (1978) A modification of the Lowry procedure to simplify protein determination in membrane and lipoprotein samples. Anal Biochem 87:206–210
17. Yohannes G, Pystynen K-H, Riekkola M-L, Wiedmer SK (2006) Stability of phospholipid vesicles studied by asymmetrical flow field-flow fractionation and capillary electrophoresis. Anal Chim Acta 560:50–56

Chapter 4

A Novel Gas Chromatographic Method for Determination of Malondialdehyde from Oxidized DNA

Takayuki Shibamoto

Abstract

Malondialdehyde (MA) is known to form from various lipids upon oxidation as one of secondary oxidation products. Determination of MA formed from lipid peroxidation has been used to examine occurrence of oxidative damages associated with many diseases, such as cancer, Alzheimer's, arthritis, inflammation, diabetes, atherosclerosis, and AIDS as well as aging. Analysis of MA is, however, extremely difficult because it is highly reactive and readily polymerized and forming adducts with biological substances such as proteins, phospholipids, and DNA (Shibamoto, J Pharm Biomed Anal 41:12–25, 2002). Gas chromatographic method using stable derivative, 1-methylpyrazole was advanced and has been successfully used to analyze MA in various lipids and lipid-rich foods. This method was also applied to determine MA formed from DNA and related compounds. The amounts found in oxidized 2′-deoxyribonucleotides were 213.8 nmol/16 mmol in 2′-deoxyguanosine, 130.6 nmol/16 mmol in 2′-deoxycytidine, 85.1 nmol/16 mmol in 2′-deoxyadenosine, and 84.5 nmol/16 mmol in thymidine. When the antioxidant activity of flavonoids and anthocyanins against calf thymus DNA oxidized with Fenton's reagent was examined using this newly developed gas chromatographic method, antioxidant activity of flavonoids and anthocyanins ranged from 48.5 % (catechin) to 29.9 % (apigenin) and from 45.0 % (callistephin) to 10.2 % (cyaniding), respectively.

Key words Antioxidant activity, Calf thymus DNA, Gas chromatography, Lipid peroxidation, Malondialdehyde

1 Introduction

Malondialdehyde (MA) has been known to form from various lipids upon oxidation [1]. Consequently, MA has been used most commonly and widely to monitor oxidation of lipids and related materials [2]. Figure 1 shows proposed formation pathways of MA. There are two possible pathways. One (A) is in vivo or autoxidation [3, 4]. The other one is that formation of low molecular weight radicals via photo or heat degradation of lipids, and subsequently these radicals combined to form MA as well as other aldehydes and ketones [2].

Formation of MA from the oxidative degradation of lipids has been studied for various subjects associated with food stability, such as thermal oxidation and autoxidation with reactive oxygen species.

Donald Armstrong (ed.), *Advanced Protocols in Oxidative Stress III*, Methods in Molecular Biology, vol. 1208,
DOI 10.1007/978-1-4939-1441-8_4,

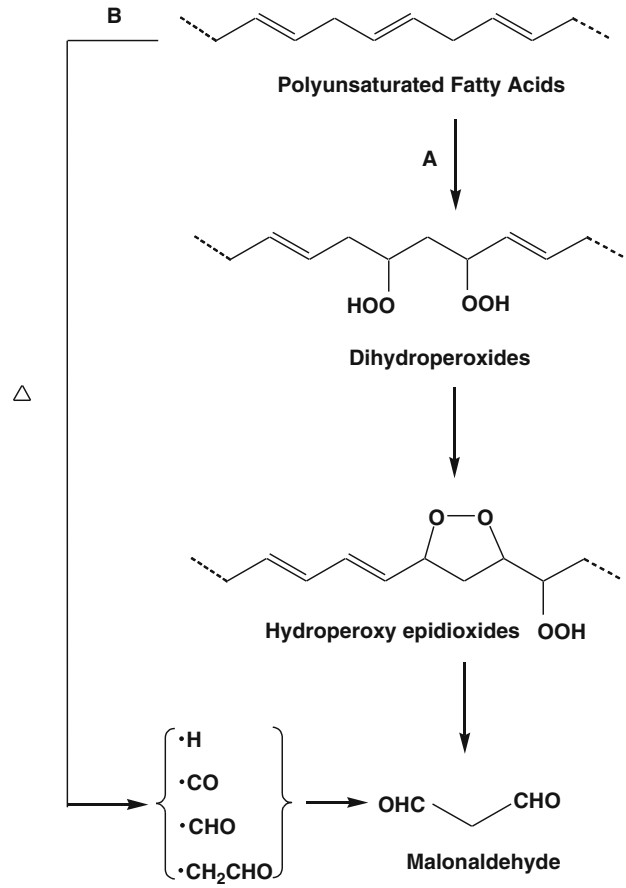

Fig. 1 Proposed formation pathways of MA

The oxidative degradation of lipids is initiated by reactive oxygen species (ROSs), including superoxide (O_2^-), singlet oxygen ($^1O_2$), triplet oxygen ($^3O_2$), hydroxyl radical ($^{\bullet}OH$), alkoxyl radical ($RO^{\bullet}$), and peroxyl radical ($ROO^{\bullet}$). The autoxidation of unsaturated fatty acids occurs slowly, initiated by a triplet oxygen ($^3O_2$), which abstracts a hydrogen atom from a methylene group of an unsaturated fatty acid and subsequently forms free radicals such as a peroxyl radical [5, 6]. Once these free radicals are formed, lipid peroxidation progresses and, consequently, many secondary oxidation products are formed as shown in Fig. 1. In addition to autoxidation, secondary lipid peroxidation products, including MA, form by heat treatments like cooking. The formation mechanisms of MA by heat involve production of many radicals, which are different from those of autoxidation because the conditions of thermal oxidation are much more intense than those of autoxidation [7].

MA has been most widely used as a biomarker to study oxidative damages associated with various diseases including cancer, Alzheimer's, arthritis, inflammation, diabetes, atherosclerosis, and

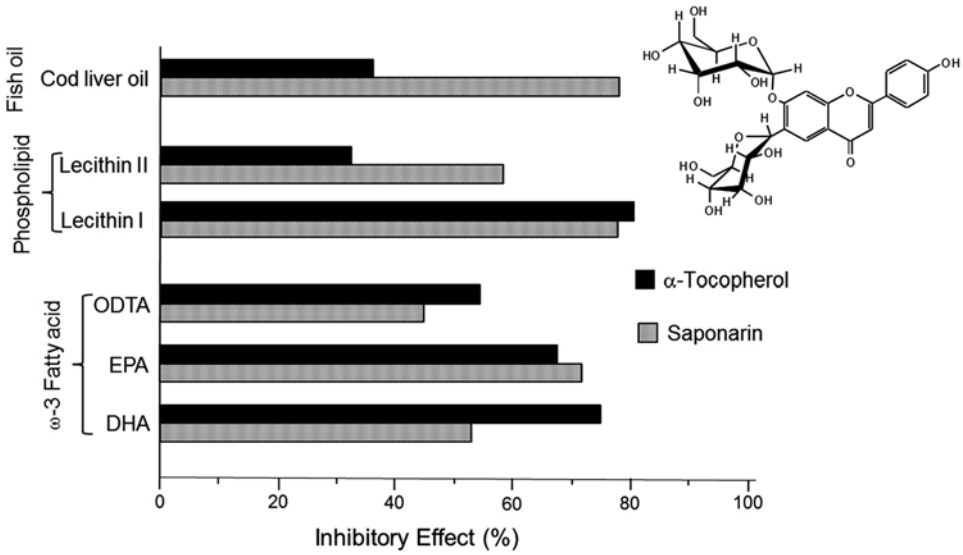

Fig. 2 Reaction of MA with *N*-methylhydrazine to yield 1-MP

AIDS as well as aging [1]. However, analysis of MA is extremely difficult because it is highly reactive and readily polymerized and forming adducts with biological substances such as proteins, phospholipids, and DNA [1]. Therefore, analysis of MA requires preparation of stable MA derivative (*see* **Notes 1–4**). Among the derivatives prepared for determination of MA, the thiobarbituric acid (TBA) derivative (MA-TBA adduct) has been the most commonly used. This adduct is determined by a spectrophotometer at 535 nm [1]. One of the major drawbacks of this method is that TBA forms adducts with many different carbonyl compounds, which absorb the same UV wavelength as is absorbed by the MA-TBA adduct. Therefore, this method is not specific to MA. It is not possible to analyze MA-TBA adduct by GC but recent development of LC/MS has achieved to determine MA-TBA adduct specifically with higher sensitivity [8].

Meantime, GC method using 1-methylpyrazole has been successfully used to analyze MA in various lipids and lipid-rich foods (*see* **Notes 5** and **6**). Reaction mechanisms of 1-methylpyrazole (1-MP) are shown in Fig. 2. The *N*-methylhydrazine derivative of MA (1-methylpyrazole) shown in Fig. 2 is an ideal chemical to be analyzed by a gas chromatograph with a nitrogen phosphorous detector (GC/NPD) because it is reasonably volatile and contains two nitrogen atoms. Moreover, MA reacts readily with *N*-methylhydrazine under mild conditions (at room temperature and pH 7). Since this method was advance in 1988 [9], trace levels of MA were successfully determined in various oxidized lipids and lipid-rich foods.

Table 1
MA analyzed by gas chromatography as 1-methylpyrazole

Sample	Oxidation method	Amount formed	References
Linolenic acid	Photo-irradiation	867 μg/g	[9]
Linoleic acid	Photo-irradiation	106 μg/g	[9]
Corn oil	Photo-irradiation	8.52–56.24 μg/g	[9]
Beef fat	Photo-irradiation	5.99–25.01 μg/g	[9]
Squalene	Photo-irradiation	< 2–176 nmol/100 g	[10]
Arachidonic acid	Photo-irradiation	5.7 μg/mg	[11]
Arachidonic acid	Fenton's reagent	4.8–27.5 nmol/mg	[12]
Ethyl arachidonate	Fenton's reagent	13.0–97.2 nmol/mg	[12]
Linoleic acid	Fenton's reagent	0.7–57.9 nmol/mg	[12]
Ethyl linoleate	Fenton's reagent	0.1–43.1 nmol/mg	[12]
Ethyl arachidonate	Microwave	8.4–11.2 nmol/mg	[13]
Ethyl linolenate	Microwave	3.5–5.3 nmol/mg	[13]
Ethyl linoleate	Microwave	1.4–1.7 nmol/mg	[13]
Ethyl arachidonate	Thermal heating	7.8–10.8 nmol/mg	[13]
Ethyl linolenate	Thermal heating	3.9–5.3 nmol/mg	[13]
Ethyl linoleate	Thermal heating	0.7–1.2 nmol/mg	[13]
Cod liver oil	Photo-irradiation	24.2–190.2 nmol/mg	[14]
Ethyl linoleate	Photo-irradiation	8.56 nmol/mg	[15]
Ethyl linolenate	Photo-irradiation	44.51 nmol/mg	[15]
Ethyl arachidonate	Photo-irradiation	59.40 nmol/mg	[15]
Cod liver oil	Fenton's reagent	61.18 nmol/mL	[16]
Probucol	Fenton's reagent	34.6–872.2 nmol/3 μmol	[17]
Cigarette	Thermal heating	19.8–36.0 mg/cigarette	[18]
Cooking oils	Thermal heating	60–745 nmol/g	[19]
Cooking oils	Thermal heating	6.7–1,070 ppm	[20]
Cod liver oils	Fenton-like reagent	95.4–837 nmol/mg	[21]

Table 1 summarizes levels of MA in samples oxidized by various methods analyzed using this method. These reports suggest that lipid peroxidation is induced by various conditions. Major source of MA is oxidized fatty acids, which are major lipids in fish oils, such as cod liver oil, and their alkyl esters. It is well known that some ω-3 polyunsaturated fatty acids, such as eicosapentaenoic

acid (EPA) and docosahexaenoic acid (DHA), present in fish oils possess cardiovascular protective effect and have been used for certain therapy [22]. However, reports indicated that these fatty acids produce readily toxic MA upon oxidation. It is obvious that fatty acids with the more unsaturations produce the more MA. Generally, amounts of MA formed by different oxidation methods are consistent. It should be noted that a drug used for atherosclerosis produced significant amount of MA (34.6–872.2 nmol/3 μmol) [17] and that MA is not just a biomarker but also known as one of the highly toxic low molecular weight carbonyl compounds [23].

After the gas chromatographic method for trace analysis of MA (MA/GC assay) was developed, many studies on antioxidant activity of many chemicals have been conducted in order to find possible prevention of oxidative damage associated with various diseases mentioned above. Table 2 shows antioxidant studies using the MA/GC assay. These results indicate that various flavonoids have potent antioxidant activity. For example, a flavonoid isolated from young green barley leaves exhibited strong antioxidant activity, which is comparable to that of α-tocopherol as shown in Fig. 3.

In addition to lipids, DNA-associated compounds, deoxynucleosides, also produced considerable amounts of MA upon oxidation [49]. Oxidative damage of DNA caused by various low molecular weight carbonyl compounds, including MA, has been known to associate with many diseases described above [50]. In vivo formation of MA adduct to *N*-terminal valine in hemoglobin and to guanine at N1, N2 in liver DNA was demonstrated using mice and radiolabeled MA [51]. Recent study reported that children living near industrial area have higher DNA damage found with analysis of MA-deoxyguanosine [52]. Therefore, the studies on a role of MA in DNA oxidation will be discussed in the present chapter [49, 53–55].

2 Materials

2.1 DNA and Related Chemicals

1. 2′-deoxyguanosine, 2′-deoxycytidine, 2′-deoxyadenosine, and thymidine were purchased from Sigma Chemical Co. (St. Louis, MO).
2. Calf thymus DNA and EDTA were obtained from Sigma-Aldrich (St. Louis, MO).

2.2 Chemicals for MA Analysis

1. *N*-methylhydrazine, 2-methylpyrazine, and 2-methylpyrazole were purchased from Sigma-Aldrich (St. Louis, MO).

2.3 Synthesis of 1-Methylpyrazole (1-MP)

1. MA (10 g) (Aldrich Chemical Co., Milwaukee, WI) was added to 300 mL of 0.1 N HCl.
2. The solution stirred for 1 h at 50 °C.

Table 2
Antioxidant studies using MA/GC assay

Testing system	Antioxidant	References
Squalene/photo-irradiation	Saponarin, α-tocopherol, and BHT. Essential oils of parsley seed, rose, celery seed, ylang-ylang, jasmine, juniper berry, patchouli, anise star, basil, bitter orange, cinnamon leaf, clove leaf, sage, and thyme	[24–27]
Squalene/Fenton's reagent	Saponarin, α-tocopherol, and BHT	[24, 25]
Ethyl linoleate/ photo-irradiation	Saponarin and α-tocopherol	[25]
Ethyl linoleate/Fenton's reagent	Naringin, galangin, rutin, and α-tocopherol	[28]
Ethyl linolenate/Fenton's reagent	Lacinilene A, naringin, galangin, rutin, and α-tocopherol	[28]
Ethyl arachidonate/ Fenton's reagent	Saponarin, ferulic acid, caffeic acid, chlorogenic acid, gallic acid, cinnamic acid, BHT, and α-tocopherol	[25, 28, 29]
Octadecatetraenoic acid/ Fenton's reagent	β-carotene, saponarin, lutonarin, BHT, and α-tocopherol	[30, 31]
Eicosapentaenoic acid/ Fenton's reagent	β-carotene, saponarin, lutonarin, BHT, and α-tocopherol	[30, 31]
Docosahexaenoic acid/ Fenton's reagent	β-carotene, saponarin, lutonarin, BHT, and α-tocopherol	[30, 31]
Lecithin I/Fenton's reagent	Saponarin, lutonarin, BHT, and α-tocopherol	[31, 32]
Lecithin II/Fenton's reagent	Saponarin, lutonarin, BHT, and α-tocopherol	[31, 32]
Cod liver oil/Fenton's reagent	Saponarin, lutonarin, α-tocopherol, BHT, eugenol, maltol, benzyl alcohol, 1-octen-3-ol, eugenyl acetate, sesamol, vanillin, ethylvanillin, pyrrole, 1-acetylpyrrole. eugenol, capsaicin, quercetin, catechin, and zeylaniin A. Extracts of mung beans, soybeans, kidney beans, azuki beans, clove bud, three species of eucalyptus leaves, brewed coffee, licorice root, onion sprouts, herbs (Tram, Voi, and Gac), roasted coffee beans, teas, and *S. zeylanicum* leaves	[33–44]
Cod liver oil/ photo-irradiation	Mixtures of essential oils: thyme/clove, thyme/cinnamon, thyme/rose, clove/rose, clove/cinnamon, and clove/ parsley. BHT and α-tocopherol	[45]
Beef homogenate/thermal heating	Extracts of sage and rosemary, and α-tocopherol	[46]
Blood plasma/Fenton's reagent	Vitamin C, saponarin, DMHF[a], and probucol. Extracts of clove bud and eucalyptus leaves	[47, 48]

[a]2,5-dimethyl-4-hydroxy-3(2H)-furanone

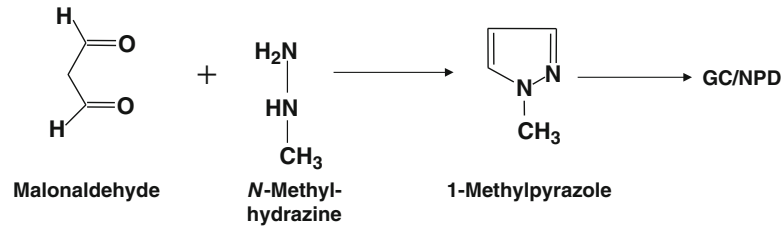

Fig. 3 Antioxidant activity of saponarin isolated from young green barley leaves tested using different lipids

3. The solution was cooled to room temperature.
4. *N*-methylhydrazine (0.3 g) in 30 mL water was added dropwise over a 10 min period with constant stirring.
5. The reaction mixture was extracted with 10 mL dichloromethane.
6. The extract was dried over anhydrous sodium sulfite.
7. Dichloromethane was removed from the extract by evaporation.
8. The colorless liquid 1-MP was obtained (1.86 g).

2.4 Isolation of Saponarin from Young Green Barley Leaves

1. Barley leaves (Hordeum vulgare L. Var. nudum Hook) harvested 2 weeks after germination (110 g) were freeze-dried.
2. The freeze-dried barley leaves were ground into powder.
3. The freeze-dried powder (20 g) was fractionated with Amberlite XAD-2 column chromatography using hexane, water/methanol (100/0, 80/20, 60/40, 40/60, 20/80, 0/100), and acetone.
4. The fraction eluted with water/methanol (40/60) was recrystallized with cold methanol twice.
5. A light yellow crude saponarin (14.5 mg) was obtained.
6. The crude saponarin (10 mg) was further purified with preparative HPLC (Develosil ODS-5) using a solvent consisted of water/methanol (70/30) at 2.5 mL/min.
7. A light yellow pure saponarin powder (6.5 mg) was obtained.

2.5 Antioxidants Used for DNA Studies

1. 2H-pyrrole, 3,4-dihydro-2,2-dimethyl-, 1-oxide (DMPO); 2H-1-benzopyran-2-carboxylic acid, 3,4-dihydro-6-hydroxy-2,5,7,8-tetramethyl-(9Cl) (Trolox®); 4H-1-benzopyran-4-one, 2-(3,4-dihydroxyphenyl)-3,5,7-trihydroxy-(9Cl) (quercetin); 4H-1-benzopyran-4-one, 5,7-dihydroxy-2-(4-hydroxyphenyl)-(9Cl) (apigenin); and 2H-1-benzopyran-3,5,7-triol, 2-(3,4-dihydroxyphenyl)-3,4-dihydro-, (2R,3S)-(9Cl) [(+)-catechin] were purchased from Sigma-Aldrich (St. Louis, MO).

2. 1-benzopyrylium, 2-(3,4-dihydroxyphenyl) 3,5,7-trihydroxy-, chloride (9Cl) (cyanidin chloride); 1-benzopyrylium, 3,5,7-trihydroxy-2-(4-hydroxyphenyl)-, chloride (9Cl) (pelargonidin chloride);1-benzopyrylium,3[{6-O-(6-deoxyl-α-L-mannopyranosyl)-β-D-glucopyranosyl}oxyl]-2-(3,4-dihydroxyphenyl)-5,7-dihydroxy-, chloride (9Cl) (keracyanin chloride); and 1-benzopyrylium, 3-(β-D-glucopyranosyloxy)-5,7-dihydroxy-2-(4-hydroxyphenyl)-, chloride (9Cl) (callistephin chloride) were bought from Extrasynthese Co. (Genay Cedex, France).

3 Methods

3.1 Analysis of MA Formed from 2′-Deoxyribonucleotides upon Oxidation

1. MA formed from DNA-related compounds; 2′-deoxyguanosine, 2′-deoxycytidine, thymidine and 2′deoxyadenosine, oxidized with Fenton's reagent was determined using gas chromatography (*see* **Notes 7**).

3.1.1 Oxidation of 2′-Deoxyribonucleotides with Fenton's Reagent

1. An aqueous solution (5 mL) containing various amounts of 2′-deoxyribonucleotides (4, 8, 12, 16, or 20 μmol) was prepared in a test tube.
2. Fenton' reagent solution (5 mL) containing 0.25 mmol Trizma buffer (pH, 7.4), 15 μmol ferrous chloride, 1.7 mmol hydrogen peroxide, and 0.75 mmol potassium chloride was added to each 2′ deoxyribonucleotide solution.
3. The solution was incubated at 37 °C for 18 h.
4. Oxidation of the samples was stopped by adding 50 μL of 4 % BHT.
5. The sample tube was covered with aluminum foil during incubation to avoid photooxidation.

3.1.2 Analysis of MA

1. A solution prepared the above was mixed with 50 μL *N*-methylhydrazine and stirred for 1 h at room temperature.
2. The reaction solution was extracted with 10 mL dichloromethane at pH 7.
3. After the extract was dried over anhydrous sodium sulfite, it was condensed to exactly 1 mL.
4. 2-methylpyrazine (4 mL) was added as a GC internal standard.
5. MA was analyzed as 1-MP by a gas chromatograph equipped with a 30 m × 0.25 i.d. (d_f = 1 mm) DB-1 bonded-phase fused silica capillary column and an NPD.

3.2 Analysis of MA Formed from Calf Thymus DNA

1. Antioxidant activities of various chemicals were determined using calf thymus DNA oxidized with Fenton's reagent under different conditions (*see* **Notes 8** and **9**).

3.2.1 Oxidation of Calf Thymus DNA with or Without Antioxidant

1. An aqueous buffer solution (5 mL) containing phosphate (20 μmol/mL), 0.5 mg/mL DNA, 0.5 μmol/mL of H_2O_2, 1.0 μmol/mL of $FeCl_2$, and 0.1 μmol/mL of antioxidant (Trolox® and DMPO) was incubated at pH 7.4 and 37 °C for 30 min.
2. A solution containing the same chemicals (5 mL) with different concentrations of Trolox® (0.06, 0.1, 0.2, or 0.6 μmol/mL) was also incubated at pH 7.4 and 37 °C for 30 min for the dose-dependent study.
3. A 5 mL aqueous NaOH solution (1 μmol/mL) containing 0.5 mg/mL of DNA, 0.5 μmol/mL of H_2O_2, 1.0 μmol/mL of $FeCl_2$, and 0.1 μmol/mL of antioxidant (quercetin, apigenin, saponarin, or catechin) was incubated at pH 7.4 and 37 °C for 30 min.
4. A 5 mL aqueous HCl solution (0.2 μmol/mL) containing 0.5 mg/mL of DNA, 0.5 μmol/mL of H_2O_2, 1.0 μmol/mL of $FeCl_2$, and 0.1 μmol/mL of antioxidant (pelargonidin, keracyanin, or callistephin) was incubated at pH 7.4 and 37 °C for 30 min.
5. A control was prepared with each buffer, NaOH, and HCl solution containing exactly the same chemicals as the above without antioxidants.
6. Oxidation of the samples was stopped by adding 50 μL of 4 % BHT.

3.2.2 Analysis of MA

1. The samples were analyzed for MA using the exactly same method described in the Subheading 3.1.2.

3.2.3 Results

1. A typical gas chromatogram of an extract is shown in Fig. 4.

3.2.3.1 MA Formed from 2′-Deoxyribonucleotides

2. Figure 5 shows the results of MA analysis in oxidized 2′-deoxyribonucleotides.
3. The amounts found in oxidized 2′-deoxyribonucleotides were 213.8 nmol/16 μmol in 2′-deoxyguanosine, 130.6 nmol/16 μmol in 2′-deoxycytidine, 85.1 nmol/16 μmol in 2′-deoxyadenosine, and 84.5 nmol/16 μmol in thymidine.

3.2.3.2 Antioxidant Activity of Various Chemicals Toward DNA Oxidation

1. The antioxidant activity of three groups (standards, flavonoids, and anthocyanins) obtained in the study on oxidation of calf thymus DNA is shown in Fig. 6.
2. Trolox® exhibited antioxidant activity with dose response.

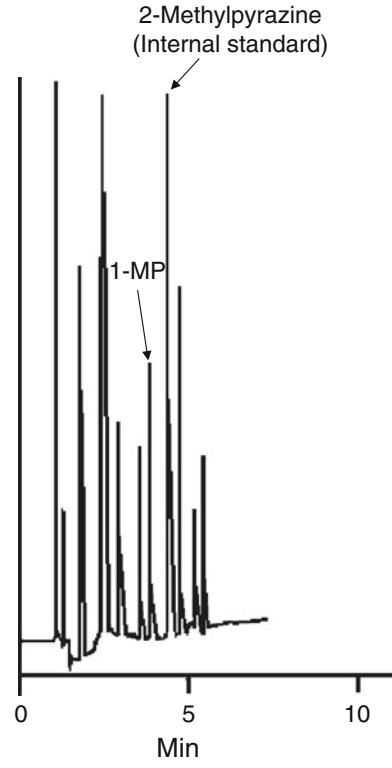

Fig. 4 Typical gas chromatogram of an extract obtained from oxidized 2′-deoxyguanosine treated with *N*-methylhydrazine (1-MP is a derivative of MA)

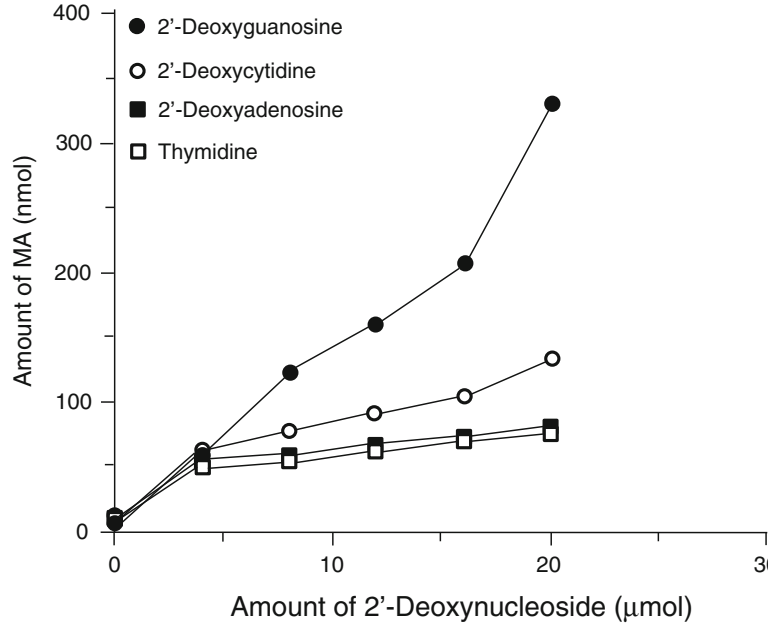

Fig. 5 Amount of MA formed in 2′-deoxynucleoside upon oxidation

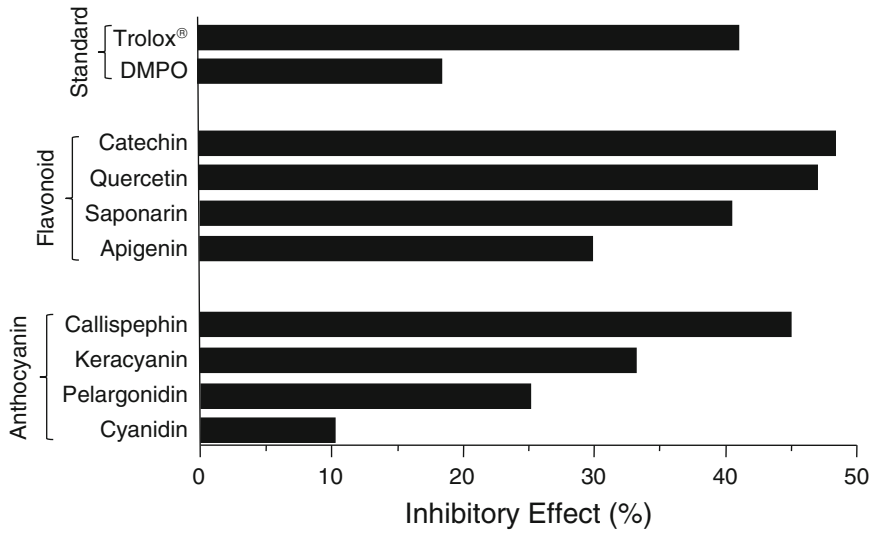

Fig. 6 Inhibitory effect of antioxidants tested using DNA/Fenton's reagent systems

3. Trolox® inhibited MA formation more (41.2 %) than DMPO (18.6 %) at a level of 0.1 μmol/mL.
4. Inhibitory effect of flavonoids ranged from 48.5 % (catechin) to 29.9 % (apigenin).
5. Callistephin (45.0 %) exhibited the highest antioxidant activity followed by keracyanin (33.2 %), pelargonidin (25.1 %), and cyaniding (10.2 %) among anthocyanins tested.

4 Notes

1. MA is extremely reactive and highly water soluble.
2. It is not possible to analyze MA directly by GC or HPLC.
3. MA requires to be derivatized for instrumental analysis.
4. MA can be derivatized with *N*-methylhydrazine readily to more stable 1-MP.
5. 1-MP is easily isolated by gas chromatography.
6. NPD detects 1-MP in pg level because it contains two nitrogen atoms.
7. A fused silica capillary column achieves baseline resolution for MA.
8. Using MA/GC assay, antioxidant studies on various samples including foods and beverages can be accomplished successfully.
9. This assay has been used successfully to examine antioxidant activity of flavonoids and anthocyanins toward oxidized DNA.

References

1. Shibamoto T (2002) Analytical methods for trace levels of reactive carbonyl compounds formed in lipid peroxidation systems. J Pharm Biomed Anal 41:12–25
2. Moon JK, Shibamoto T (2009) Antioxidant assays for plant and food components. J Agric Food Chem 57:1655–1666
3. Frankel EN, Neff WE (1983) Formation of malonaldehyde from lipid oxidation products. Biochim Biophys Acta 754:264–270
4. Pryor WA, Stanley JP (1975) A suggested mechanism for the production of malonaldehyde during the autoxidation of polyunsaturated fatty acids. Nonenzymatic production of prostaglandin endoperoxides during autoxidation (Letter). J Org Chem 40:3615–3617
5. Simic MG, Karel M (eds) (1979) Autoxidation in food and biological systems. Plenum Press, New York, pp 141–170
6. Matsuo M (1985) Formation and degradation of peroxylipids. In: Uchiyama M, Matsuo M, Sagai M (eds) Peroxide lipid in biological systems. Japan Scientific Society Press, Tokyo, pp 13–44
7. Yasuhara A, Tanaka Y, Hengel M, Shibamoto T (2003) Gas chromatographic investigation of acrylamide formation in browning model systems. J Agric Food Chem 51:3999–4003
8. Giera M, Lingeman H, Wilfried M, Niessen A (2012) Recent advancements in the LC- and GC-based analysis of malondialdehyde (MDA): a brief overview. Chromatographia 75:433–440
9. Umano K, Dennis KJ, Shibamoto T (1988) Analysis of free malondialdehyde in photoirradiated corn oil and beef fat via a pyrazole derivative. Lipids 23:811–814
10. Dennis KJ, Shibamoto T (1989) Production of malonaldehyde from squalene, a major skin surface lipid, during UV-irradiation. Photochem Photobiol 49:711–716
11. Dennis KJ, Shibamoto T (1990) Gas chromatographic analysis of reactive carbonyl compounds formed from lipids upon UV-irradiation. Lipids 25:460–464
12. Tamura H, Shibamoto T (1991) Gas chromatographic analysis of malonaldehyde and 4-hydroxy-2-(E)-nonenal produced from arachidonic acid and linoleic acid in a lipid peroxidation model system. Lipids 26:170–173
13. Wong JW, Yeo CH, Shibamoto T (1991) Determination of malonaldehyde and formaldehyde formed from fatty acid ethyl esters upon microwave and thermal heating. J Agric Food Chem 39:2260–2262
14. Niyati-Shirkhodaee F, Shibamoto T (1992) Formation of toxic aldehydes in cod liver oil after ultraviolet irradiation. J Am Oil Chem Soc 69:1254–1256
15. Nishiyama T, Hagiwara Y, Hagiwara H, Shibamoto T (1993) Inhibition of malonaldehyde formation from lipids by an isoflavonoid isolated from young green barley leaves. J Am Oil Chem Soc 70:811–813
16. Miyake T, Shibamoto T (1996) Simultaneous determination of acrolein, malonaldehyde, and 4-hydroxy-2-nonenal produced from lipids oxidized with Fenton's reagent. Food Chem Toxicol 34:1009–1011
17. Miyake T, Shibamoto T (1998) Formation of malonaldehyde in the presence of probucol, an anti-atherosclerosis drug. Food Chem Toxicol 36:841–847
18. Fujioka K, Shibamoto T (2006) Determination of toxic carbonyl compounds in cigarette smoke. Environ Toxicol 21:47–54
19. Lee SJ, Umano K, Shibamoto T, Lee KG (2005) Identification of volatile components in basil (*Ocimum basilicum* L.) and thyme leaves (*Thymus vulgaris* L.) and their antioxidant properties. Food Chem 91:131–137
20. Fujioka K, Shibamoto T (2004) Formation of genotoxic dicarbonyl compounds in dietary oils upon oxidation. Lipids 39:481–486
21. Benedet JA, Shibamoto T (2008) Role of transition metals, Fe(II), Cr(II), Pb(II), and Cd(II) in lipid peroxidation. Food Chem 107: 165–168
22. Nicholson T, Khademi H, Moghadasian MH (2013) The role of marine n-3 fatty acids in improving cardiovascular health: a review. Food Funct 4:357–365
23. Del Rio D, Stewart AJ, Pellegrini N (2005) A review of recent studies on malondialdehyde as toxic molecule and biological marker of oxidative stress. Nutr Metab Cardiovasc Dis 15: 316–328
24. Kitta K, Hagiwara Y, Shibamoto T (1992) Antioxidative activity of an isoflavonoid, 2″-O-glycosylisovitexin isolated from green barley leaves. J Agric Food Chem 40: 1843–1845
25. Yeo HCH, Shibamoto T (1992) Formation of formaldehyde and malonaldehyde by photooxidation of squalene. Lipids 27:50–53
26. Wei A, Shibamoto T (2007) Antioxidant activities and volatile constituents of various essential oils. J Agric Food Chem 55:1737–1742
27. Wei A, Shibamoto T (2010) Antioxidant/lipoxygenase inhibitory activities and chemical

compositions of selected essential oils. J Agric Food Chem 58:7218–7225
28. Miyake T, Shibamoto T (1997) Antioxidative activities of natural compounds found in plants. J Agric Food Chem 45:1819–1822
29. Lee KG, Shibamoto T, Takeoka GR, See SE, Kim JH, Park BS (2003) Inhibitory effects of plant-derived flavonoids and phenolic acids on malonaldehyde formation from ethyl arachidonate. J Agric Food Chem 51:7203–7207
30. Ogata J, Hagiwara Y, Hagiwara H, Shibamoto T (1996) Inhibition of malonaldehyde formation by antioxidants from ω-3 polyunsaturated fatty acids. J Am Oil Chem Soc 73:653–656
31. Benedet JA, Umeda H, Shibamoto T (2007) Antioxidant activity of flavonoids isolated from young green barley leaves toward biological lipid samples. J Agric Food Chem 55: 5499–5504
32. Nishiyama T, Hagiwara Y, Hagiwara H, Shibamoto T (1994) Formation and Inhibition of genotoxic glyoxal and malonaldehyde from phospholipids and fish liver oil upon lipid peroxidation. J Agric Food Chem 42:1728–1731
33. Yanagimoto K, Ochi H, Lee KG, Shibamoto T (2004) Antioxidative activities of fractions obtained from brewed coffee. J Agric Food Chem 52:592–596
34. Fujioka K, Shibamoto T (2005) Improved malonaldehyde assay using headspace solid-phase microextraction and its application to the measurement of the antioxidant activity of phytochemicals. J Agric Food Chem 53:4708–4713
35. Lee KG, Shibamoto T (2000) Antioxidant properties of aroma compounds isolated from soybeans and mung beans. J Agric Food Chem 48:4290–4293
36. Lee KG, Mitchell AE, Shibamoto T (2000) Determination of antioxidant properties of aroma extracts from various beans. J Agric Food Chem 48:4817–4820
37. Lee KG, Shibamoto T (2001) Antioxidant property of aroma extract isolated from clove bud [*Syzygium aromaticum* (L.) Merr. et Perry]. Food Chem 74:443–448
38. Lee KG, Shibamoto T (2001) Antioxidant activities of volatile components isolated from Eucalyptus species. J Sci Food Agric 81: 1573–1579
39. Tanaka A, Horiuchi M, Umano K, Shibamoto T (2008) Antioxidant and anti-inflammatory activities of water distillate and its dichloromethane extract from licorice root (*Glycyrrhiza uralensis*) and chemical composition of dichloromethane extract. J Sci Food Agri 88: 1158–1165
40. Takahashi M, Shibamoto T (2008) Chemical composition and antioxidant/anti-inflammatory activities of steam distillate from freeze-dried onion (*Allium cepa* L.) sprout. J Agric Food Chem 56:10462–10467
41. Sone Y, Moon JK, Mai TT, Thu NN, Asano E, Yamaguchi K, Otsuka Y, Shibamoto T (2011) Antioxidant/anti-inflammatory activities and total phenolic content of extracts obtained from plants grown in Vietnam. J Sci Food Agric 91:2259–2264
42. Sulaiman SF, Moon JK, Shibamoto T (2011) Investigation of optimum roasting conditions to obtain possible health benefit supplement, antioxidants from coffee beans. J Diet Supp Online: 1–8. www.informahealthcare.com/jds
43. Nam S, Jang HW, Shibamoto T (2011) Antioxidant activities of extract from teas prepared from medicinal plants, *Morus alba* L., *Camellia sinensis* L., and *Cudrania tricuspidata*, and their volatile components. J Agric Food Chem 60:9097–9105
44. Nomi Y, Shimizu S, Sone Y, Tuyet MT, Gia TP, Kamiyama M, Shibamoto T, Shindo K, Otsuka Y (2012) Isolation and antioxidant activity of Zeylaniin A, a new macrocyclic ellagitannin from *Syzygium zeylanicum* leaves. J Agric Food Chem 60:10263–10269
45. Wei A, Shibamoto T (2007) Antioxidant activities of essential oil mixture toward skin lipid squalene oxidized by UV irradiation. Cutan Ocul Toxicol 26:227–233
46. Wong WJ, Hashimoto K, Shibamoto T (1995) Antioxidant activity of rosemary and sage extracts and vitamin E in a model meat system. J Agric Food Chem 43:2707–2712
47. Miyake T, Shibamoto T (1998) Inhibition of malonaldehyde and acetaldehyde formation from blood plasma oxidation by naturally occurring antioxidants. J Agric Food Chem 46:3694–3697
48. Lee KG, Shibamoto T (2001) Inhibition of malonaldehyde formation from blood plasma oxidation by aroma extracts and aroma components isolated from clove and eucalyptus. Food Chem Toxicol 39:1199–1204
49. Miyake T, Shibamoto T (1999) Formation of malonaldehyde and acetaldehyde from the oxidation of 2′-deoxyribonucleosides. J Agric Food Chem 47:2782–2785
50. Voulgaridou GP, Anestopoulos I, Franco R, Panayiotidis MI, Pappa A (2011) DNA damage induced by endogenous aldehydes: current state of knowledge. Mutat Res 711:13027
51. Kautiainen A, Vaca CE, Granath F (1993) Studies on the relationship between hemoglobin

and DNA adducts of malonaldehyde and their stability in vivo. Carcinogenesis 14:705–708

52. Peluso M, Munnia A, Ceppi M, Giese RW, Catelan D, Rusconi F, Godschalk RW, Biggeri A (2013) Malondialdehyde-deoxyguanosine and bulky DNA adducts in schoolchildren resident in the proximity of the Sarroch industrial estate on Sardinia Island, Italy. Mutagenesis 28(3):315–321
53. Matsufuji H, Shibamoto T (2004) The role of EDTA in malonaldehyde formation from DNA oxidized by Fenton reagent system. J Agric Food Chem 52:3136–3140
54. Matsufuji H, Shibamoto T (2004) Inhibition of malonaldehyde formation in oxidized calf thymus DNA with synthetic and natural antioxidants. J Agric Food Chem 52: 5759–5763
55. Matsufuji H, Shibamoto T (2006) Formation and inhibition of genotoxic malonaldehyde from DNA oxidation controlled with EDTA. Food Chem Toxicol 44:236–241

Chapter 5

Nitric Oxide Availability as a Marker of Oxidative Stress

Dan Pierini and Nathan S. Bryan

Abstract

Nitric oxide (NO) is widely considered one of the most important molecules produced in the human body, acting as a necessary regulator in a vast array of vital physiological functions, namely, blood pressure, immune response, and neural communication. Healthy endothelium is defined by the ability to produce adequate levels of NO. Reactive oxygen species (ROS) play a major role in NO-based cell signaling. ROS can affect NO availability both from production to post-production scavenging and lead to a myriad of vascular disorders due to compromised NO functionality. In 2004, it was identified in animal models that oxidative stress plays a significant role in the development of hypertension, in part by inactivation of NO (Ghosh et al., Br J Pharmacol 141(4):562–573, 2004). It was thus concluded that NO bioavailability was reduced in the presence of ROS. We speculated that the accurate detection of NO and quantification in biological matrices is critical as a marker of oxidative stress (Bryan et al., Proc Natl Acad Sci USA 101(12):4308–4313, 2004). The elucidation of new mechanisms and signaling pathways involving NO hinges on our ability to specifically, selectively, and sensitively detect and quantify NO and all relevant NO products and metabolites in complex biological matrices. Here, we present a method for the rapid and sensitive analysis of nitrite and nitrate by HPLC as well as detection of free NO in biological samples using in vitro ozone-based chemiluminescence with chemical derivatization to determine molecular source of NO as well as ex vivo with organ bath myography. This approach ties fundamental biochemistry to functional response.

Key words Nitric oxide, Reactive oxygen species, Oxidative stress, HPLC chemiluminescence, Organ bath myography

1 Introduction

Research over the past 20 years has revealed that the loss of nitric oxide, one of the most important cellular signaling molecules the body produces, appears to be the earliest event that leads to the onset and progression of poor health outcomes, predominantly in the cardiovascular system. Cardiovascular disease continues to be the number one cause of human mortality worldwide. NO has been shown to be involved in every biological system, but it is best characterized in the cardiovascular, immune, and nervous system. There are several factors that lead to the loss of sufficient NO in the human body, and they are predominantly associated with an increase in oxidative stress particularly in the vasculature.

Donald Armstrong (ed.), *Advanced Protocols in Oxidative Stress III*, Methods in Molecular Biology, vol. 1208,
DOI 10.1007/978-1-4939-1441-8_5,

The loss of nitric oxide with age is well documented [3] and is linked to a gradual decline in endothelial function [4] at a rate of approximately 10–12 % of endothelial function per decade. Endothelial dysfunction is caused by either decreased production or increased destruction of NO, which results in decreased NO bioavailability [5]. The resultant NO deficiency creates an environment that is conducive to vascular disorders because NO plays a fundamental role in regulating a wide spectrum of healthy cardiovascular function including vasodilation for optimum circulation, inhibition of leukocyte-endothelial adhesion, and vascular smooth muscle cell migration and proliferation. Additionally, NO inhibits platelet activation, adhesion, and aggregation through several pathways. A number of studies show that insufficient NO production is associated with all major cardiovascular risk factors, such as hypertension, hyperlipidemia, type 2 diabetes, smoking, and atherosclerosis, along with a strong predictive value for future atherosclerotic disease progression [6–9].

Vascular oxidative stress, with an increased generation of reactive oxygen species (ROS), drives the mechanisms of vascular dysfunction [10]. This oxidative stress is mainly caused by an imbalance between the activity of endogenous prooxidative enzymes (such as NADPH oxidase and the mitochondrial respiratory chain) and antioxidative enzymes (such as superoxide dismutase, glutathione peroxidase, heme oxygenase, catalase, and paraoxonase) in favor of the former. Increased ROS concentrations reduce bioactive NO levels by chemical inactivation. This is often referred to as NO scavenging and is the most significant consequence of oxidative stress.

1.1 NO Concentration: Production Versus Consumption

Although there are alternative mechanisms for NO production such as reduction of nitrite to NO, the nitric oxide synthase (NOS) enzymes in the endothelium are a prime site of NO production. The NOS family of enzymes convert L-arginine to NO and citrulline in the presence of rate-limiting cofactors such as tetrahydrobiopterin (BH_4) and NADPH, FAD, and FMN, in the presence of sufficient oxygen. This is a complex pathway, and if the cofactors become limiting, then NO production from NOS may be interrupted, and instead, NOS begins to produce the free radical superoxide. This occurs in conditions of high oxidative stress where essential NOS cofactors, specifically (BH_4), becomes oxidized and causes NOS uncoupling. Superoxide (O_2^-) is a target of NO and leads to the reduction of NO concentration due to antioxidant scavenging. In this regard NO acts as a potent antioxidant. In addition, in conditions where oxygen is limited (hypoxia), the NOS enzyme can no longer maintain NO production.

Oxidative stress occurs when the formation of ROS exceeds the body's ability to metabolize and neutralize them. There are two central mechanisms for the reduction in NO bioavailability: decreased synthesis of NO and increased oxidative degradation by

reactive oxygen species (ROS). There is enormous evidence that oxidative stress plays a significant role in the pathogenesis of hypertension, in part by inactivation of NO [11]. Currently, the principal mechanism for the oxidative inactivation of NO is thought to be the reaction of NO with O_2^- to produce the potent oxidants peroxynitrite ($ONOO^-$) [12–14] and its conjugate acid, peroxynitrous acid (ONOOH).

$$O_2^- + NO \rightarrow ONOO^- + H^+ \leftrightarrow ONOOH \rightarrow NO_3^- + H^+$$

Peroxynitrite is the unstable structural isomer of nitrate, NO_3^-, but with markedly different physiological roles than NO_3^-. Peroxynitrite has been documented to induce apoptotic cell death in thymocytes, neuronal cells, and tumor cells [15], whereas nitrate is stable and is reabsorbed in the kidney for recirculation throughout the body. Commensal bacteria in the oral cavity reduce nitrate to nitrite, NO_2^-, and subsequently, NO. Evidence exists showing that in humans and animals, an increase in O_2^- and $ONOO^-$ occurs simultaneous to the reduction in NO bioavailability during vascular endothelial aging [16, 17]. Although many investigations have been performed suggesting that ONOO–/ONOOH may play an important role in several pathophysiological situations, the question of whether ONOO–/ONOOH is actually formed in vivo and exerts significant physiologic and/or pathophysiologic activity remains the subject of vigorous debate. We have also demonstrated that the ratio of nitrite and nitrate in biological tissues and blood may reflect the overall redox status of the cell and illustrate relative superoxide production [2]. Therefore, methods and strategies that quantify nitrite and nitrate as well as detect free NO gas from biological systems coupled to functional assays can provide enormous information on NO availability and oxidative stress.

2 Materials

2.1 Equipment

1. High-performance liquid chromatography: Eicom Corp, ENO-20.
2. Autosampler: Alcott 719AL.
3. Centrifuge: Eppendorf 5415D.
4. Ozone-based chemiluminescent analyzer: EcoPhysics, CLD 88Y.
5. DMT Myograph: 720MO, AD instruments.
6. PowerLab: AD instruments.

2.2 Reagents

1. *N*-ethylmaleimide: Sigma-Aldrich.
2. EDTA: Sigma-Aldrich.
3. Potassium ferricyanide: Fluka.

4. Acetylcholine was from Sigma-Aldrich, A6625.
5. R-(−)-Phenylephrine was from Sigma-Aldrich, P6126.
6. Methanol (HPLC grade): Honeywell Cat 230-4.
7. Sulfanilamide: Sigma S4251.
8. Mercuric chloride: Sigma M1136.
9. Diethyl ether: Sigma 346136.

2.3 Supplies

1. 1.5 ml centrifuge tubes: Eppendorf.
2. 1.0 ml insulin syringe with 25 gauge needle.
3. Experimental laboratory mouse.
4. Phosphate buffered saline pH 7.4.

3 Methods

3.1 Whole Blood Collection

1. Collect venous blood from humans or from experimental animals in NEM/EDTA containing tubes. *See* **Note 1** for important considerations for sample preparation.
2. Immediately spin down blood in a bench top centrifuge at 14,300 rcf (relative centrifugal force) for 7 min to prepare plasma and red blood cell pellet. *See* **Note 2**.
3. Prepare plasma samples for high-performance liquid chromatography (HPLC) and chemiluminescence detection (CLD) analysis.
   (a) HPLC: Add 1:1 volume of cold methanol to plasma; vortex and centrifuge at 13,200 rpm for 10 min to precipitate plasma proteins. Collect supernatant for HPLC analysis.
   (b) CLD: Aliquot a sample and preincubate with sulfanilamide and mercuric chloride to specifically assay nitrosothiols.
4. Prepare red cell pellet for HPLC and CLD analysis.
   (a) HPLC: Add 1:4 red cell pellet to a hypotonic lysis solution containing 10 mM NEM, 2.5 mM EDTA, and 10 mM ferricyanide. Vortex thoroughly and then add 1:1 methanol; vortex and centrifuge at 13,200 rpm for 10 min to precipitate protein. Collect supernatant for HPLC analysis.
   (b) CLD: Add 1:4 red cell pellet to a hypotonic lysis solution containing 10 mM EDTA, 2.5 mM EDTA, and 10 mM ferricyanide. Aliquot samples to tubes containing sulfanilamide and mercuric chloride for specific detection of nitrosothiols.

3.2 Tissue Extraction and Preparation

1. To determine tissue levels of NO metabolites, it is first necessary to harvest blood-free tissue for sample preparation as described above. A full blood exchange will take place by infusing physiological buffer through the apex of the left ventricle. Once all blood is removed, tissues of interest can then be harvested. *See* **Notes 3** and **4**.
2. Homogenize tissue samples and prepare samples as described above for HPLC and CLD analysis.

A representative tracing from the HPLC for the detection and quantification of nitrite is shown in Fig. 1. Figure 2 shows the

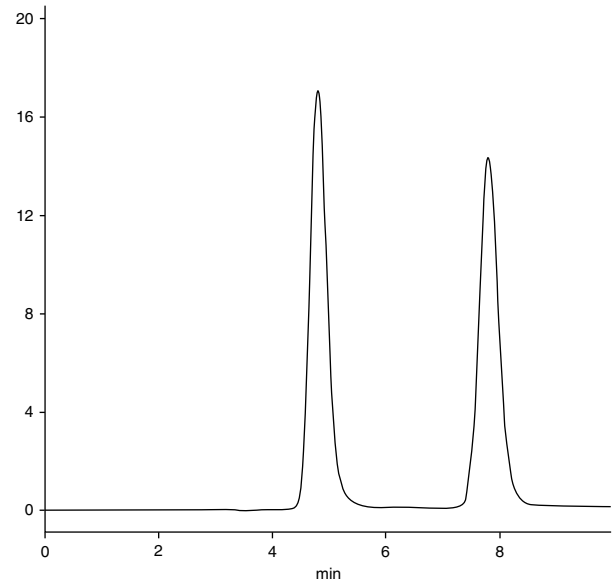

Fig. 1 The chromatogram above illustrates the HPLC analysis of nitrite and nitrate. Nitrite elutes at 5 min and nitrate at around 7 min with no interference from other molecules or anions

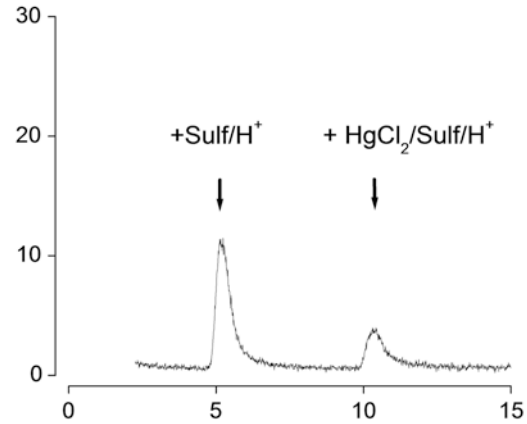

Fig. 2 The *difference in peak area between the two* represents the concentration of nitrosothiols. The *peak of the last peak* represents *N*-nitrosamine or other nitroso product

chemiluminescent detection of free NO gas after chemical derivatization with acidified sulfanilamide and mercuric chloride to detect and quantify nitrosothiols and other nitroso species. *See* **Notes 5** and **6**.

3.3 Aortic Rings Isolation for Endothelial Function

3.3.1 Tissue Organ Bath

1. Mice will be anesthetized with isoflurane to effect. A thoracotomy is performed to expose thoracic and abdominal aorta. A 25 gauge syringe is inserted into the apex of left ventricle and perfused free of blood with oxygenated Krebs-Henseleit buffer.
2. The right atrium is cut to provide an exit for blood. Abdominal aorta will be removed and cleaned of adventitia.
3. Rings will be cut into 2 mm long segments and mounted on a four-channel tissue organ bath (DMT 720MO, AD Instruments) bathed in a physiological buffer solution.
4. Vessel rings are maintained in 10 ml organ baths with oxygenated Krebs buffer (95 % O_2 and 5 % CO_2) at 37 °C. One gram pretension is placed on each aortic ring (appropriate starting tension for optimal vasomotor function as determined in previous experiments). An eight-channel octal bridge (PowerLab) and data-acquisition software (Chart version 5.2.2) are used to record all force measurements.
5. Rings are allowed to equilibrate for 80 min with the buffer in each organ bath changed every 20 min. After equilibration for 80 min, 1 μM phenylephrine is added to each ring for submaximal contraction.
6. After stabilization, endothelial agonist such as acetylcholine will be added to determine NO production and degree of vessel relaxation. After the dose response to acetylcholine, baths will be rinsed and recontracted and then treated with an exogenous source of nitric oxide and sodium nitroprusside to determine responsiveness of smooth muscle and to get a value for 100 % relaxation. This is illustrated in Fig. 3.
7. NO scavengers or antioxidant enzymes such as SOD can be added to bath to clearly illustrate the effects of reactive oxygen species on the release of NO and resulting vasodilation. This is easily performed in healthy versus models of specific disease to clearly show the effects of oxidative stress on the functional response of NO in the vasculature.

4 Notes

1. Sample preparation may be one of the most important steps in quantifying any and all NO metabolites regardless of the method employed. It is vital to the experiment that extreme

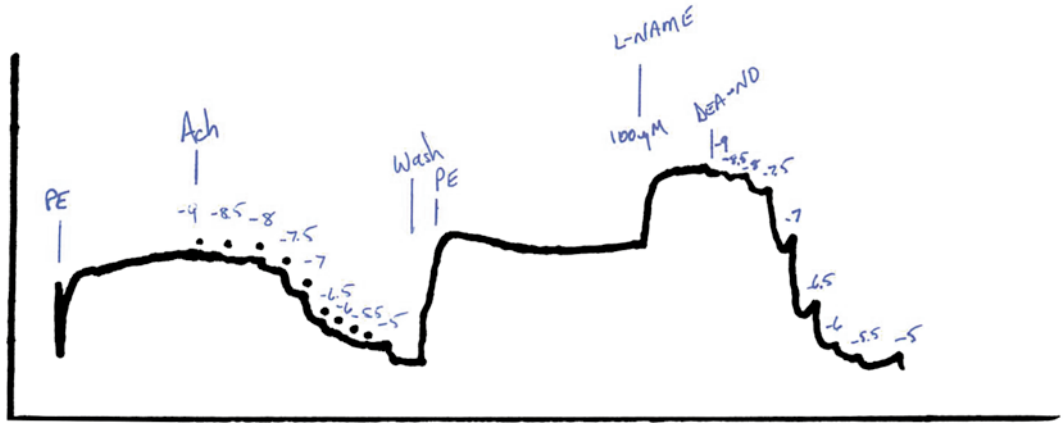

Fig. 3 The chromatogram above illustrates the vascular reactivity of two isolated aortic rings when precontracted with phenylephrine (PE) and the resulting relaxation with acetylcholine is added. This method can also allow washing of the vessel and then addition of L-NAME to block NO production in the vessels and then interrogate NOS independent sources of NO or add agents such as SOD or oxidants to determine the effects on endothelial NO production

care be taken to preserve what you are looking for and, more importantly, not to artifactually generate NO products or metabolites during sample preparation. Nitrite is rapidly metabolized to different degrees in different biological compartments by thiols and redox-active metals [18]. Nitroso/nitrosyl products are unstable and quickly decay with time [2]. This is described in Subheadings 3.1 and 3.2.

2. The blood should be immediately centrifuged to separate the plasma from the RBCs. Once blood is obtained, tissue perfusion with NEM/EDTA buffer must take place immediately to halt metabolic activity. Steady-state NO products are altered under two conditions: blood withdrawal taking too long (>20 s) and too much blood being taken. These errors will render the animal hypoxic and hypovolemic, respectively [2].
3. It is crucial to collect blood and tissue rapidly in order to preserve their integrity. This is best accomplished by perfusing tissues with an air-equilibrated isotonic solution of PBS containing 10 mM *N*-ethylmaleimide (NEM) and 2.5 mM EDTA and subsequent homogenization in the same solution. The addition of NEM/EDTA serves the purpose of blocking SH groups and inhibiting transition metal-catalyzed transnitrosation reactions, preventing artificial nitrosation, as well as thiolate- and ascorbate-mediated degradation of endogenous RSNOs and nitrite [2, 19].
4. Rapid perfusion is best attained by inserting a needle into the left ventricle and using roller pump or syringe for a full blood

exchange once blood is obtained. The inferior vena cava or right atrium should be cut to provide an exit for the blood. Hypoxia signals blood and tissue to reduce nitrite to NO, at which time nitrite will be underestimated and there will be an overestimation of nitroso/nitrosyl products as a result [2]. All steps of blood and tissue preparation should occur under reduced ambient lighting conditions (<15 lx) to minimize photolytic decomposition of tissue NO products [20].

5. It is imperative that the researcher become very efficient with the above stated procedures before any data is interpreted. When investigating blood and heart for NO metabolites, it is crucial to obtain both the blood and heart from the same animal without compromising the integrity of either sample. In this case, withdrawing blood rapidly from the anesthetized animals without causing hemolysis is ideal.
6. Tissue homogenates should be kept on ice in the dark and immediately analyzed within 2 min. It is best to analyze samples immediately on harvesting.

References

1. Ghosh M, Wang HD, McNeill JR (2004) Role of oxidative stress and nitric oxide in regulation of spontaneous tone in aorta of DOCA-salt hypertensive rats. Br J Pharmacol 141(4):562–573
2. Bryan NS et al (2004) Cellular targets and mechanisms of nitros(yl)ation: an insight into their nature and kinetics in vivo. Proc Natl Acad Sci U S A 101(12):4308–4313
3. Gerhard M et al (1996) Aging progressively impairs endothelium-dependent vasodilation in forearm resistance vessels of humans. Hypertension 27(4):849–853
4. Taddei S et al (2001) Age-related reduction of NO availability and oxidative stress in humans. Hypertension 38(2):274–279
5. Davignon J, Ganz P (2004) Role of endothelial dysfunction in atherosclerosis. Circulation 109(23 Suppl 1):III27–III32
6. Schachinger V, Britten MB, Zeiher AM (2000) Prognostic impact of coronary vasodilator dysfunction on adverse long-term outcome of coronary heart disease. Circulation 101(16): 1899–1906
7. Halcox JP et al (2002) Prognostic value of coronary vascular endothelial dysfunction. Circulation 106(6):653–658
8. Bugiardini R et al (2004) Endothelial function predicts future development of coronary artery disease: a study of women with chest pain and normal coronary angiograms. Circulation 109(21):2518–2523
9. Lerman A, Zeiher AM (2005) Endothelial function: cardiac events. Circulation 111(3): 363–368
10. Forstermann U (2010) Nitric oxide and oxidative stress in vascular disease. Pflugers Arch 459(6):923–939
11. Popolo A et al (2013) Oxidative stress in patients with cardiovascular disease and chronic renal failure. Free Radic Res 47(5): 346–356
12. Gryglewski RJ, Palmer RM, Moncada S (1986) Superoxide anion is involved in the breakdown of endothelium-derived vascular relaxing factor. Nature 320(6061): 454–456
13. Beckman JS, Koppenol WH (1996) Nitric oxide, superoxide, and peroxynitrite: the good, the bad, and ugly. Am J Physiol 271(5 Pt 1): C1424–C1437
14. Beckman JS et al (1990) Apparent hydroxyl radical production by peroxynitrite: implications for endothelial injury from nitric oxide and superoxide. Proc Natl Acad Sci U S A 87(4):1620–1624
15. Beckman JS (1996) Oxidative damage and tyrosine nitration from peroxynitrite. Chem Res Toxicol 9(5):836–844
16. Hamilton CA et al (2001) Superoxide excess in hypertension and aging: a common cause of endothelial dysfunction. Hypertension 37(2 Pt 2):529–534

17. van der Loo B et al (2000) Enhanced peroxynitrite formation is associated with vascular aging. J Exp Med 192(12):1731–1744
18. Bryan NS et al (2005) Nitrite is a signaling molecule and regulator of gene expression in mammalian tissues. Nat Chem Biol 1(5): 290–297
19. Marley R et al (2001) Formation of nanomolar concentrations of S-nitroso-albumin in human plasma by nitric oxide. Free Radic Biol Med 31(5):688–696
20. Rodriguez J et al (2003) Chemical nature of nitric oxide storage forms in rat vascular tissue. Proc Natl Acad Sci U S A 100:336–341

Chapter 6

Quantification of DNA Repair Capacity Towards Oxidatively Damaged DNA in Subcellular and Cellular Systems by a Nonradioactive Cleavage Assay

Ingrit Hamann and Andrea Hartwig

Abstract

The identification of appropriate biomarkers for oxidative stress is one major aim in molecular epidemiology. Besides the quantification of specific DNA lesions such as of 8-oxoguanine (8oxoG), another approach consists in the assessment of the repair capacity towards 8oxoG, mediated predominantly by the human 8-oxoguanine DNA glycosylase 1 (hOGG1); further processing of base excision repair involves AP endonuclease 1 (APE1). Thus, during the last few years the so-called cleavage assays have been described, investigating the incision capacity of cell extracts towards ^{32}P-labelled and 8oxoG damaged oligonucleotides. Here, we describe a sensitive nonradioactive test system based on Cy5-labelled oligonucleotides with hairpin-like structures, enabling the assessment of activities of the isolated hOGG1 and APE1 as well as their activities in extracts prepared from cultured cells or peripheral blood mononuclear cells (PBMC). This approach allows the sensitive quantification of modulating exposures, such as inhibitory metal compounds, and also the determination of interindividual differences in DNA repair capacities. The method is as sensitive and even faster as compared to the use of radioactively labelled oligonucleotides and additionally offers the advantage of reduced costs and low health risk.

Key words hOGG1, APE1, Nonradioactive cleavage assay, BER, Incision activity, Cultured cells, Human lymphocytes

1 Introduction

Reactive oxygen species (ROS) are continuously generated as by-products of normal metabolic functions such as the mitochondrial respiration or inflammatory processes. In addition, their levels can be also enhanced by exogenous agents, for example by chemical oxidants, redox active metals, or ionizing and UVA irradiation [summarized in 1]. Besides damage to cellular proteins and lipids, ROS like superoxide anions and hydroxyl radicals induce DNA damage, including oxidatively induced DNA base modifications, abasic (AP) sites, and DNA single strand breaks. 8-oxoguanine (8oxoG) is one of the most frequently formed oxidative DNA base

Donald Armstrong (ed.), *Advanced Protocols in Oxidative Stress III*, Methods in Molecular Biology, vol. 1208,
DOI 10.1007/978-1-4939-1441-8_6,

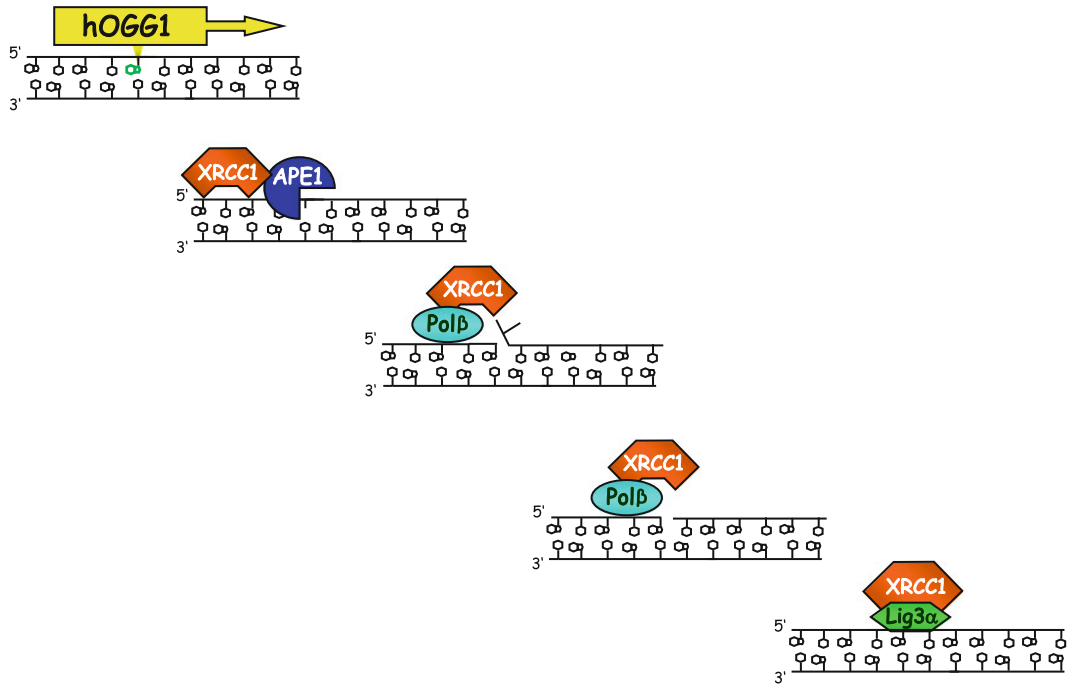

Fig. 1 Base excision repair. The repair of 8oxoG is a tightly coordinated process. After recognizing and removing the damaged base, hOGG1 remains tightly bound to the AP site until displaced by APE1 generates a 3′-OH and a 5′-deoxyribose phosphate (d-RP) terminus. DNA polymerase β cleaves the 5′-d-RP residue and fills in the gap with the appropriate nucleotide. DNA ligase III in complex with the scaffolding protein XRCC1 seals the residual nick in the final step

lesions, due to the low oxidation potential of guanine. Also, this lesion has attracted special attention because of its premutagenic property, promoting GC to TA transversions, attributable to misincorporation of adenine during replication [summarized in 2]. Thus, 8oxoG has become an established cellular biomarker of oxidative stress and has also been proposed as predictive marker for cancer, since oxidative stress is involved in the initiation, promotion and progression stages of carcinogenesis [3]. Repair of nearly all oxidatively induced DNA lesions is processed by the base excision repair (BER) pathway [4]. The repair of 8oxoG is initiated by hOGG1 [5], showing marked preference for 8oxoG/C base pairs but no nicking activity towards 8oxoG/A [6]. The repair process is tightly coordinated [7], as outlined in Fig. 1: After recognizing and removing the damaged base, hOGG1 remains tightly bound to the AP site until displaced by APE1 [8]. Next, the AP site is cleaved by APE1 generating a 3′OH and a 5′deoxyribose phosphate (dRP) terminus [9, 10]. Subsequently, DNA polymerase ß containing an inherent dRP lyase activity cleaves the 5′dRP residue and fills in the gap with the appropriate nucleotide. DNA ligase III in complex with the scaffolding protein XRCC1 seals the residual nick in the final step [11].

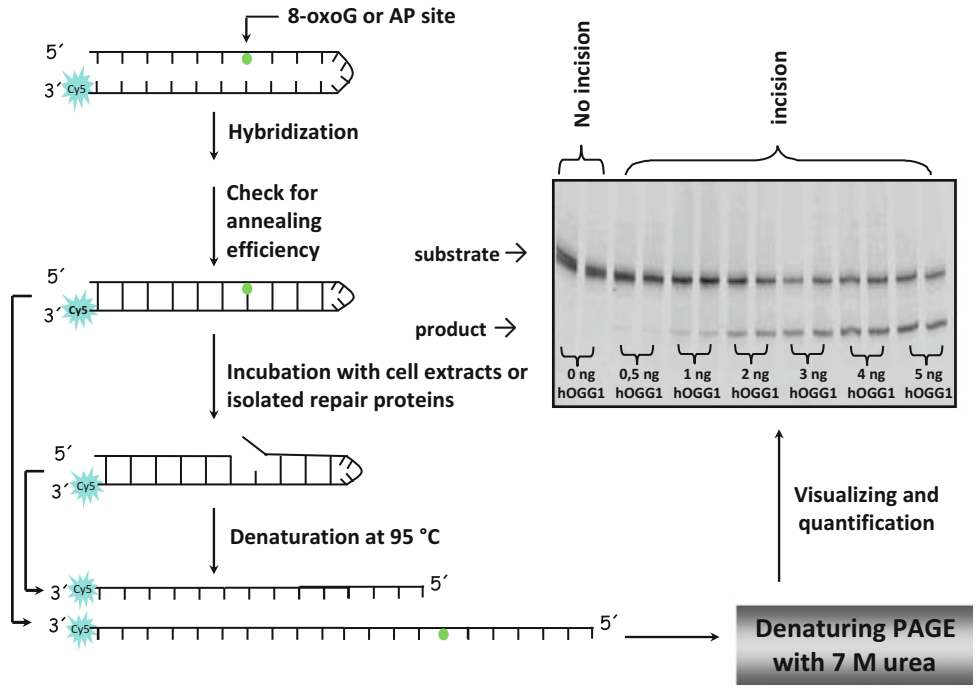

Fig. 2 Outline of the incision test system

A meta-analysis of population based studies found consistent inverse associations between cancer incidence and DNA repair capacity, which can be modified by environmental factors as well as by genetic variables and which appears to contribute to the interindividual variability in the development of cancer [12]. Hence, the direct measurement of DNA repair capacity using specific activity assays is assumed to act as important biomarker as well.

During the last few years, some functional activity assays have been described for epidemiological studies, investigating the incision capacity of cell extracts prepared from peripheral blood mononuclear cells (PBMC) towards ^{32}P-labelled and 8oxoG containing synthetic oligonucleotides. By means of these test systems an association between reduced DNA repair activity towards 8oxoG and lung cancer risk [13, 14] or risk of squamous cell carcinoma of the head and the neck [15] have been observed, while healthy individuals showed a narrow range of interindividual variation in 8oxoG-DNA glycosylase (hOGG) activity [16]. Nevertheless, only one incision assay has been described using a nonradioactively labelled oligonucleotide, which was applied for hOGG1 and APE1 overexpressing cultured cells [17]. Since for large scale epidemiological studies nonradioactive assays are preferable, we established a test system using a fluorescence-labelled oligonucleotide sensitive enough to measure the incision activity in not overexpressing cells, especially also suited for peripheral lymphocytes (Fig. 2).

We are describing here a test system based on a Cy5-labelled oligonucleotide applicable to the assessment of isolated hOGG1 and APE1 enzymes as well as to the quantification of the respective repair activities in cell extracts and cells. For example, we investigated the impact of copper sulfate on OGG activities by comparing the isolated hOGG1, cell extracts derived from A549 cells as well as extracts derived from copper-treated cells, demonstrating pronounced inhibition in the former two approaches, while copper homeostasis in intact cells prevented enzyme inhibition to a great extent [18]. Also, the effect of cadmium on hOGG1 and APE1 as a function of the cellular p53 status has been elucidated [19]. The test system is also sufficiently sensitive to examine the hOGG activity in peripheral blood mononuclear cells (PBMC). Thus, incisions activities of PBMC from different donors have been quantified and interindividual differences have been observed [18]. Altogether, the established procedure is as sensitive and even faster when compared to the radioactive technique and additionally offers the advantage of reduced costs and low health risk.

2 Materials

2.1 Hybridization of Oligonucleotides (see Notes 1 and 2)

1. Cy5-labelled oligonucleotides A, B, or C with the sequence 5′-CAATAATAACACGCXCGACCAGTCCTGCTTTTGCAGGACTGGTC GCGCGTGTTATTATTG-Cy5-3′ (A: X = 8oxoG; B: X = THF,C: X = G) were purchased from Eurogentec (Seraing, Belgium) (Fig. 3).

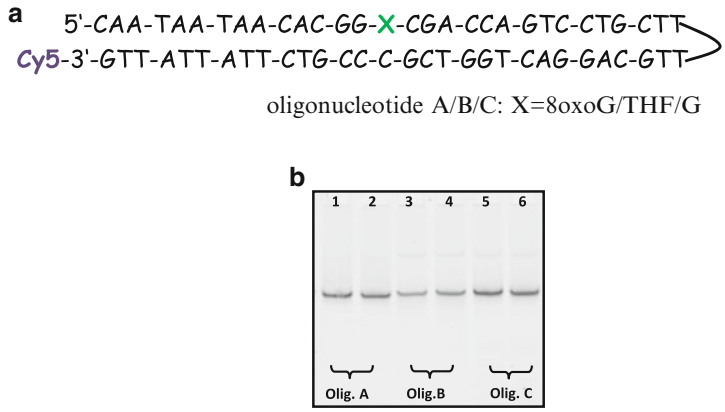

Fig. 3 Oligonucleotides. (**a**) Structures of the used oligonucleotides. The oligonucleotides used in these studies were designed to contain a TTTT hairpin loop, a Cy5 label at the 3′-end and an 8oxoG (oligonucleotide A), an AP site (oligonucleotide B), or a guanine moiety (oligonucleotide C). (**b**) Native PAGE of oligonucleotides A, B, and C after hybridization. After hybridization, annealing efficiency was checked applying 100 fmol of oligonucleotides A, B, and C, respectively, to a native PAGE. Shown is one part of a representative gel: oligonucleotide A (*lane 1* and *2*), oligonucleotide B (*lane 3* and *4*), oligonucleotide C (*lane 5* and *6*)

2. Dissolve oligonucleotides in TE buffer (100 mM Tris–HCl (pH 7.0), 10 mM EDTA). Measure concentration and labelling efficiency with a NanoDrop ND 1000, NanoDrop Technologies (Wilmington, USA) and prepare stock solutions with a concentration of 5 pmol/µl. Make aliquots and store at –20 °C.
3. For hybridization use 6 pmol of the respective oligonucleotide, add 3 µl of 1 M NaCl solution (end concentration: 50 mM) and fill with TE buffer (100 mM Tris (pH 7.0), 10 mM EDTA) to 60 µl, reaching a final oligonucleotide concentration of 100 fmol/µl.
4. While gently shaking, heat the oligonucleotide solution to 90 °C for 15 min and let it slowly cool down to 30 °C. Make aliquots and store at –20 °C.
5. Test hybridization efficiency via native PAGE.

2.2 Native PAGE

1. Prepare a 20 % polyacrylamide gel with 40 % acrylamide–bisacrylamide stock solution (19:1) and TBE buffer (50 mM Tris–borate pH 8.0, 1 mM EDTA).
2. Mix 1 µl of the respective oligonucleotide with 4 µl gel shift buffer (25 mM Hepes-KOH (pH 7.0), 30 mM KCl, 4 mM $MgCl_2$, 1 mM EDTA, 15 µM DTT, 10 % Glycerin, 45 µg/ml BSA), 8.5 µl double distilled water and 1.5 µl loading buffer (25 mM Tris–borate pH 8.0, 0.5 mM EDTA, 40 % Glycerin) and load onto the 20 % polyacrylamide gel.
3. Run for 5 h at 200 V in TBE buffer (50 mM Tris–borate pH 8.0, 1 mM EDTA) and scan gel at Typhoon Imager (GE Healthcare) and evaluate picture using Image Quant TL Software (GE Healthcare).

2.3 Preparation of Isolated hOGG1 (see Note 6)

1. Isolated hOGG1 was from New England Biolabs (Frankfurt a. M., Germany) and was provided in a storage buffer (20 mM Tris (pH 8.0), 50 mM NaCl, 1 mM EDTA, 200 µg/ml BSA, 50 % glycerol). Make aliquots and store at –20 °C.
2. For experiments prepare working solution with a concentration of 10 ng/µl, make aliquots and store at –20 °C.

2.4 Preparation of Isolated APE1 (see Note 6)

1. Isolated APE1 was from New England Biolabs (Frankfurt a. M., Germany) and was provided in a storage buffer (10 mM Tris–HCl (pH 8.0), 50 mM NaCl, 0.05 mM EDTA, 1 mM DTT, 200 µg/ml BSA, 50 % glycerol). Make aliquots and store at –20 °C.
2. For experiments prepare working solution with a concentration of 0.2 pg/µl, make aliquots and store at –20 °C.

2.5 Preparation of Whole Cell Extracts (see Notes 3–5)

1. Grow cells in 10 cm^2 dishes and treat with xenobiotica if you wish.
2. Wash with phosphate buffered saline (PBS), trypsinize, and separate in PBS with 10 % FBS.
3. Count cells and pellet by centrifugation (290 × *g*, 5 min, 20 °C). Aspirate the supernatant thoroughly and wash pelleted cells in PBS twice.
4. Aspirate the supernatant thoroughly, freeze dry cell pellets and store at −80 °C until use.
5. For cell extract preparation suspend 8×10^6 cells in 80 µl of ice cold extraction buffer (50 mM Tris–HCl (pH 7.1), 250 mM NaCl, 1 mM EDTA, 0.5 mM DTT, 20 % glycerol, 0.5 mM PMSF, 10 µg/ml aprotinin, 5 µg/ml leupeptin, 1 µg/ml pepstatin, 50 mM NaF, 1 mM Na_3VO_4) and sonicate on ice (1 s pulse [10 % amplitude] + 9 s pause, 10 cycles).
6. Remove cell debris by centrifugation at 20,800 × *g* and 4 °C for 20 min, collect the supernatants and dilute 1/5 with dilution buffer (50 mM Tris–HCl (pH 7.1), 1 mM EDTA, 0.5 mM DTT, and 20 % glycerol) reaching a final concentration of 50 mM Tris–HCl (pH 7.1), 50 mM NaCl, 1 mM EDTA, 0.5 mM DTT, and 20 % glycerol in the extracts.
7. Concentrate protein solutions by centrifugation at 20,800 × *g* and 4 °C for 60 min using Microccon filter units with a cut-off at 10 kDa (Millipore, Schwalbach, Germany).
8. Determine protein concentrations by the Bradford assay (Bio-Rad, Munich, Germany), freeze extracts and store at −80 °C until use.

3 Methods

3.1 Incision Test with Isolated hOGG1 (Fig. 4a, see Note 7)

1. For each experiment, pipet 8 µl of reaction buffer (50 mM Tris–HCl (pH 7.1), 50 mM NaCl, 0.1 µg/µl acetylated BSA) in a reaction tube.
2. Add 1 µl of isolated hOGG1 preparation (10 ng/µl) and 1 µl of a xenobiotic solution to the rim of the reaction tube.
3. Spin down to start the pre-incubation. Pre-incubate for 20 min at room temperature.
4. Note that this pre-incubation step yields in a 10-time dilution of the isolated hOGG1 preparation and the xenobiotic solution.
5. For control, use 1 µl of the diluent used for the preparation of the xenobiotic solution.
6. Now pipet 7 µl of the reaction buffer (50 mM Tris–HCl (pH 7.1), 50 mM NaCl, 0.1 µg/µl acetylated BSA) in fresh reaction tubes. Prepare a triplicate for each pre-incubation.

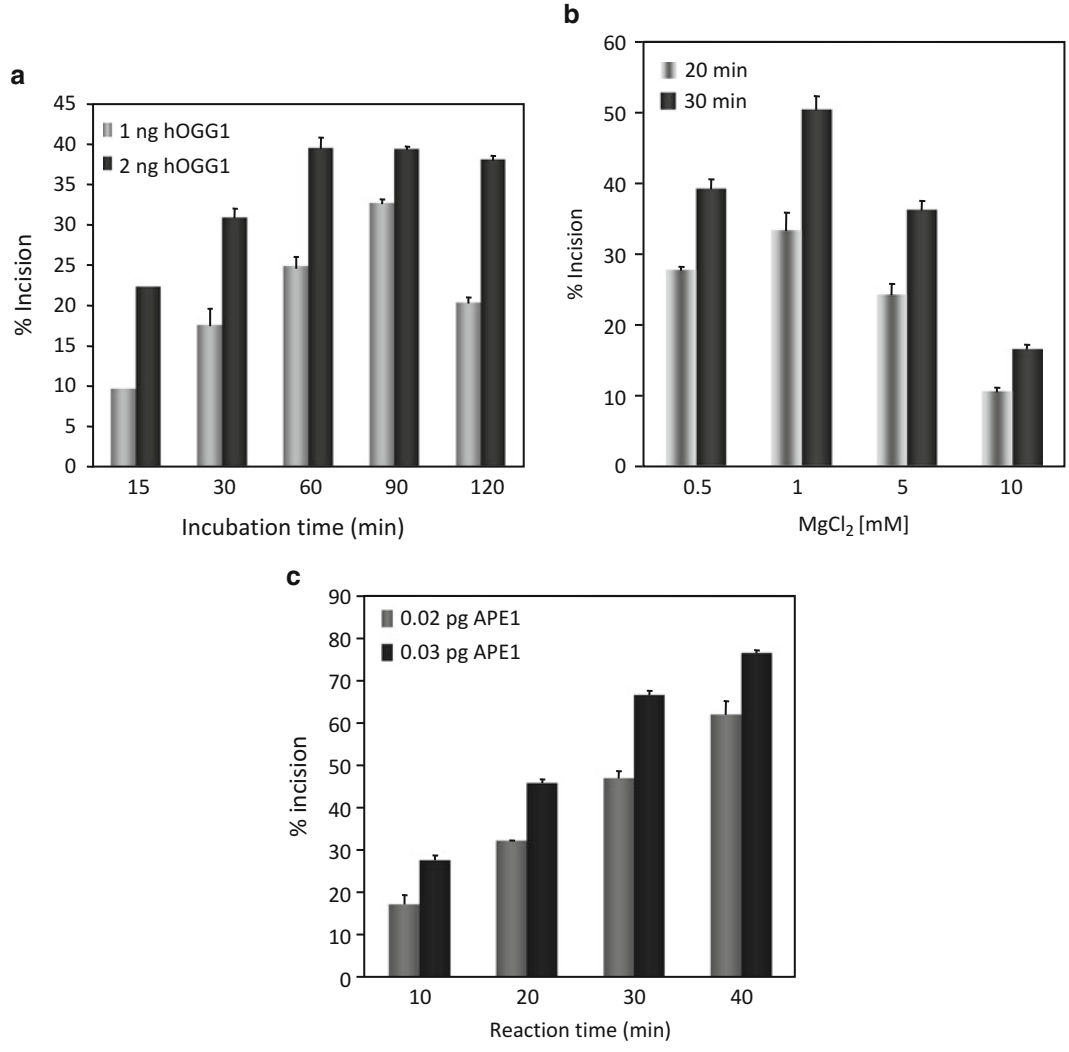

Fig. 4 Optimizations for incision assay with isolated repair proteins. (**a**) Optimization of protein amount and incubation time for incision assay with isolated hOGG1. 1–2 ng isolated hOGG1 were pre-incubated for 20 min at room temperature and then used in an incision reaction with 20 fmol oligonucleotide A for 15–120 min at 37 °C. Data are given as means of three (or two in case of 15 min) independent experiments + SD. (**b**) Optimization of $MgCl_2$ concentration and incubation time for incision assay with isolated APE1. 0.02 pg isolated APE1 were pre-incubated for 20 min at room temperature in the presence of 0.5–10 mM $MgCl_2$ and then used in an incision reaction with 20 fmol oligonucleotide B for 20–30 min at 37 °C still in the presence of 0.5–10 mM $MgCl_2$. Data are given as means of three independent experiments + SD. (**c**) Optimization of protein amount and incubation time for incision assay with isolated APE1. 0.02–0.03 pg isolated APE1 were pre-incubated for 20 min at room temperature in the presence of 1 mM $MgCl_2$ and then used in an incision reaction with 20 fmol oligonucleotide B for 10–40 min at 37 °C still in the presence of 1 mM $MgCl_2$. Data are given as means of three independent experiments + SD

7. To each tube add 0.2 µl of oligonucleotide A (100 fmol/µl) to the rim of the reaction tube, 2 µl of the pretreated isolated hOGG1 preparation (1 ng/µl) and 1 µl of the xenobiotic solution. Consider the presence of the xenobiotic solution in the pre-incubation when calculating the concentration.
8. For control, use pretreated isolated hOGG1 preparation from **step 5** and add 1 µl of the diluent instead of a xenobiotic solution.
9. To show that no unspecific incision occurs, prepare a negative control using 0.2 µl of oligonucleotide C (100 fmol/µl), pretreated isolated hOGG1 preparation from **step 5** and 1 µl of the diluent instead of the xenobiotic solution.
10. Spin down to start the incision reaction. Incubate at 37 °C for 30 min on a shaker.

3.2 Incision Test with Isolated APE1 (Fig. 4b, c, see Note 7)

1. For each experiment, pipet 8 µl of reaction buffer (50 mM Tris–HCl (pH 7.1), 50 mM NaCl, 0.1 µg/µl acetylated BSA, 1 mM $MgCl_2$) in a reaction tube.
2. Add 1 µl of isolated APE1 preparation (0.2 pg/µl) and 1 µl of a xenobiotic solution to the rim of the reaction tube.
3. Spin down to start the pre-incubation. Pre-incubate for 20 min at room temperature.
4. Note that this pre-incubation step yields in a 10-time dilution of the isolated APE1 preparation and the xenobiotic solution.
5. For control, use 1 µl of the diluent used for the preparation of the xenobiotic solution.
6. Now pipet 7 µl of the reaction buffer (50 mM Tris–HCl (pH 7.1), 50 mM NaCl, 0.1 µg/µl acetylated BSA, 1 mM $MgCl_2$) in fresh reaction tubes. Prepare a triplicate for each pre-incubation.
7. To each tube add 0.2 µl of oligonucleotide B (100 fmol/µl) and to the rim of the reaction tube 2 µl of the pretreated isolated APE1 preparation (0.02 pg/µl) and 1 µl of the xenobiotic solution. Consider the presence of the xenobiotic solution in the pre-incubation when calculating the concentration.
8. For the control, use pretreated isolated APE1 preparation from **step 5** and add 1 µl of the diluent instead of the xenobiotic solution.
9. To show that no unspecific incision occurs, prepare a negative control using 0.2 µl of oligonucleotide C (100 fmol/µl), pretreated isolated APE1 preparation from **step 5** and 1 µl of the diluent instead of the xenobiotic solution.
10. Spin down to start the incision reaction. Incubate at 37 °C for 30 min on a shaker.

3.3 Incision Test with Whole Cell Extracts

1. Establish the amount of whole cell extract to use in the incision assay to measure hOGG and APE activity, respectively. Incision activity should be as high as possible but not saturated yet (*see* Fig. 5).
2. When using A549 adenocarcinoma human alveolar basal epithelial cells, use 10 μg whole cell extract to measure hOGG incision and 5 μg to measure APE incision activity.
3. To measure hOGG incision activity, pipet 0.2 μl of oligonucleotide A (100 fmol/μl) and 10 μg whole cell extract on the rim of a prechilled reaction tube. Work on ice.
4. To measure APE incision activity, pipet 0.2 μl of oligonucleotide B (100 fmol/μl) and 5 μg whole cell extract on the rim of a prechilled reaction tube. Work on ice.
5. To reach a final volume of 10 μl, fill up with reaction buffer (50 mM Tris–HCl (pH 7.1), 50 mM NaCl, 1 mM EDTA, 0.5 mM DTT, 0.1 μg/μl acetylated BSA, 20 % glycerol).
6. For positive controls, treat oligonucleotide A (100 fmol/μl) with 2 ng of isolated hOGG1 (*see* Subheading 2.3) and oligonucleotide B (100 fmol/μl) with 0.2 pg isolated APE1 (*see* Subheading 2.4), respectively, instead of whole cell extracts.
7. For negative controls, treat oligonucleotide C (100 fmol/μl) with 2 ng of isolated hOGG1, 0.2 pg isolated APE1 (*see* Subheading 2.4) or whole cell extract.
8. Spin down to start the incision reaction.

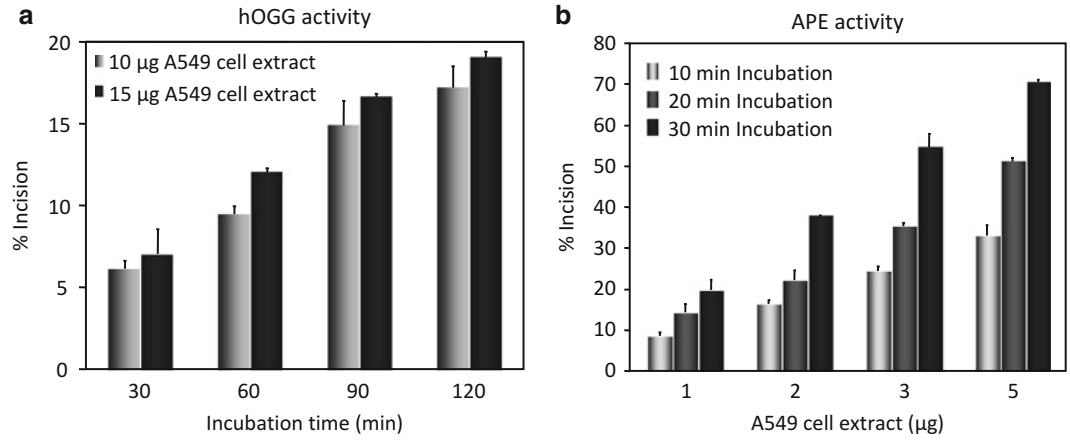

Fig. 5 Optimizations for incision assay with whole cell extract. (**a**) Optimization of protein amount and incubation time to measure hOGG activity in A549 cell extracts. 20 fmol of oligonucleotide A were treated with 10 or 15 μg A549 cell extract for 30–120 min at 37 °C. Data are given as means of three independent experiments + SD. (**b**) Optimization of protein amount and incubation time to measure APE activity in A549 cell extracts. 20 fmol of oligonucleotide B were treated with 1–5 μg A549 cell extract for 10–30 min at 37 °C. Data are given as means of three independent experiments + SD (*see* **Note 8**)

9. To measure hOGG activity, incubate at 37 °C for 90 min on a shaker, to measure APE activity, incubate at 37 °C for 20 min on a shaker.

3.4 Stop Incision Reaction

1. To terminate the incision reaction, put reaction tubes immediately on ice and add 10 µl stop solution (90 % formamide, 1 mM EDTA (pH 8.0), 0.5 % dextran blue).
2. Heat at 95 °C for 5 min to denature oligonucleotides.

3.5 Separation of Incision Products

1. Prepare a 20 % polyacrylamide gel with 40 % acrylamide–bisacrylamide stock solution (19:1), containing 7 M urea and electrophoresis buffer (89 mM Tris–borate pH 8.0, 2 mM EDTA).
2. To improve separation and band shape, flush gel slots thoroughly with electrophoresis buffer and pre-warm gels for 30 min at 50 °C.
3. Load reaction mixtures onto the gel and run in 89 mM Tris–borate (pH 8.0), 2 mM EDTA for 2 h at 15 W per gel.
4. Scan gels with a Typhoon Imager (GE Healthcare, Uppsala, Sweden).
5. Quantify incision activity using Image Quant TL software (GE Healthcare, Uppsala, Sweden).

4 Notes

1. We used an oligonucleotide which was designed to harbor a TTTT hairpin loop and a Cy5 label at the 3′ end. It turned out to be much more stable in cell extracts than usually used duplex structured oligonucleotide, probably due to protection against degradation by the loop on the one hand and by the labelled moiety on the other hand (Fig. 3).
2. After hybridization oligonucleotide aliquots can be stored at −20 °C for several months; however, quality should be tested from time to time by native PAGE (*see* Subheading 2.2).
3. For cell extract preparation, the presence of a high NaCl amount in the extraction buffer was necessary. To decrease the high salt concentration in the extracts, which had a negative impact on the incision activity, extracts had to be diluted and then concentrated again (*see* Subheading 2.5).
4. Cell pellets and cell extracts can be stored at −80 °C for at least 3 months without affecting cleavage activity.
5. When using a new cell line, establish the amount of whole cell extract to use in the incision assay to measure hOGG and APE activity, respectively. Incision activity shou.

6. Prepared working solutions of isolated hOGG1 and APE1 (*see* Subheadings 2.3 and 2.4) are stable for 1 week at –20 °C.
7. When using a new batch of enzyme, establish the enzyme amount to use in the incision assay to measure hOGG and APE activity, respectively (Fig. 4).
8. Our fluorescent method is as sensitive as and even faster than the radioactive technique, and, additionally, offers the advantage of reduced costs and low health risk. The disadvantage is that the purchase of a Fluorescence scanner like the Typhoon Imager (GE Healthcare, Uppsala, Sweden) is quite expensive.

Acknowledgements

The study was supported by the Deutsche Forschungsgemeinschaft and by the Deutsche Gesetzliche Unfallversicherung (DGUV).

References

1. David SS, O'Shea VL, Kundu S (2007) Base-excision repair of oxidative DNA damage. Nature 447:941–950
2. Klungland A, Bjelland S (2007) Oxidative damage to purines in DNA: role of mammalian Ogg1. DNA Repair (Amst) 6:481–488
3. Cooke MS, Evans MD, Dizdaroglu M, Lunec J (2003) Oxidative DNA damage: mechanisms, mutation, and disease. FASEB J 17: 1195–1214
4. Hegde ML, Hazra TK, Mitra S (2008) Early steps in the DNA base excision/single-strand interruption repair pathway in mammalian cells. Cell Res 18:27–47
5. Friedberg EC (2006) DNA repair and mutagenesis, 2nd edn. ASM Press, Washington, DC
6. Radicella JP, Dherin C, Desmaze C, Fox MS, Boiteux S (1997) Cloning and characterization of hOGG1, a human homolog of the OGG1 gene of Saccharomyces cerevisiae. Proc Natl Acad Sci U S A 94:8010–8015
7. Fortini P, Pascucci B, Parlanti E, D'Errico M, Simonelli V, Dogliotti E (2003) 8-Oxoguanine DNA damage: at the crossroad of alternative repair pathways. Mutat Res 531:127–139
8. Fortini P, Dogliotti E (2007) Base damage and single-strand break repair: mechanisms and functional significance of short- and long-patch repair subpathways. DNA Repair (Amst) 6:398–409
9. Hill JW, Hazra TK, Izumi T, Mitra S (2001) Stimulation of human 8-oxoguanine-DNA glycosylase by AP-endonuclease: potential coordination of the initial steps in base excision repair. Nucleic Acids Res 29:430–438
10. Vidal AE, Hickson ID, Boiteux S, Radicella JP (2001) Mechanism of stimulation of the DNA glycosylase activity of hOGG1 by the major human AP endonuclease: bypass of the AP lyase activity step. Nucleic Acids Res 29:1285–1292
11. Nilsen H, Krokan HE (2001) Base excision repair in a network of defence and tolerance. Carcinogenesis 22:987–998
12. Berwick M, Vineis P (2000) Markers of DNA repair and susceptibility to cancer in humans: an epidemiologic review. J Natl Cancer Inst 92:874–897
13. Paz-Elizur T, Krupsky M, Blumenstein S, Elinger D, Schechtman E, Livneh Z (2003) DNA repair activity for oxidative damage and risk of lung cancer. J Natl Cancer Inst 95:1312–1319
14. Gackowski D, Speina E, Zielinska M, Kowalewski J, Rozalski R, Siomek A, Paciorek T, Tudek B, Olinski R (2003) Products of oxidative DNA damage and repair as possible biomarkers of susceptibility to lung cancer. Cancer Res 63:4899–4902
15. Paz-Elizur T, Ben-Yosef R, Elinger D, Vexler A, Krupsky M, Berrebi A, Shani A, Schechtman

E, Freedman L, Livneh Z (2006) Reduced repair of the oxidative 8-oxoguanine DNA damage and risk of head and neck cancer. Cancer Res 66:11683–11689

16. Paz-Elizur T, Elinger D, Leitner-Dagan Y, Blumenstein S, Krupsky M, Berrebi A, Schechtman E, Livneh Z (2007) Development of an enzymatic DNA repair assay for molecular epidemiology studies: distribution of OGG activity in healthy individuals. DNA Repair (Amst) 6:45–60
17. Kreklau EL, Limp-Foster M, Liu N, Xu Y, Kelley MR, Erickson LC (2001) A novel fluorometric oligonucleotide assay to measure O(6)-methyl guanine DNA methyltransferase, methylpurine DNA glycosylase, 8-oxoguanine DNA glycosylase and abasic endonuclease activities: DNA repair status in human breast carcinoma cells overexpressing methylpurine DNA glycosylase. Nucleic Acids Res 29:2558–2566
18. Hamann I, Schwerdtle T, Hartwig A (2009) Establishment of a non-radioactive cleavage assay to assess the DNA repair capacity towards oxidatively damaged DNA in subcellular and cellular systems and the impact of copper. Mutat Res 669:122–130
19. Hamann I, Konig C, Richter C, Jahnke G, Hartwig A (2012) Impact of cadmium on hOGG1 and APE1 as a function of the cellular p53 status. Mutat Res 736:56–63

Chapter 7

Chiral Phase-HPLC Separation of Hydroperoxyoctadecenoic Acids and Their Biosynthesis by Fatty Acid Dioxygenases

Ernst H. Oliw and Anneli Wennman

Abstract

Fatty acid oxygenases are often characterized by steric analysis of their hydroxy or hydroperoxy metabolites. Chiral phase-HPLC (CP-HPLC) can be used to separate enantiomeric hydroperoxyoctadecenoic acids. This method is based on analysis of seven octadecenoic fatty acids with double bonds at positions 6*Z* to 13*Z*, which were oxidized to hydroperoxides by photooxidation. A stationary phase, Reprosil Chiral NR, was found to resolve these hydroperoxy fatty acids with 1-hydroperoxy-2-propene and with 3-hydroperoxy-1-propene elements so that the *S* hydroperoxy fatty acids consistently eluted before the *R* stereoisomers. The chiral selector has not been disclosed, but it is described as an aromatic chiral phase with π-donor and π-acceptor groups of Pirkle type. The MS^3 spectra of the hydroperoxides showed characteristic fragments, which were influenced by the distance between the hydroperoxy and the carboxyl groups and the relative position of the double bond. Octadecenoic fatty acids can be oxidized by fungal and bacterial dioxygenases to hydroperoxides with *cis* or *trans* double bond configuration. Steric analysis of the hydroperoxy metabolites can be performed by this method, and it can also be used for preparative purposes.

Key words CP-HPLC, Fatty acid dioxygenases, Fatty acid hydroperoxides, Photooxidation, Mass spectrometry

1 Introduction

Polyunsaturated fatty acids are oxygenated to hydroperoxides by lipoxygenases and by heme-dependent fatty acid dioxygenases in animals, plants, and fungi [1–3]. Enzymatic oxidation of octadecenoic acids has been reported in fungi and a few bacteria. *Pseudomonas aeruginosa* expresses a specific oleate 10*S*-dioxygenase and a diol synthase in the periplasm, which sequentially form (10*S*)-hydroperoxy-(8*E*)-octadecenoic acid (10*S*-HPOME) and (7*S*,10*S*)-dihydroxy-(8*E*)-octadecenoic acid [4]. The take-all fungus of wheat and several aspergilli oxidize oleic acid sequentially to (8*R*)-hydroperoxyoleic acid (8*R*-HPOME) and diols, e.g., (7*S*,8*S*)-dihydroxyoleic acid (7*S*,8*S*-DiHOME), 5*S*,8*R*-DiHOME, or 8*R*,11*S*-DiHOME [3, 5–7]. The key intermediate

Donald Armstrong (ed.), *Advanced Protocols in Oxidative Stress III*, Methods in Molecular Biology, vol. 1208,
DOI 10.1007/978-1-4939-1441-8_7,

in biosynthesis of the latter diols is 8*R*-HPOME, which is formed by the heme-dependent dioxygenase domains of linoleate diol synthases with both sequence and catalytic similarities to cyclooxygenases and α-dioxygenases of plants [8, 9]. Lipoxygenases with catalytic iron or manganese oxidize monoenoic fatty acids at low rates compared to these 8*R*- and 10*S*-dioxygenases [10].

CP-HPLC is now routinely used for analysis of polyunsaturated hydroxy- and hydroperoxy fatty acids, e.g., hydroxyeicosatetraenoic and hydroperoxyeicosatetraenoic acids [11]. Versatile matrices contain chiral selectors linked to cellulose or amylose, which are coated on silica, e.g., 3,5-dimethylphenyl carbamate (Chiralcel OD, Chiralpak AD, Reprosil Chiral-AM) and benzoate (Chiralcel OB). With different alcoholic modifiers, these matrices can separate a large number of hydroxy and hydroperoxy fatty acid metabolites [11]. An alternative to cellulose and amylose is an aromatic chiral selector of "Pirkle type", coated on silica (Reprosil Chiral NR; ***see* Note 1**). The latter can separate enantiomers of hydroperoxyeicosatetraenoic and hydroperoxyoctadecadienoic acids [12]. Unfortunately, there is little information on chromatographic separation of enantiomers of HOME and HPOME with derivatized cellulose and amylose as chiral selectors.

Racemic HPOME with *trans* configuration can conveniently be obtained by photooxidation and serve as racemic standards. Photooxidation generates singlet oxygen [13]. Addition of singlet oxygen to a double bond and hydrogen transfer from one of the neighboring methylene groups leads to formation of a hydroperoxide. Autoxidation will also yield HPOME with retained *cis* configuration of the double bond [14].

In this chapter we describe a method for CP-HPLC separation of enantiomers of HPOME and their identification by LC-MS^3 analysis. This method is based on hydroperoxides of seven octadecenoic acids, which were separated by CP-HPLC on Reprosil Chiral NR [15], and identified by chemical methods described by Hamberg [16]. We also illustrate that this CP-HPLC method can be used for analysis of HPOME formed by dioxygenases of bacteria and fungi. The method can also be used for preparative isolation of stereoisomers of HPOME.

2 Materials

2.1 Equipment

1. Photooxidation lamp (MIRA 63, Malmbergs Elektriska AB, Kumla, Sweden; 400 W, E40 high pressure sodium bulb) was obtained locally.
2. Analytical HPLC-MS systems for on-line UV and/or MS^3 analysis.
   The HPLC pumps were from Thermo Separation Products (P 2000) or from Spectra-Physics Analytical (ConstaMetric 3200).

The effluent was mixed post-column with the Surveyor MS pump (Thermo) for on-line MS^3 analysis in a linear ion trap mass-spectrometer (LTQ, Thermo). The effluent was subject to UV analysis in a photodiode array detector (Surveyor PDA plus, Thermo) and fractions were collected (Gilson FC 203).

3. MS and UV data were analyzed by the Xcalibur software (Thermo).

2.2 Reagents

1. Octadecenoic acids: (9*Z*)-18:1 (99 %) and (11*Z*)-18:1 (99 %) were from Larodan, and (12*Z*)-18:1 (99 %) was from Lipidox.
2. Methylene blue, *N*-hydroxyphthalimide, ceric ammonium nitrate, and α-tocopherol were from Sigma-Aldrich.
3. Kieselgel-60F254 thin layer chromatographic plates were from Merck (Darmstadt, Germany) and cartridges with silica (~0.9 g silica; Sep-Pak Classic) were from Waters.
4. Reprosil Chiral NR (8 μm; 250×2 mm) and Reprosil Chiral NR-R (8 μm; 250×4 mm; the opposite enantiomeric chiral form to the "NR" chiral selector) columns were from Dr. Maisch GmbH (Beim Brückle 14, 72119 Ammerbuch-Entringen, Germany)[1].
5. Fatty acid dioxygenases of bacterial and fungal origin were prepared as follows. Native diol synthase of *P. aeruginosa* was prepared as described [4]. Recombinant Mn-lipoxygenase was expressed in *Pichia pastoris* (strain X-33) as a secreted protein and purified as described [17, 18]. Recombinant 8-dioxygenase domain (amino acids 1–673) of 7,8-linoleate diol synthase of the take-all fungus, *Gaeumannomyces graminis*, was expressed in *Escherichia coli* as described [19].

3 Methods

3.1 Photooxidation of Octadecenoic Acids

20 mM octadecenoic acids (2–5 mg) in $CHCl_3$ with 20 μM methylene blue in a sealed glass tube were placed ~20 cm from the nitrogen lamp [13]. The tube was cooled by a fan to reduce heating from the lamp. Additional methylene blue was added from a concentrated stock solution (8 mM in methanol) when the dye was consumed, as indicated by a shift of color from blue to brownish. The reaction was followed by TLC (hexane–ethyl acetate–acetic acid, 50:50:0.1) and the fatty acids were visualized by spraying with molybdatophosphoric acid solution for TLC (Merck) before heating on a ceramic plate. About 50 % of the octadecenoic acids were usually oxidized after a few hours. The reaction was continued until at least 75 % of the acids were oxidized (***see* Note 2**). The products were purified as described in Subheading 3.3.

3.2 Autoxidation of Oleic Acid

Photooxidation will produce HPOME with *trans* configuration of the double bond, whereas autoxidation also yields HPOME with *cis* configuration. Autoxidation of oleic acid was modified from the method of Punta et al. [20]. Oleic acid (10–30 mg; 0.2 M in CH_3CN with 5–10 % α-tocopherol (w/w) in some experiments) reacted under oxygen with 40 μM *N*-hydroxyphthalimide and 20 μM ceric ammonium nitrate in CH_3CN at 37 °C for a few days under oxygen. The conversion was followed by TLC.

3.3 Separation of HPOME from Octadecenoic Acids on Silica

The photooxidized solution was evaporated to dryness under a stream of nitrogen and dissolved in 10 ml hexane–diethyl ether–acetic acid, 95:5:0.1, and applied to a silica cartridge in the same solvent. The cartridge was washed with 40 ml of this solvent to elute remaining octadecenoic acid. The HPOME were eluted in 10 ml fractions with 50 ml hexane–diethyl ether–acetic acid, 80:20:0.1. An aliquot of each fraction was assayed on TLC. The peak fractions were combined, reduced to dryness, dissolved in a small volume of hexane–isopropyl alcohol, 90:10, and diluted with hexane to 2 % isopropyl alcohol. Products from autoxidation of oleic were purified in the same way (about 5 mg per silica cartridge).

3.4 Analytical CP-HPLC Separations with In-Line LC-MS Analysis

CP-HPLC-MS analysis of HPOME was performed with the Reprosil Chiral NR column (8 μm; 250 × 2 mm), which was eluted at 0.5 ml/min with hexane–isopropyl alcohol–acetic acid, 98.8:1.2:0.01. The effluents from the column were combined with isopropyl alcohol–water (3:2) in a ratio of ~2:1 from a second HPLC pump [21] and then introduced by electrospray into a linear ion trap mass spectrometer (LTQ, Thermo) with analysis of carboxylate anions. The ion isolation width was set at 5 for anions of HPOME (m/z 313 → full scan) in the first selection and 1.5 at the final selection of MS^3 analysis of HPOME (m/z 313 → 295 → full scan). The collision energy was set at 1.7 V, and the ion tube lens at −110 to −130 V. We recorded five microscans and used the Gaussian algorithm for peak smoothing (Xcalibur Software, Thermo). Prostaglandin $F_1\alpha$ was infused for tuning.

3.5 Oxidation of Octadecenoic Acids by Fatty Acid Dioxygenases

10*S*-Dioxygenase was obtained as described and incubates with oleic acid for 5 min at room temperature. Mn-lipoxygenase (7 μg) in 0.1 M $NaBO_3$ (pH 9.0) was activated with 10 eq. 13*R*-hydroperoxyoctadecatrienoic acid and then incubated with 100 μM (12*Z*)-18:1 (40 min, 21 °C). Recombinant 8*R*-dioxygenase (the N-terminal 673 amino acids constituting the 8*R*-dioxygenase domain of 7,8-linoleate diol synthase) was incubated with 100 μM (9*Z*)-18:1 for 30 min on ice. The products were extracted on a SepPak/C_{18} cartridge and analyzed by LC-MS.

3.6 Preparative CP-HPLC with UV Analysis

Preparative CP-HPLC was performed with the Reprosil Chiral NR-R column (8 μm; 250×4 mm; eluted at 2 ml/min) and HPOME were analyzed with on-line UV detection (210 nm; PDA plus detector, Thermo). Fractions (1–2 ml) were collected, and an aliquot (2 μl) of fractions with UV absorbance was analyzed for HPOME by direct injection to the mass spectrometer in a solvent stream (0.3 ml/min) of methanol–water–acetic acid, 800:200:0.1. This method can also be used for separation of stereoisomers of 9- and 13-HPODE obtained by photooxidation of linoleic acid [12], and with UV analysis at 235 nm for detection of HPODE.

3.7 Results

3.7.1 Separation of Enantiomers of HPOME by CP-HPLC

All pairs of investigated enantiomers of HPOME were resolved on Reprosil Chiral NR. The relative retention times of HPOME with *trans* double bonds are summarized in Table 1. The absolute configuration of enantiomers of HPOME obtained following chromatography on Reprosil Chiral NR was determined by chemical methods [15, 16]. This analysis was performed with (−)-menthoxycarbonyl derivatives of the corresponding HOME methyl esters, followed by ozonolysis of the double bond, methylation, and separation and identification of the diastereoisomers by gas chromatography-mass spectrometry [16]. The results showed that the *S* stereoisomers of 14 regioisomeric HPOME with the double bond in *trans* configuration consistently eluted before the *R* stereoisomers on Reprosil Chiral NR. As far known, this elution order also applies to HPOME with *cis* double bonds (Table 1).

As illustrated in Table 1, the HPOME formed by photooxidation typically eluted from the Reprosil Chiral NR with an *S* stereoisomer

Table 1
Relative retention times of HPOME on the Reprosil Chiral NR column

18:1	HPOME(*E*)[a]			HPOME(*Z*)[b]		
Position and configuration of the hydroperoxide group						
(9*Z*)-18:1	10*S*	10*R*	9*S*	9*R*	8*S*	8*R*
	0.76	0.90	0.88	1	0.84	0.91
(11*Z*)-18:1	12*S*	12*R*	11*S*	11*R*	10*S*	10*R*
	0.71	0.82	0.86	1	0.76	0.85
(12*Z*)-18:1	13*S*	13*R*	12*S*	12*R*	11S	11*R*
	0.82	0.95	0.87	1	ND	0.87

[a]HPOME(*E*) were obtained by photooxidation, and the absolute configurations of HPOME(*E*) were determined by chemical methods after separation of enantiomers on a preparative Reprosil Chiral NR-R column

[b]HPOME(*Z*) were obtained by oxidation with the 8*R*-dioxygenase of linoleate diol synthase and Mn-lipoxygenase

with the shortest retention time and an *R* isomer with the largest, whereas the middle peaks contained *R* and *S* stereoisomers, e.g., 10*S*-HPOME eluting first and 9*R*-HPOME last, and elution of a 9*S*- and 10*R*-HPOME in between. The Reprosil Chiral NR-R column separates the isomers in the reverse order with 10*S*- and 9*R*-HPOME in the middle. By the selection of matrix, the desired 10-HPOME isomer can be eluted in the first peak and the desired 9-HPOME isomer in the last.

The separation of the 12-HPOME and 13-HPOME enantiomers is shown in Fig. 1a. 13-HPOME is formed from (12*Z*)-18:1 by Mn-lipoxygenase, and it has the same retention time as 13*R*-HPOME (Fig. 1b). 10*S*-Dioxygenase of *P. aeruginosa* oxidizes oleic acid to 10*S*-HPOME (Fig. 2a). Addition of this stereoisomer to photooxidized oleic acid with analysis of 10-HPOME by selected ion monitoring confirmed the elution order, *S* before *R* (Fig. 2a). This column also appeared to separate enantiomers of HPOME with *cis* double bond configuration. Autoxidation of oleic acid thus also yielded 8- and 11-HPOME(Z) as well as 9- and 10-HPOME. The separation of 9-HPOME is shown in Fig. 2b as well as the separation of 8-HPOME(9*Z*). 8*R*-HPOME(9*Z*) is formed by linoleate diol synthases, and addition of this compound to racemic 8-HPODE(9*Z*) confirmed the elution order, *S* before *R* (Fig. 2).

Chiral separation requires the interaction of the analyte to the chiral selector at a minimum of three positions with at least one position dependent on stereochemistry [22]. The two oxygen atoms of the hydroperoxide group and the double bond seem to interact with the chiral selector of Reprosil Chiral NR in this way (cf. the insets in Figs. 1 and 2). Interestingly, chiral separation was lost when the hydroperoxide group of HPOME was reduced to an alcohol. Enantiomers of 10-HOME(8*Z*) thus interacted with the chiral NR selector without separation, but the stereoisomers of 10-hydroxy-(8*E*,12*Z*)-octadecadienoic acid, with an addition double bond at 12Z compared with 10-HOME(8*Z*), were resolved [23], presumably by three-point interaction of the two double bonds and the hydroxyl group with the chiral selector. Enantiomers of polyunsaturated fatty acid hydroperoxides with 1-hydroperoxy-(2*E*,4*Z*)-pentene elements and additional double bonds (e.g., hydroperoxyeicosatetraenoic acids) may not elute in the same "*S*" and "*R*" order as HPOME and 9- and 13-HPODE [12].

3.7.2 Mass-Spectrometric Fragmentation of HPOME and KOME

The MS/MS spectra (m/z 313 → full scan) confirmed that HPOME were dehydrated to KOME as judged from the main ion at m/z 295 (313-18) in analogy with dehydration of other hydroperoxy fatty acids [12, 24]. Important ions in the MS^3 spectra (m/z 313 → 295 → full scan) of HPOME are summarized in Tables 2 and 3.

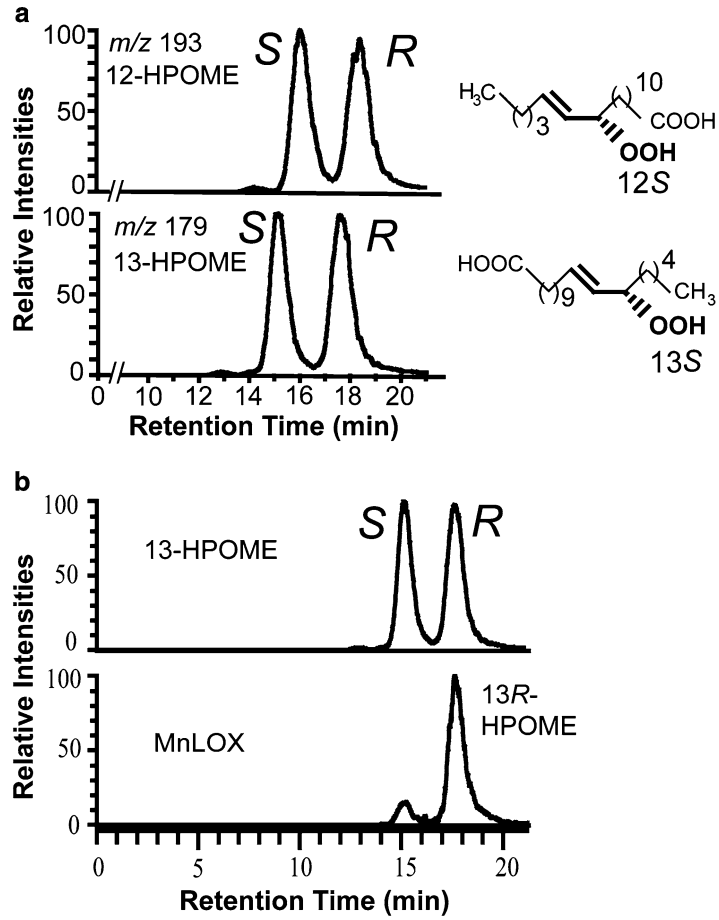

Fig. 1 CP-HPLC separation of 12- and 13-HPOME obtained by photooxidation of (12*Z*)-18:1. (**a**) The *top chromatogram* shows selective ion monitoring of the characteristic ion *m*/*z* 193 of 12-HPOME and the *bottom chromatogram* shows the characteristic ion at *m*/*z* 179 of 13-HPOME. The elution order was deduced by chemical methods [15]. The *inset* to the *right* shows in *bold* the three structural elements of HPOME likely recognized by the chiral selector. (**b**) Analysis of 13-HPOME formed by Mn-lipoxygenase. The latter oxidizes (12*Z*)-18:1 at C-11 and at C-13 with double bond migration to 13-HPOME (*bottom chromatogram*) with the same retention time as 13*R*-HPOME (*top chromatogram*)

The fragmentation pattern was influenced by the position of the hydroperoxide group in relation to the double bond and the carboxyl group. The MS^3 spectra of HPOME with their hydroperoxide groups located at the carboxylic side of a *trans* or *cis* double bond and relatively near the carboxyl group could only be explained by ions formed by a rearrangement mechanism. MS^3 analysis of 8-HPOME(9*Z*) thus yielded a rather intense signal pair at *m*/*z* 183 and 165 (Table 2). A possible fragmentation

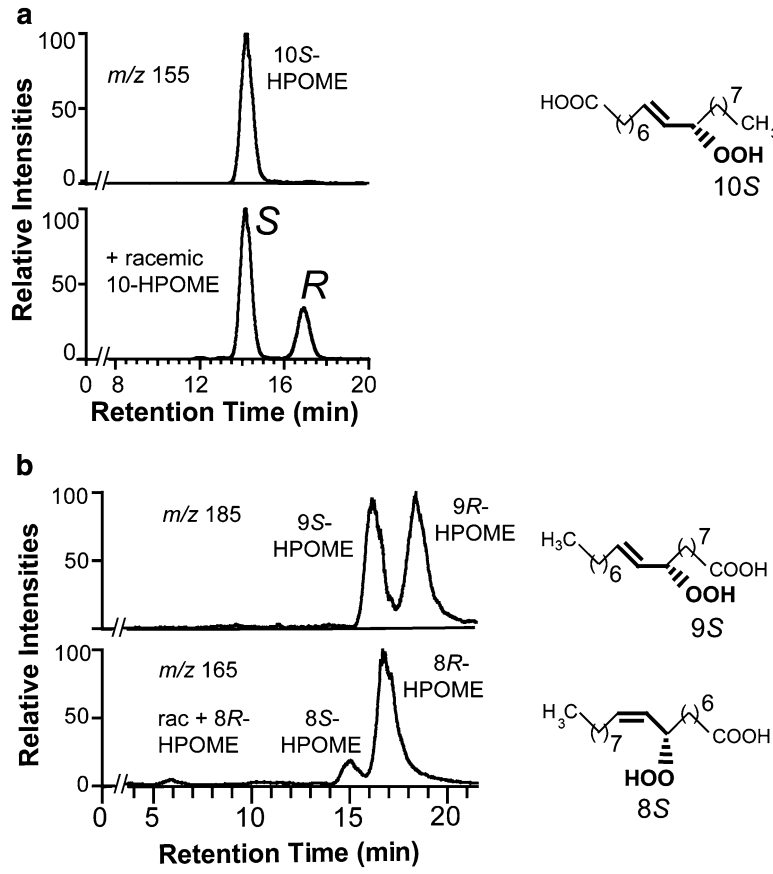

Fig. 2 Separation by CP-HPLC of stereoisomers of 10-HPOME formed by phooto-oxidation and 10*S*-dioxygenase and separation of 9- and 8-HPOME formed by autoxidation of oleic acid and 8-HPOME formed by 8*R*-dioxygenase. (**a**) The *top chromatogram* show selected ion monitoring of characteristic fragment ions of 10-HPOME, formed by 10*S*-dioxygenase, and the *bottom chromatogram* shows elution of racemic 10-HPOME with addition of 10*S*-HPOME (cf. Tables 2 and 3). (**b**) Separation of the stereoisomers of 9-HPOME (*top*) and 8-HPOME(9*Z*) (*bottom*). 8*R*-HPOME was added to identify this enantiomer. The *insets* to the *right* in (**a**) and (**b**) show in *bold* the three structural elements of HPOME likely recognized by the chiral selector

mechanism is suggested in Fig. 3a. It seems likely that the characteristic ions at m/z 183 of 8-HPOME could be due to rearrangement with loss of an uncharged species containing part of the carboxyl end with transfer of O^- to the ω end. In contrast, the MS^3 spectra of 12-HPOME(13*E*) can be interpreted with aid of keto-enol tautomerism and fragmentation by α-cleavage at the oxidized carbons as illustrated in Fig. 3b. This mechanism could also explain the fragmentation of 13-HPOME(11*E*), as illustrated in Fig. 3c. Other examples of these fragmentation mechanisms are found in Tables 2 and 3.

Table 2
Structurally important ions in the MS^3 spectra of hydroperoxides of regioisomeric octadecenoic acids with 1-hydroperoxy-2-propene functional groups

HPOME[a]	X-44	X-18	X[b]	Y-44	Y[c]
8-HPOME(9*E*)	111 (35)	137 (ND)	155 (4)	127 (30)	171 (25)
9-HPOME(10*E*)	125 (55)	151 (90)[e]	169 (10)[e]	141 (40)	185 (45)
10-HPOME(11*Z*)	139 (90)	165 (90)[e]	183 (<1)	155 (55)[e]	199 (70)
11-HPOME(12*E*)	153 (50)	179 (100)	193 (<1)	169 (20)	213 (30)
12-HPOME(13*E*)	167 (40)	193 (100)	211 (<1)	183 (10)	227 (12)

HPOME	Z-18	Z[d]
8-HPOME(9*E*)	165 (100)	183 (15)
9-HPOME(10*E*)	151 (90)[e]	169 (10)[e]
10-HPOME(11Z)	165 (90)[e]	155 (55)[e]
11-HPOME(12*E*)	123 (6)	151 (1)
12-HPOME(13*E*)	109 (1)	137 (0)

[a]The mass spectra of the corresponding hydroperoxides with a *cis* double bond were virtually identical [10]
[b]These ions (X series) were postulated as intermediates, which formed strong fragment ions after loss of water or CO_2 in some of the spectra (cf. Fig. 3a)
[c]These ions (Y series) were formed by loss of the omega end
[d]These ions (Z series) contained the omega end and gave rise to intense signals after loss of water in some spectra
[e]This ion occurs in two columns and could be formed by two different fragmentation mechanisms. The hypothetical fragmentation mechanisms of 8- and 12-HPODE are shown in Fig. 3a, b. MS^3 spectra (m/z 311 → 295 → full scan) and the base-peaks (100 %) were found at m/z 277 (295-18) unless listed in this table

Table 3
Structurally important fragmentation ions in the MS^3 spectra of hydroperoxides of regioisomeric octadecenoic acids with 3-hydroperoxy-1-propene functional groups

HPOME	X-18	X[a]	Z[b]
10-HPOME(8*E*)	137 (10)	155 (100)[c]	155 (100)[c]
11-HPOME(9*Z*)	151 (50)	169 (4)	141 (70)
12-HPOME(10*E*)	165 (100)	183 (4)	127 (30)
13-HPOME(11*E*)	179 (100)	197 (2)	113 (10)

[a]These ions (X series) contained the carboxyl group and formed fragments ions after loss of water, but only weak ions after loss of CO_2
[b]These ions (Z series) contained the omega end (cf. Fig. 3c for details)
[c]This ion occurs in two columns, and could be formed by both fragmentation mechanisms. A hypothetical fragmentation mechanism of 13-HPOME is shown in Fig. 3c. MS^3 spectra (m/z 311 → 295 → full scan) and the base-peaks were found at m/z 277 (295-18) unless listed in this table

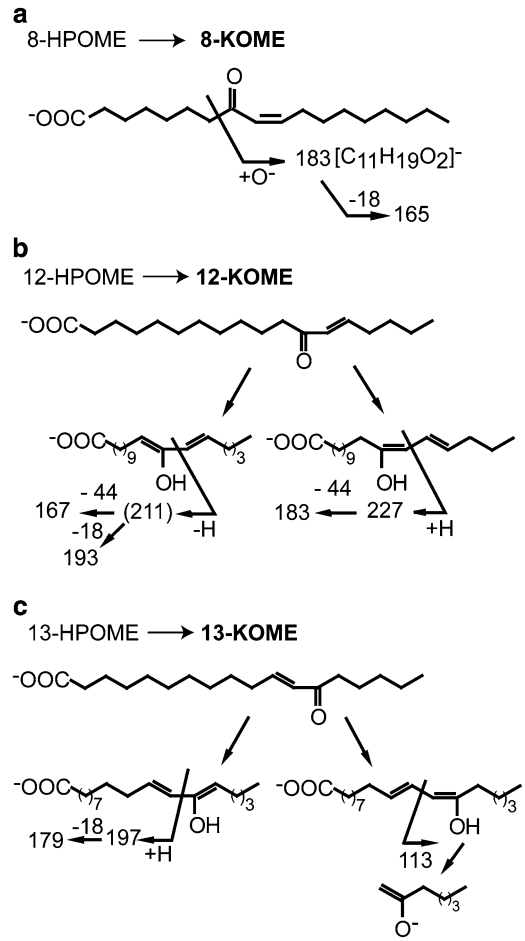

Fig. 3 Overview of the variable MS^3 fragmentation of hydroperoxides, illustrated by dehydration of 8-, 12-, and 13-HPOME to keto compounds (KOME) and their subsequent fragmentation. (**a**) Fragmentation of 8-KOME with formation of two characteristic ions by rearrangement (cf. Table 2). (**b**) Fragmentation of 12-KOME with formation of characteristic ions after keto-enol tautomerism (cf. Table 2). (**c**) Fragmentation of 13-KOME with formation of characteristic ions (cf. Table 3)

4 Notes

1. References to the separation of drugs on the Reprosil Chiral NR column and its chemical properties can be found at the home page of Dr. Maisch (http://www.dr-maisch.com/xedin.php?point=chiral_nr.html). This column can be operated both in reverse and normal phase mode, but separation of enantiomers of oxygenated fatty acids has so far only been reported in normal phase mode [12, 25][1].
2. Photooxidation and autoxidation under an atmosphere of oxygen will increase the reaction rate.

References

1. Ivanov I, Heydeck D, Hofheinz K, Roffeis J, O'Donnell VB, Kuhn H, Walther M (2010) Molecular enzymology of lipoxygenases. Arch Biochem Biophys 503:161–174
2. Andreou A, Feussner I (2009) Lipoxygenases—structure and reaction mechanism. Phytochemistry 70:1504–1510
3. Brodhun F, Feussner I (2011) Oxylipins in fungi. FEBS J 278:1047–1063
4. Martinez E, Hamberg M, Busquets M, Diaz P, Manresa A, Oliw EH (2010) Biochemical characterization of the oxygenation of unsaturated fatty acids by the dioxygenase and hydroperoxide isomerase of Pseudomonas aeruginosa 42A2. J Biol Chem 285:9339–9345
5. Brodowsky ID, Hamberg M, Oliw EH (1992) A linoleic acid (8R)-dioxygenase and hydroperoxide isomerase of the fungus Gaeumannomyces graminis. Biosynthesis of (8R)-hydroxylinoleic acid and (7S,8S)-dihydroxylinoleic acid from (8R)-hydroperoxylinoleic acid. J Biol Chem 267:14738–14745
6. Champe SP, el-Zayat AA (1989) Isolation of a sexual sporulation hormone from Aspergillus nidulans. J Bacteriol 171:3982–3988
7. Garscha U, Jernerén F, Chung D, Keller NP, Hamberg M, Oliw EH (2007) Identification of dioxygenases required for Aspergillus development. Studies of products, stereochemistry, and the reaction mechanism. J Biol Chem 282: 34707–34718
8. Su C, Sahlin M, Oliw EH (1998) A protein radical and ferryl intermediates are generated by linoleate diol synthase, a ferric hemeprotein with dioxygenase and hydroperoxide isomerase activities. J Biol Chem 273:20744–20751
9. Hamberg M, Ponce de Leon I, Rodriguez MJ, Castresana C (2005) Alpha-dioxygenases. Biochem Biophys Res Commun 338:169–174
10. Oliw EH, Jernerén F, Hoffmann I, Sahlin M, Garscha U (2011) Manganese lipoxygenase oxidizes bis-allylic hydroperoxides and octadecenoic acids by different mechanisms. Biochim Biophys Acta 1811:138–147
11. Schneider C, Yu Z, Boeglin WE, Zheng Y, Brash AR (2007) Enantiomeric separation of hydroxy and hydroperoxy eicosanoids by chiral column chromatography. Methods Enzymol 433:145–157
12. Garscha U, Nilsson T, Oliw EH (2008) Enantiomeric separation and analysis of unsaturated hydroperoxy fatty acids by chiral column chromatography-mass spectrometry. J Chromatogr B Analyt Technol Biomed Life Sci 872:90–98
13. Chacon JN, Gaggini P, Sinclair RS, Smith FJ (2000) Photo- and thermal-oxidation studies on methyl and phenyl linoleate: anti-oxidant behaviour and rates of reaction. Chem Phys Lipids 107:107–120
14. Porter NA, Mills KA, Carter RL (1994) A mechanistic study of oleate autoxidation: competing peroxyl H-atom abstraction and rearrangement. J Am Chem Soc 116:6690–6696
15. Oliw EH, Wennman A, Hoffmann I, Garscha U, Hamberg M, Jerneren F (2011) Stereoselective oxidation of regioisomeric octadecenoic acids by fatty acid dioxygenases. J Lipid Res 52:1995–2004
16. Hamberg M (1971) Steric analysis of hydroperoxides formed by lipoxygenase oxygenation of linoleic acid. Anal Biochem 43:515–526
17. Su C, Oliw EH (1998) Manganese lipoxygenase. Purification and characterization. J Biol Chem 273:13072–13079
18. Cristea M, Engström Å, Su C, Hörnsten L, Oliw EH (2005) Expression of manganese lipoxygenase in Pichia pastoris and site-directed mutagenesis of putative metal ligands. Arch Biochem Biophys 434:201–211
19. Hoffmann I, Jernerén F, Garscha U, Oliw EH (2011) Expression of 5,8-LDS of Aspergillus fumigatus and its dioxygenase domain. A comparison with 7,8-LDS, 10-dioxygenase, and cyclooxygenase. Arch Biochem Biophys 506: 216–222
20. Punta C, Rector CL, Porter NA (2005) Peroxidation of polyunsaturated fatty acid methyl esters catalyzed by N-methyl benzohydroxamic acid: a new and convenient method for selective synthesis of hydroperoxides and alcohols. Chem Res Toxicol 18:349–356
21. Cristea M, Oliw EH (2007) On the singular, dual, and multiple positional specificity of manganese lipoxygenase and its G316A mutant. J Lipid Res 48:890–903
22. Pirkle WH, Pochapsky TC (1989) Considerations of chiral recognition relevant to the liquid chromatographic separation of enantiomers. Chem Rev 89:347–362
23. Garscha U, Oliw EH (2007) Steric analysis of 8-hydroxy- and 10-hydroxyoctadecadienoic acids and dihydroxyoctadecadienoic acids formed from 8R-hydroperoxylinoleic acid by hydroperoxide isomerases. Anal Biochem 367:238–246
24. Murphy RC, Barkley RM, Zemski Berry K, Hankin J, Harrison K, Johnson C, Krank J, McAnoy A, Uhlson C, Zarini S (2005) Electrospray ionization and tandem mass spectrometry of eicosanoids. Anal Biochem 346:1–42
25. Wenzel B, Fischer S, Brust P, Steinbach J (2010) Enantioseparation of vesamicol and novel vesamicol analogs by high-performance liquid chromatography on different chiral stationary phases. J Chromatogr A 1217: 3855–3862

Chapter 8

Selenium as a Versatile Center in Fluorescence Probe for the Redox Cycle Between HClO Oxidative Stress and H_2S Repair

Zhangrong Lou, Peng Li, and Keli Han

Abstract

Selenium is a biologically important trace element and acts as an active center of glutathione peroxidase (GPx). GPx is the important antioxidant enzyme to protect organisms from oxidative damage via catalyzing the reaction between ROS and glutathione (GSH). Mimicking the oxidation–reduction cycles of the versatile selenium core in GPx, we can develop fluorescence probes to detect oxidation and reduction events in living systems. The cellular redox balance between hypochloric acid (HClO) and hydrogen sulfide (H_2S) has broad implications in human health and diseases, such as Alzheimer's disease (AD). Therefore, to further investigate the roles of this redox balance and understand the pathogenesis of neurodegenerative diseases, it is necessary to detect the redox state between HClO and H_2S in real time. We have developed a reversible fluorescence probe MPhSe-BOD for imaging of the redox cycle between HClO and H_2S based on oxidation and reduction of selenide in living cells.

Key words Selenide, Fluorescence probe, Hypochloric acid, Hydrogen sulfide, Redox, Reversible

1 Introduction

Selenium (Se) is an essential trace element exerting its biological effect through selenocysteine (Sec), which is the form of the selenium analogue of cysteine [1]. Several important selenoenzymes, such as glutathione peroxidase (GPx) [2], iodothyronine deiodinase (ID) [3] and thioredoxin reductase (TrxR) [4] all contain Sec at their active centers. Therein, GPx as an important antioxidant enzyme behaves a vital role in protecting various organisms from oxidative damage through catalyzing the reduction of ROS in the presence of glutathione [5]. Recently, numerous organoselenium compounds as GPx mimics have been synthesized to clarify the catalytic mechanism of GPx and develop effective antioxidant drugs [6]. Mimicking the GPx active site of selenium and according to the ping-pong mechanism, we can develop fluorescence probes with a versatile selenium core to detect oxidation and reduction events.

Donald Armstrong (ed.), *Advanced Protocols in Oxidative Stress III*, Methods in Molecular Biology, vol. 1208,
DOI 10.1007/978-1-4939-1441-8_8,

Hypochloric acid (HClO) is a biologically important reactive oxygen species (ROS) and has broad implications in human health and diseases. Endogenous HClO can be produced from hydrogen peroxide and chloride ions via the catalysis of the heme-enzyme myeloperoxidase (MPO) in stimulated neutrophils [7]. As a primary microbicide, HClO kills invading pathogens and plays a vital role in the human immune system. On the other hand, excessive generation of HClO can cause serious oxidative stress and destroy biomacromolecule via both oxidation and chlorination reactions [8, 9], such as lipids, proteins, and nucleic acids. Actually, under these circumstances, the antioxidant defense systems in living organisms will be activated to protect cells from the damaging of HClO. And the redox equilibrium between HClO and antioxidants has been implicated in the tissue damage, which contributes to inflammation and numerous diseases.

Hydrogen sulfide (H_2S) is a cytotoxic gas and has been proposed as a novel gasotransmitter with functions similar to that of nitric oxide and carbon monoxide recently [10]. However, evidence has demonstrated that H_2S also functioned as an antioxidant and free radical scavenger to protect cells from oxidative stress [11]. Whiteman et al. reported that H_2S can significantly inhibit HClO-induced oxidative damage to biomolecules and human SH-SY5Y cells [12]. In turn, the levels of H_2S will fluctuate in prefrontal cortex, hippocampal microglia, and neurons of Alzheimer's disease (AD) patients, where the expression of MPO is always increased [13]. It is reported by Kimura et al. that H_2S levels decreased by ~55 % in the brains of AD patients [14]. That is to say, the decreasing level of H_2S can reflect the H_2S consumption by elevated microglial and neuronal HClO production in AD patients. Consequently, it is proposed that the redox balance between HClO and H_2S is essential in human health and disease. In this regard, developing an effective technique for monitoring redox changes mediated by HClO and H_2S is necessary to further investigate the roles of this equilibrium and to understand the pathogenesis of neurodengenerative diseases.

Recently, we have developed a reversible fluorescence probe MPhSe–BOD to monitor the redox cycle between hypochlorous acid and hydrogen sulfide in solution and in living cells [15]. BODIPY dye that possesses good photostability, high extinction coefficients and fluorescence quantum yield is selected as the signal transducer of MPhSe-BOD, and 4-methyoxylphenylselanyl benzene (MPhSe) with Se center is chosen as the modulator. As mentioned above, Se is a versatile core as the GPx mimics to catalyze the oxidization/reduction reactions via a unique ping-pong mechanism. In MPhSe-BOD, Se is the active center for responding to HClO/H_2S mediated redox cycles. And the fluorescence of MPhSe–BOD is quenched due to a photoinduced electron transfer process (PET) from MPhSe to the BODPY fluorophore in the

excited state, while in Se oxidization the quenching process is blocked and the fluorescence emission is "switched on." In other words, the "off" and "on" cycles of the fluorescence signal correspond to the interconversion between "selenide" and "selenoxide," respectively. Accordingly, MPhSe–BOD can be applied to probe the redox cycles between HClO and H_2S with the fluorescence "on" and "off."

2 Materials

2.1 Equipment

1. ^{1}H NMR, ^{13}C NMR, and ^{77}Se NMR spectra were obtained on a Bruker DRX-400 spectrometer.
2. Steady-state UV/Vis spectra were measured on a Lambda 35 UV-visible Spectrophotometer (Perkin-Elmer) with 1.0-cm quartz cells.
3. Steady-state fluorescence spectra were obtained on a Fluoromax-4 Spectrofluorometer (Horiba-Jobin Yvon), with a Xenon lamp and 1.0-cm quartz cells.
4. Fluorescence images were acquired on Olympus FV1000 confocal laser-scanning microscope with an objective lens 40×.
5. In the process of synthesis of 2-(4-bromophenyl)-1,3-dioxolane, Dean-Stark trap was used to remove water azeotropically.

2.2 Reagents

1. Deuterated chloroform ($CDCl_3$) is used as the solvent in the NMR spectroscopy.
2. Common reagents or materials were of analytical reagent grade, and used without further purification except as otherwise noted.
3. Ultrapure water is used throughout the experiments.
4. 100 μL of the probe MPhSe-BOD from a 1 mM stock in acetonitrile is diluted with 20 mM phosphate buffer solution (PBS) containing 30 % acetonitrile. The final concentration of the probe MPhSe-BOD is 10 μM (*see* **Notes 1–3**).
5. Diethyl ether was dehydrated with the sodium-benzophenone system before used.
6. Tetrahydrofuran (THF) was dehydrated with the sodium-benzophenone system before used.
7. Dichloromethane was dehydrated with calcium hydride before used.
8. The peroxynitrite ($ONOO^-$) source was the 3-morpholinosydnonimine hydrochloride (Sin-1, 1 mmol/L) [16] (*see* **Notes 4–6**).

9. NO was generated in form of 3-(Aminopropyl)-1-hydroxy-3-isopropyl-2-oxo-1-triazene (NOC-5, 50 μmol/mL) [17] (*see* **Notes 4** and **5**).
10. Methyl linoleate (MeLH) and 2,2′-azobis-(2,4-dimethyl) valeronitrile (AMVN) were used to produce MeLOOH [18, 19] (*see* **Notes 4** and **5**).
11. Superoxide radicals ($O_2^{-\bullet}$) was generated by KO_2 [20]. 10 mM of KO_2 stocks were prepared in dimethylsulfoxide (DMSO) and stored at 0–5 °C (*see* **Notes 4** and **5**).
12. *tert*-butylhydroperoxide (*t*-BuOOH) and cumene hydroperoxide (CuOOH) could also use to induce ROS in biological systems [21] (*see* **Notes 4** and **5**).
13. NaOCl was the source of HClO. The concentration of NaOCl was determined based on the molar extinction coefficient at 292 nm at pH 12 ($\varepsilon_{292\,nm} = 350\ M^{-1}\ cm^{-1}$) [22] (*see* **Notes 4**, **5**, 7).
14. ·OH was generated by Fenton reaction between Fe^{II}(EDTA) and H_2O_2 quantitatively, and Fe^{II}(EDTA) concentrations represented $^{\bullet}OH$ concentrations [23] (*see* **Note 8**).
15. The reductants included glutathione (GSH), H_2S, cysteine (Cys), dithiothreitol (DTT), Fe^{2+}, $Na_2S_2O_4$, vitamin C (Vc), $NaHSO_3$, homocysteine (Hcys), alpha lipoic acid (ALA).
16. The blue fluorescent dyes Hoechst 33342 are cell permeable nucleic acid stains. The fluorescence of these dyes is very sensitive to DNA conformation and chromatin state in cells. The dyes were used according to the manufacturer's instructions.
17. 100 mM of NaHS stock in ultrapure water is the source of H_2S.
18. Phorbol myristate acetate (PMA) is used to induce a respiratory burst by activating NADPH oxidase to generate O_2^- that is converted to H_2O_2 [24]. H_2O_2 is then converted into HClO by the MPO enzymes released by the macrophage cell [7]. 1 mg/mL of PMA stocks were prepared in DMSO and stored at −20 °C.

2.3 Supplies

1. Common reagents or materials were purchased from commercial source.
2. Sin-1 was purchased from Sigma-Aldrich (Shanghai, China).
3. NOC-5 was purchased from Sigma-Aldrich (Shanghai, China).
4. The fluorescent dyes Hoechst 33342 were purchased from Sigma-Aldrich (Shanghai, China).
5. PMA was purchased from Sigma-Aldrich (Shanghai, China).
6. RAW264.7 cells (mouse macrophages cell line) were purchased from the Committee on type Culture Collection of Chinese Academy of Sciences.

3 Methods

3.1 Characterization

1. The ^{1}H NMR and ^{13}C NMR chemical shifts (δ) were reported in ppm relative to TMS (Me_4Si) as internal reference.

3.2 Synthesis of MPhSe-BOD (See Notes 9 and 10, the Synthetic Route Is Shown in Scheme 1)

3.2.1 Synthesis of 1,2-Bis(4-methoxyphenyl)diselane [25]

1. A 250 mL three-necked, round-bottomed flask was equipped with a magnetic stirrer, a pressure-equalizing dropping funnel, a condenser distillation column, and an economical Allihn condenser connected to a nitrogen source. The apparatus was vacuumized, then a stream of nitrogen was passed through the system, this operation was repeated three times.
2. The three-necked flask was suspended with 4.8 g (0.2 mol) of magnesium powder and 30 mL anhydrous diethyl ether.
3. 38 g (0.203 mol) of 4-methoxy bromobenzene was added dropwise to the flask, and the Grignard reagent of 4-methoxyphenyl magnesium bromide was obtained.

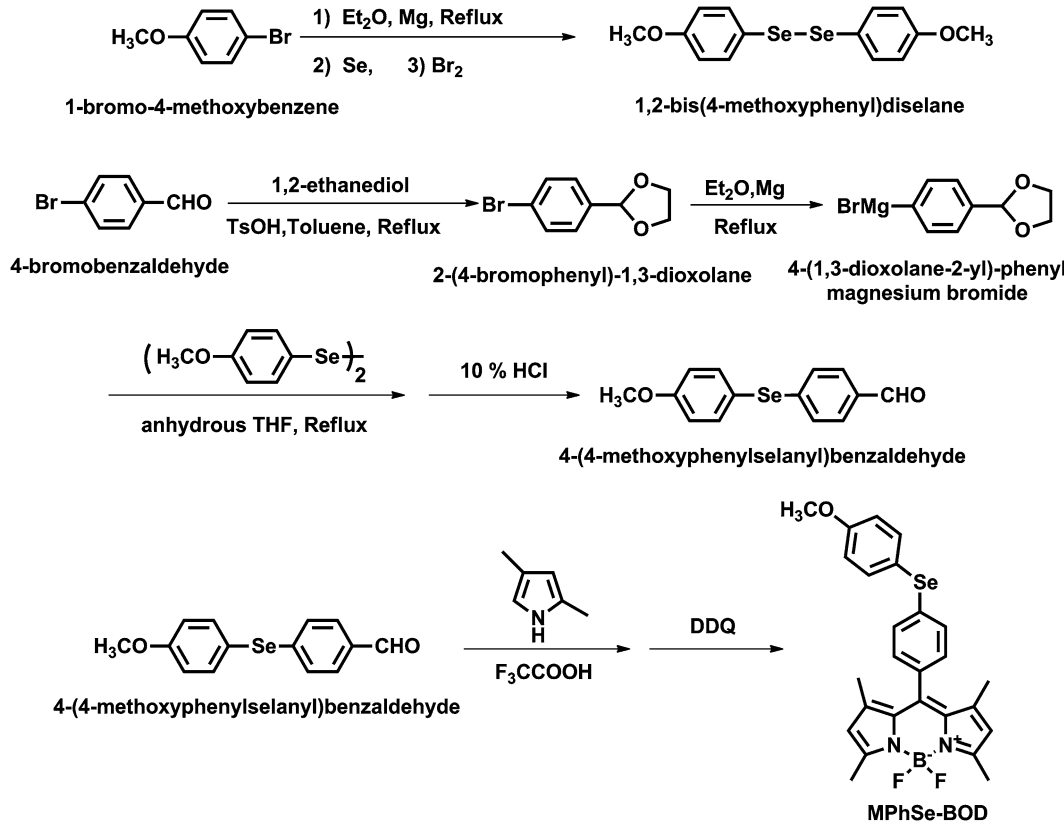

Scheme 1 Structure of MPhSe-BOD and the detection mechanism of MPhSe-BOD for HClO/H_2S induced redox cycle. *Inset* photo: (1) 10 μM probe; (2) 1 + 50 μM HClO; (3) 2 + 50 μM H_2S in 20 mM pH 7.4 PBS (30 % acetonitrile). Reproduced from reference [15] by permission of The Royal Society of Chemistry. The hyperlink to the article on the RSC Web site: http://pubs.rsc.org/en/content/articlelanding/2013/cc/c2cc37803e

4. Then 14 g (0.177 mol) of selenium (*see* **Note 11**) was added in portions at a rate sufficient to maintain a vigorous reflux through the condenser distillation column (*see* **Note 12**). The addition requires 15–30 min, after which the mixture was stirred and heated for another 30 min to ensure the selenium was dissolved completely.
5. The excess Grignard reagent was hydrolyzed with 0.6 mL of water. The generated solution was stirred and cooled to below 5 °C with ice bath. Then 5 mL of bromine was added dropwise at a rate such that the ether does not reflux (*see* **Note 13**).
6. Cooling and stirring were continued as a solution of 10.7 g of ammonium chloride in 28 mL water was added slowly.
7. The mixture was filtered, and the precipitate was washed thoroughly with 100-mL portions of ether. The combined filtrates were dried with anhydrous sodium sulfate (Na_2SO_4) and then evaporated on a rotary evaporator until dry. The acquired coarse product was purified on silica gel chromatography (200–300 mesh) eluted with dichloromethane: petroleum ether = 1:1 (v/v), the bright yellow product 4-methoxy diphenyl diselenide was collected (26.3 g, yield: 79.8 %).

   ^{1}H NMR (400 MHz, $CDCl_3$, ppm): 3.80 (s, 6H, *OCH*$_3$), 6.80 (d, 4H, *Ar-H*, *J* = 8.0), 7.50 (d, 4H, *Ar-H*, *J* = 8.0). ^{77}Se NMR (95 MHz, $CDCl_3$, ppm): 503.77. HRMS (TOF-LD+): *m/z* $C_{14}H_{14}O_2Se_2$ Calc. 373.9324, found 373.9307.

3.2.2 Synthesis of 2-(4-Bromophenyl)-1, 3-dioxolane [26]

1. In a 250 mL three-necked round-bottomed flask, 10 g (0.054 mol) of 4-bromobenzaldehyde and 0.25 g (1.45 mmol) of 4-methylbenzenesulfonic acid were dissolved in 150 mL of toluene.
2. Ethylene glycol (6 mL) was added to the flask, and the generated solution was refluxed with a Dean-Stark trap to azeotropically remove water.
3. After 10 h, the solution was allowed to cool to ambient temperature and washed twice with saturated Na_2CO_3 solution.
4. The mixture was extracted three times with ethyl acetate and the combined organic layers were dried with anhydrous sodium sulfate overnight. Then the solvent was evaporated and yellow oil was obtained. The obtained oil was purified on silica gel chromatography (200–300 mesh) eluted with dichloromethane: petroleum ether = 1:1 (v/v), the product was collected according to the determination of thin layer chromatography (TLC). After the solvent was evaporated, yellow oil of 2-(4-bromophenyl)-1,3-dioxolane was obtained (12 g, yield: 97.6 %).

3.2.3 Synthesis of 4-(4-Methoxyphenylselanyl) benzaldehyde

1. A 250 mL three necked round-bottomed flask was equipped with a magnetic stirrer, a pressure-equalizing dropping funnel, and an economical Allihn condenser connected to a nitrogen source. The air in the system was replaced with nitrogen.
2. The three-necked flask was suspended with 1.26 g (0.053 mol) of magnesium powder in 40 mL anhydrous THF.
3. 10 g (0.044 mol) of 2-(4-bromophenyl)-1,3-dioxolane was dissolved in 50 mL of anhydrous THF and the solution was added dropwise to the round-bottomed flask. Then the Grignard reagent of 4-(1,3-dioxolane-2-yl)-phenyl magnesium bromide was obtained.
4. 19.5 g (0.052 mol) of 1,2-bis(4-methoxyphenyl)diselane was dissolved in 50 mL of anhydrous dichloromethane.
5. The obtained solution in **step 4** was dropwised into the Grignard reagent in **step 3** at a rate sufficient to maintain a vigorous reflux.
6. Then the generated mixture was stirred and heated at reflux for another 2 h and the residual Grignard reagent was hydrolyzed with 3 mL of water.
7. The solvent in **step 6** was removed on a rotary evaporator. The remaining oil was dissolved in 100 mL of dichloromethane and the solution was cooled to below 10 °C in an ice bath. Then 30 mL of hydrochloric acid (the valid chlorine concentration is 10 %) was added slowly and the mixture was stirred until the deprotection reaction was finished.
8. The organic solution was dried with anhydrous Na_2SO_4 overnight and the solvent was evaporated. The remaining solid was purified on silica gel chromatography (200–300 mesh) eluted with dichloromethane: petroleum ether = 1:1 (v/v), the product was collected. After the eluent was evaporated, yellow solid of 4-(4-methoxyphenylselanyl)benzaldehyde was afforded (4.94 g, yield: 49 %).

   ^{1}H NMR (400 MHz, $CDCl_3$, ppm): 3.84 (s, 3H, O*CH*$_3$), 6.93 (d, 2H, *Ar-H*, *J* = 8.0), 7.3 (d, 2H, *Ar-H*, *J* = 8.0), 7.57 (d, 2H, *Ar-H*, *J* = 8.0), 7.65 (d, 2H, *Ar-H*, *J* = 8.0), 9.88 (s, 1H, *CHO*). ^{13}C NMR (100 MHz, $CDCl_3$, ppm): 55.35, 115.59, 117.35, 128.93, 130.01, 134.09, 138.02, 144.35, 160.63, 191.33. ^{77}Se NMR (95 MHz, $CDCl_3$, ppm): 419.14. HRMS (TOF LD$^+$) $[M+H]^+$ calcd. for $C_{14}H_{13}O_2Se$ 309.0030, found 309.0005.

3.2.4 Synthesis of MPhSe-BOD [27]

1. A 500 mL three necked round-bottomed flask was equipped with a magnetic stirrer, a pressure-equalizing dropping funnel, and an economical Allihn condenser connected to a nitrogen source. The air in the system was replaced with nitrogen.
2. The three-necked flask was suspended with 0.5 g (1.7 mmol) of 4-(4-methoxyphenylselanyl) benzaldehyde and 0.35 g

(3.4 mmol) of 2,4-dimethylpyrrole dissolved in 250 mL of anhydrous dichloromethane.

3. Five drops of trifluoroacetic acid were added and the generated solution was stirred at room temperature until there was no aldehyde through the thin-layer chromatography (TLC).
4. After the aldehyde was consumed completely, 0.39 g (1.7 mmol) of dichlorodicyanobenzoquinone (DDQ) was added, and stirring was continued for 15 min.
5. Then 1.2 g (11.9 mmol) of triethylamine and 2.65 g (18.7 mmol) of boron trifluoride diethyl ether ($BF_3{\cdot}Et_2O$) were added to the mixture in **step 4**.
6. After the reaction was continued for another 3 h. The reaction mixture was washed with water and dried with anhydrous Na_2SO_4, then the solvent was evaporated.
7. The residue was purified on preparative TLC (0.5 mm thick) eluted with dichloromethane: petroleum ether = 1:1 (v/v) and the orange solid was obtained (0.7 g, yield: 76 %). ^{1}H NMR (400 MHz, $CDCl_3$, ppm): 1.42 (s, 6H, *CH*$_3$), 2.54 (s, 6H, *CH*$_3$), 3.83 (s, 3H, O*CH*$_3$), 5.97 (s, 2H, *CH*), 6.9 (d, 2H, Ar-*H*, *J* = 8.0), 7.11 (d, 2H, *J* = 8.0, Ar-*H*), 7.39 (d, 2H, *J* = 8.0, Ar-*H*), 7.54 (d, 2H, *J* = 8.0, Ar-*H*). ^{13}C NMR (100 MHz, $CDCl_3$, ppm): 14.57, 29.71, 55.35, 115.39, 119.07, 121.28, 128.72, 130.87, 131.44, 132.92, 135.11, 136.84, 141.11, 143.03, 155.56, 160.14. ^{77}Se NMR (95 MHz, DMSO-d6, ppm): 396.82. HRMS (TOF LD+) calcd. for $C_{26}H_{25}BF_2N_2OSe$ 510.1193, found 510.1173.

3.3 Absorption and Fluorescence Analysis

1. The steady-state UV/Vis spectra of MPhSe-BOD with the different concentrations of HOCl were measured at room temperature, and the result is shown in Fig. 1.
2. The steady-state fluorescence spectra with the different concentrations of HOCl were measured at room temperature. The excitation wavelength was set to 460 nm and the emission spectra were collected ranging from 475 nm to 650 nm. The result is shown in Fig. 2.

3.4 Selectivity of MPhSe-BOD to ROS

1. The selectivity of *MPhSe-BOD* (10 μM) to ROS in fluorescence response was performed in 20 mM PBS at pH = 7.4 containing 30 % acetonitrile with the addition of different ROS (100 μM) after 5, 10, 15, 20, 25, 30, 35, 40, 45, 50, 55, 60 min.
2. The fluorescence response indicated the fluorescence intensity at 510 nm (Fig. 3).

3.5 Effect of pH Values

1. The pH of the medium is maintained by 20 mM phosphate buffer solution (PBS) at different pH value containing 30 % acetonitrile.
2. The effect of pH on the fluorescence intensity at 510 nm was investigated within the range from 4.0 to 12.0. pH values: 4.01,

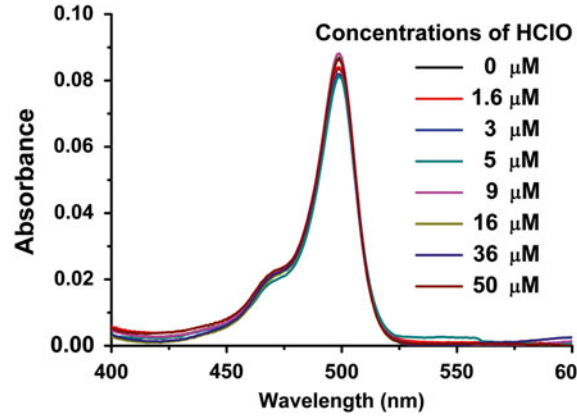

Fig. 1 Absorption response of MPhSe-BOD to different concentrations of HClO. Reproduced from reference [15] by permission of The Royal Society of Chemistry. The hyperlink to the article on the RSC Web site: http://pubs.rsc.org/en/content/articlelanding/2013/cc/c2cc37803e

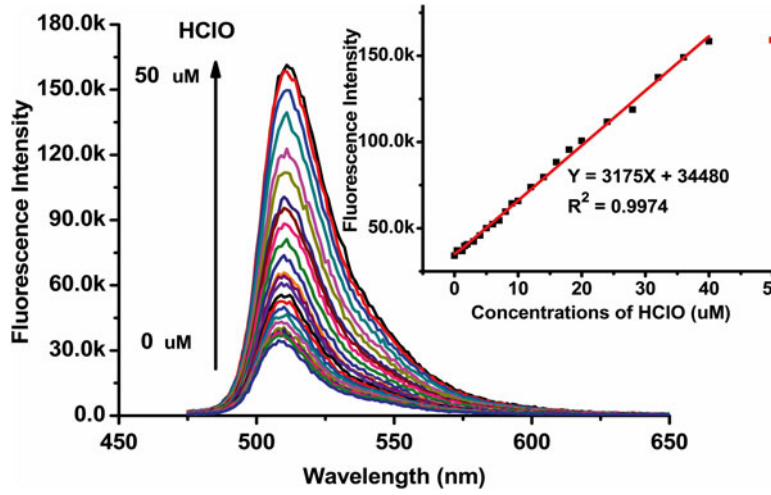

Fig. 2 Fluorescence response of MPhSe-BOD to various concentrations of HClO. *Inset*: The relationship between maximum fluorescence intensity (510 nm) and [HClO]. Reproduced from reference [15] by permission of The Royal Society of Chemistry. The hyperlink to the article on the RSC Web site: http://pubs.rsc.org/en/content/articlelanding/2013/cc/c2cc37803e

4.72, 5.12, 6.0, 6.52, 7.12, 7.4, 7.72, 8.02, 8.21, 8.5, 8.9, 9.2, 10, 11, 12.

3. The effect of pH was performed on the probe *MPhSe-BOD* (10 μM) in the absence and presence of 100 μM HClO (Fig. 4).

3.6 Selectivity of MPhSeO-BOD to Reductants

1. In the solution of 10 μM MPhSe-BOD, 100 μM of HClO was added. After equilibrating for 30 min, the fluorescence intensity at 510 nm was measured as the initial value.
2. Different reductants (100 μM) were added and the measurement was performed after 1, 5, 10. 15, 20, 25, 30 min (Fig. 5).

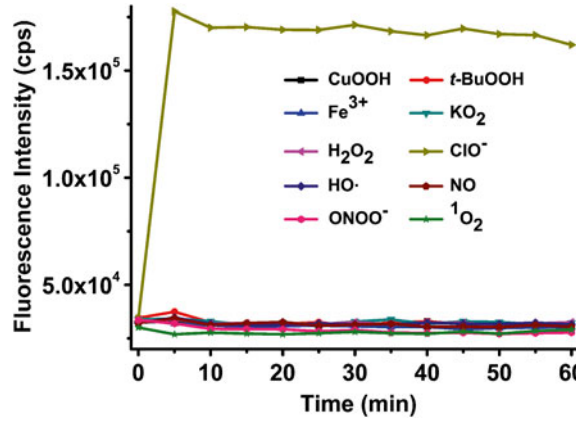

Fig. 3 Time dependent fluorescence intensity changes of MPhSe-BOD with 100 μM ROS. Reproduced from reference [15] by permission of The Royal Society of Chemistry. The hyperlink to the article on the RSC Web site: http://pubs.rsc.org/en/content/articlelanding/2013/cc/c2cc37803e

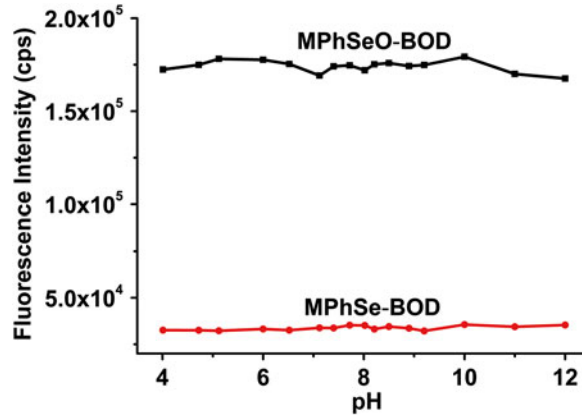

Fig. 4 Fluorescence intensity of MPhSe-BOD with the absence and presence of HClO in various pH values. Reproduced from reference [15] by permission of The Royal Society of Chemistry. The hyperlink to the article on the RSC Web site: http://pubs.rsc.org/en/content/articlelanding/2013/cc/c2cc37803e

3.7 Cell Culture and Confocal Imaging

1. Murine RAW264.7 macrophage cells (ATCC, USA) were maintained following protocols provided by the American Type Culture Collection.
2. Cells were seeded at a density of 1×10^6 cells/mL for confocal imaging in RPMI 1640 Medium supplemented with 15 % fetal bovine serum (FBS), $NaHCO_3$ (2 g/L), and 1 % antibiotics (penicillin/streptomycin, 100 U/mL). Cultures were maintained at 37 °C under a humidified atmosphere containing 5 % CO_2.

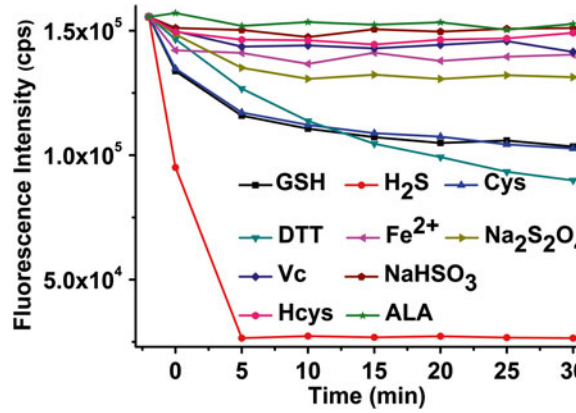

Fig. 5 Time dependent fluorescence intensity changes of MPhSeO-BOD with reductants. Reproduced from reference [15] by permission of The Royal Society of Chemistry. The hyperlink to the article on the RSC Web site: http://pubs.rsc.org/en/content/articlelanding/2013/cc/c2cc37803e

3. The cells were subcultured by scraping and seeding on 35 mm × 12 mm glass bottom cell culture dishes for laser scanning confocal imaging according to the instructions from the manufacturer.
4. For MPhSe-BOD, fluorescence images were obtained using an excitation wavelength of 488 nm and emission band from 500 nm to 600 nm.
5. For Hoechst 33342, fluorescence images were obtained using an excitation wavelength of 405 nm and emission band from 420 nm to 470 nm.
6. Prior to fluorescence imaging, the cells were washed with 20 mM PBS (pH = 7.40) for three times. The results of confocal fluorescence images of the redox cycles between HClO and H_2S in Raw 264.7 cells are shown in Fig. 6.
7. Raw 264.7 cells were incubated with MPhSe-BOD (10 μM) for 10 min, Hoechst 33342 for 5 min.
8. Incubating with 1.5 μg/mL of PMA for 30 min was used to induce the generation of HClO in Raw 264.7 cells.
9. Incubating with 100 μM of H_2S for 10 min was used to repair the oxidative stress induced by HClO in Raw 264.7 cells of **step 8**.
10. Incubating with 3.0 μg/mL of PMA for 30 min was used to induce the second generation of HClO in the Raw 264.7 cells of **step 9**.

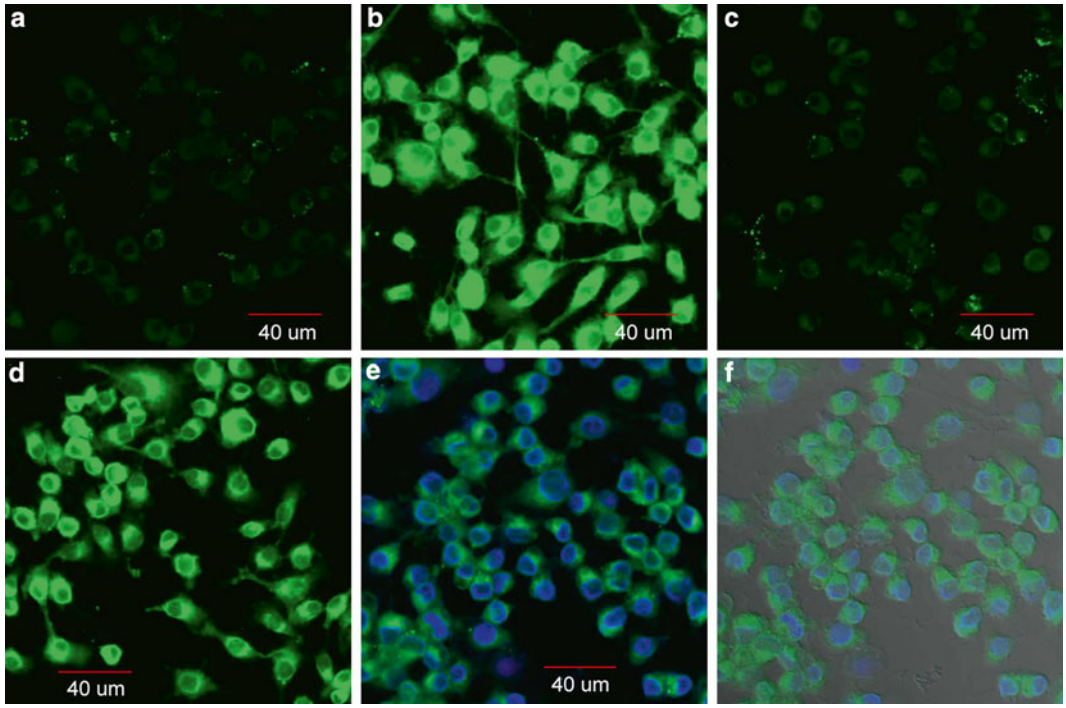

Fig. 6 Confocal fluorescence images of the redox cycles between HClO and H_2S in RAW264.7 cells. Macrophage cells were incubated with MPhSe-BOD and then treated with various stimulants at 37 °C. (**a**) Control. (**b**) Probe-loaded cells incubated with PMA. (**c**) Probe-loaded, PMA-treated cells incubated with H_2S. (**d**) Probe-loaded, PMA-treated, H_2S-incubated cells treated with a second dose of PMA. (**e**) Overlay of images showing fluorescence from MPhSe-BOD and Hoechst dye. (**f**) Overlay of bright-field, MPhSe-BOD, and Hoechst dye images. Reproduced from reference 15 by permission of The Royal Society of Chemistry. The hyperlink to the article on the RSC Web site: http://pubs.rsc.org/en/content/articlelanding/2013/cc/c2cc37803e

4 Notes

1. MPhSe-BOD is susceptible to the air, so the MPhSe-BOD solid should be stored in the nitrogen atmosphere at −20 °C.
2. The MPhSe-BOD stocks should be prepared freshly before used.
3. The PBS is beneficial to the reproduction of bacteria and should be prepared freshly before used.
4. Most ROS are strong oxidizing and care should be exercised to avoid contact with skin.
5. The ROS are unstable and the stocks should be prepared freshly before used.
6. Sin-1 in acidic solutions (>0.1 M) can be stored for at least 1 year at −80 °C without serious loss of Sin-1.
7. The valid chlorine of the commercially available NaOCl solution was 10 %.

8. The EDTA is insoluble in water at room temperature before forming the complex Fe^{2+}(EDTA), heating is allowed.
9. Caution! Most selenium compounds are toxic; care should be exercised to avoid contact with skin. All operations in the synthetic procedure should be conducted in a well-ventilated hood.
10. The selenium compounds are sensitive to the air, so the synthetic reactions should be proceeded in the nitrogen atmosphere.
11. The selenium powder is susceptible to oxygen and should be used freshly.
12. A slow stream of nitrogen should be passed through the system while the portions of selenium are added. In addition, the top of the condenser should be stoppered between additions.
13. After this step, it is no longer necessary to maintain nitrogen atmosphere of the system.

Acknowledgments

We are grateful to the National Science Foundation of China (21273234 and 21203192) and the National Basic Research Program of China (2013CB834604) for financial support.

References

1. Stadtman TC (1996) Selenocysteine. Annu Rev Biochem 65:83–100
2. Flohe L, Gunzler WA, Schock HH (1973) Glutathione peroxidase: selenoenzyme. FEBS Lett 32:132–134
3. Behne D, Kyriakopoulos A, Meinhold H et al (1990) Identification of type I iodothyronine 5′-deiodinase as a selenoenzyme. Biochem Biophys Res Commun 173:1143–1149
4. Tamura T, Stadtman TC (1996) A new selenoprotein from human lung adenocarcinoma cells: purification, properties, and thioredoxin reductase activity. Proc Natl Acad Sci U S A 93: 1006–1011
5. Rotruck JT, Pope AL, Ganther HE et al (1973) Selenium: biochemical role as a component of glutathione peroxidase. Science 179: 588–590
6. Bhabak KP, Mugesh G (2010) Functional mimics of glutathione peroxidase: bioinspired synthetic antioxidants. Acc Chem Res 43:1408–1419
7. Klebanoff SJ (2005) Myeloperoxidase: friend and foe. J Leukoc Biol 77:598–625
8. Domigan NM, Charlton TS, Duncan MW et al (1995) Chlorination of tyrosyl residues in peptides by myeloperoxidase and human neutrophils. J Biol Chem 270:16542–16548
9. Nagy P, Ashby MT (2007) Reactive sulfur species: kinetics and mechanisms of the oxidation of cysteine by hypohalous acid to give cysteine sulfenic acid. J Am Chem Soc 129: 14082–14091
10. Wang R (2002) Two's company, three's a crowd: can H_2S be the third endogenous gaseous transmitter? FASEB J 16:1792–1798
11. Lee PB, Joseph LD, Gojon G (2012) Hydrogen sulfide in biochemistry and medicine. Antioxid Redox Signal 17:119–140
12. Whiteman M, Cheung NS, Zhu YZ et al (2005) Hydrogen sulphide: a novel inhibitor of hypochlorous acid-mediated oxidative damage in the brain? Biochem Biophys Res Commun 326:794–798
13. Green PS, Mendez AJ, Jacob JS et al (2004) Neuronal expression of myeloperoxidase is increased in Alzheimer's disease. J Neurochem 90:724–733
14. Eto K, Asada T, Arima K et al (2002) Brain hydrogen sulfide is severely decreased in Alzheimer's disease. Biochem Biophys Res Commun 293:1485–1488

15. Wang BS, Li P, Yu FB et al (2013) A reversible fluorescence probe based on Se-BODIPY for the redox cycle between HClO oxidative stress and H_2S repair in living cells. Chem Commun 49:1014–1016
16. Ashki N, Hayes KC, Bao F (2008) The peroxynitrite donor 3-morpholinosydnonimine induces reversible changes in electrophysiological properties of neurons of the guinea-pig spinal cord. Neuroscience 156:107–117
17. Takayama M, Yamane H, Konishi K et al (1998) Cleavage product from the NO donor NOC-5 and inner ear hair cell damage. Acta Otolaryngol Suppl 538:12–18
18. Terao J, Nagao A, Park DK et al (1992) Lipid hydroperoxide assay for antioxidant activity of carotenoids. Methods Enzymol 213:454–460
19. Kohen R, Yamamoto Y, Cundy KC et al (1988) Antioxidant activity of carnosine, homocarnosine, and anserine present in muscle and brain. Proc Natl Acad Sci U S A 85:3175–3179
20. Albers AE, Okreglak VS, Chang CJ (2006) A FRET-based approach to ratiometric fluorescence detection of hydrogen peroxide. J Am Chem Soc 128:9640–9641
21. Nieminen AL, Byrne AM, Herman B et al (1997) Mitochondrial permeability transition in hepatocytes induced by t-BuOOH: NAD(P)H and reactive oxygen species. Am J Physiol 272:C1286–C1294
22. Morris JC (1966) The acid ionization constant of HOCl from 5 to 35°. J Phys Chem 70: 3798–3805
23. Halliwell B, Gutteridge JMC (1986) Oxygen free-radicals and iron in relation to biology and medicine-some problems and concepts. Arch Biochem Biophys 246:501–514
24. Repine JE, White JG, Clawson CC et al (1974) Influence of phorbol myristate acetate on oxygen-consumption by polymorphonuclear leukocytes. J Lab Clin Med 83:911–920
25. Reich HJ, Cohen ML, Clark PS (1988) Reagents for synthesis of organoselenium compounds-diphenyl diselenide and benzeneselenenyl chloride. Org Synth 6:533–537
26. Briggs JR, Klosin J, Whiteker GT (2005) Synthesis of biologically active amines via rhodium-bisphosphite-catalyzed hydroaminomethylation. Org Lett 7:4795–4798
27. Kollmannsberger M, Rurack K, Resch-Genger U et al (1998) Ultrafast charge transfer in amino-substituted boron dipyrromethene dyes and its inhibition by cation complexation: a new design concept for highly sensitive fluorescent probes. J Phys Chem A 102: 10211–10220

Chapter 9

Evaluation of Physical Integrity of Lipid Bilayer Under Oxidative Stress: Application of Fluorescence Microscopy and Digital Image Processing

Ran Liang, Jian-Ping Zhang, and Leif H. Skibsted

Abstract

Membrane damage as a result of oxidative stress is quantified using digital image heterogeneity analysis of single giant unilamellar vesicles (GUVs) composed of soy phosphatidylcholine (PC), which were found to undergo budding when containing chlorophyll *a* (Chl*a*) as photosensitizer in the lipid bilayer. Based on digital image heterogeneity analysis, a dimensionless scalar parameter "entropy" for the budding process was found to change linearly during an initial budding stage. Photo-induced peroxidation of PC to form linoleoyl hydroperoxides, further leading to domains of higher polarities in GUVs, was suggested to initiate the budding process. The effect on budding process of GUVs was suggested for use in assays for evaluation of potential protectors of lipid bilayer integrity under oxidative stress, and "entropy" seemed to be a valid descriptor of such membranal integrity. The one-step procedure for quantification of prooxidative effects and antioxidative protection provided by drug candidates and potential food ingredients in membranes could be easily automated for direct measurement of oxidative and antioxidative effects on cellular integrity.

Key words Antioxidation, Lipid bilayer integrity, Liposome budding, Fluorescence microscopy, Digital image processing

1 Introduction

Oxidative stress is increasingly becoming recognized as a threat to human health in relation to exposure to environmental pollution and lifelong consumption of highly processed foods, often depleted in minerals and/or vitamins [1, 2]. Oxidative stress and free radical processes are further involved in most lifestyle related diseases and may affect integrity of cellular membranes and corrupt cellular functions [3]. In principles, two strategies seem straightforward for protection of cellular membranes with one involving a decrease in exposure to agents inducing oxidative stress, while the other involves an increased integration of proper antioxidants. Both a decrease in exposure to prooxidants and an increased integration

Donald Armstrong (ed.), *Advanced Protocols in Oxidative Stress III*, Methods in Molecular Biology, vol. 1208,
DOI 10.1007/978-1-4939-1441-8_9,

of antioxidants, and the combination, call for development of methods for direct quantification of effects on membrane stability and function. Most currently available methods depend on chemical analysis after separation of individual oxidation products involving elaborated procedures.

Liposomes, first described by British hematologist, Alec D. Bangham in 1960s [4–6], are artificially prepared vesicles composed of lipid bilayers, which are made of phospholipids or other amphiphiles, and may contain small amounts of other additives. Liposomes can be prepared by self-organization of amphiphile molecules in aqueous environment, and there are generally two types of liposome preparation methods: the gentle hydration method [7] and the electroformation method [8, 9]. In recent studies, liposomes are widely used as vehicle for administration of drugs [10] and are used for simulation of biomembranes of cells and tissues [11–13]. Giant unilamellar vesicles (GUVs) are spherical shells with 5–200 μm diameters composed of a single lipid bilayer. The most important attribute of GUVs is that they are visible by optical microscopes, since GUVs equal or exceed cellular dimensions. GUVs are found to undergo a variety of "cytomimetic" morphological transformations including fusion, fission, budding, aggregation, etc. [14–16], and such morphological changes have been observed using microscopy-related techniques including phase-contrast microscopy and fluorescence microscopy [17–19].

Fluorescence microscopy combined with digital image processing and analysis enabled direct visualization of morphological changes of GUVs in late 1980s [20, 21]. Taking advantage of the fluorescence microscopy experimental setup, light-induced morphological changes of fluorescently labeled GUVs have been visualized under intense irradiation [22]. For GUVs composed of naturally occurring phospholipids, chemical reactions of unsaturated fatty acid moieties of lipid molecules, such as polymerization and (per)oxidation initiated via excited states of probes or photosensitizers, seem to be the cause of such light-induced GUV morphological changes [23–25]. Naturally occurring unsaturated phospholipids are easily oxidizable and hydroperoxides are formed as the primary oxidation products [26]. The formation of hydroperoxides is proposed to initiate the changes in lipid molecule polarity, leading to surface tension and curvature change, and eventually phase separation and budding of GUVs [27].

In our own antilipoxidation studies, the combination of fluorescence microscopy with customized digital image processing routines has enabled us to evaluate the antioxidant capacities of natural exogenous antioxidants in GUVs composed of natural soybean phospholipid mixture (predominant species: dilinoleoyl PC). The digital image processing method described above is on the basis of regional descriptors [28] characterizing heterogeneity

(randomness) of GUV images, and can take advantage of any custom-coded MATLAB programs or other commercially available software packages. Since the GUV-microscopy based experiments are performed at the level of single liposome, heterogeneity in GUV shape and size are obtained using digital image processing methods and statistics. By contrast, in classical methods, experimental data (absorbance or fluorescence emission intensity, etc.) are collected from bulk solution (or suspension) of many liposomes, and therefore the information about lipid molecule organization at the level of single liposome is unavailable.

In one of our recent studies, we prepared soybean PC GUVs with diameters 5–25 μm using reverse-phase evaporation method [29], and evaluated the antilipoxidation activities of β-carotene and rutin in this model system as lipophilic and hydrophilic antioxidants, respectively [30]. The digital image heterogeneity observed and expressed as the scalar parameter "entropy" [28] has been assigned to the budding process of GUVs under intense irradiation, and it seems to be a valid descriptor of lipid bilayer integrity under oxidative stress.

To sum up, we have developed a method which directly measures the physical integrity of the membrane of GUVs, using inverted fluorescence microscopy combined with photosensitized oxidation of membranal components oxidatively stressing the individual GUVs followed by digital image analysis to yield a single parameter for status of the physical integrity of individual GUVs. The method could be easily adopted for drug candidates and potential food ingredients. Notably, the method provides a direct one-parameter quantification of complex changes in the membranes and could be easily automated, since it involves practically no separation procedures or other "wet" chemical manipulations.

2 Materials

2.1 Equipment

Rotary evaporator (model RE-5299) was purchased from Shanghai Yarong Biochemical Instrument Factory (Shanghai, China). HP1100 HPLC system was purchased from Agilent Technologies, Inc. (Santa Clara, CA, USA). TE-2000U inversed microscope and accessories were purchased from Nikon Corporation (Tokyo, Japan).

2.2 Reagents

Natural soybean phospholipid mixture (lot. P5638, phosphatidylcholine (PC) content 14–23 %, linoleic acid content 59 %), β-carotene (lot. C9750, >93 %), and rutin (lot. R5143, >94 %) were purchased from Sigma Aldrich (St. Louis, MO, USA).

Chlorophyll *a* (Chl*a*) was extracted from fresh spinach leaves and separated using HPLC. Octadecyl silica column was used and the eluent was pure HPLC grade methanol.

100 μL of PC (0.10 M chloroform solution) was added to a 100-mL round bottom flask containing 4.9 mL chloroform and 750 μL methanol.

β-Carotene (1.0×10^{-4} M chloroform solution) and/or rutin (1.0×10^{-4} M methanol solution) used as antioxidants and Chl*a* (1.0×10^{-5} M methanol solution) used as photosensitizer were added to the flask as needed. The final concentration ratio: [PC]:[Chl*a*] = 1,500:1, [PC]:[antioxidant] = 500:1. The volume ratio of methanol and chloroform was kept 1:6.7.

35 mL of phosphate buffer solution (PBS: 0.010 M, pH 7.4) was slowly added along the flask wall. The mixture was rotary-evaporated under 20 °C and 0.010 MPa and reduced light for 2 min, yielding approximately 33 mL of opalescent GUV suspension.

3 Methods

3.1 Classic Methods

Liposomes containing lipid soluble radical initiators and/or antioxidants are prepared by lipid film rehydration with PBS containing water-soluble radical initiators and/or antioxidants. Small unilamellar vesicles (SUV) are prepared by extrusion using hydrophilic filter membranes. The suspension is thermostated under the decomposition temperature of the radical initiator used.

Azo compounds or Fenton reagents are commonly used as radical initiators. The initially formed hydroperoxides by peroxidation of polyunsaturated fatty acid moieties rearrange to form carbonylized conjugated diene with characteristic absorption at 234 nm. The peroxidation process of lipid can be followed by monitoring absorbance at 234 nm. This protocol was first published in ref. [31].

The lipoxidation process can also be followed by using of fluorescence probes. C11-BIDOPY and 6C-Fl are commonly used as fluorescence probes with characteristic emission at around 600 nm and 520 nm, respectively. The lipoxidation process can be followed by monitoring the decay of the fluorescence emission intensity. This protocol was published in refs. [32] and [33].

3.2 New Method

1. Evaluation of antilipoxidation activities of exogenic natural antioxidants at the single liposome level using fluorescence microscopy and digital image processing.

   This section describes in detail how to trace the photo-induced liposome budding process on the basis of heterogeneity analysis of microscopic images of individual GUVs. The experimental setup for inversed fluorescence microscopy, the acquisition of GUV images, the selection of region of interest (ROI), the mathematical image processing methods as well as any possible factor that affects the image quality are discussed below.

   Briefly, GUVs with typical diameters of 5–25 μm were prepared using reversed-phase evaporation method (*see*

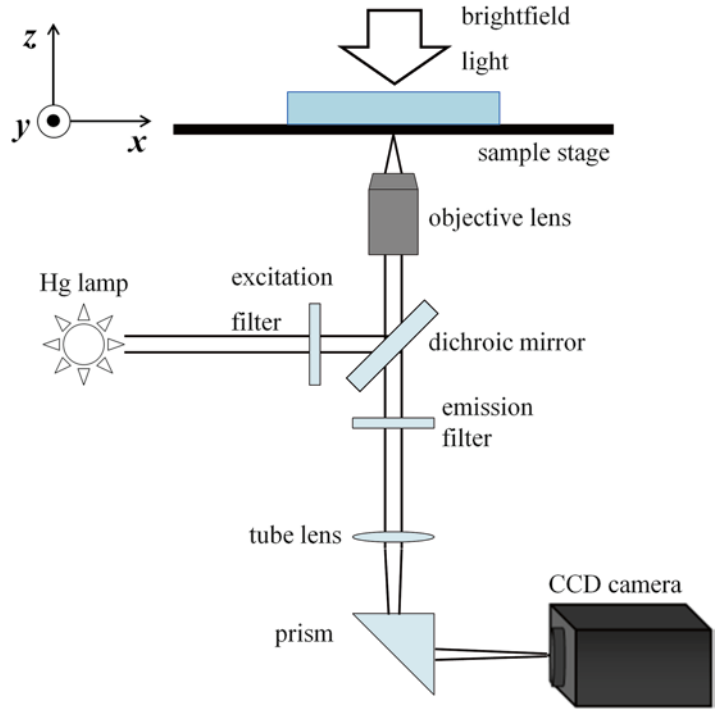

Fig. 1 Experimental setup for inversed fluorescence microscopy and digital image acquisition. Excitation wavelength range was selected by using a dichroic mirror combined with a long-pass filter. Digital images of fluorescently labeled GUVs were collected by the CCD detector

Subheading 2 and **Note 1** for details). Each 200 μL of GUV suspension (approximately 3.0×10^{-4} M) containing 1/1,500 molar fraction of photosensitizer (Chl*a*) and/or 1/500 molar fraction of antioxidants was transferred to a well of a Costar cell culturing cluster and was stabilized (adsorbed) for 2 min (*see* **Note 2**). Any operation was performed under reduced light in order to minimize undesired photodegradation.

2. The experimental setup of inversed fluorescence microscopy is shown in Fig. 1 (*see* **Note 3**). The cell culturing cluster holding the specimen was placed on the transitional stage of a Nikon TE-2000U inversed microscopy (Nikon Corporation, Tokyo, Japan) equipped with a 40× magnifying objective lens (numerical aperture 0.6, Nikon CFI Plan Fluor. ELWD). A tungsten lamp and an ultrahigh pressure mercury lamp were used as light sources for brightfield and fluorescence imaging, respectively. A 400–440 nm radiation from the mercury lamp with approximately 13 mW power was obtained by the use of a dichroic mirror combined with a band-pass filter and was focused on an area of 0.3 mm^2 on the sample to excite the Soret band of the photosensitizer (Chl*a*) (*see* **Notes 4** and **5**).

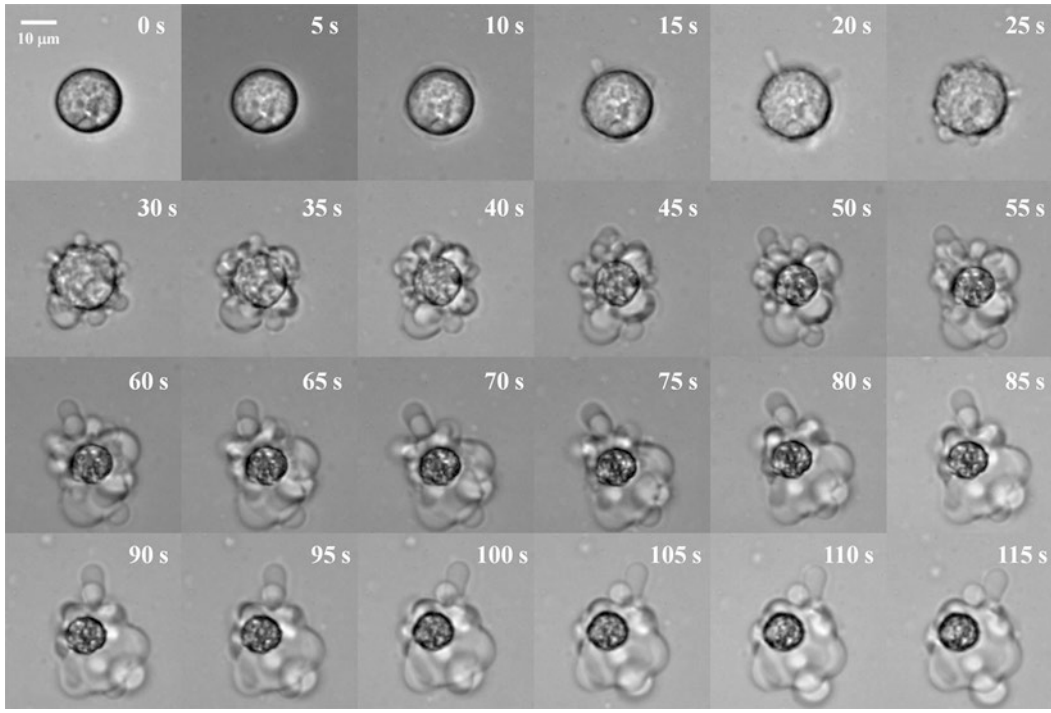

Fig. 2 Example of lateral budding of fluorescently labeled GUVs containing Chl*a* as photosensitizer ([PC]:[Chl*a*] = 1,500:1) under intense 400–440 nm radiation (15 mW/mm^2) for up to 2 min. Images were taken for every 5 s

3. Digital images were detected by a semiconductor-cooled (−70 °C) CCD (Cascade II 512, Photometrics Inc., Tucson, AZ, USA) with a resolution of 512 by 512 pixels and collected by using MetaMorph 7.0 package (Molecular Devices Inc., Sunnyvale, CA, USA).

   GUV images were collected for every 5 s before and after radiation (*see* Fig. 2 for example), with the negative-delaytime data points used as baseline. Each GUV suspension preparation was measured repeatedly for 24 times, taking advantage of the 24-well cell culturing cluster (*see* **Note 6**). GUV preparations without photosensitizer or antioxidants added were used as blank samples whereas those with photosensitizer but without antioxidants added were used as control.

4. The raw images acquired using the CCD have a dimensional resolution of 512 by 512 pixels and an intensity resolution of 16 bit. For each raw image, an area of 192 by 192 pixels containing the GUV image was selected as the region of interest (ROI). Heterogeneity analysis of the ROI was performed on the basis of Gonzalez's methods [28]. Briefly, the 16-bit intensity interval was divided into 256 bins (subintervals) by default, and the histogram counts (intensity distribution of the pixels

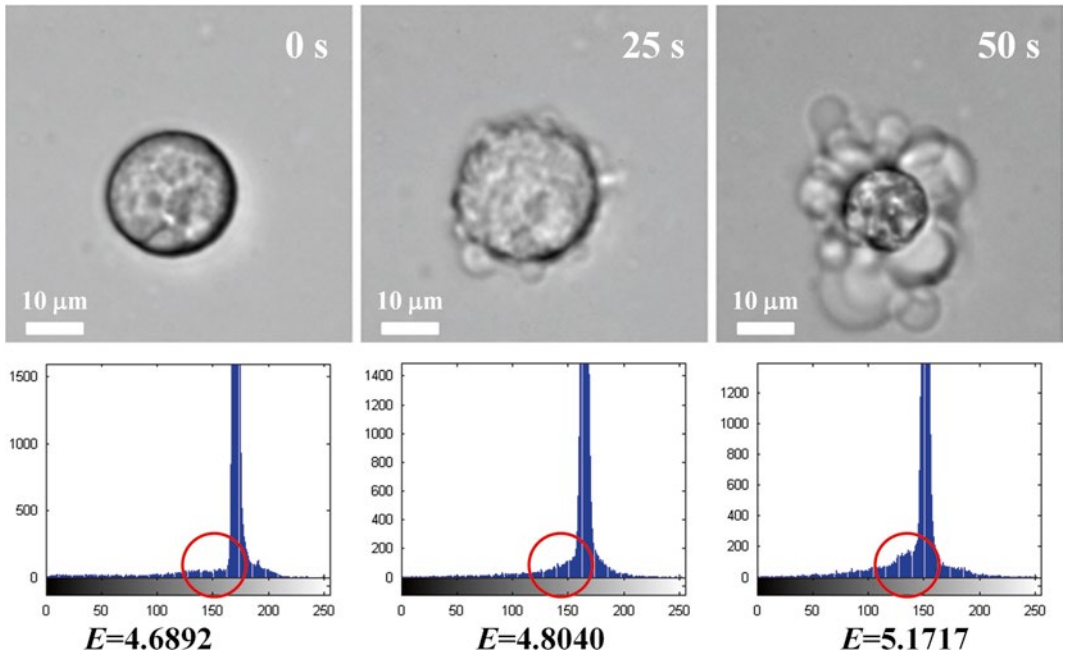

Fig. 3 Fluorescently labeled GUV ([PC]:[Chl*a*] = 1,500:1) morphologies at different irradiation times (*upper row*). Histograms of intensity distribution for each digital image are shown in *lower row*. Broadening of pixel intensity distribution in the histograms is highlighted in *circles*. The entropy of each digital image increases during the budding process

of the ROI) over the intensity subintervals were determined as the number of pixels in the ROI whose intensity (brightness) belong to the related intensity subinterval.

On the basis of the histogram (*see* Fig. 3 for example) counts over a series of subintervals, a dimensionless statistical variable, entropy (E) was defined by Gonzalez et al. [28] as

$$E = -\sum p \log_2 p$$

where p is the histogram count (number of pixels) for each intensity subinterval. Entropy is scalar, statistical measurement of image heterogeneity (randomness of intensity distribution) which is used to characterize boundary or texture of digital images.

5. For each experimental specimen, the image entropy was plotted against delay time, as is shown in Fig. 4. Certain parameters can be used to characterize the rate of liposome morphology change, such as the slopes for the initial stage on the E-t plots, or the lag phases determined as the intersect of the tangent and the time axis.

   Because the protocol is based on the morphology (change) of individual GUVs, the heterogeneity in GUV shape can be

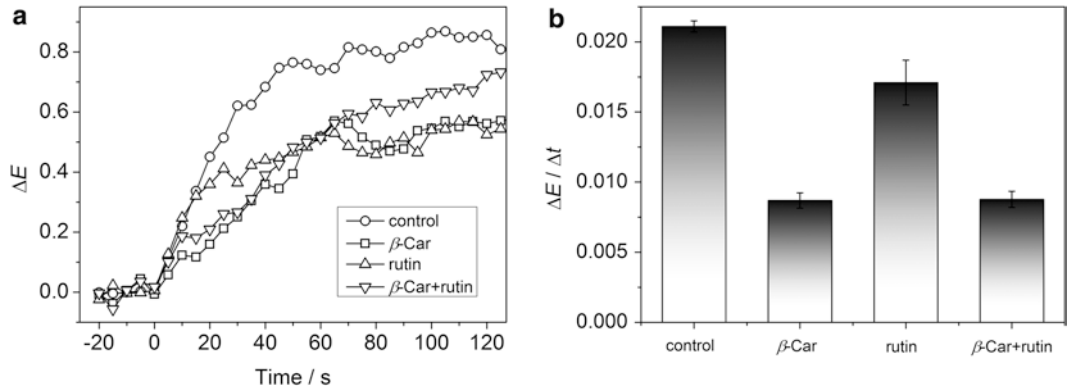

Fig. 4 (**a**) Entropy–time evaluation curves of different GUV preparations. Statistics: mean ± SD, $n = 16$. The experimental data were from ref. [30], and error bars were not shown. (**b**) The entropy change rate for each GUV preparation during the initial budding processes (0–30 s) as determined by linear regression

intuitively seen. However, this protocol has its own limitations, and improvements and refinements are needed, which could be our further study subjects (*see* **Notes 7** and **8**).

4 Notes

1. When the reverse-phase evaporation method is used for GUV preparation, chloroform and methanol are commonly chosen as the solvents, and are used to dissolve lipophilic and hydrophilic materials (lipids, photosensitizers or other radical initiators, antioxidants, etc.), respectively. The average size of GUVs is correlated to the volume ratio of the solvents. During the rotary evaporation process, the solvents should be removed completely but slowly, since GUVs are self-organized by lipid molecules in aqueous environment.
2. The GUV suspension obtained from reverse-phase evaporation is ready for microscopic observation, with or without a period of incubation, which allows further self-organization of lipid molecules and redistribution of additives. It is also worthy to notice that the addition of long-chain or rigid molecules (e.g., carotenoids or steroids), as well as any potential surfactants (amphiphilic molecules) would have significant effects on membrane properties (stability, fluidity, etc.).
3. The main advantage of the microscopy based photo-initiated GUV oxidation protocol include that such antioxidant activity evaluation is based on individual GUVs which are intuitively visualized using optical microscopes. The experiment can be carried out with basic apparatus. In classical protocols primarily based on spectrophotometric methods, the liposome preparations were required to be nearly transparent, which requires

lipid film rehydration (sonication) and further extrusion using filter membranes with large energy injection. When the classical methods require thermal radical initiation (by using azo radical initiators or Fenton reagents), such energy injection in sample preparation would have possibly triggered the reaction, making results less reliable.

4. Before initiating the liposome oxidation using the radiation from a mercury lamp, locating a target liposome using brightfield microscopy is needed. The brightfield illumination from a tungsten lamp is also used for background illumination during the whole experiment process. If chlorophylls are used as the photosensitizer (as used in our first study), the radiation from the brightfield illumination can still excite the redder absorption bands of chlorophylls, although the radiation intensity was lower than the mercury lamp, as well as the photoexcitation quantum efficiency. Therefore, the time used to find and locate a target liposome (with suitable shape and size) should be minimized.
5. Certain commonly used photosensitizers (e.g., chlorophylls or riboflavin) also emit fluorescence upon excitation. Although the sensitizers are often quickly degraded by the singlet oxygen generated by themselves, and the fluorescence intensity decayed as the quick degradation, the presence of any fluorescence significantly affect the results of digital image processing, since there is a large brightness contrast inside and outside the GUVs, given that the sensitizers are selectively distributed in the lipid phase or the aqueous phase, depending on the polarity of the sensitizers. Therefore, those sensitizers with lower fluorescence quantum yield are preferable.
6. Because the randomness of GUV morphology and budding behavior, a large number of repeated experiments (for each specimen) is essential of obtaining reliable results. Also, the long error bars on a mean ± SD statistical plotting are reasonable, which originates from the randomness mentioned above. But in most situations, this microscopy based method is still less time consuming than the classical methods using thermal radical initiation and spectrophotometric or fluorescence measurements.
7. Typically, the objective lenses used in optical microscopy experimental setups have shallow field depths, approximately 1 μm or even shallower, which are much less than the diameters of GUVs (typically >5 μm). During the experiment process, the objective lens is generally kept focused on the central intersection of GUVs precisely, in order to make the images as sharp as possible. However, Brownian motions of GUVs can significantly affect the precision of focusing. Furthermore, budding (domain formation) might occur everywhere on the surface of GUVs, and therefore the buds (domains) of GUVs

are generally blurred. The unsharpness of GUV budding images, mainly caused by Brownian motion and randomness of budding behavior, can significantly affect the results of the heterogeneity analysis, resulting in the presence of long error bars on the statistical plotting. Therefore, a large number of repeated measurements are essential of obtaining reliable results, which, however, could be easily automated.

8. The heterogeneity analysis method we have used for the protocol, i.e., the entropy, has its own limitations and can be further improved. The term entropy, as defined by Gonzalez et al. [28], is a statistical, scalar measurement of the randomness of intensity (brightness), but is based on the counts of pixels belonging to certain intensity subintervals in the ROI. The capability of texture or border recognition is desirable, and this can be the subjects of further studies.

Acknowledgements

This work has been supported by the Natural Science Foundation of China (20803091). L.H.S. is grateful for support from the Danish Research Council for Technology and Production as the grant 09-065906/FTP: Redox communication in the digestive tract.

References

1. Halliwell B (2007) Oxidative stress and cancer: have we moved forward? Biochem J 401:1–11
2. Singh N, Dhalla AK, Seneviratne C, Singal PK (1995) Oxidative stress and heart failure. Mol Cell Biochem 147:77–81
3. Amer J, Ghoti H, Rachmilewitz E, Koren A, Levin C, Fibach E (2006) Red blood cells, platelets, and polymorphonuclear neutrophils of patients with sickle cell disease exhibit oxidative stress that can be ameliorated by antioxidants. Br J Haematol 132:108–113
4. Bangham AD, Horne RW (1964) Negative staining of phospholipids and their structural modifications by surface-active agents as observed in the electron microscope. J Mol Biol 8:660–668
5. Bangham AD, Horne RW, Glauert AM, Dingle JT, Lucy JA (1962) Action of saponin on biological cell membranes. Nature 196:952–955
6. Horne RW, Bangham AD, Whittaker VP (1963) Negatively stained lipoprotein membranes. Nature 200:1340–1340
7. Reeves JP, Dowben MW (1969) Formation and properties of thin-walled phospholipid vesicles. J Cell Physiol 73:49–60
8. Angelova MI, Soléau S, Meléard P, Faucon JF, Bothorel P (1992) Preparation of giant vesicles by external AC fields. Kinetics and application. Progr Colloid Polymer Sci 89:127–131
9. Angelova MI, Dimitrov DS (1986) Liposome electroformation. Faraday Discuss Chem Soc 81:303–311
10. Torchilin VP (2006) Multifunctional nanocarriers. Adv Drug Deliv Rev 58:1532–1555
11. Dutta D, Pulsipher A, Luo W, Mak H, Yousaf MN (2011) Engineering cell surfaces via liposome fusion. Bioconjug Chem 22:2423–2433
12. Dutta D, Pulsipher A, Luo W, Yousaf MN (2011) Synthetic chemoselective rewiring of cell structures: generation of three-dimensional tissue structures. J Am Chem Soc 133:8704–8713
13. Hernandez VA, Karlsson G, Edwards K (2011) Intrinsic heterogeneity in liposome suspensions caused by the dynamic spontaneous formation

of hydrophobic active site in lipid membranes. Langmuir 27:4873–4883

14. Menger FM, Gabrielson KD (1995) Cytomimetic organic chemistry: early developments. Angew Chem Int Ed Engl 34: 2091–2106
15. Menger FM, Keiper JS (1998) Chemistry and physics of giant vesicles as biomembrane models. Curr Opin Chem Biol 2:726–732
16. Menger FM, Azov VA (2000) Cytomimetic modeling in which one phospholipid liposome chemically attacks another. J Am Chem Soc 122:6492–6493
17. Bagatolli LA (2006) To see or not to see: lateral organization of biological membranes and fluorescence microscopy. Biochim Biophys Acta 1758:1541–1556
18. Stottrup BL, Nguyen AH, Tüzel E (2010) Taking another look with fluorescence microscopy: image processing techniques in Langmuir monolayers for the twenty-first century. Biochim Biophys Acta 1798:1289–1300
19. Morales-Penningston NF, Wu J, Farkas ER, Goh SL, Konyakhina TM, Zheng JY, Webb WW, Feigenson GW (2010) GUV preparation and imaging: minimizing artifacts. Biochim Biophys Acta 1798:1324–1332
20. Haverstick DM, Glaster M (1987) Visualization of Ca^{2+}-induced phospholipid domains. Proc Natl Acad Sci U S A 84:4475–4479
21. Haverstick DM, Glaster M (1988) Visualization of domain formation in the inner and outer leaflets of a phospholipid bilayer. J Cell Biol 106:1885–1892
22. Zhao J, Wu J, Shao H, Kong F, Jain N, Hunt G, Feigenson G (2007) Phase studies of model biomembranes: macroscopic coexistence of $L\alpha + L\beta$, with light-induced coexistence of $L\alpha + Lo$ phases. Biochim Biophys Acta 1768: 2777–2786
23. Heuvingh J, Bonneau S (2009) Asymmetric oxidation of giant vesicles triggers curvature-associated shape transition and permeabilization. Biophys J 97:2904–2912
24. Ayuyan AG, Cohen FS (2006) Lipid peroxides promote large rifts: effects of excitation of probes in fluorescence microscopy and electrochemical reactions during vesicle formation. Biophys J 91:2172–2183
25. Ishii K, Hamada T, Hatakeyama M, Sugimoto R, Nagasaki T, Takagi M (2009) Reversible control of *exo*- and *endo*-budding transitions in a photosensitive lipid membrane. Chembiochem 10:251–256
26. Choe E, Min DB (2006) Chemistry and reactions of reactive oxygen species in foods. Crit Rev Food Sci Nutr 46:1–22
27. Farge E, Devaux PF (1992) Shape changes of giant liposomes induced by an asymmetric transmembrane distribution of phospholipids. Biophys J 61:347–357
28. Gonzalez RC, Woods RE, Eddins SL (2003) Digital image processing using MATLAB. Prentice Hall, New Jersey, Chapter 11, pp 426–483
29. Moscho A, Orwar O, Chiu DT, Modi BP, Zare RN (1996) Rapid preparation of giant unilamellar vesicles. Proc Natl Acad Sci U S A 93:11443–11447
30. Liang R, Liu Y, Fu LM, Ai XC, Zhang JP, Skibsted LH (2012) Antioxidants and physical integrity of lipid bilayers under oxidative stress. J Agric Food Chem 60:10331–10336
31. Klein RA (1970) The detection of oxidation in liposome preparations. Biochim Biophys Acta 210:486–489
32. Naguib YMA (1998) A fluorometric method for measurement of peroxyl radical scavenging activities of lipophilic antioxidants. Anal Biochem 265:290–298
33. Naguib YMA (2000) A fluorometric method for measurement of oxygen radical-scavenging activity of water-soluble antioxidants. Anal Biochem 284:93–98

Chapter 10

Electrochemical Detection of Glutathione S-Transferase: An Important Enzyme in the Cell Protective Mechanism Against Oxidative Stress

Manuel C. Martos-Maldonado, Juan M. Casas-Solvas, Antonio Vargas-Berenguel, and Luis García-Fuentes

Abstract

Oxidative stress arises when the antioxidant capacity of cells to clean the excess production of reactive oxygen species (ROS) decreases. Several human diseases seem to be related with an increment in the oxidative stress. In this regard, GSH present in the cells works by neutralizing ROS and other xenobiotics through the glutathione S-transferase (GST) enzyme. Thus, the level of expression of GST is an important factor in determining the sensitivity of cells to toxic chemicals or xenobiotic compounds. Therefore, the detection of GST levels is fundamental in the clinical diagnosis of ROS-related diseases. Here, we describe a methodology, based on the voltammetric properties of the ferrocene group (used as electrochemical probe), which can be applied for selective detection of GST levels in human cells. The electrochemical signal measured is associated to the specific interaction of a ferrocenyl-GSH derivate with the G- and H-sites of this enzyme.

Key words Ferrocene–glutathione conjugates, Binding, Voltammetry, Electrochemical sensors, Glutathione S-transferase

1 Introduction

Xenobiotic compounds of exogenous and endogenous origin are a substantial threat to human cells as they lead to the production of damaging highly reactive oxygen species such as superoxide anions, hydroxyl radicals, and hydrogen peroxide. These reactive oxygen species (ROS) are physiologically produced in the cell through molecular oxygen reduction to water during aerobic metabolism and indiscriminately interact with essential macromolecules such as DNA, proteins and lipids, leading to the disturbance of physiological processes. Thus, excess production or inadequate elimination of ROS lead to increased oxidative stress (OS), which seems linked to the development of some human diseases such as cardiovascular

Donald Armstrong (ed.), *Advanced Protocols in Oxidative Stress III*, Methods in Molecular Biology, vol. 1208,
DOI 10.1007/978-1-4939-1441-8_10,

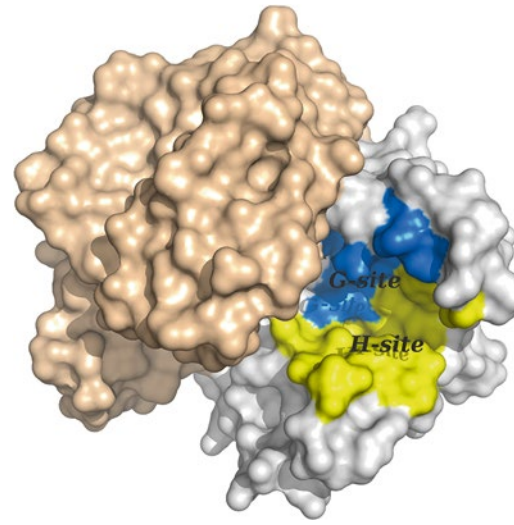

Fig. 1 Overview of homodimeric structure of human GST P1-1 from PDB entry 11GS. The subunits are shown as surfaces. The functional active site in a subunit (G- and H-site) has been enlarged for easy viewing

and respiratory diseases, cancer and inflammation-related diseases [1, 2]. The glutathione S-transferases (GSTs; EC 2.5.1.18) represent a major group of detoxification enzymes with a broad substrate specificity. All eukaryotic species possess multiple cytosolic and membrane-bound GST isoenzymes, each of which displays distinct catalytic as well as noncatalytic binding properties: the cytosolic enzymes are encoded by at least eight distantly related gene families (named as class alpha, beta, delta, mu, pi, sigma, zeta, and theta GST), whereas the membrane-bound enzymes, microsomal GST and leukotriene C_4 synthetase, are encoded by single genes and both have arisen separately from the soluble GST.

Most GSTs exist as dimeric proteins (heterodimers and homodimers) of approximately 25 kDa/subunit. Each subunit has an active site composed of two distinct functional regions: a hydrophilic G-site, which binds the physiological substrate glutathione, and an adjacent H-site which provides a hydrophobic environment for the binding of structurally diverse electrophilic substrates (Fig. 1) [3]. The G-site is highly conserved between all GSTs due to its high specificity for GSH, whereas the H-site can be quite divergent between different GSTs, and exhibits a broad and variable substrate binding specificity. Evidence suggests that the level of expression of GST is a crucial factor in determining the sensitivity of cells to a broad spectrum of toxic chemicals or xenobiotic compounds. It also appears probable that GST are regulated in vivo by reactive oxygen species (ROS), due to the fact that not only are some of the most potent inducers capable of generating free radicals by redox-cycling, but H_2O_2 has been shown to induce GST in plant and mammalian cells. Thus, induction of GST by ROS would

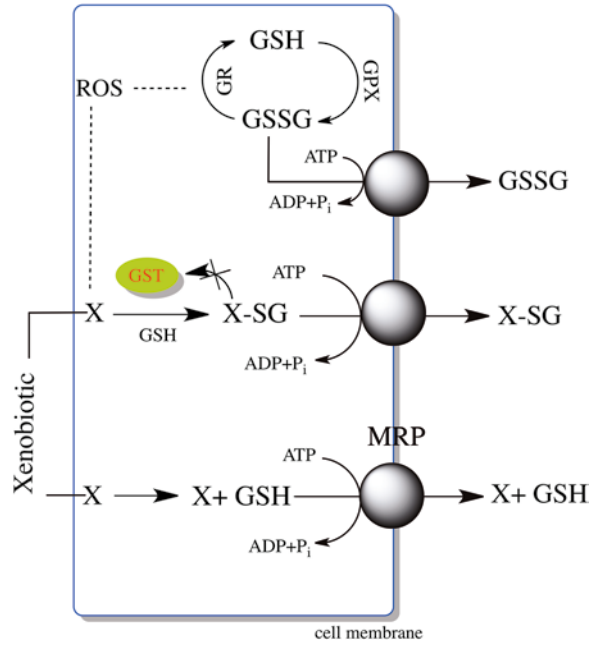

Fig. 2 Coordinate interaction between cellular GSH, glutathione S-transferase (GST) and glutathione S-conjugate efflux pump MRP. *ROS* reactive oxygen species, *GSSG* oxidized glutathione, *GPX* glutathione peroxidase, *GR* glutathione reductase, *GS-X* glutathione conjugate of X, *MRP* multidrug resistance associated protein

appear to represent an adaptive response as these enzymes detoxify some of the toxic carbonyl-, peroxide-, and epoxide-containing metabolites produced within the cell by oxidative stress [3–5]. The cells produce numerous antioxidants that counter the effects of these compounds by reducing their accumulation.

Glutathione (GSH) is an important antioxidant that protects against cellular damage caused by environmental toxins as well as from ROS-mediated injury. GSH works by neutralizing ROS and xenobiotics with the help of GST (Fig. 2); this enzyme catalyzes the conjugation of GSH to electrophilic substrates, producing compounds that are generally less reactive and more soluble [4]. This facilitates their removal from the cell via membrane-based glutathione conjugate pumps. The prevalence of GSTs, together with the evidence suggesting their importance in bioactivation and detoxification of cytotoxic and genotoxic compounds, has stimulated much research into the potential role of these enzymes in diseases. There is also substantial interest in the regulation of cellular GST activity as increased expression of GSTs in tumor cells is frequently associated with multidrug resistance [4, 6]. All these properties enhance the importance of these enzymes in the cellular metabolism, which could be used as biomarkers.

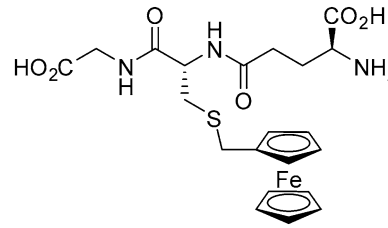

Fig. 3 Ferrocene–S-glutathione (GSFc) conjugate chemical structure

Ferrocene (Fc) is a metallocene which has attracted special attention in medicinal research since it is a neutral, chemically stable and nontoxic molecule with excellent voltammetric properties. Fc undergoes a fast and reversible or quasi-reversible one-electron oxidation at potentials which depend on the nature of the substituents attached to the cyclopentadienyl rings. Thus, Fc derivatives have found applications in different areas such as biosensors, drug research, electrocatalysis, and optoelectronics, among others [7]. Voltammetric techniques, which are simple, sensitive, and suitable for real time monitoring of chemical and biological reactions, cannot be directly used to examine the GST–GSH interactions due to the fact that GSH does not show discernible voltammetric signals. A frequent approach to study non-electroactive binding pairs by electrochemical methods is to conjugate the ligands with redox label. Following this strategy, we linked a Fc group to GSH. The resulting ferrocene–S-glutathione (GSFc) conjugate (Fig. 3) showed good redox properties and turned out to bind the enzyme stronger than native GSH itself [8, 9]. The detected electrochemical signal is associated to the specific interaction of GS- and Fc-moieties with the enzyme G- and H- sites, respectively. Such features make this GSFc conjugate an excellent candidate to be used as a redox probe for the specific detection of GST.

In this chapter, we describe a methodology for the selective detection of GST by using GSFc conjugate as electrochemical sensor in Differential Pulse Voltammetry (DPV) experiments.

2 Materials

2.1 Equipment

2.1.1 Voltammetric Experiments

1. Electrochemical measurements were carried out on a Metrohm μAutolab III potentiostat connected to an Intel Pentium Dual 2.4 GHz CPU personal computer running Eco Chimie B. V. GPES 4.9 software under Windows XP (*see* **Note 1**).
2. An electrode tip bearing a 3 mm diameter glassy carbon disk (Metrohm ref. 6.1204.300) was used as working electrode (*see* **Note 2**). Such electrode tip was fitted to an electrode shaft (Metrohm ref. 6.1241.060) through a contact pin M4/2 mm (Metrohm ref. 6.2103.120). This electrode was carefully

cleaned prior each measurement as described in Subheading 3.1. Its electrochemical effective area was determined as described in Subheading 3.2.

3. A Radiometer type P101 6×4 mm platinum sheet electrode provided with a 14/12 mm sleeve (Metrohm ref. 6.1236.020) was used as counter (or auxiliary) electrode (*see* **Notes 3–5**). This electrode was carefully cleaned prior to each measurement as described in Subheading 3.1.
4. A Ag/AgCl electrode (Metrohm ref. 6.0724.140) fitted into an electrolyte vessel with 3 mm diameter PTFE capillary and ceramic diaphragm (Metrohm ref. 6.1240.000) filled with Crison electrolyte solution Crisolyt (3 M KCl) was used as reference electrode (*see* **Notes 6** and 7).
5. Working, counter and reference electrodes were fitted into a 1–50 mL titration vessel (Metrohm ref. 6.1415.110) equipped with a mounting ring (Metrohm ref. 6.2036.000), a lid with 5 openings (Metrohm ref. 6.1414.010), and a gas inlet and overflow tube with valve (Metrohm ref. 6.1440.010) (*see* **Note 8**). Titration vessel was placed on a magnetic swing-out stirrer (Metrohm ref. 2.728.0034) and provided with an 8 mm stirring bar (Metrohm ref. 6.1903.000).
6. It is advisable to equip the titration vessel with a Faraday cage to prevent and diminish any electromagnetic noise (*see* **Note 9**).

2.2 Reagents and Chemicals

2.2.1 GSFc Preparation

1. GSFc conjugate (MW: 505.37 Da) was synthesized from reduced glutathione (GSH) and (hydroxymethyl)ferrocene as published in [9] (*see* **Note 10**). Reduced GSH, (hydroxymethyl)ferrocene and trifluoroacetic acid were purchased from Sigma-Aldrich and used without further purification.
2. A 500 μM stock solution of GSFc was prepared in 10 mM phosphate buffer, 20 mM NaCl, pH 7.2 (*see* **Note 11**).

2.2.2 GST Enzyme Preparation

1. Recombinant glutathione S-transferase (GST) was expressed and purified as reported elsewhere [10] to obtain a solution in 100 mM sodium phosphate, 0.1 mM EDTA, pH 7.0 (*see* **Note 12**). Protein concentration was measured spectrophotometrically at λ 278 nm using a molar extinction coefficient of 7.01×10^4 M^{-1} cm^{-1} for the dimer. Such solution was divided into 1 mL aliquots and stored as frozen at –80 °C (*see* **Note 13**).
2. Several fractions of the purified GST were unfrozen, joined and concentrated to ~150 μM by ultrafiltration in a centriprep-30K device from Millipore (Bedford, USA).
3. The concentrated enzyme was dialyzed twice by using pretreated dialysis membranes Spectra/Por 4 (Spectrum Labs, Inc.) at 4 °C against 10 mM phosphate buffer, 20 mM NaCl,

pH 7.2. Protein concentration of the resulting stock solution was measured as indicated above (*see* **Note 11**).

4. GST activity was measured on the dialyzed stock solution before using the enzyme in the electrochemical experiments according to Habig and Jakoby [11] (*see* **Note 14**).

3 Methods

3.1 Working and Counter Electrodes Cleaning Processes

This section described a standard protocol to clean working and counter electrodes. This step is pivotal and must be performed prior to each electrochemical experiment. Many substances are able to adsorb on electrodes, especially when glassy carbon electrodes are used as working electrodes. Any traces result in noticeable variations of the electrochemical signal, making measurements irreproducible.

1. Working glassy carbon disk electrode was first immersed in a 0.1 M HNO_3 solution for 5 min at room temperature under stirring and then rinsed with Milli-Q water.
2. Working electrode was then polished using a suitable polishing kit (Metrohm ref. 6.2802.000). Adhesive polishing cloth was stuck in a petri dish (*see* **Note 15**) and a small amount of aluminum oxide powder (grain size 0.3 μm) was placed on top and soaked with Milli-Q water to form an Al_2O_3–water slurry. The slurry was spread on the polishing cloth and the electrode surface was polished by describing fast ∞-shaped movements for 3 min. The electrode was finally exhaustively rinsed with Milli-Q water.
3. Platinum sheet counter electrode was immersed in a 50 % v/v H_2SO_4 solution at room temperature for 5 min under stirring and then rinsed with Milli-Q water.
4. Both cleaned working and counter electrodes were finally sonicated in a 1:1:1 H_2O–MeOH–CH_3CN mixture for 5 min (*see* **Note 16**).

3.2 Working Electrode Effective Area Determination

This section describes how to determinate the electrochemical effective area of the glassy carbon disk electrode [12]. Effective area of an electrode usually does not match the theoretical area which can be mathematically calculated from its geometry. Thus, the effective area of any new electrode must be determined before the first use as follows. Cyclic voltammetry (CV) experiments are used in this aim (*see* **Notes 17** and **18**). Electrodes and vessel must be cleaned before each experiment.

1. A 1 mM $Na_4Fe(CN)_6$ ($D_0 = 0.65 \times 10^{-5}$ cm^2 s^{-1}) solution containing 100 mM KCl as supporting electrolyte (*see* **Note 19**) was prepared as electroactive probe (*see* **Note 11**).

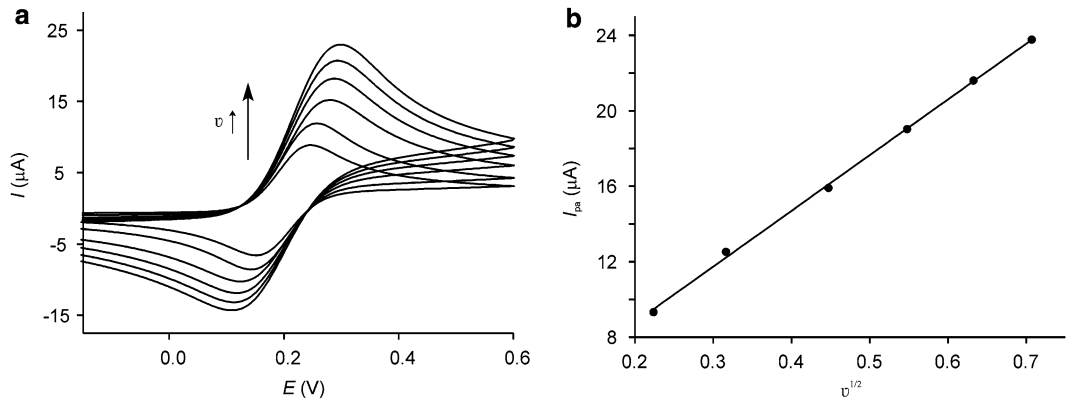

Fig. 4 (**a**) Partial cyclic voltammograms (5 scans) measured between −0.5 V and +0.6 V for 1 mM $Na_4Fe(CN)_6$ solution containing 100 mM KCl as supporting electrolyte after subtracting blank (100 mM KCl) signal at increasing scan rates (υ) from 0.05 to 0.5 V/s. An increase in the peak currents (*large arrow*) was observed as υ raised (*small arrow*). (**b**) Oxidation peak current (I_{pa}) data plotted versus $\upsilon^{1/2}$. *Solid line*: data were fitted to Randles–Ševčik equation (1) (*see* **Note 17**) in order to estimate effective area (*A*) of the working glassy carbon disk (3 mm diameter) electrode ($A = 0.038 \pm 0.006$ cm^2 in average after three measurements)

2. A 100 mM KCl solution was prepared as blank (*see* **Note 11**).
3. Blank solution (2.5 mL) was placed in the titration vessel and deoxygenated by bubbling N_2 under stirring for 3 min (*see* **Notes 20–22**).
4. CV experiments were recorded on the blank solution using −0.5 V as first vertex potential, +0.6 V as second vertex potential and 0.00244 V as step potential. Scan rate (υ) was varied from 0.05 to 0.5 V/s. Five scans were performed for each scan rate value (*see* **Note 23**).
5. $Na_4Fe(CN)_6$ solution (2.5 mL) was placed in the clean titration vessel and deoxygenated in the same condition as used for the blank solution.
6. CV experiments were recorded on the $Na_4Fe(CN)_6$ solution using the same parameters described in Subheading 3.2, **step 4**. According to Randles–Ševčik equation (1) (*see* **Note 17**), an increase in the oxidation peak current was observed as υ raised (Fig. 4).
7. Subheading 3.2, **steps 5** and **6** were repeated three times.
8. Blank signals were subtracted from those of $Na_4Fe(CN)_6$ for each υ value.
9. Oxidation peak current (I_{pa}) was measured from the voltammograms for each υ value.
10. Graphical plots of I_{pa} versus $(\upsilon)^{1/2}$ gave a straight line which was fitted to Randles–Ševčik equation (1) (*see* **Note 17**). Averaged effective area (A) of the electrode was calculated from the slope values obtained from each experiments set.

3.3 Electrochemical Detection of GST

This section describes how to detect GST enzyme using GSFc conjugate as electroactive probe. Differential pulse voltammetry (DPV) experiments are used in this aim (*see* **Note 24**). The following protocol allows not only the detection of the presence of the enzyme but also the characterization of the interaction process through its binding constant as described in Subheading 3.3, **step 8**. Electrodes and vessel must be exhaustively cleaned before each experiment.

1. A 500 μM GSFc stock solution was prepared in 10 mM phosphate buffer, pH 7.2, containing 20 mM NaCl as supporting electrolyte (*see* **Notes 11** and **19**).
2. A ~125 μM GST (concentration given as dimer) stock solution was prepared in the same buffer as described in Subheading 2.2, **item 2** (*see* **Notes 11** and **19**).
3. Different amounts of GSFc and GST stock solutions as well as pure buffer were mixed to prepare nine 2.5 mL samples containing 50 μM GSFc and increasing amounts of GST (from 0 to 90 μM). More concentrated GST samples might be needed depending on the GST source. Each sample was prepared prior to use mixing the stock solutions directly in the clean titration vessel.
4. Each sample solution was deoxygenated by bubbling N_2 under stirring for 3 min (*see* **Notes 20**–**22**).
5. A DPV experiment was recorded on each sample solution using −0.2 V as initial potential (E_i), +0.6 V as final potential (E_f), 0.02 V as step potential (ΔE_s), 0.05 V as modulation amplitude (ΔE_p), 2 s as interval time (τ), and 0.05 s as modulation time (t_p), which results in a scan rate (υ) of 0.01 V/s (*see* **Note 24**).
6. DPV voltammograms displayed a progressive decrease of the peak current intensity as the GST concentration increased (Fig. 5), indicating the binding interaction between the electroactive probe GSFc and the enzyme.
7. Oxidation peak current (I_p) was measured from the DPV voltammograms for each sample and plotted versus GST concentration to yield a nonlinear calibration curve for the detection of GST enzyme (Fig. 5) (*see* **Note 25**).
8. I_p data were fitted to a suitable binding model in order to estimate the corresponding binding constant K (*see* **Note 26**).
9. In order to estimate the limit of detection (LOD) for GST, first linear section of data were also fitted to a line (Fig. 5). LOD was defined as the lowest enzyme concentration which gives a signal variation on the oxidation peak equivalent to three times the standard deviation of the peak current measured for the solution of 50 μM GSFc in the absence of enzyme, that is, $\mathrm{LOD} = 3\sigma/b$; where σ is the standard deviation of the electrochemical signal for that solution (from 3 measurements) and b is the slope of the linear fitting [13].

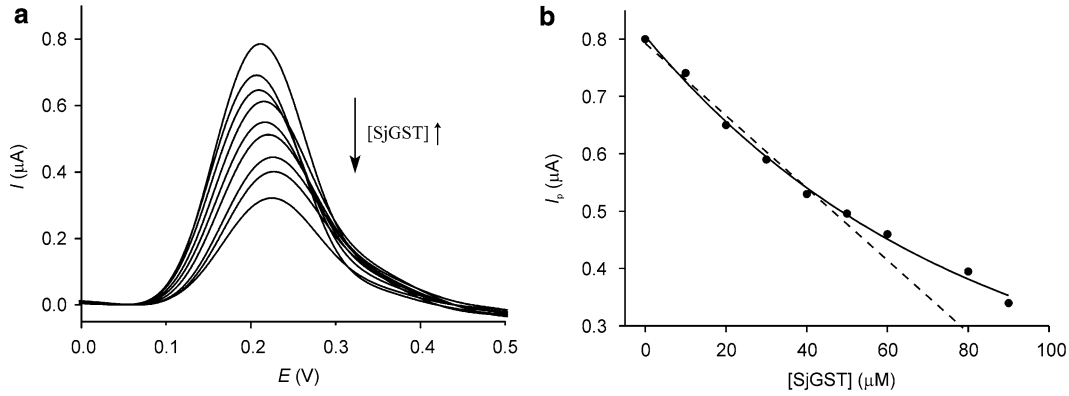

Fig. 5 (**a**) DPV curves for 50 μM GSFc in the presence of increasing amounts of *Schistosoma japonica* glutathione S-transferase (SjGST) ranging from 0 to 90 μM in 10 mM phosphate buffer, pH 7.2, containing 20 mM NaCl as supporting electrolyte. Following parameters were used: −0.2 V as initial potential (E_i), +0.6 V as final potential (E_f), 0.02 V as step potential (ΔE_s), 0.05 V as modulation amplitude (ΔE_p), 2 s as interval time (τ), and 0.05 s as modulation time (t_p), which resulted in a scan rate (υ) of 0.01 V/s. A decrease in the current intensity (*large arrow*) was observed as SjGST concentration increased (*small arrow*). (**b**) Peak current intensity (DPV) variation for GSFc oxidation versus SjGST concentration. *Solid line*: Data were fitted to a two equal and independent sites model (*see* **Note 26**) in order to estimate binding constant value ($K = (2.1 \pm 0.9) \times 10^4$ M^{-1}). *Dashed line*: The first linear section of the data was fitted to a line in order to estimate limit of detection as described in Subheading 3.3, **step 9** (LOD = 11 μM)

4 Notes

1. Metrohm μAutolab III is the most basic and affordable instrument in Autolab family, but can be used for most electrochemical techniques. Eco Chimie B. V. GPES software has recently been discontinued and replaced by the new data acquisition and analysis software package NOVA, for which the following PC configuration is recommended according with the manufacturer: Processor 2 GHz or higher, 80 Gb HDD, 2 Gb RAM, USB port, Windows XP, Vista, Windows 7, or Windows 8 (32 bit).
2. The intensity of the signal is directly proportional to the working electrode surface [14–16], and thus large working electrodes would be desirable in order to increase the sensitivity of the technique. However, it is advised to use counter electrodes larger than working ones (*see* **Note 5**), which in practice limits the size of the working electrodes that can be used. Signal intensity also increases with larger modulation amplitude (ΔE_p) (*see* **Note 24**), but larger amplitudes will also broaden the peak, lowering potential resolution. Moreover, the peaks can be distorted due to nonlinearity effects at larger amplitudes. Thus, ΔE_p value must be balanced for each particular case.

3. This electrode is no longer commercialized. Current alternative is Radiometer M241PT platinum plate electrode. Radiometer electrodes are thinner than other trademarks (7.5 mm vs. 12 mm) and thus fit better in small titration vessels such as that used in this protocol (It has to be taken into account that three electrodes and a gas inlet tube must be immersed in 2.5 mL of sample solution). However, this feature makes the electrode unable to fit in the Metrohm sleeve. The sleeve must be attached to the electrode at a suitable position in order to ensure electrode immersion is repeatable in each experiment. A drilled septum stopper, sleeve type, for 14/20-14/35 outer joints also provides a convenient performance in this aim.
4. Any convenient electrode can be used as the counter one, since its nature should have little to no effect on the electroanalytical measurement. However, it is advisable to choose inert electrodes which do not undergo electrolysis processes that would produce substances that may cause interfering reactions on the working electrode surface.
5. Many electrochemical texts recommend using a counter electrode "much larger" (*sic*) than the working electrode, so that its capacitance handles most of the current required at the reference/counter terminus [14–16]. In other words, the half-reaction occurring at the auxiliary electrode must occur fast enough so as not to limit the process at the working electrode. Otherwise, inaccuracies may arise due to the additional resistance imposed by the counter electrode, which causes an increase of the uncompensated ohmic potential drop at the working electrode. This effect may be significantly large when resistive nonaqueous media are used, but it is less important in experiments carried out in water. In addition, for most of the techniques this phenomenon can be extensively diminished in a number of ways where using a "much larger" counter electrode is not compulsory, such as setting a suitable placement for the electrodes (*see* **Note 8**) and using a high-enough concentration of supporting electrolyte (*see* **Note 19**). However, it is recommendable to employ a counter electrode reasonably bigger than the working one.
6. No bubbles must be present in the capillary tube. A Pasteur pipette should be used to fill it. Electrolyte vessel must be filled up to ensure reference electrode bulb is completely immersed in the electrolyte solution. Electrolyte level must be periodically checked and renewed.
7. When reference pack (reference electrode + electrolyte vessel) is not going to be used for a short period of time, it should be placed in a suitable beaker filled with some electrolyte solution in order to keep ceramic diaphragm and inner electrolyte solution in good conditions.
8. In order to compensate a major fraction of the cell resistance, the reference electrode should be placed as close as possible to

the working electrode [14–16]. All measurements must be carried out with the same electrodes placement and orientation.

9. External sources such as computer monitors, other instruments, or power lines generate electromagnetic fields able to interfere with the electrochemical setup, causing serious instabilities which can easily be identified due to the appearance of saw-toothed lines in the voltammograms. Commercial Faraday cages are available from a number of sources. However, a simple Faraday cage can be built by covering the titration vessel with aluminum foil connected to the grounding cable provided by the potentiostat.
10. Briefly, a solution of reduced glutathione (50 mg, 0.163 mmol) in water (2 mL) and trifluoroacetic acid (40 μL, 0.489 mmol) were added to a solution of (hydroxymethyl)ferrocene (53 mg, 0.245 mmol) in ethanol (2 mL). An excess of (hydroxymethyl) ferrocene was used in order to ensure the complete consumption of GSH and, hence, simplify the subsequent purification step. The mixture was stirred at room temperature until GSH was no longer observed by TLC (ca. 2.5 h). To follow the reaction by TLC (Merck Silica Gel $60F_{254}$ aluminum sheets) it is advisable to use $CH_3CN–H_2O$ 3:1 as eluent, where GSH exhibits $R_f = 0.3$. UV light and ethanolic sulfuric acid (5 % v/v) were used to develop TLC plates. pH was then increased to 9–10 by dropping a saturated $NaHCO_3$ aqueous solution, and the solvent was removed by rotary evaporation under vacuum. Evaporation temperature was kept below 75 °C. GSFc conjugate was finally isolated from the crude by column chromatography on silica gel using $CH_3CN–H_2O$ 5:1 as a yellow powder (86 mg, 96 %). Our experience suggests that silica gel 230–400 mesh, ASTM from Merck gives the best results in columns that use aqueous mixtures as eluents.
11. All stock solutions were always freshly prepared prior experiments using Milli-Q water (18.2 MΩcm). Stock solutions were disposed of after experiments.
12. Pure GST is also available from a number of commercial sources.
13. Purified enzyme is stable in these conditions for 3–4 months.
14. Briefly, the conjugation reaction (GSH–CDNB) was continuously recorded spectrophotometrically at λ 340 nm ($\varepsilon = 9{,}600\ M^{-1}\ cm^{-1}$) and 25 °C for 2 min on a Cary BIO 50 spectrophotometer (Varian). For the activity assay, a reaction mixture consisting in 1.5 μM GST, 1 mM GSH and 1 mM 1-chloro-2,4-dinitrobenzene (CDNB) buffered solution (final volume: 1 mL) was prepared by adding solutions of such reagents to a 0.1 M potassium phosphate buffer, pH 6.5. GST was added as an aliquot (10–20 μL) from the stock solution; volume being dependent on the concentration of that solution. GSH was added as 10 mM solution in 0.1 M potassium phosphate buffer, pH 6.5 (100 μL). CDNB was added as a freshly prepared, light-protected 20 mM ethanolic

solution (50 μL). It is assumed that the small volumes of GST and CDNB added have a negligible effect on the buffer of the reaction mixture. CDNB solution must be added the last as it marks the initiation of the reaction. One unit of GST activity was defined as the conjugation of 1 μmol of CDNB with GSH per minute at 25 °C. All GST activity assays were performed in conditions of linearity with respect to incubation time and protein concentration. Initial rate of product formed was determined from slope of the increase in absorbance per minute at λ 340 nm. These rates measured as absorbance/time were converted in concentration/time using the indicated molar absorptivity. Determined activity units were compared with the valid range for each GST source. Some commercial kits and explicative protocols for GST activity assays can also be found in the literature.

15. Petri dish provides a convenient container for the polishing cloth. It is cheap, flat, stable, easy-to-grab, and easy-to-store. Once used, aluminum oxide is wasted and the polishing cloth can be stored in the petri dish until the next use.
16. Milli-Q water and HPLC grade MeOH and CH_3CN were used. A beaker was filled up with the mixture and placed in the sonicator. The mixture may warm up during sonication. This does not affect the electrodes.
17. Briefly, cyclic voltammetry (CV) is a potential sweep method where potential is linearly varied forwards and backwards between two values (vertex potentials) with time, yielding a triangular potential waveform which causes the oxidation and subsequent reduction of the electroactive species [14–16]. The slope of the potential variation defines how fast the experiment is and is called scan rate (υ, V/s). Usually, this potential profile is repeated a number of cycles in order to reach a stationary state. Measurement of the resulting current at the working electrode during the potential scans gives a cyclic voltammogram where two curves are observed for a reversible system defined by their corresponding oxidation (or anodic) and reduction (or cathodic) peaks (Fig. 6). Each peak provides two observable, the peak potentials (E_{pa} and E_{pc} in Volts, respectively), which allow estimating the reversibility as well as formal and half-wave potentials of the system, and the peak currents (I_{pa} and I_{pc} in Amperes, respectively). For a reversible couple, the peak current is given by the Randles–Ševčik equation:

$$I_p = 0.4463\left(\frac{F^3}{RT}\right)^{1/2} n^{3/2} A C^{*} \sqrt{\upsilon D_0} \qquad (1)$$

where F is the Faraday constant (9.64853×10^4 C/mol), R is the molar gas constant (8.31447 J/mol K), T is temperature (K), n is the number of exchanged electrons, A is electrode area

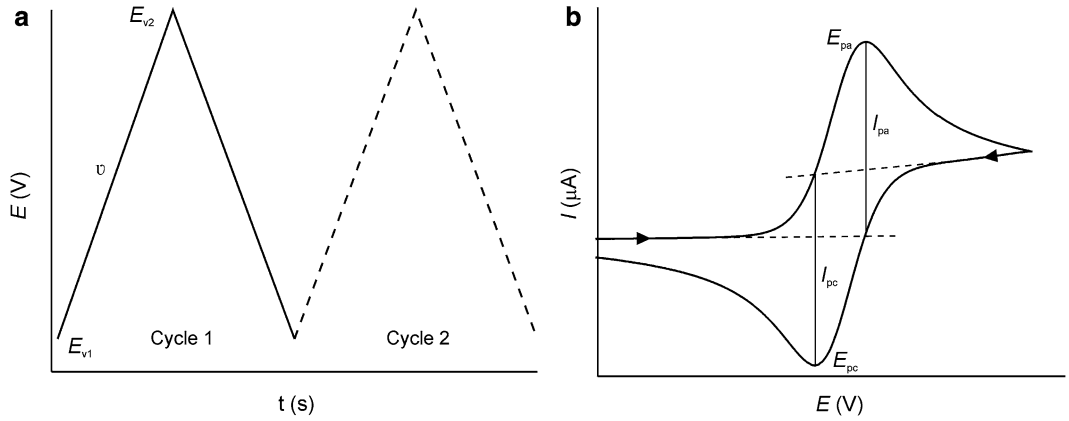

Fig. 6 (**a**) CV waveform for the oxidation of an electroactive species, where E_{v1} and E_{v2} are the vertex potential and υ (the slope of the line) is the scan rate. (**b**) Partial cyclic voltammogram for the oxidation of an electroactive species, where E_{pa} and E_{pc} are the anodic and cathodic peak potentials, respectively, and I_{pa} and I_{pc} are the anodic and cathodic peak currents, respectively

(cm^2), C^* is bulk concentration of the electroactive species (mol/cm^3), v is the scan rate (V/s), and D_0 is the diffusion coefficient (cm^2/s).

18. According to Eq. 1 (*see* **Note 17**), electrode area (A) can be calculated by measuring the peak current (I_p) at different scan rates (v) for a redox species the diffusion coefficient of which (D_0) is known.
19. Mathematical treatment for most electrochemical methods is based on the assumption that mass transport in solution is affected by a single mechanism, typically diffusion. Thus, other mass transport mechanisms such as convection and migration must be avoided. For convection suppression, sample solution must be kept completely quiet during measurement. Migration, which is the movement of ions under the influence of an electric field, is overcome by adding a large excess of an easily ionizable salt which will dissociate into inert anions and cations. These ions will be the major species affected by migration, releasing the species of interest from that effect. Such a salt is called supporting electrolyte, and must be about 100 times more concentrated that the analyte.
20. Oxygen is a redox species able to generate residual faradaic currents under certain conditions, and thus any electrochemical experiment must be performed in degassed solutions.
21. N_2 must be softly bubbled and stirring must be gentle in order to minimize foam formation, especially when any protein is present in the solution.

22. To avoid any convection effect, an equilibration time of at least 20 s should be applied after N_2 bubbling before starting measurement.
23. The characteristic peaks in a cyclic voltammogram are caused by the formation of a diffusion layer near the electrode surface which requires more than one scan to reach a stationary state. This can be seen simply comparing the voltammograms obtained after each cycle, as usually an increase in the peak currents can be observed. Strictly speaking, one should wait for the peak current to remain unchanged, but our experience suggests that after five scans peak current variations are negligible. Data must always be extracted from the last scan.
24. Briefly, differential pulse voltammetry (DPV) is a pulsed voltammetric technique where potential excitation functions are more complicated than that showed by CV (*see* **Note 17**). However, they yield much higher sensitivities (~10^{-8} M) than potential sweep methods as CV (~10^{-4} M) and thus are more adequate for analytical measurements [14–16]. DPV waveform is composed of a series of potential pulses where current is measured at two different times per pulse, before and at the end of the pulse (Fig. 7). The quantity of interest in DPV is the difference between those two values. Four parameters are needed to completely define the DPV waveform: step potential (ΔE_s), modulation amplitude (ΔE_p), interval time (τ), and modulation time (t_p). Step potential and interval time defines the scan rate (υ) as $\Delta E_s/\tau$. In addition, initial and final potentials have also to be set up. Resulting voltammograms consist

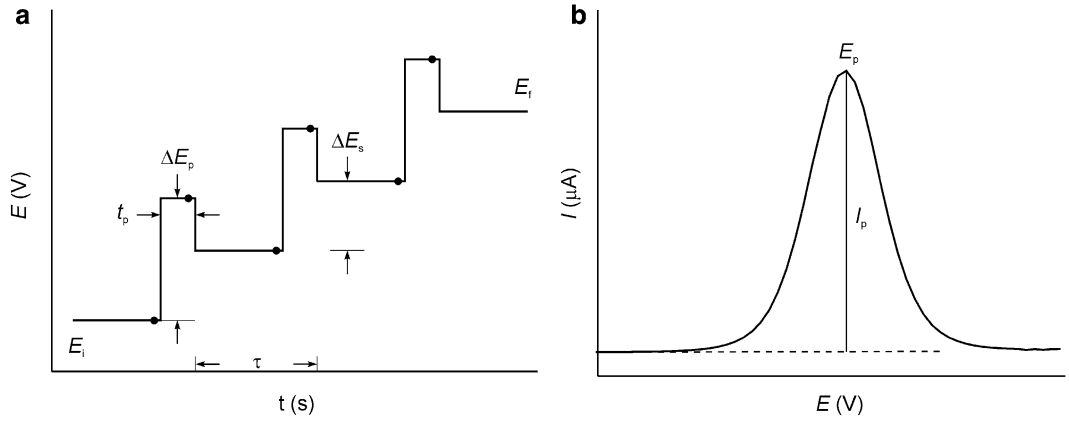

Fig. 7 (**a**) DPV waveform for the oxidation of an electroactive species, where ΔE_s is the step potential, ΔE_p is the modulation amplitude, τ is the interval time, and t_p is the modulation time. Such waveform is applied between initial (E_i) and final (E_f) potentials. Scan rate (υ) in DPV is defined as $\Delta E_s/\tau$. (**b**) DPV voltammogram for the oxidation of an electroactive species, where E_p and I_p are peak potential and peak current, respectively

of a single current peak per redox process, the height of which is directly proportional to the concentration of the corresponding electroactive species.

25. The method has a narrow linear dynamic range and should be used only as a qualitative analysis to detect the presence of GST.
26. Taking into account GST is a dimer (Fig. 1), a two equal and independent sites model was used to fit the DPV voltammetric data obtained from GSFc oxidation. The binding parameter (ν), defined as the ratio between the concentrations of bound ligand ($[L]_b$) and the total macromolecule ($[M]_t$), is expressed as:

$$\nu = \frac{[L]_b}{[M]_t} = \frac{2K[L]}{1 + K[L]} \tag{2}$$

where K and $[L]$ are the equilibrium association constant and the free ligand concentration, respectively. The latter is related to the total ligand ($[L]_t$) and the bound ligand ($[L]_b$) by the mass conservation law:

$$[L] = [L]_t - [L]_b \tag{3}$$

Under the assumptions of a reversible, diffusion-controlled electron transfer and a diffusion coefficient for the bound ligand much lower than that for the free ligand, the following approximation can be made:

$$\frac{[L]}{[L]_t} = \frac{I_p}{I_{p,0}} \tag{4}$$

where I_p and $I_{p,0}$ are the peak current in the presence and in the absence of protein, respectively. An algorithm including Eqs. 2–4 was compiled using Scientist software (Micromath Scientific Software, St. Louis, USA) to fit the experimental data.

Acknowledgments

The authors acknowledge financial support from the Spanish Ministry of Economy and Competitiveness and the EU European Regional Development Fund (Grant CTQ 2010-17848), as well as the Andalusian Regional Government (Consejería de Economía, Innovación y Ciencia, Junta de Andalucía, grants CVI-6028 and FQM-6903).

References

1. Valko M, Leibfritz D, Moncol J, Cronin MT, Mazur M, Telser F (2007) Free radicals and antioxidants in normal physiological functions and human disease. Int J Biochem Cell Biol 39: 44–84
2. Quaye IK (2012) Oxidative stress in human health and disease. In: Priti R (ed) Insight and control of infectious diseases in global scenario. InTech, Rijeka, Croatia, pp 97–120
3. Hayes JD, Flanagan JU, Jowsey IR (2005) Glutathione transferases. Annu Rev Pharmacol Toxicol 45:51–88
4. Eaton DL, Bammler TK (1999) Concise review of the glutathione S-transferases and their significance to toxicology. Toxicol Sci 49: 156–164
5. Hayes JD, McLellan LI (1999) Glutathione and glutathione-dependent enzymes represent a co-ordinately regulated defence against oxidative stress. Free Radic Res 31:273–300
6. Laborde E (2010) Glutathione transferases as mediators of signaling pathways involved in cell proliferation and cell death. Cell Death Differ 17:1373–1380
7. Fouda MFR, Abd-Elzaher MM, Abdelsamaia RA, Labib AA (2007) On the medicinal chemistry of ferrocene. Appl Organometal Chem 21:613–625
8. Martos-Maldonado MC, Quesada-Soriano I, García-Maroto F, Vargas-Berenguel A, García-Fuentes L (2012) Ferrocene labelings as inhibitors and dual electrochemical sensors of human glutathione S-transferase p 1-1. Bioorg Med Chem Lett 22:7256–7260
9. Martos-Maldonado MC, Casas-Solvas JM, Téllez-Sanz R, Mesa-Valle C, Quesada-Soriano I, García-Maroto F, Vargas-Berenguel A, García-Fuentes L (2012) Binding properties of ferrocene-glutathione conjugates as inhibitors and sensors for glutathione S-transferases. Biochimie 94:541–550
10. Yassin Z, Ortiz-Salmerón E, García-Maroto F, Barón C, García-Fuentes L (2004) Implications of the ligandin binding site on the binding of non-substrate ligands to *Schistosoma japonicum*-glutathione transferase. Biochim Biophys Acta 1698:227–237
11. Habig WH, Jakoby WB (1981) Assays for differentiation of glutathione S-transferases. Methods Enzymol 77:398–405
12. Casas-Solvas JM, Ortiz-Salmerón E, Giménez-Martínez JJ, García-Fuentes L, Capitán-Vallvey LF, Santoyo-González F, Vargas-Berenguel A (2009) Ferrocene-carbohydrate conjugates as electrochemical probes for molecular recognition studies. Chem Eur J 15:710–725
13. MacDougall D, Crummett WB (1980) Guidelines for data acquisition and data quality evaluation in environmental chemistry. Anal Chem 52:2242–2249
14. Bard AJ, Faulkner LR (2001) Electrochemical methods. Fundamentals and applications, 2nd edn. Wiley, New York, Sections 6.1, 7.3.4, and 15.6
15. Wang J (2001) Analytical electrochemistry, 2nd edn. Wiley, New York, Sections 2-1, 3-3.2 and 4-4
16. Kaifer AE, Gómez-Kaifer M (1999) Supramolecular electrochemistry. Wiley-VCH Verlag GmbH, Weinheim, Sections 1.2, 4.2 and 4.3

Chapter 11

Using Nanosensors for In Situ Monitoring and Measurement of Nitric Oxide and Peroxynitrite in a Single Cell

Tadeusz Malinski

Abstract

The cytotoxic peroxynitrite ($ONOO^-$) is an oxidation product of the cytoprotective nitric oxide (NO). Our studies support the hypothesis that the concentration ratio of NO and $ONOO^-$, $[NO]/[ONOO^-]$ can be a marker of nitroxidative imbalance, which subsequently correlates well with endothelial dysfunction and dysfunction of the cardiovascular system. Nanosensors, described here, have been used for simultaneous monitoring and measurement of NO and $ONOO^-$ release from a single endothelial cell. These nanosensors, with a diameter of 200–300 nm, can be positioned accurately in close proximity of 5–10 μm from the endothelial cell membrane. The response time of the sensors is better than a millisecond and the detection limit is 10^{-9} M, with a linear concentration response of up to about 2 μM. The application of these sensors for the measurement of the balance and imbalance of $[NO]/[ONOO^-]$ in normal and dysfunctional endothelium is demonstrated.

Key words Endothelium, Nitric oxide and peroxynitrite imbalance, Vascular nitroxidative stress, Reactive oxygen species, Nanosensors

1 Introduction

Nitric oxide (NO) is one of the smallest biological signaling molecules. NO regulates vascular homeostasis by relaxing the smooth muscle, increasing the diameter of vessels, preventing aggregation and adhesion of platelets, and leukocytes to the arterial wall [1, 2]. In addition, NO is involved in the signal transduction in the nervous system and responsible for long-term memory potentiation. Vascular NO is generated by endothelial nitric oxide synthase (eNOS), and the neuronal NO is produced by neuronal nitric oxide synthase (nNOS). Both of these enzymes are constitutive enzymes (cNOS) controlled by intracellular calcium flux. An inducible nitric oxide synthase (iNOS) is calcium independent [3].

Nitric oxide signaling is via it stimulation of guanylyl cyclase and the increase in cellular cGMP concentration. NO production

Donald Armstrong (ed.), *Advanced Protocols in Oxidative Stress III*, Methods in Molecular Biology, vol. 1208,
DOI 10.1007/978-1-4939-1441-8_11,

in the cardiovascular system is mainly controlled by physical forces of flowing blood shear stress [4]. NO can also be stimulated by chemical agonists like bradykinin, angiotensin II, acetylcholine, and many others. The half-life ($t_{1/2}$) of NO in the vasculature varies significantly. Under laminar flow of blood the $t_{1/2}$ of NO is between 3 and 10 s. However, under the turbulent ventricular flow of the blood in the heart, the half-life of NO produced by endocardium is estimated to be on the level of milliseconds [5].

In the blood, NO is mainly scavenged by hemoglobin. After axial ligation to Fe(III) in hemoglobin, NO is oxidized to NO^+ in one electron transfer reaction. Fe(III) is simultaneously reduced to Fe(II) in this reaction. NO^+ is neutralized by OH^- and converted to nontoxic nitrite ion. At very low NO concentrations in the biological systems, its reaction with molecular oxygen is slow. Therefore, the formation of the product of this reaction, nitrogen dioxide (NO_2) is negligible. NO_2 in aqueous solution, in the presence of NO, also decomposes to nontoxic nitrite. NO is a free radical of very limited reactivity. There have been, literally, thousands of scientific papers published in recent decades, which erroneously imply the toxic role of NO in the biological system. Nitric oxide is not toxic and, at its physiological concentrations, is cytoprotective [6, 7].

Nitric oxide is synthesized by NOS from L-arginine and oxygen. The physiological concentration of L-arginine is about 0.6 mM and is much higher than that needed for the production of physiological NO concentration, which is at the level of 10–50 nM in the cardiovascular system. NO produced by endothelial cells diffuses to smooth muscle cells and into the lumen of vasculature. NO is hydrophobic, therefore its diffusion is much faster in the membrane than in the aqueous phase of cytoplasm [8]. The propagation of NO in the system is enforced by the diffusion process. A gradient of concentration is needed to initiate the diffusion process. Therefore, a membrane concentration of NO in endothelial cells has to be much higher (higher than 100 nM) than at its target smooth muscle cells. A physiological concentration of NO on the level of 10 nM is needed to stimulate smooth muscle relaxation through calcium calmodulin–cGMP system. NO produced by endothelium is continuously diluted due to the diffusion process and blood flow. Under conditions of laminar blood flow, NO is transported along the arterial walls. This type of transport prevents a scavenging of NO by hemoglobin which is transported through the center of the vasculature.

One of the main scavengers of NO in the cardiovascular system is superoxide ion (O_2^-). Superoxide in endothelial cells can be generated by several sources. Three major sources are NAD(P)H oxidase, mitochondria, and nitric oxide synthase itself (Fig. 1). Under normal NO production from fully functional endothelium the generation of O_2^- by eNOS is minimal as compared to O_2^- generated

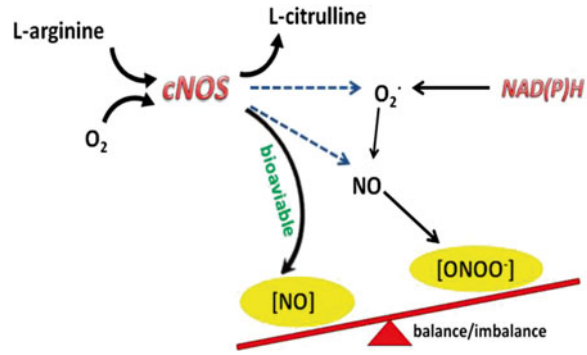

Fig. 1 A schematic diagram of nitric oxide/peroxynitrite imbalance produced by uncoupled cNOS and NAD(P)H. (Adopted from ref. [21])

by NAD(P)H or mitochondria. However, uncoupled cNOS can reduce oxygen in 1-electron reaction to produce the superoxide ion. A dimeric cNOS can be uncoupled due to a temporary shortage of L-arginine and/or O_2 substrates and/or a shortage of cofactors like tetrahydrobiopterin [9]. Temporary coupled/uncoupled cNOS can generate O_2^- and NO intermittently. NO is a potent scavenger of O_2^-, and the generation of these two radicals in close proximity makes the scavenging process extremely efficient. A reaction of O_2^- and NO is diffusion controlled ($k > 5 \times 10^9$ mol^{-1} s^{-1}) and leads to production of peroxynitrite ion ($ONOO^-$) [10, 11]. The NO can diffuse a significant distance and compete with SOD to scavenge O_2^- generated by NAD(P)H oxidase. However, the entire process is slower than the process of scavenging of NO by superoxide produced in close proximity by cNOS.

The half-life of $ONOO^-$, $t_{1/2} < 1$ s, depends on the biological environment. When generated at a high concentration, $ONOO^-$ can diffuse a short distance of a cell. Protonated $ONOO^-$ forms peroxous acid, ONOOH (pK_a 6.8) which may diffuse through cellular membrane at a distance of a few cells. Stability of $ONOO^-$ increases with an increase in pH. $ONOO^-$ can isomerize to produce nontoxic NO_3^-. However, during the diffusion process, $ONOO^-$ can collide with biological molecules and can be cleavaged into several short living highly oxidative species [12]. Figure 2 depicts some of the possible transformations of peroxynitrite/peroxous acid at physiological pH.

A cleavage of peroxynitrite can be hemolytic or heterolytic. A simple homolytic cleavage produces two radicals; $NO_2^\bullet$ and hydroxyl radical $OH^\bullet$, while heterolytic produces NO_2^+ and OH^-. $NO_2^\bullet$, $OH^\bullet$, and NO_2^+ are an extremely reactive, highly oxidative species [13]. The precise identity of oxidants derived from $ONOO^-$/ONOOH in the biological system is not well established and frequently controversial. $ONOO^-$ can also react with CO_2 to produce $O_2NOCO_2^-$ ion—a powerful oxidant [14].

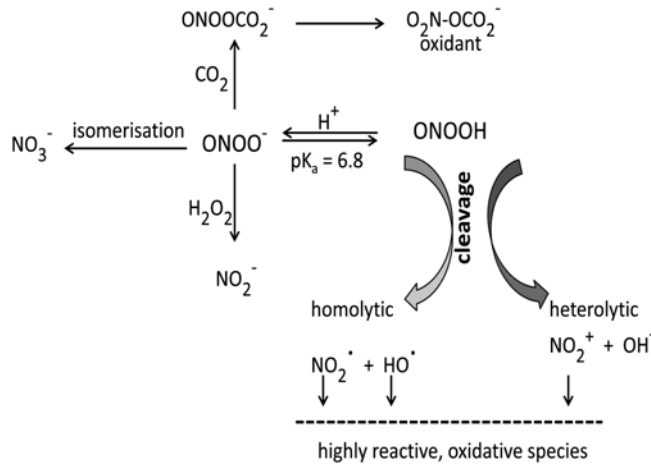

Fig. 2 A schematic diagram of selected peroxynitrite degradation pathways in biological milieu. (Adopted from ref. [21])

Apparently, $ONOO^-$ can also react with H_2O_2, and it has been suggested that the product of this reaction is nitrite. However, $OH^\bullet$ was also suggested as an intermediate of the $ONOO^-$ reaction with H_2O_2. Nitroxidative stress imposed by $ONOO^-$ on the biological system likely involves many short lived intermediaries and $OH^\bullet$ may be one of them. The oxidation power of $ONOO^-$ is highly significant and its effect on the biological system increases exponentially in the absence of cytoprotective NO. It has been well established that $ONOO^-$ can trigger a cascade of events leading to S-nitrosylation of proteins, inactivation of enzymes, apoptosis, and necrosis of cells [15]. Therefore, the balance, or imbalance, between NO and $ONOO^-$ may be an important factor in the evaluation of oxidative/nitroxidative stress in endothelial cells. This oxidative/nitroxidative stress is directly related to coupling/uncoupling of cNOS and function/dysfunction of endothelial cells. Therefore, near real-time monitoring of NO/$ONOO^-$ balance in endothelial cells is of significant importance, especially as a potential diagnostic tool for the dysfunction of the cardiovascular system.

Reactive oxygen species (ROS) and reactive nitrogen species (RNS) are the main components of oxidative/nitroxidative stress, and peroxynitrite is the most important component of nitroxidative stress. Nitroxidative stress/peroxynitrite has been implicated in lipid peroxidation and enzyme inactivation, including MnSOD inactivation and DNA damage. Peroxynitrite has high affinity to Mn(III). Therefore, the inactivation of MnSOD by $ONOO^-$ leads to the increase in O_2^- levels and an additional increase in cytotoxic peroxynitrite. The damage to cellular milieu by $ONOO^-$ may lead to cell damage, apoptosis and necrosis, DNA/RNA mutation and to a shortage of bioavailable NO in the cardiovascular and nervous system.

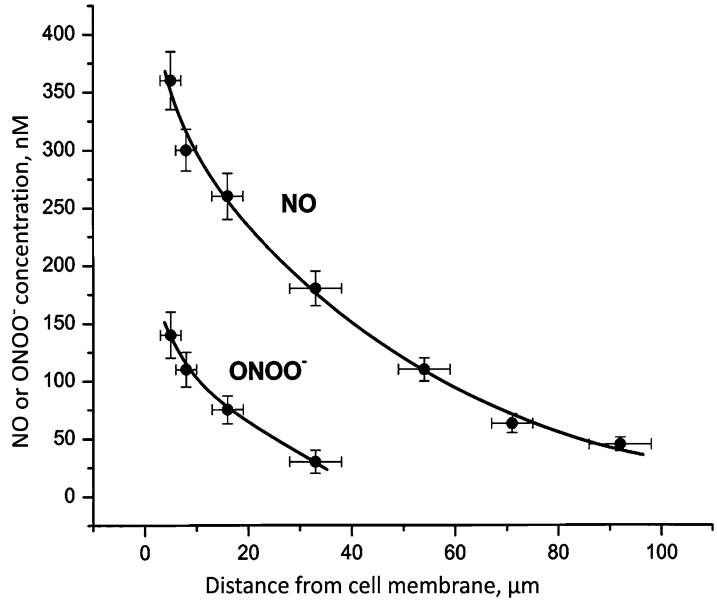

Fig. 3 Changes in NO and $ONOO^-$ concentrations as a function of the distance from the membrane of a single endothelial cell. The NO and $ONOO^-$ release from a single HUVEC (6th passage) was stimulated by calcium ionophore (Cal, 1 μM)

Deficiency of NO and overproduction of ROS has been implicated in many circulatory and neurological diseases including atherosclerosis, vasoconstriction, adhesion and thrombus formation, stroke, Parkinson's and Alzheimer's, and many others [13].

In the early 1990s, we were the first to use electrochemical nanosensors and nanosystems to measure in situ NO produced by a single endothelial cell [1, 2]. However, the direct in situ simultaneous measurement of NO and/or $ONOO^-$ is still a challenging task. Figure 3 depicts a schematic diagram of nanosensors designed in our laboratory to measure NO and $ONOO^-$. Most methods used for the determination of NO and $ONOO^-$ are indirect spectroscopic methods [15]. These indirect methods measure the products of NO and $ONOO^-$ degradation such as, NO_2^-, NO_3^-, adducts of NO to hemoglobin or spin trapping radicals. UV-spectroscopy (Griess method) is the method most frequently used to determine the level of NO as a cumulative NO_2^- and/or NO_3^- produced by NO oxidation. This method of analysis cannot differentiate between NO_2^-/NO_3^- end products of $ONOO^-$ metabolism from NO_2^-/NO_3^-, the end product of simple oxidation of NO. More importantly the analysis of NO_2^- or NO_3^- cannot provide any information about bioavailable NO. Bioavailable nitric oxide is the NO which is not rapidly oxidized and can actually diffuse and deliver the message cGMP and trigger smooth muscle relaxation. Similar problems have been noticed for the NO determination with the use of hemoglobin and UV visible

spectroscopy detection, as well as the chemiluminescence method. This may explain the high rate of misleading interpretations in many published studies covering nitric oxide. $ONOO^-$ is mostly determined by luminescence using dyes for the detection of S-Nitrosation as an indicator of $ONOO^-$. It is also a cumulative method of analysis. In addition, problems with this method arise from the fact that $ONOO^-$ is not the only source of S-Nitrosation in the biological system.

We have developed an electrochemical method of $ONOO^-$ analysis in nanoscale. A nanotechnological approach helped to miniaturize this method to be applied together with our NO nanosensors for simultaneous determination, in nanoscale, of $ONOO^-$ and NO at the same time in the same space [16, 17]. Both of the sensing devices we have developed can detect and quantify NO and $ONOO^-$ at nanomolar concentration. The detection limit of the sensors is about 10^{-9} M and response time is better than a millisecond. The miniaturization of the sensors to a nanoscale level is of crucial importance in the near real-time measurements of NO and $ONOO^-$ from a single cell.

Both NO and $ONOO^-$ can propagate through the biological system and this process is controlled by diffusion. A diffusion of hydrophobic NO is faster in the membrane than in the aqueous environment of the cytoplasm or blood. Protonated $ONOO^-$ can diffuse through the membrane, while $ONOO^-$ ion can diffuse well through aqueous environment. However, the range of the propagation of $ONOO^-$ is relatively short, due to its fast rate of degradation and low gradient of concentration. The reactivity and gradient concentration, of NO and $ONOO^-$, are important considerations in the in situ measurement of these two molecules. With the nanosensors we measured a decrease of NO and $ONOO^-$ concentration as a function of the distance from the cell membrane (Fig. 4). Both $ONOO^-$ and NO concentration decrease rapidly and the decrease is exponential. The sensors were positioned at different distances from the membrane of an endothelial cell. As expected, $ONOO^-$ concentration decreased much faster with distance, as compared to NO. Therefore, the maximal distance for measurement using fast response sensors with detection limit of 10^{-9} M will be about 90 μm for NO and about 30 μm for $ONOO^-$. These findings tell us clearly that the measurement of NO and $ONOO^-$ have to be performed, each time, at the same distance from the nanosensor, in order to obtain reproducible data. This is one of several experimental challenges in the real-time in situ measurement of NO and $ONOO^-$ in biological milieu.

The electrochemical measurements of NO and $ONOO^-$ in the membrane are possible but not recommended. That is because membrane measurement would involve physical stimulation of NO release by sensors as well as the generation of piezoelectric current overlapped with the analytical Faradaic current.

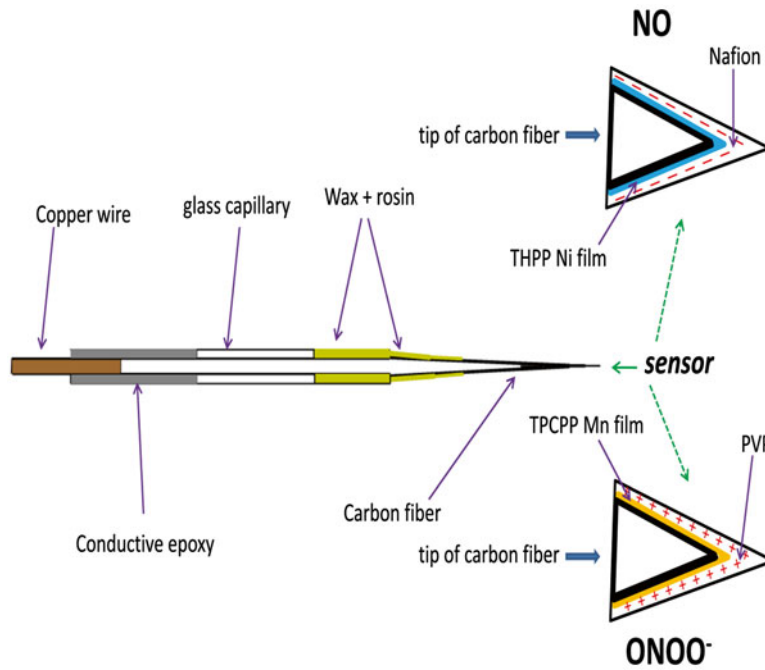

Fig. 4 A schematic design of nanosensors used for the measurement of NO and $ONOO^-$ from a single cell. The typical diameter of the tip of the sensor is about 200–300 nm

Therefore, reproducibility of NO/$ONOO^-$ concentrations directly measured on the cell membrane is rather poor.

Nanosensors developed in our laboratory [1, 16, 17] provide sufficient sensitivity and reasonable selectivity for NO or $ONOO^-$ measurement. These are electrochemical nanosensors and the sensing process involves an electron transfer between analyte to the sensor and generation of electrical current. The electrical current is a faradaic current (described by Faraday's law) controlled by diffusion of NO or $ONOO^-$ to the sensor. The faradaic diffusion controlled current is in direct linear proportion to a concentration of analyte, i.e., concentration of NO or $ONOO^-$. The selectivity of the sensors is based on specific redox potential of the analyte and on a rapid electron exchange between specific catalytic redox center Ni(III), specific for NO and Mn(III) redox center, specific for $ONOO^-$. Typical amperograms (diffusion current proportional to concentration versus time, at constant potential) are presented in Fig. 5. The amperograms were recorded at constant potential of 0.63 V versus silver/silver chloride electrodes (SSCE) for NO and –0.3 V versus SSCE for $ONOO^-$.

In the electrochemical arbitrary nomenclature, NO generated current is an anodic (positive) current and $ONOO^-$ current is cathodic (negative) current. At constant potential and the constant

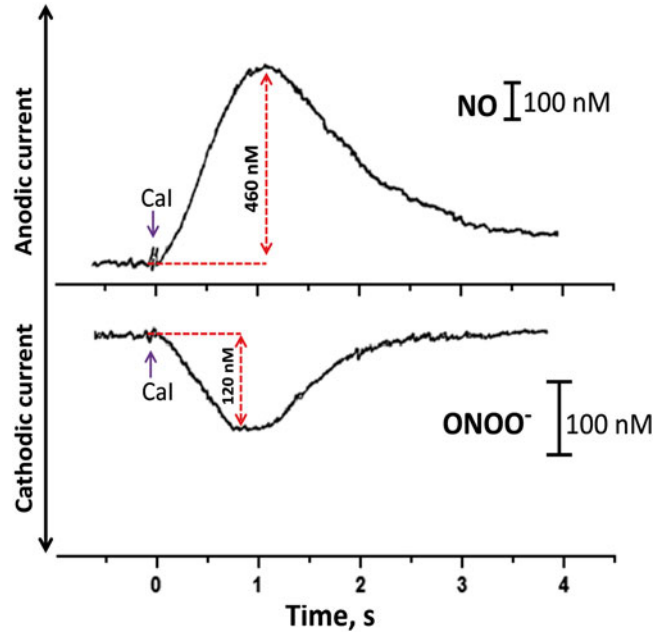

Fig. 5 A typical amperometric curves showing the change of NO and $ONOO^-$ concentration released from a single HUVEC (6th passage). The sensors were positioned about 5 ± 3 μm from the surface of an endothelial cell and the release of NO, $ONOO^-$ was stimulated with calcium ionophore (Cal, 1 μM)

concentration of analyte, this current depends on the area of the electrode sensor. Therefore, each sensor has to be calibrated before and after measurements. Two calibration methods can be used for this process; they are the dose response calibration curve and the standard addition methods.

A slope of the amperogram reflects on the rate of the NO or $ONOO^-$ production. A peak of the amperogram represents the maximal concentration. The area under the amperogram represents the total charge recorded by the nanosensor. With the application of Faraday's Law, this charge can be used to calculate the number of molecules (number of moles) reduced or oxidized on the sensor at a given time.

The validity of NO and $ONOO^-$ generated signals can be proven using several cNOS inhibitors, $ONOO^-$ scavengers, NAD(P)H inhibitors and elevated level of superoxide dismutase. The expected changes increase/decrease NO and/or $ONOO^-$ signal provide an assurance that the signal which is measured is indeed the signal generated by NO or $ONOO^-$. Also, addition of the standard solution provides additional confirmation that the signal, which is measured in the biological material is the signal generated by oxidation of NO or reduction of $ONOO^-$. Furthermore, the addition of the standard after the measurement of NO/$ONOO^-$ release from the cell can provide conformational information about the quality/

sensitivity of the sensor. The typical maximal concentrations of NO and $ONOO^-$ measured from endothelial cells in the presence of different factors affecting cNOS and NAD(P)H are presented in Fig. 7. In the presence of a nonselective inhibitor cNOS, both NO and $ONOO^-$ decreased about 80 %. As expected, SOD increased NO significantly, while $ONOO^-$ decreased. Similarly, the inhibition of NAD(P)H increased in NO and decreased in $ONOO^-$.

Both NO and $ONOO^-$ concentrations are measured in the same units, nanomol/liter (nM) and can be directly compared. This is the important feature of this method of measurement. The measured concentration from a single cell is independent of the total number of cells present in the measuring system. The maximal concentration of NO or $ONOO^-$ is not affected by the neighboring cells. However, decay in NO or $ONOO^-$ will be slower in the presence of neighboring cells.

We introduced a ratio of NO and $ONOO^-$ concentration $[NO]/[ONOO^-]$ as a convenient marker to express the balance between the two molecules in functional and dysfunctional endothelial cells [18, 19]. The scale of this marker can vary from about 3 to 7 for fully functional endothelium, and is smaller than one for dysfunctional endothelium with uncoupled eNOS. Figure 8 depicts $[NO]/[ONOO^-]$ ratio for different stages of dysfunctional endothelium which can be due to hypertension or diabetes.

2 Materials

2.1 Equipment

1. Gamry VFP Double Potentiostat/Galvanostat, USA.
2. Micromanipulator Sensapex SMX, Finland.
3. Beckman Coulter DV640 Spectrometer.

2.2 Standards

1. NO standard solution was synthesized from sodium nitrite and sulfuric acid in inert atmosphere (N_2). 50 g of $NaNO_2$ and 15 g of iron sulfate (catalyst) were mixed and H_2SO_4 (6M) was added to the mixture at the rate of 1 drop every 10 s. NO gas was purified by passing it through two columns filled with NaOH (2M and 4M NaOH) and was collected in small vials containing phosphate buffer (pH 7.4). NO standard was stored in the dark at 4 °C. The concentration of NO standard was measured with UV–Vis spectrophotometer (Beckman-Coulter) using hemoglobin (HB). Sodium hydrosulfate (NaS_2O_4) was added to the HB (10 mg in 0.5 ml H_2O_2) and kept for 30 min at 4 °C to form oxyhemoglobin (Oxy-HB). 10 μl of was placed in 3 ml cuvette with potassium phosphate buffer and absorbance was measured at wavelength 413–415 nm. Then, 10 μl of NO standard was added to Oxy-HB and the absorbance was measured again. (This protocol was published in ref. 16) (*see* **Note 1**).

2. Peroxynitrite solution was prepared from $NaNO_2$ and HCl. Approximately 500 ml of 0.6M sodium nitrite ($NaNO_2$) was mixed with equal volume of 0.6M hydrogen peroxide (H_2O_2) and 1,000 ml of 0.7M hydrochloric acid (HCl) at a temperature of 4 °C using vacuum pump. A product of this reaction is peroxynitrous acid (ONOOH). ONOOH is deprotonated in 0.9M NaOH solution at 4 °C. The absorbance of $ONOO^-$ was measured using a UV–visible spectroscopy at wavelength 303 nm. A molar absorptivity coefficient E_{302} is 1,670 M^{-1} cm^{-1} (*see* **Note 2**).

2.3 Supplies

1. Ni(II) tetrakis (3-methoxy-4-hydroxy-phenyl) porphyrin, (TMHPP) Ni was purchased from Frontier Scientific.
2. Mn(II) [2.2]paracyclophanylporphyrin, (TPCPP) Mn, was synthesized from paracyclophane-4-carbaldehyde and pyrrole, in chloroform solution. The complete synthesis, along with separational procedures, spectral properties, and metalations have been described previously [20].
3. Nafion solution 5 % (volume/volume in methanol) was purchased from Sigma-Aldrich.
4. Poly (4-vinyl-pyridine), (PVP) 1 % weight/volume in methanol was purchased from Sigma-Aldrich.
5. Conductive silver epoxy was purchased from EPO-TEK, USA.
6. Superoxide dismutase-polyethylene glycol (PEG-SOD), 3-benzyl-7-(2-benzoxazolyl), thio-1,2,3-triazolo (4,5-d) pyrimidine (VAS 2870); calcium ionophore (Cal, A23187); N^G-Methyl-L-arginine acetate salt (L-NMMA) were purchased from Sigma-Aldrich.

2.4 Cells and Animal Models

1. Human umbilical vein endothelial cells (HUVECs) were purchased as proliferating cells from Lunza (Walkersville, MD.). The cells were cultured in the MCDB-131 (Vec Technologies) complete medium at 37 °C in 5 % CO_2. The cells were propagated using an enzymatic dissociation (trypsin) procedure (maximum of 12 population doublings).
2. Spontaneously hypertensive rats (SHR) and Wistar Kyoto rats (WKY) (45–60 days old) were purchased from Harlan Laboratories (Indianapolis, IN.).

3 Methods

3.1 Preparation of the Carbon Fibers

1. Preparation of carbon fibers. The nanosensors were constructed using carbon-fiber technology. A single carbon fiber (diameter of 7 μm) was placed in a glass capillary and connected to a copper wire with conductive silver epoxy, then

stored in a vacuum oven at 40 °C for 8 h. The tip of the capillary was sealed with wax and the protruding part of the carbon fiber (about 10 mm) was covered in wax and resin mixture (10:1). Next, the tip of the wax covered carbon fiber was gradually burned using a propane micro-burn flame. This produces a cone-shaped tip of carbon fiber with the diameter of 250–300 nm. This tip was subsequently covered with the layers of sensing material(s) and used for NO and $ONOO^-$ measurement. (This protocol was published in ref. 16).

3.2 Coating of Carbon Fibers

1. For the preparation of the NO nanosensor, a monomeric TMHPP Ni solution (0.2 mM) in 0.1M NaOH was used. TMHPP Ni was polymerized electrochemically on the tip of the carbon fiber by repeated cyclic scanning of the potential from −0.20 V to +1.0 V with scan rate of 100 mV/s. About 20 scans were needed to cover the fiber with electrically conductive polymeric film of TMHPP Ni. The polymeric film of TMHPP Ni was covered with Nafion (1 %) in ethanol for 5–7 s and allowed to dry (*see* **Note 3**).

   The peroxynitrite sensor was prepared by covering the tips of the carbon fiber with T(PCP)PMn. A polymeric film was deposited from a monomeric solution of T(PCP)PMn (0.2 mM in OMSO) using continuous scan cyclic voltammetry. The potential was scanned from −0.8 V to 0.9 V versus SSCE with the scan rate of 100 mV/s. After 15–18 cycles, the tip of the carbon fiber was fully covered with the polymeric film of T(PCP)PMn. The carbon fiber tip was washed with double distilled water and dried. After that, the carbon tip was immersed in poly (4-vinyl-pyridine), (PVP) 1 % weight/volume in methanol for 10–15 s three to four times. After that, the $ONOO^-$ nanosensor was conditioned electrochemically in phosphate buffer (pH 7.4) by scanning a potential from −0.3 V to 0.9 V $ONOO^-$ nanosensors were stored in glass vials containing phosphate buffer (pH 7.4).

3.3 Calibration of Nanosensors

1. The nitric oxide sensor was calibrated by using a different concentration of standard solution of NO (range about 50 nM to 1,000 nM) in phosphate buffer (pH 7.4). A linear calibration curve was constructed from these measurements for each sensor. Also, a standard addition method was used to monitor the response of the sensor to subsequently added standard solution of NO. Typical amperograms were obtained at a constant potential of 0.63 V. Figure 6 shows the response of the nanosensor to a different concentration of NO.

   The peroxynitrite sensor was also calibrated in amperometric mode by both, the calibration curve, and the standard addition method. Amperometric response was monitored at a constant potential of +0.3 V versus SSCE (*see* **Note 4**).

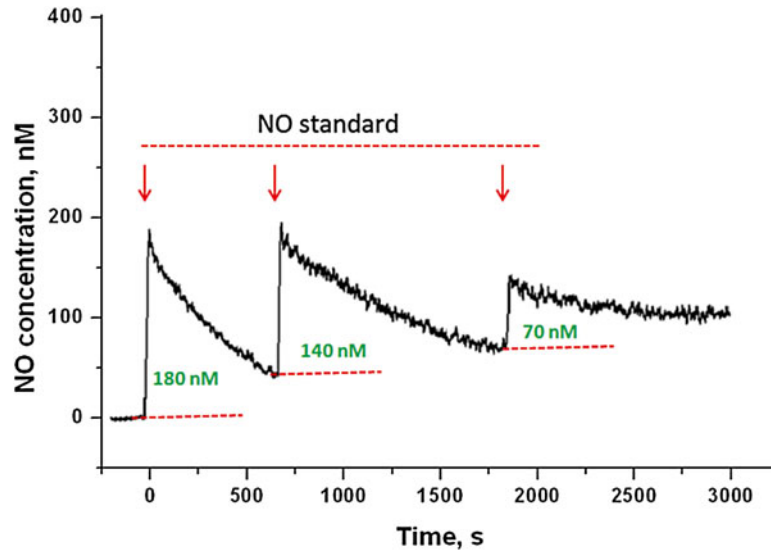

Fig. 6 The calibration signals generated by the nanosensor after subsequent injection of different concentrations of standard solution of NO into phosphate buffer (pH 7.4)

3.4 Measurement of NO and ONOO⁻ in Cells

1. A three electrode system and Gamry VFP 600 multichannel potentiostat was used to monitor NO/$ONOO^-$ release from the cells. This system consists of the nanosensor as a working electrode, silver/silver chloride as a reference electrode, and platinum wire (0.1 mm diameter) as an auxiliary electrode. A double potentiostat was used to monitor amperometric curves. Endothelial cells were suspended in MCDB-131 medium and seeded in 24-well cell culture plates and incubated at 37 °C, 5 % CO_2 and 95 % air for 1–2 days before measurements. Using stereotactic remote controlled micromanipulation, the tandem of NO/$ONOO^-$ nanosensors were positioned 50 μm above the cells and lowered to the cell membrane. A small, piezoelectric signal (picoampere, ms duration) was observed at that time. This procedure allows us to establish zero distance between the sensor and the surface of the cell. After that, the module of sensors was raised about 20 μm and moved horizontally (X Y direction) about 100–400 μm and lowered down again by about 13–15 μm. With the sensors positioned 5–7 μm from the membrane of a single endothelial cell, calcium ionophore or cNOS agonist were injected with a nanoinjector. NO/$ONOO^-$ release from the cell was monitored for 20–60 s. After about 2 min, the standard NO or $ONOO^-$ solution was added to recalibrate the sensors under the same condition which were used for single cell measurement. Finally, the sensors were gradually lowered to touch the surface of the cell with the generation of a piezoelectric signal. This operation confirmed the real distance between the given cell and the sensors. During the measurement of NO and $ONOO^-$, all the measurements were done in a Faraday cage,

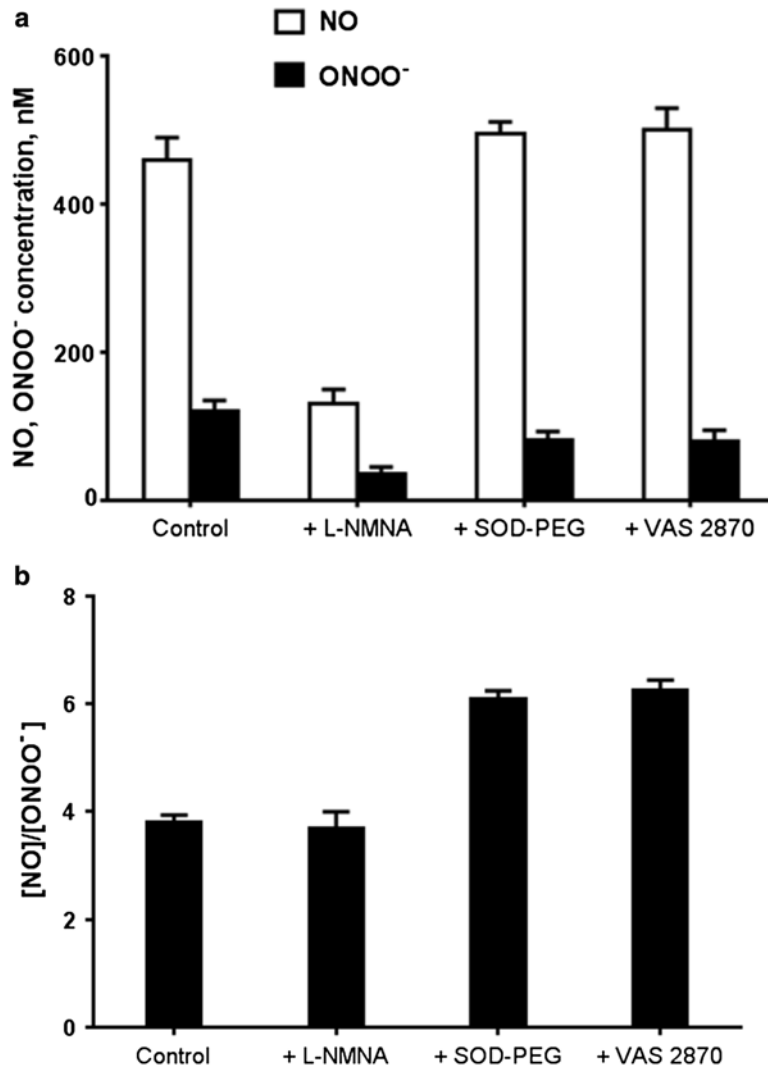

Fig. 7 Maximal calcium ionophore stimulated NO and $ONOO^-$ concentration (**a**) and [NO]/[$ONOO^-$] ratio (**b**) measured in HUVECs in the presence of L-NMMA (200 μM) PEG SOD (400 U/ml) or inhibitor of NAD(P)H oxidase (VAS 2870, 1 μM)

placed on heavy tables with a system minimizing vibrations. The typical responses recorded for the measurement of NO and $ONOO^-$ released from a single HUVEC is depicted in Fig. 5 (*see* **Note 5**).

3.5 Validation of the Methodology

1. In order to confirm that the measured signals are generated by NO and $ONOO^-$ the experiments were repeated in the presence of different attenuators of cNOS or scavengers of $ONOO^-$ or O_2^-. 10 min of incubation of endothelial cells with L-NMNA, SOD-PEG, or VAS 2870 (NAD(P)H inhibitor) significantly altered NO and $ONOO^-$ signals. The maximal NO and $ONOO^-$ concentrations are presented in Fig. 7a. As expected,

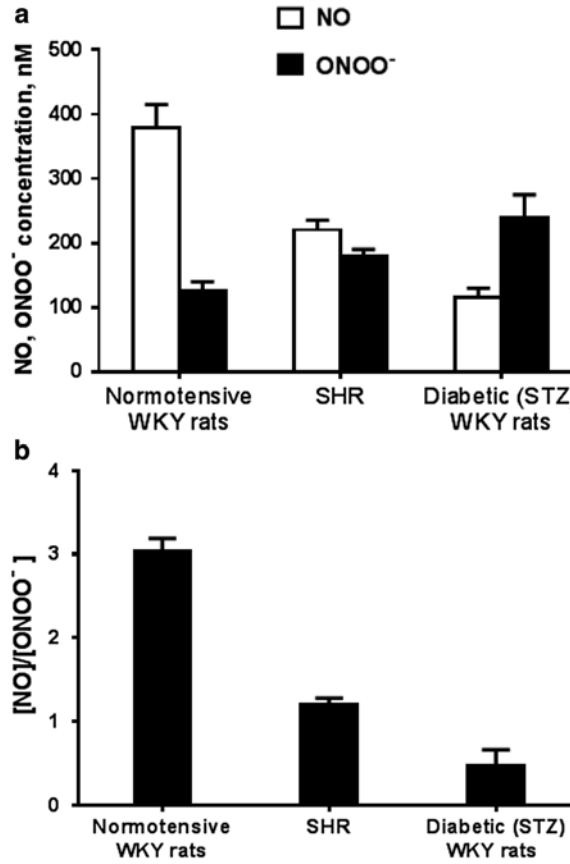

Fig. 8 Maximal NO and $ONOO^-$ concentration (**a**) and [NO]/[$ONOO^-$] ratio (**b**) measured by nanosensors. NO and $ONOO^-$ release was measured from aortic endothelial cells of normotensive WYK rats, hypertensive SHR rats, and diabetic WYK rats after stimulation with calcium ionophore (1 μM)

the nonselective NOS inhibitor, L-NMNA, reduced both NO and $ONOO^-$ concentrations by about 70 %. SOD-PEG and VAS 2870 slightly increased NO concentration and reduced $ONOO^-$ concentration by about 50 %. The inhibition of NOS by L-NMNA did not significantly change the [NO]/[$ONOO^-$] ratio as compared to control (Fig. 7b). However, a dismutation of O_2^- produced by NAD(P)H, caused an increase in [NO]/[$ONOO^-$] by about 25 % as compared to control. This data provides a clear and convincing validation of the method of simultaneous, direct, measurement of NO and $ONOO^-$ balance/imbalance produced by the endothelium (*see* **Note 6**).

3.6 Ex Vivo Measurements

1. NO and $ONOO^-$concentration was measured ex vivo in aorta of normotensive WKY rats, spontaneously hypertensive rats, SHR, and diabetic WKY rats. Maximal NO and $ONOO^-$ concentrations recorded by nanosensors are shown in Fig. 8a and

the ratio of [NO]/[$ONOO^-$] is shown in Fig. 8b. The endothelium of SHR produced about 30 % less NO and about 25 % more $ONOO^-$ than WKY rats. A further decline in NO and increase in $ONOO^-$ was observed for diabetic WKY rats where NO is about 75 % lower but $ONOO^-$ is about 50 % higher than in normotensive WKY rats. The [NO]/[$ONOO^-$] ratio reflects well on the shift in the level of nitroxidative stress compared to the level of cytoprotective NO. [NO]/[$ONOO^-$] in SHR is threefold lower than in WKY rats. For diabetic WKY rats, the ratio of [NO]/[$ONOO^-$], is below 1.0, which indicates a severe imbalance between NO and $ONOO^-$ and serious endothelial dysfunction (*see* **Note 7**).

4 Notes

1. Caution: Nitric oxide is a colorless and odorless gas and at high concentrations is extremely dangerous. All experiments with gaseous NO must be performed in a high efficiency fume hood.
2. Peroxynitrite is relatively stable in alkaline solution and can be stored in 0.9M NaOH for 6–10 months; however, a slow deterioration of $ONOO^-$ will be observed in 0.9M NaOH. Therefore, the real $ONOO^-$ standard has to be measured frequently using UV–visible spectroscopy.
3. TMHPPN: Solution should be stored at 4 °C in the dark to prevent polymerization. The thickness of deposited polymeric TMHPP Ni film significantly affects the sensitivity of the sensor. Monolayer deposition is optimal, while multilayer deposition will decrease electrical conductivity and nanosensor sensitivity.
4. The sensitivity and selectivity of NO and $ONOO^-$ nanosensors can be affected by the composition of buffers and cell culture media, temperature, electrical interference, vibration, and many other factors. Therefore, the sensors have to be calibrated frequently; at least before and after measurements in the single cell.
5. The accurate positioning of sensors in relation to the cell membrane is the most important factor in accurate and reproducible measurements of NO and $ONOO^-$ concentration. Highly accurate, remote-controlled, micromanipulators have to be used for this purpose. Also, the current generated by sensors is pA and smaller. Therefore, the entire system for measurement of NO and $ONOO^-$ has to be electrically shielded from many potential external electrical interferences. Measurements have to be performed in efficient, well-grounded Faraday's cage.
6. The system described here is designed for the measurement of NO and $ONOO^-$ after stimulation with cNOS agonists. Each of the agonists (including solutions) has to be tested with

sensors to check on the potential chemical or electrochemical interferences. Many organic solvents, including DMSO, can be easily oxidized and can produce significant amperometric signals which may interfere with NO signaling. Also, some organic solvents can damage polymeric porphyrin film. In addition, the background concentration of NO and $ONOO^-$ cannot be measured by the amperometric method. The methodology described here can only provide information concerning the increase in NO and $ONOO^-$ from its background level.

7. The accurate positioning of the sensors for measurement of NO and $ONOO^-$ from tissue is more difficult than that for a cell culture. The tissue has to be glued to the bottom of a petri dish. During this procedure, endothelial cells cannot be disturbed nor have any physical forces to be applied to their surface. The physical forces can stimulate NO and $ONOO^-$ and produce a dysfunctional endothelium. Also, in ex vivo measurement, the decay of endothelial NO and $ONOO^-$ occurs over time. After only 30 min, an aortic endothelial cell will lose about 50 % of its capacity to release NO.

References

1. Malinski T, Taha Z (1992) Nitric oxide release from a single cell measured in situ by a porphyrinic-based microsensor. Nature 358: 676–678
2. Malinski T, Radomski MW, Taha Z, Moncada S (1993) Direct electrochemical measurement of nitric oxide released from human platelets. Biochem Biophys Res Commun 194:960–965
3. Balligand JL, Ungureanu-Longrois D, Simmons WW, Pimental D, Malinski TA, Kapturczak M, Taha Z, Lowenstein CJ, Davidoff AJ, Kelly RA et al (1994) Cytokine-inducible nitric oxide synthase (iNOS) expression in cardiac myocytes. Characterization and regulation of iNOS expression and detection of iNOS activity in single cardiac myocytes in vitro. J Biol Chem 269:27580–27588
4. Kanai AJ, Strauss HC, Truskey GA, Crews AL, Grunfeld S, Malinski T (1995) Shear stress induces ATP-independent transient nitric oxide release from vascular endothelial cells, measured directly with a porphyrinic microsensor. Circ Res 77:284–293
5. Pinsky DJ, Patton S, Mesaros S, Brovkovych V, Kubaszewski E, Grunfeld S, Malinski T (1997) Mechanical transduction of nitric oxide synthesis in the beating heart. Circ Res 81:372–379
6. Kidd GA, Dobrucki LW, Brovkovych V, Bohr DF, Malinski T (2000) Nitric oxide deficiency contributes to large cerebral infarct size. Hypertension 35:1111–1118
7. Malinski T (2000) In situ detection of nitric oxide. Methods Mol Med 36:133–144
8. Malinski T, Taha Z, Grunfeld S, Patton S, Kapturczak M, Tomboulian P (1993) Diffusion of nitric oxide in the aorta wall monitored in situ by porphyrinic microsensors. Biochem Biophys Res Commun 193:1076–1082
9. Cosentino F, Patton S, D'Uscio LV, Werner ER, Werner-Felmayer G, Moreau P, Malinski T, Luscher TF (1998) Tetrahydrobiopterin alters superoxide and nitric oxide release in prehypertensive rats. J Clin Invest 101: 1530–1537
10. Huk I, Nanobashvili J, Neumayer C, Punz A, Mueller M, Afkhampour K, Mittlboeck M, Losert U, Polterauer P, Roth E, Patton S, Malinski T (1997) L-arginine treatment alters the kinetics of nitric oxide and superoxide release and reduces ischemia/reperfusion injury in skeletal muscle. Circulation 96:667–675
11. Van Der Loo B, Labugger R, Skepper JN, Bachschmid M, Kilo J, Powell JM, Palacios-Callender M, Erusalimsky JD, Quaschning T, Malinski T, Gygi D, Ullrich V, Luscher TF (2000) Enhanced peroxynitrite formation is associated with vascular aging. J Exp Med 192:1731–1744

12. Soneja A, Drews M, Malinski T (2005) Role of nitric oxide, nitroxidative and oxidative stress in wound healing. Pharmacol Rep 57 Suppl: 108–119
13. Malinski T (2007) Nitric oxide and nitroxidative stress in Alzheimer's disease. J Alzheimers Dis 11:207–218
14. Pryor WA, Lemercier JN, Zhang H, Uppu RM, Squadrito GL (1997) The catalytic role of carbon dioxide in the decomposition of peroxynitrite. Free Radic Biol Med 23: 331–338
15. Kiechle FL, Malinski T (1993) Nitric oxide. Biochemistry, pathophysiology, and detection. Am J Clin Pathol 100:567–575
16. Malinski T, Huk I (2001) Measurement of nitric oxide in single cells and tissue using a porphyrinic microsensor. Curr Protoc Neurosci Chapter 7:Unit7.14
17. Brovkovych V, Patton S, Brovkovych S, Kiechle F, Huk I, Malinski T (1997) In situ measurement of nitric oxide, superoxide and peroxynitrite during endotoxemia. J Physiol Pharmacol 48:633–644
18. Mason RP, Kalinowski L, Jacob RF, Jacoby AM, Malinski T (2005) Nebivolol reduces nitroxidative stress and restores nitric oxide bioavailability in endothelium of black Americans. Circulation 112:3795–3801
19. Kubant R, Malinski C, Burewicz A, Malinski T (2006) Peroxynitrite/nitric oxide balance in ischemia/reperfusion injury-nanomedical approach. Electroanalysis 18:410–416
20. Bennett JE, Wheeler DE, Czuchajowski L, Malinski T (1989) A novel meso-[2.2]paracyclophanyltriphenylporphyrin—electrochemical oxidation and conductive polymeric film formation. J Chem Soc Chem Comm:723–725
21. Burewicz A, Dawoud H, Jiang L-L, Malinski T (2013) Nitric oxide/peroxynitrite redox imbalance in endothelial cells measured with amperometric nanosensors. Am J Anal Chem 4:30–36

Part II

Antioxidant Technology and Application

Chapter 12

Curcuma longa Attenuates Carbon Tetrachloride-Induced Oxidative Stress in T-Lymphocyte Subpopulations

H.A. Abu-Rizq, Mohamed H. Mansour, and Mohammad Afzal

Abstract

A comparison of crude curcuminoid extract and purified curcumin was made to evaluate the immunoprotective effect of *Curcuma longa* (turmeric) Zingiberaceae. Carbon tetrachloride (CCl_4) induced selective cytolytic effects among immature (PNA^+) thymocytes and peripheral helper ($CD4^+$) T lymphocytes in the spleen were paralleled by a significant reduction in CD25, CD71, and Con A receptor expression. Treatment with curcumanoid crude extract, at two different doses, showed a significant restoration of lymphocyte viability and CD25, CD71, and Con A receptor expression in both immature (PNA+) thymocytes and splenic helper ($CD4^+$) T lymphocytes. Turmeric crude extract, at both low and high dose, was found to be more efficient as compared to purified curcumin, suggesting synergistic effect of curcumin with other components of the crude extract.

Key words *Curcuma longa*, Curcumaioids, Carbon tetrachloride, Oxidative stress, T lymphocytes

1 Introduction

Natural phenolic compounds are powerful antioxidants. These compounds accumulate in plant vacuoles and include simple phenolics to complex phenolics such as flavonoids, quinonoids, and curcuminoids. Three closely related curcuminoids have been identified from *Curcuma longa*, a common spice used throughout tropical and subtropical regions of the Southeast Asian countries. The use of Curcuma as an anti-inflammatory agent dates back to 2000 BC and curcumin was first mentioned in 1808, isolated in 1851, and its molecular structure established in 1910. The phenolic compound curcumin 1 (also known as diferuloylmethane) is the yellow pigment and apparently the main biologically active component of turmeric. It naturally occurs in the rhizomes of the perennial herb *Curcuma longa* that belongs to ginger family Zingaberaceae. Curcumin possesses a variety of pharmacological activities and therapeutic properties. Its numerous biological activities, which include alleviation of inflammation, rheumatoid arthritis, psoriasis,

Donald Armstrong (ed.), *Advanced Protocols in Oxidative Stress III*, Methods in Molecular Biology, vol. 1208,
DOI 10.1007/978-1-4939-1441-8_12, © Springer Science+Business Media New York 2015

pancreatic cancer, multiple myeloma, cystic fibrosis, and other disorders, are attributed to its powerful antioxidant properties.

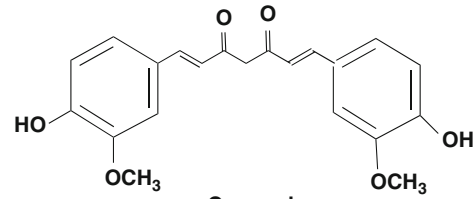

Curcumin

1.1 Oxidative Stress in the Immune System

Organs and cells of the immune system represent classical targets for oxidative stress, and have been investigated under various oxidative stress conditions. Oxidative stress is characterized by a significant decrease in thymic weight and cellularity, with a marked decrease in responsiveness of thymocytes to mitogen stimulation, indicating impairment in the cell capacity to undergo proliferation and differentiation, integral to effective T-cell responses. Within the thymus, a reduction in the number of immature thymocytes is indicative of selective modulation of migration patterns of thymocytes. This subsequently alters normal patterns of T-cell development and their migration from the thymus to peripheral blood and lymphoid tissues. In the spleen, oxidative stress is manifested by an overall decrease of white pulp cellularity, particularity within the T-cell dependent of periarteriolar lymphoid sheath.

Selective modulation of the cellular arm of the immune system has been repeatedly implicated in oxidative stress-based immunosuppression. Under these conditions, selectively targeted apoptotic signals result in an overall decrease in total T-cell numbers particularly among immature thymocytes and the $CD4^{+}CD8^{-}$ helper T-cell subpopulation in the periphery. Within the later subpopulation, oxidative stress also induces modulation of intracellular signaling pathways associated with the mitogen-activated protein kinase family, DNA methyltransferase, nuclear factor-κB, activating protein-1 involved in interleukin-2 and interleukin-2 receptor expression synthesis [1]. Oxidative stress-induced signals that inhibit interleukin-2 and interleukin-2 receptor production by T-helper lymphocytes may also reduce the expression of transferrin receptor in a negative autocrine loop, resulting in a further impairment of the lymphocyte proliferative machinery. Under oxidative imbalance, the down-modulation of membrane transferrin receptor, due to a block in receptor recycling on the cell surface, deprives lymphocytes of iron that is necessary for mitotic activity.

1.2 Cytoprotective Property of Curcuminoids

In various experimentally induced oxidative stress models, curcumin significantly suppresses oxidative stress by improving the antioxidant status and subsequent suppression of excessive lipid peroxidation [2]. Furthermore, curcumin exhibits anti-inflammatory

activities by its capacity to reduce neutrophil stimulation, and subsequent production of ROS, by blocking cyclooxygenase and lipoxygenase enzymatic pathways, as well as activating protein-1 and nuclear factor-κB activation and suppressing activation of the pro-inflammatory cytokines tumor necrosis factor-α and interleukin-1β. Among lymphocytes, curcumin has the capacity to selectively inhibit apoptosis of thymocytes, via a glutathione-dependent protective mechanism, and may modulate various immune functions by enhancing mucosal $CD4^+$ T-cells as well as B-cells.

As an *o*-Methoxyphenol, curcumin is a prototypic chain-breaking antioxidant. Its beneficial effects depend on its capacity to readily donate hydrogen atoms in oxidation reactions [3]. Similar to catechins of the flavonoids family, curcumin's capacity to act as an antioxidant depends upon its molecular structure, particularly the position and number of hydroxyl groups. Due to these structural characteristics, curcumin, and its reduced derivative tetrahydrocurcumin, have been established as effective scavengers of hydroxyl radicals, superoxide radicals, singlet oxygen, nitrogen dioxide, and nitric oxide, and as potent inhibitors of superoxide radical generation [4]. This study reports a comparative study of turmeric crude extract and purified curcumin for their protective role on T-lymphocyte subpopulations in Wistar rats subjected to CCl_4-induced oxidative stress.

2 Materials and Methods

2.1 Animal Treatment

1. Adult male Wistar rats, with an average body weight of 213.6 g, were acclimatized under laboratory conditions and randomly distributed into six groups (A–F).
2. Animals in groups B–F were given 2 ml daily dose of 0.2 % aqueous solution of CCl_4, by gavage feeding for 1 week.
3. Animals in group A (Negative control) were given a daily dose of 500 μL corn oil by gavage (emulsified in equal amount of normal saline).
4. Animals in group B were fed with CCl_4 aqueous solution for 1 week.
5. Animals in group C were fed with CCl_4 aqueous solution for 1 week followed by a daily dose of 4.28 mg curcumin emulsified in 500 μL of corn oil, during the second week.
6. Animals in group D were fed with CCl_4 aqueous solution for 1 week followed by a daily dose of 4.28 mg turmeric crude extract emulsified in 500 μL of corn oil, during the second week.
7. Animals in group E were fed with CCl_4 aqueous solution for 1 week followed by a daily dose of 8.57 mg curcumin emulsified in 500 μL of corn oil, during the second week.

8. Animals in group F were fed with CCl_4 aqueous solution for 1 week followed by a daily dose of 8.57 mg curcum crude extract emulsified in 500 μL of corn oil during the second week.

At the end of the experimental period, food and water were withdrawn 12 h before animal sacrifice by cervical dislocation. Thymuses and spleens were excised for immediate use.

2.2 Preparation of Lymphocyte Subpopulations in Suspension

1. Thymuses and spleens, excised separately from rats of the specified groups were gently teased in PBS, pH 7.2. Tissue debris was allowed to settle and lymphocytes in suspension were collected, centrifuged at $200 \times g$ for 5 min and washed.
2. Their viability was assessed by trypan blue exclusion.
3. Thymocytes were separated into PNA^+ (immature) and PNA^- (mature) lymphocytes by PNA affinity chromatography:
   (a) A fraction of purified PNA was dialyzed against coupling buffer (100 mM $NaHCO_3$ containing 150 mM NaCl, pH 7.8) and coupled to CNBr-activated Sepharose 6 MB at a concentration of 5 mg/ml beads following the manufacturer instructions.
   (b) The coupled gel (6 ml, with a coupling efficiency of 85 %) was packed in a column (1.5 × 5 cm) and equilibrated with PBS, pH 7.2. Aliquots of thymocytes in suspension (10^8 viable lymphocytes) were applied at 15 ml/h to the column and PNA^- lymphocytes recovered in the run-through fractions.
   (c) After washing with PBS, pH 7.2, PNA^+ lymphocytes bound to the column were selectively eluted with PBS, pH 7.2 containing 50 mM galactose. Both lymphocyte subpopulations were extensively washed in PBS, pH 7.2. These were counted and their viability was assessed by trypan blue exclusion.
4. Peripheral T-lymphocytes in spleen (IgM^-) were separated into subsets of helper T ($CD4^+CD8^-$) and cytotoxic T ($CD4^-CD8^+$) lymphocytes by negative selection with magnetic bead immunoabsorption:

   The standard assay involved the treatment of splenocytes (10^8) for 45 min with saturating amounts of selective biotinylated mAb (s) followed by extensive washings in PBS, pH 7.2, to remove unbound antibodies. Splenocytes were subsequently incubated with streptavidin-coated magnetic beads for 45 min and the selective bead-coated lymphocyte subsets were removed by magnetic separation. The lymphocyte subset with the reciprocal phenotype was recovered by aspiration, counted, and its viability assessed by trypan blue exclusion.

2.3 Labeling of Lymphocyte Subpopulations in Suspension

1. Viable lymphocyte subsets collected from thymus and spleen of rats in each specified group in suspension (10^6 in 25 μL PBS, pH 7.2) were separately incubated with equal volume of 25 μg/ml of biotinylated PNA, Con A, and mAbs anti-CD4, anti-CD8, anti-CD25, or anti-CD71.
2. After washing with PBS, pH 7.2, lymphocytes were treated with 25 μL streptavidin-peroxidase (at a working dilution of 1:200) followed by metal-enhanced DAB and examined by light microscopy. Assays were performed in triplicate and were paralleled by testing lymphocytes treated with biotinylated BSA. The percentage of labeled lymphocytes was determined by counting 300 lymphocytes and the reaction quantified using the formula:

$$\text{Positively} - \text{labeled lymphocyte}\,\% = \frac{100 \times \%(+\text{ve})\,\text{lymphocytes in test} - \%(+\text{ve})\,\text{lymphocytes in control}}{100 - \%(+\text{ve})\,\text{lymphocytes in control}}$$

2.4 Curcumin Extraction

1. Commercially available *Curcuma longa* rhizomes were crushed and powdered in a kitchen blender.
2. Extraction was made with chloroform using Sohxlet extractor (*see* **Note 1**).
3. Fractionation of the crude extract was made on a silica gel column packed in toluene and elution with toluene–chloroform mixtures (*see* **Note 2**).
4. Curcumin, demethoxycurcumin, and bisdemethoxy curcumin were obtained from various fractions and crystallized from toluene–methanol mixtures. Their identity was established from their spectral data. Commercially available curcumin was recrystallized before use (*see* **Note 3**).

3 Results

3.1 Lymphocyte Viability

As shown in Fig. 1a, b, the percentage viability of total thymocytes and splenocytes, in group B resulted in approximately 50 % reduction in the percentage viability of both lymphocyte populations compared to the control group A. In animals treated with either low or a higher dose of turmeric crude extract, there was a significant restoration of lymphocyte viability to control levels in both organs, regardless of the dose of turmeric crude extract used. On the other hand, treatment with purified curcumin (groups C and E) was paralleled by an equivalent restoration of lymphocyte viability but in a dose-dependent manner. Thus, a significantly higher level of lymphocyte viability was consistently observed in both organs only in rats treated with the higher dose of curcumin (group E).

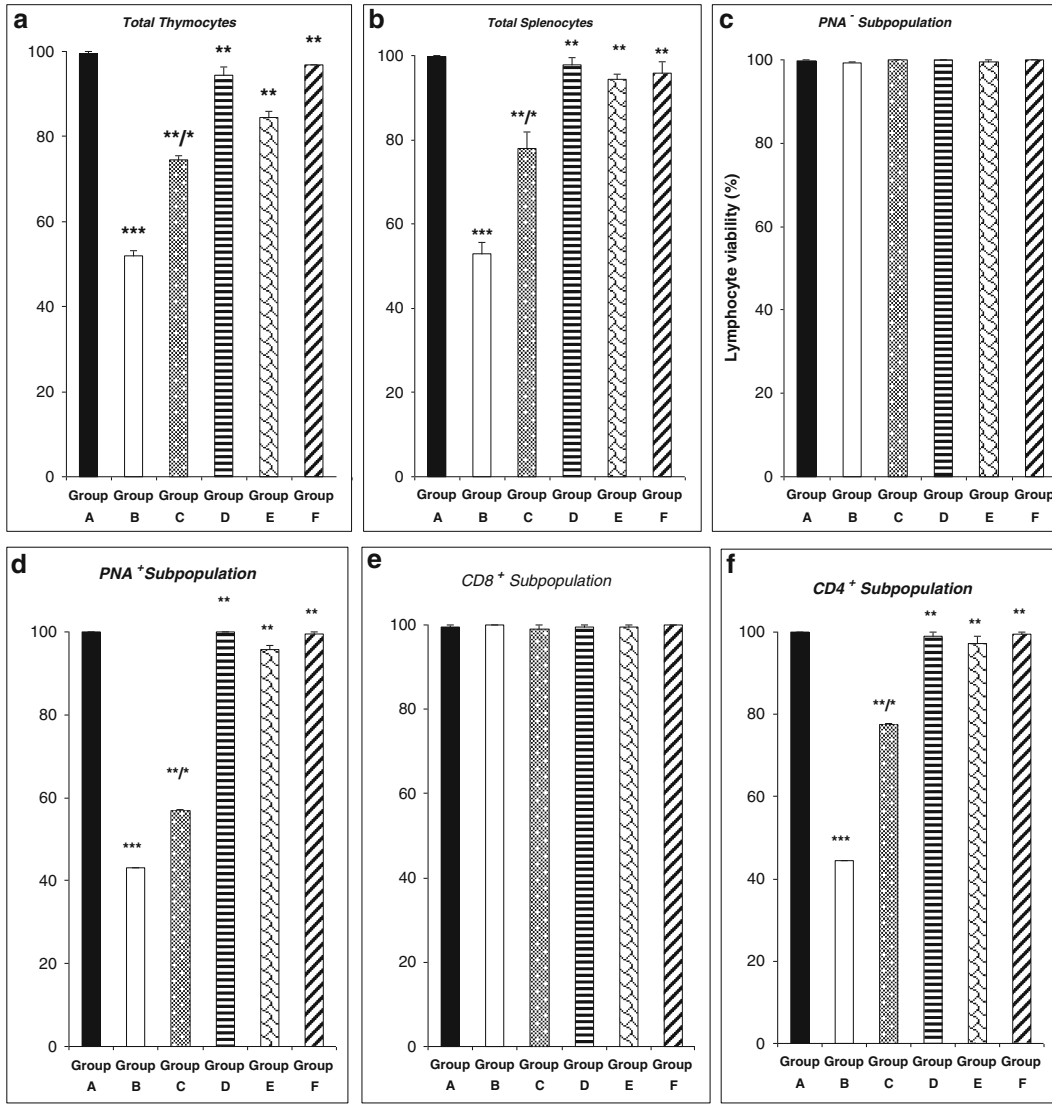

Fig. 1 Percentage of viable lymphocytes (total, PNA⁻, and PNA⁺ thymocytes; and total, CD4⁺, and CD8⁺ splenocytes) assessed by trypan blue exclusion, in untreated rats (group A), rats treated with CCl_4 (group B) and rats treated with CCl_4 followed by either low or high dose of purified curcumin (groups C and E, respectively) or turmeric acetone crude extract (groups D and F, respectively). Results are expressed as mean ± SEM of three separate sets of experiments. ***$P < 0.05$ compared with the control group A; **$P < 0.05$ compared with the CCl_4-treated group B; and *$P < 0.05$ compared with the CCl_4⁺ high dose of purified curcumin-treated group E

As shown in Fig. 1c, d, the cytolytic effect of CCl_4 was selective to only PNA⁺ (immature) thymocytes, whereas no significant difference in viability was observed among PNA⁻ (mature) thymocytes. A significant restoration of the viability of PNA⁺ thymocytes was observed among rats treated with either dose of turmeric crude extract or with the high dose of purified curcumin. In spleen, data shown in Fig. 1e, f, indicated that the cytolytic effect of CCl_4 was also selective for the CD4⁺ T-lymphocyte subpopulation compared

with the $CD8^+$ T-lymphocyte subset. A significant restoration of the viability of $CD4^+$ was, however, observed among rats treated with either dose of turmeric crude extract or with the high dose of purified curcumin in conjunction with CCl_4.

3.2 Proliferative Potential of Thymocytes and Peripheral T-Lymphocyte Subpopulations

As shown in Figs. 2a, 3a, and 4a, treatment with CCl_4 (group B) resulted in approximately 30–50 % reduction of Con A $receptor^+$, $CD25^+$, and $CD71^+$ lymphocytes, respectively, among total thymocytes. Rats treated with either low dose (group D) or high dose (group F) of turmeric crude extract showed a significant restoration of the lymphocytes expressing these receptors to control level. On the other hand, treatment with purified curcumin (groups C and E) was paralleled by an equivalent restoration of receptors expression

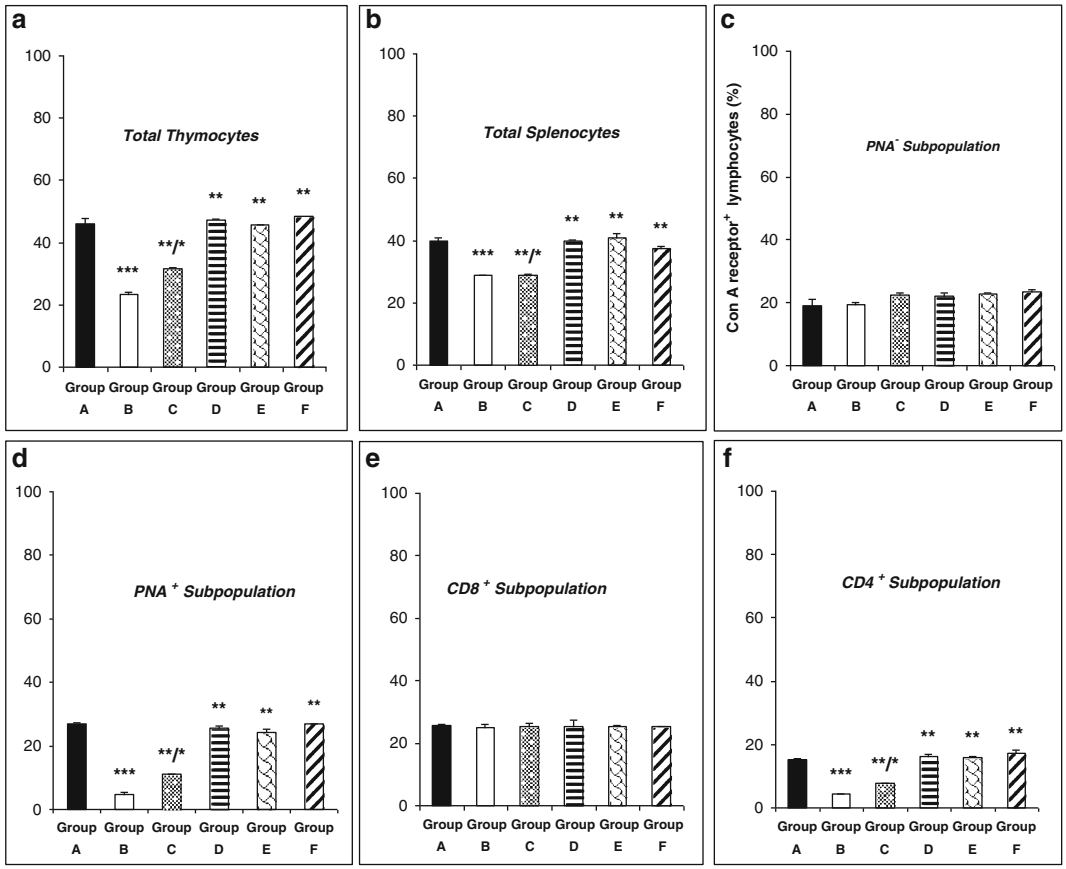

Fig. 2 Percentage of Con A receptor expression among different lymphocyte subpopulations, in control (group A), rats treated with CCl_4 (group B) and rats treated with CCl_4 followed by either low or high dose of purified curcumin (groups C and E, respectively) or turmeric acetone crude extract (groups D and F, respectively). Results are expressed as mean ± SEM of three separate sets of experiments. ***$P < 0.05$ compared with the control group A; **$P < 0.05$ compared with the CCl_4-treated group B; and *$P < 0.05$ compared with the CCl_4+ high dose of purified curcumin-treated group E

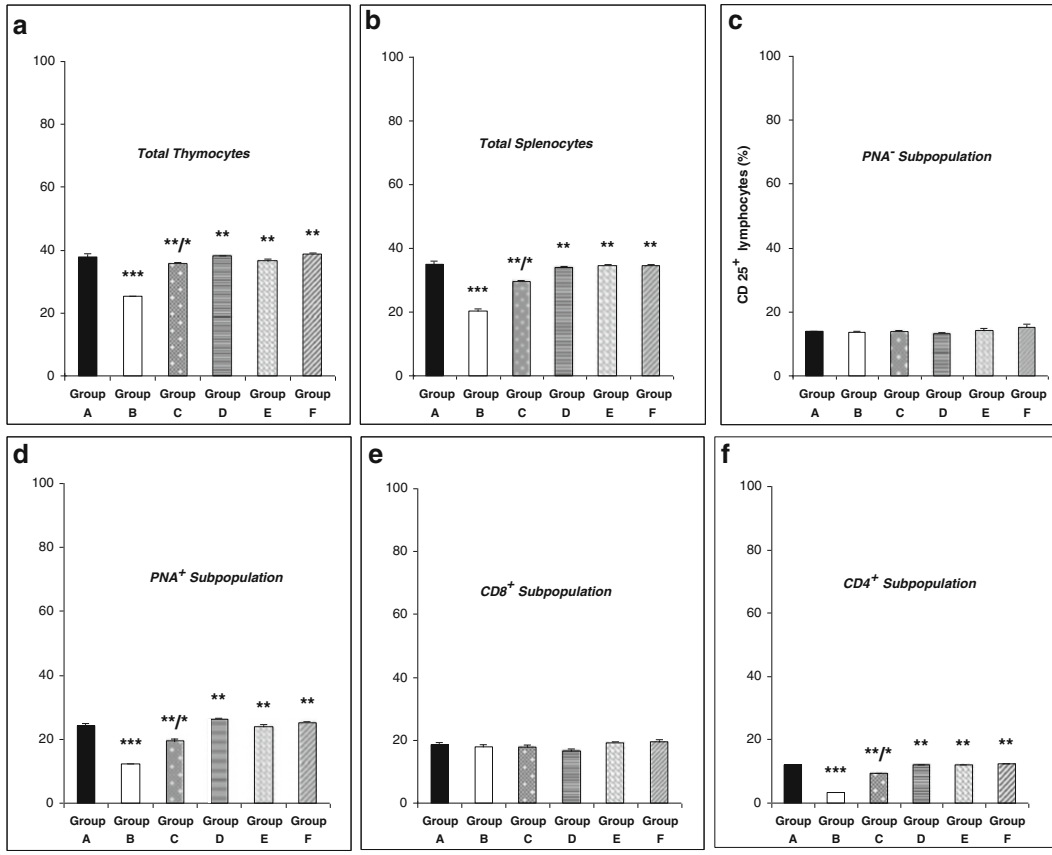

Fig. 3 Percentage of CD 25 expression among different lymphocyte subpopulations, in control (group A), rats treated with CCl_4 (group B) and rats treated with CCl_4 followed by either low or high dose of purified curcumin (groups C and E, respectively) or turmeric acetone crude extract (groups D and F, respectively). Results are expressed as mean ± SEM of three separate sets of experiments. ***$P < 0.05$ compared with the control group A; **$P < 0.05$ compared with the CCl_4-treated group B; and *$P < 0.05$ compared with the CCl_4^+ high dose of purified curcumin-treated group E

but in a dose-dependent manner. A significant restoration was observed only in rats treated with the high dose of curcumin (group E). Data in Figs. 2c, 3c, and 4c show that there was no appreciable difference in receptors expression observed among the PNA^- thymocyte subset following CCl_4 treatment alone or in conjunction with turmeric crude extract. On the other hand, abrogation of receptors expression was selective to the PNA^+ thymocyte subset following CCl_4 treatment (Figs. 2d, 3d, and 4d). A significant restoration of the percentage of lymphocytes expressing these receptors to control levels was observed among rats treated with either dose of turmeric crude extract or with the higher dose of purified curcumin. As shown in Figs. 2b, 3b, and 4b, treatment with CCl_4 (group B) resulted in approximately 50 % reduction in the percentages of the Con A $receptor^+$, $CD25^+$, and $CD71^+$

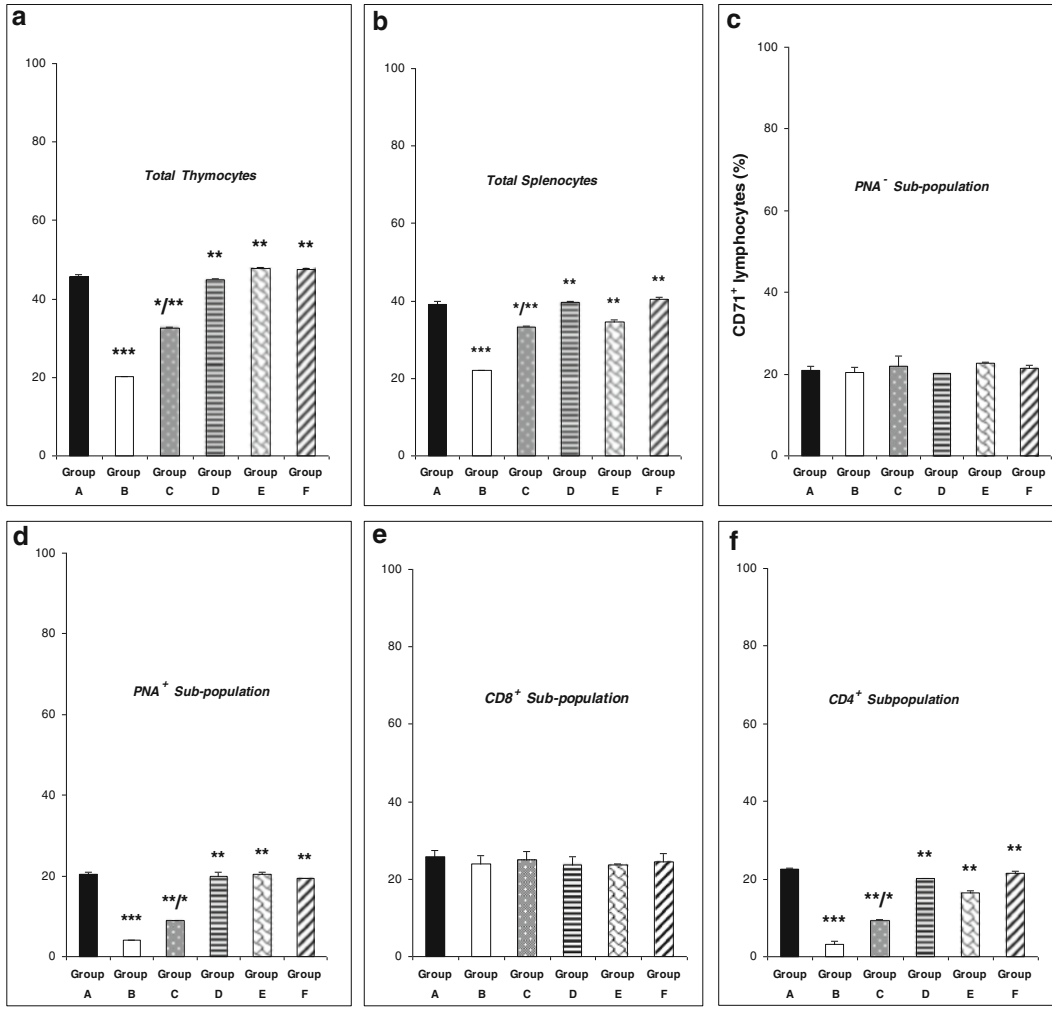

Fig. 4 Percentage of CD 71 expression among different lymphocyte subpopulations, in control (group A), rats treated with CCl_4 (group B) and rats treated with CCl_4 followed by either low or high dose of purified curcumin (groups C and E, respectively) or turmeric acetone crude extract (groups D and F, respectively). Results are expressed as mean ± SEM of three separate sets of experiments. ***$P < 0.05$ compared with the control group A; **$P < 0.05$ compared with the CCl_4-treated group B; and *$P < 0.05$ compared with the CCl_4^+ high dose of purified curcumin-treated group E

lymphocytes, respectively, among total T-lymphocytes in the spleen compared to the control group A. In rats treated with either low dose (group D) or higher dose (group F) of turmeric crude extract, there was a significant restoration of the percentage of lymphocytes expressing these receptors to control level. On the other hand, treatment with purified curcumin (groups C and E) was paralleled by an equivalent restoration of the lymphocytes expressing these receptors but in a dose-dependent manner. This significant restoration was observed only in rats treated with the higher dose of curcumin (group E). Interestingly, receptors expression among the

isolated cytotoxic $CD8^+$ T lymphocyte subset was consistently comparable to any of the specified groups of rats compared with the control group (Figs. 2e, 3e, and 4e). Among the isolated helper $CD4^+$ subset, 15 %, 12 %, and 22 % were Con A $receptor^+$, $CD25^+$, and $CD71^+$ lymphocytes, respectively, in the control group A (Figs. 2f, 3f, and 4f), and exhibited marked reduction in CCl4-treated rats (group B). A significant restoration of receptors expression was observed among rats treated with either dose of turmeric crude extract or with the high dose of purified curcumin in conjunction with CCl_4.

3.3 Discussion

In animals treated with CCl_4, almost 50 % reduction in the percentage of the viability of both total thymocytes and splenocytes was observed. This may be mainly due to the selective cytotoxic effect of CCl_4 on the PNA^+ immature thymocytes as well as the $CD4^+$ helper T-lymphocytes subset in the spleen. These results may be directly related to early observations, in which oxidative stress induces abnormal patterns of T-cell development and migration from the thymus to peripheral lymphoid organs. In other related studies, a reduction in total T-cells has been suggested due to selective apoptotic signals resulting in a significant decrease in the T-lymphocyte subpopulation with the $CD4^+$ $CD8^-$ phenotype in the periphery, which may be due to the selective oxidative stress-induced upregulated expression of tumor necrosis factor receptor-1. Within $CD4^+$ helper T-cells, oxidative stress induces modulation of intracellular signaling pathways associated with the mitogen-activated protein kinase family as well as DNA methyltransferase, nuclear factor-κB, and activating protein-1, which are collectively involved in interleukin-2 and interleukin-2 receptor synthesis [5]. This was confirmed in the present study by the selective downregulation of CD25, CD71, and Con A receptor expression observed among peripheral $CD4^+$ helper T-lymphocytes under CCl_4-induced oxidative stress. The downregulated expression of interleukin-2 and its CD 25 receptor would render the helper T-cell subpopulation unresponsive to activation and proliferation signals and more prone to apoptotic signals, which reflects its impaired capacity in coordinating both cellular and humoral arms of the immune response. Oxidative stress-induced signals may also reduce the expression of the CD 71 transferrin receptor and the Con A receptor, in a negative autocrine loop, resulting in a further impairment of the lymphocyte proliferative machinery. Under oxidative imbalance, both transferrin receptor and ferritin may be downregulated due to a block of receptor recycling on the cell surface, and hence deprive lymphocytes of iron necessary for mitotic activity. The downregulation of Con A receptor, which targets mitogenic signals to T-lymphocytes, may have far reaching effects on cytoskeletal elements mobilization and the subsequent impairment of T-lymphocytes mitotic cycle [6].

Previous studies have shown that curcuminoids, either in crude or purified preparations, are powerful antioxidants that may rescue a number of key elements in the cellular signal transduction pathways including nuclear factor-κB, c-Jun/activating protein-1 activation, and phosphorylation reactions catalyzed by protein kinases [1]. Data presented in this study support observations on the conducive properties of curcuminoids in lymphocyte viability, blastogenesis, and DNA synthesis [7, 8] and further suggest their potential in augmenting the proliferative machinery of T-lymphocytes at different stages of differentiation. However, an important facet of the present study was the significantly higher efficacy of the crude preparations, compared to purified curcumin, consistently observed in the restoration process. The capacity of curcuminoids, as potent chain-breaking antioxidants, has been attributed to the position and number of hydroxyl groups, which act as effective scavengers of hydroxyl radicals, superoxide radicals, and singlet oxygen. In line with these observations, the inclusion of bisdemethoxy curcumin (expressing 4 hydroxyl groups) and demethoxy curcumin (expressing 3 hydroxyl groups) along with curcumin (expressing 2 hydroxyl group) within the crude extract treatments (roughly in the ratio 1:1.3:2.1 by weight, respectively) may provide a plausible explanation for their higher antioxidative potency compared to the purified curcumin treatments. Besides curcumin, terpenoids present in the crude extract may be equally effective in quenching free radicals.

4 Notes

1. Powdered *curcuma longa* tubers were Soxhlet extracted till no more yellow color was present in the extract.
2. The crude extract was fractionated on silica gel (200–400 mesh size) packed in glass columns packed in toluene and eluted with increasing amount of ethyl acetate.
3. Purity of fractions was checked by TLC (Toluene–Methanol–Acetic acid 6:3:1 v/v) and the purified curcumin was recrystallized from toluene.

References

1. Mesel-Lemoine M, Cherai M, Le Gouvello S, Guillot M, Leclercq V, Klatzmann D, Thomas-Vaslin V, Lemoine FM (2005) Immune dysfunctions of cultured T lymphocytes are due to a preferential expansion of $CD4^{+}CD25^{+}$ suppressor cells. Blood 106:5199
2. Rukkumani R, Aruna K, Varma PS, Rajasekaran KN, Menon VP (2004) Comparative effects of curcumin and an analog of curcumin on alcohol and PUFA induced oxidative stress. J Pharm Pharm Sci 7:274–283
3. Fujisawa S, Atsumi T, Murakami Y, Kadoma Y (2005) Dimerization, ROS formation, and biological activity of o-methoxyphenols. Arch Immunol Ther Exp (Warsz) 53:28–38
4. Singh S, Khar A (2006) Biological effects of curcumin and its role in cancer chemoprevention and therapy. Anticancer Agents Med Chem 6:259–270
5. Tomas-Zapico C, Caballero B, Sierra V, Vega-Naredo I, Alvarez-Garcia O, Tolivia D, Rodriguez-Colunga MJ, Coto-Montes A (2005) Survival

mechanisms in a physiological oxidative stress model. FASEB J 19:3594–3595

6. Haufe D, Luther T, Kotzsch M, Knels L, Koch T (2004) Perfluorocarbon attenuates response of concanavalin A-stimulated mononuclear blood cells without altering ligand-receptor interaction. Am J Physiol Lung Cell Mol Physiol 287: L/210–L/216
7. Chakravarty AK, Yasmin H (2005) Alcoholic turmeric extract simultaneously activating murine lymphocytes and inducing apoptosis of Ehlrich ascitic carcinoma cells. Int Immunopharmacol 5:1574–1581
8. Gautam SC, Gao X, Dulchavsky S (2007) Immunomodulation by curcumin. Adv Exp Med Biol 595:321–341

Chapter 13

Prolongation of the Lag Time Preceding Peroxidation of Serum Lipids: A Measure of Antioxidant Capacity

Ilya Pinchuk and Dov Lichtenberg

Abstract

Antioxidants inhibit oxidation processes and by this affect many biological processes. This, in turn, promotes continuing efforts to synthesize new efficient antioxidants and discover compounds of natural origin capable of preventing peroxidation. Although many assays have been developed to evaluate antioxidants, the search for improved protocols is still actual. The presented protocol is based on the effect of antioxidant on the kinetics of peroxidation of lipids in human blood serum. Specifically, we evaluate the capacity of antioxidant by the relative prolongation of lag phase (delay) of copper-induced peroxidation of lipids in unfractionated serum. The main advantage of the assay is that it implements inhibition of peroxidation in physiologically relevant system. We propose expressing the results of the assay either in terms of the relative prolongation of the lag per 1 μM of antioxidant or as the concentration of antioxidant required to double the lag. To allow for comparing the results with those of other assays, these results may be normalized and expressed in terms of the unitless "TROLOX equivalents."

Key words Antioxidants, Assays, Oxidative stress, Serum lipid peroxidation

1 Introduction

Oxidative stress (OS) in humans is considered to play a pivotal role in the pathogenesis of many diseases, including cardiovascular diseases, diabetes mellitus, and neurodegenerative diseases [1]. Many of these pathologies are associated with peroxidation of oxidizable lipids in body fluids and tissues [2]. Inhibition of peroxidation can therefore be expected to suppress OS and prevent OS-related diseases [3]. Although the benefits of antioxidant supplementation, either to general population or for specific risk groups, are still debatable, the efforts to develop new potent antioxidants either of synthetic or natural origin continue. Furthermore, antioxidants prolong the shelf life of foodstuff, drugs, and other oxidizable products, which also promote the search for efficient antioxidants [4]. Evaluation of the antioxidative activity of alleged antioxidants is therefore an important part in the search for improved antioxidants.

Donald Armstrong (ed.), *Advanced Protocols in Oxidative Stress III*, Methods in Molecular Biology, vol. 1208,
DOI 10.1007/978-1-4939-1441-8_13,

The various protocols (and their numerous modifications) used for evaluation of antioxidants [5] differ with respect to the following main features (and to experimental details):

- The monitored reaction (direct interaction of free radicals with antioxidant *vs* the protection of a probe against peroxidation)
- The medium in which peroxidation is tested (homogeneous solution *vs* dispersions, such as lipoproteins or model membranes)
- The inducer of peroxidation (e.g., organic free radical generating system *vs* transition metal ions)
- The parameter measured (e.g., concentration of malondialdehyde *vs* concentration of dienic hydroperoxides)
- Kinetic aspects of the assay (kinetic experiments *vs* measurement at one predefined time-point)

Notably, the results of evaluation may depend dramatically on the specific chosen assay, which reflects the dependence of the efficiency of antioxidants on the conditions.

Here we describe the method of evaluation of antioxidant capacity based on the ability of antioxidant to delay rapid peroxidation of lipids in human serum induced by copper ions [6]. The method is based on our previously developed optimized kinetic assay for oxidizability of blood lipids in unfractionated human serum [7]. This assay allows for ex vivo estimation of OS in serum and, therefore, the method for antioxidant evaluation can be considered as (relatively) physiologically relevant [6, 8]. Being based on kinetic measurements, the protocol is free from typical artifacts of "one time-point estimate."

The protocol includes continuous spectrophotometric monitoring of copper-induced peroxidation of unfractionated serum in the UV-range at 245 nm (Fig. 1). Specifically, we monitor the accumulation of conjugated dienic hydroperoxides (B) which are the main product of peroxidation of the polyunsaturated fatty acids (and their derivatives) contained in serum lipoproteins (A):

$$\underset{\text{A}}{-CH=CH-CH_2-CH=CH-} + O_2 \rightarrow \underset{\text{B}}{-CH=CH-CH=CH-CH(OOH)-}$$

Additional products of lipoprotein peroxidation, such as 7-ketocholesterol and (poly)unsaturated carbonyl compounds also contribute to the measured optical density at 245 nm [7].

Kinetics of peroxidation in the absence of antioxidant is compared with the kinetics of peroxidation with antioxidant added to serum (Fig. 2). Addition of an antioxidant delays the rapid oxidation of serum lipids in a dose-dependent manner (Fig. 2a). The same concentrations of different antioxidants differ quantitatively in their effect on lag phase (Fig. 2b). The prolongation of the

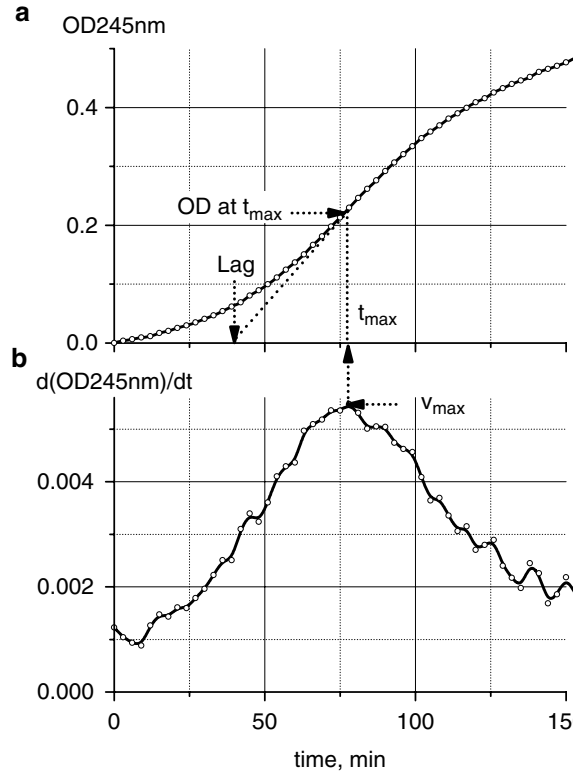

Fig. 1 A typical kinetic profile of copper-induced peroxidation of serum lipids and definition of the kinetic parameters lag, t_{max} and v_{max} used in this protocol (adopted from [6]). Panel (**a**) depicts the time course of the growth of absorbance at 245 nm (initial absorbance subtracted). Panel (**b**) is the first derivative of accumulation curve, depicted at panel (**a**), with respect to time

period of relatively slow peroxidation (lag) preceding the phase of rapid peroxidation is considered a measure of the antioxidant efficiency.

The prolongation of lag has been shown to be proportional to the concentration of antioxidant (Fig. 3). Hence, the relative prolongation of lag per unit of antioxidant concentration may serve as a quantitative measure of the capacity of the given antioxidant. Alternatively, the result of the assay may be expressed as the concentration of antioxidant required to prolong the lag by a predefined factor (e.g., to double the lag). Given the linearity of the effect of antioxidant on prolongation of lag [6], the assay can be conducted at one concentration of an antioxidant (e.g., at 2 μM). However, we recommend several measurements at different concentrations to improve the accuracy.

In relative terms, different sera give similar results. The variability of results obtained for different sera may be further reduced by normalization of the results to those obtained with a "standard

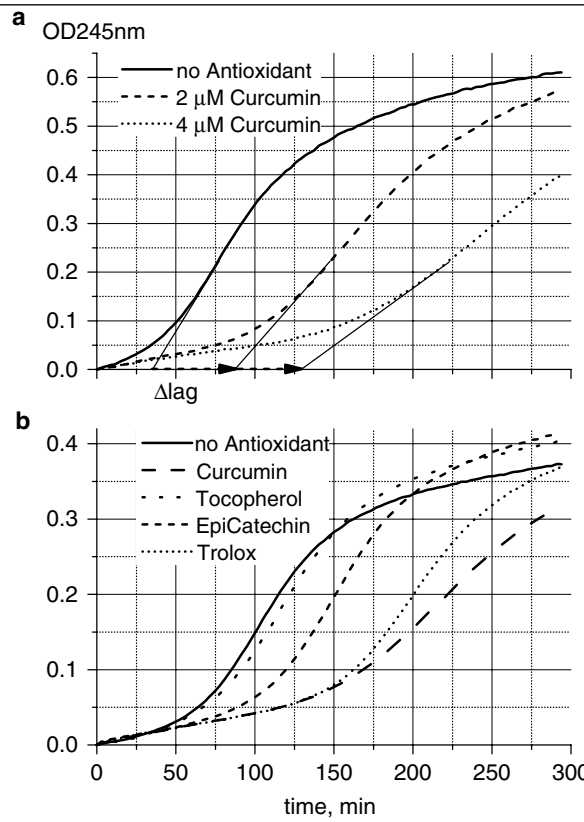

Fig. 2 The concentration-dependent effect of antioxidants on copper-induced peroxidation of serum lipids (adopted from [6]). Panel (**a**) shows the concentration-dependence of the effect of curcumin (the change of the lag is depicted by *arrows*). Panel (**b**) demonstrates the effects of the different antioxidants, added at a fixed concentration (2 μM)

antioxidant" (e.g., the water-soluble analog of α-tocopherol denoted TROLOX). In the latter case, the efficacy of the tested antioxidant is compared to the efficacy of TROLOX and the results are expressed in unitless TROLOX equivalents (TE) [4].

2 Materials

2.1 Equipment

UV-Vis spectrophotometer with linearity range up to 2 OD units at least equipped with automatic sample changer and thermostat.

2.2 Reagents

2.2.1 Preparation and Storage of Sera

Venous blood from individuals fasting for 12 h is drawn into tubes containing no anticoagulant and centrifuged at 1,000 × *g* for 20 min at 4 °C. Sera samples can either be used immediately or stored at −70 °C for several months without apparent changes of peroxidation kinetics. In the latter case samples are thawed and equilibrated before experiment at room temperature.

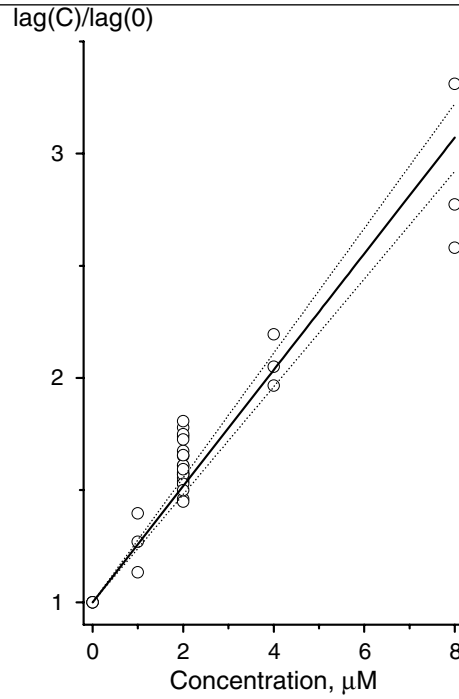

Fig. 3 The concentration-dependence of the relative prolongation of lag that is used to quantitate antioxidative effect of antioxidant on the peroxidation of serum lipids (*circles* depict results for different sera) (adopted from [6]). Data for epicatechin are given to exemplify the typical dependence. *Solid line* depicts the linear regression, *dotted lines* depict the 95 %CI. The slope of the linear regression gives *k*, the relative prolongation of lag per 1 μM epicatechin, as described in the text

2.2.2 Stock Solutions

1. Copper(II) chloride.
   5 mM solution of $CuCl_2$ in *water*.
2. Phosphate saline buffer (PBS).
   Water solution, containing 3.3 mM NaH_2PO_4, 3.3 mM Na_2HPO_4, and 146 mM NaCl with pH adjusted to 7.4.
3. Sodium citrate.
   7.5 mM solution of sodium citrate in PBS.
4. TROLOX solution.
   0.2 mM solution of TROLOX in PBS.
5. Tested Antioxidant solution.
   Water-soluble antioxidants are dissolved in PBS. Water-insoluble antioxidants are dissolved in redox-inactive, water-mixable organic solvents with negligible UV-light absobtion at 245 nm (e.g., methanol or ethanol). In the latter case, the same volume of the chosen solvent is also added to the control cuvette, containing no antioxidant.

The concentration of antioxidant is chosen to obtain the required concentration of antioxidant after final dilution (e.g., a stock solution of 0.2 mM antioxidant is prepared to obtain a final concentration of 2 μM in a cuvette of 1.5 mL volume if 15 μL aliquot is used for each cuvette). If several concentrations of the same antioxidant are tested, a stock solution can be sequentially diluted to keep the aliquot volume constant. The latter is especially important if an organic solvent is used.

2.3 Supplies

1. Quartz cuvettes with optical pathway 1 cm or any other cuvettes with minor absorbtion of the UV-light at 245 nm.
2. MS Excel © and any other software for data treatment allowing for numerical differentiation (e.g., Origin © by OriginLab).

3 Methods

3.1 Spectrophotometric Monitoring of Peroxidation Kinetics

In each experiment, a control sample containing no antioxidant and samples containing different concentrations of antioxidant and/or different antioxidants are measured simultaneously. If the aim is to obtain results in TROLOX equivalents, TROLOX is added into one of cuvettes (instead of antioxidant).

Kinetics of peroxidation of serum lipids is monitored as described in [7]. Specifically, 30 μL of serum (*see* **Note 1**) is diluted in a buffered solution containing high concentrations of citrate (144 μL of sodium citrate stock solution; final concentration 720 μM) in a quartz cuvette (optical pathway 1 cm). The stock solution(s) of antioxidant(s) are introduced into each of the cuvettes (except of the control one). Copper(II) chloride (30 μL of stock solution; final concentration 100 μM) is then added to initiate lipid peroxidation (final solution volume of 1.5 mL) (*see* **Notes 2** and **3**). The volume of PBS is calculated as the difference between final solution volume of 1.5 mL and the sum of volumes of stock solutions of sodium citrate, serum, copper chloride and antioxidant (when added). One (control) cuvette contains no antioxidant. Reference cuvette (for double beam spectrophotometer) contains PBS.

Absorbance of UV light at 245 nm should be monitored continuously during 5 h (at 3 min intervals), using a spectrophotometer equipped with an automatic cell changer and a thermostat. The time-course of the absorbance of UV light is recorded at 37 °C at 245 nm, where the contribution of albumin and of scattering of light to the spectrum is much lower than at 234 nm (absorbtion maximum for the main peroxidation product, i.e., conjugated dienic hydroperoxides) (*see* **Note 4**).

The complex kinetics of increase in the absorbance with time reflects the time dependence of the formation of hydroperoxides, 7-ketocholesterol, and other absorbing peroxidation products.

Examples for such kinetic profiles are given in Figs. 1 and 2. The initial OD is due to the absorption of light by serum components (mostly albumin and preoxidized lipids) and scattering of light by particles. Together, the observed initial OD constitutes about 1 OD unit and varies for different serum samples. Assuming that this contribution to the observed OD is relatively constant throughout the time course of peroxidation, the background OD values of the sera were subtracted from the OD measured during peroxidation. Notably, the measured OD values (less than 2 OD units) should be always within the linearity limit of the spectrophotometer.

3.2 Treatment of Experimental Data. Determination of Characteristic Parameters

The time-dependencies of optical density at 245 nm (OD245), obtained as described above (Subheading 3.1), should be exported from the spectrophotometer to an appropriate software, tabulated as a worksheet (first column—time, min; following columns—OD245 values for all sera samples). The initial optical density for each sample (OD245 value at time zero) should be subtracted from OD245 values at each time point and this "normalized" data should be plotted in coordinates of OD245 versus time.

The lag time is used as a parameter for evaluation the relative capacity of antioxidants. It can be determined either graphically (manually) or via calculations.

We define the lag as the intercept of the line, approximating the propagation phase of peroxidation (i.e., of the line with the slope equal to the maximal rate, crossing t_{max}) on the time axis (i.e., at OD = 0) (Fig. 1). The alternative definition of the lag as the time-coordinate of the crossing of two lines approximating respectively initial slow peroxidation and propagation phases is ambiguous.

As obvious from the above definition of the lag, graphical (manual) determination of lag may be conducted via drawing a tangent to the plot of OD245 versus time in the point at which the oxidation rate is maximal (Figs. 1 and 2a). Since the major part of propagation phase occurs usually with (almost) constant rate, this tangent actually represents a linear approximation of the propagation kinetics.

Alternatively, the lag may be calculated analytically. Equation 1 gives the relationship between lag and the parameters that can be readily obtained from the experimental data on the time-dependence of OD245.

$$\text{lag} = t_{max} - \frac{\text{OD}_{t_{max}}}{v_{max}} \quad (1)$$

where v_{max} is the maximal peroxidation rate $\left(\frac{d(\text{OD245})}{dt}\right)_{max}$ (in units Optical density per minute), t_{max} is the time-point at which

this maximal rate is achieved (in minutes) and $OD_{t_{max}}$ is the value of optical density at t_{max}, as depicted in Fig. 1.

Practical calculation of lag includes the following consecutive procedures (*see* also Fig. 1):

- Each of the time dependencies of OD245 adjusted for background absorbtion and scattering is differentiated with respect to time by any appropriate software for data treatment (differentiation with smoothing may be required for dizzy profiles). The outcome of the differentiation with respect to time is the time dependence of the peroxidation rate.
- The values of the maximal rate (v_{max}) and of the time at which this rate is achieved (t_{max}) are determined from the time dependencies of the peroxidation rate. Given the value of t_{max}, optical densities of $OD_{t_{max}}$ is taken from time dependencies of OD245 adjusted for background absorbtion.
- Lag values for all samples are calculated applying Eq. 1 to sets of v_{max}, t_{max}, and $OD_{t_{max}}$ for each of studied samples.

3.3 Ranking Antioxidants and Relevant Calculations

The capacity of antioxidant, as evaluated by prolongation of the lag phase, can be expressed by several interrelated parameters [6]:

- Relative prolongation of lag per 1 μM of antioxidant (k, μM^{-1}) (*see* **Note 5**)
- Concentration, required to double the lag (C_{2lag}, μM) (*see* **Note 5**)
- Concentration of TROLOX, resulting in prolongation of lag equal to prolongation caused by 1 μM antioxidant (TROLOX equivalents).

The empirical linear dependence of the relative prolongation of lag on antioxidant concentration is described by Eq. 2:

$$\frac{\mathrm{lag}(C)-\mathrm{lag}(0)}{\mathrm{lag}(0)}=\frac{\mathrm{lag}(C)}{\mathrm{lag}(0)}-1=kC \qquad (2)$$

where $\mathrm{lag}(C)$ is the lag at an antioxidant concentration of C μM (whereas $\mathrm{lag}(0)$ is the lag in the absence of antioxidant for the same serum sample). It may be concluded from Eq. 2 that

$$k=1/C_{2\mathrm{lag}} \qquad (3)$$

To calculate k, the concentration dependence of lag is analyzed after measuring lag at several concentrations of antioxidant and in the absence of antioxidant for the same serum. The slope of the linear fit of the plot of $\mathrm{lag}(C)/\mathrm{lag}(0)$ as a function of the concentration of the added antioxidant gives the value of k (Fig. 3).

The linear dependence of the relative prolongation of lag on concentration allows for evaluation of k from measuring lag at merely one concentration of antioxidant (Eq. 4):

$$k = \frac{\frac{\mathrm{lag}(C)}{\mathrm{lag}(0)} - 1}{C} \tag{4}$$

Of course, measuring k at multiple concentrations yields more precise values than the simplified method and is less likely to yield misleading results (e.g., due to the choice of the antioxidant concentration beyond the limits of linear dependence). Our experience shows that 2 μM is an optimal initial guess for the antioxidant concentration in such "one-concentration approach."

As mentioned above, $C_{2\mathrm{lag}}$ can be readily calculated from the values of k (Eq. 3). Unitless values of TROLOX equivalents (TE) may be easily computed based on $C_{2\mathrm{lag}}$ or k for antioxidant and TROLOX as given by Eq. 5:

$$\mathrm{TE} = k_{\mathrm{antioxidant}} / k_{\mathrm{TROLOX}} = C_{2\mathrm{lag(TROLOX)}} / C_{2\mathrm{lag(antioxidant)}} \tag{5}$$

Notably a higher value of k corresponds to lower $C_{2\mathrm{lag}}$ (Eq. 3). Accordingly, high antioxidant capacity results in high values of k and low values of $C_{2\mathrm{lag}}$. Similarly, high values in TE units reflect high capacity.

4 Notes

1. Only sera samples with optical density (at 50-fold dilution) of about 1 OD unit below the upper limit of the linearity range of the used spectrophotometer can be used for the assay.
2. The order of addition of the components given in this protocol (buffer—citrate—serum—antioxidant—copper chloride) should be kept thoroughly. Careful stirring of samples in the cuvettes by bubbling air via pipette after addition of copper chloride, is strongly recommended. We recommend also closing the cuvettes with plastic caps.
3. The temperature (37 °C) of the liquid in cuvettes (e.g., in reference sample) should be measured prior to addition of copper chloride. Spectrophotometric measurements begin immediately after mixing the content of the cuvettes. Control and tested samples should reside in the same compartment of the sample changer.
4. Averaging time of measurement for spectrophotometer should be as long as possible to get smooth kinetic profiles.
5. If an antioxidant of unknown composition (and molecular mass) is tested, the relative prolongation of lag should be calculated

per mass concentration rather than per molar concentration. The initial guess for preparation of antioxidant stock solution may be set to 300 Da (or higher if low concentration of active antioxidant component is expected, e.g., in samples of natural origin such as plant extracts).

Acknowledgements

We thank the Israel Science Foundation (Grant 362/02) and the Lady Davis Chair of Biochemistry for partial financial support.

References

1. Halliwell B, Gutteridge J (2007) Free radicals in biology and medicine. Oxford University Press, New York
2. Dotan Y, Lichtenberg D, Pinchuk I (2004) Lipid peroxidation cannot be used as a universal criterion of oxidative stress. Prog Lipid Res 43:200–227
3. Niki E (2011) Do free radicals play causal role in atherosclerosis? Low density lipoprotein oxidation and vitamin E revisited. J Clin Biochem Nutr 48:3–7
4. Frankel EN (2007) Antioxidants in food and biology. The Oily Press, Bridgwater, England
5. Prior RL, Wu XL, Schaich K (2005) Standardized methods for the determination of antioxidant capacity and phenolics in foods and dietary supplements. J Agric Food Chem 53: 4290–4302
6. Pinchuk I, Shoval H, Bor A, Schnitzer E, Dotan Y, Lichtenberg D (2011) Ranking antioxidants based on their effect on human serum lipids peroxidation. Chem Phys Lipids 164:42–48
7. Schnitzer E, Pinchuk I, Bor A, Fainaru M, Samuni AM, Lichtenberg D (1998) Lipid oxidation in unfractionated serum and plasma. Chem Phys Lipids 92:151–170
8. Pinchuk I, Shoval H, Dotan Y, Lichtenberg D (2012) Evaluation of antioxidants: scope, limitations and relevance of assays. Chem Phys Lipids 165:638–647

Chapter 14

Identification of (Antioxidative) Plants in Herbal Pharmaceutical Preparations and Dietary Supplements

Eric Deconinck, Deborah Custers, and Jacques Omer De Beer

Abstract

The standard procedures for the identification, authentication, and quality control of medicinal plants and herbs are nowadays limited to pure herbal products. No guidelines or procedures, describing the detection or identification of a targeted plant or herb in pharmaceutical preparations or dietary supplements, can be found. In these products the targeted plant is often present together with other components of herbal or synthetic origin.

This chapter describes a strategy for the fast development of a chromatographic fingerprint approach that allows the identification of a targeted plant in herbal preparations and dietary supplements. The strategy consists of a standard chromatographic gradient that is tested for the targeted plant with different extraction solvents and different mobile phases. From the results obtained, the optimal fingerprint is selected. Subsequently the samples are analyzed according to the selected methodological parameters, and the obtained fingerprints can be compared with the one obtained for the pure herbal product or a standard preparation. Calculation of the dissimilarity between these fingerprints will result in a probability of presence of the targeted plant. Optionally mass spectrometry can be used to improve specificity, to confirm identification, or to identify molecules with a potential medicinal or antioxidant activity.

Key words Identification of plants, Herbal pharmaceuticals, Chromatographic fingerprints, UV detection, Mass spectrometry, Similarity analysis

1 Introduction

Plant and herbs play an important role in traditional medicine and herbal-derived medicines for at least 5,300 years; the oldest documented case of the use of herbs as a medicine regards the oldest natural mummy in Europe, who was found with the woody fruits of *Piptoporus betulinus*. These fruits contain agaric acid and toxic resins and were probably used to treat *Trichuris trichiura*, an intestinal parasite [1].

The most known herbal treatments can be found in traditional Chinese medicine, but the interest in plants as a source for treatments was and is in fact worldwide. An important part of the medicines used today find their origin in herbal products from which

Donald Armstrong (ed.), *Advanced Protocols in Oxidative Stress III*, Methods in Molecular Biology, vol. 1208,
DOI 10.1007/978-1-4939-1441-8_14, © Springer Science+Business Media New York 2015

new chemical identities were isolated and later synthesized. Examples of this are acetyl salicylic acid, digoxin, morphine, paclitaxel, atropine, and vinblastine, nowadays used in allopathic medicine [2–6]. However, during the last decade, the interest in traditional medicine and herbal alternatives for allopathic treatments is growing, especially in the western world. This is due to a general trend of returning to traditional and natural products, which is exhaustively used in marketing campaigns. These campaigns are also influencing the public opinion about the choice of type of medicine. Furthermore, the concerns about the adverse effects of chemical drugs and questioning of the allopathic medicines are stimulating the popularity of herbal medicines [7].

The fast-growing industry of traditional medicines and herbal products increased the concern about the quality and the safety of these products. That is why the World Health Organization and other regulatory bodies started with programs in order to set quality parameters and guidelines to conduct quality control [7–13]. Quality control of natural products is extremely important since the effectiveness of these products depends on the concentration of certain active components they contain. However, these concentrations of active ingredients are influenced by numerous factors as the climate, cultivation conditions, harvest time, drying, storage, etc. Due to this influence, the concentrations may vary and therefore affect the activity of the product [14–23]. This may cause ineffectiveness on one hand and possible toxicity on the other, both causing a potential risk for public health.

An example of these variations can be found in the quality control of green tea. Green tea, originating from *Camellia sinensis*, is associated with many beneficial effects, like protection against cancer and cardiovascular diseases. These effects would be related to the presence of flavonoids, like epigallocatechin gallate, epigallocatechin, epicatechin gallate, and epicatechin [24–27], typically present in tea. As a consequence, one of the main quality criteria for green tea is its total antioxidant capacity, dependent on the levels of flavonoids present. These concentrations can vary dependent of external factors, like environmental parameters and storage of the dried leaves but also in function of the treatment or fermentation. The total antioxidant capacity is traditionally measured using spectroscopic techniques like the Trolox-equivalent antioxidant capacity (TEAC) assay [28, 29] or the 2.2-diphenyl-1-pikrylhydrazyl (DPPH) test [30].

The mentioned flavonoids, present in green tea, are part of a larger group of naturally occurring antioxidants. This group is commonly referred to as natural phenolics and comprises phenolic acids, tannins, stilbenes, and lignans as well. Flavonoids are highly widespread in the plant kingdom and can be divided into 6 subgroups: (a) flavones, (b) flavonols, (c) flavanols, (d) flavanones, (e) isoflavones, and (f) anthocyanins according to their chemical

structure [31]. A second large group of antioxidants, found in nature, consists of carotenoids such as β-carotene (most abundant in fruits and vegetables) and lycopene (present in tomatoes) [32]. All these compounds are increasingly drawing attention because of their potential preventive effects on chronic diseases associated with oxidative stress like cancer and cardiovascular and neurodegenerative diseases [33].

The World Health Organization (WHO) first recognized the need for regulations of traditional medicines in the national drug policies in 1978 with the declaration of Alma-Ata on primary health care needs [34]. Since then, several national agencies, but also the WHO itself and other major advisory and regulatory bodies, like the American Food and Drug Administration (FDA) and the European Medicine Agency (EMA), issued a whole series of guidelines and quality criteria in order to guarantee the quality of traditional and herbal products.

Nowadays, the quality control and assurance of herbal products and traditional medicines is based on published monographs that describe the standards to which the considered product has to comply. The WHO published a whole series of monographs in the three volumes of "WHO monographs on selected medicinal plant," which are commonly used as authoritative monographs or as basis for the development of national monographs [34–37]. These monographs were adopted by the EMA, which additionally issued a list of herbal substances for assessment, including 63 finalized monographs and products with related monographs published in some national pharmacopoeias, like the ones of Germany, France, India, and China [38]. The herbal monographs published in, for instance, the European Pharmacopoeia generally use a combination of traditional microscopic and macroscopic evaluation of the products and chromatographic techniques like thin layer chromatography for identification of certain compounds or markers, high-pressure liquid chromatography for quantification, and sometimes gas chromatography for volatile compounds [39].

The disadvantage of these monographs and the legislations at hand is that they only focus on the pure herbal product, but not on pharmaceutical preparations in which the considered medicinal plant is often present in combination with other plants and some excipients. Examples of these are the presence of green tea extract in vitamin supplements for its antioxidative properties.

Another problem and an increasing threat to public health is the counterfeiting of medicines. Counterfeiting of medicines is a problem that has existed for centuries. During the first century, Pedanius Dioscorides, a Greek physician warned about the dangers of adulterated drugs [40]. Since then, many crises of falsifications of medicines have been documented [41]. Most of these crises involved falsified herbal medicines and resulted in many lethal accidents, due to toxicity and/or lack of effectiveness.

The WHO [42] defines a counterfeit drug as "one which is deliberately and fraudulently mislabelled with respect to identity and/or source. Counterfeiting can apply to both branded and generic products and counterfeit products may include products with the correct ingredients or with the wrong ingredients, without the active pharmaceutical ingredients (APIs), with insufficient active ingredient or with fake packaging." Even if this definition is, in the first place, written for traditional allopathic medicines, it also applies for herbal medicines, which are also often counterfeited.

The threat to public health originating from counterfeited and illegal products has increased during the past decade due to the growing popularity of the Internet. On the Internet a large variety of herbal medicines, dietary supplements, or natural products can be bought, and this is often from websites disclosing their identity. Several researches clearly showed that these products could endanger the patient's safety, due to three possible problems: (a) The product does not contain the correct plants and herbs, but other more common plants are used in order to create a cheap counterfeited product. (b) The product is adulterated with synthetic drugs, often in wrong doses, which are not mentioned on the packaging. Therefore, the patient does not know that he or she is taking a synthetic medicine which may cause adverse effects and interactions with other treatments. Examples of this can be found in the literature. For example, Savaliya et al. found adulterations of the traditional Indian aphrodisiac product *Ayurvedic* with sildenafil [43]. Numerous papers describe screening methods for the detection of herbal supplements, adulterated with anorexics like sibutramine and its analogue, rimonabant [44–48]. (c) The product contains some regulated or toxic plants, since these preparations are not controlled by a regulatory body and produced without respecting any quality norms.

This chapter will deal with the identification of plants in pharmaceutical preparations. It presents a strategy for target analysis based on the fingerprint approach. Detection of a certain plant in pharmaceutical preparations, especially in the herbal products sold via the Internet, is a real challenge since they are often powdered, mixed with other powders of synthetic or herbal origin, and compressed to tablets or contained in capsules. As a result the classical microscopic and macroscopic approaches for the identification of plants cannot be applied anymore. The chromatographic fingerprint approach, an approach widely used in pharmacognosy for identification and quality control of plants [49], can be interesting for the identification of toxic or regulated plants in the herbal products considered here.

A fingerprint can be defined as a characteristic profile reflecting the complex chemical composition of an analyzed sample and can be obtained by spectroscopic, chromatographic, or electrophoretic techniques. Chromatographic fingerprints are the most informative

type of fingerprints in plant analysis, since by spreading the information contained in the sample over time, the individual compounds and their underlying information can be revealed [50]. This is also the reason why chromatographic fingerprints are an interesting approach in the detection of certain plants in mixtures of herbal and/or synthetic powders.

This chapter presents a strategy that allows the fast development of a methodology for the detection and identification of a targeted plant or herb in herbal mixtures and pharmaceutical preparations. Therefore, chromatographic fingerprints are developed using a classical HPLC with diode array detection (Subheading 3.1). Next, the obtained fingerprint is used to search for the considered plant in self-made mixtures with lactose and different herbal matrices. The purpose of this is to validate the discriminative performance of the developed fingerprint (Subheading 3.2). Optionally HPLC coupled to mass spectrometry (LC-MS) can be used to proof the specificity of the observed peaks in the chromatographic fingerprint of standards and samples and to identify some of the major signals in the fingerprint of known flavonoids or alkaloids, whether or not they are with a therapeutic value or an antioxidative potential (Subheading 3.3). In the end the developed strategy can be used to identify the targeted plant in (commercial) samples (Subheading 3.4). In order to illustrate the methodology, the identification of *Passiflora incarnata* will be used as illustration throughout this chapter.

2 Materials

2.1 Standards and Samples

1. *Passiflora incarnata*, dry extract, Fagron (Waregem, Belgium). The extract responded to the monograph of the European Pharmacopoeia [39].
2. Three authorized herbal pharmaceutical preparations, Sedanxio® (Tilman, Baillonville, Belgium), Sedinal® Plus (Melisana, Brussels, Belgium), and Dormeasan® Forte (A. Vogel, Elburg, the Netherlands), were purchased in a local pharmacy.

2.2 Reagents and Matrices

1. Methanol, high-performance LC grade; acetonitrile, high-performance LC grade; ammonium formate (99 %); formic acid (99 %); ammonium acetate; glacial acetic acid; ammonium solution (32 %).
2. Buffer 1: 0.020 M ammonium formate buffer pH 3.0.
3. Buffer 2: 0.020 M ammonium acetate buffer pH 6.0.
4. Buffer 3: a 0.020 M ammonium acetate buffer of pH 9.0.
5. Matrix 1: lactose monohydrate.

6. Matrices 2, 3, and 4: herbal matrices originating from three herbal samples previously analyzed in our laboratory and found negative for synthetic drugs. In fact all types of matrices can be used (e.g., tea or herbal infusion mixtures) if one is sure that the targeted plant is not present.

2.3 Instrumentation

1. HPLC-DAD instrument: a Waters 2695 Alliance® chromatographic system (Waters Corporation, Milford, USA). The system consisted of a quaternary pump, a temperature-controlled autosampler, and a column heater, coupled to a Waters® 2998 diode array detector (DAD). The output signal was monitored and processed using the Waters Empower2 software.
2. HPLC-MS instrument: a Surveyor® separation module of Thermo Finnigan (Waltham, USA), consisting of a quaternary pump, a temperature-controlled autosampler, and a diode array detector. The surveyor® module was coupled to a LCQ Advantage® ion trap mass spectrometer, through an electrospray ionization source. Instrument control, data collection, and data processing were performed using the Xcalibur® software. The collision energy for fragmentation was set at 30 %. Detection was done in full-scan mode and MS^2 spectra were recorded in the data-dependent scan mode.
3. Chromatographic column: an Alltech Alltima® C18, 5 μm, 250 × 3 mm (Grace Davison Discovery Sciences, Lokeren, Belgium).
4. Chromatographic method: a gradient elution method starting at 90 % buffer solution and 10 % organic modifier, which is held for 2 min. After 2 min, a linear gradient is initiated, reaching 50 % organic modifier in 5 min, followed by a plateau of 7 min. After the plateau, a linear gradient reaches 90 % of organic modifier in 6 min which is held for 5 min before returning to the initial condition in 5 min. The total run time is 30 min. Injection volume was 20 μl, column temperature 30 °C, and the flow was 0.5 ml/min. The fingerprints were recorded at a wavelength of 254 nm (*see* **Note 1**).

3 Methods

3.1 Selection Optimal Conditions

1. In the first step, it is important to select the optimal extraction solvent for the targeted plant. Therefore, 125 mg of the dry extract is extracted with 25 ml of the respective solvents. After addition of the solvent, the mixture is vortexed and placed on an ultrasonic bath for 15 min. One milliliter of the extract was filtered through a 0.45 μm PTFE filter. The filtrate is used for injection.

For herbal extracts, the following solvents are used commonly: water, ethanol, methanol, acetonitrile, and their respective mixtures with 50 % water. Of course, if justified, other extraction solvents can be selected (*see* **Note 2**).

2. Each extract is injected on the chromatographic column and the DAD fingerprints are recorded. This series of extracts is analyzed with each combination of mobile phases, i.e., two organic modifiers, methanol and acetonitrile, and three buffers (*see* Subheading 2.2). This means that the series of extracts has to be analyzed six times (three buffers × two organic modifiers).

   From these results, the optimal parameters for fingerprint recording of the targeted plant can be derived. The combination of extraction solvent and mobile phase, giving the highest number of peaks, with an area under curve above a predefined threshold (e.g., 15,000), should be selected in first instance. When several combinations give the same number of peaks, the peak shapes and the resolutions can be taken into account. If the chromatographic system is equipped with a diode array detector, the optimal wavelength for detection, giving the highest mean response over the different peaks, can also be selected. It is our experience that a wavelength of 254 nm, which is almost standard, gives very good results for the different plants tested, but the option of another wavelength is of course always possible (*see* **Note 3**).

3. The selection of the optimal parameters can be performed by using the regression approach known from the domain of experimental designs. Therefore, the results obtained are considered as a full factorial design (each combination of parameters is tested and results (number of peaks) are obtained). A regression is performed, where the response is regressed in function of the parameters (extraction solvent, pH, and organic modifier). Response surfaces can then be obtained (*see* **Note 4**). As an example, Fig. 1 shows the regression surface obtained for the optimization of the fingerprints for *Passiflora incarnata*. Figure 1a shows the number of peaks in function of the extraction solvent and the pH, using methanol as organic modifier. In Fig. 1b acetonitrile was used as organic modifier. Both surfaces clearly show that the optimum (highest number of peaks) is obtained with pH 3 using water as extraction solvent. The number of peaks is also significantly higher using methanol as organic modifier. Based on these results, it was clear that the optimal parameters were ammonium formate buffer pH3 and methanol, as mobile phase, and water, as extraction solvent.

4. After selection of the optimal conditions, the repeatability of the fingerprints should be tested. Therefore, the standard dry

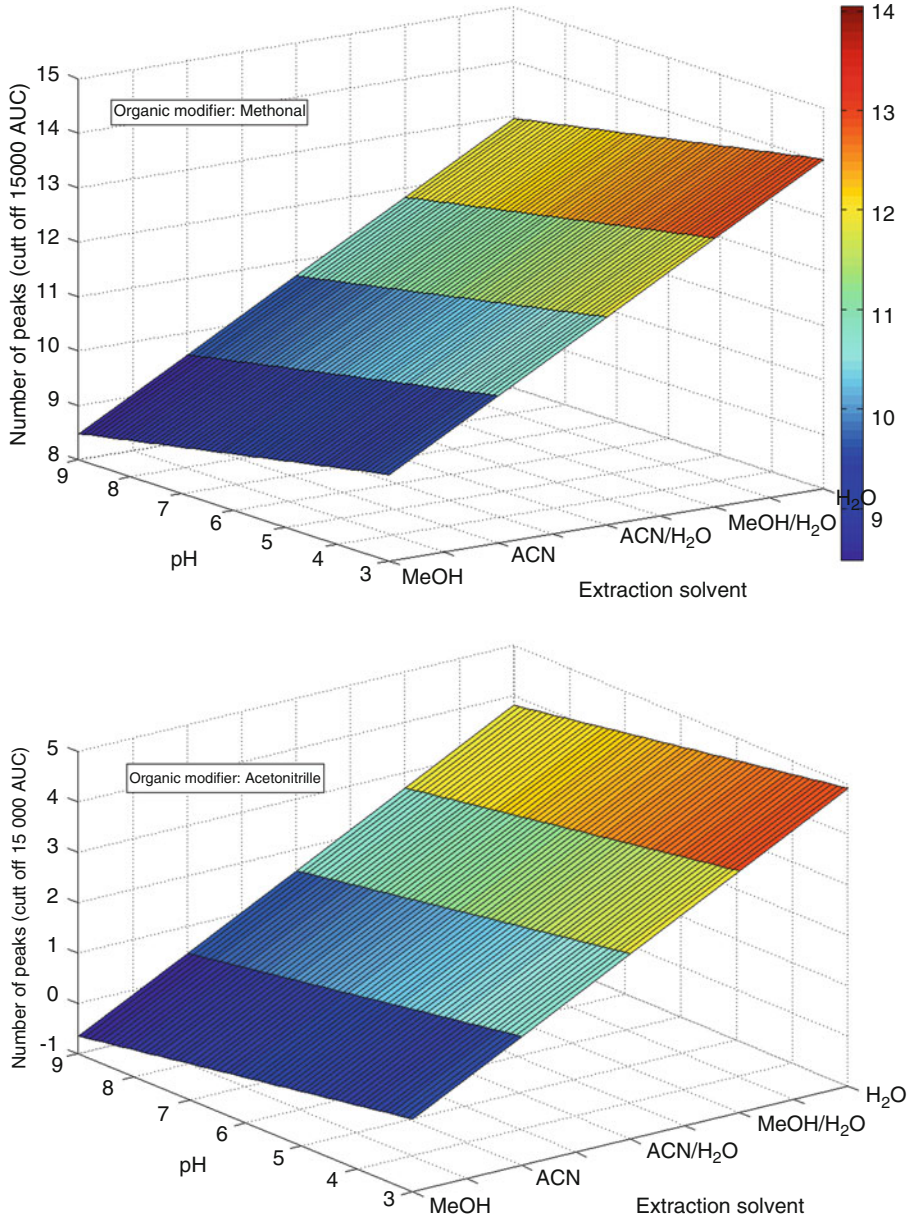

Fig. 1 Number of peaks (cutoff 15,000) in function of the pH and the extraction solvent using (**a**) methanol and (**b**) acetonitrile as organic modifier

extract should be analyzed three times during 3 days, using new extract each time. Ideally this should be performed on different batches of dry extract.

After recording the fingerprints, using the optimal conditions, a visual inspection based on overlays as well as a similarity analysis can be performed. In the most common similarity analysis,

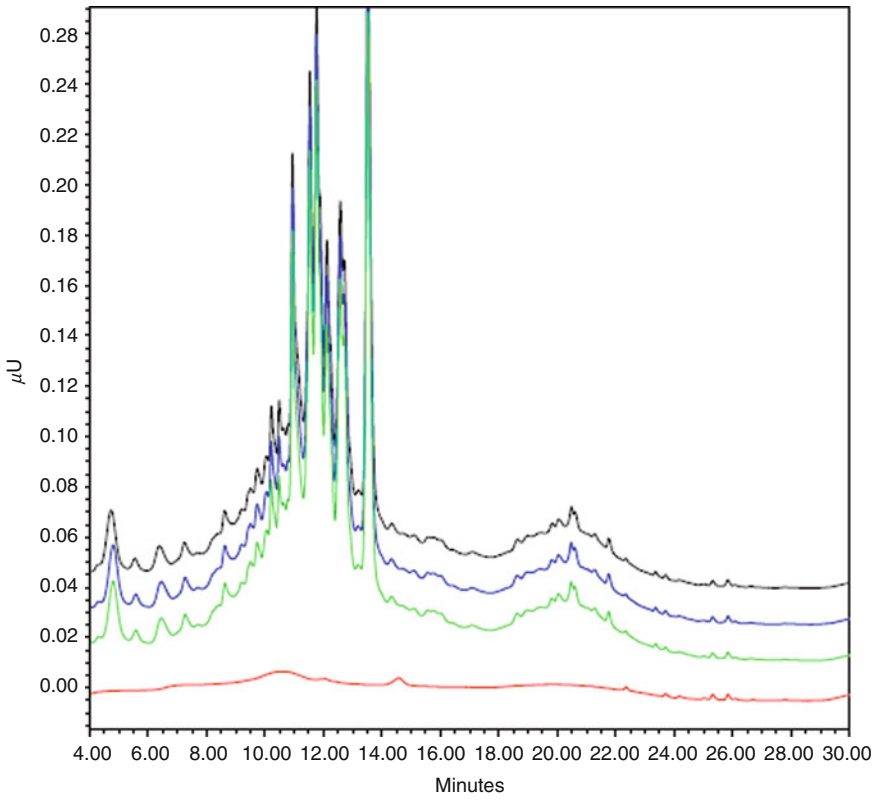

Fig. 2 Overlay of the mean fingerprint of 3 days (mean of three fingerprints a day) and a blank (*red line*)

the correlation between the chromatograms is calculated and the dissimilarity is calculated as

$$\text{Dissim} = 1 - |R|$$

with R the correlation coefficient [50].

For *Passiflora incarnata*, the overlay of the mean fingerprints of the three respective days is shown in Fig. 2. Dissimilarity values below 0.05 were obtained for each of the nine recorded fingerprints, which proof the high similarity of the fingerprints and the repeatability of the analysis.

3.2 Validation with Triturations (Spiked Samples)

1. For the dilution tests and the validation, all liquid-liquid extracts have to be performed with the selected solvent, described above. Triturations of 1/2, 1/4, and 1/10 of the dry extract were prepared with, respectively, lactose (matrix 1) and the three herbal matrices (matrices 2–4). One hundred twenty-five milligrams of the respective triturations was brought into 25 ml of selected solvent. The liquid-liquid extraction was performed as described above for the dry extract.
2. The fingerprints are recorded using the optimal conditions. Blanc solutions (extraction of lactose and the three herbal

matrices, respectively) and an extract of the standard (dry extract of the plant or herbal material) are prepared and injected together with the respective triturations.

3. Again the similarity can be evaluated based on the visual inspection of the overlays of the chromatograms and a similarity analysis. As an example, Fig. 3a shows the overlays of the fingerprints recorded for *Passiflora incarnata* and its respective triturations with lactose and three herbal matrices. Figure 3b represents the similarity matrix calculated as described in Subheading 3.1 bullet 4. In this figure the blue color represents the lowest dissimilarity or the highest similarity between the fingerprints. It can therefore be concluded that, although a lot of fingerprints are similar to the one of the dry extract (the lowest line in the plot), some are not (red color). The fingerprints with a similarity in the red zone probably suffer from matrix interferences due to the herbal matrix used for the triturations. Therefore, the visual evaluation and the similarity analysis might not be enough and a specificity test (*see* Subheading 3.3) might be necessary.

3.3 Specificity

During the validation of the developed fingerprints, it is necessary to check the specificity of the fingerprint. Therefore, fingerprint recording can be repeated using LC-MS in which the characteristic MS^2 spectra of the most important peaks can be compared between standard (dry extract) and the triturations/samples.

As an example, Fig. 4 shows the DAD fingerprint of *Passiflora incarnata* and its respective 1/10 triturations together with the MS^2 spectra of the most characteristic peaks (*see* **Note 5**).

3.4 Identification in Samples

1. To record the fingerprints for the commercial available samples, one crushed tablet or capsule content was extracted with 25 ml of the selected solvent following the same procedures as described above for the dry extract and the triturations.
2. The DAD fingerprints are recorded together with an extract of the standard (dry extract). The similarity between the fingerprints of the standard and the sample can be evaluated visually and the dissimilarity can be calculated (*see* **Notes 6** and **7**).

   As an example, the DAD fingerprints of *Passiflora incarnata* and three commercial preparations containing this plant in doses of, respectively, 80 % m/m, 3.5 % m/m, and 1.9 % m/m are shown in Fig. 5. Dissimilarities of 0.065, 0.094, and 0.189 were obtained, respectively. Based on the visual inspection as well as on the low values for dissimilarity, the presence of *Passiflora incarnata* in the commercial preparations could be confirmed.

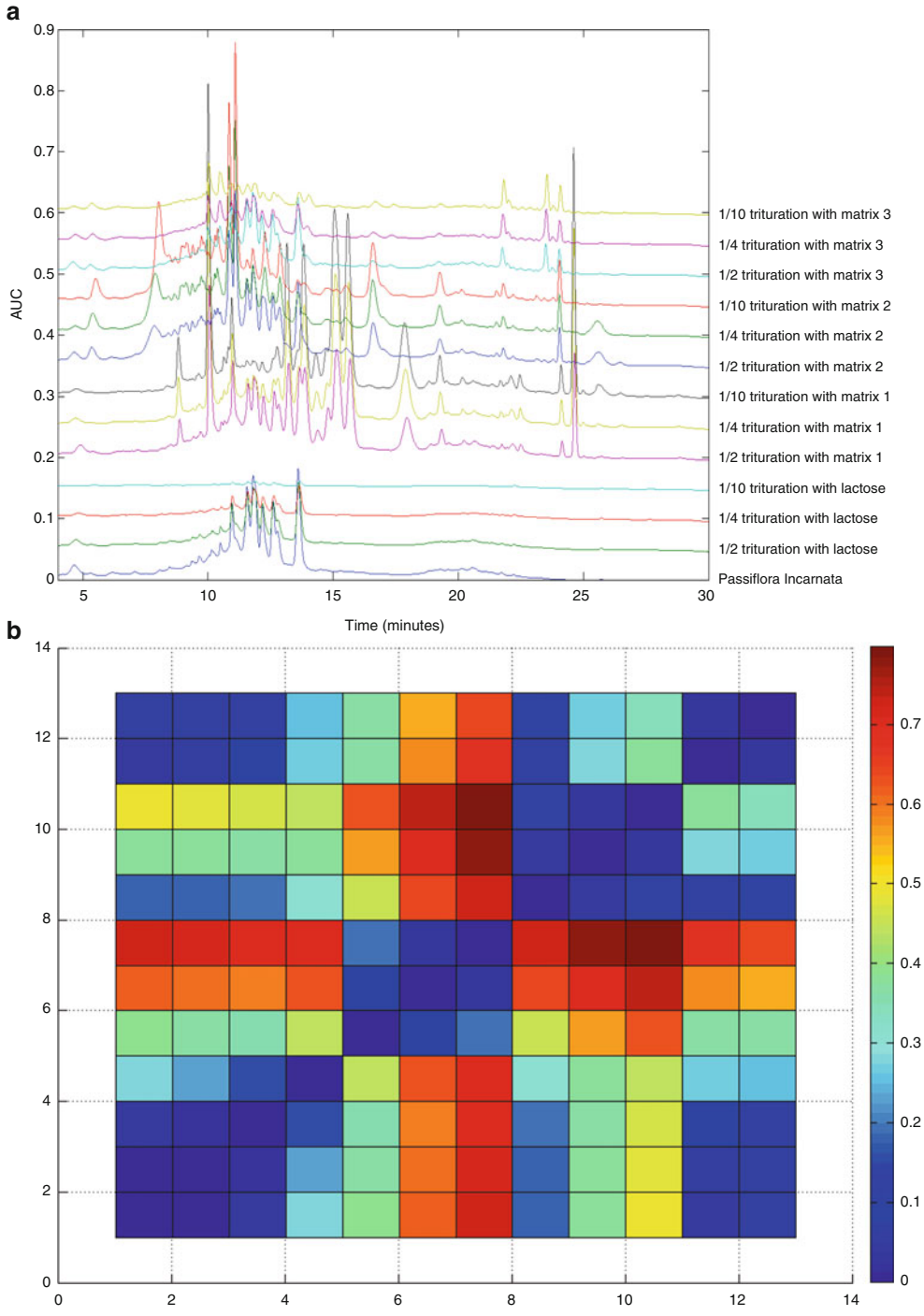

Fig. 3 (**a**) Overlay of the fingerprints for *Passiflora incarnata* and its respective triturations; (**b**) similarity matrix represented as color map

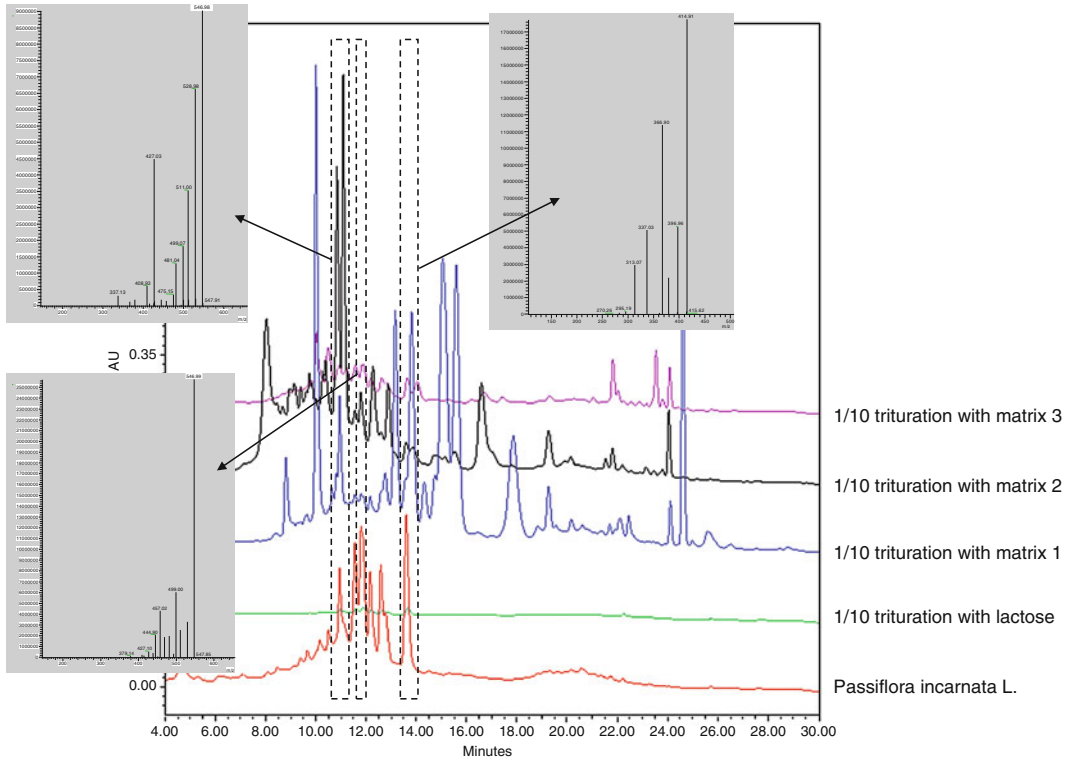

Fig. 4 Overlay of the fingerprints obtained for *Passiflora incarnata* dry extract and its respective 1/10 triturations with the MS^2 of the three most characteristic peaks

4 Notes

1. Possible adaptations to the chromatographic gradient.

   The chromatographic gradient presented in Subheading 2.3 bullet 4 is a general gradient that results in characteristic fingerprints for most of the plants tested, allowing identification of the targeted plants in formulations and dietary supplements. However, adaptations of the gradient program might be necessary or advised, for example, when the targeted plant contains some specific known alkaloids, flavonoids, or other molecules which strongly interact with the chromatographic column. In that case, another column with less interactions or a stronger gradient can be applied. On the other hand, the gradient might be too long for some plants, showing no characteristic signals anymore after a certain time point. In this situation, the gradient can be shortened, gaining time in analysis and simplifying the data treatment. Another possibility is the transfer of the method to ultra high performance liquid chromatography (UHPLC) in order to gain time and save on solvent consumption.

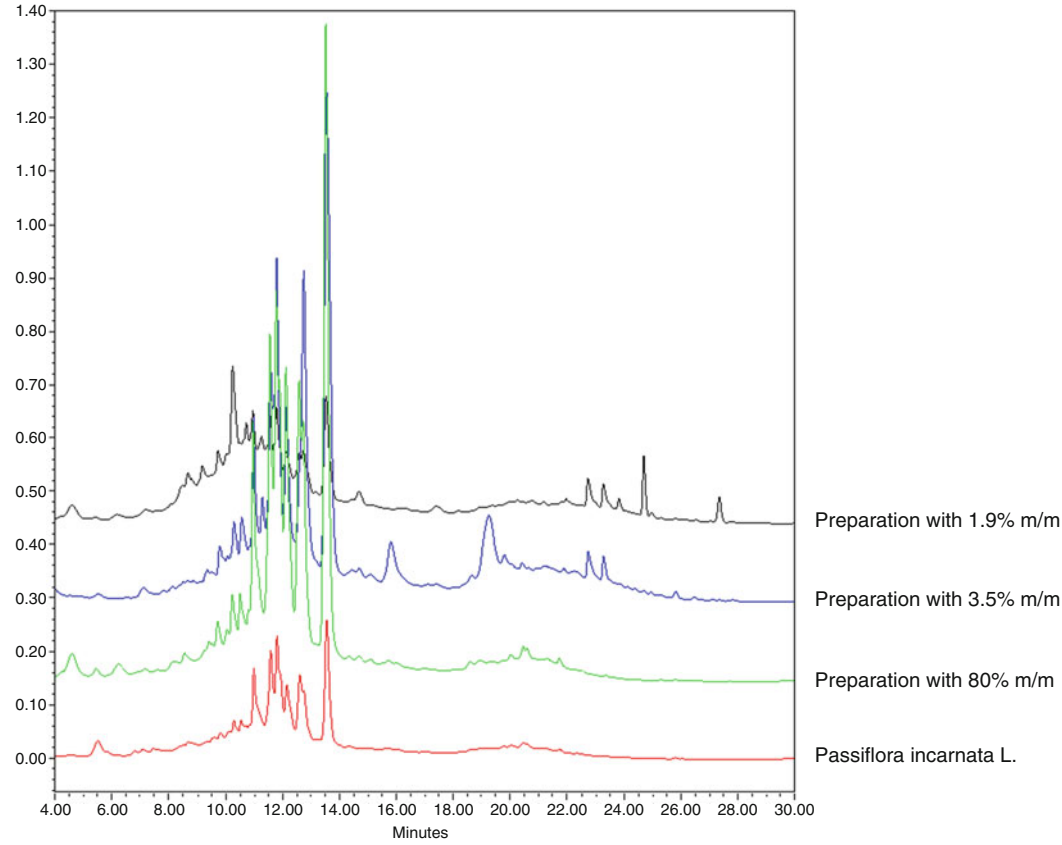

Fig. 5 Overlay of the fingerprints of *Passiflora incarnata* and three commercial preparations containing *Passiflora incarnata*

2. Lack of specificity.

   For some plants, a lack of specificity can be observed, when applying the approach as described above. Lack of specificity can be due to the choice of the extraction solvent, the time of extraction, or a problem with the chromatographic method. In the first two cases, it is advised to test other solvents and (if possible) their mixtures with water, besides the ones originally selected. If no better profiles are obtained, one should look for adaptations to the chromatographic method. For the chromatographic problems, it is advised to first look at the different wavelengths when DAD is used or when a classical UV detector is used to record a new fingerprint at a more general wavelength as 210 or 230 nm and a few wavelengths in the higher ranges. If a more specific profile is obtained, the wavelength can be optimized starting from this point. When this does not result in satisfying results, the gradient and the column might be adapted as discussed in **Note 1**.

3. Multiple fingerprints.

   In order to increase specificity, the use of a combination of fingerprints can be considered. The possibilities are endless going from using different wavelengths for the UV detection to different detection techniques (DAD, ELSD, MS) to using a set of chromatographic systems each resulting in different complementary fingerprints. For instance, the use of a combination of fingerprints on different (dissimilar) chromatographic systems was used in the quality control of green tea and more precisely in the prediction of the antioxidant capacity [51]. This way of combining fingerprints can also be valuable in the search for herbal components with antioxidative properties or medicinal activity, since it allows to acquire a very complete image of the composition of a plant and to trace the differences in composition between different species from which some have high activity and others have none [52–55]. After identification of these differences, the compounds related to it can be identified using other techniques like mass spectrometry. An example of this is the identification of potential antioxidant compounds in *Mallotus* species, belonging to the family of the *Euphorbiaceae* and used in the traditional medicine in Vietnam and China [53–55].

4. Use of experimental design.

   For the optimization of the chromatographic parameters, the use of experimental design can be valuable. In the presented approach, a general chromatographic gradient was used in which the pH of the buffer and the organic solvent were varied. Since in the first instance a limited set of extraction solvents was used, the number of injections is only 30, from which the optimal conditions could be derived. Since only a few extractions have to be prepared and the injections are, in most cases, done automatically, it was chosen to perform all experiments in order to minimize the possible loss of data. However, in some cases, researchers could be interested in varying other parameters like the gradient, chromatographic column, time of extraction, extraction temperature, etc. In this case, the optimization is more complex and the use of experimental design (optimization designs) becomes necessary. For more explanation on the use of experimental designs, the readers are referred to [50].

5. Use of MS for fingerprinting and identification confirmation.

   In the presented approach, mass spectrometry was used to check the specificity of the developed fingerprints. However, LC-MS can also be used as a fingerprinting technique on itself, replacing the UV detection by mass spectrometry. The advantages of using MS for fingerprint development are mainly the higher specificity that can be obtained and the possibility to identify the characteristic compounds observed. This identifica-

tion can be done based on the fragmentation patterns obtained for the compounds or on the exact masses, depending on the type of mass spectrometer used. Another advantage is the identification of known medicinal active components, e.g., some flavonoids known to have a high antioxidative potential and to proceed immediately with a semiquantitative analysis of these components in order to perform a quality control of the formulation analyzed. A disadvantage of such an approach, especially when the aim is to check whether or not a possible illicit preparation contains a certain plant, is the high costs of mass spectrometric analysis. Moreover, not all laboratories charged with the analysis of counterfeit products and illegal dietary supplements are equipped with expensive LC-MS instruments.

Within the approach described in this chapter, LC-MS can be used as a complementary technique for identification confirmation. When the fingerprint for a sample corresponds with the one obtained for the dry extract or standard preparations, but doubts arise, since, for example, less than 70 % match is obtained, recording the mass spectra of the most characteristic peaks of both sample and standard can then proof unambiguously the presence or non-presence of the targeted plant. As an illustration, Fig. 6 shows the fingerprints obtained in Subheading 3.4, for commercial samples containing *Passiflora incarnata* together with the MS^2 spectra. The match between the fingerprints of the samples and the dry extract, combined with the correspondence of the MS^2 spectra, leaves no doubt about the presence of *Passiflora incarnata* in the tested preparations.

6. Matrix interference.

In most cases the targeted plants are present in formulations or dietary supplements containing other powdered plants and/or synthetic powders. Due to the endless variations in matrices in which the targeted plants can be present, it is impossible to develop a generic method, ensuring 100 % identification in all different types of matrices. Especially when other plants are present, it is logical that components originating from these plants are extracted together with the characteristic compounds of the plant of interest.

Therefore, the presented approach should be used in routine analysis, like how infrared or mass spectra are used. The fingerprint is matched against the fingerprint of the targeted plant. Subsequently, a percentage of correspondence and so the probability of presence of the targeted plant are calculated. For these calculations, several different similarity measures can be applied; the calculation of the correlation between the chromatograms as discussed in Subheading 3.1 bullet 4 is the most known [56].

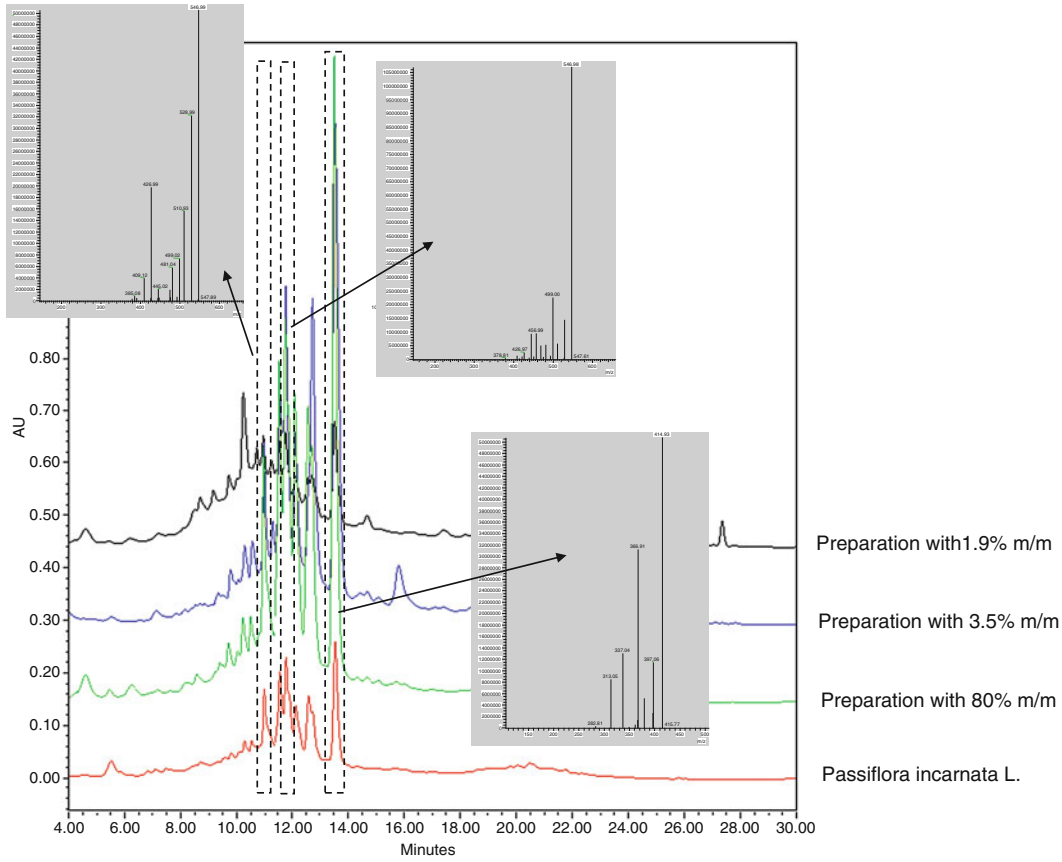

Fig. 6 Overlay of the fingerprints of *Passiflora incarnata* and three commercial preparations containing *Passiflora incarnata* together with the MS^2 spectra of the most characteristic peaks

7. Alignment of chromatograms.

Another problem that can occur when performing this type of analysis, especially when large amounts of samples are screened for the presence of a targeted plant, is the occurrence of time shifts. These time shifts can be due to column aging, temperature changes, and mobile phase changes. The shifts in time will result in lower similarity values than when no time shifts occur, resulting in bad matches with the fingerprints of the standard. Two different approaches can be used to solve or avoid this problem. A practical approach, when large amounts of samples have to be analyzed, is to reinject the extract of the dry extract or the standard preparation after each predefined number of samples. Another approach is alignment of chromatograms. This is a chemometric technique in which the successive chromatograms or fingerprints are corrected for time shifts towards a standard chromatogram. Different alignment or warping techniques exist, from which the most popular is correlation optimized warping (COW) [56].

5 General Note

The methods described in this chapter enable to screen for and identify a targeted plant. The generality of the proposed methods allows therefore also the application to herbal products with antioxidant capacity. Due to the commercial added value of adding plant extracts with antioxidant capacity to food supplements, the number of supplements containing such plants is increasing, both on the regular as on the illegal market. Applications of the above strategy allow the identification of the plants in these preparations, and if necessary the combination with MS can result in the identification of the components with antioxidative potential and a semiquantitative analysis of these components.

References

1. Aspöck H, Aver H, Picher O (1996) *Trichuris trichiura* eggs in the neolithic glacier mummy from the Alps. Parasitol Today 12:255–256
2. Fujii Y, Fujii H, Yamazaki M (1983) Separation and determination of cardiac glycosides in digitalis purpurea leaves by micro high-performance liquid chromatography. J Chromatogr 258: 147–153
3. Miller RJ, Jolles C, Rapoport H (1973) Morphine metabolism and normorphine in Papaver somniferum. Phytochemistry 12: 597–603
4. Strobel G, Stierle A, Hess WM (1994) The stimulation of taxol production in Taxus brevifolia by various growth retardants. Plant Sci 101:115–124
5. Phillipson JD, Handa SS (1976) Hyoscyamine N-oxide in Atropa belladonna. Phytochemistry 15:605–608
6. Datta A, Srivastava PS (1997) Variation in vinblastine production by Catharanthus roseus during in vivo and in vitro differentiation. Phytochemistry 46:135–137
7. World Health Organization (2002) Traditional Medicine Strategy 2002–2005, Geneva, Switzerland. http://whqlibdoc.who.int/hq/2002/who_edm_trm_2002.1.pdf. Accessed 7 May 2013
8. World Health Organization (1991) Guidelines for the assessment of herbal medicines, Geneva, Switzerland. http://whqlibdoc.who.int/HQ/1991/WHOTRM91.4.pdf. Accessed 7 May 2013
9. World Health Organization (2005) National policy on traditional medicine and regulation of herbal medicines, Geneva, Switzerland. http://whqlibdoc.who.int/publications/2005/9241593237.pdf. Accessed 7 May 2013
10. World Health Organization (2000) General guidelines for methodologies on research and evaluation of traditional medicine, Geneva, Switzerland. http://whqlibdoc.who.int/hq/2000/WHOEDMTRM2000.1.pdf. Accessed 7 May 2013
11. European Medicine Evaluation Agency (2010) Inventory of herbal substances for assessment–Alphabetical order, London, UK. http://www.ema.europa.eu/docs/enGB/documentlibrary/Other/2009/12/WC500017723.pdf. Accessed 7 May 2013
12. European Medicine Evaluation Agency (2010) Guideline on declaration of herbal substances and herbal preparations in herbal medicinal products/traditional herbal medicinal products, London, UK. http://www.ema.europa.eu/docs/enGB/document library/Scientific guideline/2009/09/WC500003283.pdf. Accessed 7 May 2013
13. European Medicine Evaluation Agency (2006) Guideline on the environmental risk assessment of medicinal products for human use, London, UK. http://www.ema.europa.eu/docs/enGB/document library/Scientificguideline/2009/10/WC500003978.pdf. Accessed 7 May 2013
14. Liang Q, Qu J, Luo G et al (2006) Rapid and reliable determination of illegal adulterant in herbal medicines and dietary supplements by LC/MS/MS. J Pharm Biomed Anal 40: 305–311
15. Cianchino V, Acosta G, Ortega C et al (2008) Analysis of potential adulteration in herbal medicines and dietary supplements for the weight control by capillary electrophoresis. Food Chem 108:1075–1081
16. Lopez-Feria S, Cardenas S, Garcıa-Mesa JA et al (2008) Classification of extra virgin olive oils according to the protected designation of

origin, olive variety and geographical origin. Talanta 75:937–943
17. Bashir HA, Abu-Goukh ABA (2003) Compositional changes during guava fruit ripening. Food Chem 80:557–563
18. Shin Y, Liu RH, Nock JF et al (2007) Temperature and relative humidity effects on quality, total ascorbic acid, phenolics and flavonoid concentrations, and antioxidant activity of strawberry. Postharv Biol Technol 45:349–357
19. Tan X, Li Q, Chen X, Wang Z et al (2008) Simultaneous determination of 13 bioactive compounds in Herba Artemisiae Scopariae (Yin Chen) from different harvest seasons by HPLC-DAD. J Pharm Biomed Anal 47:847–853
20. Chena H, Li X, Chen J et al (2010) Simultaneous determination of eleven bioactive compounds in Saururus chinensis from different harvesting seasons by HPLC-DAD. J Pharm Biomed Anal 51:1142–1146
21. Whitton PA, Lau A, Salisbury A et al (2003) Kava lactones and the kava-kava controversy. Phytochemistry 64:673–679
22. Simeoni P, Lebot V (2002) Identification of factors determining kavalactone content and chemotype in Kava (Piper methysticum Forst. f.). Biochem Syst Ecol 30:413–424
23. Naithani V, Nair S, Kakkar P (2006) Decline in antioxidant capacity of Indian herbal teas during storage and its relation to phenolic content. Food Res Int 39:176–181
24. Dufresne CJ, Farnworth ER (2001) A review of latest research findings on the health promotion properties of tea. J Nutr Biochem 12:404–421
25. Pastore RL, Fratellone P (2006) Potential health benefits of green tea (Camellia sinensis): a narrative review. Explore Diet Nutr 2:531–539
26. Wang H, Provan GJ, Helliwel K (2000) Tea flavonoids: their functions, utilization and analysis. Trends Food Sci Technol 11(2000): 152–160
27. Khan N, Mukhtar H (2007) Tea polyphenols for health promotion. Life Sci 81(2007):519–533
28. Re R, Pellegrini N, Proteggente A et al (1999) Antioxidant activity applying an improved ABTS radical cation decolorization assay. Free Radic Biol Med 26:1231–1237
29. Miller NJ, Rice-Evans CA (1996) Spectrophotometric determination of antioxidant activity. Redox Rep 2:161–171
30. Koleva I, van Beek T, Linssen J et al (2002) Screening of plant extracts for antioxidant activity: a comparative study on three testing methods. Phytochem Anal 13:8–17
31. Dai J, Mumper RJ (2010) Plant phenolics: extraction, analysis and their antioxidant and anticancer properties. Molecules 15:7313–7352
32. Paiva SAR, Russel RM (1999) β-Carotene and other carotenoids as antioxidants. J Am Coll Nutr 18:426–433
33. Yang CS, Lambert JD, Sang S (2009) Antioxidative and anti-carcinogenic activities of tea polyphenols. Arch Toxicol 83:11–21
34. Declaration of Alma-Ata (1978) International Conference on Primary Health Care, Alma-Ata, USSR. http://www.who.int/hpr/NPH/docs/declarationalmaata.pdf. Accessed 7 May 2013
35. World Health Organization (1999) WHO monographs on selected medicinal plants (Volume I), Geneva, Switzerland. http://whqlibdoc.ho.int/publications/1999/9241545178.pdf. Accessed 7 May 2013
36. World Health Organization (2003) WHO monographs on selected medicinal plants (Volume II),, Geneva, Switzerland. http://whqlibdoc.who.int/publications/2002/9241545372.pdf. Accessed 7 May 2013
37. World Health Organization (2007) WHO monographs on selected medicinal plants (Volume III),, Geneva, Switzerland. http://apps.who.int/medicinedocs/index/assoc/s14213e/s14213e.pdf. Accessed 7 May 2013
38. Committee on Herbal Medicinal Products (HMPC) (2010) Overview of assessment work – priority list, European Medicine Evaluation Agency, London, UK. http://www.ema.europa.eu/docs/enGB/documentlibrary/Other/2009/12/WC500017724.pdf. Accessed 7 May 2013
39. European Pharmacopoeia 7.0 (2010) Council of Europe. Strasbourg, France
40. World Health Organization (WHO) (1999) Counterfeit drugs—guidelines for the development of measures to combat counterfeit drugs. WHO/EDM/QSM/99.1. Geneva, Switzerland
41. Newton P, Green M, Fernande`z F et al (2006) Counterfeit anti-infective drugs. Lancet Infect Dis 6:602–613
42. WHO (2009) Sixty-second World Health Assembly Item 12.9: counterfeit medical products. http://aps.who.int/gb/ebhwa/pdf_files/A62/A62_13-en.pdf. Accessed 7 May 2013
43. Savaliya AA, Shah RP, Prasad B et al (2010) Screening of Indian aphrodisiac ayurvedic/herbal healthcare products for adulteration with sildenafil, tadalafil and/or vardenafil using LC/PDA and extracted ion LC-MS/TOF. J Pharm Biomed Anal 52:406–409
44. Kim SH, Lee J, Yoon T et al (2009) Simultaneous determination of anti-diabetes/anti-obesity drugs by LC/PDA, and targeted

analysis of sibutramine analog in dietary supplement by LC/MS/MS. Biomed Chrom 23:1259–1265

45. Stypulkowska K, Blazewicz A, Maurin J et al (2011) X-ray powder diffractometry and liquid chromatography studies of sibutramine and its analogues content in herbal dietary supplements. J Pharm Biomed Anal 56: 969–975
46. Tang MH, Chen SP, Ng SW et al (2011) Case series on a diversity of illicit weight-reducing agents: from the well-known to the unexpected. Br J Clin Pharmacol 71:250–253
47. Venhuis BJ, Vredenbregt MV, Kaun N et al (2011) The identification of rimonabant polymorphs, sibutramine and analogues of both in counterfeit Acomplia bought on the internet. J Pharm Biomed Anal 54:21–26
48. Wang J, Chen B, Yao S (2008) Analysis of six synthetic adulterants in herbal weight-reducing dietary supplements by LC electrospray ionization-MS. Food Addit Contam Part A 25:822–830
49. Tistaert C, Dejaegher B, Vander Heyden Y (2011) Chromatographic separation techniques and data handling methods for herbal fingerprints: a review. Anal Chim Acta 690:148–161
50. Massart DL, Vandeginste BGM, Buydens LMC et al (1997) Handbook of chemometrics and qualimetrics-part A. Elsevier Science, Amsterdam
51. Dumarey M, Smets I, Vander Heyden Y (2010) Prediction and interpretation of the antioxidant capacity of green tea from dissimilar chromatographic fingerprints. J Chromatogr B Analyt Technol Biomed Life Sci 878: 2733–2740
52. Deconinck E, De Leersnijder C, Custers D et al (2013) A strategy for the identification of plants in illegal pharmaceutical preparations and food supplements using chromatographic fingerprints. Anal Bioanal Chem 405:2341–2352
53. Van Hong NT, Rivière C, Hong QT et al (2011) Identification by LC-ESI-MS of flavonoids responsible for the antioxidant properties of Mallotus species from Vietnam. Nat Prod Commun 6:813–818
54. Tistaert C, Dejaegher B, Chataigné G et al (2012) Potential antioxidant compounds in Mallotus species fingerprints. Part II: fingerprint alignment, data analysis and peak identification. Anal Chim Acta 721:35–43
55. Thiangthum S, Dejaegher B, Goodarzi M et al (2012) Potentially antioxidant compounds indicated from Mallotus and Phyllanthus species fingerprints. J Chromatogr B Analyt Technol Biomed Life Sci 910:114–121
56. Deconinck E, Sacré PY, Courselle P (2013) Chromatography in the detection and characterization of illegal pharmaceutical preparations. J Chromatogr Sci. doi:10.1093/chromsci/bmt006

Chapter 15

Simultaneous Determination of Ascorbic Acid, Aminothiols, and Methionine in Biological Matrices Using Ion-Pairing RP-HPLC Coupled with Electrochemical Detector

Muhammad Imran Khan, Zafar Iqbal, and Abad Khan

Abstract

A novel highly sensitive ion-pairing reversed-phase high performance liquid-chromatography/electrochemical detection method for simultaneous determination of L-ascorbic acid, aminothiols, and methionine in biological matrices is presented. Reduced forms of the analytes are extracted from sample matrices with 10 % *m*-phosphoric acid solution$_{(aqueous)}$. To determine the total vitamin C, the total aminothiols, and the total methionine, samples are treated with tris(2-carboxyethyl)phosphine solution in 0.05 % trifluoroacetic acid solution$_{(aqueous)}$ subsequent to deproteination to reduce the oxidized forms of these compounds. Various analytes are separated on a C_{18} (250×4.6 mm, 5 μm) analytical column using methanol-0.05 % trifluoroacetic acid solution$_{(aqueous)}$ (05:95 v/v, containing 0.1 mM 1-octane sulfonic acid as the ion-pairing agent) as the isocratic mobile phase that is pumped at a flow rate of 1.5 ml/min at room temperature. The column eluents are monitored at a voltage of 0.85 V. These analytes are efficiently resolved in less than 20 min using *n*-acetyl cysteine as the internal standard.

Key words Column liquid-chromatography, Vitamin C, Aminothiols, Methionine, Electrochemical detection

1 Introduction

Vitamin C, aminothiols (cysteine, homocysteine, and glutathione), and thioethers (e.g., methionine) have a number of physiological functions and the level of these compounds in various biological matrices such as plasma and erythrocytes are valuable markers in a number of clinical situations [1, 2]. Vitamin C and glutathione are the two most active water-soluble antioxidants in many biological systems. They work in a cyclic manner to protect lipids, proteins, and other biomacromolecules from oxidative damage by neutralizing toxic peroxides and by stabilizing free radicals and other

Journal published in: Journal of Chromatography B, Vol 879, Issue 25, Pages: 2567–2575, Year of publication: 2011, doi: 10.1016/j.jchromb.2011.07.013.

Donald Armstrong (ed.), *Advanced Protocols in Oxidative Stress III*, Methods in Molecular Biology, vol. 1208,
DOI 10.1007/978-1-4939-1441-8_15,

reactive oxidants. The ratios of their reduced (ascorbic acid and glutathione, respectively) to oxidized (dehydroascorbic acid and glutathione disulfide, respectively) forms are in fact good measures of the extent of oxidative stress to which the organism is exposed [3–8]. Cysteine and methionine, on the other hand, exert their antioxidant properties by acting as direct or indirect precursors for glutathione biosynthesis, respectively. Likewise, homocysteine occurs at a pivotal metabolic juncture between pathways of methionine remethylation and transulfuration, and hyperhomocysteinemia (elevated plasma homocysteine) generally reflects the relative activity of these two pathways. Mild to moderate hyperhomocysteinemia has become a useful clinical biomarker for cardiovascular diseases [9, 10] and for folate, vitamin B_{12} (cobalamin), and/or vitamin B_6 deficiencies and several inborn folate, cobalamin, and/or methionine metabolic abnormalities [11]. Information regarding a connection between homocysteine metabolism and cognitive function, from mild cognitive decline (age-related memory loss) to vascular dementia and Alzheimer's disease has also been emerging [12]. Appropriate management of these clinical conditions thus depends on an understanding of the biochemical determinants of homocysteinemia and would be facilitated by a method that simultaneously quantify, within the same plasma sample, the vitamin C, the methionine, and the major aminothiols in both the transmethylation and transulfuration pathways.

Several papers have been published on the liquid chromatographic determination of ascorbic acid in combination with dehydroascorbic acid [13–25] and/or other compounds [25–31]. A review article has also been published on analysis of the ascorbic acid and its oxidized form [32]. Similarly, a large number of papers have been reported on the chromatographic analysis of glutathione in combination with glutathione disulfide [33–40] and/or other compounds including aminothiols and thioethers [1, 41–44]. A review paper has also been reported on determination of the glutathione and its disulfide [45]. In fact, a method for simultaneous determination of aminothiols and ascorbic acid using capillary electrophoresis has also been reported [2]. To our knowledge, except for the method reported by Khan et al. [46], no single paper has been reported so far that can simultaneously determine vitamin C, aminothiols, and thioethers. However, this paper also has a number of shortcomings including erroneous determination of cysteine and cystine concentrations due to elution with the solvent front, inability to determine the oxidized forms of homocysteine and methionine, and poor precision due to very high % residual standard deviation (% RSD) in intra- and inter-days reproducibility studies.

This study is thus designed to overcome the above mentioned shortcomings by developing a sensitive, precise, and accurate method for simultaneous determination of ascorbic acid, aminothiols, thioethers (e.g., methionine), and their oxidized forms in various

biological matrices such as plasma and erythrocytes using ion-pairing reversed-phase high performance liquid-chromatography (RP-HPLC) coupled with electrochemical (EC) detector. The proposed method is also validated according to international guidelines. Results of the study indicate that the proposed method can be efficiently utilized for analysis of both the reduced and the oxidized forms of vitamin C, aminothiols, and methionine in various biological matrices in the perspective of clinical research. Application of this method to the determination of these metabolically interrelated compounds would facilitate differential diagnosis and nutritional management of the many inborn errors of methionine metabolism and various disease states associated with oxidative stress and abnormal one-carbon metabolism. The same method can also be applied for the determination of these analytes in other sample matrices such as pharmaceuticals, dietary supplements, foodstuffs, and biological tissues.

2 Materials

2.1 Chemicals

L-Ascorbic acid ($AscH_2$; purity ≥99 %), L-cysteine (Cys; purity ≥98.5 %), L-cystine (CySS; purity ≥99.5 %), DL-homocysteine (Hcy; purity ≥95 %), L-methionine (Met; purity ≥99.5 %), L-glutathione (GSH; purity ≥98 %), (−)-glutathione disulfide (GSSG; purity ≥99 %), and *n*-acetyl-L-cysteine (NAC; purity ≥99 %).

HPLC-grade acetonitrile (purity ≥99.9 %), methanol (purity ≥99.9 %), and 1-octane sulfonic acid, sodium salt monohydrate (OSA; purity ≥98 %).

Analytical-grade chemicals such as sodium hydroxide (NaOH: purity ≥98 %), sodium chloride (NaCl: purity ≥98 %), *o*-phosphoric acid (OPA; purity 85 %), *m*-phosphoric acid (MPA; purity 100 %), monobasic potassium phosphate (KH_2PO_4; purity ≥99 %), trifluoroacetic acid (TFA; purity ≥98 %), formic acid (FA; purity 85 %), tris(2-carboxyethyl)phosphine hydrochloride (TCEP·HCl; purity ≥99 %), and phosphate buffered saline (PBS: pH 7.4).

Ultrapure water prepared by a Millipore ultrapure water system (Milford, USA).

2.2 Reagents

Prepare NaOH aqueous solution (1 M) by dissolving NaOH pellets (40 g) in ≈500 ml ultrapure water, and diluted to 1,000 ml.

Prepare monobasic potassium phosphate buffer solution (50 mM) by dissolving KH_2PO_4 (6.8 g) in ultrapure water, and dilute to ≈990 ml. Adjust the desired pH of the buffer solution with either 85 % OPA or 1 M NaOH solution$_{(aqueous)}$ before making volume to 1,000 ml with ultrapure water.

Prepare saturated NaCl solution$_{(aqueous)}$ by dissolving NaCl (30–40 g) in ≈100 ml ultrapure water.

Prepare normal saline by dissolving NaCl (0.9 g) in sufficient quantity of ultrapure water to make the final volume 100 ml.

Prepare acidified waters by adding 85 % OPA, TFA, or 85 % FA drop wise to ≈1,000 ml ultrapure water until the desired pH is achieved.

Prepare MPA solution$_{(aqueous)}$ (10 % w/v) by dissolving MPA (10 g) in sufficient quantity of ultrapure water to make the final volume 100 ml.

Prepare stock solution of the TCEP·HCl solution$_{(aqueous)}$ (10 g/ml) by dissolving TCEP·HCl (100 g) in sufficient volume of 0.05 % TFA aqueous solution to make the final volume 10 ml. This stock solution is then further diluted to get the desired concentrations (10–150 mg/ml) of the TCEP·HCl working solutions.

(**Note**: *All these chemicals and reagents can be used without further purification except mobile phases, which are vacuum filtered through 0.45 μm pore size filters*)

2.3 Instrumentation

HPLC system equipped with a pump, vacuum degasser, autosampler (or manual injector), column oven, EC detector (A single-channel EC flow cell [e.g., the Flexcell™], having effective volume of 0.5 μl, is preferred in which a three-electrode configuration is used, i.e., the maintenance free reference electrode [e.g., HyREF™], the auxiliary electrode, and the gold (Au) working electrode), interface, and computer system having data analysis software.

3 Methods

3.1 Preparation of Standard Solutions

Prepare primary stock solutions of the analytes in the aqueous component of the mobile phase and store at –20 °C in amber glass vials.

Prepare secondary stock solution of the NAC used as the internal standard (to give a final concentration of 200 ng/ml), to be added to all standard mixtures and sample matrices, by dilution of its primary stock solution with the mobile phase.

Similarly, prepare secondary stock solutions and working standard solutions (at eight concentration levels in the range of 0.2–10,000 ng/ml each containing 200 ng/ml NAC as the internal standard) of all the analytes by dilution of their primary standard solution with the mobile phase.

Prepare standard 1:1 calibration mixture containing 200 ng/ml each of $AscH_2$, Cys, Hcy, GSH, Met, and NAC as well.

3.2 Sample Collection and Handling

Collect venous blood samples (about 3 cc) from healthy subjects in precooled ethylenediaminetetraacetic acid (EDTA)-vacutainer tubes and immediately centrifuge them at 2,500×*g* for 10 min at –10 °C to separate plasma and blood cells. To prepare erythrocytes samples, remove buffy coat from blood cells and wash them with normal saline. Vortex-mix both plasma and erythrocytes samples (50 μl) with 3 ml (6 parts) of 10 % MPA solution$_{(aqueous)}$ and store in amber colored eppendorf tubes at –80 °C until analyses (*see* **Note 1**).

3.3 Sample Preparation

At the time of analysis, thaw all samples at room temperature and prepare erythrocytes hemolysates by lysing the erythrocytes by freezing–thawing two to three times.

To determine $AscH_2$, reduced aminothiols (Cys, Hcy, and GSH), and Met, pretreated samples are vigorously vortex-mixed for 2 min at room temperature and centrifuge at 2,500 × *g* for 10 min at –10 °C subsequently. Inject the resultant clear supernatants into the HPLC system after dilution with the mobile phase (*see* **Note 2**).

In order to determine vitamin C ($AscH_2$ plus dehydroascorbic acid (DHAA)), total aminothiols (total cysteine (tCys), total homocysteine (tHcy), and total glutathione (tGSH)), and total methionine (tMet), the deproteinized samples are treated with 10 μl (1/5 parts) of 20 mg/ml (70 mM) TCEP·HCl solution (in 0.05 % TFA aqueous solution) by vigorous vortex-mixing for about 5 min at room temperature. These samples are then centrifuged at 2,500 × *g* for 10 min at –10 °C before injecting the supernatant into the HPLC system (*see* **Note 3**). Representative chromatograms of various samples reduced with TCEP·HCl solution are given in Fig. 1.

Concentrations of the DHAA, the oxidized aminothiols (CySS, homocystine (HcySS), and GSSG), and methionine sulfoxide (MetO) are calculated by subtracting $AscH_2$, Cys, Hcy, GSH, and Met concentrations from concentrations of vitamin C, tCys, tHcy, tGSH, and tMet, respectively (*see* **Note 4**).

Generalized scheme for extraction of vitamin C, aminothiols, and methionine from biological matrices is summarized in Table 1.

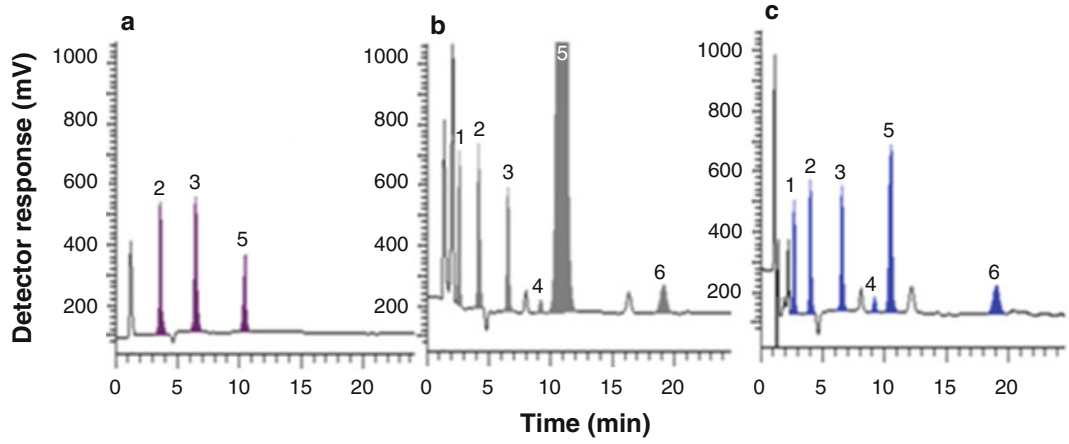

Fig. 1 Chromatograms of $AscH_2$, reduced aminothiols, and Met samples after reduction with TCEP·HCl solution. *Chromatograms:* (**a**) The standard mixture containing 200 ng/ml each of CySS, internal standard, and GSSG; (**b**) The blank erythrocyte sample containing 200 ng/ml of the internal standard; and (**c**) The blank plasma sample containing 200 ng/ml of the internal standard. *Peaks*: (1) $AscH_2$ (2.7 min); (2) Cys (4.2 min); (3) Internal standard (6.5 min); (4) Hcy (9.3 min); (5) GSH (10.75 min); and (6) Met (19.2 min)

Table 1
Generalized scheme for extraction of vitamin C, aminothiols, and methionine from biological matrices

Take 1 part (200 µl) of whole blood/plasma/erythrocytes and mix it with 1 part of 10 % MPA solution$_{(aqueous)}$ by vigorous vortex-mixing for 2 min at room temperature
(*Stabilization of the samples*)
↓
Prepare erythrocyte hemolysates by lysing the erythrocytes by freezing/thawing 2–3 times
↓
Add the internal standard solution to the samples by vigorous shaking and centrifuge these samples at 2,500×*g* for 10 min at −10 °C
Inject into the HPLC system after diluting with the aqueous component of the mobile phase (if desired) either directly or)[a]
↓
Add 1/20 parts (10 µl) of cooled TCEP·HCl solution (20 mg/ml) in the acidified aqueous component of the mobile phase and vortex-mix vigorously for 5 min at room temperature. Centrifuge samples at 2,500×*g* for 10 min at −10 °C
(*Reduction of the oxidized forms of the analytes*; *Inject into the HPLC*)[b]

[a]In case of reduced forms of the analytes
[b]In case of total analytes only

3.4 Chromatographic Analysis

Analyze samples at the following combination of chromatographic parameters. Stationary phase: Ordinary RP C_{18} (250×4.6 mm, 5 µm) analytical column protected by a pre-column guard cartridge C_{18} (30×4.6 mm, 10 µm); Mobile phase: Methanol-0.05 % TFA solution$_{(aqueous)}$ (05:95 v/v, containing 0.1 mM OSA in isocratic mode; Flow rate: 1.5 ml/min; Column oven temperature: room temperature; and Injection volume: 5 µl (*see* **Notes 5–9**).

To achieve best separation and detection, the preliminary selected parameters are evaluated on the basis of peak resolution ($R_{s;i,j}$) for the critical peak pairs "*i*" and individual tested values "*j*" of the studied parameters. The value "*j*" is selected as optimal when $R_{s;i,j}$ achieve at least the minimum acceptable value of 1.75.

Detect all analytes at 0.85 V electrical potential using the following EC detection parameters. Filter: 0.01; Polarity: positive; Range and maximum compensation: 20 nA and 2.5 µA; Offset: 10 %; and Temperature: 27 °C (room temperature) (*see* **Notes 10** and **11**).

Figure 2 shows representative chromatograms, at optimum chromatographic conditions, of the blank mobile phase, the standard 1:1 calibration mixture, the blank plasma and erythrocytes samples spiked with the internal standard, the plasma and erythrocytes

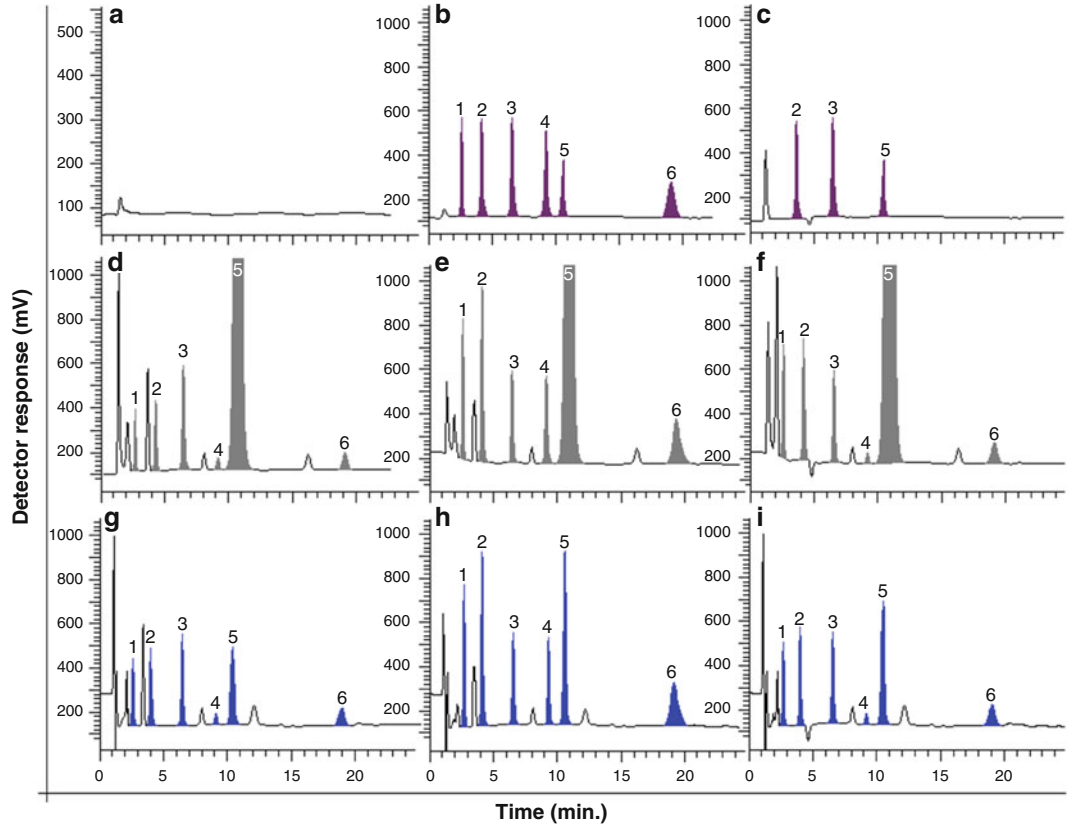

Fig. 2 Representative RP-HPLC chromatograms of different samples analyzed under optimum conditions. *Chromatograms:* (**a**) The blank mobile phase; (**b**) The standard 1:1 mixture; (**c**) The standard mixture containing 200 ng/ml each of the cystine, internal standard, and glutathione disulfide and reduced with TCEP·HCl solution; (**d**) The blank erythrocytes sample spiked with 200 ng/ml of the internal standard; (**e**) The erythrocytes sample spiked with the standard 1:1 mixture; (**f**) The blank erythrocytes sample containing 200 ng/ml of the internal standard and reduced with TCEP·HCl solution; (**g**) The blank plasma sample spiked with 200 ng/ml of the internal standard; (**h**) The plasma sample spiked with the standard 1:1 mixture; and (**i**) The blank plasma sample containing 200 ng/ml of the internal standard and reduced with TCEP·HCl solution. *Peaks*: (1) $AscH_2$ (2.7 min); (2) Cys (4.2 min); (3) NAC (6.5 min); (4) Hcy (9.3 min); (5) GSH (10.75 min); and (6) Met (19.2 min)

samples spiked with the standard 1:1 calibration mixture, and the samples reduced with TCEP·HCl solution$_{(aqueous)}$. Under the specified conditions, the mean retention times were 2.7, 4.2, 6.5, 9.3, 10.75, and 19.2 min for $AscH_2$, Cys, NAC, Hcy, GSH, and Met, respectively.

The hydrodynamic voltammograms for all analytes are depicted in Fig. 3.

3.5 Method Validation

Validate the proposed method according to international guidelines with emphasis on specificity/selectivity, linearity within the expected concentration range, accuracy in terms of % recovery,

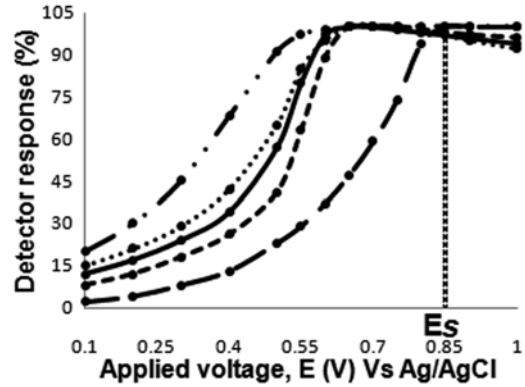

Fig. 3 Hydrodynamic voltammograms for $AscH_2$, reduced aminothiols, and Met. *Curves:* $AscH_2$ (—●··); Cys (···●··); Hcy (—●—); GSH (— ●—); and Met (—● ·). E_s is the selected voltage, 0.85 V

precision (repeatability and intermediate precision), sensitivity, robustness, and stability of solutions [47, 48].

To verify the specificity/selectivity of the method, separation of the peaks in the chromatograms of the blank solvent, the standard 1:1 calibration mixture, the blank sample matrices, and the sample matrices spiked with the standard 1:1 calibration mixture is observed.

Determine the linearity of the method by spiking various standard mixtures into sample matrices (50 µl) that are then extracted and analyzed with triplicate injections. Response ratios are then plotted as a function of spiked concentrations of the analytes and the slope, the intercept, and the correlation coefficient (r^2) are determined from the regression analysis.

To calculate % recoveries, standard mixtures, at three nominal concentration levels, are spiked into samples matrices (50 µl; $n = 5$), extracted, and analyzed with triplicate injections. Subtract the response ratios of the endogenous analytes in blank sample matrices from total response ratios in spiked samples and divide results obtained by response ratios of the analytes in the standard mixture and multiplied by 100.

Determine the sensitivity of the method as the limit of detection (LOD) and the lower limit of quantification (LLOQ) using the signal-to-noise ratio (S/N) of 3 and 10, respectively. Calculate both per ml and on-column sensitivities of the method.

Determine the injection repeatability by injecting standard 1:1 calibration mixture at least 10 times. It is expressed by repeatability of peak area and retention time and determined as mean ± standard deviation (SD) and % RSD calculated from the data obtained.

Similarly, to determine the analysis repeatability, analyze ten samples spiked with the standard 1:1 calibration mixture prepared individually from single plasma sample. Express the result by repeatability of the recovered amount and determined as mean ± SD and % RSD calculated from the data obtained.

In order to determine the intermediate precision (intra- and inter-days reproducibility), the spiked samples prepared for the accuracy/% recovery studies are analyzed three times a day (e.g., at 09:00, 16:00, and 23:00 h) and for three successive days. The result is expressed as reproducibility of the recovered amount and determined as mean ± SD and % RSD calculated from the data obtained.

Determine the robustness of the developed method by studying the effect of small deliberate variations in system parameters, like organic component of the mobile phase (±1 %), the mobile phase flow rate (±0.2 ml/min), the column oven temperature (±5 °C), and the working potential (±10 mV), on the performance of the method.

To evaluate short-term stability, peak areas of the analytes obtained at various time intervals are compared to their initial peak areas in standard solutions (stored in the freezer at –20 °C for 1 week) and spiked sample matrices (stored in the auto-sampler at room temperature for 4, 8, 12, and 24 h and in the refrigerator at 4 °C and the freezer at –20 °C for one night).

Results of various method validation parameters are summarized in Tables 2, 3, 4, 5, and 6 and Figs. 2, 4, and 5 showing that the proposed analytical method is fully validated according to international guidelines. Results of stability studies indicate that samples should be kept frozen until analysis to ensure accurate analysis of these analytes.

Table 2
Accuracy in terms of % recovery of the proposed method for simultaneous determination of $AscH_2$, reduced aminothiols, and Met

Accuracy in terms of % recovery	$AscH_2$	Cys	Hcy	GSH	Met
Spiked concentration level 1 (0.2 ng/ml each)[a]					
Plasma	97.50 ± 1.50; 1.54	97.17 ± 1.44; 1.49	96.00 ± 1.32; 1.38	97.00 ± 1.5; 1.55	97.33 ± 1.76; 1.80
Erythrocytes	97.23 ± 1.50; 1.55	97.17 ± 1.89; 1.95	96.67 ± 1.76; 1.82	96.50 ± 1.00; 1.04	97.33 ± 1.61; 1.65
Spiked concentration level 2 (500 ng/ml each)[a]					
Plasma	96.67 ± 1.22; 1.26	96.93 ± 1.40; 1.45	97.27 ± 1.21; 1.24	97.00 ± 1.00; 1.03	96.33 ± 1.29; 1.33
Erythrocytes	96.60 ± 1.56; 1.62	96.67 ± 1.50; 1.55	96.73 ± 1.21; 1.25	97.13 ± 1.10; 1.13	96.47 ± 1.51; 1.57
Spiked concentration level 3 (5,000 ng/ml each)[a]					
Plasma	98.67 ± 1.04; 1.05	98.17 ± 0.80; 0.82	98.13 ± 1.10; 1.12	98.13 ± 0.9; 0.92	98.40 ± 1.22; 1.24
Erythrocytes	98.90 ± 0.56; 0.56	98.87 ± 0.71; 0.72	98.17 ± 1.00; 1.02	98.17 ± 0.70; 0.72	98.67 ± 1.04; 1.05

Results are reported as mean ± SD; % RSD
[a] $n = 5$ (where n is the number of samples)

Table 3
Sensitivity of the proposed methods to various studied compounds

Analytes	LOD	LLOQ
$AscH_2$		
pg/ml	60	200
On-column (fg)	300	1,000
Cys		
pg/ml	55	170
On-column (fg)	275	850
Hcy		
pg/ml	50	160
On-column (fg)	250	800
GSH		
pg/ml	80	250
On-column (fg)	400	1,250
Met		
pg/ml	65	210
On-column (fg)	375	1,050

Table 4
Calibration range and linearity of the proposed method for simultaneous determination of $AscH_2$, reduced aminothiols, and Met

Parameters	$AscH_2$	Cys	Hcy	GSH	Met
Calibration range (ng/ml)	0.2–10,000				
Linearity					
Spiked plasma samples					
Regression equation	$y = 0.0019x + 0.0272$	$y = 0.0021x - 0.0028$	$y = 0.0022x - 0.0143$	$y = 0.0019x + 0.0683$	$y = 0.0019x + 0.0670$
Correlation coefficient, r^2	0.9999	0.9997	0.9996	0.9997	0.9996
Spiked erythrocyte samples					
Regression equation	$y = 0.0019x + 0.0593$	$y = 0.0020x + 0.0624$	$y = 0.0020x + 0.0243$	$y = 0.0021x + 0.0536$	$y = 0.0020x + 0.0623$
Correlation coefficient, r^2	0.9998	0.9998	0.9997	0.9998	0.9994

y is the response ratio; and x is the concentration

Table 5
Precision of the proposed method for simultaneous determination of $AscH_2$, reduced aminothiols, and Met

Parameters	$AscH_2$	Cys	Hcy	GSH	Met
Repeatability					
Injection repeatability					
Standard solution (200 ng/ml each)[a]					
Peak area	2,671,543 ± 41,700; 2	3,611,550 ± 61,138; 2	3,801,547 ± 74,302; 2	2,411,569 ± 51,272; 2	3,113,604 ± 66,909; 2
Retention time (min)	2.70 ± 0.04; 1.54	4.22 ± 0.05; 1.08	9.32 ± 0.08; 0.82	10.75 ± 0.04; 0.36	19.20 ± 0.19; 0.98
Analysis repeatability					
Spiked concentration level 1 (200 ng/ml each)[b]					
Plasma	195.0 ± 1.6[c]; 0.8	194.6 ± 3.8[c] ; 2.0	195.8 ± 3.5[c] ; 1.8	195.2 ± 2.6[c]; 1.3	195.4 ± 3.5[c]; 1.8
Intermediate precision					
Intra-day reproducibility					
Spiked concentration level 2 (0.2 ng/ml each)[d]					
Plasma	0.191 ± 0.004[c]; 1.888	0.187 ± 0.003[c] ; 1.343	0.191 ± 0.004[c]; 1.986	0.192 ± 0.004[c]; 1.878	0.189 ± 0.004[c]; 1.908
Erythrocytes	0.190 ± 0.004[c]; 1.852	0.187 ± 0.004[c]; 1.881	0.184 ± 0.004[c]; 1.905	0.190 ± 0.004[c]; 1.898	0.193 ± 0.004[c]; 1.823
Spiked concentration level 3 (500 ng/ml each)[d]					
Plasma	486.3 ± 8.7[c]; 1.8	488.7 ± 5.7[c]; 1.2	485.3 ± 6.5[c]; 1.3	486.0 ± 6.6[c]; 1.4	488.0 ± 6.6[c]; 1.3
Erythrocytes	486.0 ± 8.5[c]; 1.8	484.7 ± 7.5[c]; 1.6	483.3 ± 6.7[c]; 1.4	485.3 ± 3.5[c]; 0.7	491.3 ± 6.0[c]; 1.2
Spiked concentration level 4 (5,000 ng/ml each)[d]					
Plasma	4,876.7 ± 64.3[c]; 1.4	4,848.3 ± 63.3[c]; 1.3	4,875.0 ± 50.0[c]; 1.0	4,896.7 ± 60.5[c]; 1.2	4,930.0 ± 50.8[c]; 1.0
Erythrocytes	4,861.7 ± 32.5[c]; 0.7	4,855.0 ± 57.7[c]; 1.2	4,845.0 ± 26.5[c]; 0.5	4,880.0 ± 42.7[c]; 0.9	4,913.3 ± 55.1[c]; 1.1
Inter-days reproducibility					
Spiked concentration level 2 (0.2 ng/ml each)[d]					
Plasma	0.191 ± 0.004[c]; 1.888	0.187 ± 0.003[c]; 1.637	0.191 ± 0.004[c]; 1.986	0.189 ± 0.004[c]; 1.908	0.188 ± 0.004[c]; 2.010
Erythrocytes	0.189 ± 0.004[c]; 1.855	0.186 ± 0.004[c]; 1.938	0.184 ± 0.004[c]; 1.905	0.190 ± 0.009[c]; 1.996	0.193 ± 0.003[c]; 1.554
Spiked concentration level 3 (500 ng/ml each)[d]					
Plasma	486.3 ± 9.1[c]; 1.9	485.3 ± 8.5[c]; 1.8	483.3 ± 7.8[c]; 1.6	483.3 ± 8.7[c]; 1.8	483.3 ± 8.1[c]; 1.7
Erythrocytes	485.3 ± 8.5[c]; 1.6	483.3 ± 8.1[c]; 1.7	481.3 ± 7.5[c]; 1.6	481.3 ± 7.5[c]; 1.6	487.7 ± 6.7[c]; 1.4
Spiked concentration level 4 (5,000 ng/ml each)[d]					
Plasma	4,860.0 ± 81.8[c]; 1.7	4,861.7 ± 55.8[c]; 1.2	4,868.3 ± 46.5[c]; 1.0	4,883.3 ± 40.7[c]; 0.8	4,835.0 ± 42.7[c]; 0.9
Erythrocytes	8,438.3 ± 53.0[c]; 1.1	4,911.7 ± 80.0[c]; 1.6	4,873.3 ± 54.8[c]; 1.1	4,868.3 ± 46.5[c]; 1.0	4,823.3 ± 30.6[c]; 0.6

Results are reported as mean ± SD; % RSD

[a] $n = 10$

[b] $n = 5$

[c] Quantity recovered in ng/ml

[d] $n = 3$ (where n is the number of samples)

Table 6
Short-term stability of $AscH_2$, aminothiols, and Met samples

Analytes	Storage temperature (°C)	Standard solutions	Extracted samples	Reduced and extracted samples
$AscH_2$	30–40	–	2.0 ± 0.5^a	–
		–	7.0 ± 0.5^b	0.9 ± 0.04^c
		–	12.6 ± 0.9^d	1.2 ± 0.2^d
	4	–	1.3 ± 0.1^d	0.8 ± 0.04^d
	–20	0.2 ± 0.01^e	0.1 ± 0.03^d	0.07 ± 0.02^d
Aminothiols	30–40	–	0.5 ± 0.6^a	–
		–	2.7 ± 1.3^b	0.7 ± 0.03^c
		–	3.5 ± 0.6^d	1.1 ± 0.1^d
	4	–	0.4 ± 0.03^d	0.3 ± 0.02^d
	–20	0.2 ± 0.03^e	0.1 ± 0.03^d	0.04 ± 0.01^d
Met	30–40	–	0.5 ± 0.1^a	–
		–	0.9 ± 0.20^b	0.5 ± 0.04^c
		–	2.0 ± 0.3^d	1.0 ± 0.1^d
	4	–	0.3 ± 0.02^d	0.1 ± 0.04^d
	–20	0.1 ± 0.01^e	0.05 ± 0.01^d	0.02 ± 0.01^d

Results are reported as mean ± SD of % loss
[a]After 8 h
[b]After 12 h
[c]After 16 h
[d]After 24 h
[e]After 1 week

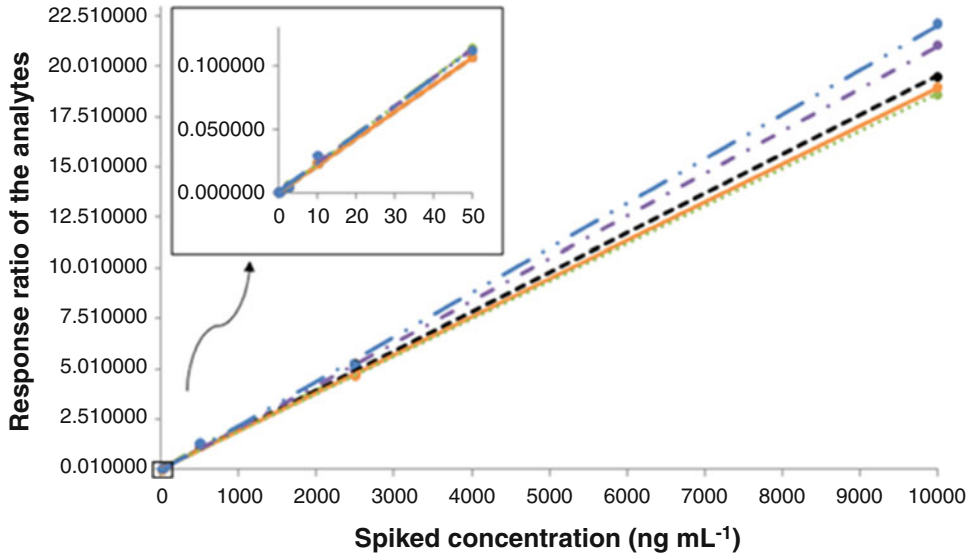

Fig. 4 Calibration curves for $AscH_2$, reduced aminothiols, and Met in plasma samples. *Curves: Dotted line* represents $AscH_2$ ($y = 0.0019x + 0.0272$, $r^2 = 0.9999$); *Solid line* represents GSH ($y = 0.0019x + 0.0683$, $r^2 = 0.9997$); *Dashed line* represents Met ($y = 0.0019x + 0.0670$, $r^2 = 0.9996$); *Dashed dotted line* represents Cys ($y = 0.0021x - 0.0028$, $r^2 = 0.9997$); and *Dashed double dotted line* represents Hcy ($y = 0.0022x - 0.0143$, $r^2 = 0.9996$). Each point is a mean of triplicate injections

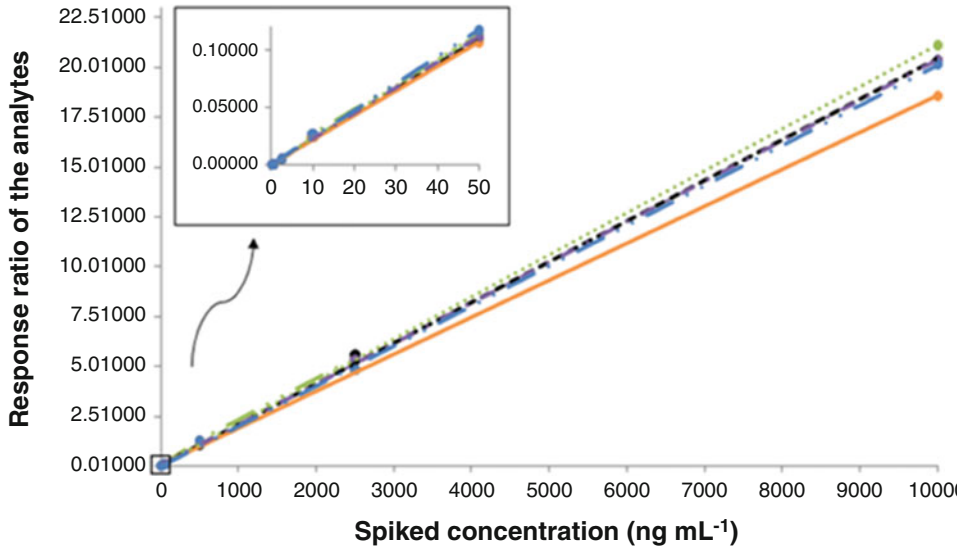

Fig. 5 Calibration curves for $AscH_2$, reduced aminothiols, and Met in erythrocytes samples. *Curves: Dotted line* represents $AscH_2$ ($y = 0.0019x + 0.0593$, $r^2 = 0.9998$); *Solid line* represents GSH ($y = 0.0021x + 0.0536$, $r^2 = 0.9998$); *Dashed line* represents Met ($y = 0.002x + 0.0623$, $r^2 = 0.9994$); *Dashed dotted line* represents Cys ($y = 0.002x + 0.0624$, $r^2 = 0.9998$); and *Dashed double dotted line* represents Hcy ($y = 0.002x + 0.243$, $r^2 = 0.9997$). Each point is a mean of triplicate injections

4 Notes

1. To ensure accurate and precise measurement of these potentially unstable compounds, different measures were taken including handling and experimental procedures well protected from light and heat; collection of the blood samples in EDTA-vacutainer tubes that have chelating properties; acidification of the plasma and the erythrocytes samples with 10 % MPA $solution_{(aqueous)}$ to prevent oxidation and hydrolysis of the analytes; immediate preservation of the plasma and the erythrocytes samples in the freezer until analyses; and reduction of the samples with water-soluble and odorless reducing agent, TCEP·HCl.
2. Stabilization, deproteination, and extraction of the plasma and the erythrocytes samples with six parts of MPA (10 % aqueous solution) obtain maximum recovery of all the analytes. To prevent column overload, samples are sufficiently diluted with the mobile phase before injection into the HPLC system.
3. TCEP·HCl concentration in slightly molar excess is usually used for reduction of thiols, and variable volumes (10–100 μl) of its solution (100–120 mg/ml) have been used for reduction purposes [49, 50]. However, using such a high concentration of TCEP·HCl solution resulted in a troublesome negative peak at

about 4.8 min in the chromatogram. To overcome this problem, lower concentrations of the TCEP·HCl solution were tried and it was found that even 10 µl (1/5 parts) of the 10 mg/ml TCEP·HCl solution was sufficient to completely reduce 50 µl (1 part) of sample matrices spiked with standard 1:1 mixture containing 5 µg/ml each of $AscH_2$, Cys, Hcy, GSH, Met, and NAC. But to ensure complete reduction, 10 µl (1/5 parts) of 20 mg/ml TCEP·HCl solution was used for reduction instead of using 10 mg/ml. On the other hand, the authors have insisted the use of BPS: pH 7.4 as the neutral medium for catalyzing its reduction reaction [49, 50]; however, according to our findings, the same reaction can occur quite efficiently in 0.05 % TFA aqueous solution. Moreover, 5 min vigorous shaking of the sample matrices with TCEP·HCl solution at room temperature was sufficient to complete the reduction reaction.

4. One should keep in mind that the error in the quantification of the oxidized forms of the analytes should be slightly high because they are determined indirectly by subtracting their reduced forms from the total concentrations obtained after reduction of the samples.
5. A routinely used RP column, Supelco Discovery® HS C_{18} (250×4.6 mm, 5 µm) was used for separation of the analytes. To avoid the reversible phase collapse (dewetting phenomenon) resulting from the prolonged use of highly aqueous mobile phases with the ordinary long-chain bonded alkyl stationary phases (octylsilane and octadecylsilane); column should be periodically conditioned with mobile phase having more than 50 % organic modifier. Alternately, this problem can be avoided by using polar embebbed or hydrophilic end-capped stationary phases [51–57].
6. Mobile phase composition is very crucial for chromatographic analysis as it significantly influences retention, height, and character of the analytical signal. Different isocratic mobile phases, consisting of methanol, acetonitrile, or acetonitrile–methanol mixtures as the organic components, pH adjusted water with TFA, FA, or OPA or KH_2PO_4 buffer, pH adjusted with OPA as the buffered/acidified aqueous components, and OSA as the ion-pairing agent, were pumped at flow rates of 0.5–2.0 ml/min.

   As far as organic component of the mobile phases is concerned, acetonitrile and methanol are the two most frequently used organic solvents in the RP-HPLC. Pure methanol in 5 % concentration was chosen because $AscH_2$, the first desirable peak in the chromatogram was difficult to retain, and was unresolved from solvent front and other unretained components even with mobile phases containing less than 5 % acetonitrile or acetonitrile–methanol (50:50 v/v) mixture as the organic components. Same was the case with Cys that was

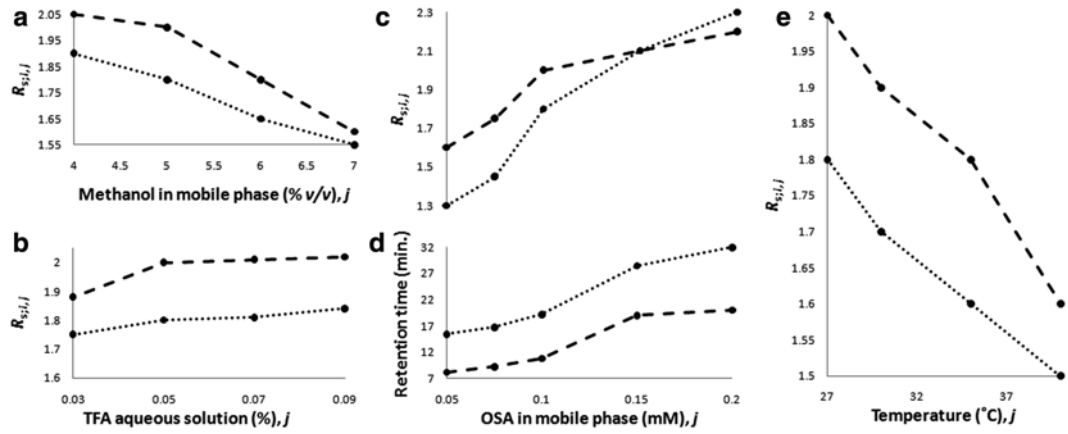

Fig. 6 Influence of (**a**) % methanol in mobile phase (v/v) on $R_{s;i,j}$; (**b**) Concentration of the TFA aqueous solution (%) on $R_{s;i,j}$; (**c**) Concentration of OSA in mobile phase (mM) on $R_{s;i,j}$; (**d**) Concentration of OSA in mobile phase (mM) on retention time; and (**e**) Column oven temperature on $R_{s;i,j}$. *Dashed line* represents $AscH_2$ and *dotted line* represents Cys, except in (**d**), where *dashed line* represents GSH and *dotted line* represents Met. For other chromatographic conditions *see* Subheading 3.4

unresolved from an unknown peak. Peak areas of all the target peaks also were comparatively more with methanol as compared to acetonitrile or acetonitrile–methanol (50:50 v/v) mixture. Influence of different concentrations of the methanol in the mobile phase (4–7 % v/v) on $R_{s;i,j}$ of the critical peak pairs (poorly retained hydrophilic components/$AscH_2$ and unknown peak/Cys) is shown in Fig. 6a.

Another important requirement for effective EC determination of the intended analytes is the presence of electrolytes (buffered aqueous component) in the mobile phase. The pH adjusted water with either 85 % OPA or 85 % FA (pH 2.0–3.5) was initially used as the acidified aqueous component of the mobile phase but it was unable to resolve the GSH peak from the Met peak even in more than 95 % concentrations. The retention time of the analytes also was not reproducible with such mobile phases. This problem of retention time fluctuation although was controlled when water was replaced with 50 mM potassium phosphate buffer, the resolution problem still persisted. Finally, the problems related to the above mentioned buffered aqueous components were solved by using 0.05 % TFA $solution_{(aqueous)}$ as the acidified aqueous component of the mobile phase. These superior properties of the TFA may be attributed to its ion-pairing properties. Influence of different concentrations (0.03, 0.05, 0.07, and 0.09 %) of 0.05 % TFA $solution_{(aqueous)}$ in the mobile phase on $R_{s;i,j}$ of poorly retained hydrophilic components/$AscH_2$ and unknown peak/Cys is shown in Fig. 6b.

In the absence of any ion-pairing agent, Cys was eluting with the solvent front and other unretained compounds even

in case of mobile phases containing only 1 % methanol. Thus to increase the retention of the analytes on the stationary phase and to allow the use of higher %age of the organic modifier in the mobile phase, OSA was used as the ion-pairing agent in the concentration range of 0.01–0.5 mM in the mobile phase (methanol-0.05 % TFA aqueous solution, 50:50 v/v). Resolution of Cys from other extraneous components was still compromised until the OSA concentration was raised to 0.1 mM, although resolution of the Cys was further improved above 0.1 mM OSA concentration; however, GSH and Met were strongly retained at higher OSA concentrations leading to longer run time. Thus OSA at a concentration of 0.1 mM in the mobile phase was optimal for the separation of $AscH_2$, reduced aminothiols, and Met. Selectivity of the mobile phase was also changed with the use of OSA, as the elution order was changed from Cys, $AscH_2$, Hcy, GSH, Met, and NAC [46] to $AscH_2$, Cys, NAC, Hcy, GSH, and Met. Influence of different concentrations of OSA in the mobile phase (0.05, 0.075, 0.1, 0.15, and 0.2 mM) on $R_{s;i,j}$ of poorly retained hydrophilic components/$AscH_2$ and unknown peak/Cys and retention times of GSH and Met is shown in Fig. 6c, d, respectively.

The selected flow rate of 1.5 ml/min was able to efficiently resolve all the analytical peaks in less than 20 min without building too much backpressure on the column (<2, 200 ± 50 psi).

7. Separation of the analytes was performed at various column oven temperatures in the range of 25–40 °C. Peak shape and height were improved and retention time decreased with increasing temperature. However, $AscH_2$ peak was not efficiently resolved from the early eluting polar hydrophilic components at temperatures above 30 °C. So depending upon these parameters, room temperature was selected to be the optimum temperature for separation of all the analytes. Influence of different temperatures (27–40 °C) on $R_{s;i,j}$ of poorly retained hydrophilic components/$AscH_2$ and unknown peak/Cys is shown in Fig. 6e.
8. Injection of higher volume of the sample (10–20 µl) resulted in broader peaks and a troublesome solvent artifact that was interfering with the peak of $AscH_2$, probably due to the elution of a very high concentration of some early eluting polar hydrophilic impurities with the mobile phase. So to overcome these problems, injection volume was kept at 5 µl.
9. Very few published methods for analysis of $AscH_2$ and/or DHAA have reported the use of internal standard. Among the various compounds that have been used as internal standard for analysis of $AscH_2$ are hydroquinone [58] and isoascorbic acid [19]. However, they may be oxidized during processing and storage leading to doubtful results [59]. Similarly, a number of compounds, including NAC, 2-mercaptopropionylglycine,

and cystamine have been used as internal standards in the analysis of glutathione and other thiols [60]. The use of NAC, however, was preferred due to its comparatively greater stability and the resultant acceptable linearity of all the analytes.

10. A voltammogram or current–voltage (I/E) relationship is the characteristic of every analyte and it gives information about the optimum working potential that can be used to improve detection sensitivity, selectivity, and reproducibility. Several approaches are used to obtain a voltammogram; however, a hydrodynamic voltammogram is the most reliable as it is taken under the real chromatographic conditions. Thus reliable information is obtained about the signal-to-noise ratio (S/N). A high working potential is required with respect to sensitivity. However, more analytes are detectable at higher working potentials. So, as to selectivity, a low working potential is favorable. On the other hand, working at a potential on the slope of the voltammogram will result in less reproducibility as not only a small fluctuation in the applied potential, but any other change in the system may result in a large variation in the current. Thus in practice, the choice of the working potential should be a compromise between sensitivity, selectivity, and reproducibility.
11. As depicted in the hydrodynamic voltammograms, 0.85 V was selected as the optimum voltage for simultaneous determination of $AscH_2$, reduced aminothiols, and Met using a single-channel EC detector. The detector response to $AscH_2$ was almost linear in the range of 0.5–1.0 V. Below 0.5 V, the detector response to it decreased considerably. On the other hand, detector response to aminothiols increased from 0.1 to 0.65 V where their maximum response was observed. Above 0.75 V, the detector response to these analytes again started to decline. As far as the Met is concerned, its maximum response was observed at 0.85 V, which then became constant up to 1.0 V.

Acknowledgement

The authors are thankful to the higher education commission (HEC), Pakistan for funding this study.

References

1. Melnyk S et al (1999) A new HPLC method for the simultaneous determination of oxidized and reduced plasma aminothiols using coulometric electrochemical detection. J Nutr Biochem 10:490–497
2. Yao X et al (2007) Simultaneous determination of aminothiols, ascorbic acid and uric acid in biological samples by capillary electrophoresis with electrochemical detection. Biomed Chrom 21:520–526
3. Victor VM et al (2009) Oxidative stress and mitochondrial dysfunction in sepsis: a potential therapy with mitochondria-targeted antioxidants. Infect Disord Drug Targets 9:376–389

4. Marí M et al (2009) Mitochondrial glutathione, a key survival antioxidant. Antioxid Redox Signal 11:2685–2700
5. Belinha I et al (2007) Quercetin increases oxidative stress resistance and longevity in Saccharomyces cerevisiae. J Agric Food Chem 55:2446–2451
6. Block KI et al (2007) Impact of antioxidant supplementation on chemotherapeutic efficacy: a systematic review of the evidence from randomized controlled trials. Cancer Treat Rev 33:407–418
7. Valko M et al (2007) Free radicals and antioxidants in normal physiological functions and human disease. Int J Biochem Cell Biol 39:44–84
8. Valko M et al (2006) Free radicals, metals and antioxidants in oxidative stress-induced cancer. Chem Biol Interact 160:1–40
9. Gerszten R, Wang T (2008) The search for new cardiovascular biomarkers. Nature 451: 949–952
10. Cushman M et al (2009) National Academy of Clinical Biochemistry Laboratory Medicine Practice guidelines: emerging biomarkers for primary prevention of cardiovascular disease. Clin Chem 55:378
11. Kerr MA et al (2009) Folate, related B vitamins, and homocysteine in childhood and adolescence: potential implications for disease risk in later life. Pediatrics 123:627–635
12. Miller AL (2003) The methionine-homocysteine cycle and its effects on cognitive diseases. Altern Med Rev 8:7
13. Behrens WA, Madère R (1987) A highly sensitive high-performance liquid chromatography method for the estimation of ascorbic and dehydroascorbic acid in tissues, biological fluids, and foods. Anal Biochem 165:102–107
14. Cerhata D et al (1994) Determination of ascorbic acid in blood serum using high-performance liquid chromatography and its correlation with spectrophotometric (colorimetric) determination. Ceská Slov Farm 43: 166–168
15. Dennison DB et al (1981) Rapid high-performance liquid chromatographic determination of ascorbic acid and combined ascorbic acid-dehydroascorbic acid in beverages. J Agric Food Chem 29:927–929
16. Esteve MJ et al (1995) Comparison of voltammetric and high performance liquid chromatographic methods for ascorbic acid determination in infant formulas. Food Chem 52:99–102
17. Keating RW, Haddad PR (1982) Simultaneous determination of ascorbic acid and dehydroascorbic acid by reversed-phase ion-pair high-performance liquid chromatography with pre-column derivatisation. J Chromatogr A 245:249–255
18. Kishida E et al (1992) Specific determination of ascorbic acid with chemical derivatization and high-performance liquid chromatography. Anal Chem 64:1505–1507
19. Kutnink MA et al (1987) An internal standard method for the unattended high-performance liquid chromatographic analysis of ascorbic acid in blood components. Anal Biochem 166: 424–430
20. Lykkesfeldt J (2000) Determination of ascorbic acid and dehydroascorbic acid in biological samples by high-performance liquid chromatography using subtraction methods: reliable reduction with tris [2-carboxyethyl] phosphine hydrochloride. Anal Biochem 282:89–93
21. Lykkesfeldt J et al (1995) Determination of ascorbic acid and dehydroascorbic acid in plasma by high-performance liquid chromatography with coulometric detection-are they reliable biomarkers of oxidative stress? Anal Biochem 229:329–335
22. Sapers GM et al (1990) Determination of ascorbic acid, dehydroascorbic acid and ascorbic acid-2-phosphate in infiltrated apple and potato tissue by high-performance liquid chromatography. J Chromatogr A 503:431–436
23. Sood SP et al (1976) High-pressure liquid chromatographic determination of ascorbic acid in selected foods and multivitamin products. Anal Chem 48:796–798
24. Tausz M et al (1996) Simultaneous determination of ascorbic acid and dehydroascorbic acid in plant materials by high performance liquid chromatography. Phytochem Anal 7:69–72
25. Teshima N et al (2001) Simultaneous flow injection determination of ascorbic acid and cysteine using double flow cell. Anal Chim Acta 438:21–29
26. Karatepe M (2004) Simultaneous determination of ascorbic acid and free malondialdehyde in human serum by HPLC-UV. LC GC N Am 22:362–365
27. Ross MA (1994) Determination of ascorbic acid and uric acid in plasma by high-performance liquid chromatography. J Chromatogr B Biomed Sci Appl 657: 197–200
28. Schüep W, Keck E (1990) Measurement of ascorbic acid and erythorbic acid in processed meat by HPLC. Z Lebensm Unters Forsch A 191:290–292
29. Thomas BR et al (1994) Mixed ion pair liquid chromatography method for the simultaneous assay of ascorbic acid, caffeine, chlorpheniramine maleate, dextromethorphan HBr monohydrate and paracetamol in Frenadol (TM) sachets. J Pharm Biomed Anal 12:85–90
30. Yuan JP, Chen F (1999) Simultaneous separation and determination of sugars, ascorbic acid and furanic compounds by HPLC-dual detection. Food Chem 64:423–427

31. Zhao B et al (2004) Simultaneous determination of vitamins C, E and beta-carotene in human plasma by high-performance liquid chromatography with photodiode-array detection. J Pharm Pharm Sci 30:200–204
32. Nováková L et al (2008) HPLC methods for simultaneous determination of ascorbic and dehydroascorbic acids. TrAC Trends Anal Chem 27:942–958
33. Anderson ME (1985) Glutathione and glutathione disulfide in biological samples. Meth Enzymol 113:548–555
34. Floreani M et al (1997) A comparison between different methods for the determination of reduced and oxidized glutathione in mammalian tissues. Free Radic Res 26:449–455
35. Klejdus B et al (2004) Sub-picomole high-performance liquid chromatographic/mass spectrometric determination of glutathione in the maize (Zea mays L.) kernels exposed to cadmium. Anal Chim Acta 520:117–124
36. Lakritz J et al (1997) Validated high-performance liquid chromatography-electrochemical method for determination of glutathione and glutathione disulfide in small tissue samples. Anal Biochem 247:63–68
37. Lenton KJ et al (1999) Analysis of glutathione and glutathione disulfide in whole cells and mitochondria by postcolumn derivatization high-performance liquid chromatography with ortho-phthalaldehyde. Anal Biochem 274: 125–130
38. Paroni R et al (1995) HPLC with o-phthalaldehyde precolumn derivatization to measure total, oxidized, and protein-bound glutathione in blood, plasma, and tissue. Clin Chem 41:448–454
39. Rellán-Álvarez R et al (2006) Direct and simultaneous determination of reduced and oxidized glutathione and homoglutathione by liquid chromatography-electrospray/mass spectrometry in plant tissue extracts. Anal Biochem 356:254–264
40. Remião F et al (2000) Simultaneous determination of reduced and oxidized glutathione in freshly isolated rat hepatocytes and cardiomyocytes by HPLC with electrochemical detection. Biomed Chromatogr 14:468–473
41. Kleinman WA (2000) Status of glutathione and other thiols and disulfides in human plasma. Biochem Pharmacol 60:19–29
42. Reed DJ et al (1980) High-performance liquid chromatography analysis of nanomole levels of glutathione, glutathione disulfide, and related thiols and disulfides. Anal Biochem 106: 55–62
43. Richie JP (1987) The determination of glutathione, cyst (e) ine, and other thiols and disulfides in biological samples using high-performance liquid chromatography with dual electrochemical detection. Anal Biochem 163:9–15
44. Bailey B et al (2010) Direct determination of tissue aminothiol, disulfide, and thioether levels using HPLC-ECD with a novel stable boron-doped diamond working electrode. Meth Mol Biol 594:327–339
45. Monostori P et al (2009) Determination of glutathione and glutathione disulfide in biological samples: an in-depth review. J Chromatogr B 877:3331–3346
46. Khan A et al (2011) A new HPLC method for the simultaneous determination of ascorbic acid and aminothiols in human plasma and erythrocytes using electrochemical detection. Talanta 84:789–801
47. Epshtein NA (2004) Validation of HPLC techniques for pharmaceutical analysis. Pharmaceut Chem J 38:212–228
48. Khan A et al (2010) Determination of lipoic acid in human plasma by HPLC-ECD using liquid-liquid and solid-phase extraction: method development, validation and optimization of experimental parameters. J Chromatogr B 878(28):2782–2788
49. Nolin TD et al (2007) Simultaneous determination of total homocysteine, cysteine, cysteinylglycine, and glutathione in human plasma by high-performance liquid chromatography: application to studies of oxidative stress. J Chromatogr B 852:554–561
50. Pfeiffer CM et al (1999) Rapid and accurate HPLC assay for plasma total homocysteine and cysteine in a clinical laboratory setting. Clin Chem 45:290
51. Meister A (1992) On the antioxidant effects of ascorbic acid and glutathione. Biochem Pharmacol 44:1905–1915
52. Przybyciel M, Majors R (2002) Phase collapse in reversed-phase liquid chromatography. LC GC N Am 20:516–523
53. Kirkland JJ (2004) Development of some stationary phases for reversed-phase HPLC. J Chromatogr A 1060:9–21
54. Kirkland JJ et al (1999) A highly stable alkylamide silica-based column packing for reversed-phase HPLC of polar and ionizable compounds. LC GC 17:634–639
55. Olsen BA (2001) Hydrophilic interaction chromatography using amino and silica columns for the determination of polar pharmaceuticals and impurities. J Chromatogr A 913:113–122
56. Majors RE, Przybyciel M (2002) Columns for reversed-phase LC separations in highly aqueous mobile phases. LC GC N Am 20:584–593
57. Nagae N et al (2002) The retention behavior of reversed-phase HPLC columns with 100 % aqueous mobile phase. LC GC N Am 20: 964–973

58. Watson DG et al (1993) Measurement of ascorbic acid in human aqueous humour and plasma and bovine aqueous humour by high-performance liquid chromatography with electrochemical detection. J Pharm Biomed Anal 11:389–392
59. Karlsen A et al (2005) High-throughput analysis of vitamin C in human plasma with the use of HPLC with monolithic column and UV-detection. J Chromatogr B 824: 132–138
60. McMenamin M et al (2009) Simultaneous analysis of multiple aminothiols in human plasma by high performance liquid chromatography with fluorescence detection. J Chromatogr B 877:3274–3281

Chapter 16

Portable Nanoparticle Based Sensors for Antioxidant Analysis

Erica Sharpe and Silvana Andreescu

Abstract

Interest in portable sensing devices has increased throughout the past decade. Portable sensors are convenient for use in remote locations and in places with limited resources for advanced instrumentation. Often such devices utilize advanced technology that allows the final user to simply deposit the sample onto the sensing platform without preparation of multiple reagents. Herein, we describe preparation and characterization of a colorimetric paper-based metal oxide sensing array designed for the field detection of polyphenolic antioxidants. This sensor is a good candidate for use in analysis of the antioxidant character of food, drink, botanical medicines, physiological fluids, and more.

Key words Paper sensor, Nanoparticle, Color analysis, Metal oxide, Antioxidant, Polyphenol, Portable, Inexpensive, Rapid

1 Introduction

In this chapter we describe the preparation, characterization, and performance evaluation of a portable paper-based sensor array for the detection of antioxidants, specifically polyphenolic compounds (PPs). This array is comprised of several individual sensors each containing a characteristic type of metal oxide sensing nanoparticles immobilized on cellulose fibers. Detection occurs through formation of colored charge transfer complexes between PPs and metal oxides. Such complexes form as a result of electron donation from hydroxyl groups of a polyphenol to surface cations on the sensing nanoparticle [1]. We directly correlate this electron donating capacity of PPs to their antioxidant activity, similarly to the way in which other popularly used assays monitor electron transfer to a metal cation as a means of indicating antioxidant activity (i.e., the ferric reducing antioxidant capacity (FRAP) [2] or the cupric ion reducing antioxidant capacity (CUPRAC) [3] assays).

Donald Armstrong (ed.), *Advanced Protocols in Oxidative Stress III*, Methods in Molecular Biology, vol. 1208,
DOI 10.1007/978-1-4939-1441-8_16,

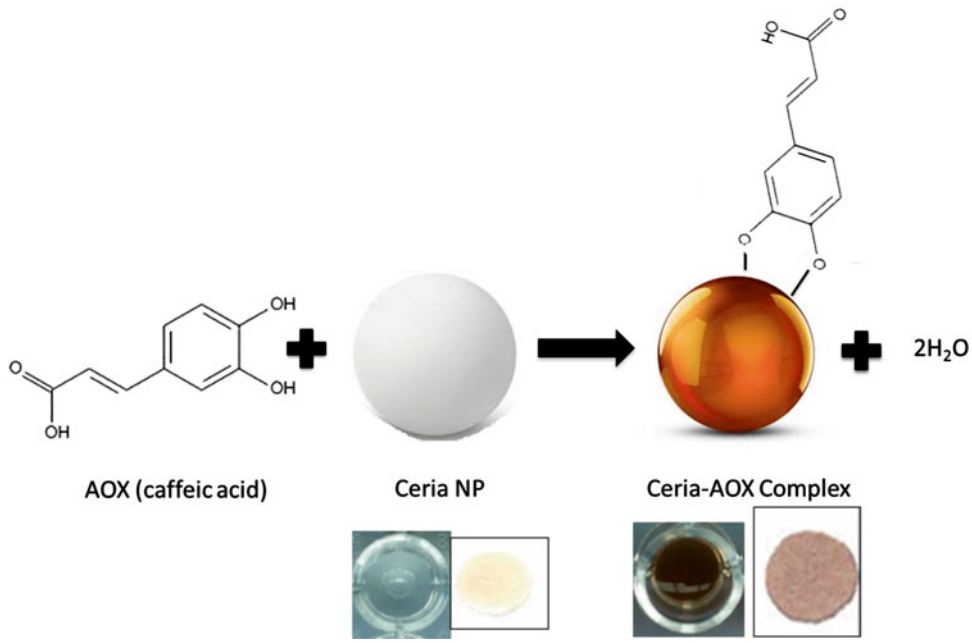

Scheme 1 Schematic of the binding mechanism between polyphenol and metal oxide nanoparticle taking place on the surface of the sensing array. This binding produces visually quantifiable color signals which are unique to each polyphenol and each metal oxide. The unique signals allow for identification of unknown samples using color matching described herein

As a result of the electron transfer from PP hydroxyl groups, highly reactive ArO· radical intermediates are formed, which subsequently bind to the surface of immobilized nanoparticles, creating charge transfer complexes with unique spectral properties. These colored charge-transfer complexes allow for visual quantification of imparted antioxidant activity both on paper and in solution (Scheme 1). It is the color production with respect to PP concentration that is used in this assay to calculate antioxidant activity with respect to an antioxidant standard, gallic acid (GA), wherein the slope of a color intensity versus concentration calibration curve is compared to that of GA to determine relative antioxidant activity in terms of GA equivalents.

In addition to assessment of PP antioxidant activity, the color responses of the metal oxide sensing array can be used to determine the identity and quantity of an active PP based on its resultant color response and respective intensity. Colorimetric responses created by each PP are unique from one another and are further differentiable depending on the sensing metal oxide involved in electron transfer and complex formation.

The unique color developments for each PP and each metal oxide has created the opportunity to formulate a large database of PP standards, which have been documented with reference to their unique color responses on metal oxide modified-paper sensing surfaces. This database can be used for sample identification in terms

of polyphenolic constitution and has been created by logging each PP color response in terms of red, green, and blue (RGB) color channels and an electronically assigned color ID code, as determined by a portable color reader, the Pantone CapSure®. Colors of fifteen polyphenol responses on four metal oxide sensor types have been documented. The four sensor types used are: zinc oxide (ZnO), iron oxide (Fe_2O_3), titanyl oxalate (Ti(IV)oxo), and ceria (CeO_2) and are used alongside one another for cross-validation of results. The documented colors can be referenced by users of the sensing array for sample identification; specifically regarding the quantity and molecular identity of the responding PP. PPs studied here represent at least one compound from each of the major families of dietary polyphenols assigned based on structural characteristics of each compound [4]. Representation of a variety of PP families provides breadth of scope to this database and creates the possibility that most samples analyzed using this technique may match an antioxidant standard contained within this database of references. The database can continue to grow as users analyze other compounds and share Pantone® ID codes through online file sharing programs.

This protocol describes the fabrication and use of this metal oxide sensing array. These sensors can be created and ready to use within an hour. The response to PP compounds is immediate, and can be analyzed within minutes. Color matching within a database of PP color standards for each metal oxide can allow for identification of the primary acting PP in a variety of samples from botanical extractions to food and drink as well as other samples.

2 Materials

2.1 Equipment

1. The Pantone CapSure® handheld color reader was used to document colorimetric responses of all polyphenol standards in terms of red, green, and blue (RGB) color intensities and unique color ID codes matching standards within a large Pantone® color database. These color IDs were used to create our own database of polyphenol standards.
2. Filter paper used as the paper platform for all sensors was medium flow rate, 11 cm diameter and purchased from Fisher Scientific.

2.2 Polyphenols and Sensing Particles

1. Antioxidant standards used to create the database include: ascorbic acid, caffeic acid, curcumin, capsaicin, ellagic acid, epigallocatechin gallate, genistein, gallic acid, keracyanin chloride, quercetin, rutin, resveratrol, rosmarinic acid, Trolox, and vanillic acid. These can be purchased from any chemical supplier.

2. Sensing nanoparticles used for paper sensor array fabrication include: CeO_2, ZnO, Fe_2O_3, and Ti(IV)oxo. CeO_2 nanoparticles (aq), of size 10–20 nm was purchased from Sigma Aldrich. ZnO nanoparticles (10–30 nm) were purchased from SkySpring Nanomaterials Inc. Fe_2O_3 (20–40 nm) was purchased from US Research Nanomaterials, Inc. Ammonium titanyl oxalate was purchased from Acros Organics.

2.3 Database of Polyphenolic Standards

1. The database of color reference standards was created using Microsoft Excel and color ID codes from the CapSure®. The "Ctrl F" function is then be used to search for ID matches for sample identification.

3 Methods

3.1 Fabrication of Metal Oxide Sensing Array

The metal oxide sensing array is comprised of four metal oxide sensors: CeO_2, ZnO, Ti(IV)oxo, Fe_2O_3. Sensor nanoparticles were immobilized following a procedure similar to that previously described for CeO_2 immobilization onto cellulose [1, 5].

1. Fe_2O_3, ZnO, and CeO_2 sensors were made by immersing 11 cm diameter filter paper rounds into baths of the various metal oxide dispersions (0.1 % Fe_2O_3 in 2.5 % HAc; 2 % ZnO in 2.5 % HAc; and 4 % : CeO_2 in 2.5 % HAc) for 1–2 min until papers were saturated *see* **Note 1**.
2. Paper rounds were dried in the oven at 100 °C for 5 min, then allowed to dry completely at room temperature.
3. Individual sensors were then cut in circular paper disks of 9/32″ diameter using a hole-puncher *see* **Note 2**.
4. Ti(IV)oxo sensors were prepared following procedures similar to those used by Xu [6]. 20 μL of 1 M titanyl oxalate salt solution was deposited onto the surface of individual circular paper sensors (9/32″ diameter) then allowed to dry completely *see* **Note 3**.
5. Before sample analysis, all sensor types (except CeO_2) were pretreated with 10 μL of 1 M NaOH, to activate -OH functionalities and increase sensitivity of polyphenol detection as described in Fig. 1.
6. GA was used as the standard for assessing reactivity of these metal oxides towards PP compounds. It was also used as the PP standard to which all antioxidant samples are compared for calculation of antioxidant activity *see* Fig. 2.

3.2 Sample Analysis and Color Documentation into Standards Database

1. Stock solutions of PP compounds were prepared at concentrations nearing their solubility limits and generally ranging from 0.02 to 20 mM. Serial 1:3 water to sample dilutions were made and deposited in triplicate onto sensors for colorimetric

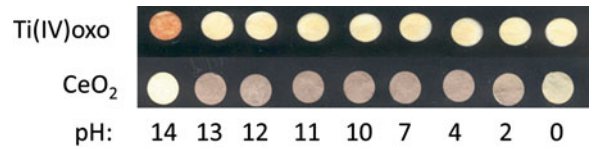

Fig. 1 Effect of pH on sensor function. A variety of metal oxide sensor types were pretreated with 10 μL of solution of various pHs ranging from 0 to 14. When sensors were dry, 5 mM GA was added to the surface to observe effects of pH on sensor sensitivity. This information was used to optimize operational conditions for each sensor type. CeO_2 and Ti(IV)oxo sensors are shown. Other metal oxide nanoparticles tested (ZnO and Fe_2O_3) followed the same trend as Ti(IV)oxo, wherein pretreatment with a strong base causes marked visible increase in sensitivity. CeO_2 was the only exception, and responded optimally in the pH range of 2–12

analysis and creation of standard calibration curves for the database.

2. Samples were analyzed by depositing 20 μL of aqueous samples onto sensing surfaces of each of four metal oxide sensor types and allowed to dry for 2 h. 10 μL of samples in volatile solvents are allowed to dry for 2 min.
3. After drying, sensors were placed onto the back of a black sheet of contact paper, with pre-cut holes (¼″ diameter) for sample framing and easy documentation within a notebook.
4. Color responses can be read once sensors are immobilized. The Pantone CapSure® handheld color analysis device was used for creation of our database due to its ability to generate unique color ID codes and RGB values that can be referenced by all users of the same device and can also be visually reproduced using Pantone inks, for a visual reference chart, if so required *see* **Note 4**.
5. Color IDs of each dilution were documented for every sample analyzed. These IDs can be later searched for sample identification.
6. A standard calibration curve was created for each PP, displaying the linear relationship of blue color intensity (BCI) to concentration of analyte *see* **Note 5**. Calibration curves created from the CapSure® system are intended for use in quantitative analysis of antioxidant samples, and also for comparison to the GA standard for calculation of antioxidant activity.

3.3 Polyphenol Constituent Identification and Quantification

1. To determine the identity of an unknown sample a systematic matching process is carried out using the unique Pantone® ID code for a sample on four sensor types. This ID code is matched within respective databases to determine possible PP identities, and matches are pared down to one true identity using the system outlined in Fig. 3. It is essential to use more than one metal

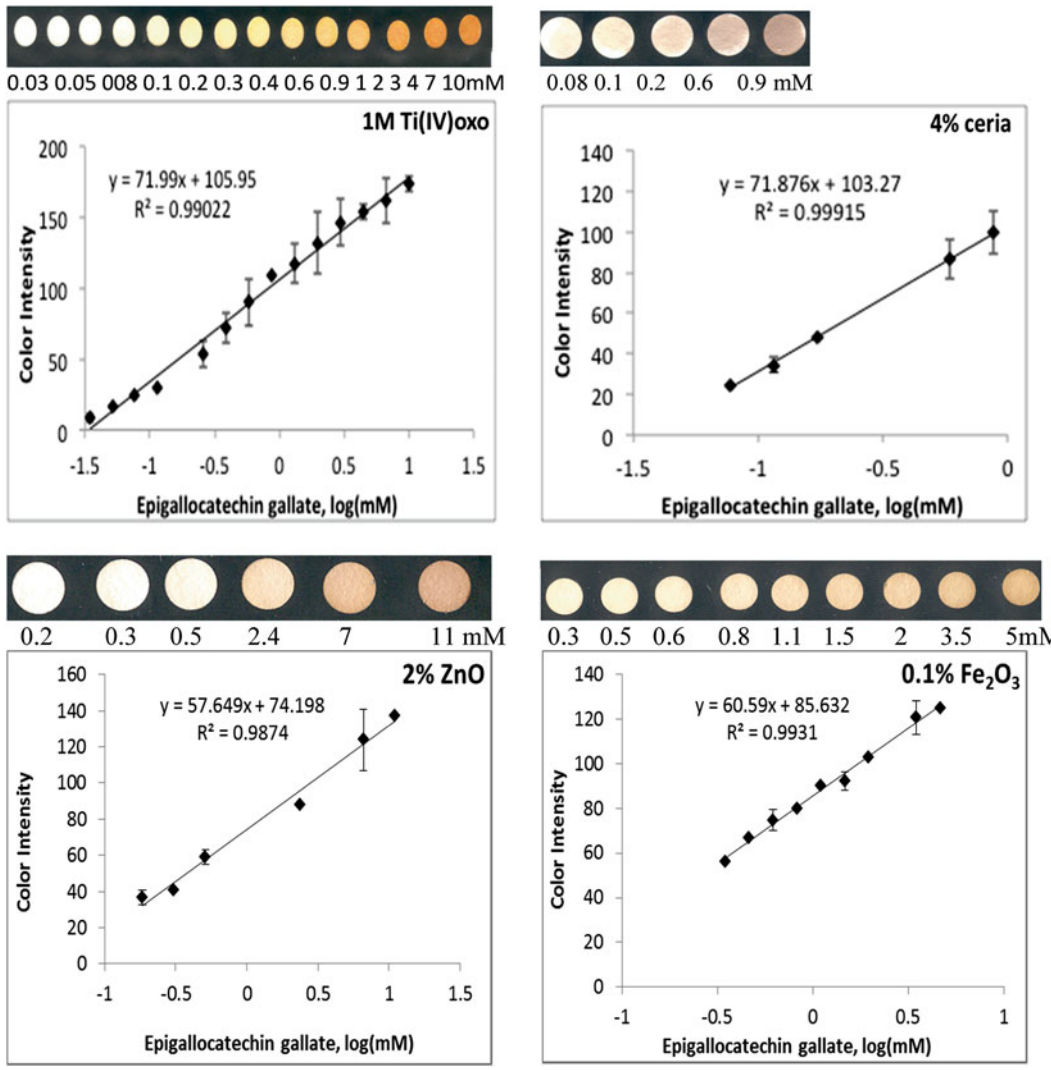

Fig. 2 Calibration curves of blue color intensity (BCI) versus concentration of one antioxidant, epigallocatechin gallate (EGCG) as an example, responding on four metal oxide sensor types, which constitute this sensing array. Metal oxide sensors depicted here include CeO_2, Ti(IV)oxo, ZnO, and Fe_2O_3. Antioxidant activity of a polyphenolic sample is calculated by comparing the slope of a calibration curve on a given sensor type to that of the GA standard on that sensor type using the equation $slope_{sample}/slope_{GA}$ = mM GAE, to give activity in terms of gallic acid equivalents

oxide sensor to determine identity of unknown solutions with increased accuracy. This is due to the fact that within any single database, multiple matches will likely appear for each ID code. These matches must be pared down using another database for validation.

2. To demonstrate the capacities of the metal oxide sensor array to determine the primary PP component of real samples and mixtures, one mixture of known composition (7 mM GA, 3 mM

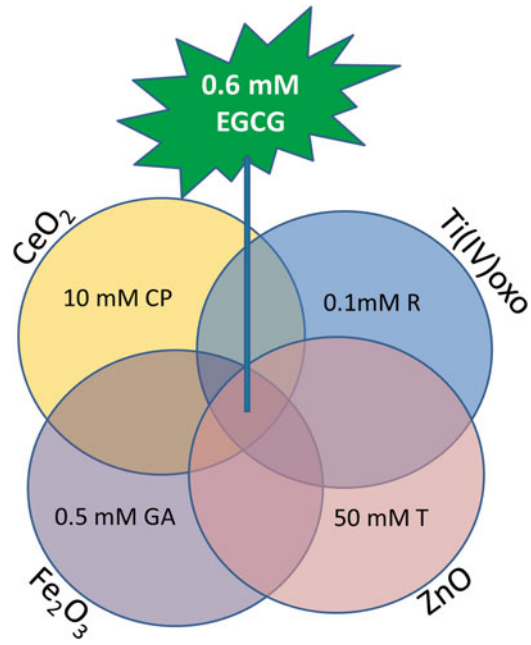

Fig. 3 Visual explanation of how to use more than one database to identify a sample in terms of molecular identity and concentration. A sample can be deposited onto two or more sensor types and analyzed using a color reader to determine its RGB color breakdown, which can be used to assign a unique color ID code. This ID code can be searched for within respective databases. Matches are placed in a pool for that sensor type as shown above by pink, blue, purple, and yellow circles representing ZnO, Ti(IV)oxo, Fe_2O_3, and CeO_2 sensors, respectively. Only those identity matches which appear in all databases are compiled and considered as possible identities for the sample in question. As seen above, using four databases, 0.6 mM epigallocatechin gallate (EGCG) was successfully identified despite signal overlap on each sensor type from other polyphenols including capsaicin (CP), gallic acid (GA), Trolox (T), and rutin (R)

ellagic acid (EA)) was analyzed and is shown here as an example of analysis using four sensor types (CeO_2, ZnO, Ti(IV)oxo, Fe_2O_3) and their respective databases.

3. Analysis of this mixture was performed using each database to determine color ID matches between PP standards and various concentrations of the mixture.
4. A calibration curve of each mixture was created and Pantone© IDs were assigned in triplicate to each concentration. IDs were matched within each respective PP database to determine the composition of the mixture.
5. PP identities and concentrations assigned to the original solution by each sensor type were calculated and compared by relating the concentrations at which the mixture and a PP

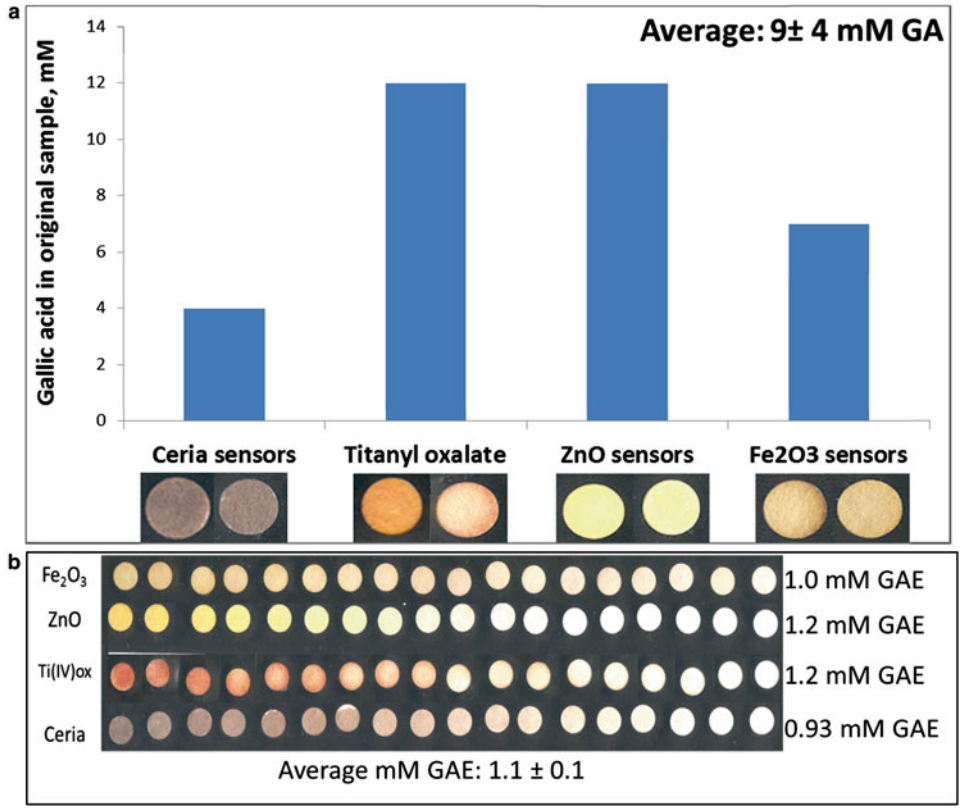

Fig. 4 Identification of the primary acting polyphenol within a laboratory-prepared mixture (7 mM GA and 3 mM EA); and quantification of antioxidant activity. (**a**) Only GA showed color matches within all four metal oxide databases. Concentration of the active antioxidant was calculated using the equation: [AOX, mM]/[sample, %] × 100 = mM AOX in original sample; and is shown on the *y*-axis. Matching sensor colors are shown below each sensor type and correspond to GA (*right*) and the sample (*left*). The sample response on four sensor types (**b**) was used to create calibration curves. Antioxidant activity was calculated by relating slopes of the calibration curves to a standard using the equation: $\text{slope}_{\text{sample}}/\text{slope}_{\text{GA}}$ = mM GAE; and is shown to the right of each sensor's colorimetric response to the sample

standard produced identical color IDs. The equation used is: (mM PP)/(% v/v mixture) X 100 = mM of responding PP in the original mixture.

6. Through comparison of results determined by four databases, select signals were eliminated. Only PP identities which appeared as a match using all sensor types were considered further.
7. If a PP identity and concentration matched for all sensor types used, said option was considered as a possible identity for the active PP component in the sample. This systematic matching using four metal oxide assays allows for semiquantitative determination of the active PP in the real sample matrix. *See* Fig. 4 for results of this mixture analysis as an example. *See* **Note 6** for further discussion.

3.4 Antioxidant Activity Calculation

1. Antioxidant activity of each sample was also analyzed in terms of GA equivalents (mM GAE) using established methods [1].
2. In brief, for antioxidant activity calculation, 10–20 serial dilutions of the sample in water (3:1) were prepared and applied to metal oxide sensors.
3. Color intensities were read using the CapSure®. BCIs were recorded and graphed versus the log (concentration, %).
4. To determine antioxidant activity of any sample, the slope of the BCI versus concentration calibration curve should be compared to that of the standard, GA using the equation: $(\text{slope}_{\text{sample}}/\text{slope}_{\text{GA}}) = \text{mM GAE}$ to determine antioxidant activity in terms of gallic acid equivalents.
5. Special care should be taken when analyzing colored samples. *See* **Note 7** for further discussion.

4 Notes

1. Sonicate Fe_2O_3 before dipping every few papers to make the dispersion more homogeneous.
2. There are visible color differences between the edges of the round paper and the center. This is delineated by the border of the beaker used to dry the sensors on. These color differences indicated non-homogenous deposition of nanoparticles on the edges as compared to the center portion of the paper. As a result, edges should be cut off of filter papers before small sensing circles are hole-punched. This will increase precision of results.
3. Ti(IV)oxo: solution containing Ti(IV)oxo salt was applied directly to pre-cut sensor disks rather than applied to the full 11 cm diameter paper before cutting to avoid disturbance and removal of resulting titanyl oxalate crystals.
4. The color reading window of the CapSure® was placed directly over the sample to block external light interferences. The RGB and Pantone© ID values are also automatically stored in the CapSure® device, which can hold up to 100 readings at a time.
5. The blue color channel is used as opposed to green or red, because it provides the most sensitive readings allowing detection of low concentrations of analyte, also responding with the greatest slope, as explained [1].
6. Most matching occurs at low concentrations of real samples/mixtures (Fig. 4). This could indicate that at these concentrations only one PP responds, due to its relatively higher concentration and binding affinity for the metal oxide as compared to other PPs in solution; which were below the LOD at the dilution where

matches appeared. The concentration of each AOX as well as the antioxidant activity (electron donating capacity) influences the ability of each PP to compete for binding sites on the sensor surface. For this reason, each sample is unique, and only those samples which have one prominently acting PP can be analyzed using this method. Separations using high-pressure liquid chromatograph (HPLC) or thin layer chromatography (TLC) or mass spectrometry (MS) could allow for separation and quantification of each individual constituent, rather than just the PP existing at the highest concentration or having the highest antioxidant activity.

7. Most colored solutions do not present a significant challenge in analysis. This is because color often comes directly from the PPs themselves. The PPs create a new color upon binding with metal oxide nanoparticles and thus, the color of solution does not cause interference. It is advised, however, to analyze colored solutions on blank paper, as a control, and to determine the dilution at which color is no longer visible on blank paper. This is the concentration below which one can confidently assign the color produced on the sensors as originating from PP reaction and not from other colored compounds in solution. In order to determine whether or not a response is specific to PPs or to the color of coexisting species at high sample concentrations, it is advisable to determine if the calibration curve remains linear over a wide range of concentrations, and to compare the colorimetric readings with the response of the sample on blank paper. A linear range indicates color specificity toward PPs. If two linear ranges are formed; the second one beginning at the concentration which has visible color on blank paper, then it can be determined that other compounds in solution maintain original color and can cause interference. In this case, the linear range for your analysis should be below the concentration at which the solution has visible color on the blank paper. This concept is explained in Fig. 5. Interferences from merlot wine, for example, are shown by a second linear range at high concentrations. Maintained linearity in acai berry juice shows an example of a colored solution which is colored only by active PPs.

Acknowledgements

This work was funded by the National Science Foundation under Grant No. 0954919. Any opinions, findings, and conclusions or recommendations expressed in this material are those of the author(s) and do not necessarily reflect the views of the National Science Foundation or Clarkson University.

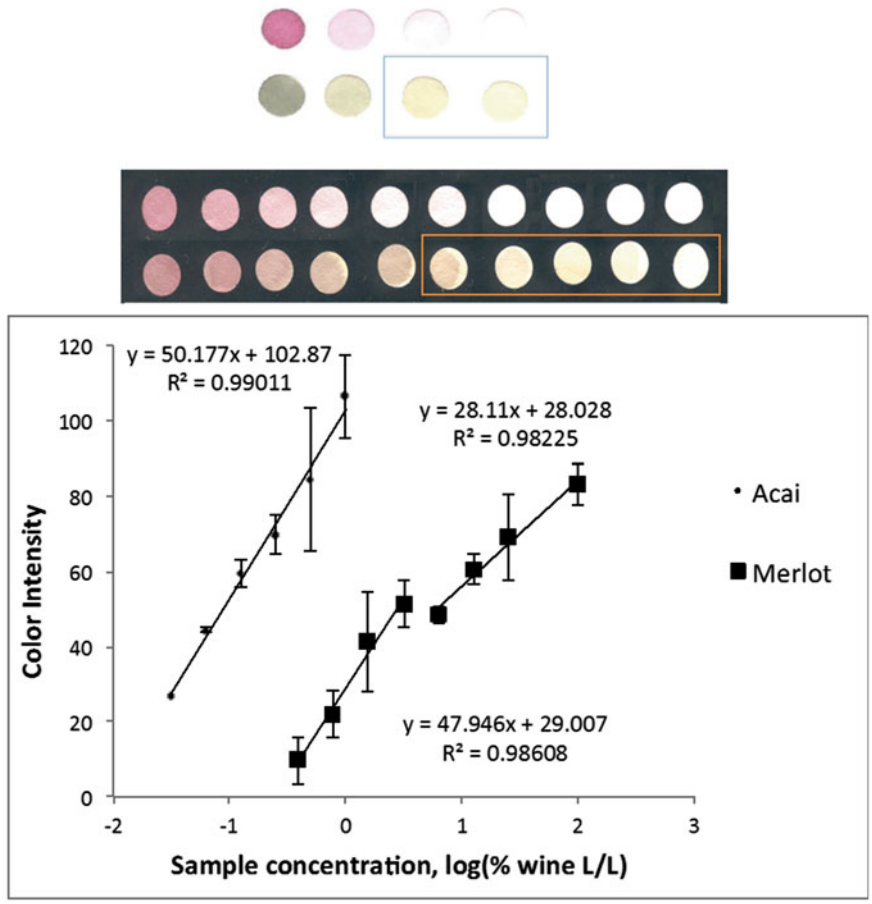

Fig. 5 Demonstration of the effect of colored compounds in solution on the linear range of a sample. Merlot is an example of a beverage which can have interference in colorimetric response from compounds in solution. Acai berry juice is an example of a colored solution which exhibits no interferences due to the fact that all colored compounds are responding as active polyphenols on the sensor surface. Adapted from [1]

References

1. Sharpe E, Frasco T, Andreescu D, Andreescu S (2013) Portable ceria nanoparticle-based assay for rapid detection of food antioxidants (NanoCerac). Analyst 138(1):249–262
2. Benzie IF, Strain J (1996) The ferric reducing ability of plasma (FRAP) as a measure of "antioxidant power": the FRAP assay. Anal Biochem 239:70–76
3. Apak R, Güçlü K, Oxyurek M, Karademir SE (2004) Novel total antioxidant capacity index for dietary polyphenols and vitamins C and E, using their cupric ion reducing capability in the presence of neocuproine: CUPRAC method. J Agric Food Chem 52(26):7970–7981
4. Tsao R (2010) Chemistry and biochemistry of dietary polyphenols. Nutrients 2(12):1231–1246
5. Ornatska M, Sharpe E, Andreescu D, Andreescu S (2011) Paper bioassay based on ceria nanoparticles as colorimetric probes. Anal Chem 83(11): 4273–4280
6. Xu M, Bunes BR, Zang L (2011) Paper-based vapor detection of hydrogen peroxide: colorimetric sensing with tunable interface. ACS Appl Mater Interfaces 3(3):642–647

Chapter 17

Fe^{3+}–Fe^{2+} Transformation Method: An Important Antioxidant Assay

İlhami Gülçin

Abstract

If we look at the multitude of varied and interesting reaction that constitute biochemistry and bioorganic chemistry, it is possible to classify a great many as either oxidation or reduction reactions. The reducing agent transfers electrons to another substance and is thus it oxidized. And, because it gives electrons, it is also called an electron donor. Electron donors can also form charge transfer complexes with electron acceptors. Reductants in biochemistry are very diverse. For example ferric ions (Fe^{3+}) are good reducing agents. Also, different bioanalytical reduction methods are available such as Fe^{3+}-ferrous ions (Fe^{2+}) reduction method, ferric reducing antioxidant power reducing assay. In this section, Fe^{3+}–Fe^{2+} transformation will be discussed. Recently there has been growing interest in research into the role of plant-derived antioxidants in food and human health. The beneficial influence of many foodstuffs and beverages including fruits, vegetables, tea, coffee, and cacao on human health has been recently recognized to originate from their antioxidant activity. For this purpose, the most commonly method used in vitro determination of reducing capacity of pure food constituents or plant extracts is Fe^{3+} reducing ability. This commonly used reducing power method is reviewed and presented in this study. Also, the general chemistry underlying this assay was clarified. Hence, this overview provides a basis and rationale for developing standardized antioxidant capacity methods for the food, nutraceutical, and dietary supplement industries. In addition, the most important advantages of this method were detected and highlighted. The chemical principles of these methods are outlined and critically discussed. The chemical principles of methods of Fe^{3+}–Fe^{2+} transformation assay are outlined and critically discussed.

Key words Antioxidant, Reducing activity, Fe^{2+} reducing ability, Bioanalytical method

1 Introduction

Oxidation is the transfer of electrons from one atom to another and represents an essential part of aerobic life and our metabolism, since oxygen is the ultimate electron acceptor in the electron flow system that produces energy in the form of ATP [1]. If we look at the multitude of varied and interesting reaction that constitute biochemistry and bioorganic chemistry, it is possible to classify a great many as either oxidation or reduction reactions. Oxidation and reduction is a theme that runs through the very core

Donald Armstrong (ed.), *Advanced Protocols in Oxidative Stress III*, Methods in Molecular Biology, vol. 1208,
DOI 10.1007/978-1-4939-1441-8_17,

of biochemistry and bioorganic chemistry. Indeed, it is difficult to think of a synthesis in laboratory or in nature, which does not use such a reaction at one stage or another. Oxidation of a biological compound may be defined as the addition of oxygen, the removal of hydrogen or the removal of electrons from that biocompound. Oxidation can be defined as the loss of electrons or an increase in oxidation state by a molecule, atom, or ion. Similarly, reduction can be described as the removal of oxygen, the addition of hydrogen, or the addition of electrons to a biocompound [2]. Oxidation and reduction is a theme that runs through the very core of biochemistry and bioorganic chemistry. Indeed, it is difficult to think of a synthesis in laboratory or in nature, which does not use such a reaction at one stage or another. Reduction is the gain of electrons or a decrease in oxidation state by a molecule, atom, or ion. Substances that have the ability to reduce other substances are said to be reductive or reducing and are known as reducing agents, reductants, or reducers. Oxidation–reduction reactions, in another word, redox reactions include all chemical reactions in which atoms have their oxidation state changed. This can be either a simple redox process, such as the oxidation of carbon to yield CO_2 or the reduction of carbon by hydrogen to a complex process such as the oxidation of glucose in the human body through a series of complex electron transfer processes [2]. However, problems may arise when the electron flow becomes uncoupled, generating free radicals. Examples of oxygen-cantered free radicals, known as reactive oxygen species (ROS), include superoxide ($O_2\cdot-$), hydroxyl ($HO\cdot$), peroxyl ($ROO\cdot$), alkoxyl ($RO\cdot$), and nitric oxide ($NO\cdot$). The hydroxyl and the alkoxyl radicals are very reactive and rapidly attack the molecules in nearby cells, and probably the damage caused by them is unavoidable and is dealt with by repair processes. On the other hand, the superoxide anion, lipid hydroperoxides, and nitric oxide are less reactive [3]. In addition to these ROS radicals, in living organisms there are other ROS nonradicals, such as the singlet oxygen ($^1O_2$), hydrogen peroxide (H_2O_2), and hypochlorous acid (HOCl) [4]. The putative reactive oxygen species (ROS), nitrogen species (ROS), and non free-radical species are shown in Table 1. ROS are continuously produced by the body's normal use of oxygen such as respiration and some cell mediated immune functions [5]. A free radical is defined as chemical species capable of independent existence, possessing one or more unpaired electrons. Free radicals are highly unstable molecules. ROS are either radicals that contain at least one unpaired electron or reactive nonradical compounds, capable of oxidizing biomolecules. Therefore, these intermediates are also called oxidants or prooxidants [6, 7]. ROS are continuously produced during normal physiologic events and can easily initiate the peroxidation of membrane lipids, leading to the accumulation of

Table 1
Reactive oxygen species (ROS), reactive nitrogen species, and non-free-radical species

Reactive oxygen and nitrogen species		Non-free-radical species	
Superoxide radical	$O_2^{\cdot-}$	Hydrogen peroxide	H_2O_2
Hydroxyl radical	HO·	Singlet oxygen	$^1O_2$
Hydroperoxyl radical	HOO·	Ozone	O_3
Lipid radical	L·	Lipid hydroperoxide	LOOH
Lipid peroxyl radical	LOO·	Hypochlorite	HOCl
Peroxyl radical	ROO·	Peroxynitrite	$ONOO^-$
Lipid alkoxyl radical	LO·	Dinitrogen trioxide	N_2O_3
Nitrogen dioxide	NO_2·	Nitrous acid	HNO_2
Nitric oxide	NO·	Nitryl chloride	NO_2Cl
Nitrosyl cation	NO^+	Nitroxyl anion	NO^-
Thiyl radical	RS·	Peroxynitrous acid	ONOOH
Protein radical	P·	Nitrous oxide	N_2O

lipid peroxides [8]. ROS at physiological concentrations may be required for normal cell function. They are also capable of damaging crucial biomolecules such as nucleic acids, lipids, proteins, polyunsaturated fatty acids, and carbohydrates. Also, they may cause DNA damage that can lead to mutations. If ROS are not effectively scavenged by cellular constituents, they can stimulate free radical chain reactions subsequently damaging the cellular biomolecules such as proteins, lipids, and nucleic acids and finally they lead to disease conditions [2, 9].

ROS are also produced in the organism as a part of the primary immune defense. Phagocytic cells such as neutrophils, monocytes, or macrophages defend against foreign organisms by synthesizing large amounts of $O_2^{\cdot-}$ or NO· as a part of their killing mechanism. Several diseases are accompanied by excessive phagocyte activation resulting in tissue damage, which is at least in part due to the activity of ROS [10]. In addition, reactive oxygen species induce some oxidative damage to biomolecules like lipids, nucleic acids, proteins, and carbohydrates. Their damage causes aging, cancer, and many other diseases [11]. As a result, ROS have been implicated in more than 100 diseases, including malaria, acquired immunodeficiency syndrome, heart disease, stroke, arteriosclerosis, diabetes, and cancer [12–15]. Also the biological pathways for endogenous formation of ROS are examples of a whole class of reactive intermediates

and their ways of generation. It should further be noted that the organism is also exposed to ROS from external sources. In living organisms, various ROS can form in different ways. Normal aerobic respiration stimulates polymorphonuclear leukocytes and macrophages, and peroxisomes appear to be the main endogenous sources of most of the oxidants produced by cells. Exogenous sources of ROS include tobacco smoke, certain pollutants, organic solvents, and pesticides [6]. With the diet many compounds of prooxidant nature, such as quinones capable of redox cycling, are delivered to the organism. Also an array of radicals is inhaled with cigarette smoke; ozone, of which increasing levels are reported due to air pollution, is an ROS, which can oxidize lipids [10].

There are various sources for specific ROS in the human organism. However, the superoxide radical anion appears to play a central role, since other reactive intermediates are formed in reaction sequences starting with $O_2 \cdot^-$. It has been estimated that about 1–3 % of the O_2 we utilize is converted to $O_2 \cdot^-$ [16, 17].

Phenolics are not active antioxidants unless substitution at either the *ortho*- or *para*-position has increased the electron density at the hydroxyl group and lowered the oxygen–hydrogen bond energy, in effect increasing the reactivity towards the lipid free radicals. Substitution in phenolic compounds at the *meta*-position has a rather limited effect. Steric and electronic effects are responsible for the antioxidant activities and stoichiometric factors of the chain-breaking phenolic antioxidants [18]. For elucidation of the hydrogen abstraction mechanism of phenolic antioxidants in the chain process of autoxidation molecular orbital theory has been applied [19].

The stability of the radical generated from flavonoid moiety relies on the hydrogen bond formed between the hydroxyl and oxygen possessing unpaired electron. The presence of a C = C double bond in ring C conjugated with a 4-oxo group is also of great importance for the delocalization of an unpaired electron. Additional antioxidant activity is assigned to the presence of a hydroxyl group at the 3- and 5-positions. An internal hydrogen bond to a 4-oxo group makes these positions kinetically equivalent [20]. Besides the two generally accepted mechanisms of phenolic antioxidants action [21], namely hydrogen atom transfer (HAT)

$$\mathrm{ArOH} \rightarrow \mathrm{ArO}\cdot + \mathrm{H}\cdot$$

and single-electron transfer followed by proton transfer (SET-PT),

$$\mathrm{ArOH} \rightarrow \mathrm{ArOH}^{+\cdot} + e^-$$

$$\mathrm{ArOH}^{+\cdot} \rightarrow \mathrm{ArO}\cdot + \mathrm{H}^+$$

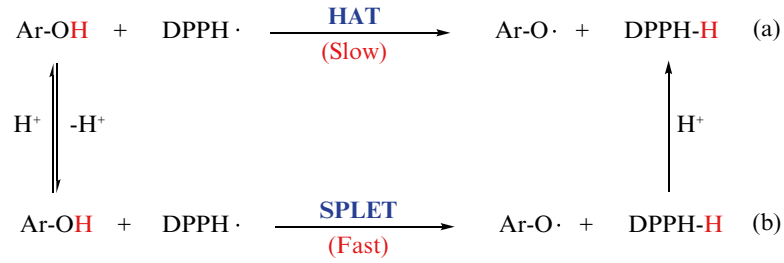

Fig. 1 Conventional hydrogen atom transfer (HAT) and sequential proton loss electron transfer (SPLET) process of a phenolic compound

Recently another important mechanism has been discovered named sequential proton loss electron transfer mechanism (SPLET).

$$\mathrm{ArOH} \rightarrow \mathrm{ArO^-} + \mathrm{H^+}$$

$$\mathrm{ArO^-} + \mathrm{ROO\cdot} \rightarrow \mathrm{ArO\cdot} + \mathrm{e^-}$$

The 7-OH group in flavonoids plays an important role as the site of ionization and of electron transfer according to sequential proton loss electron transfer (SPLET). This mechanism has been discovered recently [22–24] and takes place in two steps:

$$\mathrm{ArOH} \rightarrow \mathrm{ArO^-} + \mathrm{H^+}$$

$$\mathrm{ArOH} + \mathrm{ROO\cdot} \rightarrow \mathrm{ArO\cdot} + \mathrm{ROO^-}$$

Also, a SPLET mechanism was proposed by Litwinienko and Ingold [24]. In solvents which support ionization notably methanol among organic solvents [22], the experimental rate constant is the sum of the rate constant for the conventional HAT process (Fig. 1) and the very much larger rate constant for reaction of the radical with the phenoxide anion [24, 25], the SPLET process (Fig. 1). SPLET is favored for reactions of phenols having low pKa's with electron-deficient radicals having relatively low HAT activities and yielding product molecules having low pKa's [24].

In addition, the occurrence of SPLET in methanol and ethanol has also been clearly demonstrated by Foti et al. [24] In general, the methods for determination the antioxidant capacity of food components can deactivate radicals by two major mechanisms and were divided into two major groups: assays based on the SET reaction, and assays based on a HAT. The end result is the same, regardless of mechanism, but kinetics and potential for side reactions are different. SET based methods detect the ability of a potential antioxidant to transfer one electron to reduce any compound, including metals, carbonyls, and radicals. SET displayed through a change in color as the oxidant is reduced [26].

SET based methods measure the ability of a potential antioxidant. These methods transfer one electron to reduce any compound,

including metal ions, carbonyls and radicals [27]. SET and HAT mechanisms almost always occur together in all samples, with the balance determined by antioxidant structure and pH. SET based-methods detect the ability of an antioxidant to transfer one electron to reduce any compound, including metals, carbonyl groups and radicals:

$$AH + X\cdot \rightarrow AH^{\bullet+} + X^{-}$$

$$AH^{\bullet+} + H_2O \rightarrow A^{\bullet} + H_3O^{+}$$

$$X^{-} + H_3O^{+} \rightarrow XH + H_2O$$

$$AH + M^{3+} \rightarrow AH^{+} + M^{2+}$$

Relative reactivity in SET methods is based primarily on deprotonation [28] and ionization potential of the reactive functional group [27]. So SET reactions are pH dependent. In general, ionization potential values decrease with increasing pH, reflecting increased electron donating capacity with deprotonation. A correlation between redox potential and SET methods has been suggested [29] but not consistently demonstrated. SET reactions are usually slow and can require long times to reach completion, so antioxidant capacity calculations are based on percent decrease in product rather than kinetics. When AH^{+} has a sufficient lifetime, secondary reactions become a significant interference in assays and can even lead to toxicity or mutagenicity in vivo [30]. SET methods are very sensitive to ascorbic acid and uric acid, which are important in maintaining plasma redox tone, and reducing polyphenols are also detected. Importantly, trace components and contaminants such as metals interfere with SET methods and can account for high variability and poor reproducibility and consistency of results [31].

Relative reactivity of the SET method is based on deprotonation and in ionization potential of the reactive functional group [27, 28, 32]. Therefore, SET methods are pH-dependent. Generally, ionization potential decreases with increasing pH values, which reflects a higher electron-donating capacity with deprotonating. The antioxidant mechanism is predominantly of the electron transfer type when the ionization potential values are superior to –45 kcal/mol. The reactions based on the electron transfer are usually slow and calculations are based on product percentage decrease more than in kinetic terms. [32] The most putative SET-based method is ferric ions (Fe^{3+})-ferrous ions (Fe^{3+}) transformation assays.

2 Reducing Antioxidant Power

Reduction of a chemical is defined as a gain of electrons. Oxidation is defined as a loss of electrons. A reductant or a reducing agent is a substance that donates electrons and, thereby, causes another reactant to be reduced. An oxidant or an oxidizing agent is a substance that accepts electrons and causes another reactant to be oxidized. An oxidation is impossible without a reduction elsewhere in the system. When reduction and oxidation characterize a chemical reaction, it is called a redox reaction. Redox reactions are the main reaction of biological oxidation, the chain of chemical reactions whereby we use oxygen from air to oxidize chemicals from the breakdown of food to provide energy for living system. Reductant and oxidant are chemical terms, whereas antioxidant and prooxidant have meaning in the context of a biological system. In addition, an antioxidant that can effectively reduce prooxidants may not be able to efficiently reduce Fe^{3+}. An antioxidant is a reductant, but a reductant is not necessarily an antioxidant [2, 33].

As reported in many studies, the activities of natural antioxidants in influencing diseases are closely related to their ability to reduce DNA damage, mutagenesis, carcinogenesis, and inhibition of pathogenic bacterial growth [34].

3 Fe^{3+} Reducing Antioxidant Power-Fe^{3+}–Fe^{2+} Transformation Assay

Reducing power of bioactive compounds or food components reflects the electron donating capacity and is associated with antioxidant activity. Bioactive compounds with antioxidant effects can be reductants and inactivate oxidants [35]. The reducing capacity of a bioactive compound can be measured by the direct reduction of $Fe[(CN)_6]_3$ to $Fe[(CN)_6]_2$. Free Fe^{3+} to the reduced product leads to the formation of the intense Perl's Prussian blue complex, $Fe_4[Fe(CN^-)_6]_3$, which has a strong absorbance at 700 nm [36].

$$\mathrm{Fe(CN)_6^{3-} \xrightarrow{\text{Reductant}} Fe(CN)_6^{4-}}$$

$$\mathrm{Fe(CN)_6^{4-} + Fe^{3+} \xrightarrow{\text{Reductant}} Fe_4\left[Fe(CN)_6\right]_3}$$

An increase in absorbance of the reaction mixture would indicate an increase in the reducing capacity due to an increase in the formation of the complex. There are a number of assays designed to measure overall antioxidant activity, or reducing potential, as an indication of a host's total capacity to withstand free radical stress. The ferric ions (Fe^{3+}) reducing antioxidant power assay takes advantage of an SET in which a ferric salt is

used as an oxidant [37]. In this assay, the yellow color of the test solution changes to various shades of green and blue depending on the reducing power of antioxidant samples. The reducing capacity of a compound may serve as a significant indicator of its potential antioxidant activity [38].

Antioxidant compounds reduce Fe^{3+}-ferricyanide complexes to the ferrous (Fe^{2+}) form. The Prussian blue colored complex is formed by adding $FeCl_3$ and then ferric form (Fe^{2+}) converted to the ferrous form (Fe^{2+}). Therefore, the amount of reduction can be determined by measuring the formation of Perl's Prussian blue at 700 nm [39]. In this assay, the yellow color of the test solution changes to green or blue depending on the reducing power of the antioxidant. A higher absorbance indicates higher ferric reducing power [40].

Up to now, the most commonly used methods for in vitro determination of reducing capacity of food constituents or pure substances are ferric ions (Fe^{3+}) reducing antioxidant power assay (FRAP), Fe^{3+}–Fe^{2+} transformation assay, Both the methods are recommended for measurement of antioxidant properties of food components or pure compounds that better reflect their potential protective effects. A main objective of this overview is reviewed the chemical principles, some of its variants, recent applications as well as the advantages and shortcomings. It was suggested that bioactive component (Table 2) and different plant extracts (Table 3) could reduce likely due to higher concentrations and types of polyphenols in the extracts.

Table 2
Fe^{3+}–Fe^{2+} reducing ability of some pure compounds

Pure compounds	Fe^{3+}–Fe^{2+} reducing ability	References
BHA	1.99[a]	[41]
BHT	1.02[a]	[41]
Caffeic acid	2.77[a]	[41]
Caffeic acid phenethyl ester	1.81[a]	[42]
Cepharanthine	2.89[a]	[43]
Clove oil	1.18[a]	[44]
Curcumin	2.83[a]	[45]
Eugenol	1.18[b]	[46]

(continued)

Table 2
(continued)

Pure compounds	Fe^{3+}–Fe^{2+} reducing ability	References
Fangchinoline	1.64[a]	[42]
3-O-(β-D-glucopyranosyl)-hederagenin	0.72[b]	[47]
α-Hederin	1.41[c]	[48]
Hederasaponin-C	0.69[c]	[48]
Hederacolchiside-E	0.51[c]	[48]
Hederacolchiside-F	0.28[c]	[48]
Isomajdine	0.32[a]	[49]
L-Adrenaline	2.68[a]	[50]
L-Carnitine	0.75[b]	[5]
L-Dopa	2.22[d]	[51]
L-Tyrosine	0.38[d]	[51]
Majdine	045[a]	[49]
Melatonin	0.18[b]	[52]
Monodesmoside	0.84[b]	[53]
Morphine	1.18[c]	[54]
Oleuropein	1.23[a]	[55]
Phillyrin	0.41[a]	[55]
Pinoresinol-β-D-glucoside	0.62[a]	[55]
Pinoresinol di-β-D-glucoside	0.37[a]	[55]
Propofol	1.39[e]	[56]
Propolis	0.83[a]	[57]
Resveratrol	1.54[a]	[8]
Serotonin	2.28[c]	[58]
Silymarin	0.82[a]	[59]
Tannic acid	2.43[b]	[38]
Uric acid	0.36[a]	[60]

[a]20 μg/mL
[b]30 μg/mL
[c]75 μg/mL
[d]10 μg/mL
[e]25 μg/mL

Table 3
Reducing ability by Fe^{3+}–Fe^{2+} transformation method of some plant extracts

Plant extracts	Fe^{3+}–Fe^{2+} reducing ability	References
Anise (*Pimpinella anisum*)	0.49[a]	[61]
Basil (*Ocimum basilicum*)	0.56[b]	[62]
Bay (*Laurus nobilis*)	1.07[c]	[63]
Black Pepper (*Piper nigrum*)	0.34[b]	[64]
Broccoli (*Brassica oleracea*)	0.47[c]	[65]
Cauliflower (*Brassica oleracea*)	0.33[c]	[35]
Cherry stem (*Cerasus avium*)	1.16[c]	[66]
Clove (*Eugenia caryophyllata*)	0.62[c]	[67]
Cornelian cherry (*Cornus mas*)	0.19[c]	[68]
Duckweed (*Lemna minor*)	0.18[d]	[69]
Fennel (*Foeniculum vulgare*)	0.41[e]	[70]
Fringe tree (*Chionanthus virginicus*)	1.21[c]	[55]
Isgın (*Rheum ribes*)	0.21[c]	[71]
Kiwifruit (*Actinidia deliciosa*)	0.23[c]	[72]
Lavender (*Lavandula stoechas*)	0.51[c]	[67]
Lemon balm (*Melissa officinalis*)	1.41[c]	[73]
Liquorice (*Glycyrrhiza glabra*)	0.81[c]	[74]
Medlar (*Mespilus germanica*)	0.69[c]	[75]
Mountain mint (*Cyclotrichium niveum*)	0.24[d]	[76]
Nettle (*Urtica dioica*)	0.12[e]	[77]
Raspberries (*Rubus idaeus*)	0.66[c]	[78]
Sea buckthorn (*Hippophae rhamnoides*)	0.21[c]	[79]
Sumac (*Rhus coriaria*)	0.51[c]	[66]

[a]10 μg/mL
[b]25 μg/mL
[c]20 μg/mL
[d]30 μg/mL
[e]40 μg/mL

4 Conclusion

There are a lot of methods used in vitro determinations of reducing capacity of pure compounds, food constituents, and plant extracts. Among ones Fe^{3+} reducing ability is the putative and common method. In this study, Fe^{3+} reducing power method is reviewed and presented. Also, the general chemistry underlying this assay was clarified. Hence, this overview provides a basis and rationale for developing standardized reducing power capacity methods for the food, nutraceutical, and dietary supplement industries. In addition, the most important advantages of this method were detected and highlighted. The chemical principles of these methods are outlined and critically discussed. The chemical principles of methods of Fe^{3+}–Fe^{2+} transformation assay are outlined and critically discussed.

References

1. Davies KJ (1995) Oxidative stress: the paradox of aerobic life. Biochem Soc Symp 61:1–31
2. Gülçin İ (2012) Antioxidant activity of food constituents – an overview. Archiv Toxicol 86: 345–396
3. Ames BN, Shigenaga MK, Hagen TM (1993) Oxidants, antioxidants, and the degenerative diseases of aging. Proc Natl Acad Sci U S A 90: 7915–7922
4. Pietta PG (2000) Flavonoids as antioxidants. J Nat Prod 63:1035–1042
5. Gülçin İ (2006) Antioxidant and antiradical activities of L-Carnitine. Life Sci 78:803–811
6. Halliwell B, Gutteridge JMC (1989) Free radicals in biology and medicine, 2nd edn. Clarendon, Oxford
7. Sies H (1991) Oxidative stress: from basic research to clinical application. Am J Med 91: 31–39
8. Gülçin İ (2010) Antioxidant properties of resveratrol: a structure-activity insight. Innov Food Sci Emerg 11:210–218
9. Halliwell B, Gutteridge JMC (1990) Role of free radicals and catalytic metal ions in human disease: an overview. Meth Enzymol 186:1–85
10. Diplock AT, Charleux JL, Crozier-Willi G, Kok FJ, Rice-Evans C, Roberfroid M, Stahl W, Vina-Ribes J (1998) Functional food science and defence against reactive oxidative species. Brit J Nut 80:77–112
11. Aruoma OI (1994) Nutrition and health aspects of free radicals and antioxidants. Food Chem Toxicol 62:671–683
12. Alho H, Leinonen J (1999) Total antioxidant activity measured by chemiluminescence methods. Method Enzymol 299:3–15
13. Duh PD (1998) Antioxidant activity of burdock (*Arctium lappa* Linne): its scavenging effect on free radical and active oxygen. J Am Oil Chem Soc 75:455–465
14. Hertog MGL, Feskens EJM, Hollman PCH, Katan MB, Kromhout D (1993) Dietary antioxidant flavonoids and risk of coronary heart disease: the Zupthen Elderly study. Lancet 342:1007–1014
15. Tanizawa H, Ohkawa Y, Takino Y, Ueno A, Kageyama T, Hara S (1992) Studies on natural antioxidants in citrus species. I. Determination of antioxidant activities of citrus fruits. Chem Pharm Bull 40:1940–1942
16. Halliwell B (1996) Oxidative stress, nutrition and health. Free Radic Res 25:57–74
17. Fridovich I (1986) Superoxide dismutases. Adv Enzymol 58:61–97
18. Barclay LRC, Vinqvist MR, Mukai K, Itoh S, Morimoto H (1993) Chainbreaking phenolic antioxidants: steric and electronic effects in polyalkylchromanols, tocopherol analogs, hydroquinons, and superior antioxidants of polyalkylbenzochromanol and naphthofuran class. J Org Chem 58:7416–7420
19. Tomiyama S, Sakai S, Nishiyama T, Yamada F (1993) Factors influencing the antioxidant activities of phenols by an ab initio study. Bull Chem Soc Jpn 66:299–304
20. Bors W, Heller W, Michel C, Saran M (1990) Flavonoids as antioxidants: determination of

radical-scavenging efficiencies. Meth Enzymol 186:343–355
21. Gülçin İ, Beydemir S (2013) Phenolic compounds as antioxidants: carbonic anhydrase isoenzymes inhibitors. Mini Rev Med Chem 13:408–430
22. Litwinienko G, Ingold KU (2003) Abnormal solvent effects on hydrogen atom abstractions. 1. The reactions of phenols with 2,2-diphenyl-L-picrylhydrazyl (DPPH) in alcohols. J Org Chem 68:3433–3438
23. Litwinienko G, Ingold KU (2004) Abnormal solvent effects on hydrogen atom abstraction. 2. Resolution of the curcumin antioxidant controversy. The role of sequential proton loss electron transfer. J Org Chem 69:5888–5896
24. Foti MC, Daquino C, Geraci C (2004) Electron-transfer reaction of cinnamic acids and their methyl esters with the DPPH· radical in alcoholic solutions. J Org Chem 69: 2309–2314
25. Abraham MH, Grellier PL, Prior DV, Morris JJ, Taylor PJ (1990) Hydrogen bonding. Part 10. A scale of solute hydrogen-bond basicity using log K values for complexation in tetrachloromethane. J Chem Soc Perkin Trans 2:521–529
26. Huang D, Ou B, Prior RL (2005) The chemistry behind antioxidant capacity assays. J Agric Food Chem 53:1841–1856
27. Wright JS, Johnson ER, DiLabio GA (2001) Predicting the activity of phenolic antioxidants: theoretical method, analysis of substituent effects, and application to major families of antioxidants. J Am Chem Soc 123:1173–1183
28. Lemanska K, Szymusiak H, Tyrakowska B, Zielinski R, Soffer AEMF, Rietjens IMCM (2001) The influence of pH on the antioxidant properties and the mechanisms of antioxidant action of hydroxyflavones. Free Radic Biol Med 31:869–881
29. Ou B, Hampsch-Woodill M, Prior RL (2001) Development and validation of an improved oxygen radical absorbance capacity assay using fluorescein as the fluorescent probe. J Agric Food Chem 49:4619–4626
30. Sartor V, Henderson PT, Schuster GB (1999) Radical cation transport and reaction in RNA/DNA hybrid duplexes: effect of global structure on reactivity. J Am Chem Soc 121: 11027–11033
31. Ou B, Prior RL, Huang D (2005) The chemistry behind dietary antioxidant capacity assays. J Agric Food Chem 53:1841–1856
32. Prior RL, Wu XL, Schaich K (2005) Standardized methods for the determination of antioxidant capacity and phenolics in foods and dietary supplements. J Agric Food Chem 53: 4290–4302
33. Prior RL, Cao G (1999) In vivo total antioxidant capacity: comparison of different analytical methods. Free Radic Biol Med 27: 1173–1181
34. Roginsky V, Lissi EA (2005) Review of methods to determine chain-breaking antioxidant activity in food. Food Chem 92:235–254
35. Köksal E, Gülçin İ (2008) Antioxidant activity of cauliflower (*Brassica oleracea* L.). Turk J Agric For 32:65–78
36. Bursal E, Gülçin İ (2011) Polyphenol contents and in vitro antioxidant activities of lyophilized aqueous extract of kiwifruit (*Actinidia deliciosa*). Food Res Int 44:1482–1489
37. Gülçin İ (2009) Antioxidant activity of L-adrenaline: an activity-structure insight. Chem Biolog Interact 179:71–80
38. Gülçin İ, Huyut Z, Elmastaş M, Aboul-Enein HY (2010) Radical scavenging and antioxidant activity of tannic acid. Arab J Chem 3:43–53
39. Chung YC, Chang CT, Chao WW, Lin CF, Chou ST (2002) Antioxidative activity and safety of the 50 % ethanolic extract from red bean fermented by *Bacillus subtilis* IMR-NK1. J Agri Food Chem 50:2454–2458
40. Gülçin İ, Oktay M, Küfrevioğlu Öİ, Aslan A (2002) Determinations of antioxidant activity of lichen *Cetraria islandica* (L) Ach. J Ethnopharmacol 79:325–329
41. Gülçin İ (2006) Antioxidant activity of caffeic acid (3,4-dihydroxycinnamic acid). Toxicology 217:213–220
42. Göçer H, Gülçin İ (2011) Caffeic acid phenethyl ester (CAPE): Correlation of structure and antioxidant properties. Int J Food Sci Nut 62:821–825
43. Gülçin İ, Elias R, Gepdiremen A, Chea A, Topal F (2010) Antioxidant activity of bisbenzylisoquinoline alkaloids from *Stephania rotunda*: Cepharanthine and fangchinoline. J Enzyme Inhib Med Chem 25:44–53
44. Gülçin İ, Elmastaş M, Aboul-Enein HY (2012) Antioxidant activity of clove oil – a powerful antioxidant source. Arab J Chem 5:489–499
45. Ak T, Gülçin İ (2008) Antioxidant and radical scavenging properties of curcumin. Chem Biol Interact 174:27–37
46. Gülçin İ (2011) Antioxidant activity of eugenol-a structure and activity relationship study. J Med Food 14:975–985
47. Gülçin İ, Mshvildadze V, Gepdiremen A, Elias R (2006) Antioxidant activity of a triterpenoid

glycoside isolated from the berries of *Hedera colchica*: 3-O-(β-D-glucopyranosyl)-hederagenin. Phytother Res 20:130–134

48. Gülçin İ, Mshvildadze V, Gepdiremen A, Elias R (2004) Antioxidant activity of saponins isolated from ivy: α-Hederin, hederasaponin-C, hederacolchiside-E and hederacolchiside F. Planta Med 70:561–563
49. Gülçin İ, Gagua N, Beydemir S, Bayram R, Bakuridze A, Gepdiremen A (2012) Apoptotic, antioxidant and antiradical effects of majdine and isomajdine from *Vinca herbacea* Waldst. and kit. J Enzyme Inhib Med Chem 27:587–594
50. Gülçin İ (2009) Antioxidant activity of L-adrenaline: an activity-structure insight. Chem Biol Interact 179:71–80
51. Gülçin İ (2007) Comparison of in vitro antioxidant and antiradical activities of L-tyrosine and L-Dopa. Amino Acids 32:431–438
52. Gülçin İ, Büyükokuroğlu ME, Oktay M, Küfrevioğlu Öİ (2002) On the in vitro antioxidant properties of melatonin. J Pineal Res 33: 167–171
53. Gülçin İ, Mshvildadze V, Gepdiremen A, Elias R (2006) Screening of antioxidant and antiradical activity of monodesmosides and crude extract from *Leontice smirnowii* Tuber. Phytomedicine 13:343–351
54. Gülçin İ, Beydemir Ş, Alici HA, Elmastaş M, Büyükokuroğlu ME (2004) In vitro antioxidant properties of morphine. Pharmacol Res 49:59–66
55. Gülçin İ, Elias R, Gepdiremen A, Boyer L (2006) Antioxidant activity of lignans from fringe tree (*Chionanthus virginicus* L.). Eur Food Res Technol 223:759–767
56. Gülçin İ, Alici HA, Cesur M (2005) Determination of in vitro antioxidant and radical scavenging activities of propofol. Chem Pharm Bull 53:281–285
57. Gülçin İ, Bursal E, Şehitoğlu HM, Bilsel M, Gören AC (2010) Polyphenol contents and antioxidant activity of lyophilized aqueous extract of propolis from Erzurum, Turkey. Food Chem Toxicol 48:2227–2238
58. Öztürk Sarikaya SB, Gülçin İ (2013) Radical scavenging and antioxidant capacity of serotonin. Curr Bioact Comp 9:143–152
59. Köksal E, Gülçin İ, Öztürk Sarıkaya SB, Bursal E (2009) In vitro antioxidant activity of silymarin. J Enzyme Inhib Med Chem 24:395–405
60. Gülçin İ, Oktay M, Köksal E, Şerbetçi H, Beydemir Ş, Küfrevioglu ÖI (2008) Antioxidant and radical scavenging activities of uric acid. Asian J Chem 20:2079–2090
61. Gülçin İ, Oktay M, Kireçci E, Küfrevioğlu Öİ (2003) Screening of antioxidant and antimicrobial activities of anise (*Pimpinella anisum* L.) seed extracts. Food Chem 83:371–382
62. Gülçin İ, Elmastas M, Aboul-Enein HY (2007) Determination of antioxidant and radical scavenging activity of basil (*Ocimum basilicum*) assayed by different methodologies. Phytother Res 21:354–361
63. Elmastas M, Gülçin İ, Işıldak Ö, Küfrevioğlu Öİ, İbaoğlu K, Aboul-Enein HY (2006) Antioxidant capacity of bay (*Laurus nobilis* L.) leaves extracts. J Iran Chem Soc 3:258–266
64. Gülçin İ (2005) The antioxidant and radical scavenging activities of black pepper (Piper nigrum) seeds. Int J Food Sci Nut 56:491–499
65. Gülçin İ, Şat İG, Beydemir Ş, Küfrevioğlu Öİ (2004) Evaluation of the in vitro antioxidant properties of extracts of broccoli (*Brassica oleracea* L.). Ital J Food Sci 16:17–30
66. Bursal E, Köksal E, Gülçin İ, Bilsel G, Gören AC (2013) Antioxidant activity and polyphenol content of cherry stem (*Cerasus avium* L.) determined by LC-MS/MS. Food Res Int 51: 66–74
67. Gülçin İ, Şat İG, Beydemir Ş, Elmastaş M, Küfrevioğlu Öİ (2004) Comparison of antioxidant activity of clove (*Eugenia caryophylata* Thunb) buds and lavender (*Lavandula stoechas* L.). Food Chem 87:393–400
68. Gülçin İ, Beydemir Ş, Şat İG, Küfrevioğlu Öİ (2005) Evaluation of antioxidant activity of cornelian cherry (*Cornus mas* L.). Acta Aliment Hung 34:193–202
69. Gülçin İ, Kirecci E, Akkemik E, Topal F, Hisar O (2010) Antioxidant and antimicrobial activities of an aquatic plant: Duckweed (*Lemna minor* L.). Turk J Biol 34:175–188
70. Oktay M, Gülçin İ, Küfrevioğlu Öİ (2003) Determination of in vitro antioxidant activity of fennel (*Foeniculum vulgare*) seed extracts. Lebens Wiss Technol 36:263–271
71. Oktay M, Yıldırım A, Bilaloğlu V, Gülçin İ (2007) Antioxidant activity of different parts of ısgın (*Rheum ribes* L.). Asian J Chem 19:3047–3055
72. Bursal E, Gülçin İ (2011) Polyphenol contents and in vitro antioxidant activities of lyophilized aqueous extract of kiwifruit (*Actinidia deliciosa*). Food Res Int 44:1482–1489
73. Köksal E, Bursal E, Dikici E, Tozoğlu F, Gülçin İ (2011) Antioxidant activity of *Melissa officinalis* leaves. J Med Plant Res 5:217–222
74. Şerbetçi Tohma H, Gülçin İ (2010) Antioxidant and radical scavenging activity of aerial parts

and roots of Turkish liquorice (*Glycyrrhiza glabra* L.). Int J Food Propert 13:657–671

75. Gülçin İ, Topal F, Oztürk Sarikaya SB, Bursal E, Gören AC, Bilsel M (2011) Polyphenol contents and antioxidant properties of medlar (*Mespilus germanica* L.). Rec Nat Prod 5: 158–175
76. Gülçin İ, Tel AZ, Kirecci E (2008) Antioxidant, antimicrobial, antifungal and antiradical activities of *Cyclotrichium niveum* (Boiss.) Manden and Scheng. Int J Food Propert 11:450–471
77. Gülçin İ, Küfrevioğlu Öİ, Oktay M, Büyükokuroğlu ME (2004) Antioxidant, antimicrobial, antiulcer and analgesic activities of nettle (*Urtica dioica* L.). J Ethnopharmacol 90:205–215
78. Gülçin İ, Topal F, Çakmakçı R, Gören AC, Bilsel M, Erdoğan U (2011) Pomological features, nutritional quality, polyphenol content analysis and antioxidant properties of domesticated and three wild ecotype forms of raspberries (*Rubus idaeus* L.). J Food Sci 76:C585–C593
79. Büyükokuroğlu ME, Gülçin İ (2009) In vitro antioxidant and antiradical properties of *Hippophae rhamnoides* L. Pharmacogn Mag 4:189–195

Chapter 18

Antioxidant Activity Evaluation Involving Hemoglobin-Related Free Radical Reactivity

Augustin C. Mot, Cristina Bischin, Grigore Damian, and Radu Silaghi-Dumitrescu

Abstract

Two methods for the measurement of antioxidant capacity are described: one based on a chronometric variation of a hemoglobin ascorbate peroxidase assay and the other based on electron paramagnetic resonance (EPR) spectra collected upon alkaline treatment of ethanolic samples. The involved chemical mechanisms are discussed, alongside the most important benefits and shortcomings; the assays offer new qualitative and quantitative information on samples of biological as well as synthetic origin.

Key words Antioxidant activity assays, Hemoglobin ascorbate peroxidase assay, Electron paramagnetic resonance, Antioxidants, Natural extract, Polyphenolic compounds

1 Introduction

The variety of in vitro and in vivo methods developed to determine the antioxidant capacity of synthetic and natural products still leaves room for discussion concerning optimal biological/medical relevance—thus fostering the development of additional methods that may be more physiologically relevant [1–6].

Although most such methods relate to free radicals, it is known that the mechanism of action of antioxidants entails a variety of redox signaling pathways, beyond simple radical quenching [2, 6, 7]. Furthermore, there is evidence that in some cases, compounds that are known for their antioxidant capacity may behave as prooxidants, depending on concentration (dosage), enzymatic and chemical interaction [8, 9].

Herein two types of methods are proposed as an alternative standard test for evaluating the antioxidant capacity of the pure compounds or extracts, one based on hemoglobin ascorbate

Donald Armstrong (ed.), *Advanced Protocols in Oxidative Stress III*, Methods in Molecular Biology, vol. 1208,
DOI 10.1007/978-1-4939-1441-8_18,

peroxidase activity and the other based on electron paramagnetic resonance (EPR) spectra collected upon alkali treatment of ethanolic natural extracts.

1.1 Hemoglobin Ascorbate Peroxidase Activity (HAPX)

The peroxidase activity of hemoglobin was well studied in vivo due to its physiological and medical relevance. For instance, the products of this reaction are seen increase in athletes following physical effort; the hemoglobin + peroxide reaction has also been shown to be involved in some pathological conditions (subarrachnoid hemorrhage and rabdomyolysis). The mechanism of this reaction involve the formation of high-valent form of hemoglobin (ferryl) upon interaction of hemoglobin (regardless of starting oxidation state) and peroxide, followed by reduction of this ferryl and free radical formation within antioxidant species; the latter will be expected to be detected directly by EPR spectroscopy [10–16].

A simple kinetic model presuming that ascorbate was an active reductant maintaining the oxidative stability of hemoglobin has previously been described in detail [11]. Further, based on this reaction, a hemoglobin/ascorbate peroxidase activity inhibition assay was proposed by Mot et al. [17] to evaluate the antioxidant capacity of natural extracts (exemplified by propolis). Indeed, the propolis extract was shown to inhibit the ascorbate peroxidase activity of hemoglobin, and a direct correlation with the antioxidant capacity evaluated by the DPPH method was observed. Perfect correlation was not expected, as the DPPH quantifies those components able to react with a free radical directly, whereas the HAPX method accounts for a broader range of antioxidants primarily on redox potential.

Based on the ascorbate peroxidase activity of hemoglobin, two protocols are described here for evaluation of the antioxidant capacity of pure antioxidants or of natural extracts—first, monitoring the oxidation of ascorbate, and second, following the inhibition of ferryl formation (a chronometric procedure).

1.2 Electron Paramagnetic Resonance Spectroscopy Assay

Direct detection of free radical generated in natural extracts using the method described previously [17] is difficult to achieve as any free radical is likely to be effectively quenched by the remaining antioxidants within the solution. Production of semiquinone anion radicals during the autoxidation of polyphenolic compounds by treatment with alkali in the presence of molecular oxygen is known to often produce stable radicals, similar in nature to those generated by the antioxidants when scavenging the reactive oxygen species [18–22]. The semiquinone anion radical is further oxidized to quinone by the action of either molecular oxygen or superoxide [22]. An autocatalytic process due to comproportionation of quinone with the reduced form may produce secondary radicals by the interaction with hydroxide or other reactive species [20, 21]. Thus, treatment of natural polyphenolic-rich extracts with alkali in

presence of molecular oxygen will generate easily detectable radicals. The higher the pH, the higher the amount of radicals—and the more stable they are; a connection between the amount of the radical (EPR detected) and its antioxidant capacity was previously observed [17]. Even small traces of oxygen are enough to generate such radicals. Their EPR signatures, yields, and time dependences offer unique fingerprinting possibilities. Compared to the previously reported method based on freezing samples in liquid nitrogen [17], which only allows the evaluation of the amount of de semiquinone anion radicals at a given time point (calculating only the double integrated values of the EPR spectra), a room-temperature variation is described here, which can thus carry additional information compared to other classical parameters.

2 Materials

2.1 Equipment

2.1.1 Ascorbate Peroxidase Activity of Hemoglobin (HAPX)

1. 1 ml quartz cuvette, Hellma GmbH (Müllheim, Germany, model 108-000-10-40).
2. Cary50 UV–Vis spectrophotometer (Varian, Middleburg, The Netherlands).

2.1.2 Electron Paramagnetic Resonance Spectroscopy Assay

1. Capillary glass or quartz EPR tubes from Rainer Medizintechnik (Frensdorf, Germany).
2. Bruker EMX EPR spectrometer with continuous wave at X-band (~9 GHz), or others of comparable or better standards. The spectra will be recorded at room temperature with the following parameters: microwave power 2 mW, modulation frequency 100 kHz, modulation amplitude 0.5G, receiver gain 10^4, center field 3365G, and sweep field 70G.
3. Sephadex G-25F.

2.2 Reagents and Chemicals

2.2.1 Ascorbate Peroxidase Activity of Hemoglobin (HAPX)

1. Bovine hemoglobin may be purified according to the Antonini and Brunori [23] protocol (the pure form could be preserved in PBS buffer) or purchased from, for example, Sigma-Aldrich (Munich, Germany) (code H2500).
2. A stock solution of ferricyanide [$K_3Fe(CN)_6$]. Ferricyanide was purchased from, for example, Sigma-Aldrich (Munich, Germany, code P4066).
3. A stock solution of hemoglobin, 1 mM (in PBS buffer, pH 7.4).
4. A stock solution of hydrogen peroxide with a concentration of 60 mM (in water). Hydrogen peroxide 30 % was purchased from, for example, Merck KGaA (Darmstadt, Germany, code 107209).
5. A stock solution of 50 mM ascorbate (in water). Sodium L-ascorbate was obtained from, for example, Sigma-Aldrich (Munich, Germany, code 268550).

6. Buffer solution of 50 mM sodium acetate (pH 5.5). Sodium acetate was purchased from, for example, Merck KGaA (Darmstadt, Germany, code 106264).
7. Ethanol 96 % from, for example, Merck KGaA (Darmstadt, Germany, code 100967).

2.2.2 Electron Paramagnetic Resonance Spectroscopy Assay

1. A solution of the tested pure compounds (quercetin, kaempherol, rutin) with a concentration of 1 mM in 90 % ethanol. Quercetin (Q0125), kaempferol (K0133), and rutin (R2303) were purchased from Sigma-Aldrich (Munich, Germany).
2. A suitable concentration of tested extract should be diluted with 35 % aqueous ethanol solution, at optimal pH (11.7) and ethanol concentration (35 %).
3. A stock solution of 500 mM NaOH, yielding a pH of 11.7. NaOH was purchased from, for example, Merk KGaA (Darmstadt, Germany, code CH00304).

3 Methods

3.1 Ascorbate Peroxidase Activity of Hemoglobin (HAPX)

The HAPX assay was run according to two procedures, first (HAPX1, kinetic procedure) as described in [17] and second (HAPX2, chronometric procedure) as detailed bellow, after several preliminary experiments.

3.1.1 Monitoring the Oxidation of Ascorbate (HAPX1)

1. Ferric hemoglobin should be obtained from oxy Hb by oxidation in a $[K_3Fe(CN)_6]$: Hb ratio of 1.5:1, in order to remove excess ferricyanide they should be passed over filtration columns containing Sephadex G-25F, equilibrated with PBS at pH 7.4.
2. A solution of the tested pure compound, or natural extracts at a suitable concentration, in water or in ethanol–water mixtures (this may depend on the solubility of the sample, or on the extraction protocols applied on the biological material; in principle any water-miscible co-solvent may be used).
   The next processes should be monitored spectrophotometrically at 290 nm (*see* **Note 1**).
3. From the stock solution described on Subheading 2.1 350 μM of ascorbic acid is added to 50 mM sodium acetate buffer, pH 5.5, in a quartz cuvette, followed by the addition of 800 μM of hydrogen peroxide (*see* **Notes 2**).
4. After 20 s, 14 μM met-hemoglobin from the stock solution should be added to the reaction mixture. The kinetic profile for ascorbic acid after the addition of met-hemoglobin is linear for at least 70 s.

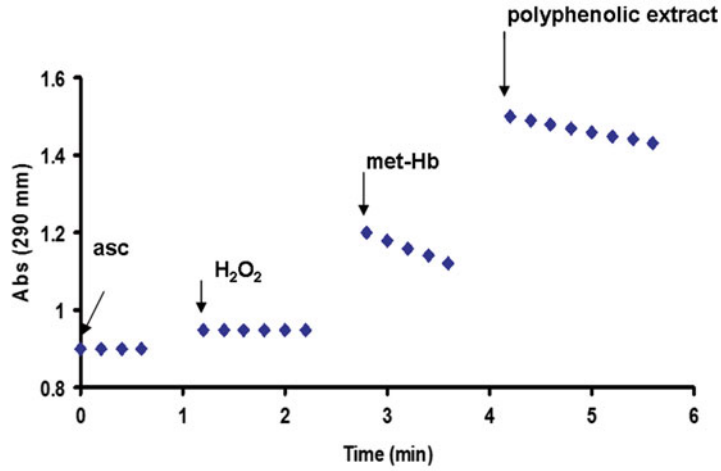

Fig. 1 Time evolution of the absorbance at 290 nm for ascorbic acid consumption in reaction with peroxide, catalyzed by hemoglobin; times of reagent addition are indicated by *arrows*

5. At 12–15 s after addition of met-hemoglobin, 5 μL of an antioxidant is added to the reaction mixture, and the 290 nm absorbance further monitored (Fig. 1). A measurable significant inhibition of the ascorbic acid consumption should be observed.

3.1.2 Inhibition of Hemoglobin Ascorbate Peroxidase Activity Assay (HAPX2, Chronometric Procedure)

1. In a quartz cuvette 979 μL of 50 mM sodium acetate pH 5.5 is added, followed by 4 μL 50 mM ascorbic acid (200 μM) (*see* **Note 2**), 4 μL 120 mM hydrogen peroxide (480 μM), and 5 μL sample (antioxidant, or natural extract)—after which the absorbance changes are monitored between 300 and 700 nm for 60 s.
2. The reaction is triggered by the addition of 8 μL 1.6 mM met hemoglobin (metHb) (12.8 μM) and further monitored for 20 min. Control experiments (no extract/antioxidant added) should also performed. The reaction should then further be monitored at both 545 nm (Fig. 2) and Soret band (405 nm) (Fig. 3) (*see* **Note 3**) until sudden changes at these wavelengths are noted; the time interval required for the lag phase is registered (T_r) (*see* **Notes 4** and **5**).

3.1.3 Electron Paramagnetic Resonance Spectroscopy (EPR) Assay

1. In a 1.5 mL Eppendorf tube 495 μL of sample should be added, followed by the rapid addition of 5 μL of 500 mM NaOH (yielding a pH of 11.7) (*see* **Note 7**).
2. Using a long needle syringe, a few tens of μL are quickly transferred to a glass capillary EPR tube so that the final volume in the capillary is 100 μL in each case (tubes should previously be marked on the outside to this end).

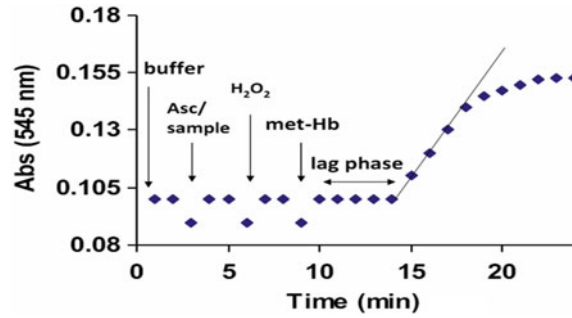

Fig. 2 Time evolution of the absorbance at 545 nm for Hb in reaction with peroxide and ascorbate with/without pure antioxidant or extract; the times of reagent addition are indicated by arrows. After met-Hb addition there is a lag phase followed by a sudden increase in the absorbance whose rate is related with the antioxidant capacity

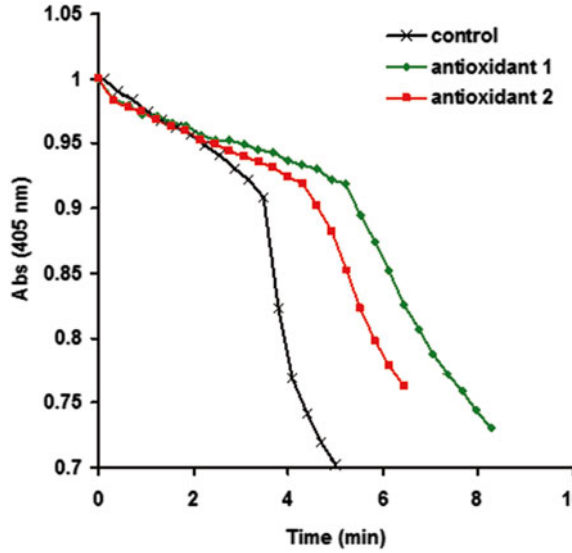

Fig. 3 Time evolution of the absorbance at 405 nm for Hb in reaction with peroxide and ascorbate for two antioxidants compared with control sample

3. The capillary is placed in the cavity of a Bruker EMX EPR spectrometer. The EPR spectra are recorded continuously every 2 or 5 min until the signal is either vanishingly small or stable (*see* **Note 6**).

In our experiments, working with a wide range of natural extracts and synthetic compounds, in order to establish the optimal conditions (NaOH concentration (pH), ethanol content and concentration of extract) the final volume (500 μL) and sodium hydroxide solution volume (5 μL) were maintained constant, but the solvent, extract and stock solution concentrations were varied. The tested pH values were 11, 11.7, 12.7, 13, 14 and the ethanol concentrations were 5, 20, 30, 50, 60, 80 % (v/v); the tested

extract concentrations were 20, 25, 35, 40, 50 % (v/v), diluted with 35 % aqueous ethanol solution (at optimal pH (11.7) and ethanol concentration (35 %) (*see* **Note 7**). The concentration of the tested pure compounds (e.g., quercetin, kaempferol, rutin) should be 1 mM in 90 % ethanol. The variation of the steady state relative concentration of free radicals species generated at different time intervals could be obtained through double integration of the experimental spectra (*see* **Note 8**).

4 Notes

1. This method has some shortcomings. Thus, when monitoring the absorbance in UV at 290 nm the degree of interference is very high and some of the oxidized compounds during the peroxidase cycle may absorb at this wavelength.
2. Due to its great affinity for hemoglobin, ascorbic acid is very important to be added in both control and samples; it may act as a mediator between antioxidant molecules which have low affinity for hemoglobin.
3. To avoid the interference at 290 nm of ascorbate oxidation with other oxidized compounds found in the extract, the reaction is better monitored at two specific wavelengths for the maximum absorption of met-Hb, at 405 or 575 nm. Here the interference is much less likely than at 290 nm. Moreover, since met-Hb absorbs as far as 630 nm in the visible region, the wavelength may be adapted widely depending on the region with which the antioxidant may interfere, if strongly colored.
4. Mixings met-hemoglobin (Hb-Fe(III)) with hydrogen peroxide in the presence of ascorbic acid leads to the formation of hemoglobin oxidized species (Hb(Fe(IV)), followed by quick reduction back to Fe(III) due to ascorbate; thus, depending of how long ascorbic acid (and tested antioxidants) is present in the mixture, hemoglobin will be present in a steady state as met form (relatively stable absorbance at 405 nm). When the ascorbic acid and other antioxidants are completed oxidized, met is rapidly transformed into ferryl (Hb(Fe(IV)) by the remaining hydrogen peroxide, producing a sudden change in UV–Vis spectra (Fig. 3). The higher the antioxidant level, the longer the time hemoglobin exists as met form.
5. A calibration curve may be used and the results can be standardized for further comparations.
6. The EPR spectra obtained under these condition are not only easily detectable within the time frame of the experiments, but also feature very clear hyperfine structure, which allows differentiation/fingerprinting between samples/chemicals (Fig. 4).
7. The extracts may be first optimized to obtain an ethanol concentration and hydroxide level to achieve a highest amount of

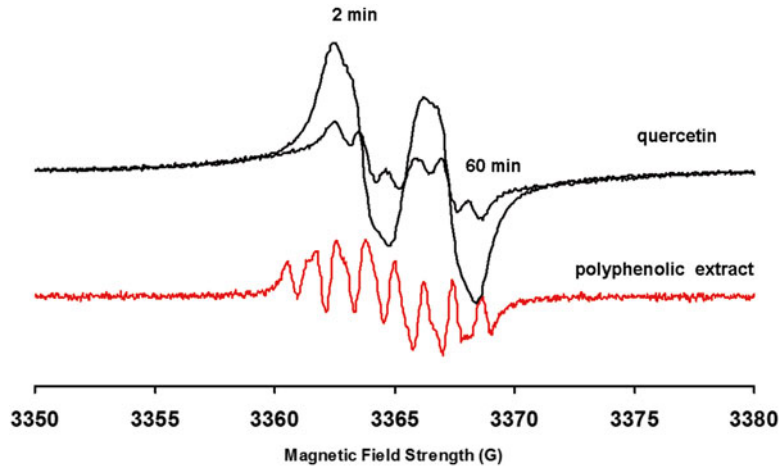

Fig. 4 EPR spectra of quercetin and a polyphenolic extract after treatment with sodium hydroxide in aerobic solution

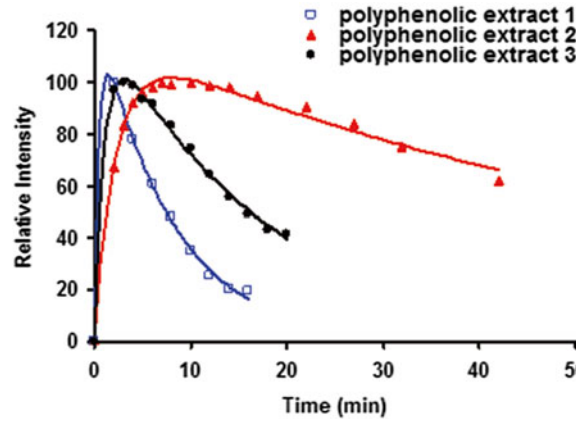

Fig. 5 Kinetic curves describing the formation and decay of radicals generated in the studied extracts after treatment with sodium hydroxide in aerobic ethanolic solution. The experimental data are fitted with the function $I(t) = A_1 * \exp(t * k_1) - A_2 * \exp(t * k_2)$, which describes the simultaneous radical formation and exponential decay

radical. Values between 35 and 45 % ethanol and pH 11.7–13.2 are usually suitable conditions for high amount of radical, with no precipitate after addition of alkali.

8. The great advantage of this method would be the kinetic approach (Fig. 5) rather than the amount of radical at a given time. The kinetic curves of the radical formation and decay for the studied extracts were detected and fitted with a function to obtain the characteristics constants (k1-radicals decay and k2-radicals growth). Correlations between these constants and the other antioxidant capacity parameters may be found, depending on the sample.

References

1. Niki E (2010) Assessment of antioxidant capacity in vitro and in vivo. Free Radical Bio Med 49:503–515
2. Jones DP (2006) Redefining oxidative stress. Antioxid Redox Signal 8:1865–1879
3. Huang D, Ou B, Prior RL (2005) The chemistry behind antioxidant capacity assays. J Agric Food Chem 53:1841–1856
4. Prior RL, Wu X, Schaich K (2005) Standardized methods for the determination of antioxidant capacity and phenolics in foods and dietary supplements. J Agric Food Chem 53:4290–4302
5. Frankel EN, Finley JW (2008) How to standardize the multiplicity of methods to evaluate natural antioxidants. J Agric Food Chem 56: 4901–4908
6. López-Alarcón C, Denicola A (2013) Evaluating the antioxidant capacity of natural products: a review on chemical and cellular-based assays. Anal Chim Acta 763:1–10
7. Carocho M, Ferreira ICFR (2013) A review on antioxidants, prooxidants and related controversy: natural and synthetic compounds, screening and analysis methodologies and future perspectives. Food Chem Toxicol 51:15–25
8. Procházková D, Boušová I, Wilhelmová N (2011) Antioxidant and prooxidant properties of flavonoids. Fitoterapia 82:513–523
9. Mot AC, Coman C, Miron C et al (2014) An assay for pro-oxidant reactivity based on phenoxyl radicals generated by laccase. Food Chem 143:214–222
10. Dunne J, Svistunenko DA, Alayash AI et al (1999) Reactions of cross-linked methaemoglobins with hydrogen peroxide. Adv Exp Med Biol 471:9–15
11. Cooper CE, Silaghi-Dumitrescu R, Rukengwa M et al (2008) Peroxidase activity of hemoglobin towards ascorbate and urate: a synergistic protective strategy against toxicity of hemoglobin-based oxygen carriers (HBOC). Biochim Biophys Acta 1784:1415–1420
12. Reeder BJ, Svistunenko DA, Cooper CE, Wilson MT (2004) The radical and redox chemistry of myoglobin and hemoglobin: from in vitro studies to human phatology. Antiox Redox Signal 6:954–966
13. Reeder BJ, Grey M, Silaghi-Dumitrescu RL et al (2008) Tyrosine residues as redox cofactors in human hemoglobin: implications for engineering nontoxic blood substitutes. J Biol Chem 283:30780–30787
14. Silaghi-Dumitrescu R, Reeder BJ, Nicholls P, Cooper CE, Wilson MT (2007) Ferryl haem protonation gates peroxidasic reactivity in globins. Biochem J 403:391–395
15. Vollard NB, Reeder BJ, Shearman JP et al (2005) A new sensitive assay reveals that hemoglobin is oxidatively modified in vivo. Free Radical Bio Med 39:1216–1228
16. Vollaard NB, Sherman JP, Cooper CE (2005) Exercise-induced oxidative stress: myths, realities and physiological relevance. Sports Med 35:1045–1062
17. Mot AC, Damian G, Sarbu C, Silaghi-Dumitrescu R (2009) Redox reactivity in propolis: direct detection of free radicals in basic medium and interaction with hemoglobin. Redox Rep 6:267–274
18. Venkataraman B, Fraenkel GK (1955) Proton hyperfine interactions in paramagnetic resonance of semiquinones. J Am Chem Soc 77:2707–2713
19. Ashworth P, Dixon WT (1972) Secondary radicals in the autoxidation of hydroquinones and quinones. J Chem Soc Perkin Trans 2: 1130–1133
20. Pedersen JA (1973) Electron spin resonance studies of oxidative processes of quinones and hydroquinones in alkaline solution; formation of primary and secondary semiquinone radicals. J Chem Soc Perkin Trans 2:424–431
21. Roginsky V, Barsukova T (2000) Kinetics of oxidation of hydroquinones by molecular oxygen. Effect of superoxide dismutase. J Chem Soc Perkin Trans 2:1575–1582
22. Eslami AC, Pasanphan W, Wagner BA, Buettner GR (2010) Free radicals produced by the oxidation of gallic acid: an electron paramagnetic resonance study. Chem Central J 4:15–19
23. Antonini E, Brunori M (1971) Hemoglobin and myoglobin in their reaction with ligands. North-Holland, Amsterdam

Chapter 19

Computational Studies on Conformation, Electron Density Distributions, and Antioxidant Properties of Anthocyanidins

Ricardo A. Mosquera, Laura Estévez, and Mercedes García Bugarín

Abstract

Computational studies carried out at density functional theory levels are able to provide reliable chemical information about medium sized compounds as anthocyanins and their aglycons (anthocyanidins). Thus, they indicate that the most stable tautomers in aqueous solution for the main anthocyanidins (excluding pelargonidin) are deprotonated at C4′ in the neutral forms, while deprotonations at C5 and C4′ characterize the most stable anions in solution. QTAIM electron density analysis (overviewed in brief in the methods section) shows that Lewis structures usually employed give rise to unreliable atomic charges. Thus: (1) The positive charge spreads throughout the whole cation, and is not localized on any specific atom or set of atoms; (2) Neutral forms can be described as enolates where the negative charge is counterbalanced in a different way to that indicated by the typical resonance forms; and (3) The negative charge of anions is mainly spread among three regions of the molecule: the two deprotonated sites and the C9-O1-C2 area. The analysis of a group of complexes formed by a model of cyanin with four common metalic cations (Mg(II), Al(II), Cu(II), Zn(II)), shows: (1) the preference for tetracoordination in Zn(II) and Cu(II) complexes, (2) higher affinity for Cu(II) than for the other metals here studied, and (3) the distortion of electron density in the cyanin ligand affects the whole molecule. This distortion can be described as a continuous polarization where, even, in some cases, the atomic electron populations of those atoms of the ligand that are more directly involved in bonding to the metal increase.

Key words Anthocyanins, Anthocyanidins, Conformational analysis, QTAIM, Electron density analysis

1 Introduction

Anthocyanins are considered as one of the most important groups of natural polyphenolic antioxidants [1]. They occur ubiquitously in vascular plants, being responsible for a large variety of colors, from orange to violet or blue, in many flowers, fruits, and grains. Anthocyanins have become a popular class of chemical compounds in everyday life, as their increased consumption has been related persistently to lower risks of cardiovascular disease.

Donald Armstrong (ed.), *Advanced Protocols in Oxidative Stress III*, Methods in Molecular Biology, vol. 1208,
DOI 10.1007/978-1-4939-1441-8_19,

Although these relationships are mainly based on epidemiological studies and much work remains to be done before definitive conclusions can be achieved [2], they certainly encouraged the research and interest on anthocyanins. Moreover, promising reports on other beneficial properties to human health, like antioxidant [3] and antitumor activity [4], as well as their natural origin, also contributed to their inclusion into the restrictive club of health-friendly substances. Among other consequences, the consumption of red fruit juices and red wines has increased during the last few decades; anthocyanins are commonly found in popular nutraceuticals, and they were proposed as food additives and/or colorants to replace synthetic dyes [5], etc.

Anthocyanins are composed by a basic structure, called anthocyanidin, bonded to one or more sugar moieties, which are usually esterificated by carboxylic acids (aliphatic or aromatic). Although the number of different anthocyanins reported nowadays exceeds 500, there are only 23 anthocyanins. Moreover, only six of them are common in higher plants: pelargonidin (Pg), peonidin (Pn), cyanidin (Cy), malvinidin (Mv), petunidin (Pt), and delphinidin (Dp) [5]. They are differentiated by the number and position of hydroxyl and methoxyl groups on their B-ring (Fig. 1). It is known that anthocyanins are much more stable than anthocyanidins (also known as aglycons) in aqueous solution. Thus, the latter hardly exist in vivo. Nevertheless, anthocyanins bioactivity is exclusively attributed to their aglycons and not to the sugar or other binding species [6].

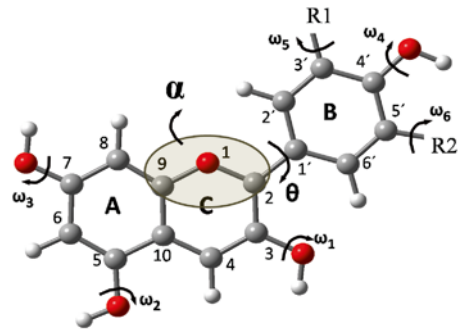

	Cy	Dp	Pg	Pn	Pt	Mv
R1	OH	OH	H	OCH_3	OCH_3	OCH_3
R2	H	OH	H	H	OH	OCH_3
NA	50%	12%	12%	12%	7%	7%

Fig. 1 IUPAC Atomic numbering, main dihedral angles (MDA), significant structural regions (A, B, and C rings and unit α = C9–O1–C2), R1 and R2 substituents, and natural abundace (NA) (taken from ref. 5) for the six most common natural anthocyanidins

In spite of their high popularity and the huge amount of interesting information collected after decades of intense research on anthocyanins, several basic aspects of their molecular structure were scarcely studied. This is also true, although more surprising because of their larger simplicity, for anthocyanidins. Some examples, we are dealing in this chapter are: (1) pH influence on the color of both anthocyanins and anthocyanidins is a well known fact, but there is not much information about which is the preferred tautomer for the neutral or anionic forms for a certain anthocyanidin [7]; (2) Cationic anthocyanidins (and all flavylium cation derivatives) are usually represented by a Lewis form leaving a positive charge on O1 (Fig. 1), which is clearly not supported (we could even say, it is discarded) by their electron density distribution [8]; (3) The immense variety of natural colors attributed to anthocyanidins arise from the small number of different anthocyanidins (six) through a phenomenon, known as co-pigmentation, where the pigments establish a molecular association with other colorless compounds (organic and/or metallic ions). Nevertheless, up to date, researchers have only determined the crystal structure for one those supramolecular associations [9] and structural studies (experimental or computational) on metal–anthocyanidin complexes are very scarce [10–12]; and (4) Most of the computational studies analyzing their antioxidant power (AP) compare O–H bond dissociation energies (BDE) and ionization potentials (IP) for a series of compounds. While AP should be enhanced by a relatively low BDE and a relative high IP [13], the radical-scavenging mechanism is affected by the protopropic equilibria involved in pH variations [14].

Our first objective was predicting how pH changes affect the conformation and tautomeric preferences of anthocyanidins. To this end, we performed density functional calculations (DFT) on diverse geometries and structures. Solvent effects were modeled in all cases with the polarizable continuum model (PCM) [15]. Once the conformational and prototropic trends were known, our next goal was related to their electronic properties. In this context we have two main objectives: (1) to describe the evolution experienced by the electron density along the prototropic equilibria; and (2) to discuss on the reliability of classical resonance structures for describing the electron density. These tasks were done by applying the Quantum Theory of Atoms in Molecules (QTAIM) developed by Bader [16, 17]. In further research, we employed models to describe several metal–anthocyanin complexes and analyze how they modify the electron density of the anthocyanidin. Finally, we also applied DFT/PCM calculations to get insight about how the radical-scavenging mechanism followed by anthocyanidins depends on pH. For the sake of brevity this issue is not reviewed here, as the computational method is described in detail in reference [14].

2 Materials

2.1 Equipment

1. We employed two computers, both of them under Linux operating system. Part of the calculations was run in the "Finisterrae" computer in the "Centro de Supercomputación Galicia" (CESGA). It has 142 nodes HP integrity rx7640 with 16 cores Itanium Montvale and 126 GB by heart each one. The rest were run in a computer owned by our group with 10 nodes HP integrity rx7640 with 16 cores Itanium Montvale and 64 GB by heart each one. Most of the calculations only require between two and four cores and 16 GB was the maximun RAM requirement. Overall, calculations described in this chapter can be run in a reasonable time on any of the workstations usually available in most of chemical research groups.

2.2 Conformational Analysis and Prototropic Equilibria

1. Programs Gaussian 03 [18] and Gaussian 09 [19] (in the revisions here cited or higher) were employed to obtain optimized geometries and molecular electronic energies (*see* **Note 1**).
2. GaussView interface program for Windows XP was employed to build initial geometries. Input and output files were transferred among computers and PCs using standard secure shell (SSH) and secure file transfer protocol (SFTP) software.

2.3 Electron Density Analysis

1. Programs Gaussian 03 [18] and Gaussian 09 [19] (in the revisions here cited or higher) were employed to obtain the electron densities associated to minimum energy geometry (*see* **Note 2**).
2. QTAIM electron density analysis were performed with the AIMPAC package originally developed in Prof. Bader's group [20], which has been slightly modified in our group to allow an easier file managing.
3. The commercial version of AIM2000 program [21] for windows XP was employed to obtain molecular diagrams.
4. Calculations with AIMPAC program were run in the same computers indicated in Subheading 2.1, while those with AIM2000 were performed in laptops and PCs.

3 Methods

3.1 Conformational Analysis of Main Cationic, Neutral, and Anionic Anthocyanidins and Prototropic Equilibria

1. Cationic anthocyanins display a different number of dihedral angles that by internal rotation around them are susceptible to connect non-equivalent minima in the potential energy surface (PES). These angles will be called main dihedral angles (MDA) in what follows. They are 4 in Pg, 5 in Cy and Pn, and 6 in Dp, Pt, and Mv and are labeled ω_1 to ω_6 in Fig. 1. As two different minima (approximately at 0 and 180°) are expected

for the independent rotation of each of these dihedral angles, cationic anthocyanidins could display 2^4 (Pg), 2^5 (Cy and Pn), and 2^6 (Dp, Pt, and Mv) different minima on the corresponding PES (*see* **Note 3**).

2. It is very convenient to establish an acronym which identifies the arrangement around each MDA (ω_1 to ω_6). For Pg, the acronym contains four letters indicating the arrangement of the four main dihedral angles in the molecule. "*s*" indicates the synperiplanar arrangement, while "*a*" refers to the antiperiplanar one [22]. Two reference atoms (one at each side of the MDA) are needed for defining "*s*" and "*a*" dispositions. To this end, we selected those with the lowest IUPAC numbering. Thus, for example, ω_1 corresponds to the C2–C3–O–H unit. Taking into account that any anthocyanidin may be in cationic, neutral, or anionic forms, a capital letter (*C*, *N*, or *A*) is inserted at the beginning of the acronym. When one of the units assigned to one MDA is deprotonated in the *N* or *A* form, the corresponding *a*/*s* letter is replaced by "-." The tautomers (each of them displaying diverse rotamers) are referred indicating if they are neutral of anionic (*N* or *A*) and the number of the C atom where the deprotonated hydroxyl/s is/are attached.
3. An initial geometry was built for all the planar conformations described above using the GaussView interface. They were subjected to full geometry optimization employing the standard B3LYP DFT functional with a usual split-valence basis set including polarization and diffuse functions (6-31++G(d,p)). While the inclusion of polarized functions in a split-valence basis set is considered a minimum requirement in order to achieve an adequate compromise between accuracy and computational cost in all species, diffuse functions are also needed to describe the long-range behavior of electron density in anions. Both molecular size and the lack of other specific problems in the structures at study do not justify the employment of higher computational levels.
4. Vibrational frequencies were computed at the same theoretical level for all the optimized structures. These calculations were performed with two objectives: (1) To characterize the geometries as minima (no imaginary frequency) or saddle points (one imaginary frequency); and (2) To estimate the zero point vibrational energies (ZPVEs) and other thermal corrections in aqueous solution [23] (*see* **Note 4**).
5. Solvent effects were considered using PCM. Complete geometry optimizations at the B3LYP/6-31++G(d,p) were carried out again with this model, using the gas phase conformers as initial geometries. PCM vibrational frequencies were not computed because of their low reliability.

Table 1
Most stable rotamers (those whose relative G_{sol} values with regard to the most stable are below 10 kJ/mol) for cation (C), neutral form (N), and anion (A) of the most common anthocyanidin in aqueous solution according to PCM B3LYP/6-31++G(d,p) optimizations. Relative values for G_{sol} (in kJ/mol) are shown in parenthesis

Pg			**Pn**		
Casaa	*N7as-s*	*A3--a*	*Casass*	*N4′asa-s*	*A54′a-s-s*
Casas (0.0)	*N5a-sa* (0.7)	*A54′a-s-* (0.2)	*Cassss* (0.2)	*N7as-ss* (0.6)	*A74′a--* (2.0)
	N3-saa (2.7)	*A74′as--* (1.7)	*Casaaa* (6.6)	*N5a-sss* (1.2)	*A3--ss* (3.3)
	N4′asa- (4.6)	*A54′s-s-* (8.7)		*N3-sass* (4.0)	*A54′a-s-a* (6.7)
				N4′asa-a (8.0)	*A74′a--* (8.6)
					A3--aa (9.8)
Cy			Dp		
Casass	*N4′asa-a*	*A54′a-s-a*	*Casaaaa*	*N4′asa-as*	*A54′a-s-as*
Casaaa (0.6)	*N7as-ss* (9.7)	*A74′--saa* (1.9)	*Casasss* (0.0)		*A74′a--s* (1.5)
		A54′s-s-a (9.0)			*A34′-sa-as* (1.8)
Pt			Mv		
Casasss	*N4′asa-ss*	*A54′a-s-ss*	*Casaasa*	*N4′asa-sa*	*A54′a-a-sa*
Casssss (0.6)	*N4′asa-as* (7.0)	*A74′a--s* (1.7)	*Casaaaa* (5.2)	*N7as-asa* (4.8)	*A74′a--a* (1.9)
Casaaaa (6.5)		*A74′a--s* (7.4)	*Casasss* (7.1)	*N5a-sasa* (5.4)	*A3--asa* (4.0)

6. The molecular Gibbs energy of the solute, G_{sol}, embedded in a continuum medium is defined as the reversible work needed to create a cavity with a suitable shape in the medium (*see* **Note 5**), and to build up the molecule in this cavity, starting from non-interacting electrons and nuclei. PCM calculates the molecular free energy considering electrostatic and non-electrostatic terms. The first one includes the electronic energy for the same molecular geometry isolated and that due to the electrostatic interactions with the solvent as modeled with PCM. The non-electrostatic terms include cavitation, dispersion, and repulsions. They depend on the cavity shape and atomic parameters that has seen diverse variations over the years.
7. Table 1 lists the most stable conformers obtained for the six main anthocyanidins in *C*, *N*, and *A* forms in aqueous solution ordered according to relative values of G_{sol} (ΔG_{sol}). According to Maxwell–Boltzmann distribution, only those rotamers with $\Delta G_{sol} < 10$ kJ/mol could be found in a nonnegligible proportion in the conformational mixture at 298 K.

8. The analysis of Table 1 indicates the following trends for anthocyanidins in aqueous solution: (1) Excluding Pg, the most stable tautomers are deprotonated at C4′ in *N* forms, while deprotonations at C4′ and C5 characterize the most stable anions; (2) Anionic and neutral forms of anthocyanidins in solution are an equilibrium between different tautomers if we exclude the *N* species of Dp and Pt, where *NC4′* tautomers are clearly preferred over the rest; and (3) Conformational variation involves more low-energy rotamers in anions than in neutral forms and cations.

3.2 QTAIM Electron Density Analysis of Main Cationic, Neutral, and Anionic Anthocyanidins and Reliability of Lewis Structures

1. QTAIM analysis usually involves the calculation of two kinds of properties: (1) point properties, which most of the times are exclusively computed at critical points (found at diverse $\mathbf{r}_c$ position vectors) of the electron density, $\rho(\mathbf{r})$, (*see* **Note 6**); and (2) integrated properties, computed for atomic basins, Ω, (*see* **Note 7**).
2. The sets of $\rho(\mathbf{r})$ critical points for the most stable rotamers indicated in Table 1, were located using the program ext94b of package AIMPAC. Among the properties computed at each BCP (*see* **Note 6**), we highlight its electron density, $\rho(\mathbf{r}_c)$, and the total energy density, $H(\mathbf{r}_c)$. The former plays a fundamental role describing the interatomic interaction. Higher values of $\rho(\mathbf{r}_c)$ indicate stronger bonds for the same pair of elements. Negative $H(\mathbf{r}_c)$ values are associated to covalent bonds or shared electron pair interactions, while positive ones are associated to ionic bonds or interactions between closed electronic shells.
3. Atomic basins are disjoint objects, whose union recovers totally the space region where the molecular electron density does not vanish. Two atomic basins are separated by interatomic surfaces (IAS), which display zero flux for the vector field of $\nabla\rho(\mathbf{r})$ (this is called the zero flux condition). The boundaries of an atom in a molecule are the IAS shared with their bonded atoms and a vanishing limit for $\rho(\mathbf{r})$ (*see* **Note 8**).
4. The electron atomic population, $N(\Omega)$, is the integrated property with the largest interest for our purposes. It allows the calculation of atomic charges, $q(\Omega)$, using Eq. 1, where $Z\Omega$ is the atomic number. Variations of $N(\Omega)$ values are used in this section to get an insight into the electron density reorganization accompanying prototropic equilibria, and are used below to describe how metal complexation modifies $\rho(\mathbf{r})$ in cyanidin.

$$q(\Omega) = Z_{\Omega} - N(\Omega) \tag{1}$$

5. Accurate obtainment of the diverse IAS in the molecule is crucial for computing reliable values of atomic electron population and charges. This accuracy is checked with diverse criteria. Two of them are very common: (1) The application of the Gauss theorem implies that integrated values of the $L(\mathbf{r})$ function, defined by Eq. 2, $L(\Omega)$, should be strictly zero when the zero flux condition is achieved. (2) Summation of $N(\Omega)$ values should recover the total number of electrons in the molecule. It has to be stressed that both are necessary conditions but none of them is sufficient by itself. Summation of atomic energies, $E(\Omega)$, (*see* **Note 9**) are also usually compared in QTAIM literature with total molecular electronic energies as another necessary condition. Absolute values of $L(\Omega)$ and $[N-\Sigma N(\Omega)]$ below 10^{-3} au or 2×10^{-3} are usually considered accurate enough.

$$L(\vec{r}) = \frac{-1}{4}\nabla^2\rho(\vec{r}) \tag{2}$$

6. Neither q(O1) nor the summation of the QTAIM atomic charge of O1 with their attached carbons, α region in Fig. 1, $q\alpha$, is positive in the cations of any of the six most common anthocyanidins [7] (Table 2). Moreover, these charges are also negative in the flavylium cation [8]. This trend, which contradicts the resonance form commonly drawn for cationic anthocyanidins (Fig. 2), is found so with $\rho(\mathbf{r})$ computed for isolated cations as with $\rho(\mathbf{r})$ obtained for PCM modeled aqueous solutions. In contrast, 45–57 % of the positive charge is spread among the hydrogens of the molecule, and around the third part of the positive charge is placed in the B ring (Table 2).

Table 2
Most significant QTAIM charges (in au multiplied by 10^3) for the most stable rotamer (Table 1) of the cationic forms of the six most common anthocyanidins

	$q\alpha$	q_{AC}	q_B	$\Sigma q(H^a)$
Pg	−36	638	362	565
Pn	−41	639	361	492
Cy	−38	641	359	512
Dp	−35	651	349	455
Pt	−38	622	378	466
Mv	−39	644	356	423

Values computed with ρ(r) obtained for PCM optimized geometries modeling aqueous solution at the B3LYP/6-31++G(d,p) level
[a]Summation is extended to hydrogens attached to C sp^2 atoms

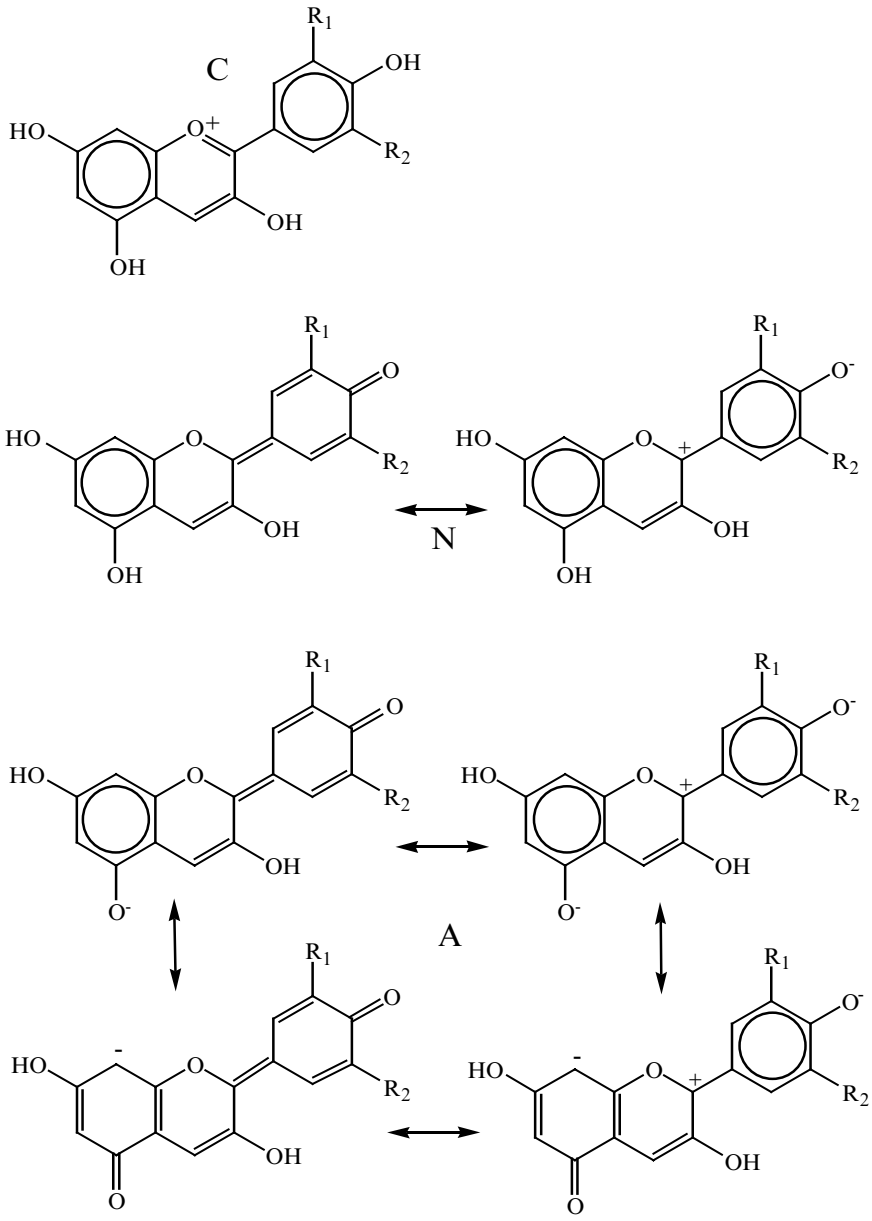

Fig. 2 Resonance forms usually employed for C, N4′, and A54′ forms of anthocyanins/anthocyanidins. Notice they are not unique, as for example there are other N4′ enolates leaving the positive charge on any of the heavy atoms of the AC system

7. Electron distribution of the neutral forms is affected by the position where the deprotonation takes place (Table 3). Thus, we observe the specific behavior of Pg (positive charge spread in AC bicycle and B ring) with regard to the common picture provided by the other five anthocyanidins

Table 3
Most significant QTAIM charges (in au multiplied by 10^3) for the most stable neutral form of the six most common anthocyanidins

	$q\alpha$	q_{AC}	q_B	$\Sigma q(H^a)$	$q(CO^-)$
Pg *N7as-s*	−124	761	239	434	−381
Pn *N4′asa-s*	−109	1,321	−321	365	−351
Cy *N4′asa-a*	−103	1,345	−345	512	−397
Dp *N4′asa-as*	−101	1,346	−346	371	−393
Pt *N4′asa-ss*	−107	1,327	−327	364	−350
Mv *N4′asa-sa*	−115	1,294	−294	332	−302

Values computed with $\rho(r)$ obtained for PCM optimized geometries modeling aqueous solution at the B3LYP/6-31++G(d,p) level
[a]Summation is extended to hydrogens attached to C sp^2 atoms

(AC positively charged while B is negative). The reason is the most stable tautomer of Pg deprotonates in the AC system (hydroxyl at C7) [24], while the deprotonation of the hydroxyl attached to C4′ (B ring) is the most favored in the remaining compounds [7]. We also stress the negative charge displayed by the deprotonated C–O group (no matter if it is in AC or B systems), pointing to a significant enolate character, which is often forgotten using the term quinoidal to refer to neutral form (Fig. 2). QTAIM analysis indicates these forms are neutral by compensation of positive and negative regions, although this is achieved is a different way to that described by the classical enolate Lewis structures [25]. Thus, once more, traditional resonance forms are not a good approximation for the electronic distribution of anthocyanidins.

8. According to QTAIM analysis, the split of positive and negative charges is still more intense in anions (Table 4). B ring is in all cases negative and the AC region becomes more positive, but displaying negative areas, like CO deprotonated groups and the α region. We also highlight that, in all cases, both deprotonated groups display similar negative charges.

3.3 Cyanin Metal Complexation (Cu(II), Zn(II), Mg(II), and Al(III))

1. In order to reduce the computational cost, we have assumed that the effect of the glucose substituents on the metal–ligand bond is negligible. Thus, cyanin was modeled replacing the glycosyl groups attached to O3 and O5 by methyls. The methyl groups are oriented with regard to the aglycon in the same disposition determined for the glycosyl groups in the X-ray diffraction study of the protocyanin crystal [9] (*see* **Note 10**).

Table 4
Most significant QTAIM charges (in au multiplied by 10^3) for the most stable anion of the six most common anthocyanidins

	$q\alpha$	q_{AC}	q_B	$\Sigma q(H^a)$	$\Sigma q(CO^-)$
Pg *A3--a*	−145	1,499	−499	289	−895
Pn *A54′a-s-s*	−143	1,503	−503	287	−856
Cy *A54′a-s-a*	−144	1,510	−510	285	−891
Dp *A54′a-s-as*	−141	1,510	−510	277	−888
Pt *A54′a-s-ss*	−147	1,493	−493	256	−850
Mv *A54′a-a-sa*	−152	1,458	−458	244	−807

Values computed with $\rho(r)$ obtained for PCM optimized geometries modeling aqueous solution at the B3LYP/6-31++G(d,p) level
[a]Summation is extended to hydrogens attached to C sp^2 atoms

2. The Cy^- anion becomes a bidentate ligand after deprotonating the hydroxyl groups attached to C3′ and C4′. This anion only has one hydroxyl group (bonded to C7) available for conformational changes. We have optimized (in gas phase and in PCM modeled aqueous solution) two initial dispositions for the –OH group bonded to C7. The *anti* arrangement (ωC6–C7–O–H = 180°) was found as the most stable one (although the relative energy for the *syn* rotamer is only 0.3 kJ/mol with PCM). The distance between O3′ and O4′ (bite distance) is 2.788 Å according to PCM results (2.805 Å in gas phase).
3. The geometries of anionic cyanidin (Cy^-), Al(III), Mg(II), Cu(II),and Zn(II) hexaaquo ions and the corresponding 1:1 $[MCy(H_2O)_n]^+$ complexes were fully optimized, both for the isolated species and for the aqueous solvated forms modeled with PCM at the B3LYP/6-31++G(d,p) level (*see* **Note 11**). The same computational level was employed to carry out single point calculations on the PCM optimized structures whenever they were not found as minima in gas phase.
4. We have only optimized (with no symmetry restrictions) hexaaqua complexes from initial O_h geometries for the four metals here considered. Excluding Cu(II), M–O bond distances are quite similar in the optimized structure allowing the description of the final structure also as O_h. In contrast, axial Cu-O distances are longer than the equatorial ones (2.305 and 2.005 Å, respectively). This fact reveals the typical strong Jahn–Teller distortions of the d^9 Cu(II) complexes [26]. Also revealed by a less symmetrical disposition of water molecules around the cation in $[Cu(H_2O)_6]^{2+}$.

5. We have concentrated on the 1:1 stoichiometry for Zn(II) and Cu(II) complexes of Cy^-, as it has been reported to be the dominant species in aqueous solutions derived from natural samples [27]. Water molecules were included in the complex in order to obtain different coordination numbers [4–6] around the metal. Thus, models for $[MCy(H_2O)_n]^+$ species with $n = 2$, 3, and 4 were optimized in different initial geometries. Tetrahedral (***T-4***) and square-planar (***SP-4***) initial dispositions for the ligands were optimized for our $[MCy(H_2O)_2]^+$ model, whereas trigonal bipyramidal (***TBPY-5***) and square pyramidal (***SPY-5***) structures were considered in our $[MCy(H_2O)_3]^+$ model, and only octahedral (***OC-6***) geometry for $[MCy(H_2O)_4]^+$ model. All of them were submitted to complete optimizations, with no symmetry restrictions, both in gas phase and in the aqueous solution simulated with PCM. Part of these initial structures was not found as minima.
6. We have performed frequency calculations on PCM optimized geometries for ***SP-4*** and ***T-4*** structures in order to obtain thermal corrections for PCM energies. Table 5 lists electronic energies thermally corrected at 298.15 K for all the optimized minima obtained with PCM, as well as those for our Cy^- model, $[M(H_2O)_6]^{2+}$, and H_2O. While ***SP-4*** and ***T-4*** energies can be compared directly, complexes with different coordination

Table 5
Electronic energies (in au and including thermal corrections at 298.15 K), for PCM modeled aqueous solution employed in the study of Cy^- metal complexation

	Mg(II)[a]	Al(III)[a,b]	Zn(II)	Cu(II)
(*SP*-4)-$[MCy(OH_2)_2]^+$			−3,038.69042[c]	−2,899.82900
(*T*-4)-$[MCy(OH_2)_2]^+$			−3,038.69034	
(*SPY*-5)-$[MCy(OH_2)_3]^+$			−3,115.11785	−2,976.25508[c]
(*OC*-6)-$[MCy(OH_2)_4]^+$	−1,613.39383	−1,655.61255	−3,191.54209[c]	−3,052.67606[c]
(*OC*-6)-$[MCy_2(OH_2)_2]$	−2,567.63868[d]	−2,609.88527[d]		
(*OC*-6)-$[MCy_3]^-$	−3,522.03139[d]	−3,564.28997[d]		
$[M(OH_2)_6]^{2+}$	−658.85606	−701.02969	−2,237.48999	−2,098.61343
Cy^-	−1,107.28203[e] −1,107.30831[d]		−1,106.86224[e]	
H_2O	−76.47178		−76.42437	

[a]B3LYP/6-311++G(2df,2p)//B3LYP/6-31++G(d,p) calculations
[b]Charge of complexes should be increased in 1 au
[c]Not minimum. Single point calculation on gas phase optimized geometry
[d]B3LYP/6-311++G(2df,2p) single point calculations
[e]C_s restricted optimization

Table 6
B3LYP/6-31++G(d.p) relative energies (including thermal corrections and CP corrections for BSSE) with regard to the most stable structure, SP-4, (in kJ/mol) in Cu(II) and Zn(II):Cy^{-1} 1:1 complexes

	Zn(II)	Cu(II)
(SP-**4**)-$[MCy(OH_2)_2]^+$	0.0	0.0
(T-**4**)-$[MCy(OH_2)_2]^+$	0.2	
(SPY-**5**)-$[MCy(OH_2)_3]^+$	1.7	3.4
(OC-**6**)-$[MCy(OH_2)_4]^+$	12.0	18.9

Water solution modeled with PCM

number require counterpoise corrections (CP) for basis set superposition error BSSE [28] (*see* **Note 12**). They were made considering the partial dissociation processes given by Eq. 3.

$$\left[\mathrm{MCy}\left(\mathrm{H_2O}\right)_n\right]^+(\mathrm{aq}) \rightarrow \left[\mathrm{MCy}\left(\mathrm{H_2O}\right)_{n-m}\right]^+(\mathrm{aq}) + m\mathrm{H_2O}(\mathrm{aq}) \qquad (3)$$

7. Tetracoordination is found as the most favored one after CP corrections for Zn(II) and Cu(II) (Table 6). For Zn(II), ***SP-4*** is very slightly preferred (only by 0.2 kJ/mol) over the ***T-4*** structure. Taking into account the reliability of the computational level employed, we can only say that both species, ***SP-4*** and ***T-4***, should be present (and interchanging dinamically) in conformational equilibrium in a room temperature aqueous solution. Moreover, the pentacoordinated ***SPY-5*** form cannot be discarded in this conformational mixture, whereas the hexacoordinated ***OC-6*** structure is really higher in energy and should not be of importance. For Cu(II), the preference over pentacoordination and hexacoordination in $[CuCy(H_2O)_n]^+$ complexes is more clear. ***SPY-5*** structure could be present in aqueous solution as a minority species, while the presence of ***OC-6*** can be considered uncommon.
8. 1:1, 1:2, and 1:3 M:L stoichiometries were considered for Al(III) and Mg(II) complexes. In all these cases, we only worked with hexacoordinated complexes based on the geometry obtained for the X-ray diffraction of the reconstructed protocyanin crystal [9]. The complex extracted from the crystal contains 3 Cy^- anions acting as bidentate ligands. For 1:1 and 1:2 complexes we replaced 1 and 2 cyanins by two and four, respectively, water molecules. Taking into account the large computational cost, we have only performed complete optimizations for 1:1 complexes, while single points calculations were carried out in the other cases.

9. The metal-binding affinity of Cy^- was computed making use of Eq. 4. CP corrections were carried out considering: (1) two fragments for the model complex, the Cy^- model and the $[M(H_2O)_n]^{2+}$ fragment; and (2) five fragments for the $[M(H_2O)_6]^{2+}$ cation, four water molecules and the $[M(H_2O)_2]^{2+}$ fragment including the two water molecules displaying the closest disposition to that adopted in $[MCy(H_2O)_2]^+$. The largest affinity of Cy^- in 1:1 stoichiometry (the most negative ΔE) is found for Cu(II) (−160.2 kJ/mol), followed by Al(II) (−146.9 kJ/mol), Zn(II) (−122.8 kJ/mol), and Mg(II) (−45.5 kJ/mol). Increasing the number of cyanins in the complex leads always (for Al(III) and Mg(II)) to more negative binding energies [12].

$$\left[M\left(H_2O\right)_6\right]^{2+}(aq)+mCy^-(aq)\rightarrow\left[MCy_m\left(H_2O\right)_{n-2m}\right]^{+}(aq)+\left(6+2m-n\right)H_2O(aq) \quad (4)$$

10. The exchange energy associated to reaction (5) shows that hexahydrated Al(III) is able to replace Mg(II) within a cyanidin complex. It has to be stressed that this exchange energy is drastically affected by solvation effects. Thus in 1:1 complexes ΔE is computed as −178.1 kcal/mol in gas phase and −28.9 kcal/mol with PCM for aqueous solution.

$$\left[MgCy_n\left(H_2O\right)_{6-2n}\right]^{(2-n)+}(aq)+Al\left(H_2O\right)_6^{3+}(aq)\rightarrow \left[AlCy_n\left(H_2O\right)_{6-2n}\right]^{(3-n)+}(aq)+Mg\left(H_2O\right)_6^{2+}(aq) \quad (5)$$

11. The evolution of $N(\Omega)$ values along complex formation reveals that all the elements in the complex (metal, cyanin, and water molecules) are altered significantly in this process (Table 7). It can be also observed that the whole electron density of cyanin is affected and not only that of the atoms directly involved in metal–ligand bonds. Thus, the electron density taken from the AC system exceeds, in all the cases studied, that retrieved from the B ring.
12. Moreover, QTAIM analysis shows that the atoms involved in metal–ligand bonds even increase their electron density in many cases. This is observed for carbons in β to M and for the oxygens of the O–M bond in Mg(II) and Al(III) complexes (Table 7). This is due to the polarization experienced by the cyanin ligand, where all the atoms distort their electron density. These distortions try to approach the electron density to the new attractor introduced in the system, in this case the metal. As reported in previous papers dealing electron density reorganization in protonations [33], the electron density moves basically through bonds, so the orientation of a bond with regard to the electron density attractor (M in this case) makes the electron density transference easier or harder [34]. Atoms that are in α or β to M transfer electron density to it but

Table 7
Variation of selected QTAIM electron populations, $\Delta N(\Omega)$, (in au and multiplied by 10^3) for selected groups of atoms in diverse 1:1 cyanin-M complexes

Complex	M	Cy $^-$	$\Sigma(H_2O)$	AC[a]	A	C	B	O3′ + O4′	C3′ + C4′	W1	W2	W3	W4
(SP-**4**)-$[ZnCy(OH_2)_2]^+$	620	−394	−225	−290	−132	−170	−104	−164	254	−109	−116		
(T-**4**)-$[ZnCy(OH_2)_2]^+$	625	−394	−231	−288	−130	−169	−106	−167	257	−101	−130		
(SPY-**5**)-$[ZnCy(OH_2)_3]^+$	657	−361	−295	−264	−119	−155	−97	−153	233	−98	−106	−91	
(OC-**6**)-$[ZnCy(OH_2)_4]^+$	662	−332	−331	−235	−105	−139	−97	−147	208	−88	−98	−71	−74
(SP-**4**)-$[CuCy(OH_2)_2]^+$	825	−555	−273	−354	−163	−207	−201	−284	323	−137	−136		
(SPY-**5**)-$[CuCy(OH_2)_3]^+$	811	−519	−292	−322	−147	−189	−197	−272	297	−123	−127	−42	
(OC-**6**)-$[CuCy(OH_2)_4]^+$	792	−495	−298	−299	−135	−176	−196	−265	274	−124	−122	−27	−25
(OC-**6**)-$[MgCy(OH_2)_4]^+$	231	−201	−30					249	479				
(OC-**6**)-$[AlCy(OH_2)_4]^{2+}$	433	−274	−159					342	759				

[a]Notice that as C9 and C10 belong both to A and C rings $\Delta N_{AC} \neq \Delta N_{A+}\Delta N_C$

they recover (sometimes more than what they give) from atoms placed further away. This is the case of C3′ and C4′ in M–Cy complexes.

13. The electron density transferred from water molecules to M is not negligible (Table 7). It reaches the 50 % of that received by M in the ***OC-6*** complex of Zn(II). The contribution taken from each water molecule is quite similar if we exclude the Jahn–Teller effect of Cu(II) complexes (***SPY-5*** and ***OC-6***), where the axial ligands, bonded by longer distances, transfer much less electron density to M.
14. Finally, while the electron density gained by M varies with the coordination number and, more slightly, with the complex geometry, it is mainly governed by metal electronegativity. Thus, $N(\mathrm{Cu}) > N(\mathrm{Zn}) > N(\mathrm{Al}) > N(\mathrm{Mg})$ (Table 7).

4 Notes

1. Molecular electronic energy denotes here the whole energy obtained for the molecular electrostatic Hamiltonian referring to electrons–nuclei relative movements. That is, the molecular electrostatic Hamiltonian once molecular translation, rotation and vibration have been separated as independent movements from the rest of energy terms. This implies that, at least, we are assuming the adiabatic approximation. We highlight that molecular electronic energy includes the internuclear repulsion energy, as well as nuclei–electron attractions and the kinetic energy associated to relative movements of electrons and nuclei. Internal energy for an ideal gas contains this electronic molecular energy, and those energies associated to molecular vibrations (e.g., using the harmonic oscillator model), rotations, and translations.
2. Electron densities are obtained from ".wfn" files created by the Gaussian programs after running single point, restricted, or full geometry optimizations for the molecule. Creation of this file is required by inserting the keyword "output = wfn" in the command line of Gaussian input file (".gjf") and by specifying the name of the ".wfn" file after a black line following the last line in the Z-matrix. Thus, for a water calculation we write the sample ".gjf" file shown in Fig. 3.
3. The number of expected minima predicted from the number of main dihedral angles is just a first estimation. Significant steric repulsions may affect one or more of the geometries of these expected minima, raising the energy high enough to alter the PES-shape, e.g., transforming one minimum into a transition state with (or not) two adjacent minima. Thus optimization to a nonplanar conformation (let us say, at $\omega_1 = 170°$)

```
#b3lyp/6-31g(d,p) opt output=wfn

example: obtaining an electron density .wfn file

0 1
O
H r1 1
H r2 1 a2 2

r1 1.0
r2 1.0
a2 104.5

water.wdn
```

Fig. 3 Sample .gjf file for obtaining a .wfn file, which is the main input for the most used QTAIM electron density analysis programs

may indicate the presence of a nearly symmetric one (at ω_1 around −170°). The two minima will be equivalent or not (and symmetric or not) depending on the planarity of the remaining main dihedral angles.

4. ZPVE and other thermal corrections to energy or enthalpy are not computed from PCM frequencies for two reasons: (1) PCM frequencies have been reported to be of very low accuracy; (2) ZPVE and other thermal corrections are expected to be rather similar in gas phase and in solution.
5. In the PCM method the solute is imbedded in a cavity of a continuum medium characterized by its dielectric constant. This cavity is created via a series of overlapping spheres centered on nuclei. The radii of the spheres are essential parameters of the method, for which several choices can be made. In this work we used the Simple United Atom Topological Model (UAO) set of solvation radii. The cavity was build up by putting a sphere around each solute heavy atom: hydrogen atoms are enclosed in the sphere of the atom to which they are bonded.
6. Gradient of the electron density, $\nabla\rho(\mathbf{r})$, is zero at any $\rho(\mathbf{r})$ critical point. These points are classified as: attractors, bond critical points (BCP), ring critical points (RCP), and cage critical points (CCP), depending on which is the signature of the Hessian matrix of $\rho(\mathbf{r})$, at the particular critical point, $H\rho(\mathbf{r}_c)$. It is, respectively −3, −1, +1, and +3 for each of these critical points. An attractor is usually placed in the surroundings of each nucleus. BCPs are roughly between every couple of nuclei connected by a bond according Lewis structures. One CCP is placed inside each cycle, while one CCP (a local minimum for $\rho(\mathbf{r})$) is placed inside each molecular cage (e.g., there is one CCP among the four V atoms of tetrahedrane).

7. An Atomic basin comprises the region of the real space defined by the set of force field lines of $\nabla\rho(\mathbf{r})$ which end at a certain attractor. One attractor is usually placed in the surroundings of each nucleus. Thus, an atom is defined by QTAIM as a certain nucleus and its basin.
8. The vanishing limit for $\rho(\mathbf{r})$ is usually taken as the 10^{-5} au electron density isosurface.
9. In QTAIM, the atomic energies, $E(\Omega)$, are atomic electronic kinetic energies $K(\Omega)$ scaled with the molecular virial ratio, $\gamma = -<V>/<K>$, which ideally should be 2. This results in: $E(\Omega) = (1-\gamma)K(\Omega)$. Although nothing assures that the value of the molecular virial ratio can be used as atomic virial [29], the reported lack of transferability of atomic energies along homologous series [29] can be solved, as shown by Cortes-Guzmán and Bader [30], making use of $E(\Omega)$ values computed with $\rho(\mathbf{r})$ distributions that follow very approximately the virial theorem, likw those obtained with the self consistent virial scaling (SCVS) method [31]. In fact, this is crucial to avoid undesirable artifacts when comparing $E(\Omega)$ values computed for molecules of different size, like what our group named "size-effect" (that is, the molecular size dependence observed for the atomic energy along a set of nearly transferable atoms) [32].
10. These orientations for the methoxyl allow avoiding important steric hindrances (anti arrangement of C2–C3–O3–CH_3 and synperiplanar one for C6–C5–O5–CH_3).
11. The same computational level was employed to carry out single point calculations on the PCM optimized structures whenever they were not found as minima in gas phase. The reason for this calculation is to obtain approximated vibrational frequencies for the isolated structure. They are employed to obtain ZPVE and other thermal corrections.
12. BSSE is due to the fact that a larger number of basis functions provides a smaller energy, thus adducts are favored over monomers and adduct formation energy is more negative than it should unless corrections for BSSE are included. The counterpoise (CP) correction which estimates the excess of stabilization of an adduct A·B in any addition reaction or process where it is formed from monomers A and B Eq. 6, is given by Eq. 7, where $E^{A\cdot B}(A)$ and $E^{A}(A)$ are, respectively, the energies computed for A with the whole set basis functions employed for A·B and those used for computing the isolated species A. Both calculations are made in the geometry of A·B for centering basis functions and positioning nuclei. $E^{A\cdot B}(B)$ and $E^{B}(B)$ are the corresponding quantities for compound B. After applying the CP correction the energy variation for the process is expressed by Eq. 8, where the non-superscripted variables

E refer to the molecule computed in its optimized geometry with its basis set.

$$\mathrm{A} + \mathrm{B} \rightarrow \mathrm{A} \cdot \mathrm{B} \tag{6}$$

$$\Delta E^{\mathrm{CP}} = \left[E^{\mathrm{A}\cdot\mathrm{B}}(\mathrm{A}) - E^{\mathrm{A}}(\mathrm{A}) \right] + \left[E^{\mathrm{A}\cdot\mathrm{B}}(\mathrm{B}) - E^{\mathrm{B}}(\mathrm{B}) \right] \tag{7}$$

$$\Delta E = E(\mathrm{A}\cdot\mathrm{B}) - E(\mathrm{A}) - E(\mathrm{B}) - \Delta E^{\mathrm{CP}} \tag{8}$$

Acknowledgements

We thank "Centro de Supercomputación de Galicia" (CESGA) for free access to its computational facilities, and financial support from Spanish Ministry of Economy through research project CTQ2010-21500.

References

1. Haslam E (1998) Practical polyphenolics. Cambridge University Press, Cambridge, UK
2. Wallace TC (2011) Anthocyanins in cardiovascular disease. Adv Nutr 2:1–7
3. Meiers S, Kemény M, Weyand U et al (2001) The anthocyanidins cyanidin and delphinidin are potent inhibitors of the epidermal growth-factor receptor. J Agric Food Chem 49: 958–962
4. Nichenametla SN, Taruscio TG, Barney DL et al (2006) A review of the effects and mechanisms of polyphenolics in cancer. Crit Rev Food Sci Nutr 46:161–183
5. Castañeda-Ovando A, Pacheco-Hernández ML, Páez-Hernández ME et al (2009) Chemical studies on anthocyanins. Food Chem 113: 859–871
6. Sakakibara H, Ashida H, Kanazawa K (2002) Simultaneous determination of all polyphenols in vegetables, fruits, and teas. Free Radical Res 36:307–316
7. Estévez L, Mosquera RA (2009) Conformational and substitution effects on the electron distribution in a series of anthocyanidins. J Phys Chem A 113:9908–9919
8. Estévez L, Mosquera RA (2008) Where is the positive charge of flavylium cations? Chem Phys Lett 451:121–126
9. Shiono M, Matsugaki N, Takeda K (2005) Structure of the blue cornflower pigment. Nature 436:791
10. Kondo T, Ueda M, Isobe M et al (1998) A new molecular mechanism of blue color development with protocyanin, a supramolecular pigment from cornflower, *Centaurea cyanus*. Tetrahedron Lett 39:8307–8310
11. Marković JMD, Veselinović DS, Baranac JM et al (2008) Spectroscopic and theoretical study of cyanidin–aluminum (III) complexes. Spectrosc Lett 41:104–115
12. Estévez L, Otero N, Mosquera RA (2011) Molecular structure of cyanidin metal complexes: Al(III) versus Mg(II). Theor Chem Acc 128:485–495
13. Wright JS, Johnson ER, DiLabio GA (2001) Predicting the activity of phenolic antioxidants: theoretical method, analysis of substituent effects, and applications to major families of antioxidants. J Am Chem Soc 123:1173–1183
14. Estévez L, Otero N, Mosquera RA (2010) A computational study on the acidity dependence of radical-scavenging mechanisms of anthocyanidins. J Phys Chem B 114:9706–9712
15. Tomasi J, Menucci B, Cammi R (2005) Quantum mechanical continuum solvation models. Chem Rev 105:2999–3094
16. Bader RFW (1990) Atoms in molecules – a quantum theory. Oxford University Press, New York, USA
17. Bader RFW (1991) A quantum theory of molecular structure and its applications. Chem Rev 91:893–928

18. Frisch MJ, Trucks GW, Schlegel HB et al. (2004) Gaussian 03, Revision E.01. Gaussian Inc., Wallingford CT, USA
19. Frisch MJ, Trucks GW, Schlegel HB et al. (2009) Gaussian 09, Revision D.01. Gaussian Inc., Wallingford CT, USA
20. Bader RFW (1995) AIMPAC: a suite of programs for the theory of atoms in molecules. McMaster University, Hamilton, ON, Canada. http://www.chemistry.mcmaster.ca/aimpac/download/download.htm
21. Biegler-König F, Schönbohm J, Bayles D (2001) AIM2000 – a program to analyze and visualize atoms in molecules. J Comp Chem 22:545–559
22. Klyne W, Prelog V (1960) Description of steric relationships across single bonds. Experientia 16:521–523
23. Rezabal E, Mercero JM, Lopez X et al (2007) A theoretical study of the principles regulating the specificity for Al(III) against Mg(II) in protein cavities. J Inorg Biochem 101: 1192–1200
24. Estévez L, Mosquera RA (2007) A density functional study of pelargonidin. J Phys Chem A 111:11100–11109
25. Estévez L, Mosquera RA (2008) Molecular structure and antioxidant properties of delphinidin. J Phys Chem A 112:10614–10623
26. Deeth RJ, Randell K (2008) Ligand field stabilization and activation energies revisited: molecular modeling of the thermodynamic and kinetic properties of divalent, first-row aqua complexes. Inorg Chem 47:7377–7388
27. Esparza I, Santamaría C, García-Mina JM et al (2007) Complexing capacity profiles of naturally occurring ligands in tempranillo wines for Cu and Zn. An electroanalytical approach for cupric casse. Anal Chim Acta 599:67–75
28. Boys SF, Bernardi F (1970) The calculation of small molecular interactions by the differences of separate total energies. Some procedures with reduced errors. Mol Phys 19:553–556
29. Mandado M, Vila A, Graña AM et al (2003) Transferability of energies of atoms in organic molecules. Chem Phys Lett 371:739–743
30. Cortes-Guzmán F, Bader RFW (2003) Transferability of group energies and satisfaction of the virial theorem. Chem Phys Lett 379:183–192
31. Lehd M, Jensen FJ (1991) A general procedure for obtaining wave functions obeying the virial theorem. J Comput Chem 12:1089–1096
32. Graña AM, Mosquera RA (1999) The transferability of the carbonyl group in aldehydes and ketones. J Chem Phys 110:6606–6616
33. González Moa M, Mandado M, Mosquera RA (2006) Eplaining the sequence of protonation affinities of cytosine with QTAIM. Chem Phys Lett 428:255–261
34. Ferro-Costas D, Mosquera RA (2013) Influence of the O-protonation in the O=C–O–Me Z preference. A QTAIM study. J Phys Chem A 117:257–265

Chapter 20

Automatic Flow Injection Analysis (FIA) Determination of Total Reducing Capacity in Serum and Urine Samples

Marcela A. Segundo, Ildikó V. Tóth, Luís M. Magalhães, and Salette Reis

Abstract

Automation of total antioxidant capacity assessment can substantially increase the determination throughput, allowing large scale studies and screening experiments. Total reducing capacity evaluation can be implemented under different chemistries, including the CUPRAC—Cupric Ion Reducing Antioxidant Capacity —assay. This assay is based on reduction of Cu(II)-neocuproine complex to highly colored Cu(I)-neocuproine complex by reducing (antioxidant) components of biological samples. In this chapter, we propose an automatic flow injection method for evaluation of total reducing capacity in serum and urine samples, attaining end-point data within 4 min using a kinetic matching strategy.

Key words Total reducing capacity, CUPRAC assay, Flow injection analysis, Biological samples, Automation

1 Introduction

Flow injection analysis (FIA) has been proposed in 1975 by Ruzicka and Hansen [1] as an automation tool for high-throughput wet chemistry analysis. The application of this technique to the evaluation of total antioxidant capacity has been reviewed [2], showing a predominance of automation of methods based on colored radicals [3, 4], electrochemical detection [5, 6], and metal reduction [7]. More recently, a Cupric Ion Reducing Antioxidant Capacity (CUPRAC)-FIA method has been proposed for the automation of determination of total reducing capacity of biological samples [8].

The CUPRAC assay was first proposed by Apak and coworkers [9]. It is based on reduction of Cu(II)-neocuproine (2,9-dimethyl-1,10-phenanthroline) complex to highly colored Cu(I)-neocuproine complex by antioxidants present in samples, namely human serum [10], food [11] and plant matrices [12]. In the FIA system depicted in Fig. 1, the chromogenic oxidizing reagent

Donald Armstrong (ed.), *Advanced Protocols in Oxidative Stress III*, Methods in Molecular Biology, vol. 1208,
DOI 10.1007/978-1-4939-1441-8_20,

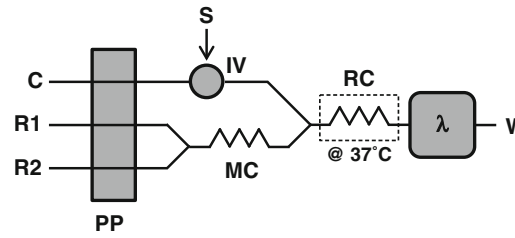

Fig. 1 FIA manifold for the assessment of total reducing capacity based on CUPRAC assay. *S* antioxidant standard solution or sample, *C* carrier (H_2O), *R1* chromogenic oxidizing reagent (8.4 mM Cu(II) + 6.3 mM Nc), *R2* ammonium acetate buffer solution 0.88 M, pH 7.0, *PP* peristaltic pump, *IV* injection valve, *MC* mixing coil (50 cm), *RC* reaction coil (600 cm) immersed in a thermostatic bath at 37 ºC, λ spectrophotometer (450 nm), *W* waste

Cu(II)-neocuproine ($[Cu(Nc)_2]^{2+}$) and buffer solution (pH 7) are premixed at the mixing coil (MC) and then this mixture is added to a 200-μL sample plug, which is inserted in the carrier stream (H_2O) by the injection valve. Afterwards, antioxidant(s) reduce the oxidizing reagent to Cu(I)-neocuproine ($[Cu(Nc)_2]^{+}$) complex along the reaction coil. The amount of colored complex formed is detected spectrophotometrically at 450 nm.

One of the problems of determining the antioxidant capacity using the FIA technique is the underestimation of total antioxidant capacity, fostered by incomplete reaction. In fact, FIA systems rely on non-equilibria conditions, where the analytical readouts are taken after the same reaction time for samples and standards, conditions which are most frequently far from reaction end-point conditions. To circumvent this issue, several strategies have been proposed, including the application of a mathematical model to estimate the end-point antioxidant capacity [13], the measurement of initial rates of reaction [14], and the kinetic matching approach [15].

The kinetic matching approach consists of selecting a standard with a kinetic behavior similar to that presented by the target samples. Therefore, the antioxidant capacity value will not depend on the reaction time selected, as schematically represented in Fig. 2. This approach was applied to the FIA-CUPRAC assay [8], using uric acid as kinetic matching standard for urine and serum samples. As shown in Fig. 2, when Trolox, a fast reacting compound is applied as standard, the antioxidant capacity of the urine sample will increase along reaction time, because its components are still reacting, as opposite to Trolox. When a kinetic matching standard is applied, the antioxidant capacity value is the same for any reaction time as reaction for both standard and sample are still taking place at similar rates.

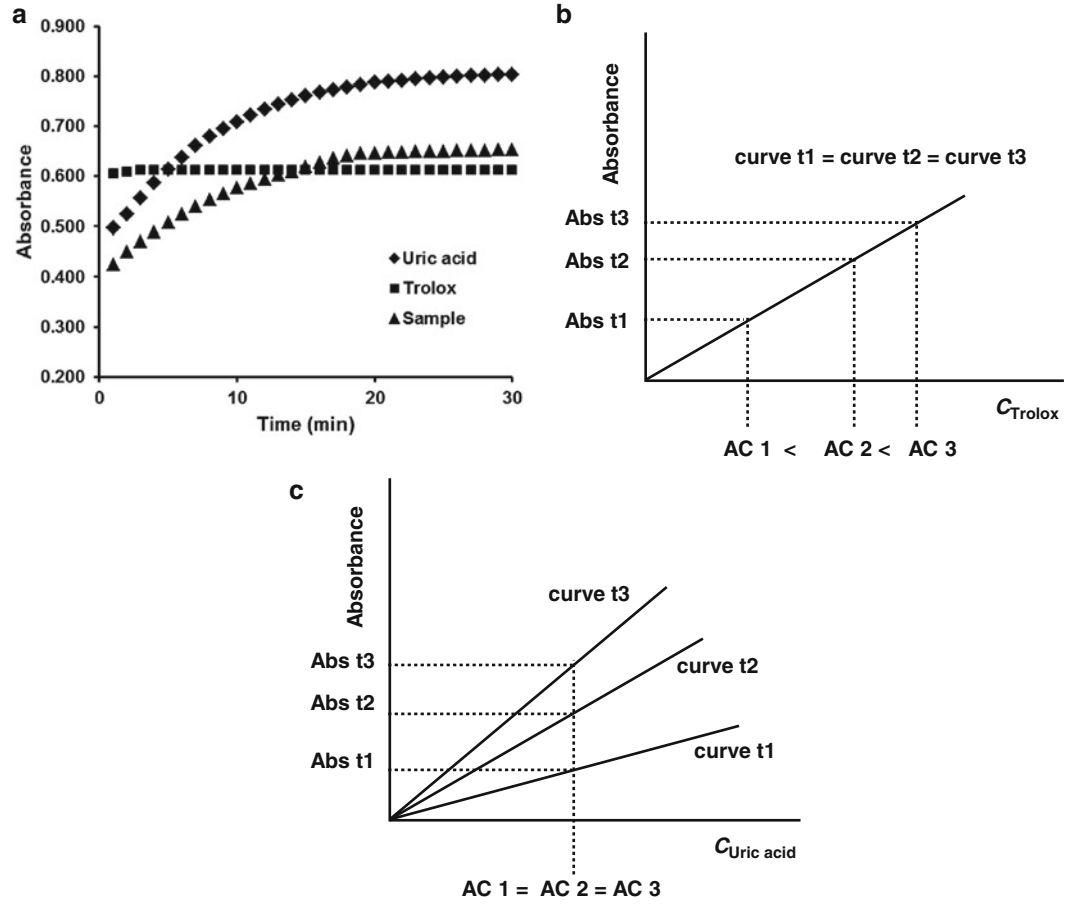

Fig. 2 Schematic representation of kinetic matching approach implementation. (**a**) Kinetic profile for CUPRAC reaction using uric acid (100 μM), Trolox (135 μM), and urine sample (1:40 dilution) using the microplate technique [8]; (**b**) Diagram for interpolation of sample absorbance (Abs t_i) at Trolox calibration curves at different reaction times, providing different values of antioxidant capacity; (**c**) Diagram for interpolation of sample absorbance (Abs t_i) at uric acid (kinetic matching standard as observed at (**a**)) calibration curves at different reaction times, providing the same antioxidant capacity value

2 Materials

2.1 Flow Injection Apparatus

Flow injection systems should contain the following components (*see* **Note 1**):

1. Multichannel peristaltic pump, with at least three channels, equipped with propulsion tubes (*see* **Note 2**).
2. Rotary injection valve (6-port) equipped with 200 μL loop.
3. Polytetrafluoroethylene (PTFE) tubing (*see* **Note 3**).
4. Y-shaped low-pressure connectors and fittings (*see* **Note 4**).
5. Spectrophotometric detector ($\lambda = 450$ nm) equipped with flow-through cell.

6. Thermostatic water bath set at 37 °C.
7. Chart strip recorder or signal processing unit (*see* **Note 5**).

2.2 Solutions

1. Chromogenic oxidizing solution of $[Cu(Nc)_2]^{2+}$ (8.4 mM Cu(II) + 6.3 mM Nc): dissolve 1.432 g of copper(II) chloride dihydrate ($CuCl_2 \cdot 2H_2O$) and 1.655 g of 2,9-dimethyl-1,10-phenanthroline hydrochloride monohydrate (neocuproine hydrochloride monohydrate, Nc, *see* **Note 6**) in Milli-Q H_2O (*see* **Note 7**) and dilute to 1,000 mL.
2. 0.88 M ammonium acetate buffer (pH 7.0): dissolve 67.84 g of anhydrous ammonium acetate (NH_4CH_3COO) in water, adding enough 2 M NaOH or 2 M HCl to give the required pH and making up the volume to 1,000 mL.
3. 2 M NaOH solution: dissolve 4 g of NaOH in 50 mL of water.
4. 2 M HCl solution: add 16 mL of concentrated HCl (37 % *w/w*) to 84 mL of water (*see* **Note 8**).
5. 1.0 mM uric acid stock solution: dissolve 16.81 mg in 20 mL of 0.01 M NaOH. The excess of base is neutralized by dropwise addition of 0.01 M HCl until reaching pH 7.0. The volume is then completed to 100 mL with water.
6. 0.01 M NaOH solution: dilute 2 M NaOH solution 200 times (e.g., 1 mL of 2 M NaOH solution added to 199 mL of water).
7. 0.01 M HCl solution: dilute 2 M HCl solution 200 times (e.g., 1 mL of 2 M HCl solution added to 199 mL of water).
8. 20, 50, 100, and 200 μM uric acid stock solution: appropriate dilution of stock solution in Milli-Q water.

3 Methods

In the flow injection system described here, the reaction between the antioxidants present in samples and $[Cu(Nc)_2]^{2+}$ takes place at reaction coil RC (Fig. 1) at 37 °C, where sample introduced in the system by a rotary valve is mixed with the buffered reagent coming from the mixing coil MC (Fig. 1). After a mean residence time of about 4 min at RC (calculated from the flow rate and volume contained in RC) and connecting tubing, the mixture sample/$[Cu(Nc)_2]^{2+}$ reaches the detector, where the spectrophotometric signal corresponding to the $[Cu(Nc)_2]^{+}$ formed is attained. The total analysis time is about 4 min, providing a determination throughput of ca. 15 h^{-1}.

3.1 Operation of Flow Injection System

1. Assemble the flow system as depicted in Fig. 1 (*see* **Note 9**).
2. Introduce the pumping tubes into the solutions and start the pump (*see* **Note 10**).

3. Fill all the lines with the appropriate solutions (*see* **Note 11**) and check the flow rate in each channel (*see* **Note 12**). It should be about 0.54 mL/min in the channel filled with water and about 0.23 mL/min in the channels filled with $[Cu(Nc)_2]^{2+}$ and buffer solutions (*see* **Note 13**). Wait until a stable baseline signal is attained before starting analysis.
4. Perform the analytical procedure (Subheading 3.2) for all samples.
5. After finishing the analytical procedure, wash the system for 20 min, using water in all channels. Leave all tubing filled with water if the system is to be used within a week. If not, emptying the tubing and disassembling the system is recommended.

3.2 Analytical Procedure and Calibration

1. Fill the loop of the rotary valve (load position) with solution to be tested (*see* **Note 14**).
2. Inject the test solution by changing the injection valve position. Wait until a maximum value of absorbance (peak) is attained before returning the injection valve to the load position.
3. Refill the loop and inject the same test solution once again when the absorbance signal returns to its baseline value. Repeat this procedure until achieving at least three replicate measurements for the same test solution.
4. Perform the calibration by injecting the uric acid standards (*see* **Note 15**).

3.3 Sample Analysis

1. Proceed as described in Subheading 3.2, diluting the sample before sample introduction (*see* **Notes 16** and **17**).
2. Interpolate the maximum peak height on the calibration curve established with uric acid standards. Results will be expressed in mM of uric acid equivalents, after multiplication by the dilution factor applied. To convert these values to TEAC (Trolox equivalent antioxidant capacity), the values should be multiplied by 1.74 (*see* **Note 18**).

4 Notes

1. Commercial flow injection and sequential injection systems are available from several manufacturers, namely, FIAlab Instruments (Bellevue, Washington, USA), Burkard Scientific (Middlesex, UK), Lachat Instruments (Loveland, Colorado, USA), GlobalFIA (Fox Island, Washington, USA).
2. The flow rate is defined by the rotation speed of the peristaltic pump and by the internal diameter of the pumping tubing. For this particular application, two tubing diameters are necessary in order to provide a given flow rate and 2.3 times of this value.

This can be attained using, for instance, Gilson (Villiers-Le-Bel, France) PVC pumping tubes with color codes black/black (0.76 mm i.d.) and grey/grey (1.29 mm i.d.).

3. FIA systems usually employ tubing with 0.8 mm of internal diameter and 1.6 mm of external diameter. Generally, 1 m of this tubing contains 502 μL. Tubing with 0.5 mm or 1.0 mm of internal diameter can also be applied, but its length should be adapted, considering that 1 m contains 196 and 785 μL, respectively.
4. These connectors and fittings are also commercially available from Omnifit (Cambridge, UK) and Gilson (Villiers-Le-Bel, France), among other suppliers.
5. Traditionally, FIA systems do not require computer control, with analytical data recorded in strip recorders, where peak height is manually measured. However, nowadays most detection systems have already incorporated data processing features.
6. Other forms of neocuproine are available, namely neocuproine anhydrous, neocuproine hemihydrate, and neocuproine hydrate. Anhydrous neocuproine can be used, but it is sparingly soluble in water, requiring a previous dissolution in acetone (ca. 10 mL) before adding the aqueous solvent. Neocuproine hydrate does not have the exact number of hydration water molecules defined; therefore it is not possible to measure its accurate amount from the mass. For this methodology, the ratio between Cu(II) and neocuproine is important, so the use of this solid should be avoided.
7. Water used in the preparation of the solutions and buffers should be of high quality, such as water obtained from Milli-Q systems (resistivity > 18 MΩ cm) to avoid contamination and consequent interference by trace metals.
8. If using concentrated HCl at 32 % *w*/*w*, HCl volume is 19 mL and water volume is 81 mL.
9. The reaction coil should be kept at 37 °C. Therefore, it can be immersed in a water bath or other type of heating system can be applied (Peltier heater, for instance).
10. Check that solutions are aspirated by removing the pumping tubing a few times from the solution, allowing air bubbles to enter the tubing. Observe the movement of air bubbles along the system and if flow pulses (short stops of flow) exist, change the pressure exerted from the pump braces into the pumping tubing until no pulses are visible. If any of the solutions are not aspirated, check if the pump braces are correctly adjusted.
11. Discard or filtrate solutions that present suspend particles because they can block the flow system tubing.
12. Check the flow rate by placing the pumping tubing in a measuring cylinder filled with water. Determine the volume of

water aspirated during ten minutes, which will correspond to ten times the flow rate expressed as mL/min.

13. If necessary adjust the flow rate by changing the rotation speed of the pump.
14. To fill the injection loop, test solution can be aspirated through an extra pumping tubing placed in the peristaltic pump or it can be aspirated by an external syringe.
15. The sensitivity should be about 3.6 mM^{-1}. If such value is not attained, prepare new solutions of uric acid. If the problem persists, check the system performance using Trolox standards (25–300 μM), which should provide a sensitivity of 2.8 mM^{-1}.
16. Urine samples should be filtrated before analysis using 0.45 μm filters. Human serum should be diluted 75–100 times, while urine samples should be diluted 20–60 times using water as diluent. Check for the existence of suspended solids of precipitates. In this case, filter the diluted sample before introducing it in the FIA system.
17. Blank measurements can be taken to assess the intrinsic absorption from sample components. These measurements are performed by assessing the analytical signal for the lowest dilution of test sample replacing $[Cu(Nc)_2]^{2+}$ solution by Milli-Q water. If a blank value is >0.010, use more diluted samples.
18. This factor is established by the ratio between the slope of calibration curves obtained for uric acid (7.11 mM^{-1}) and Trolox (4.08 mM^{-1}) at end-point conditions [8, 15].

Acknowledgements

L.M. Magalhães and I.V. Tóth thank FSE (Fundo Social Europeu) and MCTES (Ministério da Ciência, Tecnologia e Ensino Superior) for the financial support through the POPH-QREN program. The authors also acknowledge to the Fundação para a Ciência e a Tecnologia for the financial support through Strategic Project PEst-C/EQB/LA0006/2013.

References

1. Ruzicka J, Hansen EH (1975) Flow injection analyses. 1. New concept of fast continuous-flow analysis. Anal Chim Acta 78(1):145–157
2. Magalhães LM, Santos M, Segundo MA, Reis S, Lima JLFC (2009) Flow injection based methods for fast screening of antioxidant capacity. Talanta 77(5):1559–1566
3. Bukman L, Martins AC, Barizao EO, Visentainer JV, Almeida VD (2013) DPPH assay adapted to the FIA system for the determination of the antioxidant capacity of wines: optimization of the conditions using the response surface methodology. Food Anal Methods 6(5):1424–1432
4. Pellegrini N, Del Rio D, Colombi B, Bianchi M, Brighenti F (2003) Application of the 2,2′-azinobis(3-ethylbenzothiazoline-6-sulfonic acid) radical cation assay to a flow

injection system for the evaluation of antioxidant activity of some pure compounds and beverages. J Agric Food Chem 51(1):260–264

5. Chen J, Gorton L, Akesson B (2002) Electrochemical studies on antioxidants in bovine milk. Anal Chim Acta 474(1–2): 137–146
6. Mannino S, Brenna O, Buratti S, Cosio MS (1998) A new method for the evaluation of the 'antioxidant power' of wines. Electroanalysis 10(13):908–912
7. Shpigun LK, Arharova MA, Brainina KZ, Ivanova AV (2006) Flow injection potentiometric determination of total antioxidant activity of plant extracts. Anal Chim Acta 573:419–426
8. Ribeiro JPN, Magalhães LM, Reis S, Lima JLFC, Segundo MA (2011) High-throughput total cupric ion reducing antioxidant capacity of biological samples determined using flow injection analysis and microplate-based methods. Anal Sci 27(5):483–488
9. Apak R, Guclu K, Ozyurek M, Karademir SE (2004) Novel total antioxidant capacity index for dietary polyphenols and vitamins C and E, using their cupric ion reducing capability in the presence of neocuproine: CUPRAC method. J Agric Food Chem 52(26): 7970–7981
10. Apak R, Guclu K, Ozyurek M, Karademir SE, Altun M (2005) Total antioxidant capacity assay of human serum using copper(II)-neocuproine as chromogenic oxidant: the CUPRAC method. Free Radic Res 39(9):949–961
11. Bener M, Ozyurek M, Guclu K, Apak R (2010) Development of a low-cost optical sensor for cupric reducing antioxidant capacity measurement of food extracts. Anal Chem 82(10): 4252–4258
12. Alpinar K, Ozyurek M, Kolak U, Guclu K, Aras Q, Altun M, Celik SE, Berker KIJ, Bektasoglu B, Apak R (2009) Antioxidant capacities of some food plants wildly grown in Ayvalik of Turkey. Food Sci Technol Res 15(1):59–64
13. Magalhães LM, Segundo MA, Reis S, Lima JLFC (2006) Automatic method for determination of total antioxidant capacity using 2,2-diphenyl-1-picrylhydrazyl assay. Anal Chim Acta 558(1–2):310–318
14. Walker RB, Everette JD (2009) Comparative reaction rates of various antioxidants with ABTS radical cation. J Agric Food Chem 57(4): 1156–1161
15. Magalhães LM, Barreiros L, Maia MA, Reis S, Segundo MA (2012) Rapid assessment of endpoint antioxidant capacity of red wines through microchemical methods using a kinetic matching approach. Talanta 97:473–483

Chapter 21

Mass Spectrometry Detection of Isolevuglandin Adduction to Specific Protein Residues

Casey D. Charvet and Irina A. Pikuleva

Abstract

The aging process seems to be associated with oxidative stress and hence increased production of lipid peroxidation products, including isolevuglandins (isoLGs). The latter are highly reactive γ-ketoaldehydes which can form covalent adducts with primary amino groups of enzymes and proteins and alter the properties of these biomolecules. Yet little is currently known about amino acid-containing compounds affected by isoLG modification in different age-related pathological processes. To facilitate the detection of these biomolecules, we developed a strategy in which the purified enzyme (or protein) of interest is first treated with authentic isoLG in vitro to evaluate whether it contains reactive lysine residues prone to modification with isoLGs. The data obtained serve as a basis for making the "GO/NO GO" decision as to whether to pursue a further search of this isoLG modification in a biological sample. In this chapter, we describe the conditions for the in vitro isoLG modification assay and how to use mass spectrometry to identify the isoLG-modified peptides and amino acid residues. Our studies were carried out on cytochrome P450 27A1, an important metabolic enzyme, and utilized iso[4]levuglandin E_2 as a prototypical isoLG. The isoLG-treated cytochrome P450 was subjected to proteolysis followed by liquid chromatography-tandem mass spectrometry for peptide separation and analysis by Mascot, a proteomics search engine, for the presence of modified peptides. The developed protocol could be applied to characterization of other enzymes/proteins and other types of unconventional posttranslational protein modification.

Key words Isolevuglandin, γ-ketoaldehyde, Posttranslational modification, Mass spectrometry, Multiple reaction monitoring, CYP27A1, Mascot

1 Introduction

Isolevuglandins (isoLGs) are a family of extremely reactive γ-aldehydes named for their levulinaldehyde nucleus and prostaglandin-like structure [1]. These compounds were discovered in the 1980s and shown initially to form through spontaneous rearrangement of prostaglandin H_2 [2, 3]. Later, isoLGs were also found to arise via free radical oxidation of arachidonic acid [1, 4–6]. While the rearrangement of prostaglandin H_2 produces only levuglandin E_2 (Fig. 1a), the free radical oxidation yields a large array of

Donald Armstrong (ed.), *Advanced Protocols in Oxidative Stress III*, Methods in Molecular Biology, vol. 1208,
DOI 10.1007/978-1-4939-1441-8_21,

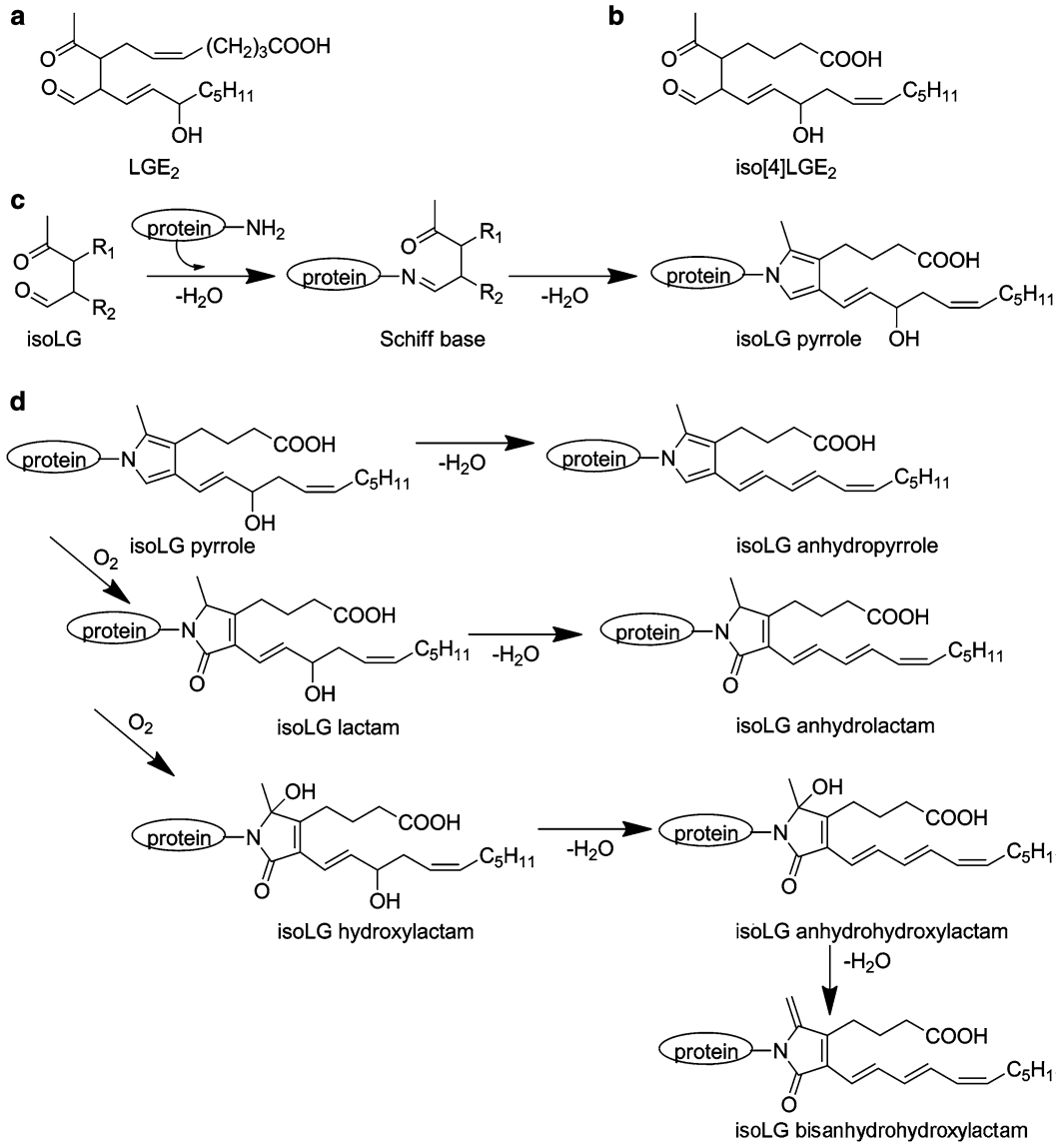

Fig. 1 Isolevuglandins and their adducts with proteins. (**a**) The structures of LGE_2 and (**b**) iso[4]LGE_2. (**c**) IsoLGs react with lysyine residues in proteins to form a reversible Schiff base which then rapidly cyclizes to form a stable pyrrole adduct. (**d**) The initial pyrrole adduct may oxidize to isoLG lactams and isoLG hydroxylactams. The adducts may also dehydrate to the anhydro forms. Adapted from [7]

regioisomers and stereoisomers of isoLGs such as iso[4]levuglandin E_2 (iso[4]LGE_2) (Fig. 1b) [7]. The isoLGs are many times (up to 1,000-fold) more reactive than most other lipid oxidation products avidly binding to primary amines in biomolecules and forming different types of adducts (Fig. 1c, d) [5, 6, 8]. The existence of these different adducts makes investigation of posttranslational

modification with isoLGs difficult. Before our work, little was known about which adducts were most abundant. A major benefit of using mass spectrometry (MS) to analyze isoLG adduction is that MS is capable of recognizing and distinguishing these multiple adduct oxidation forms.

IsoLG adducts have been used as a biomarker of long-term oxidative stress. The products of isoLG modification are elevated in the serum of patients with renal disease, atherosclerosis, and age-related macular degeneration (AMD) and also present in a disease-affected tissue such as trabecular meshwork of glaucoma patients and brain of individuals diagnosed with Alzheimer's disease [9–14]. Of importance is that isoLG modification may not simply be a biomarker but also a causative agent because of the deleterious impact on the properties of the modified biomolecules [13, 15–17]. We were interested in establishing whether a specific enzyme, cytochrome P450 27A1 (CYP27A1), is modified by isoLGs in aged human retina and how this modification affects the enzyme activity [17, 18]. CYP27A1 is a ubiquitously expressed mitochondrial sterol 27-hydroxylase which acts on multiple substrates and thereby participates in several metabolic pathways such as cholesterol removal from extrahepatic tissues, bioactivation of vitamin D_3 in the kidney and production of bile acids in the liver (reviewed in ref. 19). However, the role of CYP27A1 in the retina is not yet fully understood and is currently under investigation in this laboratory [17, 18, 20, 21]. To search for CYP27A1-isoLG adducts in human retina, we decided to assess first whether this enzyme could be modified by isoLGs in vitro under the conditions when varying isoLG amounts are used and purified recombinant CYP27A1 is reconstituted in phospholipid vehicles that model the enzyme's natural membrane environment [17]. The effect of isoLG treatment on enzyme activity was evaluated as well [17, 18]. Subsequent MS analysis enabled the identification of the modified CYP27A1 peptides, most reactive lysine residues and most abundant isoLG adducts [17]. These results were used for a search of the isoLG-modified CYP27A1 peptides in human retina by multiple reaction monitoring (MRM) [17]. MRM is a technique wherein a mass spectrometer fragments the peptides obtained after proteolytic protein digestion and is set up to detect multiple transitions, or pairs of a peptide ion and peptide-fragment ions derived from the fragmentation of this peptide. MRM can unambiguously identify specific peptide modifications in complex biological samples and quantify these modifications with high accuracy (if internal standards are available). MRM, however, requires prior knowledge of the specific sites of modification and structure of the adducts formed. Herein, we describe how to obtain this information from the studies in vitro.

2 Materials

2.1 Equipment

1. An Ultimate 3000 LC system was from Dionex (Sunnyvale, CA) with a C_{18} Acclaim PepMap 100 column (0.075 × 150 mm), also from Dionex.
2. A hybrid Fourier transform ion cyclotron resonance (FTICR)/linear ion trap mass spectrometer, a LTQ FT Ultra, was from Thermo Scientific (San Jose, CA).
3. The Mascot search engine was from Matrix Science (Boston, MA).

2.2 Reagents and Chemicals

1. IsoLGs are not commercially available and must be custom synthesized. We obtained iso[4]LGE_2 from our collaborator Dr. R. Salomon (Case Western Reserve University) [22]. A 3 mM stock of iso[4]LGE_2 was prepared in methanol and stored at −20 °C under nitrogen.
2. The protein of interest is either obtained in the laboratory or purchased from a vendor. We heterologously expressed and purified recombinant human CYP27A1 by ourselves as described [23]. The protein concentration was 37 μM, and the buffer was 50 mM potassium phosphate (KP_i), pH 7.2, 20 % glycerol (*see* **Note 1**). To avoid repeated freezing–thawing, the protein was divided into 20 μL aliquots and stored at −80 °C.
3. Sequencing grade chymotrypsin and trypsin for proteolytic digestion were from Promega (Madison, WI). The lyophilized enzymes were reconstituted immediately prior to use at 0.1 mg/μL per manufacturer's instructions.
4. Ammonium bicarbonate (50 mM, pH 7.8) and solutions of dithithreitol (DTT) and iodoacetamide (IAA) on this buffer were prepared immediately prior to use and the excess was discarded (*see* **Note 2**).

3 Methods

3.1 Iso[4]LGE2 Treatment of CYP27A1

1. Iso[4]LGE_2 in methanol (1.150 μmol in 383 μL) was dispensed into a glass tube (*see* **Note 3**). The methanol was then evaporated with flowing nitrogen.
2. The resulting iso[4]LGE_2 residue was dissolved in 100 μL of 50 mM KP_i, pH 7.2, 100 μM diethylenetriaminepentaacetic acid (DTPA, *see* **Note 4**). The solution was vortexed two times for 5 s with a 10 min-interval.
3. The purified CYP27A1, 5 nmol of in 135 μL, was placed in a separate glass tube and diluted with 765 μL of 50 mM KP_i, pH 7.2, 100 μM DTPA.

4. The CYP27A1 solution was transferred to the tube containing the iso[4]LGE_2 solution. The tube was capped and placed in an orbital shaker (30 rpm) at room temperature for 60 min. A sample omitting iso[4]LGE_2 was used as the untreated control.
5. Glycine, 25 μL of 100 mM stock in 50 mM KP_i, pH 7.2, was added to the reaction mixture to stop CYP27A1 modification with iso[4]LGE_2 by neutralizing unreacted isoLG.
6. The reaction mixture was divided into 100 μL aliquots and flash-frozen in liquid nitrogen and stored at −80 °C.

3.2 Proteolytic Digestion

To maximize protein sequence coverage, we performed two types of digests, in-gel and in-solution, and for each used two types of proteases, trypsin and chymotrypsin.

3.2.1 In-Gel Digestion

In-gel digestion was followed the standard protocol [24].

1. The sample of iso[4]LGE_2-treated CYP27A1, 15 pmol in 20 μL, was subjected to 10 % SDS-PAGE along with untreated control and molecular weight standards.
2. The gel was stained with Coomassie blue and, for the sample lanes (isoLG treated CYP27A1 and untreated control), the stained region corresponding to proteins with molecular mass between 50 and 60 kDa was excised with razor blade (*see* **Note 5**). Each excised band was diced into 1 mm^3 cubes and transferred to a separate 1.5 mL microcentrifuge tube.
3. The gel pieces were destained in 100 μL of 50 mM ammonium bicarbonate–acetonitrile (1:1 vol/vol) for 30 min with occasional vortexing for 5 s.
4. The gel pieces were dehydrated by the addition of 500 μL acetonitrile until the pieces became small, hard, and opaque (about 10 min). The liquid was removed by pipetman, taking care not to poke or aspirate the gel pieces (*see* **Note 6**).
5. The gel pieces were covered with 100 μL of 20 mM DTT for 30 min to reduce CYP27A1. The liquid was then removed, and the gel pieces were dehydrated as in **step 4**.
6. The gel pieces were covered with 100 μL of 100 mM IAA to alkylate CYP27A1. This procedure was carried out in the dark for 20 min followed by liquid removal, and gel dehydration as in **step 4**. The gel pieces were air-dried for 5 min.
7. Chymotrypsin or trypsin was added to the dried gel pieces at a protease to CYP27A1 ratio of 1:50 (w/w) in a final volume of 50 μL of 50 mM ammonium bicarbonate, pH 7.8. The proteolysis proceeded for 22 h at 37 °C with shaking at 60 rpm.
8. The resultant peptides were extracted by incubating the gel pieces with 100 μL of 50 % acetonitrile containing 5 % formic acid for 15 min in a shaker at 37 °C. The tube was centrifuged

for 5 s at 500 rpm to spin down the solution from the cap and sides. The solution was aspirated by pipetman and transferred to new microfuge tube, where it was dried in a vacuum concentrator. The tube was stored at −20 °C until MS analysis.

3.2.2 In-Solution Digestion

In-solution digestion followed the standard protocol [25].

1. Iso[4]LGE$_2$-treated CYP27A1, 2 nmol in 400 μL, was dialyzed overnight against 1,000 volumes of 50 mM KP$_i$, pH 7.2, 100 μM DTPA, 0.2 M NaCl (*see* **Note 7**).
2. The protein sample was concentrated to a volume of 5 μL in an Amicon Ultracentrifugal filter (regenerated cellulose, 50-kDa molecular mass cutoff, EMD Millipore, Billerica, MA) and transferred to a clean microfuge tube. Crystalline urea (4.8 mg) was added to the protein solution, resulting in a final volume of 10 μL.
3. DTT (2.5 μL of 100 mM stock) was added to the protein solution to reduce CYP27A1. The incubation was carried out for 30 min at room temperature. Then IAA (1.5 μL of 250 mM stock) was added to alkylate the protein for 30 min in the dark. The final volume at this point was 14 μL.
4. The protein solution was diluted tenfold with 126 μL of 10 mM Tris–HCl, pH 8.0, containing 3 μg chymotrypsin or trypsin at a protease to CYP27A1 ratio of 1:50 (w/w). The protein was digested for 22 h at 37 °C with shaking at 60 rpm (*see* **Note 8**).
5. Protein digest (667 pmol in 47 μL) was applied to an Ultra-Micro C$_{18}$ PrepTip from the Nest Group (Southborough, MA), and the flow through fraction discarded. Sample loading, washes, and peptide elution were according to the manufacturer's instructions. Acetonitrile (50 μL of 80 % (V/V) aqueous solution) was applied two times to the tip to elute peptides. The eluates were combined in a clean microfuge tube, and dried in a vacuum concentrator. The tube was stored at −20 °C until MS analysis.

3.3 LC-MS/MS Analysis

1. The dried peptides were dissolved in 12 μL of 2 % aqueous acetonitrile containing 0.1 % formic acid. One-sixth (2 μL) of this solution was injected into the LC-MS system. Peptides were eluted with a 2–80 % gradient of aqueous acetonitrile containing 0.1 % formic acid over a 50 min period at a flow rate of 300 nL/min and directed into the nanospray source with the following source parameters: ion spray voltage of 2,400 V and an interface capillary heating temperature of 200 °C.
2. Full mass spectra were acquired from the FTICR detector, and the tandem mass spectra (MS/MS) of the eight most intense ions generated by the linear ion trap were recorded in

data-dependent acquisition mode (*see* **Note 9**) with normalized collision energy of 35 eV, an isolation width of 2.5 Da, and activation Q of 0.25.

3.4 Identification of Iso[4]LGE$_2$ Adducts

This section describes how to identify the sites of iso[4]LGE$_2$ modification from the MS/MS data using the Mascot Search Engine (*see* **Note 10**).

1. The set of all possible iso[4]LGE$_2$ modifications was created by connecting to the university Mascot server. From the welcome page, "Configuration Editor" was clicked, followed by "Modifications", then the "Add New Modification" button. The "Add Modification" page presents form fields to fill in the title, full name, and composition of the modification. When listing the composition of the iso[4]LGE$_2$ adduct formula, it is important to subtract 2 hydrogen atoms to account of the two hydrogen atoms that are eliminated from the ε-amino group upon its reaction with iso[4]LGE$_2$. For example, the lactam adduct has a formula of $C_{20}H_{30}O_4$, but must be entered into Mascot as $C_{20}H_{28}O_4$. All 7 modifications (Table 1) were entered in this manner.
2. A new database containing the primary sequence of only CYP27A1 was created by selecting "Configuration Editor" from the welcome page, followed by "Database Maintenance", to load the "Edit Database Definitions" page. CYP27A1 was entered for "Name", and the full path and filename to a fasta file containing the primary sequence of mature human CYP27A1 was entered into "Path". All other options were left as the default.

Table 1
IsoLGE$_2$ adduct formulas in Mascot. Formulas are as they were entered in Mascot and account for the 2 hydrogen atoms lost from lysine in the reaction with iso[4]LGE$_2$

Adduct	Adduct formula	Δ Monoisotopic mass (Da)
Pyrrole	$C_{20}H_{28}O_3$	316.20
Anhydropyrrole	$C_{20}H_{26}O_2$	298.19
Lactam	$C_{20}H_{28}O_4$	332.20
Anhydrolactam	$C_{20}H_{26}O_3$	314.19
Hydroxylactam	$C_{20}H_{28}O_5$	348.19
Anhydrohydroxylactam	$C_{20}H_{26}O_4$	330.18
Bisanhydrohydroxylactam	$C_{20}H_{24}O_3$	312.17

3. After launching the Mascot Daemon (the application for submitting jobs to the Mascot server), the Parameter Editor tab was selected (Fig. 2). The custom CYP27A1 database was selected in the Database box, and the "Select Modification"

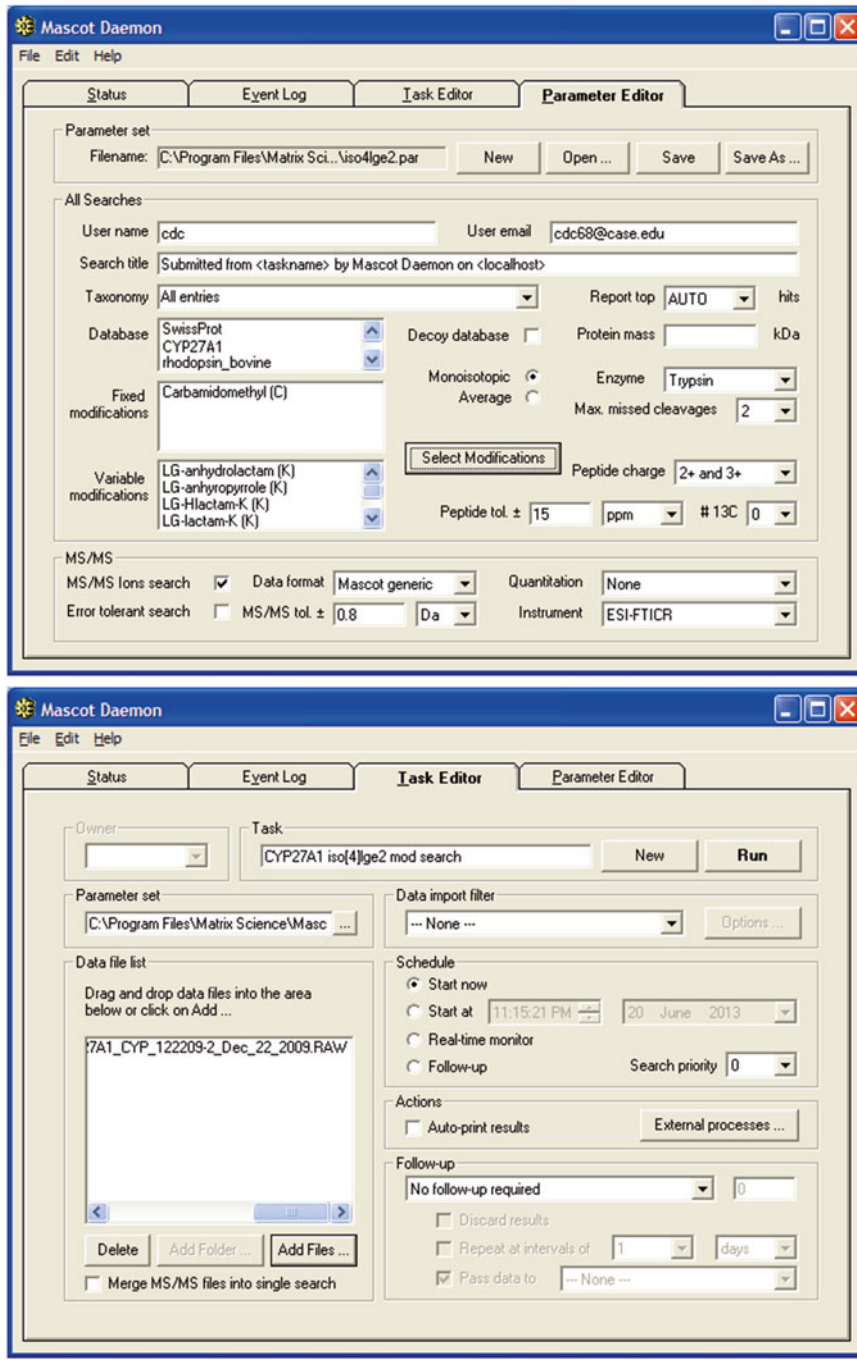

Fig. 2 Configuration of the parameter editor and task editor tabs in Mascot Daemon software for the identification of isoLG-modified lysine residues

button was clicked. "Carbamidomethyl (C)" was selected and added under "Fixed Modification", while "Oxidation (M)" and the 7 new iso[4]LGE_2 adducts were selected and added under "Variable Modifications". Either trypsin or chymotrypsin was selected as for the "Enzyme" with "Max missed cleavages" set to 2. The remaining parameters were set as follows: monoisotopic, selected; peptide charge, 2+ and 3+; peptide tolerance, 15 ppm; MS/MS ions search, checked; data format, Mascot generic, MS/MS tolerance, 0.8 Da; quantitation, none; instrument, ESI-FTICR. The parameter set was saved as "iso4lge2. par".

4. To submit the MS/MS data files for searching, the Task Editor tab was selected in Mascot Daemon (Fig. 2). The "iso[4]lge2. par" parameter set was loaded by clicking the "…" button under "Parameter Set". Next, under "Data file list", the MS/MS file was added. All other parameters were as default and the search was started by clicking "Run."
5. Mascot identified in the isoLG-trated CYP27A1 MS/MS spectra which corresponded to the enzyme peptides both with and without isoLG modification. Modified residues were underlined in the peptide sequence and the detected modification displayed (Fig. 3a). Clicking on a specific query loaded the MS/MS spectra for examination and confirmation of the modification (Fig. 3b). The presence of the modified residues in isoLG-treated CYP27A1 and lack of modification in untreated control was used as the basis for the next set of experiments (*see* **Note 11**).

3.5 Concluding Remarks

The search for unconventional protein modification in a biological sample is extremely difficult if preliminary in vitro data on the type of the adduct formed and residue(s) modified are unavailable. Herein we described how to obtain this in vitro data and simultaneously gain insight into whether a protein of interest could have this type of modification in vivo. Our data indicate that a good prerequisite for the subsequent analysis of a biological sample is when the protein of interest is amenable to the modification in vitro after a short incubation (<1 min) with low molar excesses of the modifying agent (<2-fold). The most reactive lysine residues will also likely be modified in a biological sample [17, 18]. Protein location in a cell should also be considered and modeled in vitro, e.g., by insertion into liposomes, followed by the modification. If the protein is still amenable to the modification, studies of a biological sample are warranted and should utilize an internal standard to obtain unambiguous results. This internal standard can also be generated based on the information provided by the in vitro experiment. In the case of CYP27A1, the most abundant adduct was the isoLG lactam. Thus, collectively, the in vitro modification

a

Query	Observed	Mr(expt)	Mr(calc)	Delta	Miss	Score	Expect	Rank	Unique	Peptide
7312	628.3683	1882.0831	1882.0815	-0.1572	1	39	2e-005	1		K.VVLAPETGELKSVAR.I + LG-lactam-K (K)

b **Peptide View**

MS/MS Fragmentation of VVLAPETGELKSVAR

Found in gi|4503211, cytochrome P450, family 27, subfamily A, polypeptide 1 precursor [Homo sapiens]

Match to Query 7312: 1882.083072 from(628.368300,3+)

Title: CHA1223A2LC3_CYP27A1_CYP_122209-2_Dec_22_2009.8130.8130.3.dta

Data file C:\[redacted]\CHA1223A2LC3_CYP27A1_CYP_122209-2_Dec_22_2009.RAW

Click mouse within plot area to zoom in by factor of two about that point

Or, Plot from 100 to 1600 Da Full range

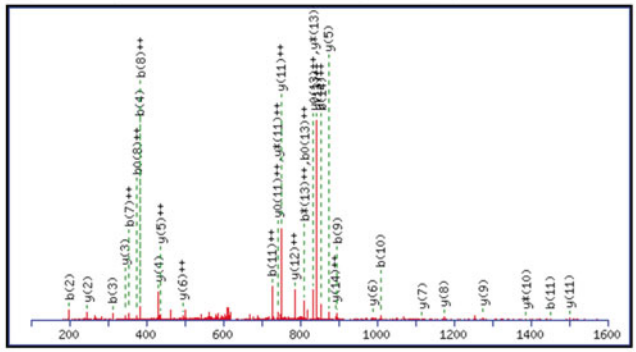

Monoisotopic mass of neutral peptide Mr(calc): 1882.0815
Fixed modifications: Carbamidomethyl (C)
Variable modifications:
K11 : LG-lactam-K (K)
Ions Score: 39 **Expect:** 2e-005
Matches (Bold Red): 33/132 fragment ions using 74 most intense peaks

#	b	b^{++}	b*	b^{*++}	b^{0}	b^{0++}	Seq.	y	y^{++}	y*	y^{*++}	y^{0}	y^{0++}	#
1	100.0757	50.5415					V							15
2	**199.1441**	100.0757					V	1784.0204	**892.5138**	1766.9939	884.0006	1766.0099	883.5086	14
3	**312.2282**	156.6177					L	1684.9520	**842.9796**	1667.9255	**834.4664**	1666.9414	**833.9744**	13
4	**383.2653**	192.1363					A	1571.8679	**786.4376**	1554.8414	777.9243	1553.8574	777.4323	12
5	480.3180	240.6627					P	**1500.8308**	**750.9191**	1483.8043	**742.4058**	1482.8203	**741.9138**	11
6	609.3606	305.1840			591.3501	296.1787	E	1403.7781	702.3927	**1386.7515**	693.8794	1385.7675	693.3874	10
7	710.4083	**355.7078**			692.3978	346.7025	T	**1274.7355**	637.8714	1257.7089	629.3581	1256.7249	628.8661	9
8	767.4298	**384.2185**			749.4192	**375.2132**	G	**1173.6878**	587.3475	1156.6612	578.8343	1155.6772	578.3423	8
9	**896.4724**	448.7398			878.4618	439.7345	E	**1116.6663**	558.8368	1099.6398	550.3235	1098.6558	549.8315	7
10	**1009.5564**	505.2819			991.5459	496.2766	L	**987.6237**	**494.3155**	970.5972	485.8022	969.6132	485.3102	6
11	**1451.8396**	**726.4234**	1434.8131	717.9102	1433.8290	717.4182	K	**874.5397**	**437.7735**	857.5131	429.2602	856.5291	428.7682	5
12	1538.8716	769.9395	1521.8451	761.4262	1520.8611	760.9342	S	**432.2565**	216.6319	415.2300	208.1186	414.2459	207.6266	4
13	1637.9400	819.4737	1620.9135	**810.9604**	1619.9295	**810.4684**	V	**345.2245**	173.1159	328.1979	164.6026			3
14	1708.9772	**854.9922**	1691.9506	846.4789	1690.9666	845.9869	A	**246.1561**	123.5817	229.1295	115.0684			2
15							R	175.1190	88.0631	158.0924	79.5498			1

Fig. 3 The MS/MS fragmentation report generated by Mascot consists of several panes of data. (**a**) The first page of the report displays a listing of search queries with each query line containing information about statistics (e.g., score), peptide sequence and detected modification. Clicking a query number (in *underlined blue*) loads the corresponding peptide report for that query (**b**). The peptide report displays the sequence of the identified peptide (in *red*) in the first line and indicates that it belongs to CYP27A1 in the second line. The next lines display information about the MS/MS scan number examined by the software (highlighted in *yellow*), the mass of the precursor ion from the full MS scan (highlighted in *cyan*), and the *m/z* and charge state of the peptide ion (highlighted in *light green*). The spectrum (*red*) in the black box is the full MS/MS scan of the fragmented peptide ion, while the *green dashed* lines point to the labels indicating the identity of the ions. Below the spectrum are more data regarding the peptide, including any variable modifications detected by the software.

of protein of interest could provide a lot of information for making the "GO/NO GO" decision and essential for successful identification of the unconventional protein modification in a biological sample. While this method is focused on a single protein and does not represent a "shotgun" approach, the advantage of our strategy is that it enables the investigation of a low abundance enzyme. In contrast, "shotgun" strategies usually pick up only the most abundant targets, e.g., structural proteins.

4 Notes

1. Buffer composition may vary based on the protein to be modified. However, buffers containing primary amines, e.g., Tris, must be avoided as they will compete with lysine residues to react with iso[4]LGE_2.
2. The pH of ammonium bicarbonate upon dissolution is 7.8 and is not adjusted further.
3. The amount of iso[4]LGE_2 in this experiment, 1.150 μmol, represented a tenfold molar excess over the lysine residue content in 5 nmol of CYP27A1, which contains 23 lysine residues per molecule. If such excess of isoLG does not modify a protein of interest in vitro, this protein is unlikely to be modified by isoLGs in vivo when other proteins are present and the isoLG to protein ratios are much smaller. However, if a high isoLG to protein ratio does lead to isoLG adduction, the next step is to use lower concentration of isoLGs (*see* **Note 11**).
4. DTPA was included in the buffer as an iron chelating agent. Contamination of buffers and glassware with iron could lead to the formation of reactive oxygen species and confound results.
5. In our experiments, the iso[4]LGE_2-treated CYP27A1 had slower electrophoretic migration than the untreated control whose molecular weight is ~57 kDa.

Fig. 3 (continued) The report indicates that an isoLG lactam modification was detected at K11 in the peptide (highlighted in *magenta*). Beneath this text is a table displaying the *m*/*z* of the predicted fragment ions, with the sequence of the peptide displayed (in *bold blue*) vertically down the center column of the table, and the b-series (peptide fragments numbered from and containing the N-terminus) and y-series (peptide fragments numbered from and containing the C-terminus) ion numbering vertically down the *left-hand* and *right-hand* side columns, respectively. Experimentally observed ions matching the predicted *m*/*z* are shown in *bold red*. Identification of both b- and y-series fragment ions which include the modified lysine residue (b11, b13, b14, and y5–y14), as reflected in their *m*/*z* values, and those without it (b2–b4, b7–b10, and y2–y4) provides even stronger evidence that the identity of the peptide and location of the isoLG adduct are correct

6. Gel-loading pipeteman tips are ideal for removing or transferring liquid in microfuge tubes with gel pieces. Holding the tip against the bottom of the tube prevents aspiration of gel pieces. Regular tips with wider openings are prone to clogging by aspiration of gel pieces.
7. Detergent, glycerol, and other additives present in protein solution along with precipitated protein could create problems (e.g., high column pressure and electrospray source clogging) during the subsequent peptide separation by LC and MS/MS analysis.
8. If the in-solution digest contains protein precipitate, the protease should be added in two portions, a half of the amount to start the digest, and the other half 11–12 h later. Sonication by microtip at 10 % power, 20 % duty cycle with a Digital Sonifier S-450D from Branson Ultrasonics (Danbury, CT) may also help disperse larger precipitates and thus facilitate the proteolysis.
9. Data-dependent acquisition is an operational mode on Thermo Scientific mass spectrometers capable of MS/MS wherein the software automatically selects the 4–8 most intense ions present in the full MS scan for subsequent full MS/MS analysis. Instruments from other vendors with MS/MS capabilities usually offer this mode in their software as well.
10. This section requires creation of a custom database and custom modifications on the Mascot server which is usually installed at universities/companies with mass spectrometry facilities. Please consult with the administrator of your Mascot system if you are not authorized to make changes to the system configuration or are not comfortable with process.
11. Identification of the CYP27A1 lysine residues susceptible to modification was a starting point for a number of additional experiments including quantitative MRM. For example, CYP27A1 was incubated with much lowers concentration of isoLGs (a twofold molar excess over the protein lysine residue content) for 30 s, 5 min, 15 min, 60 min, and 120 min, to study the kinetics of modification and identify the most reactive lysine residues [17, 18]. We found that the lysine residues most amenable to modification could be identified after only a 30 s-incubation with isoLGs [18]. We also studied the effect of CYP27A1 incorporation into phospholipid vesicles prior to isoLG treatment as CYP27A1 is a membrane-bound protein (hence some of its lysine residues may not be available for modification in vivo). Indeed, association with liposomes restricted iso[4]LGE_2 modification of CYP27A1 to a smaller set of residues with one of the most reactive residues being then found modified by isoLGs in a biological sample [17].

Another finding was that the isoLG-lactam adduct was the most abundant form in vitro and the form we observed in vivo [17, 18], while the pyrrole and anhydropyrrole adducts were never detected. Finally, by mutating the most reactive residues to arginines, which do not usually interact with isoLGs, we were able to demonstrate that isoLG modification at one specific site could greatly reduce enzyme activity [18]. Another application of these data would be the synthesis of a custom peptide corresponding to the sequence of the tryptic or chymotryptic peptides which contained the modified lysine residue. This synthesized peptide could then be modified by stable isotope labeled iso[4]LGE_2, purified, and used as an internal standard for quantifying isoLG modification of a specific protein in biological samples. Alternatively, the peptide could be isotope labeled, e.g., with ^{15}N, and be modified by unlabeled isoLG.

Acknowledgements

We thank the National Institutes of Health (the EY018383 grant to I.A.P. and the T32 EY007157 fellowship to C.D.C.). I.A.P. is the recipient of a Jules and Doris Stein Professorship from the Research to Prevent Blindness. We are grateful to Robert G. Salomon for his enthusiastic collaboration.

References

1. Salomon RG, Miller DB (1985) Levuglandins: isolation, characterization, and total synthesis of new secoprostanoid products from prostaglandin endoperoxides. Adv Prostaglandin Thromboxane Leukot Res 15:323–326
2. Salomon RG, Miller DB, Zagorski MG et al (1984) Prostaglandin endoperoxides. 14. Solvent-induced fragmentation of prostaglandin endoperoxides. New aldehyde products from PGH2 and a novel intramolecular 1,2-hydride shift during endoperoxide fragmentation in aqueous solution. J Am Chem Soc 106:6049–6060
3. Miller DB, Raychaudhuri SR, Avasthi K et al (1990) Prostaglandin endoperoxides. 25. Levuglandin E2: enantiocontrolled total synthesis of a biologically active rearrangement product from the prostaglandin endoperoxide PGH2. J Org Chem 55:3164–3175
4. Salomon RG, Subbanagounder G, Singh U et al (1997) Oxidation of low-density lipoproteins produces levuglandin-protein adducts. Chem Res Toxicol 10:750–759
5. DiFranco E, Subbanagounder G, Kim S et al (1995) Formation and stability of pyrrole adducts in the reaction of levuglandin E2 with proteins. Chem Res Toxicol 8:61–67
6. Salomon RG, Sha W, Brame C et al (1999) Protein adducts of iso[4]levuglandin E2, a product of the isoprostane pathway, in oxidized low density lipoprotein. J Biol Chem 274:20271–20280
7. Salomon RG (2005) Distinguishing levuglandins produced through the cyclooxygenase and isoprostane pathways. Chem Phys Lipids 134:1–20
8. Kobierski ME, Kim S, Murthi KK et al (1994) Synthesis of a pyrazole isostere of pyrroles formed by the reaction of the .epsilon.-amino groups of protein lysyl residues with levuglandin E2. J Org Chem 59:6044–6050
9. Li W, Laird JM, Lu L et al (2009) Isolevuglandins covalently modify phosphatidylethanolamines in vivo: detection and quantitative analysis of hydroxylactam adducts. Free Radic Biol Med 47:1539–1552

10. Poliakov E, Brennan ML, Macpherson J et al (2003) Isolevuglandins, a novel class of isoprostenoid derivatives, function as integrated sensors of oxidant stress and are generated by myeloperoxidase in vivo. FASEB J 17:2209–2220
11. Salomon RG (2005) Levuglandins and isolevuglandins: stealthy toxins of oxidative injury. Antioxid Redox Signal 7:185–201
12. Salomon RG, Kaur K, Batyreva E (2000) Isolevuglandin-protein adducts in oxidized low density lipoprotein and human plasma: a strong connection with cardiovascular disease. Trends Cardiovasc Med 10:53–59
13. Govindarajan B, Laird J, Salomon RG et al (2008) Isolevuglandin-modified proteins, including elevated levels of inactive calpain-1, accumulate in glaucomatous trabecular meshwork. Biochemistry (Mosc) 47:817–825
14. Zagol-Ikapitte I, Masterson TS, Amarnath V et al (2005) Prostaglandin H(2)-derived adducts of proteins correlate with Alzheimer's disease severity. J Neurochem 94:1140–1145
15. Fukuda K, Davies SS, Nakajima T et al (2005) Oxidative mediated lipid peroxidation recapitulates proarrhythmic effects on cardiac sodium channels. Circ Res 97:1262–1269
16. Stavrovskaya IG, Baranov SV, Guo X et al (2010) Reactive gamma-ketoaldehydes formed via the isoprostane pathway disrupt mitochondrial respiration and calcium homeostasis. Free Radic Biol Med 49:567–579
17. Charvet C, Liao WL, Heo GY et al (2011) Isolevuglandins and mitochondrial enzymes in the retina: mass spectrometry detection of post-translational modification of sterol-metabolizing CYP27A1. J Biol Chem 286: 20413–20422
18. Charvet CD, Laird J, Xu Y et al (2013) Posttranslational modification by an isolevuglandin diminishes activity of the mitochondrial cytochrome P450 27A1. J Lipid Res 54: 1421–1429
19. Pikuleva IA (2006) Cytochrome P450s and cholesterol homeostasis. Pharmacol Ther 112: 761–773
20. Heo G-Y, Bederman I, Mast N et al (2011) Conversion of 7-ketocholesterol to oxysterol metabolites by recombinant CYP27A1 and retinal pigment epithelial cells. J Lipid Res 52: 1117–1127
21. Omarova S, Charvet CD, Reem RE et al (2012) Abnormal vascularization in mouse retina with dysregulated retinal cholesterol homeostasis. J Clin Invest 122:3012–3023
22. Subbanagounder G, Salomon RG, Murthi KK et al (1997) Total synthesis of Iso[4]-levuglandin E2. J Org Chem 62:7658–7666
23. Pikuleva IA, Bjorkhem I, Waterman MR (1997) Expression, purification, and enzymatic properties of recombinant human cytochrome P450c27 (CYP27). Arch Biochem Biophys 343:123–130
24. Shevchenko A, Tomas H, Havlis J et al (2007) In-gel digestion for mass spectrometric characterization of proteins and proteomes. Nat Protoc 1:2856–2860
25. Lee MS (2012) Mass spectrometry handbook. Wiley, Hoboken, NJ

Chapter 22

Preoxiredoxin Family Members (Prx3 and Prx4) and Pregnancy Disorder (Recurrent Pregnancy Loss)

Behrouz Gharesi-Fard

Abstract

Placenta is a pregnancy unique tissue, and proper formation of placenta is a key phenomenal step for success of a pregnancy. Peroxiredoxins (Prxs) are a family of antioxidant proteins. This family is composed of six members, among which Peroxiredoxin 3 (Prx3) and Peroxiredoxin 4 (Prx4) are expressed by cytotrophoblast cells and play an important role in the implantation and a normal placentation through their antioxidant activities.

Although the presence of autoantibody against several peroxiredoxin family members was reported before, there was no report regarding the presence of antibodies against Prx3 or Prx4 in human pregnancy miscarriage. So for the first time we hypothesize and indicate that uncontrolled oxidative stress, due to anti-peroxiredoxins antibodies, may affect the proper formation of the placenta and lead to placentation-related pregnancy disorders such as miscarriage. Our results indicate that two placental proteins, Prx3 and Prx4, may act as new placental immune targets. Considering the role of antioxidant defense in the protection of placenta from oxidative stress, production of antibodies against peroxiredoxins 3 and 4 may introduce a new autoimmune hypothesis for miscarriages, which is needed to be tested in the future works.

Key words Peroxiredoxin 3, Peroxiredoxin 4, Placenta, Miscarriage

1 Introduction

Peroxiredoxins (Prxs) are a family of antioxidant proteins. In 1994, for the first time a family of thiolredoxin-dependent peroxidase reductase proteins was described [1]. This group of proteins is now known as peroxiredoxins family. Members of this family are antioxidant enzymes, which perform their antioxidative role by peroxidase activity as well as recovery and neutralization of hydrogen peroxide, nitrogen peroxide, and hydroperoxides [2]. This family is composed of six members, among which Peroxiredoxin 3 (Prx3) and Peroxiredoxin 4 (Prx4) are expressed by cytotrophoblast cells and play an important role in the implantation and a normal placentation through their antioxidant activities [2–5]. Peroxiredoxin 3 is expressed by different placental cells including cytotrophoblast,

Donald Armstrong (ed.), *Advanced Protocols in Oxidative Stress III*, Methods in Molecular Biology, vol. 1208,
DOI 10.1007/978-1-4939-1441-8_22, © Springer Science+Business Media New York 2015

deciduas, and stromal cells [5]. Several studies have shown the important role of Prx3 in normal placentation or defense against oxidative stress. Knockout mouse model for Prx3 shows pathological changes in placentation [6]. Peroxiredoxin 4 is also expressed by cytotrophoblast cells in human placenta [4]. Downregulation of Prx4 may affect trophoblast invasion and placenta formation and predispose women to pregnancy disorders such as miscarriage [7]. Oxygen tension is one of the major regulators of trophoblast cell proliferation and differentiation during placentation [8]. First-trimester placenta is under oxidative stress due to high oxygen tension in this period of placentation [9]. Antioxidative systems such as peroxiredoxin family members may play a critical role in the neutralization of the oxidative stress. While the presence of autoantibody against several peroxiredoxin family members was reported before [10, 11], there was no report regarding the presence of antibodies against Prx3 or Prx4 in human pregnancy miscarriage. So for the first time we hypothesize and indicate that uncontrolled oxidative stress, due to anti-peroxiredoxins antibodies, may affect the proper formation of the placenta and lead to placentation-related pregnancy disorders such as miscarriage [12].

2 Materials

2.1 Instruments and Kits

Ettan IPGphor II Isoelectric Focusing Unit, Amersham, USA.
Dual gel electrophoresis system, SCIE Plus, UK.
Image Scanner (Power Lux 1120 UFG), Amersham, USA.
Semidry blotter (Multiphor II) system, Pharmacia, USA.
Real-Time PCR system (7500 Fast), ABI, USA.
Microcentrifuge (5415R), Eppendorf, Germany.
Centrifuge (Universal 320R), Hettich, Germany.
Nitrogen Tank (XC47/11-6), MVE, USA.
Freezer (JD300L, −70 °C), Jahl, Iran.
Power supply (EPS 100), Paya Pajoohesh, Iran.
PH meter (T-7DE Digital), Horiba, Japan.
Spectrophotometer, Pharmacia, USA.
Deionized water producer (Direct Q3), Millipore, Germany.
Vortex, Clay Adams, USA.
Balance, Sartorius, Germany.
Electrophoresis system, Paya Pajoohesh, Iran.
U.V. Transilluminator, Sigma, USA.
MALDI-TOF/TOF 4800 Mass spectrometer ABI, USA.
ImageMaster 2D Platinum Software version 5, Amersham, USA.
Sampler 1–10, 10–100, 100–1,000 μl, Socorex, Switzerland.

In-Gel-Digest Kit (Millipore, USA) contains:

Vial 1: (25 mM ammonium bicarbonate, 5 % acetonitrile).

Vial 2: (25 mM ammonium bicarbonate, 5 % acetonitrile).

Vial 3: Trypsin resuspension solution (1 mM HCl).

Vial 4: Trypsin buffer (25 mM ammonium bicarbonate).

Vial 5: Trypsin.

Vial 6: Extraction/Wash solution (0.2 % TFA).

Vial 7: Elution Solution (0.1 % TFA, 50 % acetonitrile).

2-D Quant Kit, Amersham, UK.

cDNA synthesis kit (Fermentas) CinnaGen, Iran.

2.2 Placenta Samples

For collection of the placenta samples we used the following protocol:

1. Immediately after caesarian section, five different areas of the placenta were punched, each about 500 mg.
2. All five pieces were pooled.
3. The collected tissue was washed using cold normal saline in a sterile petri dish to eliminate any contaminating blood.
4. Protease inhibitor cocktail was used in washing solution to inhibit protease activities.
5. After three rounds of washing the remaining blood or saline was removed using a filter paper.
6. The washed tissue was aliquoted into five separated parts and stored in liquid nitrogen until extraction.

2.3 Serum Samples

All sera were aliquoted and kept at –70 °C until used.

3 Methods

3.1 Protein Extraction

Total protein from the placental tissue was extracted using the following protocol:

1. The placental samples were removed from nitrogen tank.
2. The weight of the tissue was measured and adjusted to 500 mg.
3. The tissue was powdered under N_2 gas, mixed and homogenized with a lysis buffer containing 8 M urea, 2 % CHAPS, 2 % DTT in Tris–HCl 5 mM (pH = 7.6). Five milliliters of lysis buffer was used for 500 mg of the placental tissue.
4. After 10 min incubation on ice, the samples were centrifuged at $15{,}000 \times g$ for 1 h at 4 °C.
5. The supernatant were collected, aliquoted, and stored at –70 °C until 2D-PAGE analysis.

3.2 Measuring the Protein Content

2-D Quant Kit (Amersham, UK) was used for the protein assay, because many of the reagents used in the preparation of protein samples for 2D-PAGE are incompatible with other protein assays such as Bradford and Lowry methods. This procedure is compatible with common sample preparation reagents such as DTT, 8 M urea, CHAPS, and IPG Buffer. The assay is based on the specific binding of copper ions to proteins. Precipitated proteins are resuspended in a copper-containing solution and unbound copper was measured with a colorimetric reagent.

1. A serial standard solution of BSA (0, 10, 20, 30, 40, 50 μg) and at least two dilutions of the sample were prepared (these dilutions must be fitted to standard curve).
2. 500 μl of precipitant solution was added to each sample and standard.
3. After vortexing the tubes were incubated for 2–3 min in room temperature.
4. For better precipitation 500 μl of the co-precipitant was added to each tube, briefly vortexed and centrifuged at 10,000 × *g* for 5 min.
5. Supernatants were decanted and the tubes were briefly centrifuged again and the remaining supernatants were removed using a micropipette.
6. 100 μl of copper solution plus 400 μl of deionized water was added to each tube and vortexed to dissolve precipitated proteins.
7. After adding 1 ml color reagent, the tubes were incubated at room temperature for 15–20 min.
8. Absorbances were read within 40 min at 480 nm using water as the reference.
9. At the end protein concentration of the samples were calculated by plotting a standard curve.

3.3 2D-PAGE

IPGphore II systems were used for isoelectric focusing (IEF). Linear precast 18 cm IPG strips (5–8) were used for IEF.

3.3.1 First Dimension Electrophoresis (Isoelectric Focusing)

1. A total volume of 340 μl protein mixtures including 8 M urea, 2 % CHAPS, 2 % DTT, 2 % IPG buffer, and 0.001 % bromophenol blue was applied on the IPG strips and covered by cover fluid.
2. The concentration of the protein sample is dependent on type of the IPG strip and staining method.
3. The best results concentration was obtained from 150–200 and 400–500 μg protein for silver and Coomassie blue staining gels respectively.
4. The strips were actively rehydrated for 16 h at 70 V.

5. After rehydration the strip cover fluid was changed and isoelectric focusing (IEF) was performed on the strips at 20 °C to reach appropriate voltage.
6. The strips were focused at total of 42,000–45,000.

3.3.2 Second Dimension Electrophoresis

The focused strips were equilibrated in equilibration buffer (6 M urea, 50 mM Tris–HCl pH 8.8, 30 % v/v glycerol, 2 % SDS, and 0.001 % bromophenol blue) containing 65 mM dithiothreitol (DTT) for 15 min at 37 °C followed by another 15 min incubation in equilibration buffer containing 135 mM iodoacetamide at room temperature.

A twin gel electrophoresis system (SCIE Plus, UK) was used for the second dimension.

1. The strips were placed on the top of a 15 % SDS-PAGE gel.
2. The strips were sealed using 0.5 % agarose and run first at a constant voltage of 50 V for 60 min followed with 200 V constant voltages for next 5–6 h until the bromophenol blue line reached the bottom of the gels.
3. For minimizing the variation, two gels were run and stained simultaneously.

3.4 Immunoblotting

After 2D-PAGE, protein spots were transferred to a PVDF membrane using a semidry blotter system (Amersham, UK).

1. PDVF membranes were equilibrated in absolute methanol for 30 s, and then washed with deionized water.
2. Blotting was performed under 1.5 mA current/cm^2 of the PVDF blot paper area for 75 min. For minimizing the variation, normal and cases placentas in each group were transferred simultaneously.
3. After transfer, the PVDF membranes were blocked with 3 % BSA in TBST buffer (500 mM NaCl, 20 mM Tris–HCl, 0.05 % Tween 20, pH = 7.5) overnight at 4 °C or 2 h at 37 °C.
4. After blocking, the membranes were incubated with 1/50 diluted sera (pooled sera from three to five different individuals) in TBST buffer at room temperature for 2 h or overnight at 4 °C.
5. The membranes were washed five times, each for 5 min in TBST buffer and the shaker speed was adjusted at 75 RPM.
6. Anti-human whole immunoglobulin or anti-human IgG (conjugated with horseradish peroxidase, Sigma, USA) 1/2,000 diluted in TBST buffer was used as secondary antibodies. The incubation time for conjugated antibodies was 1 h on a shaker.

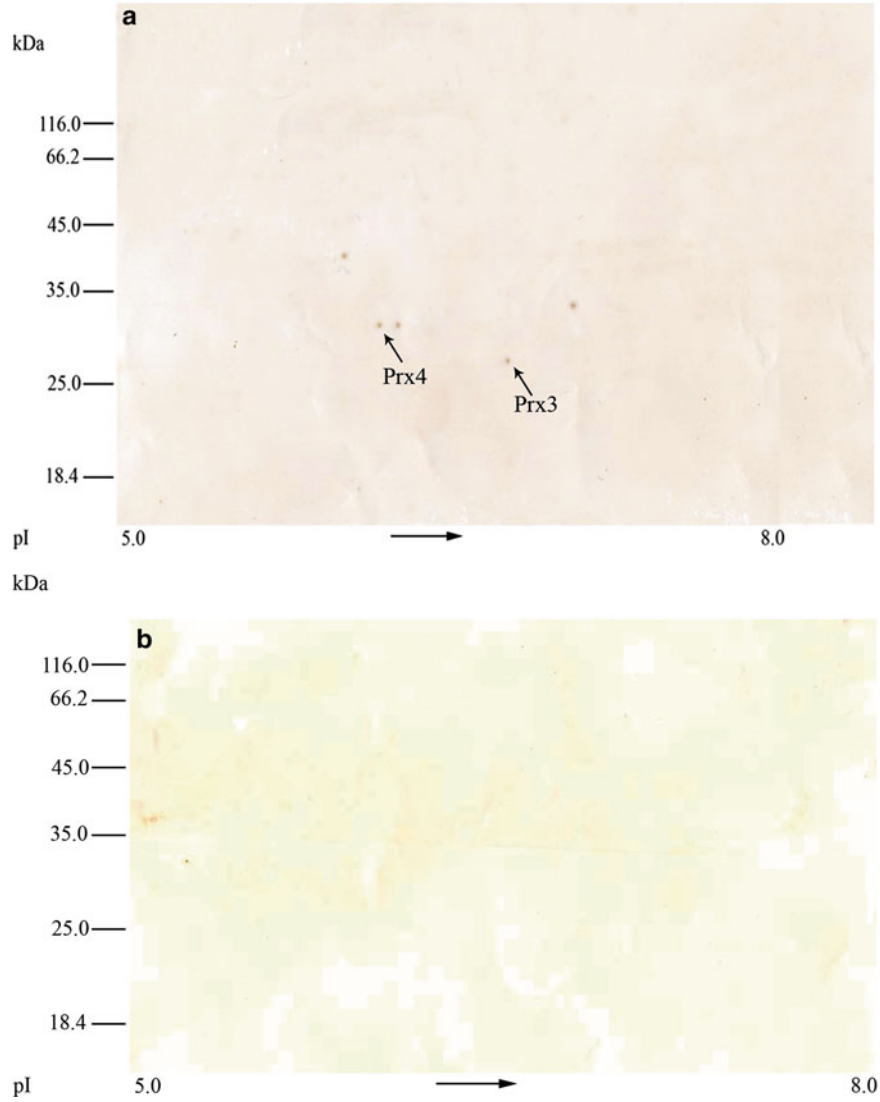

Fig. 1 Representative pictures of PVDF membranes (15 %, pI 5–8 linear) blotted with pooled sera. (**a**) Picture of a PVDF membrane blotted with pooled sera from recurrent pregnancy loss patients including all differentially blotted spots in which the location of Peroxiredoxin 3 and Peroxiredoxin 4 spots is indicated. (**b**) Picture of a PVDF membrane blotted with pooled sera from normal women excluding all differentially blotted spots

7. The membranes were then washed five times as previously noted.
8. SIGMAFAST 3,3′-diaminobenzidine (DAB, Sigma, USA) tablets were used to visualize of protein spots (Fig. 1). For minimizing the variation, normal and cases sera in each group were immunoblotted simultaneously.

3.5 Gel Staining

The gels were stained with silver nitrate [13] or colloidal Coomassie Brilliant Blue G-250 as previously described by Neuhoff et al. [14].

For silver nitrate staining, after 2D-PAGE:

1. The gels were fixed in a fixation solution containing 40 % methanol and 10 % acetic acid v/v for 15 min.
2. The fixation solution was changed and the gels were fixed again in the fresh fixation solution for 15 min (alternatively the gels might be fixed in fixation solution overnight).
3. After the fixation the gels were sensitized in a solution containing 25 % methanol, 6.8 % w/v sodium acetate, and 0.2 % sodium thiosulfate for 30 min.
4. The gels were then washed with Milli-Q water five times, each for 8 min. Fresh 2.5 % w/v silver nitrate solution prepared in Milli-Q water was used for staining. The gels were stained in staining solution for 20 min.
5. After staining the gels were washed twice with Milli-Q water, each about 1 min.
6. Fresh developing solution contained 2.5 % w/v sodium bicarbonate and 0.04 % v/v formaldehyde was used as developer.
7. After about 4 min, development was stopped using 1.5 % w/v EDTA as stopping solution.
8. The gels were kept in stopping solution for 10 min and then washed two times (each 5 min) with Milli-Q water.
9. After washing, the gels were scanned or stored in deionized water at 4 °C.

Colloidal Coomassie Brilliant Blue G-250 staining was based on Neuhoff et al. method [14].

1. The gels were washed briefly with Milli-Q water and stained overnight for the first round in a staining solution containing, 10 % w/v ammonium sulfate, 2 % v/v ortho-phosphoric acid, 0.125 % w/v Coomassie Brilliant Blue G-250, and 20 % v/v methanol (shaking the gels during incubation significantly will improve the staining result).
2. After the first round of staining, the gels were transferred into neutralizing solution contained, 0.1 M Tris–HCl (pH = 6.5, adjusted by phosphoric acid and incubated for 3 min).
3. Destaining was performed in 25 % v/v methanol for less than 1 min.
4. The gels were then transferred and remained in fixation solution containing 20 % w/v ammonium sulfate in Milli-Q water overnight.

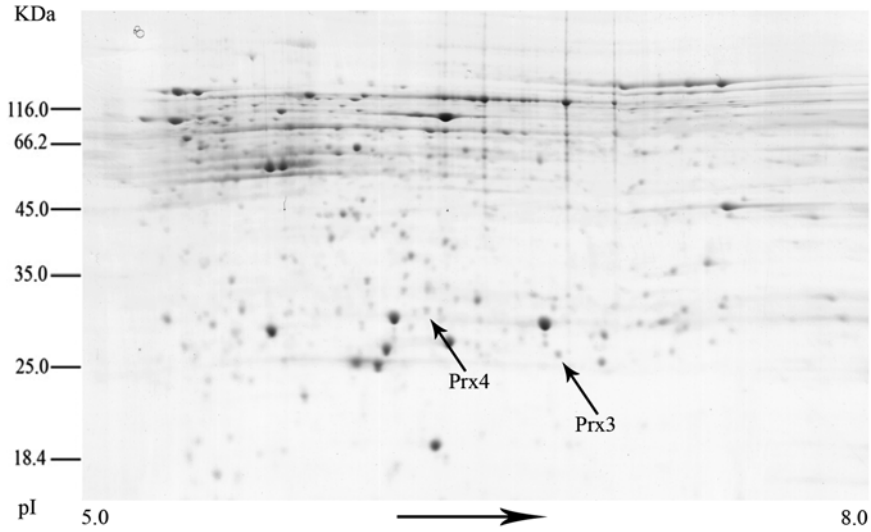

Fig. 2 Representative picture of a Coomassie Brilliant Blue-stained 2D-PAGE gel (15 %, pI 5–8 linear) in which two correspondence proteins related to spots in Fig. 1 (Peroxiredoxin 3 and Peroxiredoxin 4) are labeled

5. For obtaining the best staining result, the gels were stained in three rounds by repeating all the mentioned steps except the last one (fixation).
6. The gels were scanned immediately and stored in Milli-Q water for extremely 1 week before picking the desirable protein spots (Fig. 2).

3.6 Spot Picking and MALDI-TOF/TOF Analysis

Desirable protein spots were manually picked from colloidal Coomassie Blue stained gels using scalpel. The slices were placed into individual tubes and kept at −70 °C until performing mass analysis.

MALDI TOF/TOF technique was used for identification of the spots. Mass spectrometry analyses were performed in the Sir Henry Wellcome Functional Genomics Facility, University of Glasgow using the following protocol:

1. Destaining:
   The gels were diced into small pieces and placed into 1.5 ml micro tubes. The gel pieces were first washed with 25 mM ammonium bicarbonate (ABC) for 30 min at room temperature followed by twice washing in 50 % acetonitrile (ACN)/25 mM ammonium bicarbonate for 30 min. In each step the supernatants were discarded. Samples were dehydrated using 100 % ACN and supernatants were discarded (After dehydration, the gel pieces should shrink and appear white).
2. Reduction and alkylation:
   Fresh Dithiothreitol (DTT) and Iodoacetamide (IDD) were used for reduction and alkylation, respectively. At first 10 mM

DTT in 25 mM ABC was added to samples and incubated at 60 °C in a water bath for 60 min. After incubation supernatants were discarded and IDD solution (55 mM in 25 mM ABC) was added and incubated at room temperature in dark for 45 min. Supernatants were discarded and the gel pieces were washed with 25 m M ABC and then with 2 mM ABC/50 % ACN, each for 10 min. The gels were then dehydrated with 100 % ACN in 60 °C for 30 min.

3. Digestion and peptide extraction:
   The gel pieces were covered with trypsin (10 mg/ml in 25 mM ABC, 5 % ACN) and digestion was performed at 37 °C overnight. Liquid phase was collected and the gel pieces were washed for further 10 min with 50 % ACN/25 mM ABC and pooled with the first extract. The peptide extracts were dried and resuspended in 10 μl of 0.1 % trifluoroacetic acid (TFA).
4. Mass analysis:
   MALDI TOF/TOF technique was used for Mass analysis. Mass spectrometric analysis was performed in IDA mode (Analyst QS software, Applied Biosystems), selecting the four most intense ions for MS/MS analysis.

3.7 Database Search

Database search was based on the National Center for Biotechnology Information database (NCBI: http://www.ncbi.nlm.nih.gov) using the Mascot program search algorithm (http://www.matrixscience.com). Search settings allowed one missed cleavage with trypsin and two modifications (carbamidomethylation of cysteine and oxidation of methionine). The spots were considered to be successfully identified when at least five peptide masses were matched with a mass accuracy better than 30 ppm (part per million).

The mass accuracy (ppm) parameter indicates the difference between calculated and observed mass in Dalton. One ppm means 1/1,000,000 difference.

Moreover, MASCOT protein scores of greater than 66 were considered statistically significant ($p < 0.05$). MASCOT protein score value corresponds to a 5 % significant level and depends on database size. If the score of a spot exceeds this level, it means that the confidence interval for correct identification is above 95 %.

3.8 Western Blot Analysis for Confirming the Mass Results

To confirm the mass results, western blot technique was used for the detection of desirable protein spots (Prx3 and Prx4) using appropriate mAb (Abcam). For western blotting of each protein:

1. Two 2D gels were simultaneously run in a twin gel electrophoresis system (SCIE Plus, UK).
2. One gel was stained with CBB, while the other was transferred onto PVDF membrane using a semidry transfer system (Pharmacia).

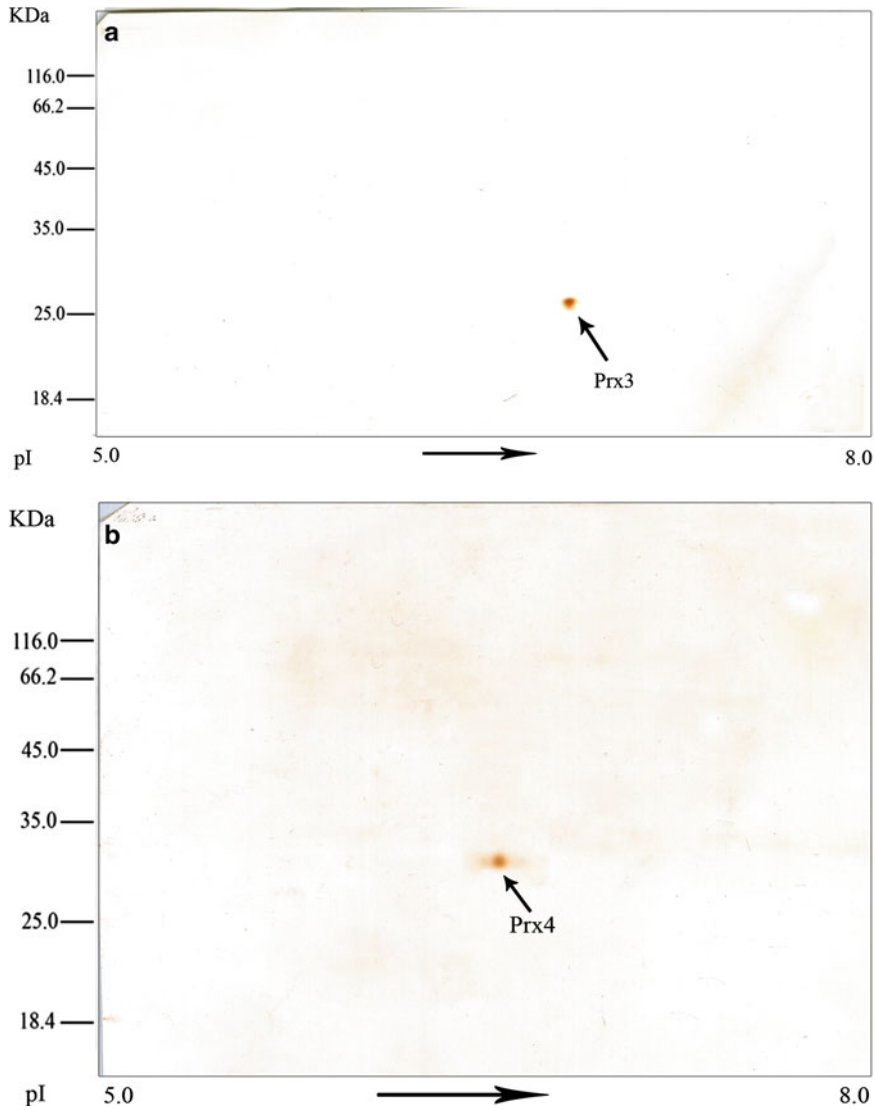

Fig. 3 Representative pictures of PVDF membranes (15 %, pI 5–8 linear) blotted with monoclonal antibody. (**a**) Picture of a PVDF membrane which is blotted with monoclonal antibody to Peroxiredoxin 3. (**b**) Picture of a PVDF membrane which is blotted with monoclonal antibody to Peroxiredoxin 4

3. The appropriate mAbs (ab40468 for Prx3 and ab93947 for Prx4; Abcam) were used for blotting of PVDF membrane-transferred protein spots.
4. Finally, the location of each blotted spot was compared with manually excised spot from CBB-stained gel (Fig. 3).

3.9 RT-PCR

To confirm the mass results we analyzed the presence of some selected differentially expressed proteins at mRNA levels, using RT-PCR technique.

3.9.1 RNA Extraction

Total RNA was extracted from placental samples using self-made guanidinium acid phenol–chloroform method. RNA extraction solution contained 4 M guanidinium thiocyanate, 25 mM sodium citrate, 0.5 % w/v lauroylsarcosine, 0.1 M 2-mercaptoethanol, pH 7.0. The procedure was as follows:

1. After removing the placenta sample from liquid nitrogen, 1 ml of RNA extraction solution was mixed with 50 mg of tissue in a 2 ml microtube and incubated at room temperature for 5 min.
2. 50 μl of sodium acetate (2 M, pH 4.0) was added and the tube was inverted to mix.
3. 500 μl of DEPC water saturated phenol was added and the tube was inverted to mix.
4. 200 μl chloroform was added and the tube was shook vigorously, incubated at room temperature for 2 min, and centrifuged at 13,000 × *g* for 20 min.
5. The top aqueous phase was transferred into a new tube and precipitated by isopropanol and washed in ethanol.
6. The concentration of RNA was measured by optical density using a Picodrop instrument.

3.9.2 cDNA Synthesis

cDNA was synthesized using cDNA synthesis kit (Fermentas, CinnaGen), using the following procedure:

1. One microgram of total RNA was mixed in a microtube with 0.5 μg random hexamer primer in DEPC water in a total of 12 μl final volume, mixed and incubated at 70 °C for 5 min.
2. The tube was chilled on ice, then 4 μl of 5× reaction buffer along with 1 μl Ribonuclease inhibitor plus and 2 μl of 10 mM dNTPs was added and incubated at 25 °C for 5 min.
3. 200 units of Reverse transcriptase enzyme was added into tube. The final tube volume was 20 μl.
4. The tube was incubated first at 25 °C for 10 min. This short incubation will facilitates primer annealing to the template and producing much longer cDNA molecules.
5. The tube was incubated at 42 °C for 60 min to enhance reverse transcriptase activity.
6. The reaction was stopped by heating the tube at 70 °C for 10 min and chilling on ice.

3.9.3 PCR

Polymerase chain reaction was done using a 5530 Eppendorf Master Cycler as thermal cycler. 18S rRNA was used as RNA extraction and cDNA synthesis control gene.

The sequences of primers and PCR conditions are presented in Table 1.

The amplified products were monitored by electrophoresis in 2–2.5 % agarose gel after GelRed staining (Fig. 4).

Table 1
RT-PCR condition and primer sequences

Gene	PCR conditions	Primer sequence
Peroxiredoxin 3	35 cycle: 94 °C 30 s, 57 °C 30 s, 72 °C 30 s, 250 ng cDNA, 200 µmol dNTP	5′-AGGTTCTGGTCTTGCACTAAGAGG-3′ 5′-GACGCTCAAATGCTTGATGACTCCA-3′
Peroxiredoxin 4	35 cycle: 94 °C 30 s, 57 °C 30 s, 72 °C 30 s, 250 ng cDNA, 200 µmol dNTP	5′-TCGAAGACAAGGAGGACTTGGGC-3′ 5′-AGAGACCTCTAAGAGTGTGGCCTG-3′
18S rRNA[a]	35 cycle: 94 °C 30 s, 57 °C 30 s, 72 °C 30 s, 250 ng cDNA, 200 µmol dNTP	5′-CTCAACACGGGAAACCTCAC-3′ 5′-AAATCGCTCCACCAACTAAGAA-3′

[a]From ref. [15]

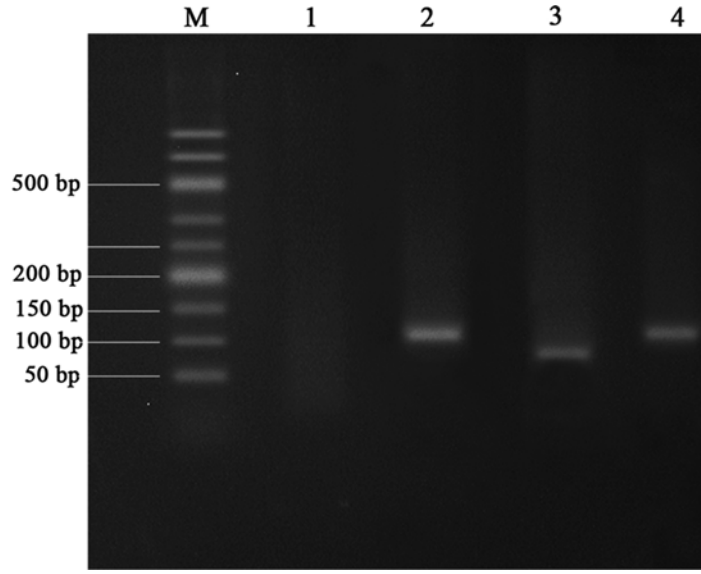

Fig. 4 Representative picture of an agarose gel (3 %) that indicates the electrophoresis results of reverse transcriptase polymerase chain reaction products for Peroxiredoxin 3 (Prx3), Peroxiredoxin 4 (Prx4), and 18S rRNA. *M*, size marker, *line 1*, negative control, *line 2*, 18S rRNA as positive control (114 bp), *line 3*, Prx3 (70 bp), and *line 4*, Prx4 (119 bp)

References

1. Chae HZ, Chung SJ, Rhee SG (1994) Thioredoxin-dependent peroxide reductase from yeast. J Biol Chem 269(44):27670–27678
2. Nelson KJ, Knutson ST, Soito L, Klomsiri C, Poole LB, Fetrow JS (2011) Analysis of the peroxiredoxin family: using active-site structure and sequence information for global classification and residue analysis. Proteins 79:947–964
3. Tavender TJ, Bulleid NJ (2010) Peroxiredoxin IV protects cells from oxidative stress by

removing H2O2 produced during disulphide formation. J Cell Sci 123:2672–2679

4. Hoang VM, Foulk R, Clauser K, Burlingame A, Gibson BW, Fisher SJ (2001) Functional proteomics: examining the effects of hypoxia on the cytotrophoblast protein repertoire. Biochemistry 40:4077–4086
5. Ejima K, Nanri H, Araki M, Koji T, Shibata E, Kashimura M, Ikeda M (2000) Expression of mitochondrial thioredoxin-dependent antioxidant protein, SP-22, in normal human and inflammatory mouse placentae. Placenta 21:847–852
6. Li L, Shoji W, Oshima H, Obinata M, Fukumoto M, Kanno N (2008) Crucial role of peroxiredoxin III in placental antioxidant defense of mice. FEBS Lett 582:2431–2434
7. Garrido-Gomez T, Dominguez F, Lopez JA, Camafeita E, Quinonero A, Martinez-Conejero JA, Pellicer A, Conesa A, Simon C (2011) Modeling human endometrial decidualization from the interaction between proteome and secretome. J Clin Endocrinol Metab 96:706–716
8. Bose P, Kadyrov M, Goldin R, Hahn S, Backos M, Regan L, Huppertz B (2006) Aberrations of early trophoblast differentiation predispose to pregnancy failure: lessons from the antiphospholipid syndrome. Placenta 27:869–875
9. Lash GE, Postovit LM, Matthews NE, Chung EY, Canning MT, Pross H, Adams MA, Graham CH (2002) Oxygen as a regulator of cellular phenotypes in pregnancy and cancer. Can J Physiol Pharmacol 80:103–109
10. Karasawa R, Ozaki S, Nishioka K, Kato T (2005) Autoantibodies to peroxiredoxin I and IV in patients with systemic autoimmune diseases. Microbiol Immunol 49:57–65
11. Iwata Y, Ogawa F, Komura K, Muroi E, Hara T, Shimizu K, Hasegawa M, Fujimoto M, Tomita Y, Sato S (2007) Autoantibody against peroxiredoxin I, an antioxidant enzyme, in patients with systemic sclerosis: possible association with oxidative stress. Rheumatology (Oxford) 46:790–795
12. Gharesi-Fard B, Jafarzadeh L, Ghaderi-shabankareh F, Zolghadri J, Kamali-Sarvestani E (2013) Presence of autoantibody against two placental proteins, peroxiredoxin 3 and peroxiredoxin 4, in sera of recurrent pregnancy loss patients. Am J Reprod Immunol 69(3):248–255
13. Yan JX, Wait R, Berkelman T, Harry RA, Westbrook JA, Wheeler CH, Dunn MJ (2000) Modified silver staining protocol for visualization of proteins compatible with matrix-assisted laser desorption/ionization and electrospray ionization-mass spectrometry. Electrophoresis 21:3666–3672
14. Neuhoff V, Arold N, Taube D, Ehrhardt W (1998) Improved staining of proteins in polyacrylamide gels including isoelectric focusing gels with clear background at nanogram sensitivity using Coomassie Brilliant Blue G-250 and R-250. Electrophoresis 9:255–262
15. Vanderlelie J, Gude NM, Perkins AV (2008) Antioxidant gene expression in preeclamptic placentae: a preliminary investigation. Placenta 29:519–522

Chapter 23

Substituted Pyridoindoles as Biological Antioxidants: Drug Design, Chemical Synthesis, and Biological Activity

Lucia Kovacikova, Magdalena Majekova, and Milan Stefek

Abstract

Great effort has been devoted to design and synthesize biologically active and pharmacologically acceptable antioxidants. Although a number of efficient antioxidant compounds have been designed, synthesized, and tested in animals, none of them have demonstrated sufficient efficacy in human clinical trials without undesirable side effects. Thus new pharmacologically applicable antioxidants have been sought for. Substituted pyridoindoles represent a broad spectrum of pharmacologically active substances including highly effective scavengers of reactive oxygen species. The hexahydropyridoindole scaffold represents a valuable lead with a great deal of knowledge on molecular mechanisms of free radical scavenging, on bioavailability and toxicity. Its modification may yield congeners tailored according to specific requirements for antiradical efficacy, lipophilicity, and basicity, meeting the aim of providing a pharmacologically practicable antioxidant drug as exemplified by the novel derivative SMe1EC2.

Key words Antioxidant, Pyridoindoles, γ-Carbolines, Oxidative stress, Scavenger, Free radical

1 Introduction

Treatment of free radical pathologies by antioxidants has been supported by studies in relevant animal models. Thus far, however, pharmacological use of antioxidants in the therapy of oxidative stress-related diseases has not found satisfactory application in clinical practice [1–15]. This may be due to an insufficient efficacy of the antioxidants available, their unsuitable pharmacokinetics, lack of selectivity, presence of adverse side effects, and their toxicity. New pharmacologically applicable antioxidants therefore are still in demand.

Substituted pyridoindoles (γ-carbolines) represent a broad spectrum of pharmacologically active substances with specific effect on the cardiovascular and nervous systems. Some of the substances from this structural cluster have been utilized in clinical practice, e.g., the antihistaminic drug dimebon, 2,8-dimethyl-5-[2-(6-methyl-3-pyridinyl)ethyl]-2,3,4,5-tetrahydro-1*H*-pyrido[4,3-b]

Donald Armstrong (ed.), *Advanced Protocols in Oxidative Stress III*, Methods in Molecular Biology, vol. 1208,
DOI 10.1007/978-1-4939-1441-8_23,

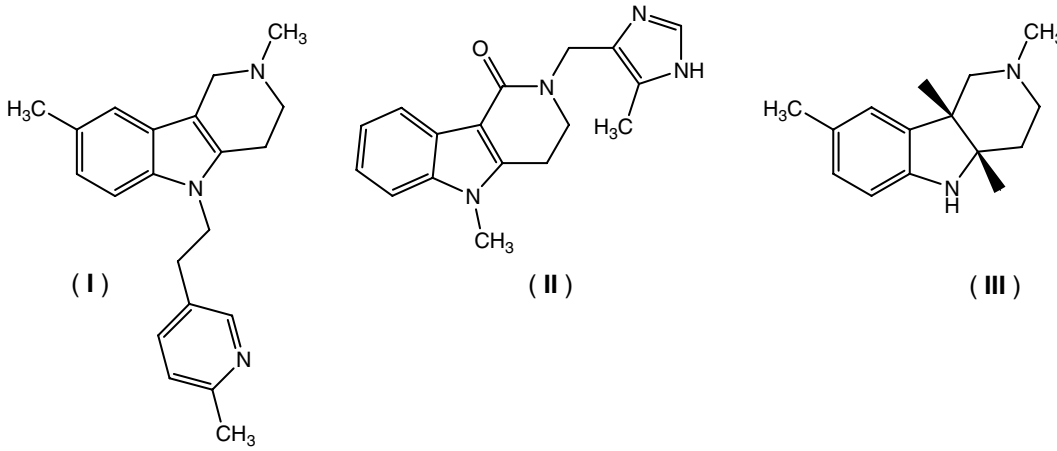

Fig. 1 Chemical structure of dimebon (**I**), alosetron (**II**), and stobadine (**III**)

indole (**I**, Fig. 1, ref. 16) alosetron, 2-[(5-methyl-4-imidazolyl) methyl]-2,3,4,5-tetrahydro-1H-pyrido[4,3-b]indole-1-one (**II**, Fig. 1, ref. 17), or the neuroleptic carbidine or its less toxic left-spinned enantiomer with specific antiarrhythmic effect—stobadine, (-)4a, 9b-(cis)-2,8-dimetyl-2,3,4,4a,5,9b-hexahydro-1H-pyrido[4,3-b] indole (**III**, Fig. 1, ref. 18).

Stobadine, originally developed and tested for its antiarrhythmic action [19], was soon recognized as an efficient antioxidant and free radical scavenger, including hydroxyl, peroxyl, and alkoxyl radicals, as well as an efficient quencher of singlet oxygen [20–31]. Pulse-radiolysis studies showed that one-electron oxidation of stobadine (**III**) resulted in deprotonation of the indoline nitrogen to give a resonance-stabilized nitrogen-centered radical [22]. Protective effects of stobadine were proved in a variety of experimental models of "free-radical diseases," including ischemic cardiovascular disorders, ischemia–hypoxia mediated cerebral damage, radiation injury, pseudohypoxic consequences of hyperglycemia under diabetes mellitus, etc. Stobadine was found to protect tissues from free radical-mediated injury via inhibiting oxidative damage to lipids, proteins, and nucleic acids [6].

Considering stobadine as a leading compound, a number of structurally related hexahydropyridoindole congeners have been designed, synthesized, and characterized [6]. Modification of the stobadine molecule by aromatic electron donating substitution was found to enhance the intrinsic free radical scavenging activity. Variation of the N2 substituent afforded a synthetically accessible way to modulate the biological availability without affecting significantly the free radical scavenging activity. In the group of substituted hexahydropyridoindoles, the findings on structure–activity relationships of the antioxidant protection of lipids and proteins are of particular importance. Knowledge on molecular mechanisms of free radical scavenging, along with the ability to predict oral

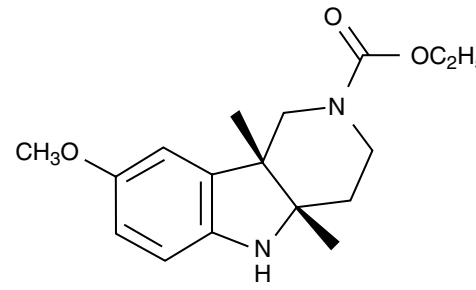

(IV)

Fig. 2 Chemical structure of SMe1EC2 (**IV**)

bioavailability and toxicity, renders stobadine-related pyridoindoles prospective agents for potential pharmacological interventions to treat free radical pathologies.

Among the novel derivatives, the compound SMe1EC2 (**IV**, Fig. 2) has been subject of extensive preclinical studies. It revealed significant neuroprotection in the murine model of acute head trauma [32, 33] and in vitro rat hippocampal slices exposed to transient hypoxia–reoxygenation [34–36]. Under conditions of experimental diabetes of rats, SMe1EC2 attenuated endothelial injury and restored the reduced endothelium mediated relaxation in diabetic animals [37]. SMe1EC2 improved the viability of HT22 neuronal cells in culture exposed to high glucose and attenuated indices of oxidative stress [38]. The compound protected efficiently rat pancreatic INS-1E β cell cultures against cytotoxic effects of hydrogen peroxide [39]. Preclinical toxicology tests revealed a remarkably low acute toxicity of SMe1EC2 in mice, regardless the way of administration [32]. Contrary to stobadine, SMe1EC2 did no possess any α-adrenolytic action [32]. In a prenatal developmental toxicity study in rats, SMe1EC2 demonstrated neither embryotoxic nor teratogenic effects on rat fetuses and no signs of maternal toxicity were found [40].

SMe1EC2 was projected with the aim to increase the free radical scavenging activity compared to the parent stobadine by substituting the aromatic methyl group by the more electron-donating methoxy group. At the same time, for the sake of bioavailability improvement, basicity decrease was achieved by replacement of the methyl substituent in position N2 by an appropriate acyl substituent, designed so that the lipophilicity of the parent molecule would not change significantly.

One of the most elaborated methods to prepare 2,3,4,5-tetrahydro-1H-pyrido[4,3-b] indoles is Fischer indole synthesis [41], which is based on the reaction of arylhydrazines and 4-piperidones in acid environment. The disadvantage of this method is the use of arylhydrazines, which are instable, highly toxic, and mutagenic. In the technological process their use puts

great demand on working safety and environment protection. The method yields uniform products only for symmetrically substituted arylhydrazines or 4-piperidones. The use of non-symmetric 3-substituted arylhydrazines leads to a non-selective reaction and to production of regioisomers [42]. In the case of 2-substituted derivatives, transposition and elimination of functional groups occur on the aromatic skeleton in position 2, in relation to hydrazine function [43]. These facts often complicate the isolation and decrease the yield of the product.

SMe1EC2 was found to rapidly react with DPPH, its activity being about three times higher than that of equimolar stobadine and comparable with that of the standard trolox (Fig. 3). DPPH, as a weak hydrogen atom abstractor, is considered a good kinetic model for peroxyl radicals [44]. In homogeneous cell-free systems, antioxidant activity reflects an intrinsic chemical reactivity towards radicals. In a group of structurally related antioxidants, the free radical scavenging activity can be predicted by means of quantum chemical calculations within the appropriate model as exemplified by structure–activity relationships found for a series of homologic pyridoindoles [45]. In this case, bond dissociation energy (BDE) of indoline hydrogen was found the most predictive parameter for DPPH scavenging. For SMe1EC2 the value of BDE was lower by 29.0 kJ/mol in comparison with stobadine, underlining more efficient scavenging of DPPH by SMe1EC2 (Fig. 3).

In membranes, however, the relative reactivity of antioxidants may be different since it is determined also by additional factors such as mutual location of the antioxidant and radicals at the

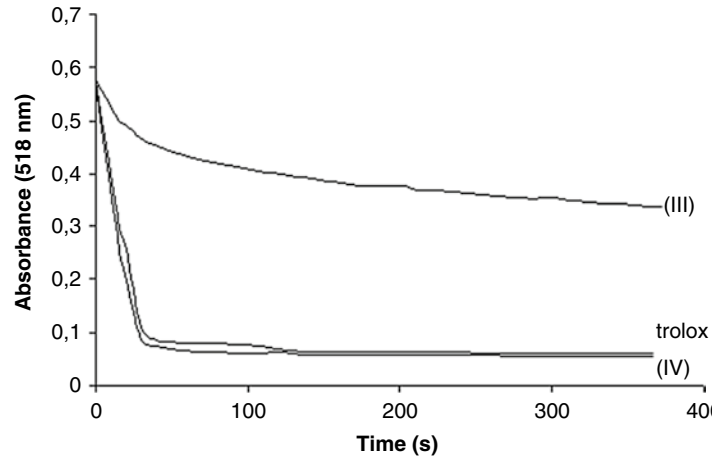

Fig. 3 Time dependence of absorbance decrease of ethanolic solution of DPPH radical (50 μM) in the presence of the antioxidant tested (50 μM) at $\lambda_{max} = 518$ nm. The figure shows the typical records obtained from spectrophotometer working in a kinetic mode preset to 15-s scanning interval. Adopted from ref. [48]

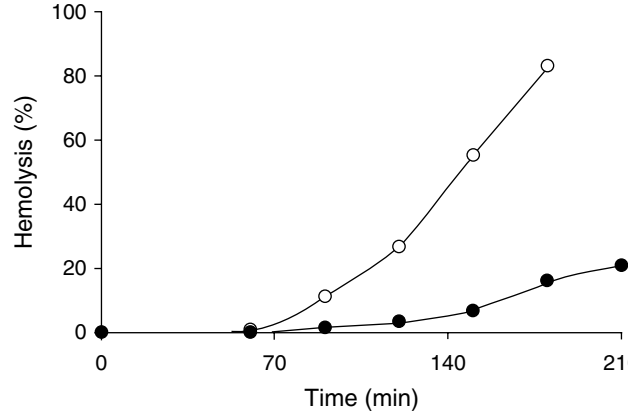

Fig. 4 Typical hemolysis curves induced by t-BuOOH. Erythrocyte suspensions (1.5 %) were incubated with 250 μM tBuOOH in the absence (*line with open circle*) or presence of 2.5 μM SMe1EC2. Record from two independent experiments. Adopted from ref. [48]

membrane, ruled predominantly by their actual distribution ratios between water and lipid compartments. Isolated rat erythrocytes were used as a cellular model to test the antioxidant action of SMe1EC2. Peroxidation of plasma membrane, eventually resulting in hemolysis, was induced by lipophilic t-BuOOH, generating peroxyl radicals intracellularly [46, 47]. At the concentrations studied, SMe1EC2 showed an inhibition period (lag phase) in the kinetic curves of hemolysis (Fig. 4).

The presence of a distinct lag phase is indication of a much higher reaction rate of antioxidant molecules with initiating radicals compared to the rate of chain propagation. SMe1EC2 exceeded stobadine in its antioxidant action when lipophilic t-BuOOH was used to initiate the hemolysis (Fig. 5).

When the hydrophilic azoinitiator AAPH was used to initiate hemolysis, SMe1EC2 was found significantly less efficient than stobadine [48]. To account for the apparent discrepancy, the variance of basicity of SMe1EC2 versus stobadine should be taken into consideration, as indicated below.

Obviously, when considering biological availability of a drug in general, the molecule has not only to be lipophilic enough, as characterized by the corresponding log*P*, but also neutral at the actual pH, to be able to penetrate into the lipid phase. Based on partition coefficients of SMe1EC2 and stobadine, their molecules are of a very similar lipophilicity, characterized by the respective log*P* values of 1.95 and 1.79 (calculated by the Palas software). At pH 7.4, however, with regard to the variance of basicity of the proton-binding center represented by the piperidine (N2) nitrogen, their actual distribution ratios may differ profoundly. The indoline nitrogen, with very low p*K*a (for stobadine $pK_{a_1} = 3.2$) [49], remains unprotonated at pH 7.4.

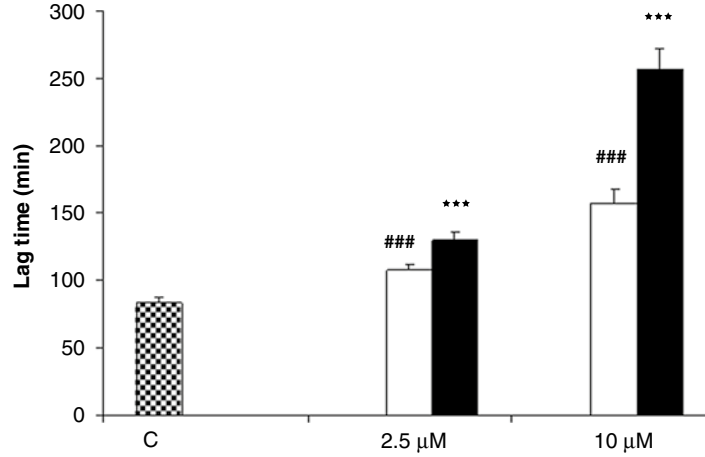

Fig. 5 SMe1EC2 (*filled bar*) and stobadine (*open bar*) protect rat erythrocytes against t-BuOOH-induced hemolysis. Results are presented as means ± SD from three to six experiments. $^{***}p < 0.001$ versus (▓) and (*open bar*), $^{###}p < 0.001$ versus (▓), parametric Student's *t*-test for independent samples. Adopted from ref. [48]

For stobadine, as a high basicity N-methyl derivative with $pKa_2 = 8.5$, [49], an acidobasic equilibrium with respect to the piperidine nitrogen is expected to be strongly shifted to its protonation at pH 7.4 (92.1 % participation of the protonated form as calculated for its $pKa_2 = 8.5$). The high degree of protonation of the N-methyl derivatives at physiological pH is expected to be reflected by low actual distribution ratios in spite of rather high partition coefficients (e.g., for stobadine, calculated $\log D = -0.05$ vs. $\log P = 1.95$; experimental $\log D = 0.57 \pm 0.03$ at pH 7.4) [23]. In contrast, for the SMe1EC2 molecule, the acyl substituent at N2 lowers the basicity of this site profoundly. According to calculations, its p*K*a value corresponding to piperidinic nitrogen may be expected to be around –3.7, while p*K*a of the indoline nitrogen remains as low as 5.4. Therefore the protonation of both nitrogens in SMe1EC2 is negligible at physiological pH, which is reflected by high actual distribution ratios at pH 7.4, reaching almost the value of the partition coefficient (calculated $\log D = 1.78$ vs. $\log P = 1.79$).

The above mentioned acidobasic equilibria of the compounds studied may have major consequences for their overall antioxidant action at cellular level. When peroxyl radicals were generated in the medium outside the red blood cells by thermal decomposition of the hydrophilic AAPH initiator, stobadine was found to be more efficient than SMe1EC2. On the other hand, when peroxyl radicals were generated inside the red blood cells, by degradation of the lipophilic t-BuOOH, it was SMe1EC2 that was found more protective compared to stobadine.

On balance then, a high antiradical efficacy of SMe1EC2, a novel hexahydropyridoindole derivative, was proved. Both in the DPPH test and in the system of t-BuOOH/isolated erythrocytes, which is considered a useful model for membrane perturbations characteristic of endogenously generated oxidative disorders, SMe1EC2 significantly exceeded the parent stobadine in its antioxidant action.

Considering the reported results of preclinical studies of SMe1EC2 showing its profound neuroprotective effects and low toxicity, the compound represents an example of a potential antioxidant drug. In addition, the present outcomes in the context of preceding findings indicate that the hexahydropyridoindole structure represents an interesting scaffold. Its modification may yield congeners tailored according to specific requirements for antiradical efficacy, lipophilicity, and basicity, meeting the aim of providing a pharmacologically practicable antioxidant drug.

2 Materials

2.1 Equipment

1. Centrifuge.
2. Spectrophotometer.

2.2 Reagents and Chemicals

Preparation of the tetrahydropyridoindole 3 *by Fischer indole synthesis (Reaction scheme on Fig. 6)*

2.2.1 Synthesis of SMe1EC2

1. Ethyl-4-oxopiperidine-1-carboxylate was obtained from Fluka.
2. 4-Methoxyphenylhydrazine was purchased from Avocado.
3. HCl, dichloromethane and ethanol were purchased from local commercial sources.
4. Pyridine was purchased from Sigma-Aldrich.
5. The mixture of 4-methoxyphenylhydrazine hydrochloride (**1**, 112 g, 0.643 mol) and ethyl-4-oxopiperidine-1-carboxylate (**2**, 110 g, 0.643 mol) in pyridine (207 ml) was refluxed under argone atmosphere during 6 h (*see* **Note 1**).

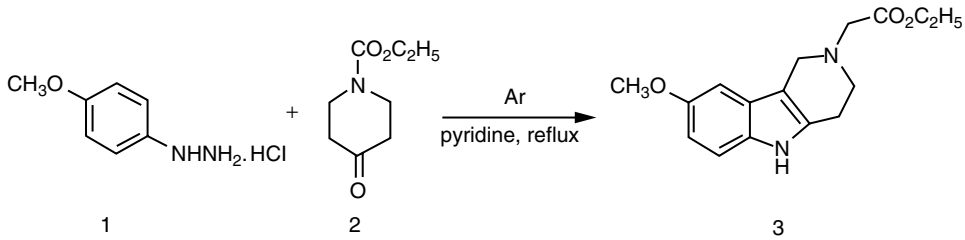

Fig. 6 Reaction scheme for Fischer indole synthesis of the unsaturated precursor (**3**) of SMe1EC2 (**IV**)

6. The developed NH_4Cl salt was filtered off, washed with pyridine and the filtrate was evaporated under reduced pressure to dryness.
7. The crude product was dissolved in CH_2Cl_2 (400 ml) and washed with water (3 × 100 ml, *see* **Note 2**).
8. The organic layer was dried ($MgSO_4$), concentrated under reduced pressure and crystallized from ethanol at −5 °C to give the product (**3**, 163.9 g, 92.9 %).
9. Structure identification: *mp* = 159–161 °C (EtOH). *Elementary analysis* $C_{15}H_{18}N_2O_2$ (Mw 274.29): calc (%) C 65.68, H 6.61, N 10.21 found (%) C 65.47, H 6.89, N 10.16. *MS m/z* (%) = 274 (M^+, 48), 245 (100), 229 (4), 201 (22), 173 (39), 158 (34), 130 (7), 103 (5), 77 (6). R_t = 9.414 min. *Purity* > 99 % (*see* **Note 3**). ^{1}*H-NMR* (300 MHz, $CDCl_3$, 25 °C): 1.30 (t, 3H, CH_3CH_2), 2.85 (t, 2H, H-4), 3.85 (bs, 5H, H-3, CH_3O), 4.20 (q, 2H, CH_2CH_3), 4.75 (s, 2H, H-1), 6.75 (d, 1H, H-9), 7.25 (d, 1H, H-6), 10.80 (s, NH). ^{13}*C-NMR* (75 MHz, DMSO-d_6, 25 °C): 14,80 (CH_3CH_2), 23.30 (C-4), 41.24 (C-1,C-3), 55.50 (CH_3O-8), 61.00 ($C\ H_2CH_3$), 99.70 (C-9), 105.60 (C-9b), 110.50 (C-7), 111.60 (C-6), 125.60 (C-4a), 131.00 (C-9a), 133.23 (C-5a), 153.31 (C-8), 155.30 (CO).

2.2.2 Preparation of the Hexahydropyridoindole SMe1EC2 (IV) by Reduction of the Tetrahydropyridoindole 3 (Reaction Scheme on Fig. 7)

1. Trifluoroacetic acid (TFA) was obtained from Sigma-Aldrich.
2. $NaBH_4$ was purchased from Sigma-Aldrich.
3. The magnetically stirred and cooled solution (−5 to 0 °C) of **3** (0.05 mol) in TFA (100 ml) was gradually added during a 1-h period by $NaBH_4$ (2.0 equiv.).
4. The reaction mixture was stirred for 30 min at 0 °C and then, after removing the cooling bath, the stirring was continued for 2.5 h at room temperature.
5. The reaction mixture was carefully poured into an ice-cold solution of NaOH (70 g) in water (105 ml), with the final pH being approx. 10.

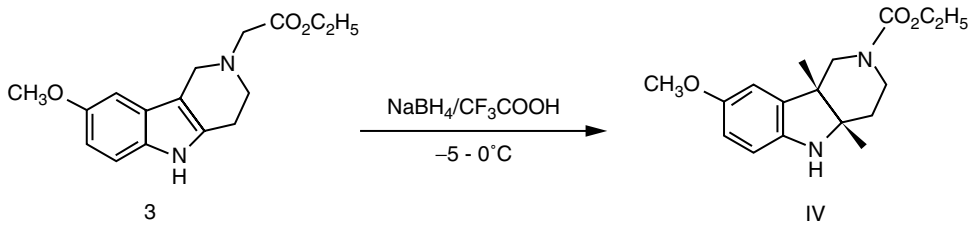

Fig. 7 Reaction scheme for reduction of compound **3** into SMe1EC2 (**IV**)

6. The product base was taken up in CH_2Cl_2 by repeated extraction. The combined organic phases were washed with brine, dried (anhydrous $MgSO_4$), filtered through a short column of silica gel and concentrated under reduced pressure to dryness.
7. The residue (1 g) was dissolved in dry ether (15 ml) and the solution was bubbled by gaseous HCl under stirring at −5 to 0 °C (*see* **Note 4**).
8. After finishing the reaction, the mixture was stirred at room temperature for 30 min and then let crystallize at −5 °C for 2 h (*see* **Note 5**).
9. The crystals were filtered, washed with a small volume of dry ether and dried at 90 °C during a 1-h period to give pure hydrochloride of **IV** (80.7 %).
10. Structure identification: *mp* = 82–84 °C (*n*-hexane for isolated base), 174–179 °C (MeOH/EtOH for hydrochloride salt). *Elementary analysis* for base $C_{15}H_{20}N_2O_3$ (Mw 276.33) and hydrochloride salt $C_{15}H_{21}ClN_2O_3$ (Mw 312.79): calc (%) C 57.60, H 6.76, N 8.95 found (%) C 57.36, H 7.02, N 8.74. *MS m/z* (%) = 276 (M^+, 100), 231 (4), 173 (50), 160 (46), 146 (12), 132 (12), 116 (38), 100 (12), 77 (7), 56 (12), 44 (42). R_t = 7.220 min. *Purity* > 99 % (*see* **Note 3**). *^{1}H-NMR* (300 MHz, DMSO-d_6, 60 °C): 7.24 (t, 3H, CH_3CH_2O), 7.74, 1.90 (m, m, 1H, 1H, H-4,4′), 3.26 (om, 1H, H-9b), 3.40 (om, 1H,H-1), 3.44 (om, 2H, H-3,3′), 3.72 (s, 3H, CH_3O), 3.79 (om, 1H, H-1′), 3.95 (m, 1H, H-4a), 4.71 (q, 2H, CH_3CH_2O), 5.32 (bs, 1H, NH), 6.57 (d, 1H, H-6), 6.67 (dd, 1H, H-7), 6.83 (d, 1H, H-9). *^{13}C-NMR* (75 MHz, DMSO-d_6, 60 °C): 14.61 (CH_3CH_2O), 27.16 (C-4), 38.77 (C-3), 40.54 (C-9b), 42.32 (C-1), 55.12 (CH_3O-8), 56.24 (C-4a), 60.41 (CH_3CH_2O), 109.25 (C-6), 110.37 (C-9), 112.68 (C-7), 131.54 (C-9a), 145.78 (C-5a), 151.85 (C-8), 154.90 (CO).

2.2.3 DPPH Test

1. DPPH was obtained from Sigma-Aldrich.
2. UV-grade ethanol was purchased from local commercial source.
3. Stobadine was synthesized at the Institute of Experimental Pharmacology and Toxicology, Slovak Academy of Sciences, and was available as a dihydrochloride.
4. Trolox was purchased from Sigma-Aldrich.

2.2.4 t-BuOOH Induced Hemolysis

1. *tert*-Butyl hydroperoxide (t-BuOOH) was purchased from Sigma-Aldrich.
2. Male Wistar rats, 8–9 weeks old, weighing 200–250 g, were used. The animals came from the Breeding Facility of the Institute of Experimental Pharmacology and Toxicology,

Dobra Voda (Slovak Republic). The study was approved by the Ethics Committee of the Institute and performed in accordance with the Principles of Laboratory Animal Care (NIH publication 83-25, revised 1985) and the Slovak law regulating animal experiments (Decree 289, Part 139, July 9th 2003).

2.2.5 Spartan '08 Program

1. Program was obtained from Wavefunction, Inc., Irvine, CA, 2009.

3 Methods

3.1 DPPH Test

1. Ethanolic solution of DPPH (50 μM) was incubated in the presence of a compound tested (50 μM; water solution, *see* **Note 6**) at laboratory temperature. The absorbance decrease at $\lambda_{max} = 518$ nm during the first 50-s interval was taken as a measure of the antiradical activity (*see* **Note 7**).

3.2 t-BuOOH Induced Hemolysis

1. To prepare packed erythrocytes, the animals in light ether anesthesia were killed by exsanguination of the carotid artery. The blood was collected in 3.8 % sodium citrate (1 vol. of sodium citrate: 9 vol. of blood) and centrifuged at $500 \times g$ for 15 min at 4 °C. Plasma and white blood cells were removed by aspiration (*see* **Note 8**).
2. The retrieved erythrocytes were washed three times with 6 vol. of ice-cold phosphate buffered saline (PBS, for composition *see* **Note 9**). The entire procedure was conducted at 0–4 °C. After the last washing, the red blood cells were used for further studies.
3. The hemolysis studies were performed in rat erythrocyte suspensions in PBS with the hematocrit of 1.5 %.
4. SMe1EC2 and stobadine were dissolved in PBS directly. Further dilutions were made with PBS. The compounds studied were added from stock solutions in PBS to the erythrocyte suspensions to the final concentrations as reported. Controls received an equivalent volume of PBS alone.
5. Mixtures were then pre-incubated for 30 min at 37 °C.
6. t-BuOOH (250 μM final concentration) was added to the samples and incubation continued at 37 °C up to 4 h.
7. Aliquots were withdrawn after different time periods and the reaction was terminated by cooling the suspensions in an ice bath, followed by centrifugation at $700 \times g$ for 10 min.
8. The degree of hemolysis was estimated by spectrophotometry of the hemoglobin released into the supernatant fraction (*see* **Note 10**).

9. The results were calculated as percentage of hemolysis. Total hemolysis (100 %) was obtained by incubation of control erythrocytes in 10 mM hypotonic phosphate buffer, pH 7.4 (1.9 mM NaH_2PO_4, 8.1 mM Na_2HPO_4) at 37 °C for 1 h.
10. Lag period was determined as an *x*-axis intersection of the ascending part of the semilogarithmic plot "hemolysis (%) versus log*t*".

3.3 Quantum Chemical Calculations

1. The optimal geometries of the compounds and their relevant indolyl radicals were obtained by the program package Spartan '08 (*see* **Note 11**).
2. The systematic MMFF94 (*see* **Note 12**) conformational search was performed for both molecules and subsequently the low conformers were reoptimized by the semiempirical AM1 (*see* **Note 13**) and then by DFT method using the B3LYP (*see* **Note 14**) functional and the 6-31G*basis set.
3. The piperidine ring was taken in the chair conformation with nitrogen in the equatorial position.
4. BDE values were obtained as a difference of the energy of the particular structure (E) and its relevant indolyl radical (E_R), i.e., $BDE = E - E_R$.

4 Notes

1. Ethyl-4-oxopiperidine-1-carboxylate was added slowly, under permanent mixing and cooling, during 15 min into the solution of 4-methoxyphenylhydrazine hydrochloride in freshly distilled and dried pyridine.
2. The washings were performed by using 10 % (w/w) water solutions of HCl (first), Na_2CO_3 (second), and NaCl (third).
3. Purity checked by gas chromatography under the following conditions: Hewlett Packard GC HP 5980 instrument. Column HP-5 (12 m × 0.2 mm × 0.33 μm). Splitless injection at 220 °C. Column temperature programed from 120 to 210 °C with gradient 30°/min; from 210 to 260 °C with gradient 10°/min and from 260 to 300 °C with gradient 30°/min. Mass detector MSD HP 5970B, temperature of detector 260 °C, carrier gas helium (0.2 ml/min).
4. Accidental insoluble particles were filtered off. Absolute dryness of ethanol and HCl is a must.
5. The mixture was let to reach ambient temperature before filtering.
6. SMe1EC2 and stobadine hydrochlorides were dissolved directly in distilled water. Trolox was suspended in distilled water and titrated with 5 mM KOH till complete dissolution.

7. During the 50-s interval used, an approximately linear decrease of DPPH absorbance was observed, which was considered a good assessment of the initial velocity of the radical reaction.
8. The erythrocyte suspensions used in the experiments were prepared daily.
9. Phosphate buffered saline (PBS) pH 7.4, consisted of 1.9 mM NaH_2PO_4, 8.1 mM Na_2HPO_4, and 150 mM NaCl.
10. Since a great deal of oxyhemoglobin degradation into methemoglobin occurs under t-BuOOH-induced free radical attack, empirical equations of Winterbourn [50] based on absorbance maxima at 577 nm and 630 nm were used for determination of total hemoglobin released as follows:

$$[\text{Total hemoglobin}] = [\text{Oxyhemoglobin}] + [\text{Methemoglobin}]$$
$$[\text{Oxyhemoglobin}] = 66A_{577} - 80A_{630}$$
$$[\text{Methemoglobin}] = 279A_{630} - 3A_{577}.$$

11. The starting structures were constructed by *Model Kit* of the program package Spartan '08 [51]. The piperidine ring was built manually to maintain the geometry in the chair conformation with nitrogen in the equatorial position, as it was observed by X-ray structural analysis for stobadine [52]. After the construction, the structures were undergone simple optimization (modul *E*—minimize, which occurs on panel menu).
12. The optimal conformers were calculated by conformational search in menu *Setup/Calculations* with Equilibrium Conformer chosen for *Calculate* window. The molecular mechanics method and force field MMFF94 [53] were chosen together with the key parameter SEARCHMETHOD = SYSTEMATIC for the *Options*. After the calculation, the optimal conformer was obtained.
13. The optimal conformers were firstly undergone by geometry optimization in the semiempirical method AM1 [54]. In menu *Setup/Calculations* value Equilibrium Geometry was chosen for Calculate window. Default values were kept for optimization limits (no key values in *Options* parameters). The pre-optimization with the semiempirical method was included in order to accelerate the last step of quantum-chemical calculations.
14. At last, the geometries were optimized by the DFT method using the B3LYP functional and the 6-31G*basis set [55]. Likewise with the calculations with semiempirical method, also this method was used with default values for optimization limits.

Acknowledgments

This study was supported by the grant VEGA 2/0067/11.

References

1. Bandyopadhyay D, Chattopadhyay A, Ghosh G, Datta A (2004) Oxidative stress-induced ischemic heart disease: protection by antioxidants. Curr Med Chem 11(3):369–387
2. Kovacic P, Somanathan R (2005) Neurotoxicity: the broad framework of electron transfer, oxidative stress and protection by antioxidants. Curr Med Chem-CNS Agent 5(4):249–258
3. Cherubini A, Ruggiero C, Morand C, Lattanzio F, Dell'Aquila G, Zuliani G, Di Iorio A, Andres-Lacueva C (2008) Dietary antioxidants as potential pharmacological agents for ischemic stroke. Curr Med Chem 15(12): 1236–1248
4. Aldini G, Vistoli G, Stefek M, Chondrogianni N, Grune T, Sereikaite J, Sadowska-Bartosz I, Bartosz G (2013) Molecular strategies to prevent, inhibit and degrade advanced glycoxidation and advanced lipoxidation end products. Free Radic Res 47 Suppl 1:93–137
5. Augustyniak A, Bartosz G, Cipak A, Duburs G, Horakova L, Luczaj W, Majekova M, Odysseos AD, Rackova L, Skrzydlewska E, Stefek M, Strosova M, Tirzitis G, Venskutonis PR, Viskupicova J, Vraka PS, Zarković N (2010) Natural and synthetic antioxidants: an updated overview. Free Radic Res 44(10): 1216–1262. doi:10.3109/10715762.2010.508495, Review
6. Juranek I, Horakova L, Rackova L, Stefek M (2010) Antioxidants in treating pathologies involving oxidative damage: an update on medicinal chemistry and biological activity of stobadine and related pyridoindoles. Curr Med Chem 17(6):552–570, Review
7. Carrizzo A, Forte M, Damato A, Trimarco V, Salzano F, Bartolo M, Maciag A, Puca AA, Vecchione C (2013) Antioxidant effects of resveratrol in cardiovascular, cerebral and metabolic diseases. Food Chem Toxicol. doi:10.1016/j.fct.2013.07.021
8. Yang Y, Karakhanova S, Werner J, Bazhin AV (2013) Reactive oxygen species in cancer biology and anticancer therapy. Curr Med Chem 20(30):3677–3692
9. Montero AJ, Jassem J (2011) Cellular redox pathways as a therapeutic target in the treatment of cancer. Drugs 71(11):1385–1396
10. Miller E, Wachowicz B, Majsterek I (2013) Advances in antioxidative therapy of multiple sclerosis. Curr Med Chem 20(37):4720–4730
11. Rosenbaugh EG, Savalia KK, Manickam DS, Zimmerman MC (2013) Antioxidant-based therapies for angiotensin II-associated cardiovascular diseases. Am J Physiol Regul Integr Comp Physiol 304(11):R917–R928
12. Zamora PL, Villamena FA (2013) Pharmacological approaches to the treatment of oxidative stress-induced cardiovascular dysfunctions. Future Med Chem 4:465–478
13. Musso G, Anty R, Petta S (2013) Antioxidant therapy and drugs interfering with lipid metabolism: could they be effective in NAFLD patients? Curr Pharm Des 19(29):5297–5313
14. Myung SK, Ju W, Cho B, Oh SW, Park SM, Koo BK, Park BJ, Korean Meta-Analysis Study Group (2013) Efficacy of vitamin and antioxidant supplements in prevention of cardiovascular disease: systematic review and meta-analysis of randomised controlled trials. BMJ 346:f10
15. Xu YJ, Tappia PS, Neki NS, Dhalla NS (2014) Prevention of diabetes-induced cardiovascular complications upon treatment with antioxidants. Heart Fail Rev 19(1):113–121
16. Shadurskij KS (1985) USSR patent 1 138 164
17. Baker DE (2005) Rationale for using serotonergic agents to treat irritable bowel syndrome. Am J Health Syst Pharm 62(7):700–711
18. Stolc S, Bauer V, Benes L, Tichy M (1983) Medicine with antiarrhythmic and antihypoxic activity and its method of preparation. Patents: CS 229 067, SWED. 8204693-9, BELG. 894148, SWISS 651 754, BRD P-3231088, SPAIN 553 017, JAP. 151 4040
19. Benes L, Stolc S (1989) Stobadine. Drugs Future 14:135–137
20. Ondrias K, Misik V, Gergel D, Stasko A (1989) Lipid peroxidation of phosphatidylcholine liposomes depressed by the calcium channel blockers nifedipine and verapamil and by the antiarrhythmicantihypoxic drug stobadine. Biochim Biophys Acta 1003:238–245
21. Stefek M, Benes L (1991) Pyridoindole stobadine is a potent scavenger of hydroxyl radicals. FEBS Lett 294:264–266

22. Steenken S, Sunquist AR, Jovanovic SV, Crockett R, Sies H (1992) Antioxidant activity of the pyridoindole stobadine. Pulse radiolytic characterization of one-electron-oxidized stobadine and quenching of singlet molecular oxygen. Chem Res Toxicol 5:355–360
23. Kagan VE, Tsuchiya M, Serbinova E, Packer L, Sies H (1993) Interaction of the pyridoindole stobadine with peroxyl, superoxide and chromanoxyl radicals. Biochem Pharmacol 45: 393–400
24. Horakova L, Briviba K, Sies H (1992) Antioxidant activity of the pyridoindole stobadine in liposomal and microsomal lipid-peroxidation. Chem Biol Interact 83(1): 85–93
25. Stefek M, Masarykova M, Benes L (1992) Inhibition of cumene hydroperoxide-induced lipid peroxidation by a novel pyridoindole antioxidant in rat liver microsomes. Pharmacol Toxicol 70:407–411
26. Stefek M, Trnkova Z (1996) The pyridoindole antioxidant stobadine prevents alloxan-induced lipid peroxidation by inhibiting its propagation. Pharmacol Toxicol 78:77–81
27. Kyselova Z, Rackova L, Stefek M (2003) Pyridoindole antioxidant stobadine protected bovine serum albumin against the hydroxyl radical mediated cross-linking in vitro. Arch Gerontol Geriatr 36(3):221–229
28. Stefek M, Kyselova Z, Rackova L, Krizanova L (2005) Oxidative modification of rat lens proteins by peroxyl radicals in vitro: protection by the chain-breaking antioxidants Stobadine and Trolox. Biochim Biophys Acta 1741(1–2): 183–190
29. Horakova L, Schaur RJ, Balgavy P, Egger G (1995) Interaction of stobadine with alkoxyl and stable free radicals. Redox Rep 1: 369–372
30. Misik V, Ondrias K, Stasko A (1999) EPR spectroscopy of free radical intermediates of antiarrhythmic-antihypoxic drug stobadine, a pyridoindole derivative. Life Sci 65(18–19):1879–1881
31. Rackova L, Stefek M, Majekova M (2002) Structural aspects of antioxidant activity of substituted pyridoindoles. Redox Rep 7(4):207–214
32. Stolc S, Povazanec F, Bauer V, Majekova M, Wilcox AL, Snirc V et al (2010) Pyridoindole derivatives with antioxidant properties: synthesis, therapy and pharmaceutical remedies. Slovak Patent Agency P 287506
33. Stolc S, Snirc V, Majekova M, Gasparova Z, Gajdosikova A, Stvrtina S (2006) Development of the new group of indole-derived neuroprotective drugs affecting oxidative stress. Cell Mol Neurobiol 26(7–8):1495–1504
34. Gasparova Z, Janega P, Babal P, Snirc V, Stolc S, Mach M et al (2009) Effect of the new pyridoindole antioxidant SMe1EC2 on functional deficits and oedema formation in rat hippocampus exposed to ischaemia in vitro. Neuro Endocrinol Lett 30:574–581
35. Gasparova Z, Ondrejickova O, Gajdosikova A, Gajdosik A, Snirc V, Stolc S (2010) Oxidative stress induced by the Fe2+/ascorbic acid system or model ischemia in vitro: effect of carvedilol and pyridoindole antioxidant SMe1EC2 in young and adult rat brain tissue. Interdiscip Toxicol 3:122–126
36. Gasparova Z, Snirc V, Stolc S (2010) The new pyridoindole antioxidant SMe1EC2 and its intervention in hypoxia/hypoglycemia-induced impairment of longterm potentiation in rat hippocampus. Interdiscip Toxicol 4: 56–61
37. Sotnikova R, Nedelcevova J, Navarova J, Nosalova V, Drabikova K, Szocs K et al (2011) Protection of the vascular endothelium in experimental situations. Interdiscip Toxicol 4:20–26
38. Rackova L, Snirc V, Jung T, Stefek M, Karasu C, Grune T (2009) Metabolism-induced oxidative stress is a mediator of glucose toxicity in HT22 neuronal cells. Free Radic Res 43: 876–886
39. Rackova L, Cumaoglu A, Bagriacik EU, Stefek M, Maechler P, Karasu C (2011) Novel hexahydropyridoindole derivative as prospective agent against oxidative damage in pancreatic β cells. Med Chem 7:711–717
40. Ujhazy E, Dubovicky M, Ponechalova V, Navarova J, Brucknerova I, Snirc V et al (2008) Prenatal developmental toxicity study of the pyridoindole antioxidant SMe1EC2 in rats. Neuro Endocrinol Lett 29(5):639–643
41. Robinson B (1982) The Fischer indole synthesis. Wiley, New York
42. Ockenden DW, Schofield K (1957) Indoles. Part V. The Fischer cyclisation of some meta-substituted arylhydrazones. J Chem Soc: 3175. doi: 10.1039/JR9570003175
43. Murakami Y, Watanabe T, Yokoyama Y et al (1993) Fischer indolization of variously ortho-substituted phenylhydrazones (Fischer indolization and its related compounds. XXV). Chem Pharm Bull 41(11):1910–1919
44. Blois MS (1958) Antioxidant determinations by the use of a stable free radical. Nature 181:1199–1200

45. Rackova L, Snirc V, Majekova M, Majek P, Stefek M (2005) Free radical scavenging and antioxidant activities of substituted hexahydropyridoindoles. Quantitative structure-activity relationships. J Med Chem 49(8):2543–2548
46. Trotta RJ, Sullivan SG, Stern A (1983) Lipid peroxidation and haemoglobin degradation in red blood cells exposed to t-butyl hydroperoxide. The relative roles of haem- and glutathione-dependent decomposition of t-butyl hydroperoxide and membrane lipid hydroperoxides in lipid peroxidation and haemolysis. Biochem J 212(3):759–772
47. Thornalley PJ, Trotta RJ, Stern A (1983) Free radical involvement in the oxidative phenomena induced by tert-butyl hydroperoxide in erythrocytes. Biochim Biophys Acta 759(1–2):16–22
48. Stefek M, Milackova I, Juskova-Karasova M, Snirc V (2013) Antioxidant action of the hexahydropyridoindole SMe1EC2 in the cellular system of isolated red blood cells in vitro. Redox Rep 18(2):71–75
49. Stefek M, Benes L, Zelnik V (1989) N-oxygenation of stobadine, a gamma-carboline antiarrhythmic and cardioprotective agent: the role of flavin-containing monooxygenase. Xenobiotica 19:143–150
50. Winterbourn CC (1990) Oxidative reactions of hemoglobin. Methods Enzymol 186: 265–272
51. Shao Y, Molnar LF, Jung Y, Kussmann J, Ochsenfeld C, Brown ST, Gilbert ATB, Slipchenko LV, Levchenko SV, O'Neill DP, DiStasio RA Jr, Lochan RC, Wang T, Beran GJO, Besley NA, Herbert JM, Lin CY, Van Voorhis T, Chien SH, Sodt A, Steele RP, Rassolov VA, Maslen PE, Korambath PP, Adamson RD, Austin B, Baker J, Byrd EFC, Dachsel H, Doerksen RJ, Dreuw A, Dunietz BD, Dutoi AD, Furlani TR, Gwaltney SR, Heyden A, Hirata S, Hsu C-P, Kedziora G, Khalliulin RZ, Klunzinger P, Lee AM, Lee MS, Liang WZ, Lotan I, Nair N, Peters B, Proynov EI, Pieniazek PA, Rhee YM, Ritchie J, Rosta E, Sherrill CD, Simmonett AC, Subotnik JE, Woodcock HL III, Zhang W, Bell AT, Chakraborty AK, Chipman DM, Keil FJ, Warshel A, Hehre WJ, Schaefer HF, Kong J, Krylov AI, Gill PMW, Head-Gordon M (2006) Advances in methods and algorithms in a modern quantum chemistry program package. Phys Chem Chem Phys 8(27):3172–3191, Spartan '0 8. Irvine, CA: Wavefunction; Inc.; 2009; http://www.wavefun.com/products/spartan.htm
52. Kettmann V, Benes L, Tichy M (1985) (-)-Cis-2,8-dimethyl-1,2,3,4,4A,9b-hexahydro-2h-pyrido[4,3-b]indolium(S,S)-2,3-Di-O-Benzoyltartrate(2-). A new antiarrhythmic drug. Acta Cryst C 41(2):208–210
53. Halgren TA (1996) Merck molecular force field. I. Basis, form, scope, parameterization, and performance of MMFF94. J Comput Chem 17(5–6):490–519
54. Dewar MJS, Zoebisch EG, Healy EF, Stewart JJP (1985) Development and use of quantum mechanical molecular models. 76. AM1: a new general purpose quantum mechanical molecular model. J Am Chem Soc 107(13): 3902–3909
55. Becke AD (1993) Density-functional thermochemistry. III. The role of exact exchange. J Chem Phys 98(7):5648–5652

Chapter 24

Measuring Antioxidant and Prooxidant Capacity Using the Crocin Bleaching Assay (CBA)

Stella A. Ordoudi and Maria Z. Tsimidou

Abstract

The Crocin Bleaching Assay (CBA) appears in literature as an in vitro method for measuring antioxidant and prooxidant capacity of model dietary antioxidants, food formulations, pharmaceuticals, and biological samples. The assay is based on simple competitive reactions between a colored probe, crocin, and the test compounds/constituents for scavenging peroxyl radicals generated after thermolysis of a water-soluble azo-initiator. So far, several researchers in the fields of food chemistry, nutrition and clinical biochemistry have sporadically addressed critical views about advantages, limitations and potential field of CBA application. This chapter presents step-by-step critical aspects of CBA in order to assist standardization of its performance. Detailed procedures for calculation of two attributes of peroxyl radical scavenging reactions, the relative rate constant and "total antioxidant capacity", are also presented.

Key words Peroxyl radical scavenging, Crocin bleaching, Total antioxidant capacity, Phenolic antioxidants

Abbreviations

ABTS	2,2′-Azino-bis(3-ethylbenzothiazoline-6-sulphonic acid)
AE	Antiradical efficiency
AUC	Area under curve
DPPH	1,1-Diphenyl-2-picrylhydrazyl
EC_{50}	Efficient concentration for scavenging 50 % of DPPH radical
ORAC	Oxygen radical absorbance capacity
PDO	Protected designation of origin
RP-HPLC	Reversed phase high performance liquid chromatography
TEC_{50}	Time required to reach EC50
UV–Vis	Ultraviolet–visible

Donald Armstrong (ed.), *Advanced Protocols in Oxidative Stress III*, Methods in Molecular Biology, vol. 1208,
DOI 10.1007/978-1-4939-1441-8_24,

1 Introduction

Among the methods that are based on competitive reactions and are currently appraised for assessment of antioxidant and prooxidant capacity, the beta-carotene and the crocin bleaching assays are the only ones that utilize carotenoids as probes of oxidation. In particular, the Crocin Bleaching Assay (CBA) can be performed in both aqueous and non-aqueous environment using an appropriate azo-initiator, which is thermally decomposed to produce peroxyl radicals at a constant rate [1–7]. The majority of CBA applications concern hydrophilic radical scavengers (pure compounds, plant polar extracts and biological fluids). For this reason, this chapter presents step-by-step critical aspects of this assay in order to assist standardization of its performance.

In principle, peroxyl radicals, formed by thermal decomposition of azo-initiators in the presence of oxygen, react with *crocin*. Under this collective name, a mixture of structurally similar yellow-orange esters of crocetin (8,8′-diapocarotene-8,8′-dioic acid) with sugar and/or methyl moieties is expected. When the source of crocins is saffron, i.e., the dried stigmas of *Crocus sativus* L. used worldwide as a spice [8], the major compound (>60 %) is crocetin-di-β-D-gentiobioside or crocin 1 (Fig. 1).

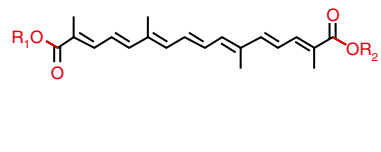

all-*trans*-

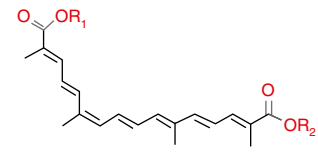

13-*cis*-

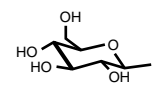

β-D-glucosyl- (A)

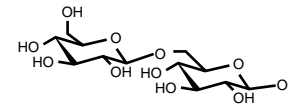

β-D-gentiobiosyl- (B)

Group	Crocetin ester
$R_1 = R_2$= **B**	*trans*- or *cis*- di-(β-D- gentiobiosyl) (crocin l)-
R_1 = **B,** R_2= **A**	*trans*- or *cis*- (β-D- gentiobiosyl)-(β-D- glucosyl)-
$R_1 = R_2$= **A**	*trans*- or *cis*- di -(β-D- glucosyl)-
R_1 = **B,** R_2= **H**	*trans*- or *cis*- mon -(β-D- gentiobiosyl)-
R_1 = **A,** R_2= **H**	*trans*-mon-β-D- glucosyl-
$R_1 = R_2$= **-CH_3**	di -methyl-
R_1 = **H**, R_2 = **H**	**crocetin**

Fig. 1 Major crocetin esters that are present in CBA probe solution [9]

The result of the reaction is the disruption of the extended system of conjugated double bonds. Bleaching (loss of color) follows mainly three mechanistic routes; electron transfer, hydrogen atom abstraction and adduct formation as described in reactions 1 [10, 11] (where ROO•: peroxyl radicals)

$$\begin{aligned} &\mathrm{ROO}^{\bullet} + \mathrm{CAR(H)} \rightarrow \mathrm{ROO}^{-} + \mathrm{CAR}^{\bullet+} \\ &\mathrm{ROO}^{\bullet} + \mathrm{CAR(H)} \rightarrow \mathrm{ROOH} + \mathrm{CAR}^{\bullet} \\ &\mathrm{ROO}^{\bullet} + \mathrm{CAR} \rightarrow \mathrm{ROO{-}CAR}^{\bullet} \end{aligned} \quad (1)$$

Loss of color is monitored at 440 nm. Strong radical scavengers competitively intercept the peroxyl radicals, leading to a reduction in the rate of crocin bleaching. In contrast, strong oxidative species may induce discoloration of the probe. The overall bleaching rate can be thus, calculated; In particular, the bleaching rate in the absence of antioxidants (V_0) is described as $V_0 = k_{crocin} \times [\mathrm{ROO}^{\bullet}] \times [\mathrm{crocin}]$ whereas in the presence of test antioxidants (V) becomes $V = V_0 \times \frac{k_{\mathrm{crocin}} \times [\mathrm{crocin}]}{k_{\mathrm{crocin}} \times [\mathrm{crocin}] + k_{\mathrm{AOX}} \times [\mathrm{AOX}]}$. The effect of the test compounds is generally evaluated by testing conformity of these values to a simple competitive kinetic model according to which $\frac{V_0}{V} = 1 + \frac{k_{\mathrm{AOX}}}{k_{\mathrm{crocin}}} \times \frac{[\mathrm{AOX}]}{[\mathrm{crocin}]}$ (Stern–Volmer equation) where [AOX] and [crocin] are the concentrations of the tested antioxidant and crocin, and k_{AOX} and k_{crocin} are rate constants for reaction of the ROO• radicals with AOX and with crocin, respectively. Results can be then expressed as relative rate constant or as percentage of inhibition [12, 13].

With regard to antioxidant activity assessment, *reactivity* and *capacity* of test antioxidants and/or radicals deriving from parent compounds are considered as two distinct terms. Roginsky and Lissi [14] stated that "reactivity characterizes the starting dynamics of antioxidation at a certain concentration of an antioxidant or antioxidant mixture" whereas "capacity gives the information about the duration of antioxidative action." CBA reactions that are consistent with the Stern–Volmer competition kinetic model allow a good estimation of k_{rel} values. CBA describes peroxyl radical reactivity better than other probe-based assays that utilize only one concentration of antioxidants [15], or are based on more complex kinetic models that result in information of no clear physical meaning [16]. Apart from reactivity, the "total antioxidant capacity" of complex mixtures can be assessed using a modified CBA protocol. A procedure proposed for the assessment of the prooxidant capacity of food constituents involves their reaction with crocin in the absence of radical initiators.

In this case, results are expressed as the ratio between reduction in absorbance for a given time interval ($\Delta A_{5\text{min}}$) and sample weight (g) or concentration (g/L) [17–19].

CBA shows a strong potential for adaptation to automate, high-throughput analysis as well as for hyphenation with HPLC technique [20, 21]. In comparison to the beta-carotene bleaching assay, CBA is based on a simple competitive reaction model that can be used to obtain quantitative and reproducible results [14, 22]. Its low frequency of use is based on two attributes that are considered as drawbacks. The concern that crocin being a mixture of compounds rather than a pure one will be alleviated in this work. The fact that crocin absorbs light at 430–440 nm, where other food constituents may also absorb is a realistic limitation similar to those for other radical scavenging assays [23].

2 Materials

2.1 Instrumentation

1. Dual beam UV–Vis spectrophotometer equipped with a temperature control device and software for automatic data recording, storage, and treatment. Plastic, glass, or quartz (1 cm pathlength) cuvettes.
2. HPLC system equipped with a UV–Vis or a Diode-array detector and a RP C18, 4 μm column (125 mm×4 mm i.d.) [e.g., Superspher 100 or equivalent].
3. pH meter (0.01 pH resolution).

2.2 Reagents

1. Any commercial raw saffron or commercially available crocin preparation of guaranteed authenticity (e.g., PDO "Krokos Kozanis," www.saffran.gr) or laboratory-purified crocin-1 (*see* **Note 1**).
2. 2,2′-azobis (2-amino-propane) dihydrochloride, (AAPH, >98 %) (e.g., Fluka Chemie, Buchs, Switzerland).
3. Ultrahigh purity water of maximum 5.5 μS/cm conductivity at 25 °C (e.g., Millipore Milli-Q system).
4. Phosphate buffered saline (PBS) (0.01 M, pH 7.4).
5. HPLC-grade methanol and acetonitrile (e.g., Riedel de Haën, Seelze, Germany).
6. Diethyl ether (stabilized with ethanol, free from butylated hydroxytoluene, peroxides or any other prooxidant/antioxidant) (e.g., Panreac Química, Barcelona, Spain).
7. 6-Hydroxy-2,5,7,8-tetramethylchroman-2-carboxylic acid (Trolox, 97 %) (e.g., Aldrich Chemical Co, Steinheim, Germany).

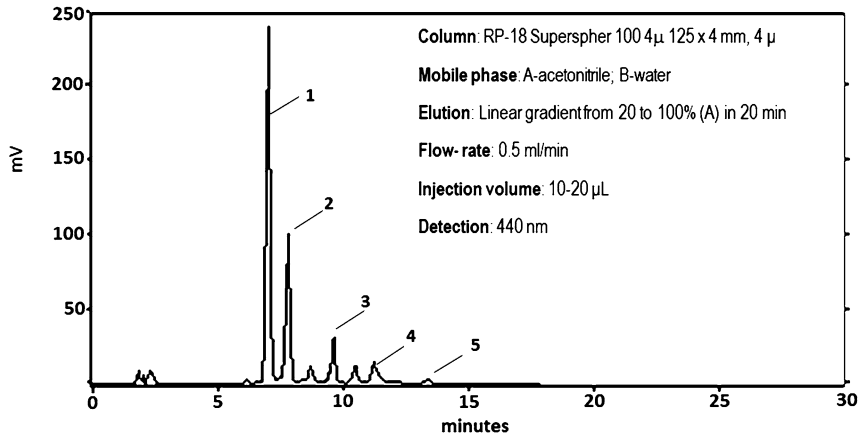

Fig. 2 Typical HPLC profile of saffron aqueous or methanol extracts at 440 nm. (1) *trans*-di-(β-D-gentiobiosyl) crocetin (crocin-1); (2) *trans*-(β-D-gentiobiosyl)-(β-D-glucosyl)crocetin; (3) *cis*-di-(β-D-gentiobiosyl)crocetin; (4) *trans*-mono-β-D-gentiobiosyl crocetin; (5) *trans*-mono-β-D-glucosyl crocetin. (adapted with permission from ref. 13. Copyright (2006) American Chemical Society)

3 Methods

3.1 Probe Preparation

3.1.1 Purity Control and Cleanup Procedure of Saffron Powder

1. In case of unlabelled saffron material, examine the HPLC profile of aqueous or methanol extracts at 440 nm according to the conditions shown in Fig. 2. A typical HPLC profile of authentic saffron at 440 nm is shown in the same figure.
2. Grind ~1 g of dehydrated red stigmas in a spice blender to obtain a fine powder (<500 μ). Sample handling should be done away from direct exposure to light. Storage in dark-colored or foil-covered glassware is strongly recommended.
3. Place 0.5 g saffron powder in a heart-shaped flask, add 15 mL diethyl ether, vortex for 5 min to extract impurities and decant the supernatant. Repeat washing process twice more.
4. Remove residual ether from the saffron residue by evaporation under a nitrogen stream to obtain purified saffron.

3.1.2 Preparation of Working Solution

1. Suspend purified saffron in 25 mL methanol (HPLC grade), vortex for 5 min and filter through a PTFE syringe filter (0.45 μm porous size). Methanol is suggested as the solvent of choice since it ensures satisfactory crocin yield, easier solvent removal under reduced pressure, and avoidance of mold growth.
2. Store the filtrate at −18 °C for a maximum of 1 month and use as the crocin stock solution.
3. Transfer 1 mL of crocin stock solution into a glass container and dilute with approximately 50 mL of methanol in order to prepare the crocin working solution A. Follow the next steps to adjust the concentration.

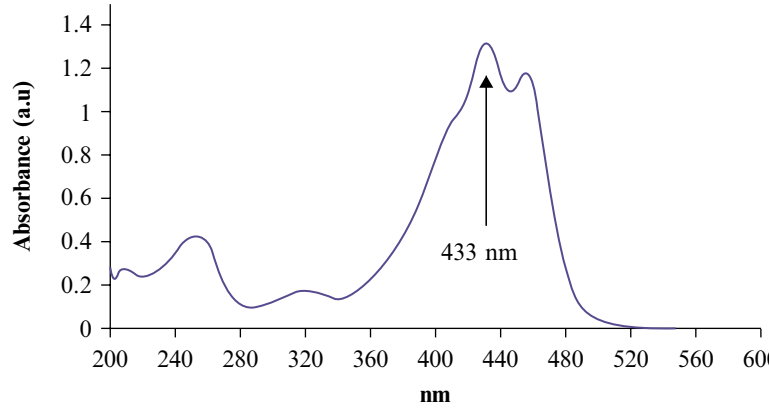

Fig. 3 Typical UV–Vis profile of the *crocin* working solution in methanol ([crocin] = 10 μM)

4. Remove an aliquot of the working solution A and dilute with methanol by 1:10 v/v (working solution B) in order to measure the absorbance value at 433 nm (*see* **Note 2**).
5. Calculate crocin concentration from the Lambert-Beer equation ($A = \varepsilon \times b \times C$) using extinction coefficient ε_{MeOH} = 133,000 M^{-1} cm^{-1} (λ_{max} = 433 nm) [24]. Do not use the extinction coefficient for crocin in water $\varepsilon_{H_2O} = 89{,}000 M^{-1} cm^{-1}$ (λ_{max} = 440 nm) [25]. As long as A_{433} value falls between 1.27 and 1.39 (a.u) (or $A_{450} \sim 1.10$) crocin concentration in the working solution B will be 10 ± 0.5 μM. The working solution A is now suitable for use with no need for volume adjustment. A typical UV–Vis spectrum of a methanolic solution containing 10 μM of crocin is shown in Fig. 3.
6. If $A_{433} > 1.39$ (a.u): dilute working solution A accordingly and repeat **step 5**.
7. If $A_{433} < 1.27$ (a.u.): add a small aliquot of *crocin* stock solution to the working solution A and repeat **step 5**.

3.2 Preparation of the Azo-Initiator Solution

The AAPH reagent should be stored frozen (−18 °C) and dry (seal with moisture-impermeable tape).

1. Prepare phosphate buffered saline (PBS) solution (0.01 M, pH 7.4): Weigh 0.24 g KH_2PO_4, 1.44 g Na_2HPO_4, 0.2 g KCl, and 8 g NaCl and transfer to a 1 L volumetric flask. Fill the flask with ultrahigh purity water. pH value will normally vary between 7.4 ± 0.6 % (n = 7) without adjustment. Store PBS solution at 4 °C and use it within 1 month. Check pH before each use and adjust as necessary.
2. Weigh 0.339 g AAPH (or 0.05 g for the microplate-based assay) into a 10 mL volumetric flask.

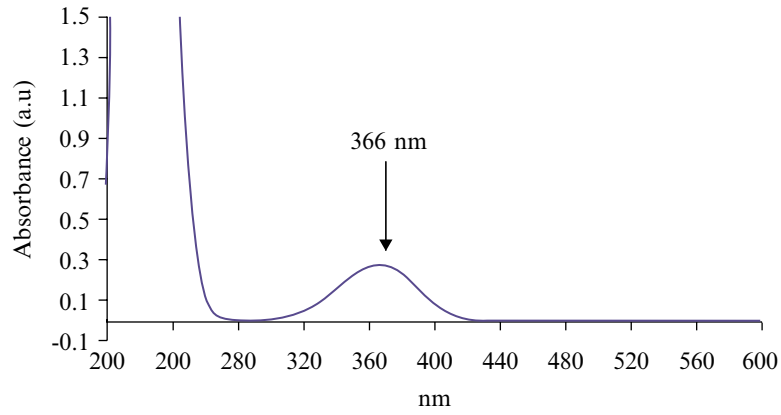

Fig. 4 Typical UV–Vis profile of the AAPH solution in PBS (12.5 mM, pH 7.4)

3. Add phosphate buffered saline (PBS) solution and fill to mark.
4. Prepare the colorless stock AAPH solution daily. To avoid thermolysis, store at 4 °C between experiments conducted on the same working day.
5. A typical UV–Vis spectrum of the AAPH solution in PBS (12.5 mM = 3.39 mg/mL) is shown in Fig. 4.

3.3 Preparation of the Reference and Test Antioxidant (AOX) Compounds Stock Solution

Calculate the partition coefficient values of test compounds in *n*-octanol–water (expressed as log*P*) using a suitable software (*see* **Note 3**). Calculated values are then compared with that calculated for Trolox.[1] Compounds with log*P* value lower than that of Trolox can be tested in the aqueous CBA environment.

Prepare stock solutions of pure compounds in methanol (unless otherwise stated) so that final concentration to be 0.5 mM.

3.4 Preparation of Plant Extracts

1. Follow the extraction protocol that is suggested according to the plant material composition.
2. Evaporate the solvent under vacuum or a nitrogen stream.
3. Add methanol or water–methanol mixtures to adjust the concentration of extract in mg dry material/L (*see* **Note 4**). Skip **steps 2** and **3** in case extraction and analysis solvents are the same.
4. Store at –18 °C until analysis.

[1] e.g., CS ChemDraw Ultra, Chemical Structure Drawing Standard, 1985–1998, Cambridge Soft Corp. (Calculate Log*P* using Brotos' Fragmentation Method; $\text{Log}P_{\text{Trolox}} = 3.18$).

3.5 Preparation of Serum Samples

1. Collect blood samples in K_2EDTA tubes after fasting for 12 h according to the objectives of the study.
2. Centrifuge at 2,000 × *g* for 15 min.
3. Separate the serum aliquots and use immediately or store at −80 °C for a maximum of 1 month.

3.6 Crocin Bleaching Assay: Kinetic Approach for Determining Reactivity of Antioxidants with Peroxyl Radicals

The kinetic approach is proposed for pure compounds or extracts of known concentration of total AOX, expressed as mM of Trolox or other reference compound [26]. The procedures detailed below are based on the manual protocols for CBA developed by Tubaro et al. [1], as modified and validated by Ordoudi and Tsimidou [13]. In brief, antioxidants are added to the ROO•—crocin reaction at a range of concentrations, bleaching rates in the absence (V_0) and presence of AOX (V) are calculated and V_0/V ratios are plotted against concentration ratios of the tested antioxidant and crocin ([AOX]/[Crocin]); linear curves are then generated according to the simple competitive kinetic model $\frac{V_0}{V} = 1 + \frac{k_{AOX}}{k_{crocin}} \times \frac{[AOX]}{[crocin]}$ and their slopes representing relative rate constants for each antioxidant ($k_{rel} = k_{AOX}/k_{crocin}$) are calculated.

Along with instrumentation described in Subheading 2.1, the kinetic protocol requires a timer, 5 mL-volumetric flasks and micropipettes.

1. Set up spectrophotometer to report or record absorbance at 440 nm. Set the cell heater at 39.5 ± 0.5 °C. Blank the spectrophotometer against PBS.
2. Determine spectral interferences between crocin and the test antioxidant. Record the optical spectra of control samples not containing AAPH over the range 415–470 nm, where crocin triplet appears. In case of overlapping peaks with those of the test antioxidants, dilute AOX stock solutions.
3. Transfer 0.5 mL crocin working solution A (*see* Subheading 3.1.2) to a 5 mL-volumetric flask (*see* **Note 5**).
4. Add specified amount of antioxidant (final concentration 1–100 μM, *see* **Note 6**). Start the reaction ($t = 0$ min) by adding 0.5 mL AAPH solution (*see* Subheading 3.2). Immediately start the timer. Fill the flask to 5 mL volume with PBS and stir by vigorous inversion for ~30 s.
5. Transfer about half of each test mixture to a 3 mL thermostated, optical 1 cm-cuvette placed in the spectrophotometer.
6. Begin recording the absorbance values at 440 nm (λ_{max} of crocin in aqueous solutions) exactly 1 min after the addition of initiator, and continue for a period of 10 min. Data points should be recorded at least every 6 s (or more often) in order to obtain kinetic curves (*see* **Note 7**).

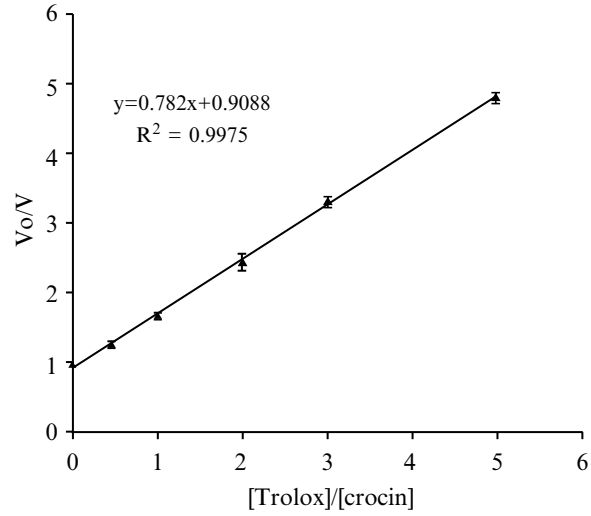

Fig. 5 Linear regression curve for Trolox. The slope represents the relative rate constant for the reaction with peroxyl radicals in the presence of crocin

7. Repeat **steps 4–6**, analyzing a range of concentrations (at least four) of pure compound or mixture to generate a concentration curve for each test antioxidant.

3.6.1 Calculation of Relative Rate Constants

Relative rate constants were found particularly useful in structure–activity relationship studies among closely related phenols and derivatives [23, 27–30].

1. From the optical data, calculate
   (a) $V_0 = \Delta A_0/\Delta t$: absorbance decrease during 10 min reaction in the absence of AOX.
   (b) $V = \Delta A/\Delta t$: absorbance decrease during 10 min reaction in the presence of AOX.
   (c) V_0/V: relative bleaching rate.
2. Plot relative bleaching rate values (V_0/V) against [AOX]/[crocin] over the full range tested, as illustrated for Trolox in Fig. 5. Provided that *y*-intercept is ca. 1.0, and the curve is linear, the slope value corresponds to the relative rate constant one ($k_{rel} = k_{AOX}/k_{crocin}$) of the competitive reaction (*see* **Note 8**).
3. Divide k_{rel} by the k_{rel} of Trolox analyzed under identical conditions to express results as "Trolox Equivalent Values" "TEV_{krel}."

3.6.2 Alternative Methods for Calculating and Expressing Results

Expression of results as "% Inhibition" of crocin bleaching is useful to prioritize individual compounds or even extracts. It requires only one level of AOX to be tested and provides a quite rapid preliminary assessment of reactivity. The disadvantage is that, if the wrong concentration is selected, an incorrect picture (too low, too high) of test compound reactivity may be generated.

1. Calculate $V_0 = \Delta A_0/\Delta t$ and $V = \Delta A/\Delta t$ at a single concentration equivalent to that of crocin ([AOX]/[crocin] = 1) within 10 min of reaction with peroxyl radicals (*see* Subheading 3.1.1).
2. Calculate the protective effect of antioxidants using $\%Inh = 100 \times (V_0 - V)/V$.
3. Divide the $\%Inh_{AOX}$ by the respective value of Trolox [13] to express results as "Trolox Equivalent Values" ($TEV_{\%Inh}$).

3.6.3 Method Performance Control

1. Saffron of different origin (Iranian, Greek, Spanish, Indian) or commercial grade can be found in the market [9]. As long as authenticity is guaranteed, the RP-HPLC profile of saffron extracts at 440 nm should only vary in the levels of individual crocins [13]. Consequently, stock solutions preparation as described in Subheading 3.1.2 may need adjustment to suppress this source of uncertainty. In practice, variation in raw saffron characteristics due to different origin and commercial grade was not found critical for the CBA performance as exemplified for Trolox (Fig. 6). In all cases, data from six-point linear regression curves ($n = 5$) were fit to the Stern–Volmer equation ($r^2 = 0.951$–0.998). Moreover, slope along with intercept values were of the same size and not always statistically different as illustrated in Fig. 6.
2. The use of initial AAPH and crocin concentrations that correspond to a molar ratio value of 1250 ensures a standard overall decrease in A_{440} values of the control solution (typically by 72–90 % within 10 min). By changing this ratio value the rate of crocin bleaching was affected as shown in Fig. 7. In a standardized protocol it is possible to use any molar ratio of $[AAPH]_0/[crocin]_0$ as long as (a) absorbance of probe into the control solution at time zero and in the end of the selected

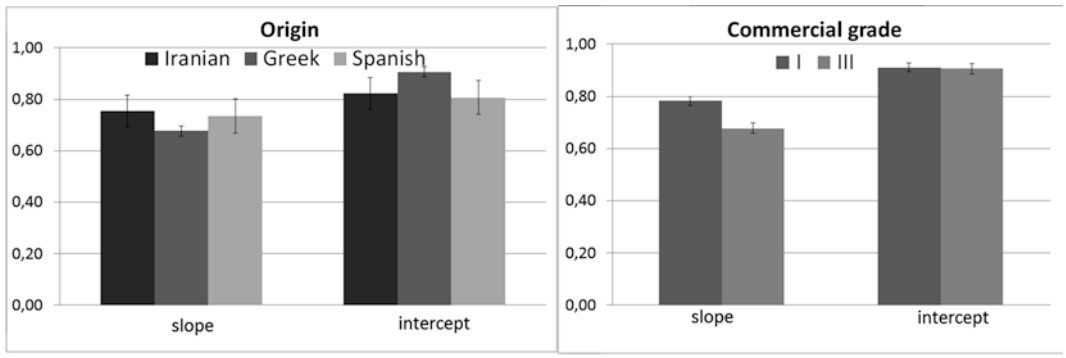

Fig. 6 CBA performance on the relative ROO• scavenging activity of Trolox (data from six-point linear regression curves, $n = 5$) after adjustment of probe concentration

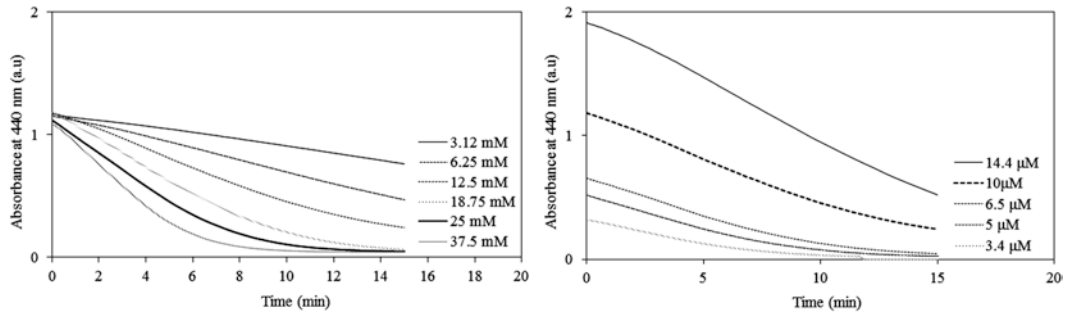

Fig. 7 Effect of (**a**) the initial AAPH concentration when $[crocin]_0 = 10$ μM and (**b**) the initial crocin level when $[AAPH]_0 = 12.5$ mM on the kinetics of crocin bleaching ($T = 40$ °C)

monitoring period lies within the optimal linear range of the spectrophotometer used and (b) % reduction of initial absorbance value is 60–80 %.

3. The intra-day repeatability *of* k_{rel} values (as % CV) for Trolox or other selected phenolic compounds should be less than 10 %. The intra-day repeatability of relative bleaching rates ($\Delta A_0/\Delta A$) should be also calculated for [Trolox]/[crocin] ratios equal to 0, 1, 2, and 3 at random days. Reported values for the respective CV ranges were 2.5–6.1 %, 1.8–5.1 %, 4.1–7.5 %, and 3.9–10.6 %, respectively [29]. Inter-day reproducibility values (as % CV) that have been calculated at ten random days within 3 months of analysis were found 9.4, 11.0, 12.5, and 13.0 % for the abovementioned ratios, respectively.
4. So far there is no way to assess "*accuracy*" for any antioxidant activity assay since there is not agreement among scientists about "reference" method or even a "reference" compound [31]. To appreciate CBA performance compare data produced by the same analysts for various methods, which give evidence for an antioxidant property, e.g., radical scavenging, redox potential, chelating effect. Such data are available for CBA, ORAC, DPPH, and ABTS assays for a series of well-known antioxidants and presented in Table 1 [26]. It has to be stressed that no pair of applied methods resulted in the same order of activity for gallic acid, caffeic acid, sinapic acid, isoeugenol, uric acid, ascorbic acid, and Trolox.

3.7 Crocin Bleaching Assay: Total Antioxidant Capacity (TAC) Approach

The TAC approach is often associated with applications to biological fluids using various antioxidant assay protocols. A manual CBA procedure for the estimation of TAC has been developed by Lussignoli et al. [32], later modified and validated by Kampa et al. [20]. In brief, pure antioxidants or complex mixtures are added to the ROO•—crocin reaction at a range of concentrations (usually w/v or volumes of complex mixtures), curves relating [AOX] to the inhibitory effect are generated and the IC_{50} values (concentration corresponding to 50 % inhibitory effect) are calculated.

Table 1
Prioritization of a series of AOX according to their radical scavenging activity using different in vitro assays (adapted with permission from ref. 26. Copyright (2007) American Chemical Society)

	In vitro radical scavenging assay				
	CBA (% Inh[a])	ORAC (ΔAUC[b])	DPPH· (EC_{50}[c])	(AE[d])	$ABTS^{+\cdot}$ (slope[e])
Gallic acid	2	4	1	2	1
Caffeic acid	1	1	2	2	4
Sinapic acid	1	3	3	3	2
Isoeugenol	5	2	4	2	3
Ascorbic acid	3	6	2	1	5
Uric acid	4	5	N[f]	N	5
Trolox	4	4	2	2	5

[a]% Inhibition at final [AOX] = 10 μM
[b]$\Delta AUC = AUC_{AOX} - AUC_{control}$ at final [AOX] = 1.0 μM
[c]Efficient [AH] for scavenging 50 % of [DPPH•]
[d]AE values [$AE = 1/(EC_{50} \times TEC_{50})$]
[e]Activity is expressed as the slope value of a linear curve describing the dependence of activity as a function of [AH]
[f]*N* not determined

3.7.1 Manual Procedure

This procedure requires a timer, micropipettes, microplates with flat-bottom wells, a shaking incubator and a microplate reader with filters at 450 nm. Software for automatic data recording greatly facilitates assays but is not a prerequisite (data can be recorded manually).

1. Transfer 100 μL crocin working solution A (*see* Subheading 3.1.2) to wells of a microplate reader.
2. Add 50 μL of the test antioxidant solution in PBS to each reaction well.
3. Prepare wells with reagent blanks consisting of crocin, test antioxidants, and PBS (100, 50, and 100 μL, respectively) to run in parallel with test compounds.
4. Incubate the plate in the shaking incubator at 37 °C for 10 min.
5. Start reactions by adding 100 μL AAPH (5 mg/mL = 5.9 mM, preheated for 5 min) to each test well, but not to blanks.
6. Incubate the plate in a water-bath at 37 °C for 60–75 min (*see* **Note 9**).
7. Read the absorbance of each well at 450 nm in a plate reader.

3.7.2 Calculation of IC_{50}

1. Calculate the % inhibition of bleaching using the equation % $Inh = 100 \times (\Delta A_0 - \Delta A)/\Delta A_0$ where ΔA_0, ΔA are defined as differences in the absorbance values of blank solutions (AAPH-free) minus those of test solutions at $t = 65$–70 min, in the absence and presence of AOX, respectively. Trolox may be

analyzed simultaneously as a reference antioxidant. Expression similar to that in Subheading 3.1.2 can be also adopted.

2. Plot % Inh values versus concentration (w/v) of pure compounds or volumes of complex mixtures (biological fluids). This dose-inhibition curve was found to be sigmoidal for all AOX tested. Semi-log plots are then used to generate linear regression curves and simplify calculations. The above are clearly illustrated in Fig. 8 for a series of well-known AOX.
3. From the graphs, calculate the antioxidant concentration required to inhibit crocin bleaching by 50 % (IC_{50}). In the case of mixtures, express IC_{50} values as μg of test mixture per volume of microplate (w/v).
4. Express results as "Total Antioxidant Capacity" (TAC), the reciprocal of IC_{50}

$$TAC = 1/IC_{50}$$

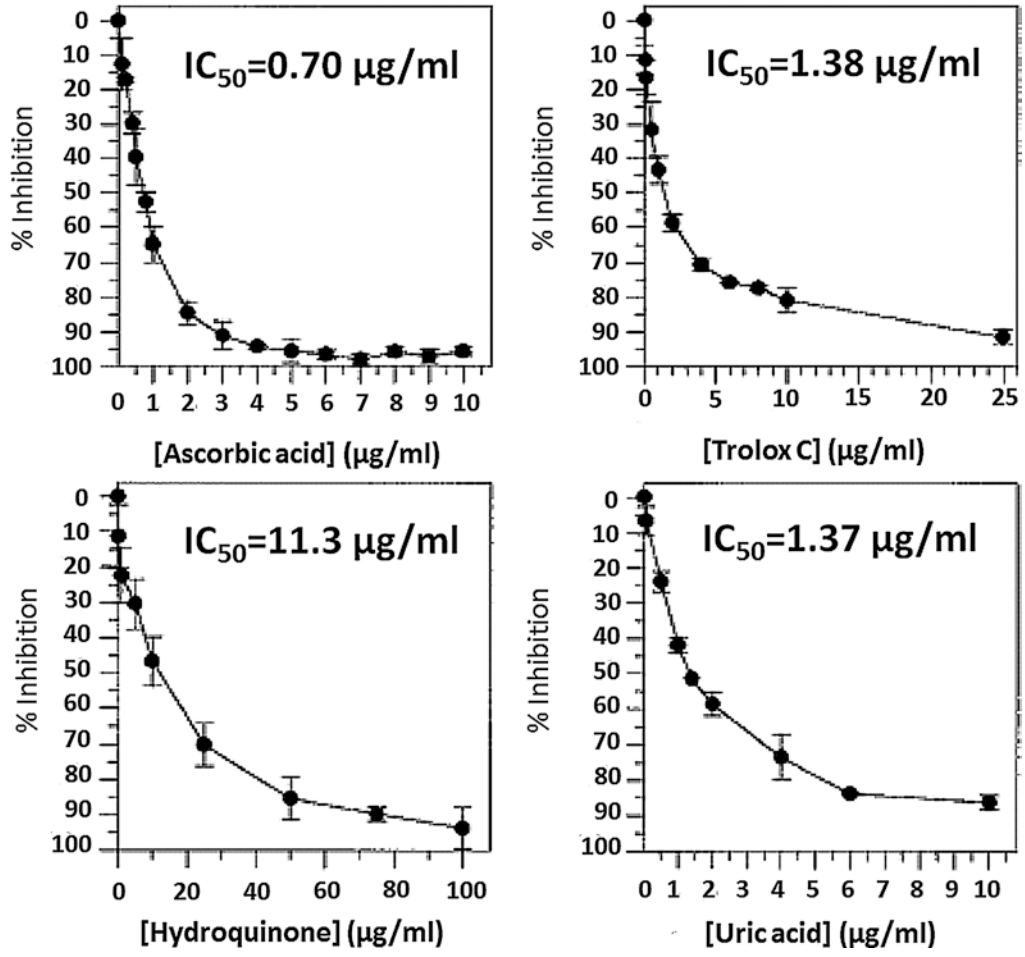

Fig. 8 Dose-inhibition curves of well-known antioxidants (adapted with permission from ref. 32. Copyright (1999) Academic Press)

3.7.3 Automated Procedure

A fully automated CBA procedure using an Olympus AU 400 high throughput analyzer [20] has been validated and used for the evaluation of Total Antioxidant Capacity in blood of patients with chronic disorders (inflammatory bowel, primary biliary cirrhosis, chronic hepatitis C, and viral HCV cirrhosis) [33, 34] and in organs of aged mice [35]. Results are expressed as in Subheading 3.7.2.

4 Notes

1. A semi-preparative RP-HPLC method for isolation of crocin-1 from saffron extracts is described by Kyriakoudi et al. [36]. In brief, separation can be achieved on a Nucleosil 100 C_{18} (250 mm × 10 mm i.d., 7 μm) chromatographic column with gradient elution by water (A)–methanol (B) mixture (30–100 % B in 30 min) at a flow rate of 3.0 mL/min. Detection wavelength is set at 350 nm.
2. In case of using microplate readers at 450 nm, prepare a more concentrated working solution A, e.g., by dilution with 20 mL of methanol and then proceed to **step 4** (*see* Subheading 3.1.2).
3. Partition coefficients in *n*-octanol–water can be also calculated experimentally using a mixture of chloroform–methanol–acetic acid (19:1:0.5, v/v/v) as the development system. The procedure is described by Nenadis et al. [37].
4. Concentration can be also expressed as mg total AOX content/kg extract.
5. Prepare the test solutions just before analysis in order to avoid prolonged exposure to light.
6. Concentration range depends on the type of AOX tested (structure, composition). Typically, for highly active radical scavengers such as flavonoids, hydroxycinnamic acids, and their derivatives, concentrations of 1–10 μM are sufficient; less potent compounds may require much higher levels of addition, e.g., 10–90 μM [25].
7. Analysis time per sample is ~12 min. Multiple samples can be analyzed in sequence or using microplate readers, as suggested by Lussignoli et al. [32].
8. CBA data for thirty-nine phenolic compounds all fitted to the Stern–Volmer equation for simple competitive reactions: $\frac{V_0}{V} = 1 + \frac{k_{AOX}}{k_{crocin}} \times \frac{[AOX]}{[crocin]}$ and generated linear plots with regression coefficients (r^2) between 0.964 and 0.999.

If the *y*-intercept value or the slope are close to zero then the test antioxidants most probably act as very poor free-radical scavengers or as prooxidants [29].

9. Under the conditions of the TAC protocol $[AAPH]_0/[crocin]_0$ value is approximately 590, so longer monitoring period is required to achieve a drop in A_{450} values by 60–80 %.

References

1. Tubaro F, Micossi E, Ursini F (1996) The antioxidant capacity of complex mixtures by kinetic analysis of crocin bleaching inhibition. J Am Oil Chem Soc 73:173–179
2. Toniolo R, Tubaro F, Ursini F et al (2003) An electroanalytical investigation on the redox properties of calcium antagonist dihydropyridines. Electroanal 15:855–861
3. Pizzale L, Bortolomeazzi R, Vichi S et al (2002) Antioxidant activity of sage (Salvia officinalis and S fruticosa) and oregano (Origanum onites and O. indercedens) extracts related to their phenolic compound content. J Sci Food Agric 82:1645–1651
4. Finotti E, Paoletti F, Bertone A et al (1998) Antioxidant capacity determination of extra virgin olive oils unsaponifiable fraction by crocin bleaching inhibition method. Nahrung 42:324–325
5. Finotti E, D'Ambrosio M, Paoletti F et al (2000) Synergistic effects of α-tocopherol, β-sitosterol and squalene on antioxidant activity assayed by crocin bleaching method. Nahrung 44:373–374
6. Dalla Libera A, Scutari G, Boscolo R et al (1998) Antioxidant properties of clozapine and related neuroleptics. Free Radic Res 29:151–157
7. Finotti E, Di Majo D (2003) Influence of solvents on the antioxidant property of flavonoids. Nahrung 47:186–187
8. International Organisation for Standardization (2011) ISO 3632-1, saffron (Crocus sativus L) part 1 specifications. Geneva, Switzerland
9. Ordoudi SA, Tsimidou MZ (2004) Saffron quality, effect of agricultural practices, processing and storage. In: Dris R (ed) Harvest and quality evaluation of food crop. Kluwer Academic Publishers, Dordrecht, pp 215–218
10. El-Agamey A, Lowe GM, McGarvey DJ et al (2004) Carotenoid radical chemistry and antioxidant/pro-oxidant properties. Arch Biochem Biophys 430:37–48
11. Krinsky NI, Johnson EJ (2005) Carotenoid actions and their relation to health and disease. Mol Asp Med 26:459–516
12. Bors W, Michel C, Saran M (1984) Inhibition of the bleaching of the carotenoid crocin. A rapid test for quantifying antioxidant activity. Biochim Biophys Acta 796:312–319
13. Ordoudi SA, Tsimidou MZ (2006) Crocin bleaching assay step by step: observations and suggestions for an alternative validated protocol. J Agric Food Chem 54:1663–1671
14. Roginsky V, Lissi EA (2005) Review of methods to determine chain-breaking antioxidant activity in food. Food Chem 92:235–254
15. Tubaro F, Ghiselli A, Rapuzzi P et al (1998) Analysis of plasma antioxidant capacity by competition kinetics. Free Radic Biol Med 24:1228–1234
16. Pino E, Lissi EA (2001) Quantitative treatment of the kinetics of free-radical-mediated amage. Protection by free-radical scavengers. Helv Chim Acta 84:3677–3685
17. Calligaris S, Manzocco L, Anese M et al (2004) Effect of heat-treatment on the antioxidant and pro-oxidant activity of milk. Int Dairy J 14:421–427
18. Manzocco L, Calligaris S, Nicoli MC (2002) Assessment of pro-oxidant activity of foods by kinetic analysis of crocin bleaching. J Agric Food Chem 50:2767–2771
19. Woffenden HM, Ames JM, Chandra S et al (2002) Effect of kilning on the antioxidant and prooxidant activities of pale malts. J Agric Food Chem 50:4925–4933
20. Kampa M, Nistikaki A, Tsaousis V et al (2002) A new automated method for the determination of the total antioxidant capacity (TAC) of human plasma, based on the crocin bleaching assay. BMC Clin Pathol 2:3
21. Bountagkidou O, van der Klift EJC, Tsimidou MZ et al (2012) An on-line high performance liquid chromatography-crocin bleaching assay for detection of antioxidants. J Chrom A 1237: 80–85
22. Huang D, Ou B, Prior RL (2005) The chemistry behind antioxidant capacity assays. J Agric Food Chem 53:1841–1856

23. Ordoudi SA, Tsermentseli SK, Nenadis N et al (2011) Structure-radical scavenging activity relationship of alkannin/shikonin derivatives. Food Chem 124:171–176
24. Weber F, Grosch W (1976) Co-oxidation of a carotenoid by the enzyme lipoxygenase: influence on the formation of linoleic acid hydroperoxides. Z Lebensm Unters Forsch 161: 223–230
25. Speranza G, Dada G, Manitto P et al (1984) 13-cis-crocin: a new crocinoid of saffron. Gazz Chim Ital 114:189–192
26. Nenadis N, Lazaridou O, Tsimidou MZ (2007) Use of reference compounds in antioxidant activity assessment. J Agric Food Chem 55:5452–5460
27. Natella F, Nardini M, De Felice M et al (1999) Benzoic and cinnamic acid derivatives as antioxidants, structure-activity relation. J Agric Food Chem 47:1453–1459
28. Bortolomeazzi R, Sebastianutto N, Toniolo R et al (2007) Comparative evaluation of the antioxidant capacity of smoke flavouring phenols by crocin bleaching inhibition, DPPH radical scavenging and oxidation potential. Food Chem 100:1481–1489
29. Ordoudi SA, Tsimidou MZ (2006) Crocin bleaching assay (CBA) in structure-radical scavenging activity studies of selected phenolic compounds. J Agric Food Chem 54:9347–9356
30. Bountagkidou OG, Ordoudi SA, Tsimidou MZ (2010) Structure-antioxidant activity relationship study of natural hydroxybenzaldehydes using in vitro assays. Food Res Int 43: 2014–2019
31. Frankel EN, Finley JW (2008) How to standardize the multiplicity of methods to evaluate natural antioxidants. J Agric Food Chem 56:4901–4908
32. Lussignoli S, Fraccaroli M, Andrioli G (1999) A microplate based colorimetric assay of the total peroxyl radical trapping capability of human plasma. Anal Biochem 269:38–44
33. Koutroubakis IE, Malliaraki N, Dimoulios PD et al (2004) Decreased total and corrected antioxidant capacity in patients with inflammatory bowel disease. Dig Diseas Sci 49: 1433–1437
34. Notas G, Miliaraki N, Kampa M et al (2005) Patients with primary biliary cirrhosis have increased serum total antioxidant capacity measured with the crocin bleaching assay. World J Gastroenterol 11:4194–4198
35. Li XL, Ma YL, Liu XJ (2007) Effect of the *Lycium barbarum* polysaccharides on age-related oxidative stress in aged mice. J Ethnopharm 111:504–511
36. Kyriakoudi A, Chrysanthou A, Mantzouridou F et al (2012) Revisiting extraction of bioactive apocarotenoids from *Crocus sativus* L. dry stigmas (saffron). Anal Chim Acta 755:77–85
37. Nenadis N, Zhang HY, Tsimidou M (2003) Structure-antioxidant activity relationship of ferulic acid derivatives: effect of carbon side chain characteristic groups. J Agric Food Chem 51:1874–1879

Chapter 25

Simultaneous Determination of the Endogenous Free α-Lipoic Acid and Dihydrolipoic Acid in Human Plasma and Erythrocytes by RP-HPLC Coupled with Electrochemical Detector

Muhammad Imran Khan, Zafar Iqbal, and Abad Khan

Abstract

A highly sensitive, precise, and accurate reversed-phase high performance liquid-chromatography/electrochemical detection method for simultaneous determination of the endogenous free α-lipoic acid and dihydrolipoic acid in biological matrices is presented. The two analytes are extracted from samples with acetonitrile–10 % *m*-phosphoric acid solution$_{(aqueous)}$ (50:50 v/v). To determine the total lipoic acid, samples are treated with tris(2-carboxyethyl)phosphine solution in phosphate buffer: pH 2.5 with 85 % *o*-phosphoric acid prior to deproteination. The two analytes are separated on a C_{18} (150×4.6 mm, 5 μm) analytical column using acetonitrile-50 mM phosphate buffer: pH 2.5 with 85 % *o*-phosphoric acid (35:65 v/v) as the isocratic mobile phase pumped at a flow rate of 2.0 ml/min at the column oven temperature of 35 °C. The column eluents are monitored at a potential of 0.9 V. These analytes are efficiently resolved in <7 min.

Key words Column liquid-chromatography, α-Lipoic acid, Dihydrolipoic acid, Electrochemical detection

1 Introduction

Alpha-lipoic acid (α-LA; 1,2-dithiolane-3-pentanoic acid; $C_8H_{14}O_2S_2$), an organosulfur derivative of octanoic acid, is a naturally occurring medium chain fatty acid compound having powerful antioxidant properties [1–4]. Being soluble in both water and fats, it is widely distributed in both cellular membranes and the cytosol [5]. When absorbed from the diet, α-LA is rapidly reduced to its dithiol form, dihydrolipoic acid (DHLA) in many tissues [6, 7]. Like α-LA, DHLA is also an antioxidant, probably more potent

Journal published in: Chromatographia, Vol 73, Issue 9, Pages: 929–939, Year of publication: 2011, doi: 10.1007/s10337-011-1997-3.

Donald Armstrong (ed.), *Advanced Protocols in Oxidative Stress III*, Methods in Molecular Biology, vol. 1208,
DOI 10.1007/978-1-4939-1441-8_25,

than its oxidized counterpart. The DHLA/α-LA couple has a redox potential (ΔE) of –320 mV, which means that DHLA has one of the highest antioxidant potentials known in biological systems [8]. The ratio of DHLA to α-LA is also a good measure of the oxidative stress to which an organism is exposed [4]. The total lipoic acid (tLA; sum of the α-LA and DHLA) content of the biological samples consists of the free LA, weakly protein bound LA via hydrogen bonds, and strongly protein bound LA (lipoyllysine) via covalent bonds. However, various physiological functions of the LA (both α-LA and DHLA) are attributed to their free forms (free and weakly protein bound) [9].

Several methods have been published on the chromatographic analysis of either total, free, or bound α-LA in various sample matrices such as foodstuffs [9], dietary supplements [10], and biological samples [11–16]. Similarly, very few methods [17–23] are available for simultaneous determination of the total α-LA and its reduced form, DHLA in biological samples after oral administration. But to our knowledge, no single method has been reported so far that is capable of determining the endogenous free α-LA and DHLA simultaneously. Moreover, the problem with these methods is that they do not differentiate clearly between total and free LA as drastic hydrolysis conditions have been used for their extraction that are able to extract covalently bound LA but degrade the free LA and these available methods also are not simple and reliable because these molecules do not possess strong chromophores to permit the use of conventional ultraviolet–visible (UV–Vis) or fluorescence (FL) detectors. To overcome these problems, few derivatization reagents were used to determine them by FL detection [18, 19]. However, such derivatization is laborious and expensive. Another approach applied for simultaneous analysis of these compounds was the use of pulse electrochemical (EC) [17, 20] and coulometric detection [21–23] techniques. However, these methods were not sensitive enough to be applied to the measurement of these endogenous thiols.

To overcome the inherent problems in the analysis of the free LA, a sensitive, precise, and accurate method for simultaneous determination of the endogenous free α-LA and DHLA using reversed-phase high performance liquid-chromatography (RP-HPLC) coupled with EC detector is presented in this chapter. Likewise, the procedure used for their extraction from various biological matrices such as plasma and erythrocytes is also very simple and reliable as milder extraction conditions are utilized. The proposed method have been used for assessment of the oxidative stress through monitoring of the endogenous free α-LA and DHLA concentrations and their ratio in various biological matrices of human volunteers. The same method can also be applied to other sample matrices such as dietary supplements, foodstuffs, and biological tissues with slight modification in the sample preparation.

2 Materials

2.1 Chemicals

DL-α-Lipoic acid (α-LA: purity ≥99 %) and reduced lipoic acid (DHLA: purity ≥98 %).

Ultrapure water prepared by a Millipore ultrapure water system (Milford, USA).

HPLC-grade methanol (MeOH: purity ≥99.9 %) and acetonitrile (ACN: purity ≥99.9 %).

Analytical-grade monobasic potassium phosphate (KH_2PO_4: purity ≥99 %), *o*-phosphoric acid (OPA: purity 85 %), sodium hydroxide (NaOH: purity ≥98 %), sodium chloride (NaCl: purity ≥98 %), trifluoroacetic acid (TFA: purity ≥98 %), glacial acetic acid (GAA: meeting USP test specifications), *m*-phosphoric acid (MPA: purity 100 %), dichloromethane (DCM), diethylether (DEE), ethyl acetate (EA), tris(2-carboxyethyl)phosphine hydrochloride (TCEP·HCl: purity ≥99 %), and phosphate buffered saline (PBS: pH 7.4).

2.2 Reagents

Prepare the NaOH aqueous solution (1 M) by dissolving NaOH pellets (40 g) in ≈500 ml ultrapure water, and diluted to 1,000 ml.

Prepare monobasic potassium phosphate buffer solution (50 mM) by dissolving KH_2PO_4 (6.8 g) in ultrapure water, and diluted to ≈990 ml. The desired pH of the buffer solution is then adjusted with either 85 % OPA or 1 M NaOH solution$_{(aqueous)}$ before making volume to 1,000 ml with ultrapure water.

Prepare the saturated NaCl solution$_{(aqueous)}$ by dissolving NaCl (30–40 g) in ≈100 ml ultrapure water.

Prepare the normal saline by dissolving NaCl (0.9 g) in sufficient quantity of ultrapure water to make the final volume 100 ml.

Prepare the acidified waters by adding 85 % OPA, TFA, or 85 % FA drop wise to ≈1,000 ml ultrapure water until the desired pH is achieved.

Prepare the GAA solution$_{(aqueous)}$ (0.5 % v/v) by diluting GAA (0.5 ml) with sufficient quantity of ultrapure water to make the final volume 100 ml.

Prepare the MPA solution$_{(aqueous)}$ (10 % w/v) by dissolving MPA (10 g) in sufficient quantity of ultrapure water to make the final volume 100 ml.

Prepare stock solution of the TCEP·HCl solution$_{(aqueous)}$ (10 g/ml) by dissolving TCEP·HCl (100 g) in sufficient quantity of KH_2PO_4, pH 2.5 with 85 % OPA to make the final volume 10 ml. This stock solution is then further diluted to get the desired concentrations (10–150 mg/ml) of the TCEP·HCl working solutions.

(*Note: All these chemicals and reagents can be used without further purification except mobile phases, which are vacuum filtered through 0.45 μm pore size filters*)

2.3 Instrumentation

HPLC system equipped with a pump, vacuum degasser, autosampler (or manual injector), column oven, EC detector (A single-channel EC flow cell [e.g., the Flexcell™] is preferred in

which a three-electrode configuration can be used: the maintenance free reference electrode [e.g., HyREF™], the auxiliary electrode, and the gold (Au) working electrode. The Flexcell has an effective volume of 0.5 μl), interface, and computer system having data analysis software.

3 Methods

3.1 Preparation of Standard Solutions

Prepare stock solutions of the analytes by dissolving their weighed amounts in ACN and store at −20 °C in amber glass vials. At the time of analysis, dilute these stock solutions with mobile phase to give standard mixtures of the α-LA and DHLA in the range of 0.1–500 and 0.25–1,000 ng/ml, respectively.

3.2 Sample Handling

Draw blood samples from subjects in precooled ethylenediaminetetraacetic acid (EDTA)-vacutainer tubes. Separate these samples into plasma and blood cells immediately by centrifugation at 1,500 × *g* for 10 min at −10 °C. Prepare erythrocytes samples by removal of the buffy coat from the blood cells and then wash them with normal saline. Store all samples at −80 °C until analyses.

All handling and experimental procedures should be carried out well protected from light and heat because these thiol compounds are prone to oxidation.

3.3 Sample Preparation

Thaw both plasma and erythrocytes samples to room temperature. Erythrocytes hemolysates are then prepared by lysing the erythrocytes by freezing–thawing two to three times.

To determine the free α-LA and DHLA separately, sample matrices are deproteinized with ACN–10 % MPA solution$_{(aqueous)}$ (50:50 v/v) by vigorous vortex-mixing. These samples were then centrifuged and the supernatants obtained were collected in separate eppendorf tubes, which were then directly injected into the HPLC system after dilution with the aqueous component of the mobile phase, if desired (*see* **Notes 1–3**).

In case of determining the tLA, the deproteination step is preceded by the reduction of the α-LA to DHLA, which is accomplished by the addition of TCEP·HCl solution to the samples (*see* **Note 4**).

A comprehensive scheme for extraction of the α-LA and the DHLA and the tLA from plasma and erythrocytes hemolysates is given in Table 1.

Comparative recoveries of the two analytes with various extraction solvents/procedures are given in Table 2 showing that maximum recoveries of the two analytes can be efficiently obtained by a simple one step protein precipitation (PP) extraction procedure, consisting of a deproteination and extraction with three parts of ACN–10 % MPA solution(aqueous) (50:50 v/v) and the subsequent volume make up with the aqueous component of the mobile phase.

Table 1
Scheme for the extraction of α-LA and DHLA and the tLA from the biological matrices

Take 1 part (200 µl) of whole blood/plasma/erythrocyte hemolysate
↓
Add 1/20 parts (10 µl) of cooled TCEP·HCl solution (20 mg/ml or 70 mM) in 50 mM KH_2PO_4 buffer: pH 2.5 with 85 % OPA and vortex-mix vigorously for 5 min at room temperature
(*Reduction of the α-LA to DHLA*)[a]
↓
Add 3 parts (600 µl) of the cooled protein denaturing solvent(s), vortex-mix vigorously for 5 min, and centrifuge at 2,500 × *g* at −9 °C for 10 min
(*Protein precipitation and extraction of thiols*)
↓
Transfer the supernatant layer to another tube
(*Inject into the HPLC system either directly after diluting it with the aqueous component of the mobile phase, if desired or*)
↓
Add 10 parts (1000 µl) of the cooled organic solvent(s), vortex–mix vigorously for 5 min, and centrifuge at 2,500 × *g* at −9 °C for 10 min. Collect the supernatant and repeat this extraction process twice with the residue using fresh extraction solvent(s). Combine the supernatant organic layers and evaporate to dryness under the stream of nitrogen gas
(*Selective extraction of thiols*)
↓
Reconstitute the residue in 5 parts (1000 µL) of the aqueous component of the mobile phase by vortex-mixing vigorously for 1 min
(*Solvent exchange*)

[a]In case of tLA only

Table 2
Recovery of α-LA and DHLA from human plasma and erythrocyte samples with various extraction procedures/solvents

Extraction procedures/solvents	% Recovery (mean ± SD)	
	α-LA[a]	DHLA[a]
Protein precipitation (PP) methods		
Acetonitrile		
Plasma	90 ± 3	88 ± 3
Erythrocytes	87 ± 3	85 ± 3
Methanol		
Plasma	49 ± 4	58 ± 2
Erythrocytes	44 ± 3	61 ± 2

(continued)

Table 2
(continued)

Extraction procedures/solvents	% Recovery (mean ± SD)	
	α-LA[a]	DHLA[a]
0.5 % GAA solution$_{(aqueous)}$		
Plasma	71 ± 2	67 ± 3
Erythrocytes	70 ± 1	59 ± 2
10 % MPA solution$_{(aqueous)}$		
Plasma	83 ± 3	80 ± 2
Erythrocytes	80 ± 2	75 ± 1
Acetonitrile–0.5 % GAA solution$_{(aqueous)}$ (50:50 v/v)		
Plasma	91 ± 3	88 ± 3
Erythrocytes	88 ± 3	86 ± 3
Acetonitrile–10 % MPA solution$_{(aqueous)}$ (50:50 v/v)		
Plasma	98 ± 1	98 ± 2
Erythrocytes	97 ± 1	98 ± 1
Liquid–liquid extraction (LLE) methods		
Diethyl ether		
Plasma	75 ± 3	68 ± 3
Erythrocytes	72 ± 2	65 ± 2
Ethyl acetate		
Plasma	80 ± 2	75 ± 2
Erythrocytes	78 ± 2	72 ± 2
Dichloromethane		
Plasma	95 ± 1	78 ± 2
Erythrocytes	94 ± 2	74 ± 1

[a] $n = 3$ (where n is the number of samples)

3.4 Chromatographic Analysis

Analyze samples at the following combination of chromatographic parameters. Stationary phase: Ordinary RP C_{18} (150 × 4.6 mm, 5 μm) analytical column protected by a pre-column guard cartridge C_{18} (30 × 4.6 mm, 10 μm); Mobile phase: ACN-50 mM KH_2PO_4 buffer: pH 2.5 with 85 % OPA (35:65 v/v) in isocratic mode; Flow rate: 2.0 ml/min; Column oven temperature: 35 °C; and Injection volume: 5 μl (*see* **Notes 5–10**).

Detect the two analytes at 0.9 V electrical potential using the following EC detection parameters. Filter: 0.01; Polarity: positive; Range and maximum compensation: 20 nA and 2.5 μA; Offset: 10 %; and Temperature: 35 °C (*see* **Notes 11** and **12**).

Figure 1 shows representative chromatograms, at optimum chromatographic conditions and detection parameters, of various samples reduced with TCEP·HCl solution (a, b, and c), the blank mobile phase (d), the blank erythrocytes (e) and plasma (f) samples, the standard mixture (g), and the erythrocytes (h) and plasma (i) samples spiked with the standard mixture. Under the specified

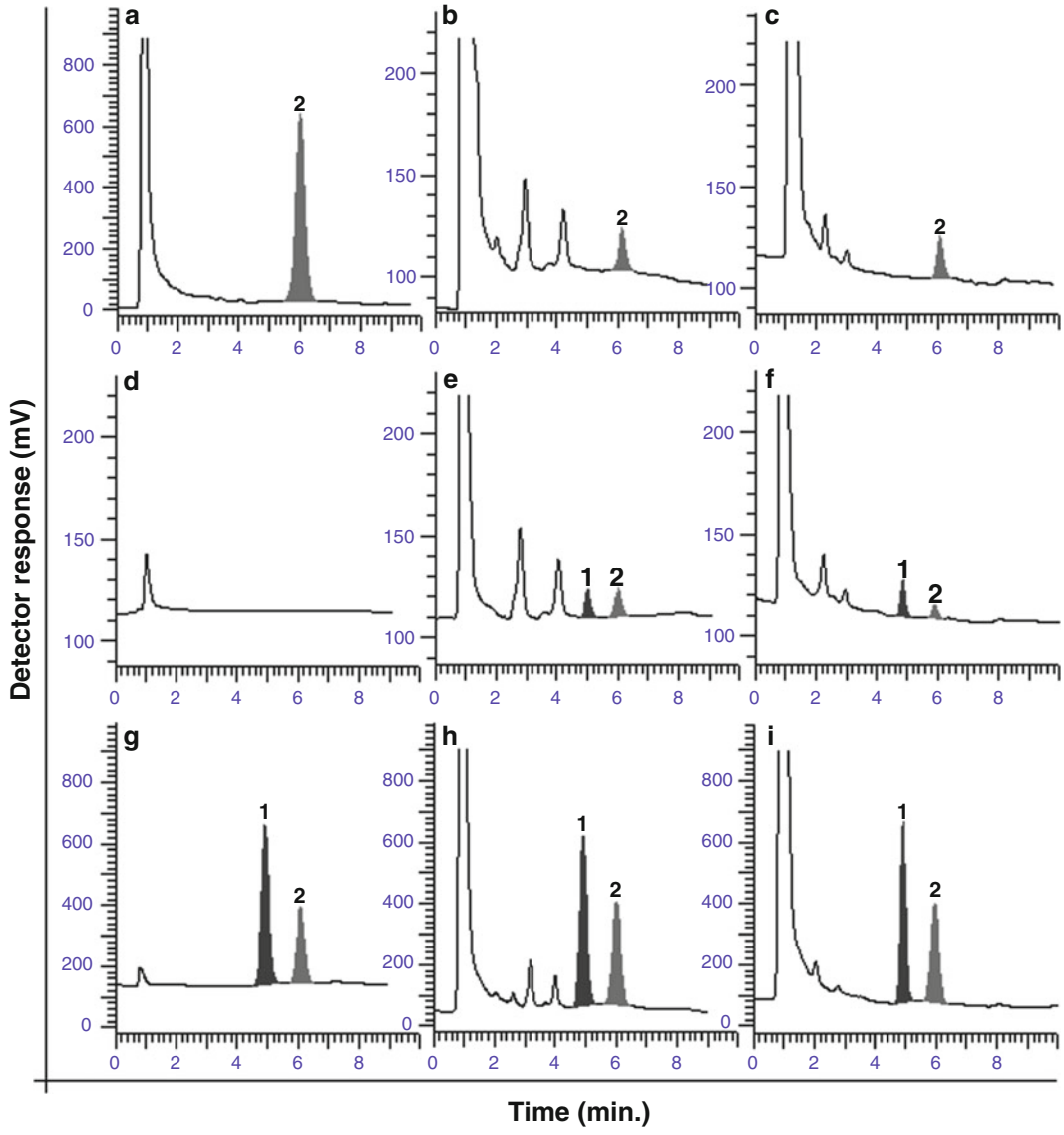

Fig. 1 Representative RP-HPLC chromatograms of different samples analyzed under optimum conditions. *Chromatograms:* (**a**) The standard mixture containing 100 ng/ml of the α-lipoic acid and dihydrolipoic acid each reduced with TCEP·HCl solution; (**b**) The blank erythrocytes sample reduced with TCEP·HCl solution; (**c**) The blank plasma sample reduced with TCEP·HCl solution; (**d**) The blank mobile phase; (**e**) The blank erythrocytes sample; (**f**) The blank plasma sample; (**g**) The standard mixture containing 100 ng/ml of the α-lipoic acid and dihydrolipoic acid each; (**h**) The erythrocytes sample spiked with the standard mixture containing 100 ng/ml of the α-lipoic acid and dihydrolipoic acid each; and (**i**) The plasma sample spiked with the standard mixture containing 100 ng/ml of the α-lipoic acid and dihydrolipoic acid each. *Peaks*: (1) α-lipoic acid (4.95 min) and (2) Dihydrolipoic acid (6.0 min)

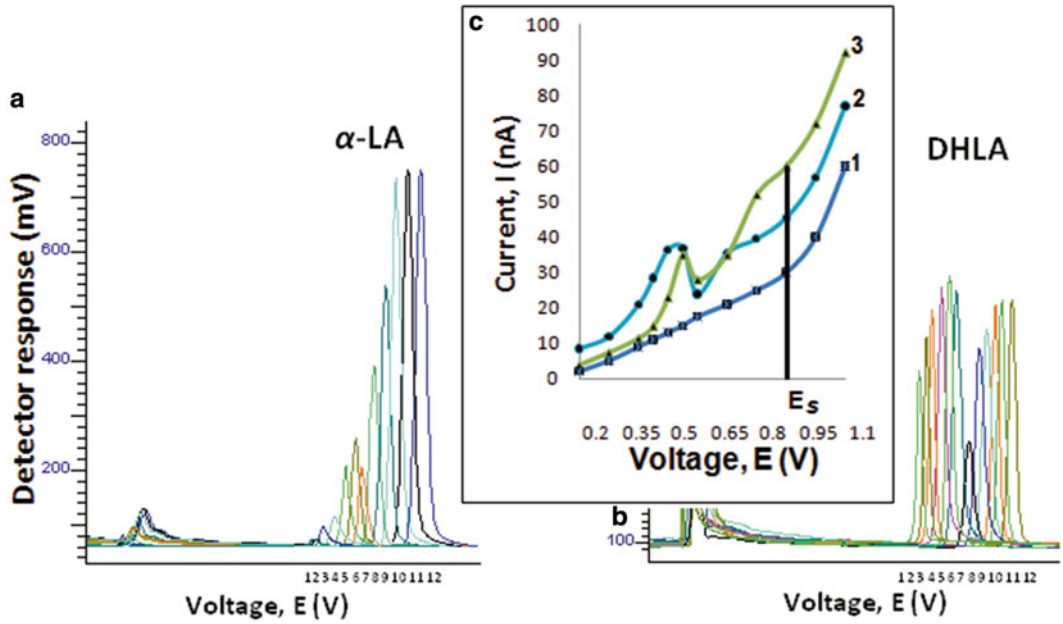

Fig. 2 Hydrodynamic voltammograms for the α-lipoic acid and dihydrolipoic acid. *Chromatograms:* (**a**) Detector response (mV) versus voltage, *E* (V) relationship for the α-lipoic acid and (**b**) Detector response (mV) versus voltage, *E* (V) relationship for the dihydrolipoic acid. *Voltammograms:* (**c**) Total current (nA) versus voltage, *E* (V) relationship for the two analytes: (1) Baseline current; (2) Dihydrolipoic acid; and (3) α-Lipoic acid. While, *E*s is the selected voltage, 0.9 V. *Peaks:* (1) At 0.2 V; (2) At 0.3 V; (3) At 0.4 V; (4) At 0.45 V; (5) At 0.5 V; (6) At 0.55 V; (7) 0.6 V; (8) At 0.7 V; (9) At 0.8 V; (10) At 0.9 V; (11) At 1.0 V; and (12) At 1.1 V

conditions, the mean retention times were 4.95 and 6.0 min for α-LA and DHLA, respectively.

Hydrodynamic voltammograms for the two analytes are given in Fig. 2.

3.5 Method Validation

Validate the chromatographic method according to international guidelines with emphasis on specificity/selectivity, recovery, sensitivity, linearity within the expected concentration range, precision (repeatability and intermediate precision), stability of solutions, and robustness [24, 25].

To verify the specificity/selectivity of the method, the separation of peaks in the chromatograms of the blank solvent, the blank sample matrices, the standard mixture, and the sample matrices spiked with the standard mixture is confirmed.

For recovery studies, standard mixtures, at three nominal concentration levels, are spiked into samples matrices (200 µl; $n=5$), extracted, and analyzed with triplicate injections. Peak areas of endogenous thiols are subtracted from total peak areas in spiked sample matrix and results obtained are divided by peak areas of corresponding standard mixtures and multiplied by 100 to get % recovery.

The sensitivity of the method is evaluated by determining the limit of detection (LOD) and lower limit of quantification (LLOQ)

using the signal-to-noise (*S/N*) approach. The LOD is the minimum concentration that produces response equal to at least three times the value of the noise and the LLOQ is the minimum concentration whose response is not less than ten times the value of the noise. Both per ml and on-column sensitivity of the method is determined.

To determine the linearity of the method, various standard mixtures are spiked into sample matrices (200 µl), which are then extracted and analyzed with triplicate injections. The peak areas of analytes are then plotted as a function of spiked concentrations of the analytes and the slope (m), the intercept (b), and the correlation coefficient (r^2) are determined from the regression analysis.

To determine the injection repeatability, mixed standard solution is injected at least ten times. It is expressed by repeatability of peak area and retention time and determined as the mean ± standard deviation (SD) and the percent residual standard deviation (% RSD) calculated from the data obtained.

Similarly, analysis repeatability is determined by analyzing ten samples prepared individually from single plasma sample spiked with the standard mixture. The result is expressed by repeatability of the recovered amount and determined as the mean ± SD and the % RSD calculated from the data obtained.

In order to determine the intermediate precision (intra-day and inter-days reproducibility), the spiked samples prepared for the recovery studies are analyzed three times a day at 0, 7, and 14 h and for three successive days. The result is expressed as the reproducibility of the recovered amount and determined as the mean ± SD and the % RSD calculated from the data obtained.

To determine the robustness of the developed method, effect of small deliberate variations in system parameters like the organic component of the mobile phase (±2 %), the mobile phase flow rate (±0.2 ml/min), the column oven temperature (±5 °C), and the working potential (±10 mV) are studied.

Short-term stability study of the analytes is evaluated in:

- Standard solutions stored in the freezer (at –20 °C) for 1 week, brought to room temperature, and then injected within 1 h after thawing.
- Extracted sample matrices stored in the auto-sampler at room temperature (30–40 °C) after the first injection cycle and then reinjected after 4, 8, 12, and 24 h.
- Extracted sample matrices stored over-night in the refrigerator (at 4 °C) and the freezer, brought to room temperature, and then injected within 1 h after thawing.

Results of various method validation parameters are summarized in Tables 3, 4, 5, 6, and 7 and Fig. 1 and 3, showing that the proposed analytical method is fully validated according to international guidelines. However, samples should be kept refrigerated or frozen until analysis in order to determine the two analytes accurately.

Table 3
Accuracy in terms of % recovery of the proposed method for simultaneous determination of α-LA and DHLA

Accuracy in terms of % recovery	α-LA	DHLA
Spiked concentration level 1 (α-LA 1 and DHLA 2 ng/ml)[a]		
Plasma	98.07 ± 1.30; 1.33	98.21 ± 1.08; 1.10
Erythrocytes	97.77 ± 0.92; 0.94	98.72 ± 0.65; 0.66
Spiked concentration level 2 (α-LA 10 and DHLA 50 ng/ml)[a]		
Plasma	98.74 ± 0.90; 0.91	98.72 ± 0.65; 0.66
Erythrocytes	97.33 ± 0.35; 0.36	98.48 ± 0.67; 0.68
Spiked concentration level 3 (α-LA 100 and DHLA 500 ng/ml)[a]		
Plasma	98.72 ± 0.54; 0.55	98.28 ± 0.56; 0.57
Erythrocytes	98.69 ± 0.48; 0.48	97.81 ± 0.40; 0.40

Results are reported as mean ± SD; % RSD
[a] $n = 5$ (where n is the number of samples)

Table 4
Sensitivity of the proposed method for simultaneous determination of α-LA and DHLA

Analytes	LOD	LLOQ
α-Lipoic acid		
Per ml (pg)	30	100
On-column (fg)	150	500
Dihydrolipoic acid		
Per ml (pg)	75	250
On-column (fg)	375	1,250

Table 5
Calibration range and linearity of the proposed method for simultaneous determination of α-LA and DHLA

Parameters	α-LA	DHLA
Calibration range (ng/ml)	0.1–500	0.25–1,000
Linearity		
Spiked plasma samples		
Regression equation	$y = 28{,}303x + 119$	$y = 11{,}623x + 9{,}185$
Correlation coefficient, r^2	0.999	0.999
Spiked erythrocyte samples		
Regression equation	$y = 28{,}735x + 52{,}975$	$y = 11{,}519x + 16{,}299$
Correlation coefficient, r^2	0.999	0.999

y is the peak area and x is the concentration

Table 6
Precision of the proposed method for simultaneous determination of α-LA and DHLA

Precision	α-LA	DHLA
Repeatability		
Injection repeatability		
Standard solution (α-LA and DHLA 100 ng/ml each)[a]		
Peak area	30,53,754 ± 63,680; 2.09	12,08,721 ± 20,329; 1.68
Retention time (min)	4.95 ± 0.03; 0.6	6.00 ± 0.04; 0.70
Analysis repeatability		
Spiked concentration level 1 (α-LA and DHLA 100 ng/ml each)[b]		
Plasma	99.61 ± 1.36[c]; 1.36	99.17 ± 1.30[c]; 1.31
Erythrocytes	98.29 ± 1.55[c]; 1.57	98.36 ± 0.88[c]; 0.90
Intermediate precision		
Intra-day reproducibility		
Spiked concentration level 2 (α-LA 1 and DHLA 2 ng/ml)[d]		
Plasma	0.98 ± 0.01[c]; 1.40	1.95 ± 0.04[c]; 2.15
Erythrocytes	0.97 ± 0.02[c]; 1.92	1.92 ± 0.01[c]; 0.42
Spiked concentration level 3 (α-LA 10 and DHLA 50 ng/ml)[d]		
Plasma	9.65 ± 0.10[c]; 0.98	48.52 ± 0.27[c]; 0.56
Erythrocytes	9.52 ± 0.07[c]; 0.72	48.20 ± 0.21[c]; 0.43
Spiked concentration level 4 (α-LA 100 and DHLA 500 ng/ml)[d]		
Plasma	96.10 ± 1.01[c]; 1.05	492.76 ± 2.54[c]; 0.52
Erythrocytes	96.96 ± 0.80[c]; 0.82	489.13 ± 1.19[c]; 0.24
Inter-days reproducibility		
Spiked concentration level 2 (α-LA 1 and DHLA 2 ng/ml)[d]		
Plasma	0.97 ± 0.01[c]; 0.79	1.96 ± 0.03[c]; 1.76
Erythrocytes	0.98 ± 0.02[c]; 1.65	1.91 ± 0.02[c]; 0.91
Spiked concentration level 3 (α-LA 10 and DHLA 50 ng/ml)[d]		
Plasma	9.58 ± 0.15[c]; 1.58	48.43 ± 0.42[c]; 0.87
Erythrocytes	9.61 ± 0.17[c]; 1.80	47.79 ± 0.76[c]; 1.59
Spiked concentration level 4 (α-LA 100 and DHLA 500 ng/ml)[d]		
Plasma	95.72 ± 1.58[c]; 1.64	491.00 ± 4.34[c]; 0.88
Erythrocytes	95.85 ± 0.59[c]; 0.62	451.53 ± 5.40[c]; 1.10

Results are reported as mean ± SD; % RSD
[a] $n = 10$
[b] $n = 5$
[c] Quantity recovered in ng/ml
[d] $n = 3$ (where n is the number of samples)

4 Notes

1. Although recovery of the α-LA with liquid–liquid extraction (LLE) procedure using dichloromethane as the extraction solvent [13] was comparable with that obtained with the selected PP method, DHLA was not efficiently extracted by LLE as compared to PP, which may be attributed to its poor partitioning into nonpolar solvents due to its greater polarity [16]. Other disadvantages of the LLE methods over PP methods are that these procedures are multistep, laborious, and time-consuming.

Table 7
Short-term stability of α-LA and DHLA samples

Analytes	Storage temperature (°C)	% Loss		
		Standard solutions	Extracted samples	Reduced and extracted samples
α-LA	30–40	–	0.07 ± 0.03^{a}	–
		–	0.15 ± 0.05^{b}	–
		–	0.50 ± 0.10^{c}	–
		–	0.78 ± 0.04^{d}	–
	4	–	0.14 ± 0.04^{d}	–
	−20	0.09 ± 0.01^{e}	0.07 ± 0.03^{d}	–
DHLA	30–40	–	0.35 ± 0.05^{a}	0.07 ± 0.02^{a}
		–	2.5 ± 0.50^{b}	0.14 ± 0.04^{b}
		–	5.00 ± 0.50^{c}	0.24 ± 0.04^{c}
		–	12.83 ± 0.76^{d}	0.41 ± 0.04^{d}
	4	–	0.43 ± 0.03^{d}	0.14 ± 0.04^{d}
	−20	0.14 ± 0.04^{e}	0.2 ± 0.03^{d}	0.06 ± 0.02^{d}

Results are reported as mean ± SD
[a]After 4 h
[b]After 8 h
[c]After 12 h
[d]After 24 h
[e]After 1 week

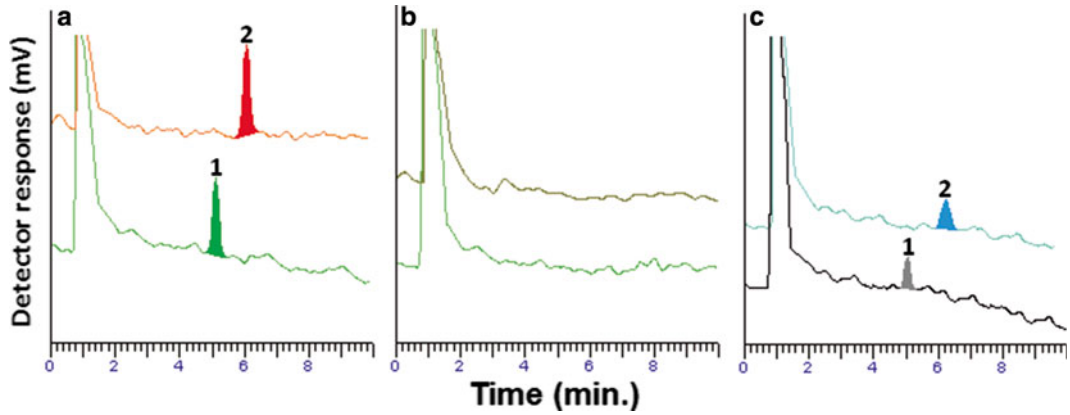

Fig. 3 RP-HPLC chromatograms showing peaks of the α-lipoic acid (peak *1*) and dihydrolipoic acid (peak *2*) at the level of LLOQ (a) and LOD (c)

2. Solid-phase extraction (SPE) procedures have also been reported for the extraction of the α-LA from complex sample matrices [12, 13, 15, 17, 20] and these procedures offer comparable recoveries and clear chromatograms. However, SPE is a much more expensive procedure than the LLE and PP.

3. The use of milder extraction conditions is advantageous over using drastic acid, base, and enzymatic hydrolytic procedures (summarized in the review article by Kataoka [26]) because such conditions result in the release of undesired bound LA as well. Moreover, LA tends to become oxidized to its thiosulfinate or thiosulfonate form by drastic hydrolysis resulting in poor recovery of the analytes [26].
4. Treatment of sample matrices with 10 μl (1/20 parts) of 20 mg/ml (70 mM) TCEP·HCl solution in 50 mM KH_2PO_4 buffer: pH 2.5 with 85 % OPA by vigorous vortex-mixing for about 5 min at room temperature was sufficient to completely reduce the α-LA to DHLA.

   TCEP·HCl concentration in slightly molar excess is usually used for reduction of thiols and variable volumes (10–100 μl) of TCEP·HCl solution (100–120 mg/ml) have been used for reduction purpose [27, 28]. However, using such a high concentration of TCEP·HCl solution results in a troublesome peak at the solvent front that suppresses other peaks in the chromatogram. To overcome this problem, lower concentrations of the TCEP·HCl solution were tried and it was found that even 10 μl (1/20 parts) of the 10 mg/ml TCEP·HCl solution was sufficient to completely reduce 200 μl (1 part) of sample matrices spiked with 50 μl (1/4 parts) of the 5 μg/ml α-LA solution. But to ensure complete reduction, 10 μl (1/20 parts) of 20 mg/ml TCEP·HCl solution was used for reduction instead of using 10 mg/ml.

   Researchers have insisted the use of BPS: pH 7.4 as the neutral medium for catalyzing the reduction of the α-LA to DHLA [27, 28]; however, according to our findings, the same reaction can occur quite efficiently in 50 mM KH_2PO_4 buffer: pH 2.5 with 85 % OPA.

   Vigorous shaking of the sample matrices with TCEP·HCl solution at room temperature for 5 min is sufficient to complete the reduction reaction.
5. Depending upon the nature of the analytes, a routinely used RP column, C_{18} (150 × 4.6 mm, 5 μm) can be efficiently utilized for the separation of the α-LA and DHLA. Although the use of a longer column (250 mm) has also been reported for the analysis of the α-LA [13], a shorter column offers the advantages of lesser mobile phase consumption and shorter run time over the longer column without affecting peaks resolution.
6. Different isocratic mobile phases, consisting of MeOH, ACN, or MeOH-ACN mixture (50:50 v/v) as the organic and pH adjusted water with either TFA or 85 % OPA or 50 mM KH_2PO_4 buffer: pH adjusted with 85 % OPA (pH 2.0–3.5) as the aqueous buffered components, were utilized.

Of the various organic components, better results are obtained with pure ACN as compared to pure MeOH or their 50–50 mixture because the retention times of the analytes are longer with both MeOH and MeOH–ACN (50:50 v/v) even with mobile phases containing 50 % organic modifier. A mobile phase containing not more than 35 % ACN is able to resolve the two peaks efficiently. Using higher than 35 % of ACN results in poor resolution of the two peaks. In fact the two peaks co-elute when 50 % or higher ratio of the ACN is used.

As far as buffered aqueous component of the mobile phase is concerned, most favorable results were obtained with 50 mM KH_2PO_4 buffer: pH adjusted with 85 % OPA. The pH adjusted water with TFA can also be used as the buffered aqueous component of the mobile phase; however, it causes ugly post peak dips, which are actually the characteristic of PED techniques. Likewise, there were significant inter-run differences in the retention times of the analytes in case of the pH adjusted water with OPA.

As far as pH of the mobile phase was concerned, tailing in peaks was observed above pH 2.7. However, when pH was decreased to 2.7, the tailing was almost negligible. Below this pH, peaks were symmetrical and were unaffected in the range of 2.6–2.0. So pH 2.5 was selected to be the optimum pH for simultaneous determination of the α-LA and DHLA.

7. The mobile phase was pumped at various flow rates in the range of 1.0–2.5 ml/min but the selected flow rate of 2.0 ml/min was able to efficiently resolve the two analytical peaks in less than seven min without building too much backpressure on the column.
8. Separation of the analytes was performed at various column oven temperatures in the range of 25–40 °C. Peak shape and height were improved and retention time decreased with increasing temperature up to 35 °C without affecting peak area and resolution. Above 35 °C, peak area and resolution were adversely affected and background current was too much raised, although retention time of the analytes was further decreased. So depending upon these parameters, 35 °C was selected to be the optimum temperature for the separation of the two analytes.
9. Injection of higher volume of the sample (10–20 µl) resulted in broader peaks and a troublesome solvent artifact, probably due to the elution of a very high concentration of some early eluting polar hydrophilic impurities with the mobile phase. So to overcome these problems, injection volume was kept at 5 µl.

10. As far as internal standard (IS) was concerned, several sulfur-containing compounds such as *n*-acetyl cysteine, cefixime, and cefdinir and naproxen sodium were tried but none of them obtained favorable results under the optimum chromatographic conditions for the two analytes. Thus the two analytes were quantified from the calibration curve (external standard method) without using any IS.
11. A voltammogram or current–voltage (*I/E*) relationship is the characteristic of every analyte and it gives information about the optimum working potential that can be used to improve detection sensitivity, selectivity, and reproducibility. Several approaches are used to obtain a voltammogram; however, a hydrodynamic voltammogram is the most reliable as it is taken under the real chromatographic conditions. Thus reliable information is obtained about the signal-to-noise ratio (*S/N*). A high working potential is required with respect to sensitivity. However, more analytes are detectable at higher working potentials. So, as to selectivity, a low working potential is favorable. On the other hand, working at a potential on the slope of the voltammogram will result in less reproducibility as not only a small fluctuation in the applied potential, but any other change in the system may result in a large variation in the current. Thus in practice, the choice of the working potential should be a compromise between sensitivity, selectivity, and reproducibility.
12. Hydrodynamic voltammograms for the two analytes show that the two analytes behave anomalously from the standard voltammogram in the range of 0.5–0.6 V. Detector response to α-LA increased from 0.2 to 0.55 V. It then decreased slightly at 0.6 V. However, it again increased from 0.7 to 0.9 V where its maximum response was observed. Above 0.9 V, the detector response to α-LA became constant. On the other hand, detector response to DHLA increased from 0.2 to 0.5 V where its maximum response was observed. Above 0.5 V, detector response to it decreased and reached to its lowest value at 0.6 V. It then increased again up to 0.9 V but never achieved its highest value observed at 0.5 V. Moreover, detector response was fluctuating in the range of 0.4–0.6 V and peaks were much broader and tailed in the range of 0.2–0.7 V.

Acknowledgement

The authors are thankful to the higher education commission (HEC), Pakistan for funding this study.

References

1. Chidlow G et al (2002) [alpha]-Lipoic acid protects the retina against ischemia-reperfusion. Neuropharmacology 43:1015–1025
2. Gurer H et al (1999) Antioxidant role of [alpha]-lipoic acid in lead toxicity. Free Radic Biol Med 27:75–81
3. Holmquist L et al (2007) Lipoic acid as a novel treatment for Alzheimer's disease and related dementias. Pharmacol Ther 113:154–164
4. Packer L et al (1995) Alpha-lipoic acid as a biological antioxidant. Free Radic Biol Med 19:227–250
5. Navari-Izzo F et al (2002) Lipoic acid: a unique antioxidant in the detoxification of activated oxygen species. Plant Physiol Biochem 40:463–470
6. Constantinescu A, Pick U (1995) Reduction and transport of lipoic acid by human erythrocytes. Biochem Pharmacol 50:253–261
7. Smith A et al (2004) Lipoic acid as a potential therapy for chronic diseases associated with oxidative stress. Curr Med Chem 11:1135–1146
8. Ramakrishnan N et al (1992) Radioprotection of hematopoietic tissues in mice by lipoic acid. Radiat Res 130:360–365
9. Durrani AI et al (2010) Determination of free [alpha]-lipoic acid in foodstuffs by HPLC coupled with CEAD and ESI-MS. Food Chem 120:1143–1148
10. Durrani A et al (2007) [alpha]-Lipoic acid in dietary supplements: Development and comparison of HPLC-CEAD and HPLC-ESI-MS methods. J Pharm Biomed Anal 45:694–699
11. Trivedi R et al (2004) Determination of lipoic acid in rat plasma by LC MS/MS with electrospray ionization: assay development, validation and application to a pharamcokinetic study. Biomed Chromatogr 18:681–686
12. Teichert J, Preiß R (1995) Determination of lipoic acid in human plasma by high-performance liquid chromatography with electrochemical detection. J Chromatogr B 672:277–281
13. Khan A et al (2010) Determination of lipoic acid in human plasma by HPLC-ECD using liquid-liquid and solid-phase extraction: method development, validation and optimization of experimental parameters. J Chromatogr B 878:2782–2788
14. Chen J et al (2005) Quantification of lipoic acid in plasma by high-performance liquid chromatography-electrospray ionization mass spectrometry. J Chromatogr B 824:249–257
15. Teichert J, Preiß R (2002) High-performance liquid chromatographic assay for [alpha]-lipoic acid and five of its metabolites in human plasma and urine. J Chromatogr B 769:269–281
16. Chng HT et al (2010) A sensitive LC/MS/MS bioanalysis assay of orally administered lipoic acid in rat blood and brain tissue. J Pharm Biomed Anal 51:754–757
17. Teichert J, Preiß R (1997) High-performance liquid chromatography methods for determination of lipoic and dihydrolipoic acid in human plasma. Methods Enzymol 279:159–166
18. Haj-Yehia AI et al (2000) Determination of lipoic acid and dihydrolipoic acid in human plasma and urine by high-performance liquid chromatography with fluorimetric detection. J Chromatogr A 870:381–388
19. Satoh S et al (2007) Simultaneous determination of [alpha]-lipoic acid and its reduced form by high-performance liquid chromatography with fluorescence detection. J Chromatogr B 854:109–115
20. Teichert J, Preiß R (1992) HPLC-methods for determination of lipoic acid and its reduced form in human plasma. Int J Clin Pharmacol Ther Toxicol 30:511
21. Han D et al (1995) Analysis of reduced and oxidized lipoic acid in biological samples by high-performance liquid chromatography. Methods Enzymol 251:315
22. Handelman GJ et al (1994) [alpha]-Lipoic acid reduction by mammalian cells to the dithiol form, and release into the culture medium. Biochem Pharmacol 47:1725–1730
23. Sen CK et al (1999) Determination of oxidized and reduced lipoic acid using high-performance liquid chromatography and coulometric detection. Methods Enzymol 299:239
24. Epshtein N (2004) Validation of HPLC techniques for pharmaceutical analysis. Pharmaceut Chem J 38:212–228
25. Khan MI et al (2010) Optimization and validation of RP-LC/UV–VIS detection method for simultaneous determination of fat-soluble antioxidant vitamins, all-trans-retinol and -tocopherol in human serum: effect of experimental parameters. Chromatographia 77:577–586
26. Kataoka H (1998) Chromatographic analysis of lipoic acid and related compounds. J Chromatogr B Biomed Sci Appl 717:247–262
27. Pfeiffer CM et al (1999) Rapid and accurate HPLC assay for plasma total homocysteine and cysteine in a clinical laboratory setting. Clin Chem 45:290
28. Nolin TD et al (2007) Simultaneous determination of total homocysteine, cysteine, cysteinylglycine, and glutathione in human plasma by high-performance liquid chromatography: application to studies of oxidative stress. J Chromatogr B 852:554–561

Chapter 26

Aryl-Acetic and Cinnamic Acids as Lipoxygenase Inhibitors with Antioxidant, Anti-inflammatory, and Anticancer Activity

Dimitra Hadjipavlou-Litina and Eleni Pontiki

Abstract

Cinnamic acids have been identified as interesting compounds with cytotoxic, anti-inflammatory, and antioxidant properties. Lipoxygenase pathway, catalyzing the first two steps of the transformation of arachidonic acid into leukotrienes is implicated in several processes such as cell differentiation, inflammation and carcinogenesis. Development of drugs that interfere with the formation or effects of these metabolites would be important for the treatment of various diseases like asthma, psoriasis, ulcerative colitis, rheumatoid arthritis, atherosclerosis, cancer, and blood vessel disorders. Till now, asthma consists of the only pathological case in which improvement has been shown by lipoxygenase LO inhibitors. Thus, the research has been directed towards the development of drugs that interfere with the formation of leukotrienes.

In order to explore the anti-inflammatory and cytotoxic effects of antioxidant acrylic/cinnamic acids a series of derivatives bearing the appropriate moieties have been synthesized via the Knoevenagel condensation and evaluated for their biological activities. The compounds have shown important antioxidant activity, anti-inflammatory activity and very good inhibition of soybean lipoxygenase while some of them were tested for their anticancer activity.

Key words Cinnamic acids, Antioxidants, Lipoxygenase inhibitors, Inflammation, Oxidative stress, Cancer

1 Introduction

Cinnamic acids have been identified as interesting targets with cytotoxic, anti-inflammatory, and antioxidant properties. The cinnamoyl moiety is present in a variety of biologically active substances as highlighted by several studies [1, 2]. Especially, 2′-hydroxycinnamaldehyde and the analogue 2′-benzoyloxycinnamaldehyde induce apoptosis in cancer cells via the induction of cellular reactive oxygen species (ROS) [3]. Recently antitumor activities of various cinnamic acid derivatives were explored by many research groups [4–7]. Moreover, many natural products and synthetic compounds act as anti-inflammatory agents via the

Donald Armstrong (ed.), *Advanced Protocols in Oxidative Stress III*, Methods in Molecular Biology, vol. 1208,
DOI 10.1007/978-1-4939-1441-8_26,

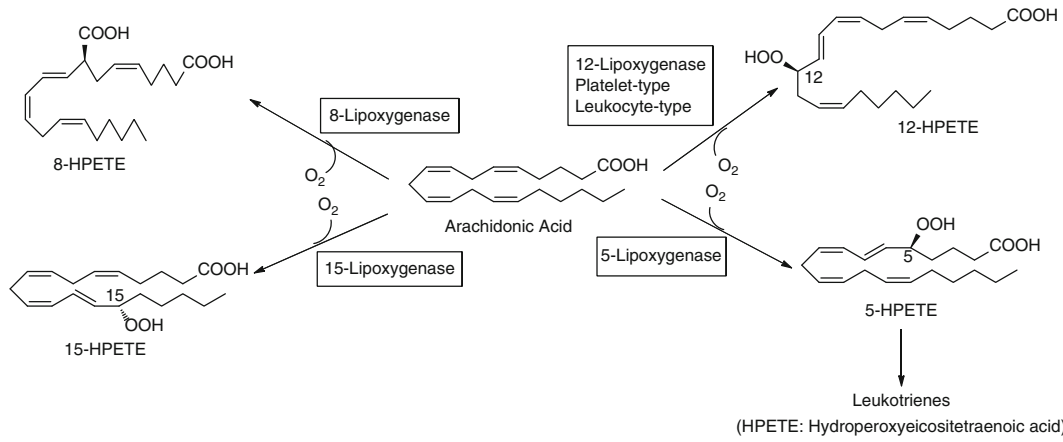

Fig. 1 Classification of LO in mammals and their products from arachidonic acid metabolism

lipoxygenase (LO) pathway by reducing the active site iron thereby uncoupling the catalytic cycle of the enzyme. Thus, phenols like nordihydroguaretic acid, caffeic acid, flavonoids, coumarins, or compounds like phenidone are efficient 5-LO inhibitors in vitro and in vivo [8, 9].

Lipoxygenases (LOs) include several members and constitute a family of dioxygenases containing one non-heme iron atom per molecule, which oscillates between Fe^{2+} (inactive enzyme) and Fe^{3+} (active form) during the catalytic cycle. They catalyze the oxygenation of polyunsaturated fatty acids containing a (1Z, 4Z)-penta-1,4-diene system to the corresponding hydroxyperoxy derivatives [10]. LOs act via a complicated free radical mechanism and with respect to their positional specificity of arachidonic acid oxygenation they are categorized: 5-LOs, 8-LOs, 9-LOs, 11-LOs, 12-LOs, and 15-LOs [11, 12] (*see* Fig. 1).

It has been found that LOs are implicated in several processes such as cell differentiation, inflammation, and carcinogenesis. Development of drugs that interfere with the formation or effects of these metabolites would be important for the treatment of various diseases like asthma, psoriasis, ulcerative colitis, rheumatoid arthritis, atherosclerosis, cancer, and blood vessel disorders [8, 13–15].

Inflammation represents a risk and causative factor for several types of cancer. The functional relationship between arachidonic acid metabolism, inflammation, and carcinogenesis has been extensively examined in numerous molecular studies, revealing potential novel targets like metabolizing enzymes [16, 17]. LO-catalyzed products may activate transcription factors of the peroxisome proliferator-activated receptor/PPAR family, or may interact with specific transmembrane G protein-coupled cell surface receptors in an autocrine or paracrine manner [18, 19].

Moreover, under "oxidative stress" conditions, reactive oxygen species (ROS) in the form of superoxide anion, hydroxyl radical and hydrogen peroxide, attack various biological macromolecules (proteins, enzymes, DNA, etc.) or indirectly may interfere with mechanisms of DNA repair [20]. Oxidative stress can activate signal transduction pathways, leading to the expression of genes, including those for growth factors, inflammatory cytokines, chemokines, cell cycle regulatory molecules, and anti-inflammatory molecules [21].

It is of increasing interest that the treatment of the above-mentioned pathophysiological conditions could benefit from multifunction molecules combining the above activities. Our group has explored the cytotoxic and anti-inflammatory effects of antioxidant acrylic/cinnamic acids associated with their pro-oxidant effects [16–19]. The antioxidant, anti-inflammatory, and anticancer properties of aryl-acetic–cinnamic acids are known to be influenced to a great extent by the substitutions of the aryl ring and the double bond.

LO inhibitors present a valuable target for the treatment of various diseases such as asthma, inflammation, cancer, cardiovascular diseases, etc. Detailed information on the classification and characterization of the LOs family of enzymes is provided by two reviews of our group, the first one covers the literature from the disclosure of LO until mid 2005, while the second one covers the principal literature for LO inhibitors from 2005 until 2011 [25, 26].

In this report, we focus on our contribution to the design and synthesis of aryl-acetic and cinnamic acids by presenting the methodology we have used.

2 Materials

2.1 Equipment

The described reactions and purification protocols have been performed using standard equipment available in synthetic organic chemistry laboratories.

2.2 Reagents

1. All the chemicals used were of analytical grade and commercially available by Merck, Fluka, and Aldrich Chemical Co. Milwaukee, WI, (USA).
2. All starting materials were obtained from commercial sources and used without further purification.
3. Melting Points (uncorrected) were determined on a MEL-Temp II (Lab. Devices, Holliston, MA, USA).
4. UV–Vis spectra were obtained on a Perkin-Elmer 554 beam spectrophotometer and on a Hitachi U-2001 spectrophotometer.

5. Infrared spectra (film as Nujol mulls) were recorded with a Shimadzu FTIR-8101M.
6. The ^{1}H Nucleic Magnetic Resonance (NMR) spectra were recorded at 300 MHz on a Bruker AM 300 spectrometer (Bruker Analytische Messtechnik GmbH, Rheinstetten, Germany) in $CDCl_3$ or DMSO using tetramethylsilane as an internal standard unless otherwise stated. ^{13}C-NMR spectra were obtained at 75 MHz on a Bruker AM 300 spectrometer in $CDCl_3$ or DMSO solutions with tetramethylsilane as internal reference unless otherwise stated.
7. Elemental analyses were obtained on an acceptable range (±0.4 %) in a Perkin-Elmer 240B CHN analyzer (The Perkin-Elmer Corporation Ltd.).
8. Reactions were monitored by thin-layer chromatography (TLC) by Fluka, on aluminum cards precoated with 0.2 mm of silica gel and fluorescent indicator.

3 Methods

3.1 Synthetic Method of Phenyl-Substituted Aryl-Acetic Acids

Title compounds were prepared by a by a Knoevenagel reaction, as illustrated in Scheme 1, according to literature methods [22–24]. A suitable aldehyde (0.015 mol) was condensed with phenylacrylic acid (0.015 mol) and acetic acid anhydride (10 mL) in the presence of triethylamine (5 mL) (*see* **Note 1**). The reaction mixture was refluxed for 5 h (*see* **Note 2**). The solution was poured into 2 N HCl, then on ice and the formed precipitate was collected by filtration and recrystallized from 50 % aqueous ethanol. In case that no precipitate was formed an extraction with 3×100 mL

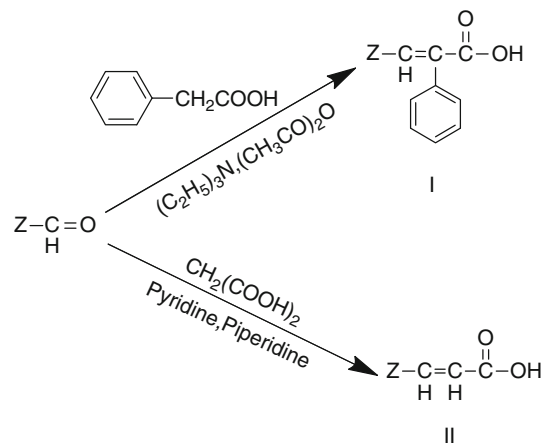

Scheme 1 Synthesis of substituted aryl-acetic acids

$CHCl_3$ was made and the organic phase was collected, dried over Mg_2SO_4 and evaporated to dryness affording a residue that was recrystallized from 50 % aqueous ethanol (*see* **Note 3**).

3.2 Synthetic Method of Aryl-Acetic Acids

Title compounds were prepared, as illustrated in Scheme 1, by a Knoevenagel condensation of the suitable aldehyde with malonic acid. Malonic acid (0.01 mol) was dissolved in 1.12 mL of pyridine and the aldehyde (0.01 mol) and piperidine (0.01 mol) were added (*see* **Note 1**). The mixture was refluxed until the emission of CO_2 stopped (*see* **Note 2**). Then the solution was poured into 2 N HCl and then on ice. The formed precipitate was collected by filtration and recrystallized from water or from 3:1 water/ethanol mixture. If no precipitate was formed an extraction with 3×100 mL $CHCl_3$ or CH_2Cl_2 was made and the organic phase was collected, dried over Mg_2SO_4, and evaporated to dryness affording a residue that was recrystallized from aqueous ethanol (*see* **Note 3**) [22–24].

3.3 Synthesized Compounds

3.3.1 Phenyl-Substituted Aryl-Acetic Acids (See Fig. 2)

3-(3-Phenoxy-phenyl)-2-phenyl-acrylic acid (1i)
According to the general synthetical procedure I, using 3-phenoxy-benzaldehyde. A precipitate was formed, which was filtered and recrystallized from 50 % aqueous ethanol, to the final pure product. Reaction yield: 56 %.

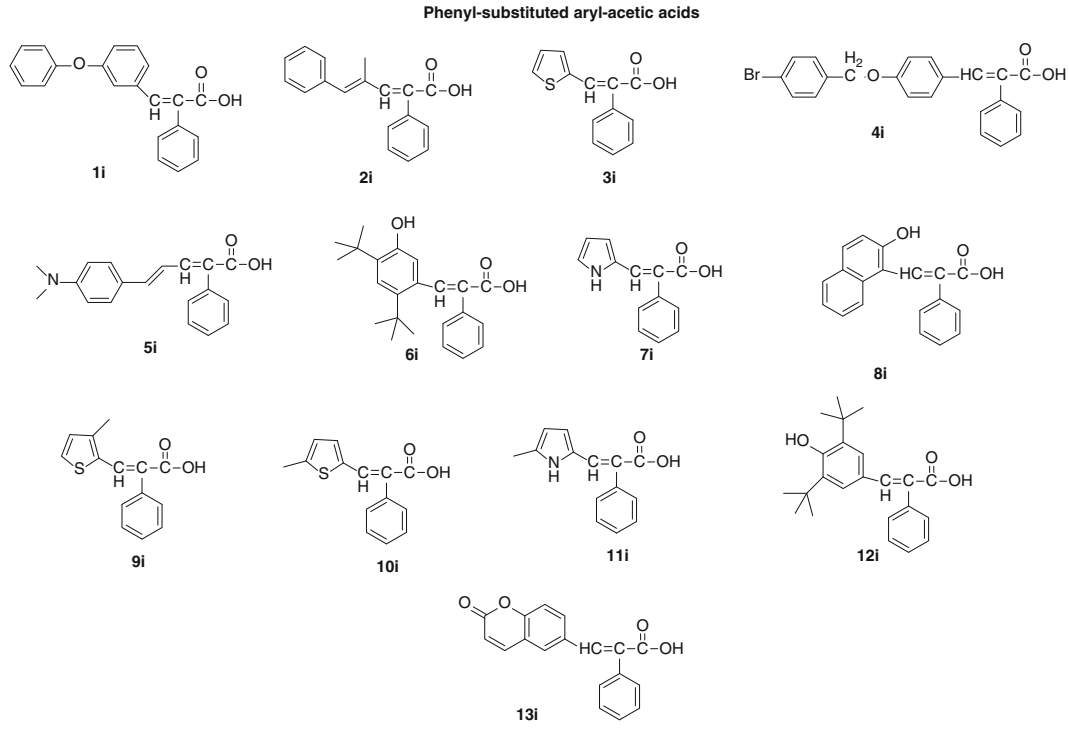

Fig. 2 Phenyl-substituted aryl-acetic acids

4-Methyl-2,5-diphenyl-penta-2,4-dienoic acid (2i)
According to the general synthetical procedure I, using 2-methyl-3-phenylacrylaldehyde. After adding ice and HCl acid, no precipitate was formed. The acidic solution was extracted with 3×100 mL $CHCl_3$. The organic layers were collected, combined and dried over Mg_2SO_4. The product in a liquid form was distilled and purified to the final one. Reaction yield: 91 %.

2-Phenyl-3-thiophen-2-yl-acrylic acid (3i)
According to the general synthetical procedure I, using thiophene-2-carbaldehyde. A precipitate was formed, which was filtered and recrystallized from 50 % aqueous ethanol, to the final pure product. Reaction yield: 47 %.

3-[4-(4-Bromo-benzyloxy)-phenyl]-2-phenyl-acrylic acid (4i)
According to the reported general procedure I, using 4-(4-bromobenzyloxy-benzaldehyde. A precipitate was formed, which was filtered and recrystallized from 50 % aqueous ethanol, to the final pure product. Reaction yield: 53 %.

5-(4-Dimethylamino-phenyl)-2-phenyl-penta-2,4-dienoic acid (5i)
According to the general synthetical procedure I, using 3-(4-(dimethylamino)phenyl)acrylaldehyde. A precipitate was formed, which was filtered and recrystallized from 50 % aqueous ethanol, to the final pure product. Reaction yield: 37 %.

3-(3,5-Di-tert-butyl-2,4-dihydroxy-phenyl)-2-phenyl-acrylic acid (6i)
According to the general synthetical procedure I, using 3,5-di-tert-butyl-2-hydroxybenzaldehyde. A precipitate was formed, which was filtered and recrystallized from 50 % aqueous ethanol, to the final pure product. Reaction yield: 73 %.

2-Phenyl-3-(1H-pyrrol-2-yl)-acrylic acid (7i)
According to the general synthetical procedure I, using 1H-pyrrol-2-yl carboxaldehyde. A precipitate was formed, which was filtered and recrystallized from 50 % aqueous ethanol, to the final pure product. Reaction yield: 25 %.

3-(2-Hydroxy-naphthalen-1-yl)-2-phenyl-acrylic acid (8i)
According to the general synthetical procedure I, using 2-Hydroxy-naphthalen-1-yl carboxaldehyde. A precipitate was formed, which was filtered and recrystallized from 50 % aqueous ethanol, to the final pure product. Reaction yield: 53 %.

3-(3-Methyl-thiophen-2-yl)-2-phenylacrylic acid (9i)
According to the general synthetical procedure I, using 3-methyl-thiophene-2-carbaldehyde. A precipitate was formed, which was

filtered and recrystallized from 50 % aqueous ethanol, to the final pure product. Reaction yield: 28 %.

3-(5-Methyl-thiophen-2-yl)-2-phenylacrylic acid (10i)
According to the general synthetical procedure I, using 5-methyl-thiophene-2-carbaldehyde. A precipitate was formed, which was filtered and recrystallized from 50 % aqueous ethanol, to the final pure product. Reaction yield: 43 %.

3-(5-Methyl-furan-2-yl)-2-phenylacrylic acid (11i)
According to the general synthetical procedure I, using 5-methyl-furan-2-carbaldehyde. A precipitate was formed, which was filtered and recrystallized from 50 % aqueous ethanol, to the final pure product. Reaction yield: 46 %.

3-(3,5-Di-tert-butyl-4-hydroxyphenyl)-2-phenylacrylic acid (12i)
According to the general synthetical procedure I, using 3,5-di-tert-butyl-4-hydroxybenzaldehyde. A precipitate was formed, which was filtered and recrystallized from 50 % aqueous ethanol, to the final pure product. Reaction yield: 72 %.

3-(2-Oxo-2H-chromen-6-yl)-2-phenyl-acrylic acid (13i)
According to the general synthetical procedure I, using 2-oxo-2H-chromen-6-carboxaldehyde, prepared from the oxidation of 6-methyl-2H-chromen-2-one with SeO_2. A precipitate was formed, which was filtered and recrystallized from 50 % aqueous ethanol, to the final pure product. Reaction yield: 36 %.

3.3.2 Substituted Aryl-Acetic Acids (See Fig. 3)

3-(3-Phenoxy-phenyl)-acrylic acid (1ii)
According to the general synthetical procedure II, using 3-phenoxy-benzaldehyde. A precipitate was formed, which was filtered and recrystallized from 50 % aqueous ethanol, to the final pure product. Reaction yield: 56 %.

4-Methyl-5-phenyl-penta-2,4-dienoic acid (2ii)
According to the general synthetical procedure II, using 2-methyl-3-phenylacrylaldehyde. After adding ice and HCl acid, no precipitate was formed. The acidic solution was extracted with 3×100 mL $CHCl_3$. The organic layers were collected, combined and dried over Mg_2SO_4. The product in a liquid form was distilled and purified to the final one. Reaction yield: 82 %.

3-Thiophen-2-yl-acrylic acid (3ii)
According to the general synthetical procedure II, using thiophene-2-carbaldehyde. A precipitate was formed, which was filtered and recrystallized from 50 % aqueous ethanol, to the final pure product. Reaction yield: 85 %.

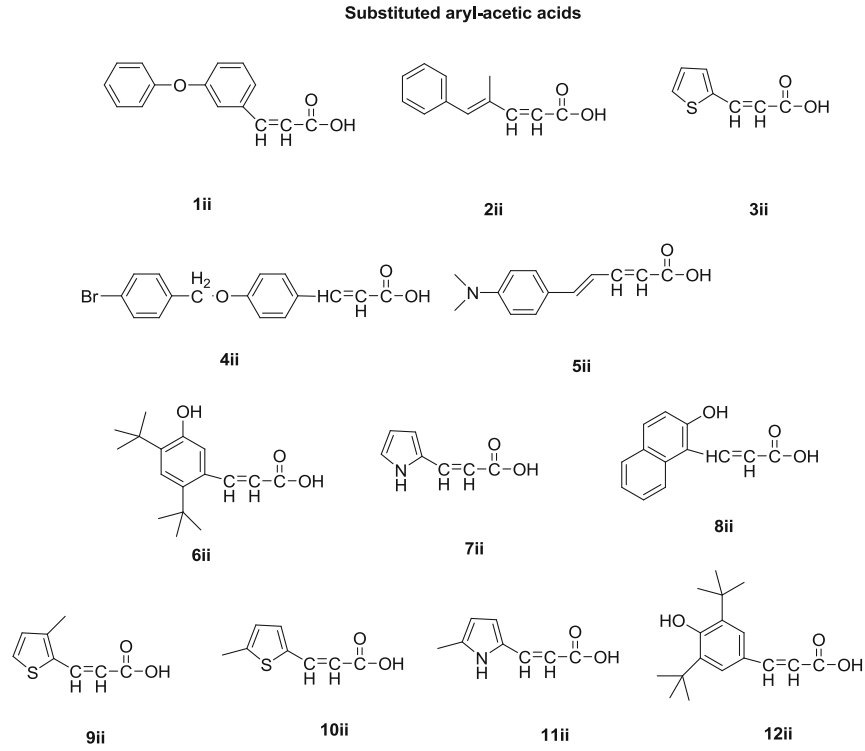

Fig. 3 Substituted aryl-acetic acids

3-[4-(4-Bromo-benzyloxy)-phenyl]-acrylic acid (4ii)
According to the reported general procedure II, using 4-(4-bromobenzyloxy-benzaldehyde. A precipitate was formed, which was filtered and recrystallized from 50 % aqueous ethanol, to the final pure product. Reaction yield: 53 %.

5-(4-Dimethylamino-phenyl)-penta-2,4-dienoic acid (5ii)
According to the general synthetical procedure II, using 3-(4-(dimethylamino)phenyl)acrylaldehyde. A precipitate was formed, which was filtered and recrystallized from 50 % aqueous ethanol, to the final pure product. Reaction yield: 37 %.

3-(3,5-Di-tert-butyl-2,4-dihydroxy-phenyl)-acrylic acid (6ii)
According to the general synthetical procedure II, using 3,5-di-tert-butyl-2-hydroxybenzaldehyde. After work up no precipitate was formed. The product in a liquid form was distilled and purified to the final one. Reaction yield: 46 %.

3-(1H-Pyrrol-2-yl)-acrylic acid (7ii)
According to the general synthetical procedure II, using 1H-pyrrol-2-yl carboxaldehyde. A precipitate was formed, which was filtered

and recrystallized from 50 % aqueous ethanol, to the final pure product. Reaction yield: 60 %.

3-(2-Hydroxy-naphthalen-1-yl)-acrylic acid (8ii)
According to the general synthetical procedure II, using 2-Hydroxy-naphthalen-1-yl carboxaldehyde. A precipitate was formed, which was filtered and recrystallized from 50 % aqueous ethanol, to the final pure product. Reaction yield: 72 %.

3-(3-Methylthiophen-2-yl)acrylic acid (9ii)
According to the general synthetical procedure II, using 3-methyl-thiophene-2-carbaldehyde. A precipitate was formed, which was filtered and recrystallized from 50 % aqueous ethanol, to the final pure product. Reaction yield: 59 %.

3-(5-Methylthiophen-2-yl)acrylic acid (10ii)
According to the general synthetical procedure II, using 5-methyl-thiophene-2-carbaldehyde. A precipitate was formed, which was filtered and recrystallized from 50 % aqueous ethanol, to the final pure product. Reaction yield: 64 %.

3-(5-Methylfuran-2-yl)acrylic acid (11ii)
According to the general synthetical procedure II, using 5-methyl-furan-2-carbaldehyde. A precipitate was formed, which was filtered and recrystallized from 50 % aqueous ethanol, to the final pure product. Reaction yield: 75 %.

3-(3,5-Di-tert-butyl-4-hydroxyphenyl)acrylic acid (12ii)
According to the general synthetical procedure II, using 3,5-di-tert-butyl-4-hydroxybenzaldehyde. A precipitate was formed, which was filtered and recrystallized from 50 % aqueous ethanol, to the final pure product. Reaction yield: 27 %.

3.4 Results

3.4.1 Antioxidant Activity

A number of assays have been used for the measurement of the antioxidant activity. Each method relates to the generation of different radical, acting through a variety of mechanisms and the measurement of a range of end points at a fixed time intervals. The antioxidant activity of the tested compounds is determined using different protocols and compared to appropriate reference compounds:

Determination of the Reducing Activity of the Stable Radical 1,1-Diphenyl-Picrylhydrazyl (DPPH) [22–24]

The reducing abilities of the novel derivatives were determined by the use of the stable radical DPPH after 20 and 60 min (indicating the radical scavenging ability in an iron-free system) (Table 1).

Table 1
Interaction % with DPPH (RA %); competition % with DMSO for hydroxyl radical ($HO^{\cdot}$ %)

	RA % 0.05 mM		RA % 0.1 mM		$HO^{\cdot}$ (%)		
Compd.	**20 min**	**60 min**	**20 min**	**60 min**	**0.001 mM**	**0.01 mM**	**0.1 mM**
1i	50.6	93.9	60.3	60.5	no	no	97.1
1ii	72.4	66.2	72.2	94.8	no	no	90.2
2i	98.6	92.1	99.7	71.5	94.3	97.2	97.7
2ii	75.1	86.1	75.6	55.3	94.2	98.7	nd
3i	72.7	93.4	70.8	68.8	91.3	93.9	94.3
3ii	70.2	94	76.3	62.5	no	87.9	87.1
4i	77.6	77.1	85.4	97.3	no	71.1	91.6
4ii	74.7	72.9	81.8	93.5	no	91.2	90.5
5i	82	74.4	94	81.5	99.1	96.7	93.3
5ii	85	87.6	88.2	89.9	no	no	95.3
6i	24	36	28	35	95	92	*
6ii	32	38	37	44	91	96	83
7i	22	29	23	35	86	96	88
7ii	26	32	25	33	no	94	*
8i	29	37	26	32	97	94	86
8ii	32	38	34	42	90	100	99.4
9i	1.7	no	5.9	2.8	nt	99.8	99.8
9ii	3.2	no	3.2	2.5	nt	98.9	97.9
10i	3.6	2.9	6.7	4.9	nt	99.3	97.8
10ii	3.5	1.0	4.4	4.3	nt	99.8	100
11i	3.2	1.4	3.6	4.8	nt	98.1	99.6
11ii	4.8	3.0	8.6	7.6	nt	99.8	99.5
12i	2.8	5.3	7.6	12.2	nt	97.8	100
12ii	28.1	26.9	31.6	36.9	nt	100	99.4
13i	76.1	81.6	66.4	91.5	no	96.2	96.7
BHT			31.3	60			
NDGA	84.8	83.1	81.0	82.6			
Caffeic acid			9.3	9.02			
Trolox					nt	73.4	88.2

no no action under the experimental conditions, *nt* not tested, *nd* not determined, *problems of dissolution under the experimental conditions

Competition of the Tested Compounds with DMSO for Hydroxyl Radicals [22–24]

The cytotoxicity of $O_2^{\cdot-}$ and H_2O_2 in living organisms is mainly due to their transformation into $^{\cdot}OH$ reactive radical and $^1O_2$. Hydroxyl radicals are among the most reactive oxygen species and are considered to be in part responsible for tissue damage occurring in inflammation.

The competition of the new acids with DMSO for $^{\cdot}OH$ radicals generated by the Fe^{3+}/ascorbic acid system expressed as percent inhibition of formaldehyde production was used for the evaluation of their radical scavenging activity (Table 1).

Non-enzymatic Assay of Superoxide Radicals: Measurement of Superoxide Radical Scavenging Activity [22–24]

An additional assay was performed to evaluate the radical scavenging property of our compounds, on non-enzymatically generated superoxide anion radicals (Table 2).

ABTS$^{+\cdot}$: Decolorization Assay for Antioxidant Activity [24]

Generation of the ABTS (2,2′-azinobis-(3-ethyl-benzothiazoline-6-sulfonic acid) radical cation, formed the basis for a further determination of the antioxidant activity of our compounds (Table 3).

Heme Protein-Dependent Lipid Degradation [22–24]

The compounds are tested for their ability to inhibit lipid peroxidation using the model of the peroxidation of arachidonic acid by a mixture of heme and H_2O_2. Mixing heme proteins with H_2O_2 generates powerfully oxidizing activated heme species and radicals on amino-acids side chains that can cause lipid peroxidation (Table 2).

Table 2
% Inhibition of heme dependent lipid peroxidation (LP %); % superoxide radical scavenging activity ($O_2^{\cdot-}$)

Compd.	A % LP-1 mM	$O_2^{\cdot-}$(%) 0.1 mM	$O_2^{\cdot-}$ (%) 1 mM
1i	32.1	no	no
1ii	37.8	67.9	72.3
2i	11.5	75.4	*
2ii	31.4	88.8	66.6
3i	0.60	52.1	*
3ii	29.5	82.1	95.7
4i	4.50	92.1	100
4ii	59.6	90	100
5i	no	92.5	100
5ii	no	69.2	100

(continued)

Table 2
(continued)

Compd.	A % LP-1 mM	$O_2^{-\cdot}$(%) 0.1 mM	$O_2^{-\cdot}$ (%) 1 mM
6i	71	61	nt
6ii	71	97	nt
7i	60	90	nt
7ii	73	85	nt
8i	74	96	nt
8ii	69	93	nt
9i	35.5	no	100
9ii	1.2	57.1	nt
10i	55.8	no	100
10ii	1.2	no	66.7
11i	49.2	50.0	nt
11ii	7.9	14.3	nt
12i	39.3	85.7	nt
12ii	54.1	35.7	nt
13i	23.1	70	71
Caffeic acid	21.9		86.1
NDGA	26.1		

no no action under the experimental conditions, *dissolution problems

Inhibition of Linoleic Acid Peroxidation [24]

Azo compounds generating free radicals through spontaneous thermal decomposition are useful for in vitro studies of free radical production. The water soluble 2,2′-azobis (2-amidinopropane) hydrochloride (AAPH) has been extensively used as a clean and controllable source of thermally produced alkylperoxyl free radicals (Table 3).

3.4.2 In Vitro Enzymatic Inhibitory Activity of LO and COX-1

Soybean Lipoxygenase Inhibition Study In Vitro [22–24]

Compounds were evaluated for the inhibition of soybean LO (SLO) by the UV-based enzyme assay of Taraporewala and Kauffman [27]. While one may not extrapolate the quantitative results of this assay to the inhibition of mammalian 5-LOX, it has been shown that inhibition of plant LO activity by NSAIDs is qualitatively quite similar to their inhibition on the rat mast cells LO and this assay may be used as a qualitative or semi-quantitative screen for such activity. The compounds presented very good inhibitory activity against SLO (Table 4).

Table 3
$ABTS^{+\cdot}$—decolorization ($ABTS^{+\cdot}$ %) and inhibition of linoleic acid peroxidation (AAPH) assays

Compd.	$ABTS^{+\cdot}$% 0.1 mM	AAPH% 0.1 mM
9i	18.8	20.1
9ii	41.7	64.9
10i	41.1	37.5
10ii	44.2	73.4
11i	65.6	32.6
11ii	37.1	74.9
12i	60.3	60.1
12ii	53.9	74.8
Trolox	88.0	63.0
Ascorbic acid	95.8	nt

nt not tested

In Vitro Cyclooxygenase-1 (COX-1) Inhibition Study [22, 24]

Compounds were examined for their inhibitory activity towards COX-1. They resulted moderately active and no correlation was observed between the anti-inflammatory activity and COX-1 inhibition (Table 4).

3.4.3 In Vivo Anti-inflammatory Activity: Inhibition of the Carrageenin-Induced Edema [22–24]

The in vivo anti-inflammarory effects of the tested acids were assessed by using the carrageenin-induced rat paw edema (CPE) model as percentage of weight decrease at the right hind paw. The induced edema is a nonspecific inflammation highly sensitive to NSAIDs and it is largely accepted as a useful tool for studying new anti-inflammatory agents [28]. It reliably predicts the anti-inflammatory potency of the NSAIDs and detects during the second phase of inflammation process that they are anti-inflammatory agents as a result of inhibition of prostaglandin amplification [29] (Table 4).

3.4.4 In Vitro Anticancer Activity [30]

There is a close association between inflammation and cancer. Aryl-acetic acids have been tested in different human tumor cell lines: HT-29 (colon), OAW-42 (ovarian), A-549 (lung), and BT-20 (breast) and normal cells [31]. On the basis of the in vitro testing results, most of these compounds with different substitution patterns exhibited significant anticancer activity Table 5.

Table 4
Inhibition % of induced carrageenin rat paw edema (CPE %); in vitro inhibition of soybean lipoxygenase (LO) (IC_{50}); in vitro inhibition of cyclooxygenase-1 (COX-1 %)

Compd.	CPE (%)[a], 0.01 mM	LO, IC_{50} (μM)	COX-1 %, 1 mM
1i	70.9*	no	57.8
1ii	41.6*	66	nt
2i	44.1**	no	100
2ii	49.0**	95	nt
3i	65.5*	242	nt
3ii	42.7**	98	nt
4i	62.3*	81	nt
4ii	44.4*	89	nt
5i	57.2**	96	nt
5ii	61.8*	79	nt
6i	43.4**	65	nt
6ii	45.7**	425	nt
7i	49.8*	70	nt
7ii	29.5*	170	nt
8i	25.2*	0.01 mM (66.3 %) 0.1 mM (70.4 %)	nt
8ii	44.1*	415	nt
9i	21.0**	310	75
9ii	63.0**	255	37.5
10i	53.0*	290	12.5
10ii	77.5*	280	75
11i	34.0*	240	nt
11ii	10.0*	315	nt
12i	43.0*	100	nt
12ii	2.0*	220	nt
13i	37.9*	75	15.1
Caffeic acid		600	
Sc-560			57.8
Indomethacin	47*		100
NDGA		515	

[a]Each value represents the mean of two independent experiments with 5 animals in each group, statistical studies were done with student's *T*-test
*$p<0.01$, **$p<0.05$; *no* no action under the experimental conditions

Table 5
Anticancer activity data of aryl-acetic acids

Compd.	IC_{50} (HT-29)	IC_{50} (A-549)	IC_{50} (OAW-42)	IC_{50} (BT-20)	IC_{50} (MRC-5)
1i	114.21	118.71	101.67	n.e.[a]	132.67
1ii	126.9	116.92	214.82	126.83	183.45
4i	109.27	107.05	65.5	n.e.	93.03
4ii	142.28	158.32	163.58	135.43	172.27
5i	78.86	146	137.94	n.e.	116.45
5ii	134.34	112.71	258.5	133.88	238.94
6i	101.39	232.23	191.94	n.e.	231.50

IC_{50} refers to the concentration of the compounds (in μM) required for 50 % growth inhibition of human cancer cells of several types
[a]*n.e.* not evaluated

4 Notes

1. It is better to work in a low scale (using small quantities of the reactants). Otherwise the reaction time is increased significantly.
2. After the heating period sometimes an amount of tar is produced. In this case we have used decolorizing carbon before recrystallization.
3. The recrystallization from 50 % aqueous ethanol must be undertaken with care. It is better to use a dilute ethanolic solution of the acid, leave it to come to the room temperature and then to pour carefully the water, to succeed the 50 % dissolution and a good rate of recrystallization. Otherwise an emulsion is derived. In this case evaporation takes place to dryness affording a residue that is recrystallized from the beginning.

References

1. Yoshimatsu K, Yamaguchi A, Yoshino H, Koyanagi N, Kitoh K (1997) Mechanism of action of E7010, an orally active sulfonamide antitumor agent: inhibition of mitosis by binding to the colchicine site of tubulin. Cancer Res 7:208–3213
2. Hideki Tanaka H, Ohshima N, Ikenoya M, Komori K, Katoh F, Hidaka H (2003) HMN-176, an active metabolite of the synthetic antitumor agent HMN-214, restores chemosensitivity to multidrug-resistant cells by targeting the transcription factor NF-Y. Cancer Res 63: 6942–6947
3. Han DC, Lee MY, Shin KD, Jeon SB, Kim JM, Son KH, Kim HC, Kim HM, Kwon BM (2004) 20-Benzoyloxycinnamaldehyde induces apoptosis in human carcinoma via reactive oxygen species. J Biol Chem 279:6911–6920
4. Bandgar BP, Gawande SS, Bodade RG, Totre JV, Khobragade CN (2010) Synthesis and biological evaluation of simple methoxylated chalcones as anticancer, anti-inflammatory and antioxidant agents. Bioorg Med Chem 18: 1364–1370
5. Cheng JH, Huang AM, Hour TC, Yang SC, Pu YP, Lin CN (2010) Antioxidant xanthone

derivatives induce cell cycle arrest and apoptosis and enhance cell death induced by cisplatin in NTUB1 cells associated with ROS. Eur J Med Chem 46:1222–1231

6. Kanagalakshmi K, Premanathan M, Priyanka R, Hemalatha B, Vanangamudi A (2010) Synthesis, anticancer and antioxidant activities of 7-methoxy-isoflavanone and 2,3-diarylchromanones. Eur J Med Chem 45:2447–2452
7. Karali N, Guzel Ö, Özsov N, Özbey S, Salman A (2010) Synthesis of new spiroindolinones incorporating a benzothiazole moiety as antioxidant agents. Eur J Med Chem 45: 1068–1077
8. Ford-Hutchinson AW, Gresser M, Young RN (1994) 5-Lipoxygenase. Annu Rev Biochem 63:383–417
9. Batt DG (1992) 5-Lipoxygenase inhibitors and their anti-inflammatory activities. Prog Med Chem 29:1–63
10. Kühn H (2007) Lipoxygenases. In: Marks F, Fürstenberger G (eds) Prostaglandins, laukotrienes and other eicosanoids: from biogenesis to clinical application. Wiley, Weinheim, Germany
11. Webb EC (1992) Enzyme Nomenclature 1992. Recommendations of the nomenclature Committee of the International Union of Biochemistry and Molecular Biology on the nomenclature and classification of the enzymes. Acad Press, San Diego, CA
12. Kuhn H (2000) Structural basis for the positional specificity of lipoxygenases. Prostaglandins Other Lipid Mediat 62:255–270
13. Kuhn H, Chaitidis P, Roffeis J, Walther M (2007) Arachidonic acid metabolites in the cardiovascular system: the role of lipoxygenase isoforms in atherogenesis with particular emphasis on vascular remodeling. J Cardiovasc Pharmacol 50:609–620
14. Pace-Asciak CR, Asotra S (1989) Biosynthesis, catabolism, and biological properties of HPETEs, hydroperoxide derivatives of arachidonic acid. Free Radic Biol Med 7:409–433
15. Radmark O, Samuelsson B (2007) 5-Lipoxygenase: regulation and possible involvement in atherosclerosis. Prostaglandins Other Lipid Mediat 8:162–174
16. Grivennikov SI, Greten FR, Karin M (2010) Immunity, inflammation, and cancer. Cell 140:883–899
17. Grivennikov SI, Karin M (2010) Inflammation and oncogenesis: a vicious connection. Curr Opin Genet Dev 20:65–71
18. Brash AR (1999) Lipoxygenases: occurrence, functions, catalysis, and acquisition of substrate. J Biol Chem 274:23679–23682
19. Norel X, Brink C (2004) The quest for new cysteinylleukotriene and lipoxin receptors: recent clues. Pharmacol Ther 103:81–94
20. Vera-Ramirez L, Sanchez-Rovira P, Ramirez-Tortosa MC, Ramirez-Tortosa CL, Granados-Principal S, Lorente JA, Quiles JL (2011) Free radicals in breast carcinogenesis, breast cancer progression and cancer stem cells. Biological bases to develop oxidative-based therapies. Crit Rev Oncol Hematol 80: 347–368
21. Reuter S, Gupta SC, Chaturvedi MM, Aggarwal BB (2010) Oxidative stress, inflammation, and cancer: how are they linked? Free Radic Biol Med 49:1603–1616
22. Pontiki E, Hadjipavlou-Litina D (2006) Antioxidant and anti-inflammatory activity of aryl-acetic and hydroxamic acids as novel lipoxygenase inhibitors. Med Chem 2:251–264
23. Pontiki E, Hadjipavlou-Litina D (2007) Synthesis and pharmacochemical evaluation of novel aryl-acetic acids inhibitors of lipoxygenase and antioxidants and anti-inflammatory agents. Biorg Med Chem 15: 5819–5827
24. Pontiki E, Hadjipavlou-Litina D, Litinas K, Nicolotti O, Carotti A (2011) Design, synthesis and pharmacobiological evaluation of novel acrylic acid derivatives acting as lipoxygenase and cyclooxygenase-1 inhibitors with antioxidant and anti-inflammatory activities. Eur J Med Chem 46:191–200
25. Pontiki E, Hadjipavlou-Litina D (2005) Lipoxygenases (LOs): an heterogenous family of lipid peroxidizing enzymes implicated in cell differentiation, inflammation, asthma, carcinogenesis, atherogenesis. An interesting target for the development of promising drugs. Curr Enh Inh 1:309–328
26. Pontiki E, Hadjipavlou-Litina D (2013) Targeting lipoxygenases (LOs): drug design and discovery. Curr Enz Inh 9:89–105
27. Taraporewala IB, Kauffman JM (1990) Synthesis and structure-activity relationships of anti-inflammatory 9,10-dihydro-9-oxo-2-acridine-alkanoic acids and 4-(2-carboxyphenyl)aminobenzenealkanoic acids. J Pharm Sci 79:173–178
28. Winter CA (1965) Anti-inflammatory testing methods: comparative evaluation of indomethacin and other agents. In: Garattini S, Dukes MNG (eds) International symposium on non-steroidal anti-inflammatory drugs. Excerpta Medica Foundation, Amsterdam
29. Kuroda T, Suzuki F, Tamura T, Ohmori K, Hosoe H (1992) A novel synthesis and potent antiin-

flammatory activity of 4-hydroxy-2(1H)-oxo-1-phenyl-1,8-naphthyridine-3-carboxamides. J Med Chem 5:1130–1136

30. Pontiki E, Hadjipavlou-Litina D, Geromichalos G, Papageorgiou A (2009) Anticancer activity and quantitative-structure activity relationship (QSAR) studies of a series of antioxidant/anti-inflammatory aryl-acetic and hydroxamic acids. Chem Biol Drug Des 74:266–275
31. Papazisis KT, Geromichalos GD, Dimitriadis KA, Kortsaris AH (1997) Optimization of the sulforhodamine B colorimetric assay. J Immunol Methods 208:151–158

Chapter 27

Liquid Chromatography and Mass Spectrometry for the Analysis of N-β-Methylamino-L-alanine with 6-Aminoquinolyl-*N*-Hydroxysuccinimidyl Carbamate

W. Broc Glover, Steven A. Cohen, and Susan J. Murch

Abstract

Numerous studies in the past decade have identified N-β-methylamino-L-alanine (BMAA) as a putative environmental neurotoxin. Produced by cyanobacteria and accumulated at different levels of the trophic system, BMAA has been detected in the brain tissue of human patients that died from progressive neurodegenerative disease. Research into the mechanism of neurotoxicity has been hampered by conflicting results and disagreement in the literature over analytical methods used for quantification and detection. While several research approaches have been tested, the use of the derivatizing reagent 6-aminoquinolyl-N-hydroxysuccinimidyl carbamate is presented here as an effective and selective means for the analysis of BMAA and two co-occurring biological isomers, DAB and AEG, by liquid chromatography and tandem mass spectrometry.

Key words BMAA, AEG, DAB, Amino acid analysis, 6-Aminoquinolyl-*N*-hydroxysuccinimidyl carbamate, Derivatization, AQC, Liquid chromatography, Tandem mass spectrometry

1 Introduction

Shortly after the Second World War, early reports began to appear describing a high frequency of amyotrophic lateral sclerosis (ALS) on the Micronesian island of Guam [1, 2]. Known as "lytico" by the indigenous Chamorro population [3], ALS was so common that nearly every household was affected by the disease [3]. While spatial clustering was readily observed, initial studies found no genetic correlation between those affected within the population [4]. Subsequent studies indicated that prevalence of the disease was based on neither viral infection nor nutrient deficiency [4].

In the early 1960s, the work of ethnobotanist Marjorie Whiting revealed that a preference for the traditional diet may have been involved in the onset of the disease [5], indicating, for the first time, a possible link between chronic exposure to an environmental toxin and the onset of neurodegenerative disease. The seeds of the indigenous

Donald Armstrong (ed.), *Advanced Protocols in Oxidative Stress III*, Methods in Molecular Biology, vol. 1208,
DOI 10.1007/978-1-4939-1441-8_27,

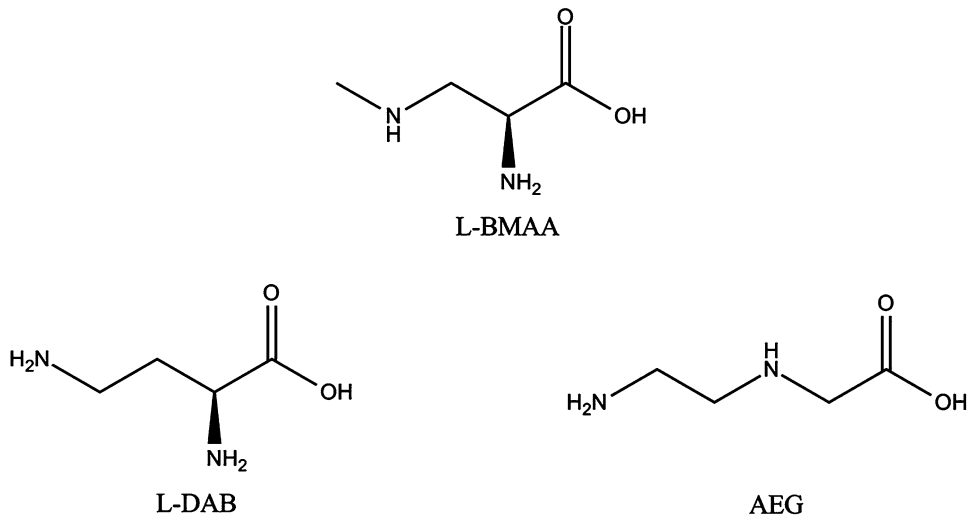

Fig. 1 The chemical structure of the isomeric amino acids BMAA, DAB, and AEG

cycad tree (*Cycas micronesica*), traditionally used to make a flour by the Chamorros, were found to contain high levels of an amino acid that eventually came to be known as N-β-methylamino-L-alanine (BMAA; Fig. 1) [6]. It was initially hypothesized that BMAA was produced by the cycads and was unique to these trees. Animal experiments demonstrated that ingestion of high levels of BMAA induced acute neurotoxicity, but cessation of exposure was followed by a concurrent loss of the associated symptoms [6, 7]. Duncan and coworkers argued that the doses used in the animal studies were much greater than the Chamorro would have consumed in Guam [8] and research in this area was virtually suspended. Renewed research began in the early 2000s with the hypothesis that BMAA could be accumulated at different trophic levels in the ecosystem and the traditional Chamorro food chain [9]. In addition, it was discovered that BMAA was produced not by cycad trees, but by an extremely taxonomically diverse set of cyanobacteria that live symbiotically in the roots of the cycad trees [10, 11]. Given both the ubiquity of cyanobacteria throughout the world and the environmental changes currently underway that may induce widespread proliferation of cyanobacteria, the implications for human health have become readily apparent. Our 2004 study reported significant levels of BMAA in the brain tissue of Canadian autopsy patients that died from Alzheimer's disease (AD) [12]. Subsequent studies have quantified BMAA in brain tissues of patients who died of AD and amyotrophic lateral sclerosis (ALS) [13]. However, other studies have reported conflicting results and some controversy was generated by studies that failed to detect BMAA in autopsy brain tissues of neurodegenerative patients.

In addition to its association with neurodegenerative diseases, recent works by several researchers have linked BMAA levels with oxidative stress. For example, Lobner et al. showed in 2007 that BMAA at concentrations as low as 10 μM can potentiate neuronal injury caused by other known neurotoxins [14], while Liu et al. validated the threefold activity of BMAA described by Lobner, and postulated that BMAA may induce oxidative stress via inhibition of the cystine/glutamate antiporter system Xc−, resulting in glutathione depletion and oxidative stress [15]. BMAA intake has also been linked by several groups to increases in reactive oxygen species (ROS) [15–18]. One possible explanation for BMAA's influence is the observation that it can inhibit antioxidative stress response enzymes such as catalase, glutathione peroxidase, and glutathione reductase [19]. They found that increasing ROS content in cells was correlated with increasing BMAA concentration, with a fivefold increase in ROS at an exposure concentration of 50 mg/L [19]. Given the potential for disease causation, and the challenges of measuring low levels of an unusual amino acid such as BMAA, developing appropriate analysis methods is essential.

Over 50 papers on the quantification of BMAA have now been published [20], but there has been a great deal of controversy over analytical methods [21]. Analysis of BMAA is complicated by the low levels of BMAA, a range of different sample matrices, different and conflicting methods, limited method information and potential isomers that complicated the analysis viz. diamino butyric acid (DAB) [22] and *N*-(2-aminoethyl)glycine (AEG) [23] (Fig. 1). Traditional amino acid analysis used ion-exchange chromatography to separate amino acids prior to post-column ninhydrin derivatization [21]. More recently, pre-column derivatization and reverse phase separations have become more common and offer increased sensitivity and selectivity, particularly for the analysis of isomeric compounds [22]. A variety of suitable derivatizing agents are available for amino acids with 6-aminoquinolyl-N-hydroxysuccinimidyl carbamate (AQC) most commonly used for analysis of BMAA (Fig. 2) [21]. An advantage of AQC is the unique product ions that can be generated from each of the isomers of BMAA (Fig. 3) in MS/MS experiments, thereby allowing for highly selective analysis of individual species. There is a need for sensitive, highly selective detection methods to decrease the risk of both false positives and negatives and it is essential that methods must differentiate the isomers but also take into account the potential adducts that may be formed [24].

At present, the ability to advance the science behind BMAA research has been significantly troubled by so many conflicting reports; to move the science behind BMAA research forward, a consensus on sound, rugged analytical methods will be necessary. The material presented here will serve as a framework for others new to the analysis of BMAA, and will strive to point out common pitfalls in the analysis.

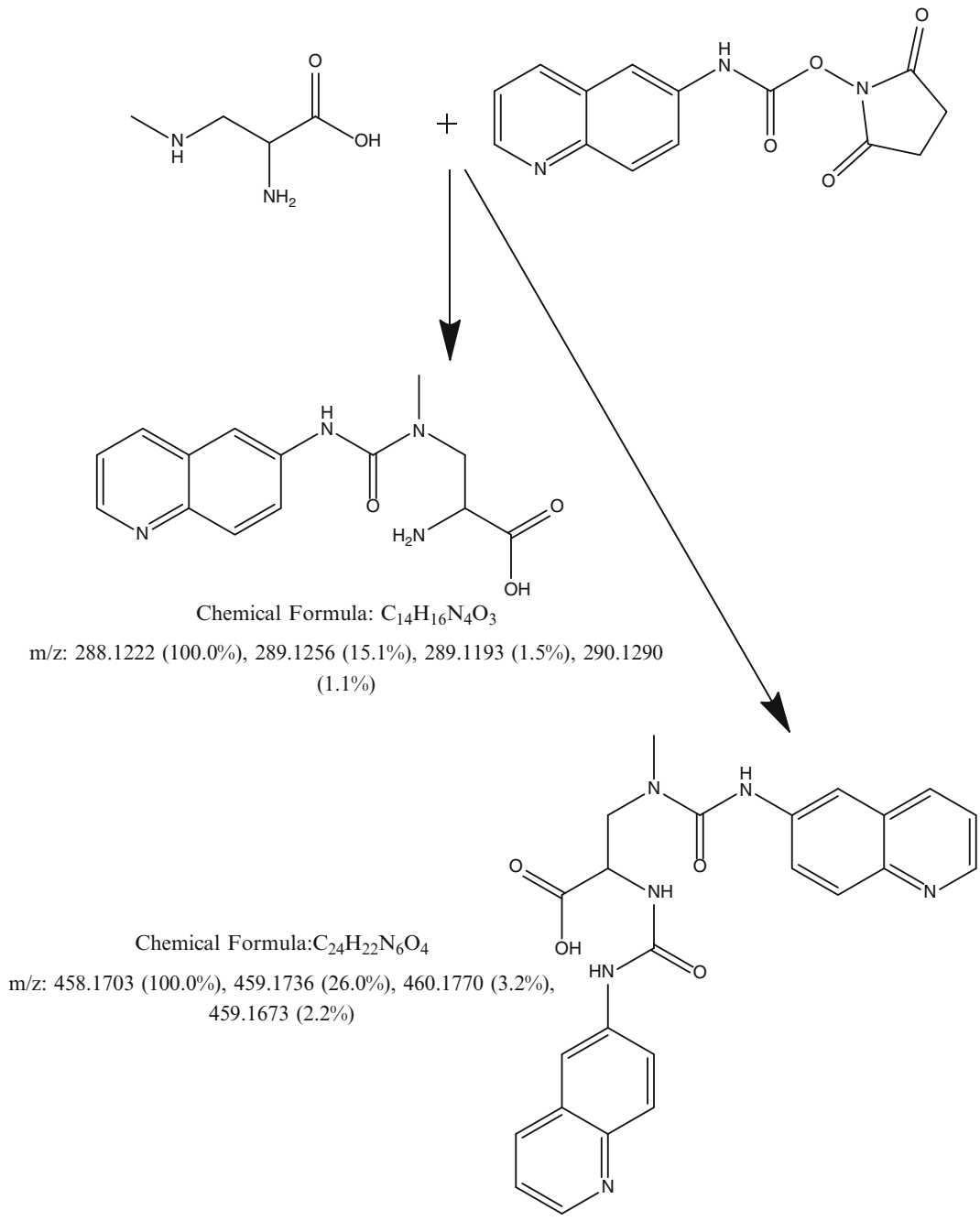

Fig. 2 Reaction scheme for the AQC derivatization reaction of BMAA

2 Materials

2.1 Hydrolysis

1. Class A1 borosilicate glass vial (4 mL) with a screw cap and PTFE-lined septum, available from most general laboratory supply companies.

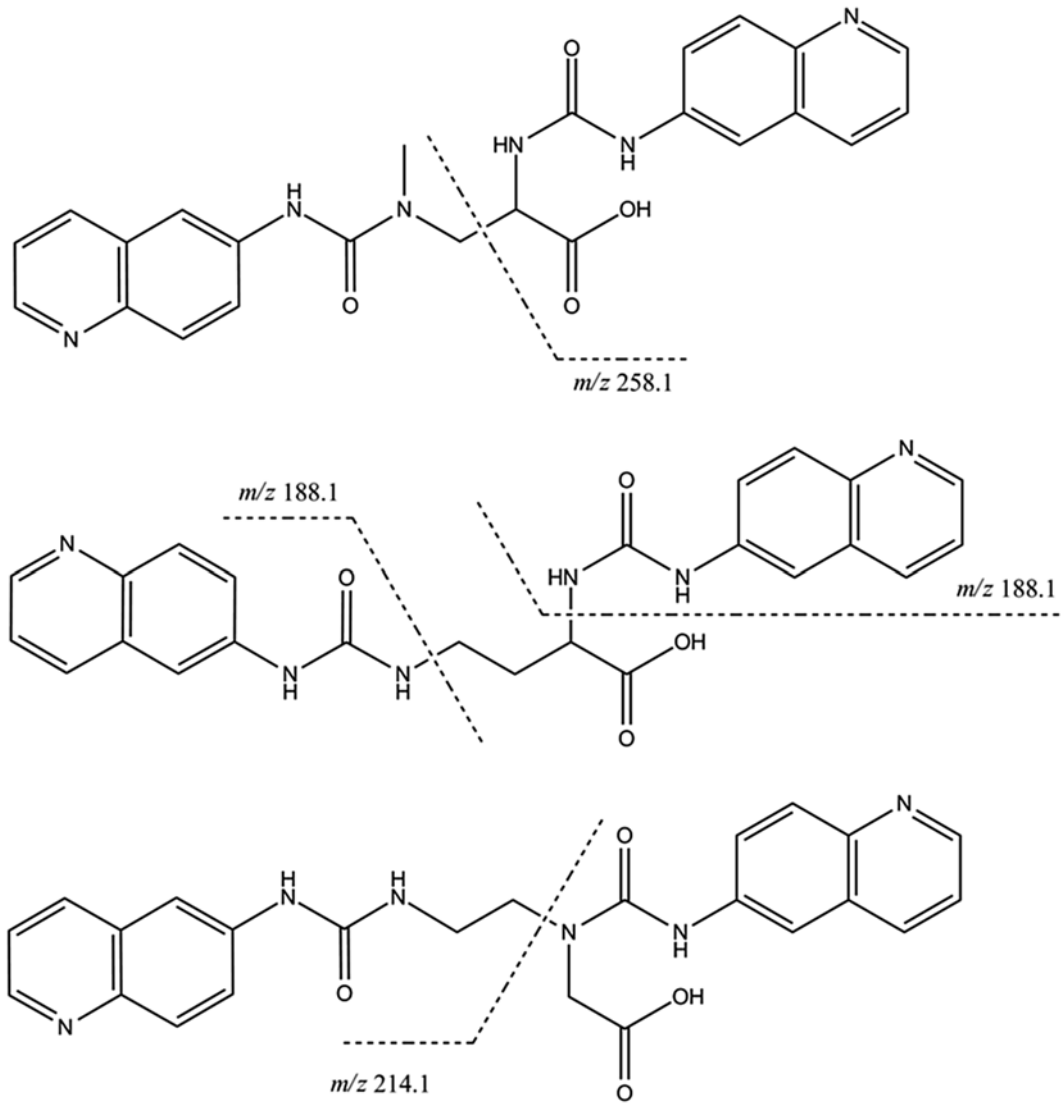

Fig. 3 Unique fragmentation patterns for BMAA (*top*), DAB (*middle*), and AEG (*bottom*) as seen in MS/MS experiments

2. 6N HCl; 10N HCl was purchased from Sigma-Aldrich and diluted down using LC-MS grade water (≤18.2 MΩ resistance).
3. 20 mM HCl, made from the same stock HCl solution and LC-MS grade water above.
4. BMAA and DAB standards were purchased from Sigma-Aldrich.
5. AEG was purchased from TCI Chemicals (Japan).
6. High purity pressurized N_2 gas (≥99.9 %) with an adjustable-flow outlet nozzle.

7. Dry block heater capable of reaching temperatures no lower than 110 °C.

2.2 Derivatization

1. AQC reagent powder; comes as a lyophilized powder (AccQ-Tag Amino Acid Analysis Kit; Waters Corporation). 1 mL of the supplied Reagent A should be used to reconstitute the reagent; it will likely need to be heated (10 min, 50 °C) to ensure it is completely dissolved.
2. 0.2 M sodium $borate_{(aq)}$ supplied with the AccQ-Tag Kit. If more is required, it should be adjusted to a pH of 8.8 prior to use.
3. 250 µL spring-loaded glass inserts for 2 mL autosampler vials.
4. 2 mL autosampler vials.
5. Caps with pre-slit PTFE/silicone septa.

2.3 Chromatographic/ Mass Spectrometric Analysis

1. Acetonitrile (LC-MS grade).
2. Methanol (LC-MS grade).
3. Formic acid (99.9 %).
4. Ammonium formate (99.999 % trace metal basis).
5. Waters 150 × 2.1 mm, 1.7 µm C18, 130 Å, BEH column.
6. Binary UPLC or UHPLC system (capable of operating at backpressures of up to 12,000 psi), with an in-line degasser, autosampler, and column heater (*see* Subheading 3.3).

3 Methods

3.1 Hydrolysis

1. 50 mg of sample was weighed out into a glass vial.
2. 1,000 µL of 6N HCl were added (*see* **Note 1**).
3. N_2 gas was layered over the sample for 30 s before the vials were sealed as tightly as possible (*see* **Note 2**).
4. Vials were incubated in a dry block heater for 18 h at 110 °C to induce hydrolysis of the protein. The wells of the heating block should match the vial size as closely as possible to ensure even and consistent heating throughout hydrolysis.
5. The sample vials were removed from the heating block and allowed to cool to ambient temperature.
6. 400 µL of sample were removed from each vial and cleared using 0.22 µm centrifugal filters (5 min at 14,600 × *g*) (*see* **Note 3**).
7. 100 µL of filtrate from each sample was transferred to a 1.5 mL microcentrifuge tube and placed in a freeze dryer for 24 h.
8. Once dry, all samples were stored at −20 °C prior to analysis. As the 100 µL aliquot provides more than enough sample for

analysis, the remaining filtrate can be either discarded or stored at −80 °C should the drying process ever need to be repeated.

3.2 Derivatization

1. 1 mL of 20 mM HCl was added to each sample vial and vortexed vigorously.
2. 60 µL of 0.2M borate buffer was added to 250 µL inserts in 2 mL autosampler injection vials.
3. 20 µL of each reconstituted sample was then added to each insert.
4. Finally, 20 µL of the AQC reagent was added to each vial. The vials were capped and vortexed 3 times (*see* **Note 4**).
5. Vials were left for 10 min at room temperature prior to transfer to an autosampler tray. Reaction can proceed to 2 potential products viz. single and double derivatized BMAA (Fig. 2). For assays in which amino acids other than BMAA, DAB and AEG were being analyzed, the autosampler vials should be incubated at 55 °C for 10 min (*see* **Note 5**). Isomers were identified by characteristic ion fragments (Fig. 3).

3.3 Chromatographic/Mass Spectrometric Analysis

1. The UPLC system was equilibrated with 99.1 % Eluent A for 15 min prior to injection of the first sample. Short re-equilibration times afford no change in retention for subsequent injections.
2. Chromatographic separation was carried out using the following gradient (Table 1). Separation was completed on a Waters 150×2.1 mm, 1.7 µm C18 BEH column using a Waters Acquity I-Class UPLC. The flow rate was 0.65 mL/min. with a column temperature of 45 °C. Compounds were eluted with 0.2 % formic acid in 20 mM ammonium formate (A) and 0.1 % formic acid in acetonitrile (B). Isomers were clearly separated by reverse phase chromatography (Fig. 4).
3. Post-column, the eluent was shunted to a triple quadrupole mass spectrometer with an electrospray source operated in positive mode. Instrument parameters will need to be optimized individually for each analytical instrument performing the analysis to guarantee maximum sensitivity. Of particular note, however, is the capillary voltage; in order to generate the highest possible signal from the parent ion, low capillary voltages appear to have significant impact on the abundance of the parent ion species (*see* **Note 6**). Multiple reaction monitoring (MRM) was scheduled such that data was collected for no less than 1.5 min on either side of the observed peaks. This allowed for the establishment of a well-defined baseline for use in quantification (Fig. 4). Fragmentation of AQC derivatives of BMAA, DAB and AEG give characteristic daughter ions as qualifiers. 459.0 > 119.0 transition resulting from loss of the fluorophore tag from all three chemical species. 459.0 > 171.0 fragmentation is again seen in all three species, as are the transitions from 459.0 > 289.1. 459.0 > 258.0 fragmentation is exclusive to

Table 1
UPLC gradient separation method for AEG, BMAA, and DAB

Flow rate (mL/min)	Time (min)	%A	%B	Curve
0.700	–	99.9	0.1	6
0.700	0.50	99.9	0.1	6
0.700	6.75	90.0	10.0	6
0.700	7.50	85.0	15.0	6
0.700	7.55	15.0	85.0	6
0.700	8.55	15.0	85.0	6
0.700	9.00	99.9	0.1	6
0.700	10.00	99.9	0.1	6

BMAA, while the transitions 459.0 > 188.0 and 459.0 > 214.0 are characteristic of DAB and AEG, respectively (*see* **Note 6**).

4. Since BMAA and its analogues are all present at very low levels, incomplete derivatization can significantly hamper the analysis. Lack of complete derivatization will result in large detector responses for all of the highly abundant amino acids present even without complete derivatization, but may very easily lead to false negatives for low abundance species such as BMAA. To ensure that near or complete derivatization has been achieved, special monitoring practices can be put into place. Specifically, both the single and double-derivatized forms of lysine, one of only a handful of amino acids that form double-derivatives when reacted with AQC, can be monitored. Shown in Fig. 5, both of the single-derivatized forms of lysine appear as early eluting compounds at 2.5 and 3.1 min, and can be monitored using the transition m/z 317.3 > 171.0. The fully derivatized form of lysine elutes quite late in this method, with a retention time of 7.5 min, and, as expected, appears as only a single peak. This transition can be monitored using the transition m/z 478.2 > 171.0. To ensure complete derivatization occurred, these peaks should be checked during data processing; if peaks resulting from the single-derivatized form of lysine are found, then the sample should be diluted appropriately and re-analyzed (*see* **Note 7**). Alternatively, the same sample concentration can be used, but with a larger volume of AQC used in the preparation process.

4 Notes

1. The optimal amount of 6N HCl added to a given type of sample depends on the composition of that sample. Some samples, particularly soft tissue, will already contain a relatively high level

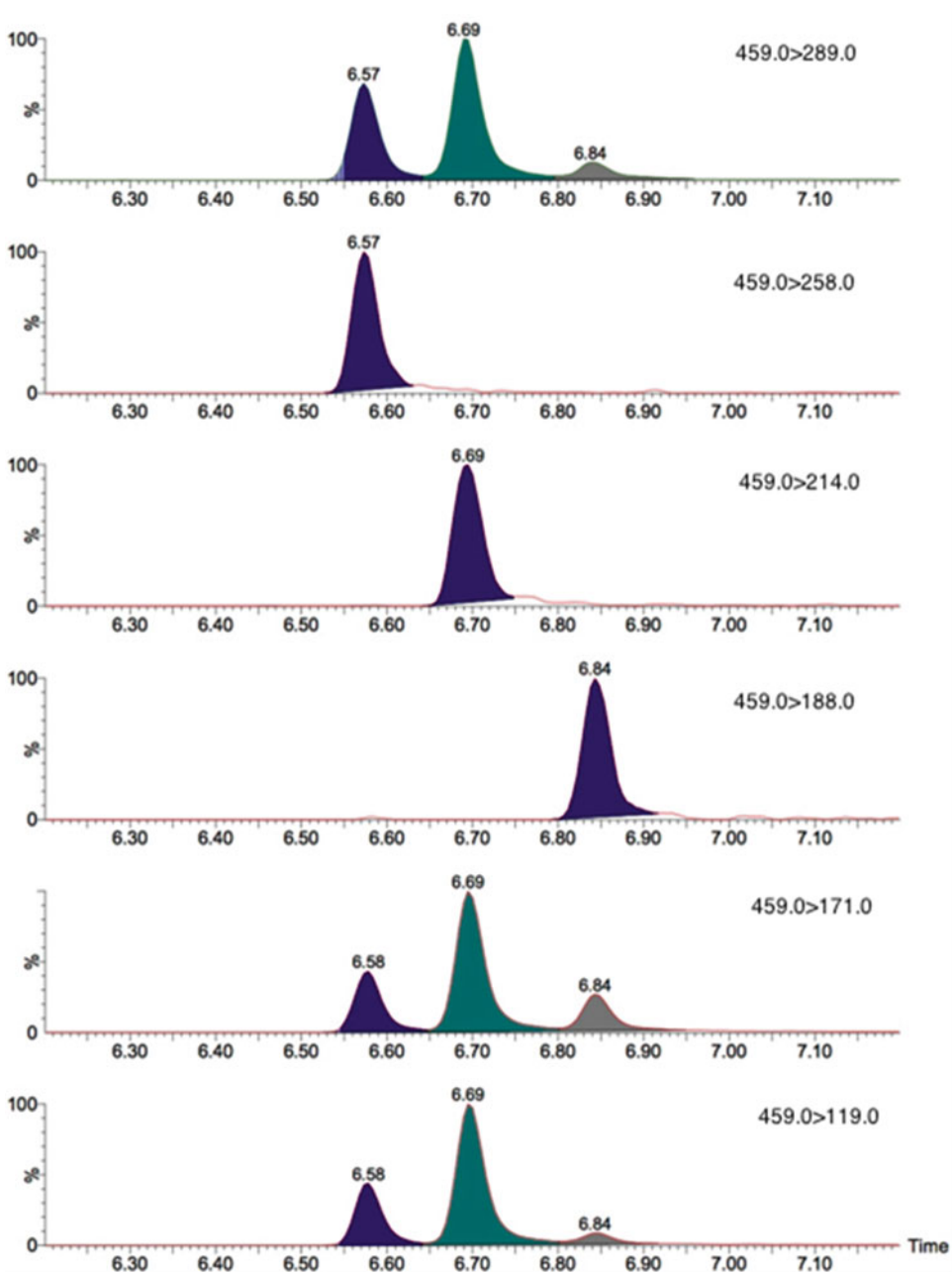

Fig. 4 Chromatographic separation of AEG, BMAA, and DAB, respectively, on a Waters 150 × 2.1 mm, 1.7 μm C18 BEH column using a Waters Acquity I-Class UPLC according to the chromatographic method described

of water; in this case, as little as 400 μL will be required to fully dissolve the sample. In the other extreme, for hygroscopic samples such as powders, up to 1 mL of 6N HCl will be required to dissolve the sample. If a less-than-optimal amount is added, it is likely that hydrolysis of peptide bonds will be incomplete. Should this happen, recovery of the filtrate will be negatively effected, as will the measured amount of analyte in the sample.

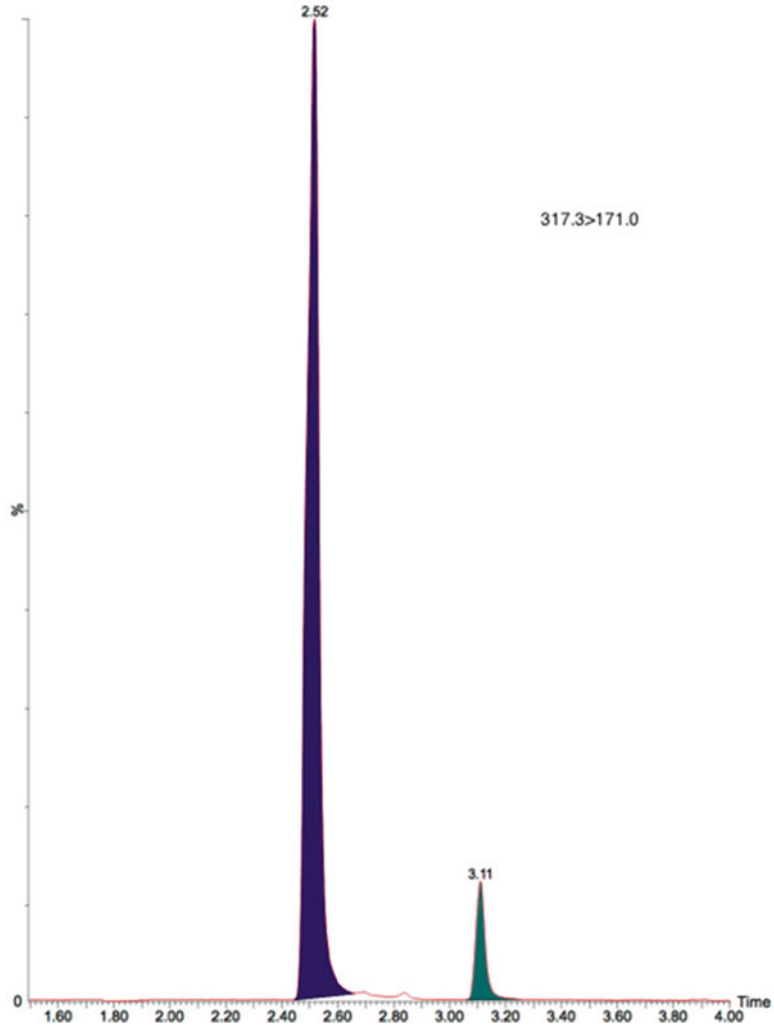

Fig. 5 Lysine reacted with only one molecule of AQC leads to a single-derivatized form that elutes early in the chromatographic run; because lysine can be derivatized in two separate locations, two readily separated peaks can be found in the chromatogram

2. Layering high-purity N_2 gas (>99.9 %) over the sample displaces atmospheric oxygen, thus preventing oxidation of the amino acids during the hydrolysis process. As the AQC derivatization reaction requires a free amine to proceed, the reaction will not go forward for those amino acids in the sample have been oxidized. To remove as much oxygen as possible from the sample, it is best to use a gas line with a small opening, such as a 1 mL pipette tip, with a very flow rate. This allows placement of the tip near the surface of the acid without significant perturbation of the sample itself. Additionally, placing the tip near the side of the vial ensures the present atmosphere will be displaced,

leaving as little oxygen as possible. Once this process in complete, the vial should be capped as quickly and tightly as possible to prevent reentry of atmospheric oxygen into the vial.

3. It is important to not let the hydrolysis vials sit for a significant length of time between cooling of the samples and centrifugal filtration. Due to the ion-exchange character exhibited by many types of glass, amino acids will irreversibly bind to many glass surfaces given time. The remaining acid in the sample should prevent significant losses due to this adsorption, but it is best not to allow these samples to sit for long periods, as this only introduces another source of error into the analysis.
4. The derivatizing reagent 6-aminoquinolyl-*N-hydroxysuccinimidyl* carbamate is moisture sensitive and has a very short half-life in water (approximately 15 s), but reacts with primary and secondary amines on the order of milliseconds. As a result, it is important to mix a sample as quickly as possible upon addition of the derivatizing reagent. Failure to do so will yield high levels of the water hydrolysis product, AMQ, with only minimal amounts of fully reacted amino acids; analytically, this will result in falsely low levels of not just BMAA and its isomers, but all amino acids as a whole.
5. It is recommended to incubate all samples derivatized with AQC to 55 °C for 10 min. While the derivatization reaction occurs almost instantaneously, in one case, more specifically, tyrosine, a side product is generated during the reaction that will convert to the expected product spontaneously. At room temperature, however, this conversion proceeds with a half-life of approximately 30 min. This can be overcome by heating samples as described. While tyrosine is the only known amino acid to behave in this manner, there may be many more, particularly as research increasingly moves into non-protein amino acids. If the analysis is being conducted specifically for BMAA and its known isomers, this incubation period is unnecessary; the samples can be injected within 1–2 min of derivatization.
6. It should be noted that derivatized BMAA forms both the $[M+H]^+$ and $[M+2H]^{2+}$ ions very easily in electrospray ionization, particularly at low mobile phase pH values. As such, the parent ion selected could also be the doubly protonated form (m/z 230); the MS/MS spectra obtained are identical. It is also worth noting that because low mass interferences may be more prominent in this range than at a higher m/z value, which may in turn have an impact on the signal-to-noise, and therefore the limit of detection, should these values be used for parent ion selection.
7. It is inevitable that, even when enough of the AQC reagent is present to fully react all amino acids present, that a very small fraction of amino acids will undergo partial or no derivatization.

In the case of lysine, very small amounts of the single-derivatized form will still be present. To get around this, a rough approximation of derivatization completeness can be carried out: the peak area of the first two signals can be summed and divided by the peak area of the fully reacted lysine signal (Fig. 5). While not particularly quantitative due to the lack of standard curves available for the single-derivatized forms, this will produce an approximate ratio of incomplete to completely derivatized lysine, an assumption that can be extended to the entire sample. Should derivatization be less than 90 % efficient, it is recommended that the sample be further diluted and reanalyzed.

References

1. Arnold A, Edgren DC, Paladino VS (1953) Amyotrophic lateral sclerosis: fifty cases observed on Guam. J Nerv Ment Dis 117:135–139
2. Koerner DR (1952) Amyotrophic lateral sclerosis on Guam: a clinical study and review of the literature. Ann Intern Med 37: 1204–1220
3. Kurland LT, Mulder DW (1954) Epidemiologic investigations of amyotrophic lateral sclerosis. 1. Preliminary report on geographic distribution with special reference to the Mariana Islands, including clinical and pathologic observations. Neurology 4:438–448
4. Reed W, Plato C, Elizan T, Kurland LT (1966) The amyotrophic lateral sclerosis/parkinsonism-dementia complex: a ten year follow up on Guam. Am J Epidemiol 83:54–73
5. Whiting MJ (1963) Toxicity of cycads. Econ Bot 17:270–302
6. Vega A, Bell EA (1967) a-amino-methylamio-propionic acid, a new amino acid from seeds of Cycas circinalis. Phytochemistry 6:759–762
7. Ludolph A, Hugon J, Nunn PB, Roy DN, Spenser PS (1988) Clinical and electrophysiological features of the primate motor system disease induced by BMAA—a neurotoxin in the Guam Cycad plant. Electroencephalogr Clin Neurophysiol 69:P18
8. Duncan MW, Steele JC, Kopin IL, Markey SP (1990) 2-amino-3-(methylamino)-propanoic acid (BMAA) in cycad flour: an unlikely cause of amyotrophic lateral sclerosis and Parkinsonism-dementia of Guam. Neurology 5:767–772
9. Cox PA, Sacks OW (2002) Cycad neurotoxins, consumption of flying foxes, and ALS-PDC disease in Guam. Neurology 58:956–959
10. Cox PA, Banack SA, Murch SJ (2003) Biomagnification of cyanobacterial neurotoxins through the ecosystem: implications for ALS-PDC in Guam. Proc Natl Acad Sci U S A 100(23):13380–13383
11. Cox PA, Banack SA, Murch SJ, Rasmussen U, Tien G, Bidigare RR, Metcalf JS, Morrison LF, Codd GA, Bergman B (2005) Diverse taxa of cyanobacteria produce beta-N-methylamino-L-alanine, a neurotoxic amino acid. Proc Natl Acad Sci U S A 102:5074–5078
12. Murch SJ, Cox PA, Banack SA, Steele JC, Sacks OW (2004) Occurrence of ß-methylamino-l-alanine (BMAA) in ALS/PDC patients from Guam. Acta Neurol Scand 110:267–269
13. Pablo J, Banack SA, Cox PA, Johnson TE, Papapetropoulos S, Bradley WG, Buck A, Mash DC (2009) Cyanobacterial neurotoxin BMAA in ALS and Alzheimer's disease. Acta Neurol Scand 120:216–225
14. Lobner D, Piana PM, Salous AK, Peoples RW (2007) β-N-methylamino-l-alanine enhances neurotoxicity through multiple mechanisms. Neurobiol Dis 25:360–366
15. Liu XQ, Rush T, Zapata J, Lobner D (2009) β-N-methylamino-l-alanine induces oxidative stress and glutamate release through action on system Xc−. Exp Neurol 217:429–433
16. Rao SD, Banack SA, Cox PA, Weiss JH (2006) BMAA selectively injures motor neurons via AMPA/kainate receptor activation. Exp Neurol 201:244–252
17. Cucchiaroni ML, Viscomi MT, Bernardi G, Molinari M, Guatteo E, Mercuri NB (2010) Metabotropic glutamate receptor 1 mediates the electrophysiological and toxic actions of the cycad derivative {beta}-N-Methylamino-L-alanine on substantia nigra pars compacta DAergic neurons. J Neurosci 30:5176–5188
18. Chiu AS, Gehringer MM, Braidy N, Guillemin GJ, Welch JH, Neilan BA (2013) Gliotoxicity of the cyanotoxin, β-methyl-amino-L-alanine

(BMAA). Sci Rep 3:1482. doi:10.1038/srep01482

19. Esterhuizen-Londt M, Pflugmacher S, Downing TG (2011) The effect of b-N-methylamino-L-alanine (BMAA) on oxidative stress response enzymes of the macrophyte Ceratophyllum demersum. Toxicon 57:803–810
20. Glover WB, Murch SJ (2013) Analysis of ß-methylamino-l-alanine for environmental and food samples. Recent Adv Phytochemistry 44:149–174
21. Cohen SA (2012) Analytical techniques for the detection of a-amino-b-methylamino-propionic acid. Analyst 137:1991–2005
22. Banack SA, Downing TG, Spácil Z, Purdie EL, Metcalf JS, Downing S, Esterhuizen M, Codd GA, Cox PA (2010) Distinguishing the cyanobacterial neurotoxin β-N-methylamino-L-alanine (BMAA) from its structural isomer 2,4-diaminobutyric acid (2,4-DAB). Toxicon 56:868–879
23. Banack SA, Metcalf JS, Jiang L, Craighead D, Ilag LL, Cox PA (2012) Cyanobacteria produce N-(2-aminoethyl)glycine, a backbone for peptide nucleic acids which may have been the first genetic molecules for life on Earth. PLoS One 7:e49043
24. Glover WB, Liberto CM, McNeil WS, Banack SA, Shipley PR, Murch SJ (2012) Reactivity of β-methylamino-L-alanine in complex sample matrices complicates detection and quantification by mass spectrometry. Anal Chem 84: 7946–7953

Part III

Gene Expression

Chapter 28

Intracellular Distribution of Glutathionylated Proteins in Cultured Dermal Fibroblasts by Immunofluorescence

Stefania Petrini, Valentina D'Oria, and Fiorella Piemonte

Abstract

S-glutathionylation is a mechanism of signal transduction by which cells respond effectively and reversibly to redox inputs. The glutathionylation regulates most cellular pathways. It is involved in oxidative cellular response to insult by modulating the transcription factor Nrf2 and inducing the expression of antioxidant genes (ARE); it contributes to cell survival through nuclear translocation of NFkB and activation of survival genes, and to cell death by modulating the activity of caspase 3. It is involved in mitotic spindle formation during cell division by binding cytoskeletal proteins thus contributing to cell proliferation and differentiation. Glutathionylation also interfaces with the mechanism of phosphorylation by modulating several kinases (PKA, CK) and phosphatases (PP2A, PTEN), thus allowing a cross talk between the two processes of signal transduction. Glutathionylation of proteins may also act on cell metabolism by modulating enzymes involved in glycosylation, in the Krebs cycle and in mitochondrial oxidative phosphorylation. Perturbations in protein glutathionylation status may contribute to the etiology of many diseases, thus it is clear the importance to visualize the distribution of glutathionylated proteins in subcellular compartments. This chapter describes the immunofluorescence technique that permits simultaneous detection of glutathionylated proteins and their localization in cellular compartments, using multiple stained cell samples. By confocal laser microscopy analysis of the immunofluorescent cells it is possible to obtain detailed information of submicroscopic structures inside cells and tissues, and to perform correct co-localization analysis between two proteins. The association between glutathione, nuclear lamina, and cytoskeleton has been investigated by employing a helpful assay consisting on the in situ extraction of the cellular matrix from cultured dermal fibroblasts followed by multiple stainings with several primary antibodies.

This protocol can be used for the detection of the intracellular distribution and expression of interest proteins and can be customized for a large variety of cells and tissues.

Key words Dermal fibroblasts, Glutathionylation, Nuclear lamina, Cytoskeleton, In situ extracted matrix, Immunofluorescence, Confocal microscopy

1 Introduction

S-glutathionylation is a mechanism of signal transduction by which cells respond effectively and reversibly to redox inputs. Glutathione is the most abundant non-enzymatic antioxidant in cells, where it plays an important role against oxidative stress-induced cell injury [1].

Donald Armstrong (ed.), *Advanced Protocols in Oxidative Stress III*, Methods in Molecular Biology, vol. 1208,
DOI 10.1007/978-1-4939-1441-8_28,

It is a tripeptide composed of cysteine, glutamic acid, and glycine, with an active group represented by the thiol (–SH) of cysteine residue. Intracellularly, total glutathione can be free or bound to proteins. Free glutathione is present mainly in its reduced form (GSH), which can be converted to the oxidized form (GSSG) during oxidative stress. In mammalian cells, the redox status depends on the relative amounts of the reduced and oxidized glutathione (GSH/GSSG), with GSH normally exceeding GSSG. The oxidation of a small amount of GSH is enough to dramatically alter this ratio, causing the thiol groups of some intracellular proteins to be modified by a process known as S-glutathionylation [2, 3]. Several studies have supported the fundamental role of glutathionylation in numerous pathophysiological processes [3–6], requiring the development of techniques able to separate and identify glutathionylated proteins in distinct cellular compartments.

Many proteins may undergo glutathionylation [4, 6–8]. Several are enzymes involved in various pathways of carbohydrate/energy metabolism. Some glutathionylated proteins belong to the class of cytoskeletal proteins, and some are involved in transcription, translation and degradation [5, 9]. Among the cytoskeletal proteins, actin has been found to be glutathionylated in human platelets [10], erythrocytes [11], hepatocytes and in T lymphocytes [12], after exposure to oxidants. The glutathionylation of tubulin has also been demonstrated in vitro by using the purified protein [13]. Other proteins are involved in the assembly of ribosomal proteins, such as the nucleophosmin, or in the proteasomal degradation, like cyclophilin. Growing evidence, furthermore, indicates glutathionylation, as a modulatory mechanism able to regulate several transcription factors (Nrf2 and NF-kB) and to interfere with the phosphorylation/dephosphorylation mechanism by interacting with kinases (PKA and CK) and/or phosphatases (PP2A and PTEN) [9]. Protein glutathionylation is also involved in cell proliferation and differentiation by contributing to the mitotic spindle formation during cell division. However, besides the physiological role in redox signaling, some proteins become glutathionylated under conditions of oxidative and nitrosative stress [4], thus becoming a sensor of tissue redox status. Indeed, in the last years, glutathionylated proteins have also been investigated as possible biomarkers of oxidative stress in human diseases and the extent of protein glutathionylation may indicate the evolution of the disease, acquiring a diagnostic/prognostic value. Significant increases of glutathionylated proteins, for instance, have been found in hyperlipidemia, chronic renal failure, and diabetes mellitus [7]. Furthermore, evidence for a dysfunction of glutathione metabolism has been proposed for the pathogenesis of several neurodegenerative diseases, such as Parkinson's disease, Alzheimer's disease, Friedreich's ataxia, and Amyotrophic lateral sclerosis [14–16].

Protein-S-glutathionylation it has been evaluated in human cell lines both in steady state and under cell proliferation [17–21],

as well as to verify its role as a sensor of oxidative stress [21, 22]. In particular, an association of glutathionylated proteins with nuclear lamina, endoplasmic reticulum (ER), and cytoskeletal filaments has been found by using confocal laser microscopy [21]. In subconfluent dermal fibroblasts, the intracellular compartmentalization of glutathionylated proteins suggests a clear association between glutathione and protein components of nuclear lamina (Fig. 1), endoplasmic reticulum (Fig. 1), and cytoskeleton (Fig. 2). Further, the confocal laser microscopy analysis of the immunofluorescent cells allows to obtain detailed information of submicroscopic structures inside cells and tissues, and to perform correct colocalization analysis between two proteins (*see* insets in Fig. 1).

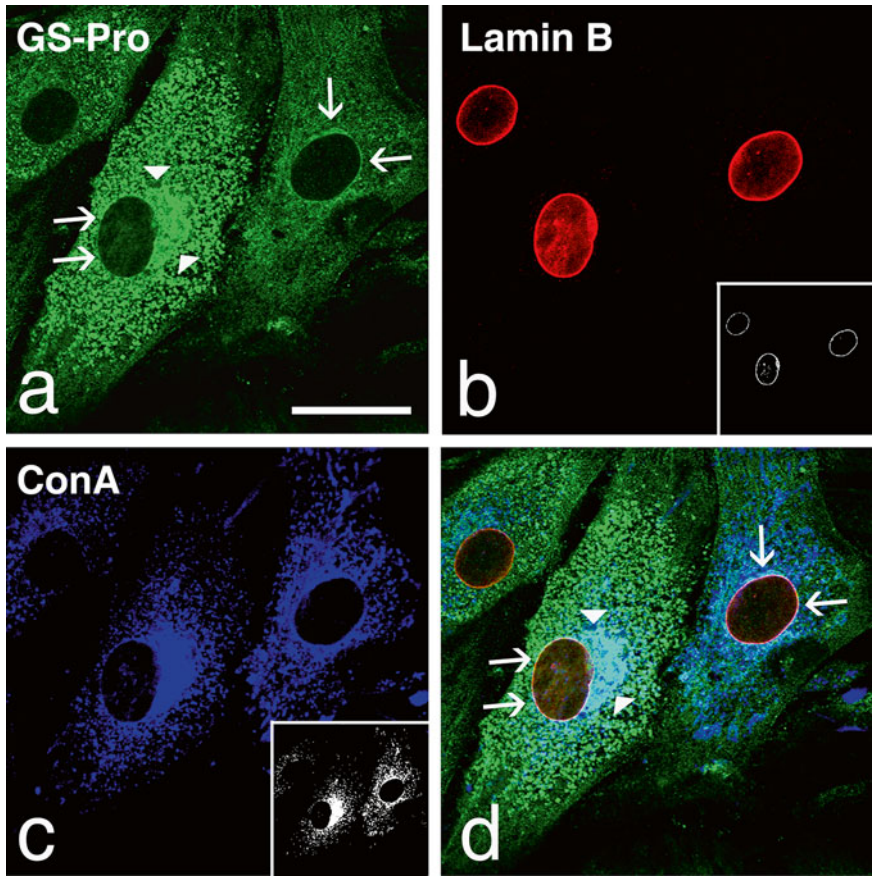

Fig. 1 Intracellular distribution of glutathionylated proteins in cultured dermal fibroblasts. Confocal imaging of glutathionylated proteins (*green* in **a**) and multiple staining with markers of the nuclear lamina (lamin B, *red* in **b**) or endoplasmic reticulum (ConA, pseudocolored in *blue* in **c**), and their colocalization masks (*insets* in **b** and **c**). GS-Pro is thickened around nuclei (*arrows*) and shows a clear colocalization with the nuclear lamina (white spots in the *inset* in **b**). The GS-Pro distribution is concentrated around nuclei (*arrowheads*), interspersed in the cytoplasm, and codistributed with the endoplasmic reticulum cisternae (colocalization mask in the *inset* in **c**, and merge signal in **d**). Magnification bar: 40 μm (Modified from Fig. 1 in ref. 21)

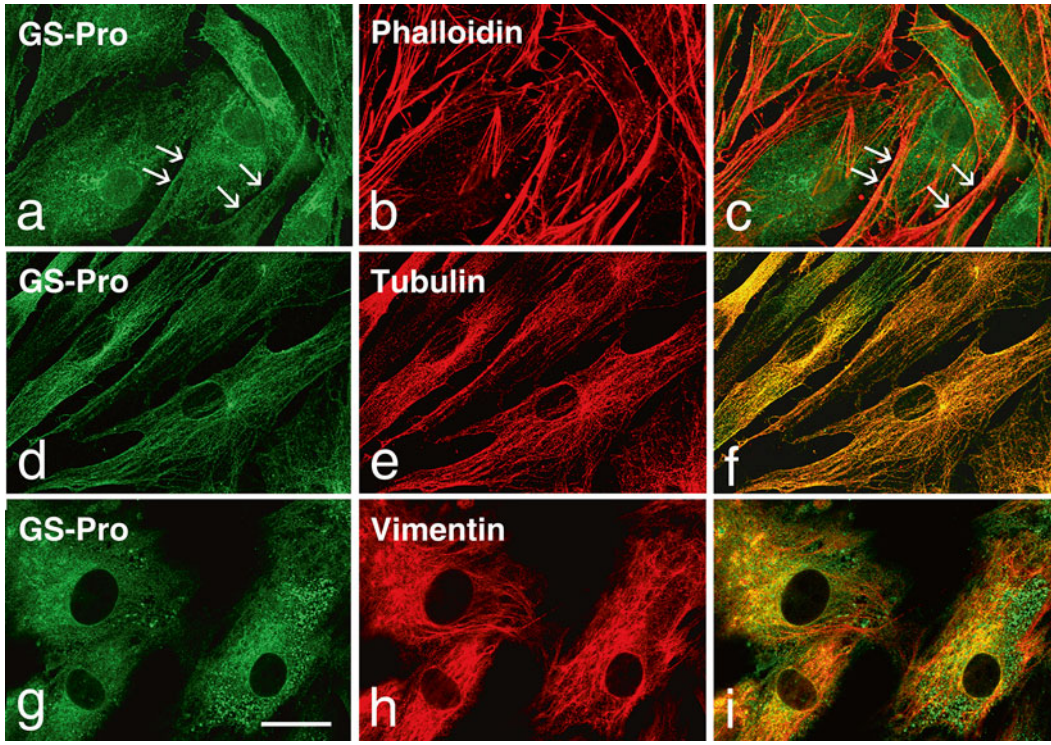

Fig. 2 The cytoskeleton-S-glutathionylation in cultured dermal fibroblasts. Confocal analysis of GS-Pro (*green* in **a**, **d**, **g**) immunolabelling and its colocalization (merge images in **c**, **f**, **i**) with markers of actin filaments (phalloidin in **b**, stress fibers visualized by *arrows*), microtubules (tubulin in **e**), and intermediate filaments (vimentin in **h**). Magnification bar: 40 μm (Modified from Fig. 4 in ref. 21)

We describe the technique of indirect immunofluorescence that permits the detection of glutathionylated proteins using a monoclonal antibody anti-glutathionylated proteins (GS-Pro) and their localization in intracellular compartments. Using multiple stained cell samples with antibodies recognizing different cellular districts, such as nuclear lamina, endoplasmic reticulum, and cytoskeleton, it is possible to define the intracellular distribution of the glutathionylation process in cultured dermal fibroblasts in steady state condition. Further, the tight association between glutathione, nuclear lamina, and cytoskeleton may be analyzed by the employment of the in situ extraction assay [23] of the cellular matrix from cultured cells (Fig. 3) that allows to discard cytosol, organuli, endoplasmic reticulum cisternae, nucleoplasm, and DNA, saving nuclear lamina and cytoskeleton only. After fixation, these extracted matrix samples may be processed for immunocytochemistry and labeled with antibodies directed against GS-Pro, nuclear lamina, and cytoskeleton components.

We describe a helpful assay that can be employed for detection of the intracellular distribution and expression of interest proteins and can be customized for a large variety of cells and tissues.

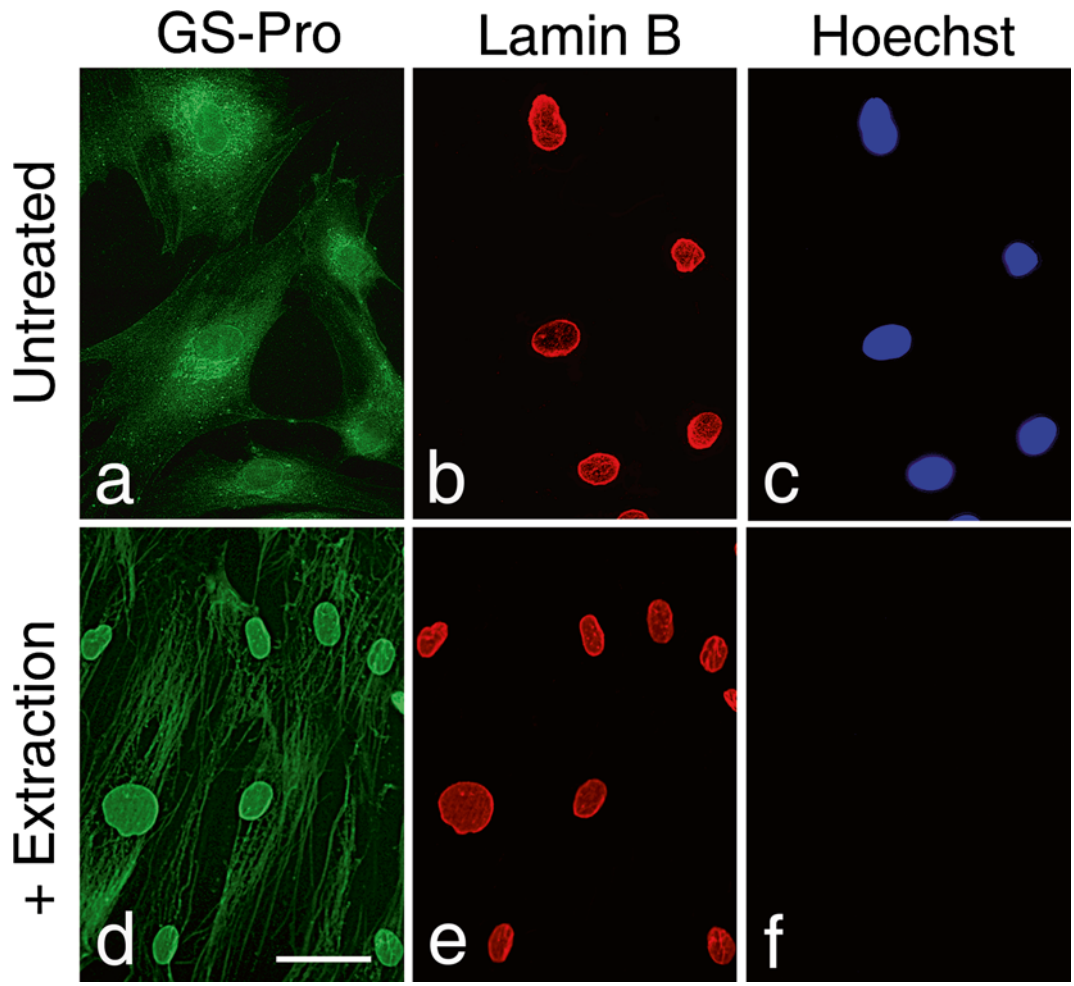

Fig. 3 The glutathionylation is strictly associated with the nuclear lamina and the cytoskeleton. Epifluorescence microscopy of unextracted (**a**–**c**) and extracted cultured fibroblasts (**d**–**f**) using GS-Pro (**a**, **d**) and lamin B (**b**–**e**) antibodies. In untreated cells, glutathionylated proteins are distributed around nuclei, interspersed in subcellular compartments and in correspondence to cytoskeleton components (**a**). After matrix extraction, cells show a brilliant staining of cytoskeletal filaments and of the nuclear lamina (**d**) as supported by double-labeling with lamin B antibody (**e**). Nuclear counterstaining with Hoechst (**c**, **f**) confirms the DNA digestion by DNAse I in extracted cells (**f**). Magnification bar: 50 μm (Modified from Fig. 2 in ref. 21)

2 Materials

2.1 Reagents for Cell Culture

1. Primary culture fibroblasts, obtained from human skin biopsy after mechanical dissociation, are seeded (1×10^4) in chamber slides with 8 wells (BD Falcon glass culture slides, code 354118) and grown in culture medium until semi-confluence.
2. Culture medium: Dulbecco's modified Eagle's medium (D-MEM, Gibco Life Technologies) supplemented with 10 % fetal bovine serum (FCS, Gibco Life Technologies) and antibiotics (25 units/ml penicillin, 25 μg/ml streptomycin, and 0.3 μg/ml amphotericin B).

2.2 Reagents for Immunofluorescence

1. Phosphate buffered solution (PBS) 10×: dissolve 80 g of NaCl, 2 g of KCl, 11.5 g of Na_2HPO_4 (anhydrous), and 2 g of KH_2PO_4 in 1 L beaker with 900 ml of distillated H_2O (dH_2O). Dilute 10 times and check pH to be 7.2 (adjust pH using 1 M NaOH and/or 1 M HCl).
2. Paraformaldehyde powder is toxic and it is required to wear mask and gloves as fumes and contact are dangerous. Use the chemical hood when preparing this fixative solution. Discard formaldehyde by emptying into hazardous waste container stored in chemical waste hood. Paraformaldehyde preparation (8 % formaldehyde): dissolve 8 g of paraformaldehyde powder in 50 ml of dH_2O and place on hot plate (do not bring temperature above 55–58 °C). Mix for about 30 min, then turn the heat off and add one-two drops of 1 M NaOH to clear the solution. Mix for 10 min, cool it down and filter it using filter paper such as Whatman #1. Store in opaque container at 4 °C. Use within 1 month, otherwise it will decompose. 4 % formaldehyde solution (50 ml) is prepared by mixing 25 ml of 8 % formaldehyde with 5 ml of 10× PBS and 20 ml of dH_2O. Store in opaque container at 4 °C. Use within 24 h.
3. Permeabilization solution: dissolve 0.15 % of Triton-X 100 (Sigma-Aldrich) in 100 ml of 1× PBS.
4. Dilution buffer: PBS 1× containing 1 % bovine serum albumine (BSA, from Sigma-Aldrich).
5. Blocking solution: 5 % non-immune goat-serum (NGS, Sigma-Aldrich) in dilution buffer.
6. Fluorescence Mounting Medium can be prepared in the lab and help to reduce fading of immunofluorescence during microscopy. Add 9 parts of glycerol (Sigma-Aldrich) to 1 part 1× PBS. Usually an antiquenching agent is added (such as 1 % DABCO or 4 % n-propyl gallate). The pH should be adjusted to 8.5–9.0. Mix well preventing the formation of bubbles, filter, and store at 4 °C. Alternatively, commercially available mounting media can be purchased from several companies (such as Invitrogen, DAKO, Vector Labs, Sigma-Aldrich).
7. Lectins: they are plant-derived proteins that bind specific carbohydrate modifications with high affinity. (a) *Phalloidin* is a fungal toxin that selectively labels polymeric and oligomeric forms of actin (filamentous actin or F-actin) and not monomeric actin. Dissolve 1 mg phalloidin-TRITC (P1951, Sigma-Aldrich) in 1 ml methanol and store at –20 °C. Stain cells with working solution of fluorescent phalloidin (dilution of 1:100 in PBS) for 60 min, at RT, in the dark. (b) *Concanavalin A* (ConA) selectively binds to α-mannopyranosyl and α-glucopyranosyl residues, primarily in the endoplasmic reticulum. Dissolve 5 mg ConA conjugated to Alexa Fluor 633

(C21402, Invitrogen) in 1 ml of 0.1 M sodium bicarbonate (pH 8.3). Divide the solution into aliquots and freeze at –20 °C. Stain cells with working solution of fluorescent ConA: prepare a dilution of 1:100 in PBS, then centrifuge the ConA conjugate solution briefly in a microcentrifuge before use, and use the supernatant. Incubate cells for 60 min at RT, in the dark.

8. Primary antibodies: (a) Mouse monoclonal anti-GS-Pro (Code 101-A, clone D8, Virogen, Watertown, MA). It is recommended to aliquot the antibody in small volume aliquots and store them at –20 °C for up to 1 year and avoid repeated freeze–thaw cycles. Prepare working solution of 10 ng/ml in the dilution buffer. (b) Goat polyclonal anti-vimentin (sc-7557, Santa Cruz Biotechnology, Temecula, CA). Prepare a working solution of 20 ng/ml in the dilution buffer. (c) Goat polyclonal anti-lamin B (sc-6216, Santa Cruz Biotechnology, Temecula, CA). Prepare a working solution of 20 ng/ml in the dilution buffer. (d) Sheep polyclonal anti-tubulin (Code ATN02, from Cytoskeleton, Denver, CO, USA). Reconstitute the antibody following the manufacturer instructions. A 1:100 working dilution of antibody can be used.
9. Secondary antibodies: Goat anti-mouse $F(ab')^2$ immunoglobulins conjugated to Alexa Fluor 488 (code A11017, from Invitrogen) used at 1:500 working dilution. Donkey anti-goat immunoglobulins conjugated to Alexa Fluor 555 (code A21432, from Invitrogen) used at 1:500 dilution. Donkey anti sheep IgG (H + L) conjugated to Alexa Fluor 555 (code A21436, from Invitrogen). Usually antibodies conjugated to fluorochromes must be stored at –4 °C up to 1 year, and protected by light. All the working solutions of secondary antibodies must be prepared and centrifuged in a microcentrifuge before use, then use the supernatant.
10. Nuclear counterstain: Hoechst 33342 (H3569, 10 mg/ml, Invitrogen). Before use, dilute 1 μl of Hoechst in 10 ml of 1× PBS (final dilution of 10 μg/ml), store at 4 °C and use within 24 h.
11. Solutions for in situ matrix extraction procedure:
    (a) *Tris–HCl buffer (10 mM):* dissolve 1.22 g Trizma-base (Sigma-Aldrich) in 800 ml of dH_2O. Adjust pH to 7.4 with conc. HCl, then adjust volume to 1,000 ml.
    (b) *TBS-5 buffer*: dissolve 150 mM NaCl (1.75 g) and 5 mM $MgCl_2$ (0.41 g) in 200 ml of Tris–HCl buffer (10 mM, pH 7.4).
    (c) *Stock solutions reagents for permeabilization buffer*:
        - Prepare 0.2 M of sodium tetrathionate (NaTT) in 5 ml of dH_2O, make aliquots with 100 μl and store at –20 °C.

- Dissolve 0.1 M of phenylmethylsulfonyl fluoride (PMSF) in 5 ml acetone, make aliquots with 100 µl and store at –20 °C.
- Dissolve 1 mg/ml of leupeptin in dH_2O. Dissolve 1 mg/ml of aprotinin in dH_2O.

For all these reagents it is recommended to make aliquots of 100 µl and store them at –20 °C.

(d) *TBS-5 permeabilization buffer*: Add to 9 ml of TBS-5 buffer, 100 µl NaTT from 0.2 M stock (yielding a final NaTT concentration of 2 mM), 100 µl PMSF from 0.1 M stock (yielding a final PMSF concentration of 1 mM). Then, add 1 aliquot (100 µl) of leupeptin (final concentration of 10 µg/ml) and 1 aliquot (100 µl) of aprotinin (final concentration of 10 µg/ml). Finally, add 100 µl NP40 (1 %) and adjust volume to 10 ml with TBS-5 buffer.

(e) *DNA digestion buffer*: dissolve 0.01 mg/ml DNase I (Roche) in TBS-5 buffer (yielding a concentration of 20 U/ml).

(f) *NaCl extraction buffer*: before use, dissolve 5.8 g NaCl in 50 ml TBS-5 yielding a final concentration of 2 M.

3 Methods

When cells reach the semi-confluence, they were processed for immunofluorescence (*see* **Note 1**). Each immunofluorescence staining must be performed in at least duplicate to confirm the results.

3.1 Immunocytochemistry by Indirect Immunofluorescence

3.1.1 Intracellular Distribution of Glutathionylated Proteins (GS-Pro Single Staining)

1. Transfer the coverslip with adherent cells from incubator to a lab bench, discard the culture medium, and wash for 5 min in PBS.
2. Add ice cold 4 % paraformaldehyde in PBS into each well and fix for 10 min at 4 °C.
3. Rinse samples 2 × 5 min in PBS.
4. Permeabilize the cells by adding 0.15 % Triton X-100 in PBS for 10 min (RT).
5. Wash for 2 × 5 min in PBS.
6. Apply 5 % non-immune goat-serum (serum from the same host as the secondary antibody is raised in) in PBS to block unspecific staining (*see* **Note 2**). Incubate in a humid chamber for approximately 30 min.
7. Drain off the serum blocking solution and apply the primary antibody (mouse anti-GS-Pro) diluted in PBS supplemented with 0.1 % BSA (*see* **Note 3**). Place slides horizontally in a humid chamber and incubate overnight at 4 °C.

8. Rinse samples 3 times in PBS for 10 min.
9. Incubate with the secondary antibody (goat $F(ab')^2$ anti-mouse IgG conjugated to Alexa Fluor 488: *see* **Note 4**) for 60 min at RT. Protect from light.
10. Rinse 3 times in PBS for 5 min (*see* **Note 5**).
11. The nuclei are counterstained with blue-fluorescent Hoechst at the dilution of 10 μg/ml in PBS for 5 min (in the dark, at RT).
12. Wash for 2 × 5 min in PBS.
13. Remove the chamber from the slide following the manufacturer instructions. Apply 25 μl of mounting medium in each well and mount with a 24 × 60 mm coverslip. Gently remove the excess media with a paper towel and allow to mounting media to dry. Store the slides in the dark at 4 °C.
14. Examine with a confocal microscope and capture images within the next month as fluorescent signals fade over time. Best results are immediately after staining.

3.1.2 Compartimentalization of GS-Pro Distribution (Multiple Stainings)

In double-multiple labeling immunofluorescence, after the previous **step 10**, samples stained with anti-GS-Pro antibody may be incubated with a second primary antibody, overnight (goat anti-lamin B) or for 1 h (sheep anti-tubulin or goat anti-vimentin), or with lectins (ConA, phalloidin).

Association of GS-Pro with Nuclear Lamina and RER

After washes in PBS, the multiple staining was carried out as follows:

1. Apply the primary antibody (goat anti-lamin B) diluted in dilution buffer. Place slides horizontally in a humid chamber and incubate overnight at 4 °C.
2. Rinse samples 3 times in PBS for 10 min.
3. Incubate with the secondary antibody (donkey anti-goat conjugated to Alexa Fluor 555; *see* **Note 6**) for 60 min at RT. Protect from light.
4. Rinse 3 times in PBS for 5 min.
5. Incubate with Alexa Fluor 633 ConA for 60 min at RT in the humid chamber.
6. Rinse 3 times in PBS for 5 min.
7. Incubate with Hoechst for 5 min (in the dark, at RT).
8. Wash for 2 × 5 min in PBS.
9. Mount samples following the procedure described in previous **step 13**.
10. Examine with a confocal microscope and capture images within the next month.

Association of GS-Pro with the Cytoskeleton

To study the cytoskeletal distribution of glutathionylated proteins, double immunostaining of GS-Pro labeled cells with antibodies against microtubules (tubulin) and intermediate filaments (vimentin), or lectins detecting filaments of actin (such as phalloidin).

After washes in PBS, samples previously labeled with anti-GS-Pro antibody were double-stained to detect:

Microtubules:

1. Apply the primary antibody (sheep anti-tubulin) diluted in dilution buffer. Place slides horizontally in a humid chamber and incubate overnight at 4 °C.
2. Rinse samples 3 times in PBS for 10 min.
3. Incubate with the secondary antibody (donkey anti-sheep conjugated to Alexa Fluor 555) for 60 min at RT. Protect from light and incubate in a humid chamber.
4. Rinse 3 times in PBS for 5 min.
5. After counterstaining with Hoechst (5 min, in the dark, at RT) and PBS washes, samples were mounted following the procedure described in previous **step 13**, and examined with a confocal microscope.

Intermediate filaments:

1. Apply the primary antibody (goat anti-vimentin) diluted in dilution buffer. Place slides horizontally in a humid chamber and incubate overnight at 4 °C.
2. Rinse samples 3 times in PBS for 10 min.
3. Incubate with the secondary antibody (donkey anti-goat conjugated to Alexa Fluor 555) for 60 min at RT. Protect from light.
4. Rinse 3 times in PBS for 5 min.
5. Repeat previous **step 5**.

F-actin filaments:

1. Apply the rhodamine phalloidin diluted in PBS. Place slides horizontally in a humid chamber and incubate for 60 min, at RT.
2. Rinse samples 3 times in PBS for 5 min.
3. Mount chamber with coverslip following the previous **step 5**.

3.2 In Situ Matrix Extraction Procedure

Subconfluent cells grown on chamber slides are processed as follows:

1. Wash in D-MEM without serum (5 min).
2. Wash once in PBS (5 min).
3. Incubated with TBS-5 permeabilization buffer for 15 min, at RT.
4. Rinse 2 times in TBS-5 for 5 min.

5. Digestion with DNase I, for 60 min at RT.
6. Wash 2 times in TBS-5 for 5 min.
7. Double extraction in NaCl in TBS-5 (5 min).
8. Wash for 2 × 5 min in TBS-5.
9. Rinse once in PBS.
10. Fixation in ice cold 4 % paraformaldehyde in PBS for 10 min at 4 °C.
11. In situ extracted matrix samples may be processed for immunocytochemistry (*see* **Note 7**) and labeled with antibodies against GS-Pro and lamina B (*see* Fig. 3), following Subheading 3.1 reported above.

3.3 Confocal Laser Microscopy Imaging

In this work, the confocal imaging is performed on Olympus Fluoview FV1000 confocal IX81 inverted microscope (Olympus Europa GMBH), equipped with green argon-ion (458–488 and 515 nm) laser, red Helium-Neon (543 and 633 nm) laser as well as a 405-nm diode laser, using 60× (1.42 numerical aperture) oil objective.

3.3.1 Optical Sectioning

Single sections are acquired with FV10-ASW software, using the following acquisition parameters: (a) scanning mode format of 1024 × 1024 pixels; (b) pixel size of 0.21 μm; (c) sampling speed of 40 μs/pixel.

The images are acquired with bandpass emission filter sets appropriate for Alexa Fluor 488 (BA505-525), Alexa Fluor 555 (BA560-620), and Hoechst (BA430-460). In double-multiple labeling, fluorochromes unmixing is performed by acquisition of automated-sequential collection of multichannel images, in order to reduce spectral crosstalk between channels (*see* **Note 8**). After their conversion in TIFF format, images are processed with Photoshop software version 9.0 (Adobe Systems Inc., San Jose, CA).

3.3.2 Colocalization Analysis

Colocalization analysis compares the spatial localization of two proteins that are identified by fluorescence immunocytochemistry, to verify if they occupy the same pixel location. Proper guidelines are required for preparation and acquisition of samples for qualitative and quantitative colocalization analysis. Qualitative colocalization may be represented by *dye-overlay* (visualization of yellow pixels in a red-green merged image) and *threshold-overlap* (only those pixels that show certain red pixel intensity and green pixel intensity above a certain threshold value are highlighted) techniques. In this work, colocalization masks (visualized as white areas/spots, *see* insets in Fig. 1) for dual stained samples are obtained using the FV10-ASW software with the threshold-based approach (*see* **Note 9**). Qualitative colocalization should be accompanied by quantitative analysis that includes a number of respective coefficients to evaluate colocalization (*see* refs. 24, 25 as tutorial guides).

4 Notes

1. It is important to consider the confluence status of the cell culture, as in proliferating condition the total GS-Pro fluorescence increases in the early phases of growth and significantly drops when cells reach confluence (*see* ref. 21).
2. Alternatively, blocking may be carried out with 5 % bovine serum albumine when secondary antibodies produced by different species are used in multiple stainings. It is important to include a control sample to test nonspecific signal of immunohistochemical reagents by omitting primary antibody from the dilution buffer.
3. Once the procedure has started the cells should not dry during the incubation and washing steps. Drying out results in nonspecific staining. All incubation steps are carried out in a humid chamber. Use 100–150 μl blocking solution or antibody per well- or just sufficient to cover cells completely.
4. It is recommended to use $F(ab')^2$, or Fab-fragments of a given secondary antibody as they do not contain the Fc-region of IgG. The Fab/$F(ab')^2$-type antibodies do not bind to Fc receptors that may be present in a given tissue or cell type thus giving a reduced background. For the Green channel, it is recommended to use Alexa Fluor 488 that has the same spectral characteristics as fluorescein (FITC) or Cy2.
5. After this step, cell nuclei may be counterstained with Hoechst, or samples may be processed for double-multiple labelings.
6. For the Red channel, it is recommended to use Alexa Fluor 555 that has the same spectral characteristics as tetramethyl rhodamine (TRITC), or Alexa Fluor 594 that has the same spectral characteristics as Texas Red.
7. This technique allows discarding cytosol, organuli, endoplasmic reticulum cisternae, nucleoplasm and DNA, saving nuclear lamina and cytoskeleton only. By this method it is possible to confirm the tight association of GS-Pro with nuclear lamina and cytoskeleton.
8. It is important that each group of image, for each set of experiment, will be processed and analyzed using the same settings (i.e. laser power and detector amplification).
9. However, analysis tools for visualization and quantification of colocalization are freely available via the software ImageJ (N.I.H. USA, http://rsbweb.nih.gov/ij/, using the JACoP plugin: http://rsbweb.nih.gov/ij/plugins/colocalization.html).

Acknowledgments

We gratefully thank *Maney Publishing* and *Redox Report* journal for the permission to reuse part of material (Figs. 1, 2, and 4) originally inserted in ref. [21] (article URL: http://www.ingentaconnect.com/content/maney/rer/2012/00000017/00000002/art00003; URLs for the online version of "Redox report" journal: www.maneypublishing.com/journals/rer and http://www.ingentaconnect.com/content/maney/rer).

We thank the Italian Ministry of Health (Ricerca Corrente) for financial support of this work.

References

1. Dickinson DA, Forman HJ (2002) Glutathione in defense and signaling: lessons from a small thiol. Ann N Y Acad Sci 973:488–504
2. Chai YC, Ashraf SS, Rokutan K, Johnstone RB, Thomas JA (1994) S-thiolation of individual human neutrophil proteins including actin by stimulation of the respiratory burst: evidence against a role for glutathione disulfide. Arch Biochem Biophys 310:273–281
3. Desagher S, Glowinski J, Premont J (1996) Astrocytes protect neurons from hydrogen peroxide toxicity. J Neurosci 16:2553–2562
4. Cotgreave IA, Gerdes RG (1998) Recent trends in glutathione biochemistry. Glutathione-protein interactions: a molecular link between oxidative stress and cell proliferation? Biochem Biophys Res Commun 242:1–9
5. Klatt P, Lamas S (2000) Regulation of protein function by S-glutathionylation in response to oxidative and nitrosative stress. Eur J Biochem 267:4928–4944
6. Fratelli M, Demol H, Puype M, Casagrande S, Eberini L, Salmona M, Bonetto V, Mengozzi M, Duffieux F, Miclet E, Bachi A, Vandekerckhove J, Gianazza E, Ghezzi P (2002) Identification by redox proteomics of glutathionylated proteins in oxidatively stressed human T lymphocytes. Proc Natl Acad Sci U S A 99:3505–3510
7. Giustarini D, Rossi R, Milzani A, Colombo R, Dalle-Donne I (2004) S-glutathionylation: from redox regulation of protein functions to human diseases. J Cell Mol Med 8:201–212
8. Pastore A, Tozzi G, Gaeta LM, Bertini E, Serafini V, Di Cesare S, Bonetto V, Casoni F, Carrozzo R, Federici G, Piemonte F (2003) Actin glutathionylation increases in fibroblasts of patients with Friedreich's ataxia: a potential role in the pathogenesis of the disease. J Biol Chem 43:42588–42595
9. Pineda-Molina E, Klatt P, Vazquez J, Marina A, Garcia de Jacoba M, Perez-Sala D, Lamas S (2001) Glutathionylation of the p50 subunit of NF-kB: a mechanism for redox-induced inhibition of DNA binding. Biochemistry 40:14134–14142
10. Dalle-Donne I, Giustarini D, Colombo R, Milzani A, Rossi R (2005) S-glutathionylation in human platelets by a thiol-disulfide exchange-independent mechanism. Free Radic Biol Med 38:1501–1510
11. Mawatari S, Murakami K (2004) Different types of glutathionylation of hemoglobin can exist in intact erythrocytes. Arch Biochem Biophys 421:108–114
12. Fratelli M, Demol H, Puype M, Casagrande S, Villa P, Eberini L, Vandekerckhove J, Gianazza E, Ghezzi P (2003) Identification of proteins undergoing glutathionylation in oxidatively stressed hepatocytes and hepatoma cells. Proteomics 3:1154–1161
13. Landino LM, Moynihan KL, Todd JV, Kennett KL (2004) Modulation of the redox state of tubulin by the glutathione/glutaredoxin reductase system. Biochem Biophys Res Commun 314:555–560
14. Schulz JB, Lindenau J, Seyfried J, Dichgans J (2000) Glutathione, oxidative stress and neurodegeneration. Eur J Biochem 267:4904–4911
15. Piemonte F, Pastore A, Tozzi G, Tagliacozzi D, Santorelli FM, Carrozzo R, Casali C, Damiano M, Federici G, Bertini E (2001) Glutathione in blood of patients with Friedreich's ataxia. Eur J Clin Invest 31:1007–1011
16. Sparaco M, Gaeta LM, Santorelli FM, Passarelli C, Tozzi G, Bertini E, Simonati A, Scaravilli F, Taroni F, Duyckaerts C, Feleppa M, Piemonte F (2009) Friedreich's ataxia: oxidative stress and cytoskeletal abnormalities. J Neurol Sci 287:111–118

17. Markovic J, Borrás C, Ortega A, Sastre J, Viña J, Pallardó FV (2007) Glutathione is recruited into the nucleus in early phases of cell proliferation. J Biol Chem 282(28):20416–20424
18. Pallardó FV, Markovic J, García JL, Viña J (2009) Role of nuclear glutathione as a key regulator of cell proliferation. Mol Aspects Med 30:77–85
19. Brennan JP, Miller JIA, Fuller W, Wait R, Begum S, Dunn MJ, Eaton P (2006) The utility of N, N-biotinyl glutathione disulfide in the study of protein S-glutathiolation. Mol Cell Proteomics 5:215–225
20. Lim SY, Raftery MJ, Goyette J, Geczy CL (2010) S-Glutathionylation regulates inflammatory activities of S100A9. J Biol Chem 285(19):14377–14388
21. Petrini S, Passarelli C, Pastore A, Tozzi G, Coccetti M, Colucci M, Bianchi M, Carrozzo R, Bertini E, Piemonte F (2012) Protein glutathionylation in cellular compartments: a constitutive redox signal. Redox Rep 17(2):63–71
22. Jones DP, Go YM (2010) Redox compartmentalization and cellular stress. Diabetes Obes Metab 12(2):116–125
23. Squarzoni S, Sabatelli P, Ognibene A, Toniolo D, Cartegni L, Cobianchi F, Petrini S, Merlini L, Maraldi NM (1998) Immunocytochemical detection of emerin within the nuclear matrix. Neuromuscul Disord 8:338–344
24. Bolte S, Cordelieres FP (2006) A guided tour into subcellular colocalization analysis in light microscopy. J Microsc 224:213–232
25. Zinchuk V, Grossenbacher-Zinchuk O (2011) Quantitative colocalization analysis of confocal fluorescence microscopy images. Curr Protoc Cell Biol Chapter 4:Unit 4.19. doi: 10.1002/0471143030.cb0419s52

Chapter 29

New Analytical Strategies Applied to the Determination of Coenzyme Q10 in Biological Matrix

Mario Contin, Sabrina Flor, Manuela Martinefski, Silvia Lucangioli, and Valeria Tripodi

Abstract

In the last few years the importance of Coenzyme Q10 (CoQ10) determination has gained clinical relevance. CoQ10 is a redox-active, lipophilic substance integrated in the mitochondrial respiratory chain which acts as an electron carrier for the production of cellular energy. In addition, it is recognized as a primary regenerating antioxidant playing an intrinsic role against oxidative damage. There are some reports of low CoQ10 levels in a number of disorders, such as cancer, muscular, neurodegenerative, cardiological, and reproductive diseases. Therefore, it is a priority to develop analytical methodologies for evaluating CoQ10 in matrices of greater importance for the correct diagnosis of diseases, simple enough to be used in routine clinical laboratories.

In this chapter two recently developed techniques, capillary electrophoresis and microHPLC, for the analysis of CoQ10 in biological matrices, are studied.

Key words Coenzyme Q10, Capillary electrophoresis, micro-HPLC, Plasma, Platelet, Muscle

1 Introduction

Coenzyme Q10 (CoQ10) (2, 3-dimethoxy-5-methyl-6-decaprenyl-1,4-benzoquinone) is a redox-active, lipophilic substance integrated in the mitochondrial respiratory chain where it acts as an electron carrier for the production of cellular energy (Fig. 1) [1]. In addition, CoQ10 is known as a powerful antioxidant agent able to protect circulating proteins and cell membranes against oxidative damage [2, 3].

Although the importance of CoQ10 in mitochondrial function is well established, the significance of CoQ10 deficiency has recently achieved clinical relevance. In this sense, CoQ10 determination has acquired clinical significance as a biomarker, particularly for metabolic and oxidative stress abnormalities [1, 4]. Human CoQ10 deficiency can be classified as primary or secondary deficiency resulting in a series of heterogeneous diseases. Primary CoQ10 deficiency seems to be relative rare and has been associated with mutations of diverse

Donald Armstrong (ed.), *Advanced Protocols in Oxidative Stress III*, Methods in Molecular Biology, vol. 1208,
DOI 10.1007/978-1-4939-1441-8_29,

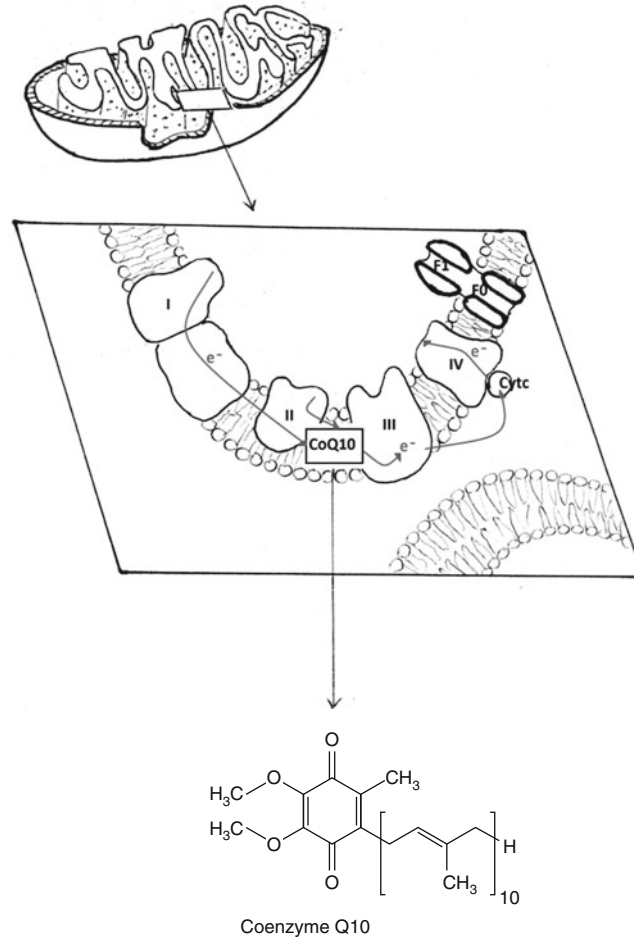

Fig. 1 Schematic illustration of mitochondrial Coenzyme Q10 localization

genes involved in its biosynthesis [5, 6]. Growing evidence supports that secondary or acquired CoQ10 deficiency is more common. Low plasma levels of CoQ10 have been reported in a number of disorders, including cancer, muscular, neurodegenerative, cardiological, and reproductive diseases [7–12], among others. For these reasons, the determination of CoQ10 in biological samples and the study of the correlation of its levels with states of deficiency are very important for diagnosis and therapeutics [2, 3, 8, 13, 14].

However, the low concentration of CoQ10 in plasma, the complexity of this matrix and two molecular properties necessary for CoQ10 function (the high hydrophobicity and easy oxidation) make the analysis of CoQ10 technically challenging [1]. Many procedures have been reported to quantitate CoQ10 in plasma: HPLC with ultraviolet (UV) or electrochemical detection (ECD) [2, 14–23]; HPLC coupled to mass spectrometry [24], and also voltammetric [25]; chemioluminiscent [26]; fluorimetric [27]; and spectrophotometric methods [28].

The focusing of this chapter is to describe two recently developed techniques: one by capillary electrophoresis and the other by microHPLC, for the analysis of CoQ10 in biological matrices. These methods show multiples advantages respect to those previously reported.

Capillary electrophoresis (CE) is a powerful technique with relevant characteristic of performance such as simplicity, very high resolution in short times of analysis and low cost of operation and it has become an alternative methodology applied to the analysis of compounds in different matrices [29]. CE is applied into several modes being electrokinetic chromatography (EKC) one of the most used for analysis in biological matrices. In EKC, selectivity is achieved by the partitioning of analytes between mobile phase (usually a buffer) and a pseudostationary phase (PSP), which may be micelles (MEKC), vesicles (VEKC), polymers or droplets in the case of a microemulsions (MEEKC) [29].

Microemulsions are dispersed systems consisting of nanometer size droplets of an inmiscible liquid, stabilized by surfactant and co-surfactant molecules [30]. Microemulsions can be prepared as water droplets in an oil phase (W/O) or oil droplets in a water phase (O/W). Microemulsions have been used as a new EKC system with unique selectivity because they have many potential advantages such as high stability, ability to interact with a wide range of hydrophobic and hydrophilic compounds, transparency, and easy preparation [31–33].

Traditional MEEKC systems employ sodium dodecyl sulfate (SDS), a single-chain structure tensioactive, as the surfactant. However, resolution of some hydrophobic compounds using only SDS as surfactant can be unsuccessful [34].

In a previous work, we have developed a microemulsion system based on sulfosuccinate sodium (AOT) as a tensioactive agent applied to the simultaneous analysis de natural and synthetic estrogen. The use of a double chain and hydrophobic surfactant as AOT in a MEEKC system allowed the analysis of estrogens with different hydrophobicity in a single run [35].

Taking into account the experience in the developed of microemulsion systems and the high hydrophobicity of the CoQ10, a new MEEKC system has been developed based on the use of two surfactants, AOT and cholic acid (CA, bile acid) applied to the quantification of CoQ10 in plasma samples (Figs. 2) [36]. This new microemulsion system resulted to be a simple and suitable analytical method for the separation of CoQ10 from the plasma components (Fig. 3).

Another strategy to analyze this complex molecule is to turn traditional HPLC methods into microanalytical developments. HPLC is the most affordable, easy to operate, and workable to adapt into microsystems. We describe here an optimized method by microHPLC which is fast, simple, and highly sensitive [13, 37].

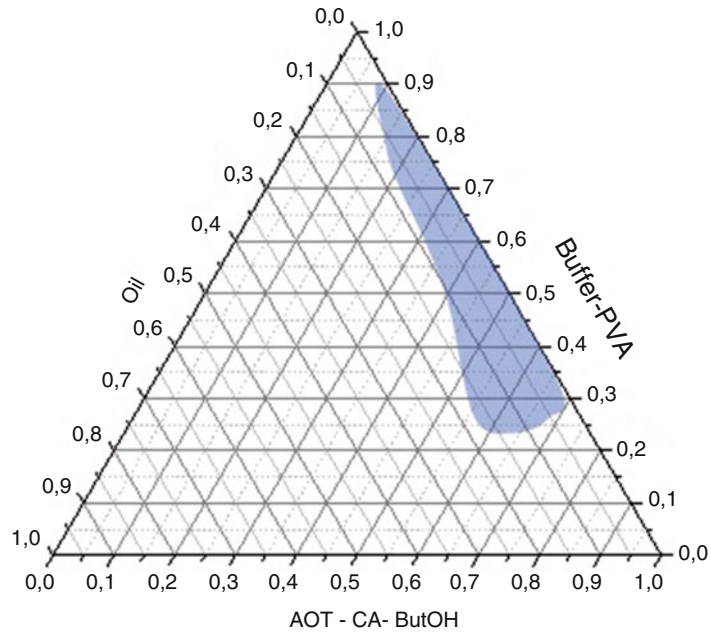

Fig. 2 Ternary phase diagram AOT–CA–Octane–Butanol–PVA–Tris buffer. *Shaded area* corresponds to the proportions of components obtained with the formation of a microemulsion o/w

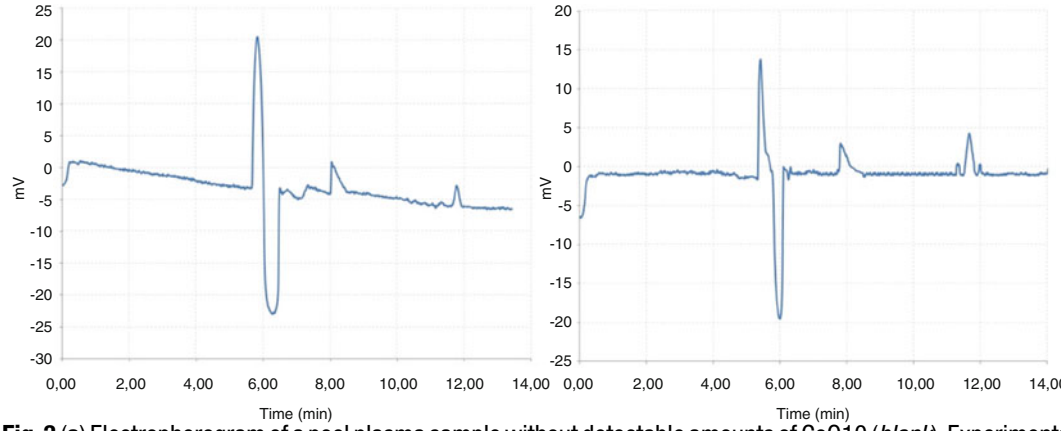

Fig. 3 (**a**) Electropherogram of a pool plasma sample without detectable amounts of CoQ10 (*blank*). Experimental conditions are described in the text. (**b**) Electropherogram of a plasma sample of a healthy subject (0.56 mg/mL of CoQ10). Experimental conditions are described in the text

In this sense, one of the current trends of advanced analytical chemistry is the miniaturization of the analytical procedures. Ultrafast separations, consumption of small amounts of both samples and reagents, as well as high sensitivity and easy automatization are some of the most important goals to achieve [38]; therefore, the miniaturization of the HPLC columns allows the performance of CoQ10 analysis with these features. Fast HPLC employs short columns of 2–5 cm of length with a conventional internal diameter

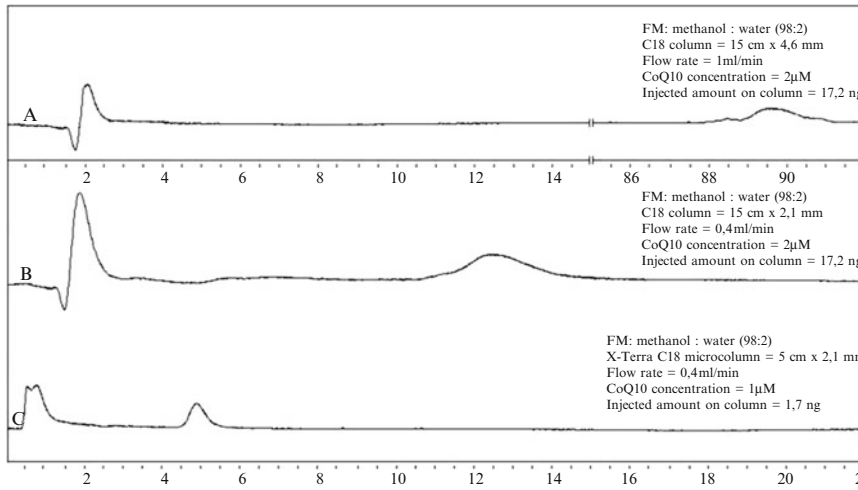

Fig. 4 Comparison of analysis of CoQ10 standard using different HPLC columns. Retention time in parentheses. (**a**) Traditional C18-column (15.0 cm 4.6 mm i.d.). Mobile phase: methanol–water (98:2, v/v), flow rate: 1.0 mL/min. CoQ10 standard: 2.0 μM. (**b**) Microbore C18-column (15.0 cm × 2.1 mm i.d.). Mobile phase: methanol–water (98:2, v/v), flow rate: 0.3 mL/min. CoQ10 standard: 2.0 μM. (**c**) XTerra C18 microcolumn (50 mm × 2.1 mm i.d.). Mobile phase: methanol–water (98:2, v/v), flow rate: 0.3 mL/min. CoQ10 standard: 1.0 μM

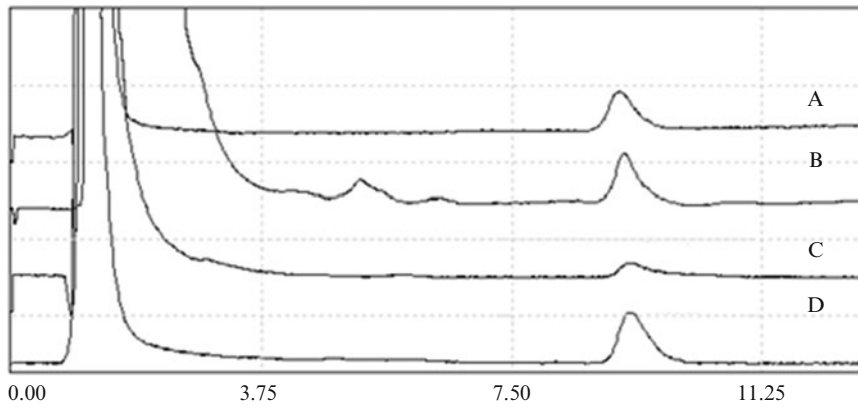

Fig. 5 CoQ10 microHPLC analysis. (**a**) CoQ10 standard of 1.4 μM, (**b**) plasma of healthy volunteers: 0.8 μM, (**c**) healthy volunteer platelet: 333.0 pmol/10^9platelet, (**d**) porcine heart muscle 234.0 μg/g tissue

(i.d.) of 4.6 mm while microbore HPLC uses columns of 1–2 mm i.d. In microHPLC the use of reduced diameter columns increases the number of the orical plates, which leads to a higher efficiency achieving better LODs and LOQs, comparables with those described for HPLC with electrochemical detection (Fig. 4).

Although CoQ10 is often analyzed in plasma, it has recently been shown that in some cases, plasma CoQ10 does not accurately reflect the intracellular concentration and it would be necessary to determine it in other matrices such as platelet and muscle [39], so the developed microHPLC method will be described coupled with each sample preparation required to analyze CoQ10 (Fig. 5) [37].

2 Materials

2.1 Equipment

2.1.1 Capillary Electrophoresis

Analysis were carried out in P/ACE™ MDQ CE system equipped with diode array detector (190–600 nm) and data were processed by Karat V.8 software.

2.1.2 Micro-HPLC

Analysis were carried out in an HPLC Thermo Scientific equipped with a quaternary pump (P4000), temperature control, a vacuum degasser (SCM 1000), a dual UV detector (UV2000), an automatic injector (AS3000).

2.2 Reagents and Chemicals

1. CoQ10 standard stock solution

   25.0 mg of CoQ10 were accurately weighted in a 25.0 mL volumetric flask, and dissolved in ethanol, in order to obtain a final concentration of 1.0 mg/mL. The stock solution was protected from light and stored at −20 °C till 2 months.

2. CoQ10 working standard solution

   CE: 1.0 mL of *Stock Solution* was diluted in 50.0 mL volumetric flask with diluent at a final concentration of 20 μg/mL.

   HPLC: Working standard solution of 1 μg/mL was obtained by appropriate dilution of *Stock Solution* with ethanol.

3. Background electrolyte
   144 mg of AOT, 100 mg of octane, and 850 mg of butanol were manually stirred until complete dissolution of AOT (phase A) (*see* **Notes 1–4**).

   Separately 400 mg of CA and 10 mg of PVA were dissolved in 8.5 g of 10 mM Tris buffer, pH 9.00 (phase B) (*see* **Notes 3–6**).

   Finally, in order to obtain a microemulsion system, phase B was added drop to drop to the phase A under a slowly shirring. The solution was let to stand until obtain a clear solution.

4. *Benzoquinone solution:* 20.0 mg of benzoquinone were accurately weighted in an epperdorf, and dissolved in 5.0 mL of 1-propanol. The solution was prepared every day protected from light.

5. *Ultrapure water* was obtained from an EASY pure™ RF equipment. All solutions were filtered through a 0.45 μm nylon membrane and degassed before use.

6. Diluent solutions

   Sterile diluent solution: Diluent (sterile solution of diethylaminoethyl p-aminobenzoate 85 mM and sodium chloride 31 mM) was used for platelet count.

   CE Diluent was consisted of 10 mM Tris buffer, pH 9.00 with a 15 % of ethanol (*see* **Note 7**).

2.3 Supplies

1. *ChromQuest* Chromatography Data System software was used for the chromatographic analysis.
2. *Capillary:* An uncoated fused-silica capillary of 60 cm × 75 μm i.d (50 cm to the detector) was employed (*see* **Note 8**).
3. *Xterra microcolumn*: 50 mm × 2.1 mm i.d, 3.5 μm particle size with a guard column Xterra (10 mm × 2.1 mm i.d, 3.5 μm particle size) was employed.

3 Methods

3.1 Capillary Electrophoresis

Electrophoretic parameters: The capillary temperature was kept at 25 °C, and UV detection wavelength was set at 210 nm. Samples were injected by pressure 1 psi during 5 s and electrophoretic system was operated under positive polarity and a constant voltage of 26 kV.

3.1.1 Sample Pretreatment

1. 2.0 mL of whole blood was taken from fasting people and collected in heparinized tube, immediately processed and centrifuged a 2,000 × *g* for 10 min at 4 °C. Plasma was collected, placed in a capped polypropylene tube and immediately stored at −80 °C.
2. Before the analysis, the samples were allowed to thaw at room temperature. Firstly, 600 μL of plasma was supplemented with 1,200 μL of cold 1-propanol, stirred with vortex for 2 min and centrifuged at 9,000 × *g* for 10 min at 4 °C to spin down the protein precipitate (*see* **Note 9**).
3. Next, the supernatant was transferred to another tube and evaporated to dryness under stream of nitrogen.
4. The dry residue was dissolved in 60 μL of 10 mM Tris buffer, pH 9.00 containing 15 % ethanol and then injected into the CE equipment. A tenfold enrichment of CoQ10 in the plasma samples was finally obtained (*see* **Note 10**).

3.1.2 Capillary Pre-conditioning

1. Before be used for first time, the capillary was rinsed by pressure (30 psi) with potassium hydroxide 0.5 M for 3 min; potassium hydroxide 0.1 M for 3 min; and finally with water 5 min.
2. At the beginning of each day, the capillary was rinsed by pressure (30 psi) with potassium hydroxide 0.1 M for 3 min; water 3 min; and finally with BGE for 5 min.
3. Between runs, the capillary was rinsed by pressure (30 psi) with potassium hydroxide 0.1 M for 1 min; water 1 min, and finally with BGE for 3 min.

3.2 Micro-HPLC

Chromatographic conditions: 10 μL injection volume, column temperature of 30 °C, isocratic mobile phase of methanol 10 % and flow rate of 0.4 mL/min. UV-detection was performed at 275 nm.
Sample Pretreatment

3.2.1 Plasma

1. 2.0 mL of whole blood was taken from fasting people and collected in heparinized tube, immediately processed and centrifuged a 2,000 × *g* for 10 min at 4 °C. Plasma was collected, placed in a capped polypropylene tube and immediately stored at −80 °C.
2. Before the analysis, the samples were allowed to thaw at room temperature.
3. 100 μL of heparinized plasma was supplemented with 50 μL benzoquinone stirred with vortex for 2 min and let to stand, protected from light, for 5 min (*see* **Note 11**).
4. Next, 150 μL cold 1-propanol was added, centrifuged, and the organic layer was evaporated to dryness under a stream of nitrogen (*see* **Notes 12** and **13**).
5. The dry residue was dissolved in 50 μL ethanol, sonicated for 5 min vortexed for 1 min (*see* **Note 14**), centrifuged for 2 min at 9,000 × *g*, and injected into HPLC equipment.

3.2.2 Platelets

1. 2.5 mL of whole blood was taken from fasting people and collected in citrated tube (9:1 relation blood–anticoagulant).
2. Platelet rich plasma (PRP) was obtained by decantation up to obtain about 30 % of total volume, the tube is allowed to stand for 2 h at room temperature (*see* **Note 15**).
3. PRP was placed in an eppendorf and the volume obtained was accurately measured. Then this was homogenized and an aliquot of 10 μL was taken for platelets count (*see* **Note 16**).
4. PRP was centrifuged at 9,000 × *g* for 10 min at room temperature, the supernatant was removed and the pellet was immediately stored at −80 °C (*see* **Note 17**).
5. Before the analysis, the samples were allowed to thaw at room temperature.
6. Pellet was supplemented with 50 μL of the benzoquinone solution stirred with vortex for 2 min and let to stand, protected from light, for 5 min (*see* **Note 11**).
7. Next, 150 μL cold 1-propanol was added, centrifuged and the organic layer was evaporated to dryness under a stream of nitrogen (*see* **Notes 12** and **13**).
8. The dry residue was dissolved in 50 μL ethanol, sonicated for 5 min vortexed for 1 min (*see* **Note 14**), centrifuged for 2 min at 9,000 × *g* and injected into HPLC equipment.
9. *Platelets count*: Manual platelet count was carried out in Neubauer chamber.

3.2.3 Muscle

1. 100.0 mg of skeletal muscle was accurately weighted and homogenized with 3.0 mL cold 1-propanol on ice bath (*see* **Note 18**).

2. The mixture was then vortex-mixed for 1 min, sonicated and transferred to a polypropylene tube stirred with vortex for 2 min, sonicated for 5 min and centrifuged at 2,000 × *g* for 20 min.
3. To 950 μL from the supernatant 50 μL of the benzoquinone solution was added and allowed to stand protected from light for 5 min.
4. The mixture was ultracentrifuged at 9,000 × *g* for 10 min and injected directly into the HPLC system (*see* **Note 19**).

4 Notes

1. In BGE preparation it is important that the surfactant, co-surfactant, and the oil phase are manually stirred. It has been demonstrated that mechanical stirring disables microemulsions systems based on AOT. This could be due to the fact that the drops of oil obtained after mechanically stirring vary in size and morphology compared to those obtained with manual stirring (Fig. 6).
2. Butanol showed to be the most adequate co-surfactant to stabilize the microemulsion but high concentration of this component not only produced higher migration times but also disturbed the peak shapes.
3. Optimal concentration of AOT was 1.4 % w/w and 4 % CA for complete resolution and adequate stability of the microemulsion.
4. Longer migration time of analytes was obtained at higher concentrations of AOT and CA.
5. Resolution was poorer at CA concentration lower than 4 %.
6. The best peak shape and stability of baseline were observed at 0.1 % PVA, but at higher PVA concentrations the UV signal was reduced.
7. Sample diluents: it was observed that 15 % of ethanol showed an appropriate solubilization of the analyte and good peak shapes.
8. A capillary of 60 cm length and 75 μm id at 20 kV of voltage was employed because good resolution together with adequate intensity of current could be achieved during the run.
9. Pretreatment of sample was found necessary because some components of the plasma interfere in the quantitation of CoQ10 and also reduce the capillary life time.

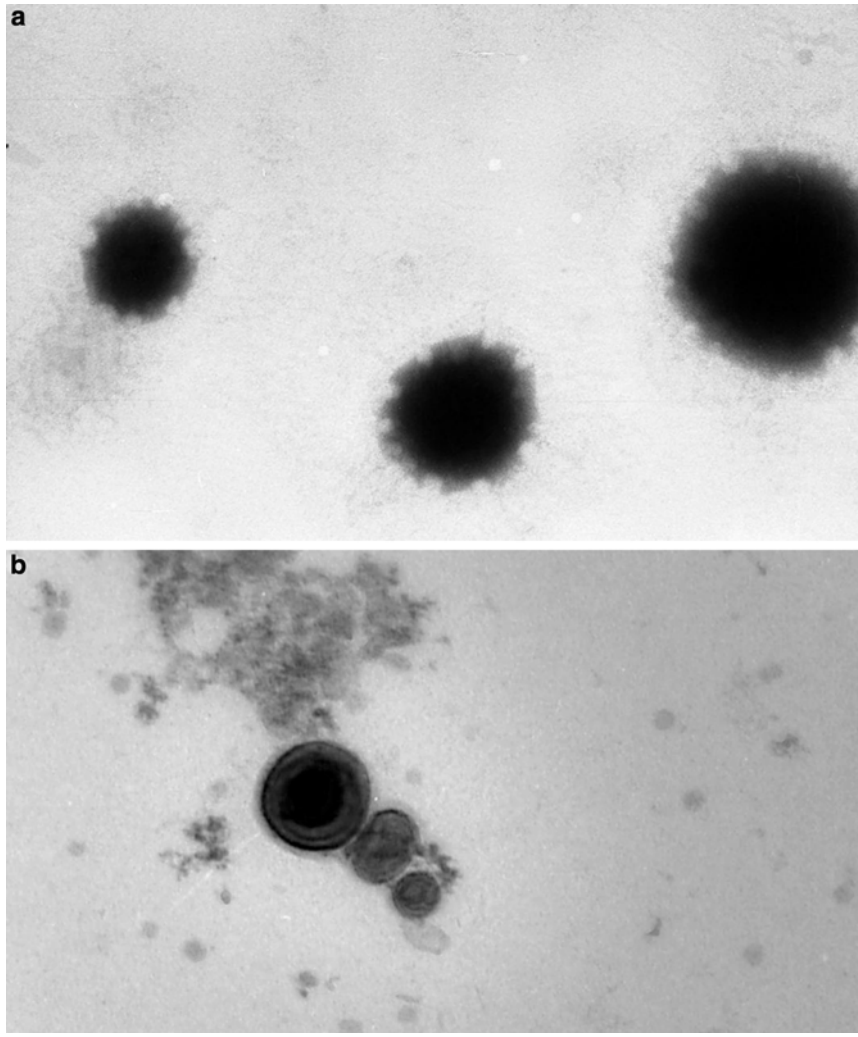

Fig. 6 (**a**) TEM microemulsion AOT–Octane–Butanol–Tris Buffer, sonicated. (30 kX) and (**b**) TEM microemulsion AOT–Octane–Butanol–Tris Buffer without sonication. (30 kX)

10. To increase sensitivity and to improve the sample preparation before injection, it was necessary to evaporate hexane to dryness and finally to dissolve the residue in 60 μL of 10 mM Tris buffer, pH: 9.00–15 % ethanol.
11. Is important that after adding benzoquinone to completely oxidized CoQ10, the sample remains in the darkness for 5 min.
12. It was shown that the use of 1-propanol fulfills the function of protein precipitant as well as an efficient solvent for extraction of CoQ10 without presence of interferents.
13. Sample evaporation and reconstitution turn out to be the key steps, and it is very important to perform a careful evaporation.

14. When reconstituted, it is important to sonicate for 5 min, then vortex for 2 min and then centrifuge.
15. Regarding the sample preparation to determine CoQ10 in platelets it is very important to maintain the sample at room temperature and the use of polypropylene material.
16. Platelets counts were performed by duplicate, obtaining about 400,000 platelets/μL.
17. After obtaining the platelets pellet, supernatant should be removed completely, because this will directly influence the determination of CoQ10 (positive interference with CoQ10).
18. Using small pieces of a muscle biopsy (5 mg) an appropriate assay is able to be achieved. In that case a proportional volume of 1-propanol should be used.
19. A similar procedure for the determination of CoQ10 in muscle has been successfully employed in other tissues, such as liver, brain, and heart in animal models.

References

1. Barshop B, Gangoiti J (2007) Analysis of coenzyme Q10 in human blood and tissues. Mitochondrion 7:89–93
2. Jiang P, Wu M, Zheng Y et al (2004) Analysis of coenzyme Q(10) in human plasma by column-switching liquid chromatography. J Chromatogr B Analyt Technol Biomed Life Sci 805(2): 297–301
3. Armstrong JS, Whiteman M, Rose P et al (2003) The Coenzyme Q10 analog decylubiquinone inhibits the redox-activated mitochondrial permeability transition: role of mitochondrial [correction mitochondrial] complex III. J Biol Chem 278(4):49079–49084
4. Miles MV, Tang PH, Liles L et al (2008) Validation and application of an HPLC-EC method for analysis of coenzyme Q10 in blood platelets. Biomed Chromatogr 22: 1403–1408
5. Quinzii C, Naini A, Salviati L et al (2006) A mutation in para-hydroxybenzoate-polyprenyltransferase (COQ2) causes primary coenzyme Q10 deficiency. Am J Hum Genet 78:345–349
6. Rötig A, Mollet J, Rio M et al (2007) Infantile and pediatric quinone deficiency diseases. Mitochondrion 7 Suppl:S112–S121
7. CooperJ M, Korlipara LV, Hart PE et al (2008) Coenzyme Q10 and vitamin E deficiency in Friedreich's ataxia: predictor of efficacy of vitamin E and coenzyme Q10 therapy. Eur J Neurol 15(12):1371–1379
8. Molineux S, Young J, Florkowshi C et al (2008) Coenzyme Q10: is there a clinical role and a case for measurement? Clin Biochem Rev 29(2):71–78
9. Cobanoglu U, Demir H, Cebi A et al (2011) Lipid peroxidation, DNA damage and coenzyme Q10 in lung cancer patients—markers for risk assessment? Asian Pac J Cancer Prev 12(6):1399–1403
10. Cooney RV, Dai Q, Gao YT et al (2011) Low plasma coenzyme Q(10) levels and breast cancer risk in Chinese women. Cancer Epidemiol Biomarkers Prev 20(6):1124–1130
11. El-ghoroury EA, Raslan HM, Badawy EA et al (2009) Malondialdehyde and coenzyme Q10 in platelets and serum in type 2 diabetes mellitus: correlation with glycemic control. Blood Coagul Fibrinolysis 20(4):248–251
12. Littarru GP, Tiano L (2010) Clinical aspects of coenzyme Q10: an update. Nutrition 26: 250–254
13. Contin M, Lucangioli S, Martinefski M et al (2011) Miniaturized HPLC-UV method for analysis of coenzyme Q10 in human plasma. J Liq Chrom Relat Tech 34:2485–2494
14. Tang PH, Miles MV, DeGrauw A et al (2001) HPLC analysis of reduced and oxidized coenzyme Q(10) in human plasma. Clin Chem 47(2):256–265
15. Grossi G, Bargossi AM, Fiorella PL et al (1992) Improved high-performance liquid chromatographic method for the determination of

coenzyme Q10 in plasma. J Chromatogr 593: 217–226

16. Okamoto T, Fukunaga Y, Ida Y et al (1988) Determination of reduced and total ubiquinones in biological materials by liquid chromatography with electrochemical detection. J Chromatogr 430:11–19
17. Mosca F, Fattorini D, Bompadre S et al (2002) Assay of coenzyme Q(10) in plasma by a single dilution step. Anal Biochem 305:49–54
18. Karpińska J, Mikołuć B, Motkowski R et al (2006) HPLC method for simultaneous determination of retinol, alpha-tocopherol and coenzyme Q10 in human plasma. J Pharm Biomed Anal 42:232–236
19. Breihaupt D, Kraut S (2006) Simultaneous determination of the vitamins A, E, their esters and coenzyme Q_{10} in multivitamin dietary supplements using an RP-C30 phase. Eur Food Res Technol 222:643–649
20. Andersson S (1992) Determination of coenzyme Q by non-aqueous reversed-phase liquid chromatography. J Chromatogr 606:272–276
21. Edlund PO (1988) Determination of coenzyme Q10, alpha-tocopherol and cholesterol in biological samples by coupled-column liquid chromatography with coulometric and ultraviolet detection. J Chromatogr 425(1):87–97
22. Wang Q, Lee B, Ong C (1999) Automated high-performance liquid chromatographic method with precolumn reduction for the determination of ubiquinol and ubiquinone in human plasma. J Chromatogr B Biomed Sci Appl 726:297–302
23. Tang P, Miles M, Miles L et al (2004) Measurement of reduced and oxidized coenzyme Q9 and coenzyme Q10 levels in mouse tissues by HPLC with coulometric detection. Clin Chim Acta 341:173–184
24. Hansen G, Christensen P, Tüchsen E et al (2004) Sensitive and selective analysis of coenzyme Q10 in human serum by negative APCI LC-MS. Analyst 129:45–50
25. Michalkiewicz S (2008) Voltammetric determination of coenzyme Q10 in pharmaceutical dosage forms. Bioelectrochemistry 73:30–36
26. Battino M, Ferri E, Girotti S et al (1991) Free radical scavenging activity of coenzyme 0 measured by a chemiluminescent assay. Anal Chim Acta 255:367–371
27. Rokos JA (1973) Determination of ubiquinone in subnanomole quantities by spectrofluorometry of its product with alkaline ethylcyanoacetate. Anal Biochem 56:26–33
28. Karpińska J, Mikołuć B, Piotrowska-Jastrzebska J (1998) Application of derivative spectrophotometry for determination of coenzyme Q10 in pharmaceuticals and plasma. J Pharm Biomed Anal 17:1345–1350
29. Lucangioli S, Tripodi V (2012) Applications of capillary electrophoresis to the clinical and pharmaceutical analysis. In: He Z (ed) Capillary electrophoresis: fundamentals, techniques and applications, Chap 9. Nova Science, New Orleans, LA, pp 187–209
30. Trotta M, Gallarate M, Pattarino F et al (1999) Investigation of the phase behaviour of systems containing lecithin and 2-acyl lysolecithin derivatives. Int J Pharm 190:83–89
31. Marsh A, Clark B, Broderick M et al (2004) Recent advances in microemulsion electrokinetic chromatography. Electrophoresis 25: 3970–3980
32. Broderick M, Donegan S, Power J et al (2005) Optimisation and use of water-in-oil MEEKC in pharmaceutical analysis. J Pharm Biomed Anal 37:877–884
33. Huie CW (2006) Recent applications of microemulsion electrokinetic chromatography. Electrophoresis 27:60–75
34. Lin JM, Nakagawa M, Uchiyama K et al (2002) Comparison of three different anionic surfactants for the separation of hydrophobic compounds by nonaqueous capillary electrophoresis. Electrophoresis 23:421–425
35. Tripodi V, Flor S, Carlucci A et al (2006) Simultaneous determination of natural and synthetic estrogens by EKC using a novel microemulsion. Electrophoresis 27:4431–4438
36. Lucangioli S, Flor S, Contin M et al (2009) A capillary electrophoretic system based on a novel microemulsion for the analysis of coenzyme Q10 in human plasma by electrokinetic chromatography. Electrophoresis 30: 1899–1905
37. Contin M, Martinefski M, Lucangioli S et al (2011) Sistema cromatográfico miniaturizado para la determinación de coenzima Q10 en plasma, músculo y plaquetas. Acta Bioquim Clín Latinoam 45(2):273–278
38. Ascenio RM, Hernandez BJ, Rocco A et al (2009) Food analysis: a continuous challenge for miniaturized separation techniques. J Sep Sci 32(21):3764–3800
39. Niklowitz P, Menke T, Andler W et al (2004) Simultaneous analysis of coenzyme Q10 in plasma, erythrocytes and platelets: comparison of the antioxidant level in blood cells and their environment in healthy children and after oral supplementation in adults. Clin Chim Acta 342:219–226

Chapter 30

Binding and Cytotoxic Trafficking of Cholesterol Hydroperoxides by Sterol Carrier Protein-2

Albert W. Girotti and Tamas Kriska

Abstract

Redox-active cholesterol hydroperoxides (ChOOHs) generated by oxidative stress in eukaryotic cells may propagate cytotoxic membrane damage by undergoing one-electron reduction or, at low levels, act as mobile signaling molecules like H_2O_2. We discovered that ChOOHs can spontaneously translocate between membranes or membranes and lipoproteins in model systems, and that this can be accelerated by sterol carrier protein-2 (SCP-2), a nonspecific lipid trafficking protein. We found that cells overexpressing SCP-2 were more susceptible to damage/toxicity by 7α-OOH (a free radical-generated ChOOH) than control cells, and that this correlated with 7α-OOH delivery to mitochondria. The methods used for obtaining these results and for establishing that cellular SCP-2 binds and traffics 7α-OOH are described in this chapter.

Key words Cholesterol hydroperoxide (ChOOH), Sterol carrier protein-2 (SCP-2), SCP-2 inhibitors, Cytotoxic ChOOH trafficking

1 Introduction

Like natural phospholipids (PLs), non-esterified cholesterol (Ch) can respond to a concentration gradient by departing from a given membrane or lipoprotein (donor) and transferring to another one, the initial rate for Ch being much greater than that for PLs [1]. Such transfer plays an important role in membrane biogenesis/homeostasis and lipoprotein remodeling [1, 2]. At relatively low total membrane lipid concentrations, spontaneous Ch transfer is known to occur via an aqueous transit pool rather than via collisions between donor and acceptor membranes [1, 2]. Ch departure from the donor compartment is typically rate limiting, but this rate can be increased by intracellular transfer proteins acting as facilitators of desorption from donor membranes or as delivery vehicles to acceptors [1, 3, 4]. At least two types of Ch transfer protein have been identified and characterized: (a) those of the steroidogenic acute regulatory (StAR) family, which are highly specific for sterol-type

Donald Armstrong (ed.), *Advanced Protocols in Oxidative Stress III*, Methods in Molecular Biology, vol. 1208,
DOI 10.1007/978-1-4939-1441-8_30,

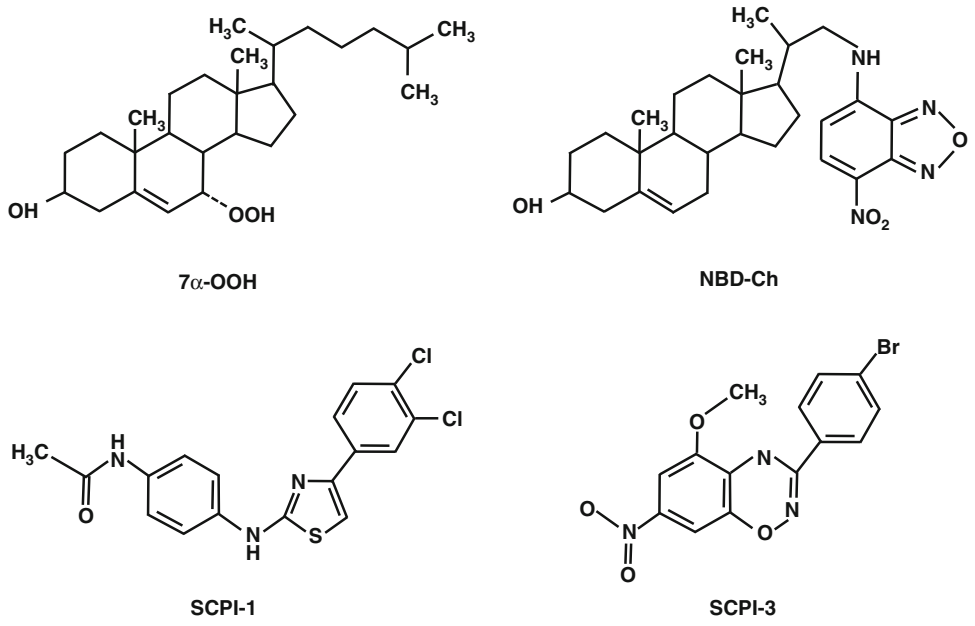

Fig. 1 Chemical structures of 7α-OOH, NBD-Ch, SCPI-1, and SCPI-3

ligands [5], and (b) sterol carrier protein-2 (SCP-2), a nonspecific transporter which can bind fatty acids and phospholipids as well as Ch and other sterols [6, 7].

As an unsaturated lipid, Ch is susceptible to oxidative modification under conditions of biological oxidative stress, giving rise to hydroperoxides (ChOOHs) and other oxidized species [8, 9]. 3β-hydroxycholest-5-ene-7α-hydroperoxide (7α-OOH), shown in Fig. 1, and its β-epimer are prominent ChOOH intermediates generated by free radical-mediated (chain) lipid peroxidation in oxidatively stressed membranes and lipoproteins [9, 10]. If the rate 7α- and 7β-OOH formation in a cell membrane outpaces that of detoxification by type-4 glutathione peroxidase (the only enzyme now known to be capable of this), these peroxides become more available for iron-catalyzed one-electron reduction to oxyl radicals [10, 11]. The latter may then trigger free radical-mediated (chain) lipid peroxidation, which exacerbates oxidative damage [10]. Several years ago, we discovered that these reactions are not necessarily limited to the membrane of ChOOH origin, but can extend to other membranes by way of ChOOH translocation through the aqueous phase [12, 13]. Using model membrane donor–acceptor systems, we showed that 7α-OOH, for example, translocated more rapidly than unoxidized Ch and that this was further accelerated by recombinant SCP-2 [14]. When isolated mitochondria were used as acceptors, the accelerated transfer resulted in greater mitochondrial damage/dysfunction as assessed by loss of transmembrane

potential [14]. Similar effects of SCP-2 were observed with other ChOOH isomers and also with various PLOOHs [14]. Subsequent studies showed that SCP-2-overexpressing hepatoma cells internalized liposome-delivered 7α-OOH and transferred it to mitochondria more rapidly than controls, and this resulted in more extensive membrane depolarization and apoptotic cell killing [15]. These findings were consistent with SCP-2 involvement in elevated 7α-OOH cytotoxicity, but did not establish whether the protein actually interacted with and transported the hydroperoxide as it entered cells. In a recent study, we used two competitive inhibitors of Ch binding to SCP-2 [16], denoted SCPI-1 and SCPI-3 (Fig. 1), to demonstrate that the protein does, in fact, bind 7α-OOH as it enters cells [17]. The methods we developed for preparing 7α-OOH, challenging cells with it, and measuring its cellular uptake and toxicity in the absence versus presence of SCPI-1 or SCPI-3 are described.

2 Materials

2.1 Equipment

The following general types of equipment are used for carrying out the protocols described: a CO_2 incubator for maintaining cells in culture, a laminar flow hood, thin layer chromatography (TLC) chambers, a TLC hair-line sample applicator, high performance liquid chromatography (HPLC) equipment with normal and reverse-phase columns, phosphorimaging equipment, a confocal fluorescence microscope, and a fluorescence plate reader. Specific details are provided in Subheading 3.

2.2 Reagents and Supplies

Sigma Chemical Co. (St. Louis, MO) supplied most of the routine chemicals and reagents, including cholesterol (Ch), 3-(4,5-dimethylthiazolyl-2-yl)-2,5-diphenyltetrazoliumbromide (MTT), 5,5′,6,6′-tetrachloro-1,1′,3,3′-tetraethyl-benzimidazolyl-carbocyanine iodide (JC-1), Dulbecco's modified Eagle's medium (DMEM), fetal bovine serum (FBS), and other cell culture materials. 1-palmitoyl-2-oleoyl-*sn*-glycero-3-phosphocholine (POPC) was obtained from Avanti Polar Lipids (Alabaster, AL) and [4-^{14}C]Ch (~55 mCi/mmol) from Amersham Biosciences (Arlington Heights, IL). Molecular Probes (Eugene, OR) supplied the 22-[*N*-(7-nitrobenz-2-oxa-1,3-diazol-4-yl)amino]-23,24-bisnor-5-cholen-3β-ol (NBD-Ch) and 4,4-difluoro-5-(4-phenyl-1,3-butadienyl)-4-bora-3a,4a-diaza-*s*-inda-cene-3-undecanoic acid (C11-BODIPY). *N*-(4-{[4-(3,4-dichlorophenyl)-1,3-thiazol-2-yl]amino}phenyl) acetamidehydrobromide (SCPI-1) and 3-(4-bromophenyl)-5-methoxy-7-nitro-4H-1,2,4-benzoxadiazine (SCPI-3) were obtained from ChemBridge Hit2Lead Chemical Store (San Diego, CA). All aqueous reagent solutions were prepared with deionized glass distilled water.

2.3 SCP-2-Expressing Cells

Two SCP-2-overexpressing transfectant clones are represented, one (SC2F) derived from mouse L-cell fibroblasts and the other (SC2H) from rat hepatoma cells; both were obtained originally from Dr. F. Schroeder (Texas A&M University) as a research gift. SC2F and SC2H cells express ~3-fold and ~7-fold more SCP-2 protein, respectively, than their wild type or vector controls [14]. The cells are grown under standard culture conditions (humidified 37 °C incubator with 5 % CO_2), using DMEM, 10 % FBS, penicillin (100 U/ml), streptomycin (0.1 mg/ml), and geneticin (G418, 0.35 mg/ml) selection agent. The latter is removed at the second cell passage before an experiment.

3 Methods

3.1 Preparation of Unlabeled and Radiolabeled 7α-OOH

7α-OOH is prepared by dye-sensitized photoperoxidation of Ch in liposomal membranes (*see* **Note 1**). Large unilamellar vesicles (100 nm diameter LUVs) are prepared by a lipid extrusion method [18]. A mixture of dimyristoyl phosphatidylcholine (DMPC), Ch, and dicetylphosphate (DCP) in pre-set amounts (*see* below) in chloroform is dried to a film under argon and then under vacuum overnight (*see* **Note 2**). After hydration in PBS, followed by five freeze–thaw cycles, the resulting multilamellar vesicles are passed at least 10-times through a double layer of 0.1 μm polycarbonate filters (Nucleopore, Pleasanton, CA), using an Extruder apparatus (Lipex Biomembranes, Vancouver, BC) at room temperature. The resulting LUVs, typically consisting of 2.5 mM DMPC, 2.0 mM Ch, and 0.25 mM DCP in bulk phase PBS (5 ml) (*see* **Note 3**), are placed in a thermostatted 50-ml beaker, treated with a potent photosensitizer such as aluminum phthalocyanine disulfonate (25 μM), and irradiated at 4 °C, using a 90 W quartz-halogen lamp positioned as close as possible above the LUV suspension. The suspension is stirred continuously at a low rate to ensure uniform light and oxygen exposure. 7α-OOH yield after a 1 h irradiation period is typically 1–2 % or 0.1–0.2 μmol [19]. 7α-OOH is separated from other ChOOHs by two HPLC steps: first, reverse-phase HPLC using a C18 column and methanol–isopropanol–acetonitrile–water (70:12:11:7 by vol) as the mobile phase and second, normal-phase HPLC using a silica column with hexane–isopropanol (95:5 by vol) as the mobile phase, 212 nm UV detection being used in each case. Finally isolated material is confirmed as 7α-OOH by proton-NMR, quantified by iodometic analysis, and stably stored in isopropanol at −20 °C. Radiolabeled 7α-OOH ([^{14}C]7α-OOH) is prepared similarly, using [4-^{14}C]Ch as the starting material. Additional details are as reported previously [19, 20].

3.2 Preparation of 7α-OOH-Containing Liposomes

Small unilamellar vesicles (50 nm SUVs) are used as delivery vehicles for assessing 7α-OOH uptake by cells, subcellular distribution, and toxicity (*see* **Note 4**). A suitable lipid formulation is DMPC–7α-OOH–Ch–DCP (49:25:25:1 by mol) at 5 mM total lipid prepared in metal ion-depleted PBS (*see* **Note 3**). The SUVs are fabricated by an extrusion method (cf. Subheading 3.1) using 0.05 μm polycarbonate filters in this case. Fully formed vesicles are stored under argon at 4 °C and used experimentally within 2 days.

3.3 Determination of 7α-OOH Uptake and Cytotoxicity in SCP-2-Expressing Cells

This section outlines well-established methodology for challenging cells with a ChOOH, in this case 7α-OOH, how cell uptake and SCP-2-dependent distribution of the hydroperoxide can be determined, and how the peroxidative damage and cellular dysfunction that it initiates can be assessed.

3.3.1 Cell Challenge with Liposomal 7α-OOH

1. Twenty four hours before and experiment, SC2H and VC cells are seeded into 12-well plates at a density of 10^5 per well so as to reach ~60 % confluency at experiment time (*see* **Note 5**).
2. After rinsing twice with RPMI medium, the wells are overlaid with SUV 7α-OOH in serum-free RPMI, using up to 75 μM peroxide in bulk suspension (*see* **Note 6**).
3. After 3 h of incubation, cells are washed free of SUVs, overlaid with 1 % serum-containing RPMI, and incubated for an additional 20 h (*see* **Note 7**).
4. The medium is aspirated and cells are treated with MTT (0.5 mg/ml) in DMEM for 4 h. The level of formazan produced (which reflects number of viable cells) is determined by dissolving the blue crystals in isopropanol and measuring absorbance at 570 nm [21].
5. Published data [15] showed that SC2H cells were more sensitive to 7α-OOH than VC (Fig. 2b)

3.3.2 Uptake and Subcellular Distribution of 7α-OOH

1. SC2H and VC cells (5×10^5 per dish) are seeded into 10-cm dishes 2 days before and experiment. The Ch level of both cell types are reduced by growing them in RPMI containing 5 % lipoprotein-deficient serum for 12 h before a peroxide challenge.
2. The cells are freed of serum-containing medium by rinsing twice with RPMI alone, then overlaid with 25 μM SUV [^{14}C]7α-OOH and incubated for 3 h.
3. Cells are then washed twice with ice-cold PBS, recovered by scraping, and centrifuged at $180 \times g$ for 10 min at 4 °C. Supernatant fractions are discarded and cell pellets are resuspended and incubated in ice-cold hypo-osmotic buffer (10 mM HEPES, 2 mM $MgCl_2$, 1 mM DTT, 150 mM sucrose,

2 mM EDTA, 0.1 % serum albumin, pH 7.4) for 5 min. Cells are lysed by Dounce homogenization using 10–15 passes. Immediately thereafter, osmolarity is restored and the lysate is layered onto a buffered 10-step sucrose gradient ranging from 12 to 83 % (w/w) [22]. Centrifugation at 15,000 × *g* is carried out for 3 h at 4 °C to separate nuclear, mitochondrial, microsomal, and cytosolic fractions, each of which is analyzed for protein content. Other details are as specified previously [22].

4. Each fraction is extracted with 0.8 ml of cold chloroform–methanol (2:1, v/v) and the recovered lipid portion is dried under N_2, dissolved in hexane–isopropanol (97:3, v/v), and applied to a high-performance silica gel TLC plate (EM Science, Gibstown, NJ) in a hairline N_2 stream using a programmable applicator (Camag Scientific, Wilmington, NC). The plate is chromatographed with benzene–ethyl acetate (1:1, v/v), and analyzed by phosphorimaging using a Storm 860 storage phosphor system (Molecular Dynamics, Sunnyvale, CA). A [^{14}C]7α-OOH standard of known specific radioactivity is used for data quantification. *See* ref. [23] for additional details.
5. Published findings [15] showed that SC2H cells not only internalized [^{14}C]7α-OOH faster than VC cells, but delivered it preferentially to mitochondria compared with other compartments (nuclei, endoplasmic reticulum, cytosol) (Fig. 2a).

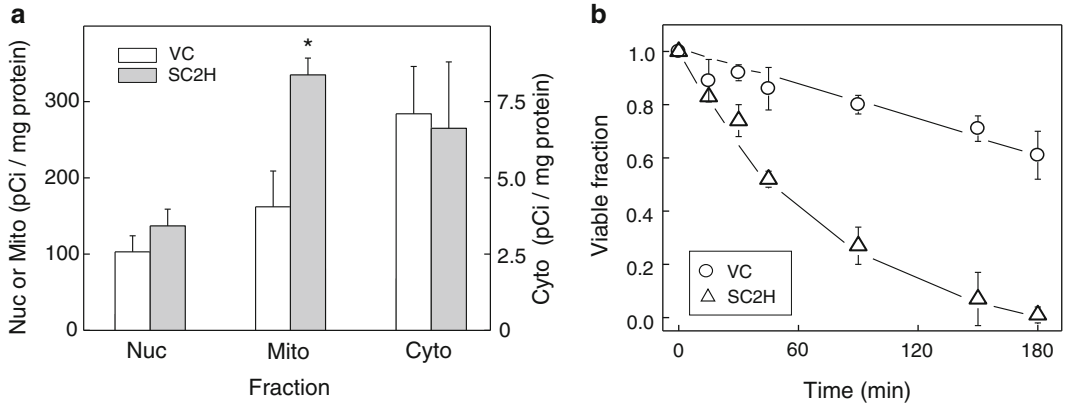

Fig. 2 7α-OOH uptake, subcellular distribution, and cytotoxicity determined for SC2H cells. (**a**) Uptake and distribution. SC2H and vector control (VC) cells that had been pre-incubated for 12 h in medium containing lipoprotein-deficient serum were incubated for 3 h with SUV [^{14}C]7α-OOH (25 μM, 30 nCi/ml) in RPMI medium, then washed and homogenized. Subcellular fractions (nuclear, mitochondrial, microsomal, and cytosolic) were separated by sucrose density gradient centrifugation and analyzed for total protein. Lipids were extracted from each fraction and subjected to HPTLC-PI for determination of specific radioactivity. *Significantly greater than corresponding VC; $p < 0.01$. (**b**) Cytotoxicity. SC2H and VC cells were incubated with SUV 7α-OOH (25 μM) for increasing times up to 3 h, then washed free of SUVs, overlaid with 1 % FBS-containing RPMI, and checked for viability by MTT assay 20 h later. Data points are means ± SE ($n = 6$). Adopted from ref. [15]

3.3.3 Use of C11-BODIPY as a Lipid Peroxidation Probe

In this subsection, a protocol is described on how to use the lipophilic fluorophore C11-BODIPY [24] as a reporter of free radical lipid peroxidation occurring in a specific subcellular compartment.

1. SC2H and VC cells seeded in 12-well plates are incubated with SUV 7α-OOH for various periods up to 3 h at 37 °C. Immediately after the cells were cleared of SUVs and washed with DMEM, C11-BODIPY was introduced.
2. Stock C11-BODIPY is prepared by dissolving 1 mg in 50 μl of dimethylformamide (DMF). The DMF solution is added to 10 ml of FBS to give a final probe concentration of 200 μM. Cells in DMEM are treated with 5 μM C11-BODIPY for 30 min at 37 °C.
3. After treatment, cells are washed and overlaid with DMEM and examined by fluorescence microscopy, using 488 nm excitation with 590 nm (red) and 530 nm (green) emission filters for observing the unoxidized and oxidized probe, respectively. Photographs are taken of representative zones and the ratio of oxidized to non-oxidized probe is determined using MetaMorph™ software. The red fluorescence value for cells treated with 7α-OOH for 0-min is taken as 100 %.
4. Confocal fluorescence microscopy is used for assessing the subcellular localization of any lipid peroxidation observed by conventional fluorescence microscopy. SC2H cells grown on coverslips in a 12-well plate are exposed to 75 μM SUV 7α-OOH for 3 h, then washed and overlaid with DMEM containing 2 μM C11-BODIPY and 0.5 μM MitoTracker Deep Red (from a 1 mM stock solution in dimethyl sulfoxide). After 30 min in the dark, the cells are washed with PBS, fixed with 4 % paraformaldehyde, washed again, and mounted on a slide using Fluoromount-G medium. A Leica DMRE microscope equipped with TCS SP2 scanner (Leica Microsystems, Heidelberg GmbH) can be used for confocal microscopy. The respective excitation and emission wavelengths are as follows: C11-BODIPY (488 nm, 507–535 nm); MitoTracker Deep Red (633 nm, 660–680 nm). At least 100-fold magnification is necessary to visualize subcellular organelles.
5. Reported findings [15] showed more rapid probe oxidation in SC2H cells than VC cells (Fig. 3a), and this occurred mainly in mitochondria (Fig. 3b).

3.3.4 Measurement of Mitochondrial Membrane Potential

Loss of mitochondrial membrane potential ($\Delta\Psi m$) serves as a direct indicator of mitochondrial damage and dysfunction. A sensitive fluorometric method for measuring $\Delta\Psi m$ status in relation to 7α-OOH challenge is described.

1. SC2H and VC cells seeded in 12-well plates are challenged with 75 μM SUV 7α-OOH as described above. At various times up to 3 h after challenge, cells were washed with PBS

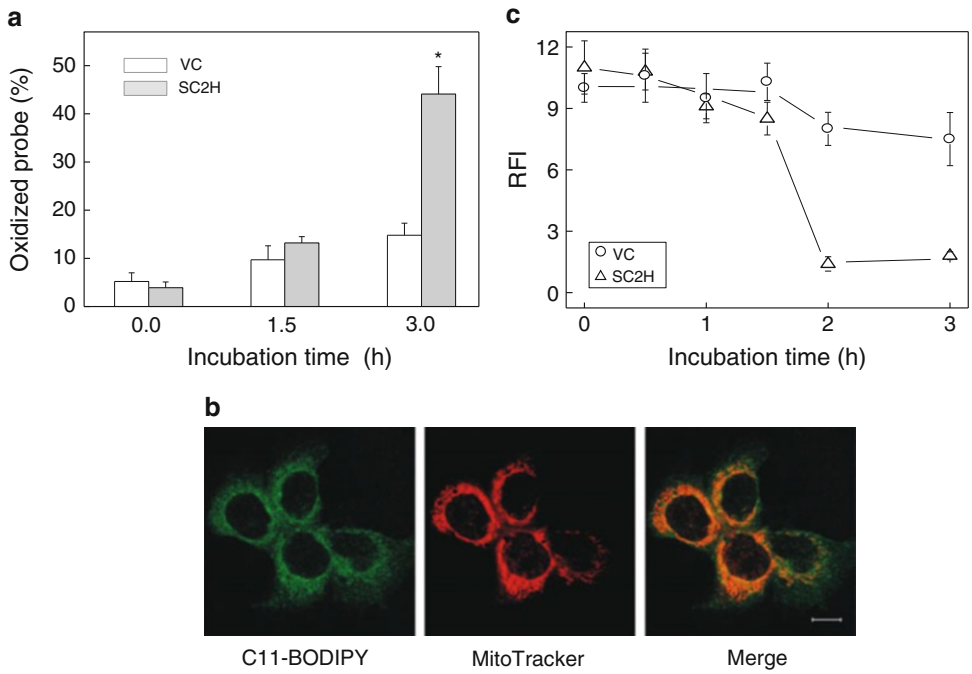

Fig. 3 Mitochondrial membrane peroxidative damage and depolarization in 7α-OOH-treated SC2H cells. (**a**) Lipid peroxidation. SC2H and VC cells at ~60 % confluency in DMEM were incubated with 25 μM SUV 7α-OOH for the indicated times, then washed, treated with 5 μM C11-BODIPY for 30 min, washed again, and examined by fluorescence microscopy, using 488 nm excitation with 590 nm (*red*) emission for non-oxidized probe and 530 nm (*green*) emission for oxidized probe. *Plot* shows integrated fluorescence intensities as percent oxidized C11-BODIPY. *Significantly greater than VC; $p < 0.001$. (**b**) Confocal micrographs of SC2H cells stained with 2 μM C11-BODIPY and 0.5 μM MitoTracker Deep Red after 3 h exposure to 25 μM SUV 7α-OOH. Bar: 10 μm. (**c**) JC-1-determined ΔΨm of SC2H (*open up pointing triangle*) and VC (*circle*) cells after incubation with 25 μM SUV 7α-OOH for the indicated times. *RFI* relative fluorescence intensity: 590 nm/530 nm. Adopted from ref. [17]

and overlaid with DMEM containing 2 μM JC-1, ratiometric ΔΨm probe [25]. After 30 min of incubation at 37 °C, cells were washed again, overlaid with DMEM alone, and checked for fluorescence emission intensity at 590 nm (red) versus 530 nm (green) fluorescence using 488 nm excitation measured in a plate reader, e.g., the Cytofluor™ fluorescence plate reader (Bedford, MA). Strong 590 nm and weak 530 nm emission reflects a high ΔΨm, whereas the opposite reflects a low ΔΨm. Time course changes is the 590 nm/530 intensity ratio for 7α-OOH-challenged SC2H cells are illustrated in Fig. 3c [15].

2. Published observations [15] indicated a more rapid ΔΨm loss in 7α-OOH-treated SC2H cells than VC (Fig. 3c).

3.4 Evaluation of SCP-2 Inhibitor (SCPI) Effects

This section describes how SCP-2 inhibitors can be used to assess SCP-2 involvement in 7α-OOH uptake by SCP-2-expressing cells, intracellular distribution of the hydropeoxide, and its damaging/cytotoxic effects. Two different transfectant clones that overexpress SCP-2 are represented: fibroblast-derived SC2F and hepatoma-derived SC2H, along with their respective vector control clones. A method for confirming that SCPIs actually bind to SCP-2 in competition with Ch, and for determining whether 7α-OOH also does this, is also described.

3.4.1 Protection Against 7α-OOH-Induced Cell Killing

1. Cells are grown to ~60 % confluency in 12-well plates. One hour before peroxide addition, cells are switched to serum-free medium and treated with SCPI-1 or SCPI-3 in increasing concentrations, using freshly prepared stock solutions in dimethyl sulfoxide (DMSO). Controls without either inhibitor receive a matching concentration of DMSO, which is kept below 0.5 % (v/v) for all incubations.
2. For the peroxide challenge, the cells are cleared of medium and overlaid with 7α-OOH-containing SUVs in DMEM, using a range of initial 7α-OOH concentrations up to ~200 μM in bulk medium (*see* **Note 8**). SCPI-1 and SCPI-3 are included so that their initial levels are maintained.
3. After a given incubation period at 37 °C, e.g., 4 h, the SUVs are removed, cells are overlaid with 1 % FBS-containing medium, and incubated for an additional 20 h, after which viability is assessed by MTT assay [21].
4. Published data involving this methodology [17] showed that SCPI-1 at ~6 μM and SCPI-3 at ~21 μM maximally protected SC2F cells against 7α-OOH-induced loss of viability, as measured by MTT assay (Fig. 4). Similar strong SCPI protection against 7α-OOH cytotoxicity was observed for SC2H cells (Fig. 4) (*see* **Notes 9** and **10**).

3.4.2 Inhibition of 7α-OOH Uptake

1. The procedure for measuring 7α-OOH taken up by cells in the absence versus presence of an SCPI is similar to that described in Subheading 3.3.2. A stock preparation of DMPC–[^{14}C]7α-OOH–Ch–DCP (49:25:25:1 by mol) SUVs containing 1.25 mM hydroperoxide (15–20 nCi/ml) has been used [17].
2. Sub-confluent cells in 10-cm culture dishes are incubated with 6 μM SCPI-1 or 21 μM SCPI-3 for 1 h, then with the SUVs at an initial [^{14}C]7α-OOH concentration of 100 μM. At various times points, SUVs are removed and cells are washed, recovered by scraping into PBS, sampled for protein determination, then extracted with chloroform–methanol (2:1 v/v), as described [19, 20].

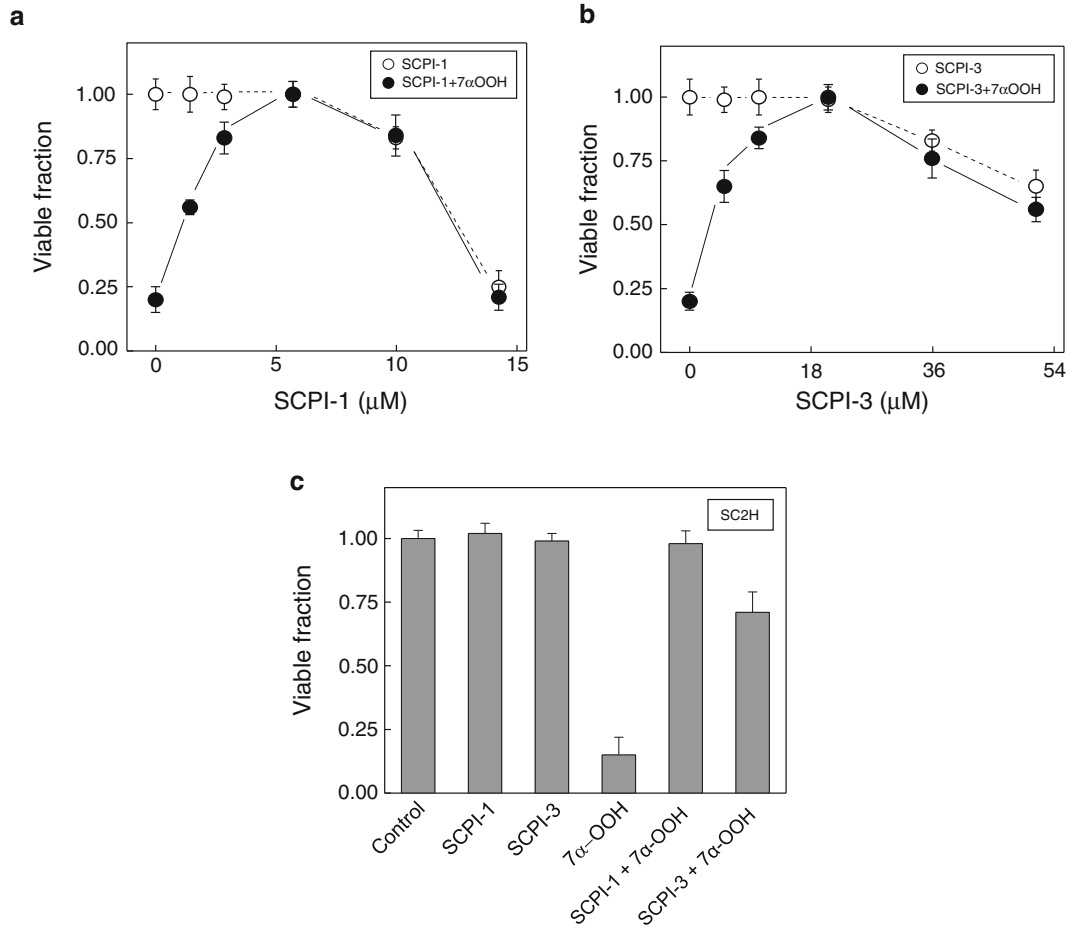

Fig. 4 SCPI protection against 7α-OOH-induced losses in cellular viability. SC2F cells in serum-free DMEM were incubated with SCPI-1 (**a**) or SCPI-3 (**b**) alone in increasing concentrations, or SCPI-1 (**a**) or SCPI-3 (**b**) in the presence of 75 μM SUV 7α-OOH. After 4 h, SUV-containing medium was replaced with 1 % FBS-containing DMEM with either SCPI present, and assessed for viability by MTT assay 20 h later. (**c**) Viability assessment of SC2H cells 20 h after a 4 h challenge with 75 μM SUV 7α-OOH in the absence versus presence of 6 μM SCPI-I or 21 μM SCPI-3. Means ± SD of values from four replicate experiments are plotted in each panel. From ref. [17]

3. Lipid-containing lower phases are dried under an argon stream, dissolved in 25 μl of hexane–isopropanol (93:7 v/v), and analyzed for [^{14}C]7α-OOH and its alcohol product ([^{14}C]7α-OH) by high-performance thin layer chromatography with phosphorimaging detection (HPTLC-PI), using benzene–ethyl acetate (1:1, v/v) as the mobile phase [23] (*see* **Note 11**). A known amount of starting SUVs is analyzed alongside to allow expression of cellular uptake of 7α-OOH in molar terms.
4. Published results [17] involving these methods showed a time-dependent increase in SUV [^{14}C]7α-OOH uptake by SC2F cells; the SCPIs reduced this substantially (Fig. 5a, b) as well as

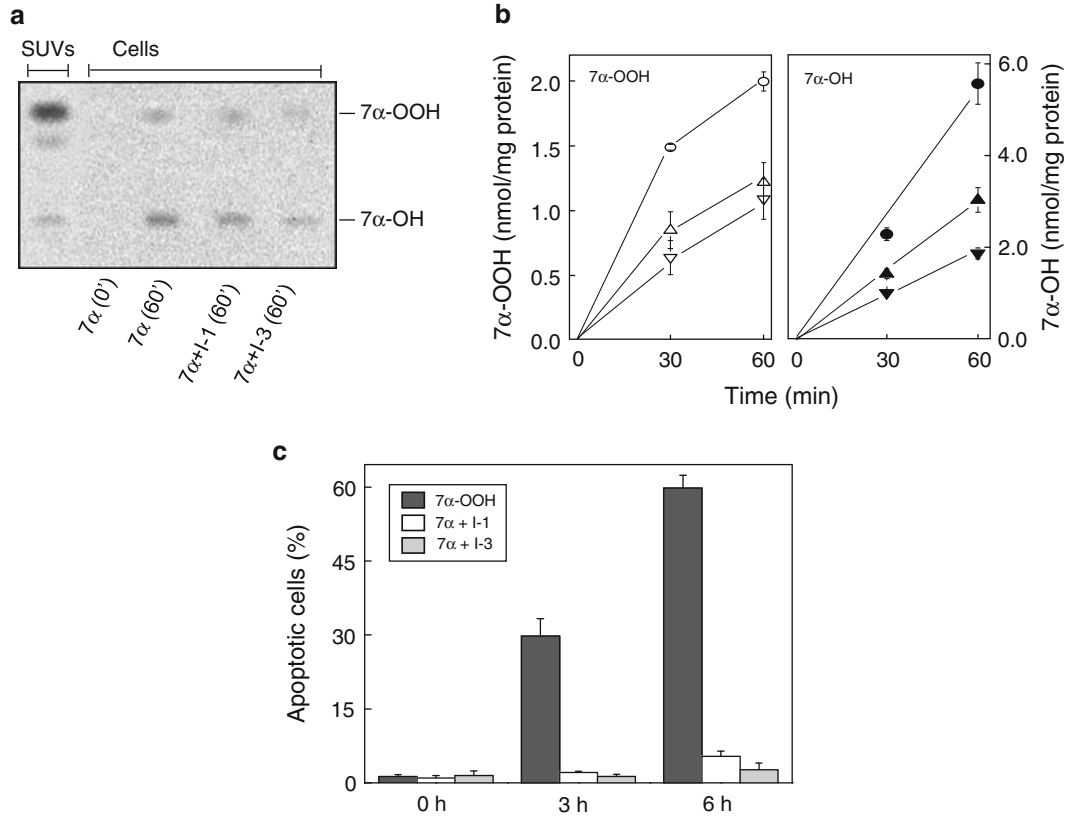

Fig. 5 SCPI inhibition of 7α-OOH uptake and apoptotic killing of SC2F cells. (**a**, **b**) Cells at ~60 % confluence in 10-cm dishes were either not treated or treated with DMPC–[^{14}C]7α-OOH–Ch–DCP (49:25:25:1 by mol) SUVs (105 μM hydroperoxide, 1.5 nCi/ml) in the absence or presence of 6 μM SCPI-1 or 21 μM SCPI-3. After 30 min and 60 min of incubation at 37 °C, SUV-containing medium was removed and after a wash with cold PBS, cells were recovered, extracted with chloroform–methanol (2:1, v/v), and lipid fractions were analyzed by HPTLC-PI. (**a**) Phosphorimaging patterns of [^{14}C]7α-OOH and [^{14}C]7α-OH immediately after, 30-min after, and 60-min after SUV addition to cells. (**b**) Time course of analyte accumulation in cells; *left panel*: 7α-OOH in the absence (*circle*) or presence of SCPI-1 (*open up pointing triangle*) or SCPI-3 (*open down pointing triangle*). *Right panel*: 7α-OH accumulation in the absence (*circle*) or presence of SCPI-1 (*filled up pointing triangle*) or SCPI-3 (*filled down pointing triangle*). Plotted data are means ± deviation of values from duplicate experiments. (**c**) Apoptosis. SC2F cells were incubated with 175 μM SUV 7α-OOH in the absence (7α-OOH) versus presence of 6 μM SCPI-1 (7α + I-1) or 21 μM SCPI-3 (7α + I-3). At the indicated times, apoptotic cell counts were determined by Ho staining with fluorescence microscopy. From ref. [17]

the accompanying accumulation of [^{14}C]7α-OH. (The alcohol appeared to arise mainly from hydroperoxide reduction in the cellular compartment rather than extracellular compartment.) These findings suggest that the SCPI cytoprotective effects observed in Fig. 4 were due to inhibitor interference with 7α-OOH uptake and distribution by SCP-2.

3.4.3 Inhibition of 7α-OOH-Induced Apoptosis

1. A nuclear fluorescence staining method is used to assess 7α-OOH-provoked apoptosis and how this is affected by SCIs.
2. SC2F cells grown to ~60 % confluency in 6-well plates are incubated in the absence or presence of 6 μM SCPI-1 or 21 μM SCPI-3 for 1 h and then to 175 μM SUV 7α-OOH in the absence or presence of either SCPI.
3. After 0, 3, and 6 h of incubation at 37 °C, the SUV-containing medium is removed, cells are washed with PBS, then incubated for 20 min in the presence of 5 μM Hoechst 33258 (Ho), which detects apoptotic cells, and 50 μM Propidium Iodide (PI), which detects necrotic cells [26].
4. Cells are examined with an inverted fluorescence microscope, using a DAPI filter for visualizing Ho fluorescence and a Texas Red filter for PI fluorescence. The number of Ho- versus PI-stained nuclei in 5 viewing fields of ~100 cells each are determined for each experimental sample.
5. Reported findings [17] revealed that SC2F cells died mainly by apoptosis during exposure to 7α-OOH over a 6 h period, and that both SCPIs effectively prevented this (Fig. 5c).

3.4.4 SCI and 7α-OOH Competitive Binding to Recombinant SCP-2

1. Competition between SCPI and Ch for binding to isolated SCP-2 is assessed by using the Ch-conjugated fluorescent probe NBD-Ch (Fig. 1) [16]. Competitive binding of 7α-OOH and NBD-Ch to SCP-2 can be assessed similarly. Because this has been observed [17], it suggests that the results obtained with SCP-2-expressing SC2H and SC2F cells [15, 17] were due to actual binding and trafficking of 7α-OOH by cellular SCP-2.
2. Recombinant SCP-2 is prepared using an *E. coli* strain carrying a plasmid encoded for the 13.2 kDa human protein (provided by F. Schroeder, Texas A&M University as a gift). Details about protein isolation, storage, and recovery are as described [14].
3. For determining SCPI binding, one prepares in a quartz fluorescence cuvette a 2.0 ml reaction mixture containing 5 μM recombinant SCP-2, 1.25 μM NBD-Ch, and SCPI-1 or SCPI-3 in increasing concentrations from 0.2 to 10 μM in 10 mM sodium phosphate, 0.1 mM EDTA, 0.1 mM desferrioxamine (pH 7.4). NBD-Ch and the SCPIs are added together from freshly prepared 1 mM stock solutions in dimethylformamide (DMF), the final concentration of DMF not exceeding ~0.25 %. A reference mixture prepared alongside contained everything except SCPI.

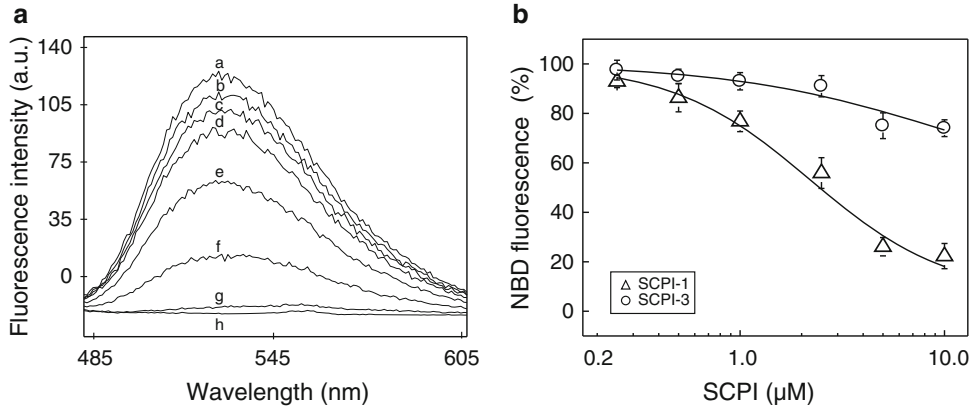

Fig. 6 SCPI competition with NBD-Ch for binding to recombinant SCP-2. (**a**) Fluorescence emission spectra for NBD-Ch (1.25 μM) in the presence of recombinant SCP-2 (5 μM) without SCPI-1 (trace a) or with SCPI-1 in increasing concentrations up to 10 μM (traces b-f). Trace g: NBD-Ch alone; trace h: SCP-2 alone. Each solution contained ~0.25 % (v/v) DMF, the NBD-Ch and SCPI-1 solvent. (**b**) Integrated fluorescence spectra from (**a**) and a similar experiment using 0–10 μM SCPI-3. Values are plotted as a function of increasing SCPI concentration relative to the non-SCPI control. Means ± SD of values from four experiments are shown. From ref. [17]

4. A scanning spectrofluorometer such as the Model QM-7SE from Photon Technology International (Ontario, Canada) is used for data acquisition.
5. After 5 min of incubation at 37 °C with slow magnetic stirring, emission spectra between 480 nm and 610 nm are recorded, using 460 nm excitation with band-pass slits of 5 nm and 7 nm for excitation and emission, respectively.
6. Observed fluorescence peaks are integrated and reductions in peak area caused by an SCPI relative to the reference are calculated using a program such as the Prism 4.0 from GraphPad Software Inc. (San Diego, CA).
7. Reported data [17] showed that the fluorescence intensity of NBD-Ch increased dramatically when it was bound to SCP-2 (Fig. 6a), the integrated peak area of scan a (NBD-Ch + SCP-2) being nearly 30-times greater than that of scan g (NBD-Ch alone). When included with NBD-Ch and SCP-2, the SCPIs reduced fluorescence yield in a concentration-dependent manner, the IC_{50} values for SCPI-1 and SCPI-3 being ~3.3 μM and ~6.5 μM, respectively (Fig. 6b). Thus, SCPI-1 was found to bind more tightly to SCP-2 than SCPI-3. Analogous competitive binding determinations for 7α-OOH revealed that its avidity for SCP-2 was ~1/4 that of SCPI-1 [17].

4 Notes

1. None of the known ChOOHs, including 7α-OOH and 7β-OOH, are available from commercial sources, so preparation via peroxidation of parent Ch is necessary; the method described is highly efficient, giving excellent overall ChOOH yields.
2. DMPC and DCP are non-oxidizable lipids and, therefore, do not compete with Ch for photoperoxidation. DCP imposes a net negative charge on the liposomes, thereby hindering their tendency to aggregate over time.
3. Phosphate-buffered saline (PBS) is 25 mM sodium phosphate, 125 mM sodium chloride (pH 7.4) that is treated with Chelex-100 before use to prevent any metal ion-catalyzed Ch oxidation or 7α-OOH decomposition in liposome preparations.
4. It is inadvisable to simply add a ChOOH in some organic solvent (methanol, isopropanol) to cells, as much of the peroxide may either aggregate in the aqueous compartment or on the cell surface, giving spurious results. Slow ChOOH translocation from liposomal donors is the preferred delivery method for reproducible results.
5. It is important to maintain a uniform confluency from well to well in order to obtain consistent experimental results. Significant variation from a given value may result in a greater or lower cytotoxicity (for lower or higher cell counts, respectively).
6. SC2H cells become detached at bulk 7α-OOH concentrations significantly greater than 75 μM, which should be avoided.
7. A relatively low serum concentration (1 %) is used to minimize growth of both control and stressed cells, thereby simplifying viability determinations.
8. Under the conditions described, no significant detachment occurs during cell exposure to 7α-OOH, even at 200 μM for up to 6 h.
9. SCPI-1 and SCPI-3 at concentrations higher than ~6 μM and ~21 μM, respectively, exhibited increasing cytotoxicity on their own (Fig. 4).
10. It is important to note that SCPI-1 and SCPI-3 did not protect cells against the cytotoxic effects of the non-lipid hydroperoxides H_2O_2 and *tert*-butyl hydroperoxide, neither of which is an SCP-2 ligand [17].
11. HPTLC-PI is more sensitive than scintillation counting and also provides information about extent of [^{14}C]7α-OOH reduction to [^{14}C]7α-OH.

References

1. Phillips MCW, Johnson WJ, Rothblat GH (1987) Mechanisms and consequences of cellular cholesterol exchange and transfer. Biochim Biophys Acta 906:223–276
2. Brown RE (1992) Spontaneous lipid transfer between organized lipid assemblies. Biochim Biophys Acta 1113:375–389
3. Zilversmit DB (1984) Lipid transfer proteins. J Lipid Res 25:1563–1569
4. Wirtz KWA (1991) Phospholipid transfer proteins. Annu Rev Biochem 60:73–99
5. Soccio RE, Breslow JL (2003) StAR-related lipid transfer (START) proteins: mediators of intracellular lipid metabolism. J Biol Chem 278:22183–22186
6. Scallen TJ, Pastuszyn A, Nohad BJ, Chanderbhan R, Kharroubi A, Vanhouny GV (1985) Sterol carrier and lipid transfer proteins. Chem Phys Lipids 38:239–261
7. Gallegos AM, Atshaves BP, Storey SM, Starodub O, Petrescu AD, Huang H, McIntosh AL, Martin GG, Chao H, Kier AB, Schroeder F (2001) Gene structure, intracellular localization, and functional roles of sterol carrier protein-2. Prog Lipid Res 40:498–563
8. Smith LL, Teng JI, Kulig MJ, Hill FL (1973) Sterol metabolism XXIII. Cholesterol oxidation by radical-induced processes. J Org Chem 38:1763–1765
9. Girotti AW (2002) Cholesterol-derived hydroperoxides: generation and reactivity in biological systems. In: Fleischer S (ed) Sterols and oxysterols: chemistry, biology, and pathobiology. Research Signpost, Kerala, pp 121–139
10. Girotti AW (1998) Lipid hydroperoxide generation, turnover, and effector action in biological systems. J Lipid Res 39:1529–1542
11. Thomas JP, Maiorino M, Ursini F, Girotti AW (1990) Protective action of phospholipid hydroperoxide glutathione peroxidase against membrane-damaging lipid peroxidation. J Biol Chem 265:454–461
12. Vila A, Korytowski W, Girotti AW (2000) Dissemination of peroxidative stress via intermembrane transfer of lipid hydroperoxides; model studies with cholesterol hydroperoxides. Arch Biochem Biophys 380:208–218
13. Vila A, Korytowski W, Girotti AW (2001) Spontaneous intermembrane transfer of various cholesterol-derived hydroperoxide species: kinetic studies with model membranes and cells. Biochemistry 40:14715–14726
14. Vila A, Levchenko VV, Korytowski W, Girotti AW (2004) Sterol carrier protein-2-facilitated intermembrane transfer of cholesterol- and phospholipid-derived hydroperoxides. Biochemistry 43:12592–12605
15. Kriska T, Levchenko VV, Korytowski W, Atshaves BP, Schroeder F, Girotti AW (2006) Intracellular dissemination of peroxidative stress: internalization, transport, and lethal targeting of a cholesterol hydroperoxide species by sterol carrier protein-2-overexpressing hepatoma cells. J Biol Chem 281:23643–23651
16. Kim MS, Wessely V, Lan Q (2005) Identification of mosquito sterol carrier protein-2 inhibitors. J Lipid Res 46:650–657
17. Kriska T, Pilat A, Schmitt JC, Girotti AW (2010) Sterol carrier protein-2 (SCP-2) involvement in cholesterol hydroperoxide cytotoxicity as revealed by SCP-2 inhibitor effects. J Lipid Res 51:3174–3184
18. Meyer LD, Hope MJ, Cullis PR (1986) Vesicles of variable size produced by a rapid extrusion procedure. Biochim Biophys Acta 858:161–168
19. Korytowski W, Bachowski GJ, Girotti AW (1991) Chromatographic separation and electrochemical determination of cholesterol hydroperoxides generated by photodynamic action. Anal Biochem 197:149–156
20. Korytowski W, Geiger PG, Girotti AW (1999) Lipid hydroperoxide analysis by high-performance liquid chromatography with mercury cathode electrochemical detection. Methods Enzymol 300:23–33
21. Mossman T (1983) Rapid colorimetric assay for cellular growth and survival: application to proliferation and cytotoxicity assays. J Immunol Methods 65:55–63
22. Srinivas KS, Chandrasekar G, Srivastava R, Puvanadrishnan R (2004) A novel protocol for the subcellular fractionation of C3A hepatoma cells using sucrose density gradient centrifugation. J Biochem Biophys Methods 60:23–27
23. Korytowski W, Wrona M, Girotti AW (1999) Radiolabeled cholesterol as a reporter for assessing one-electron turnover of lipid hydroperoxides. Anal Biochem 270:123–132
24. Drummen GPC, Van Liebergen LCM, Op den Kamp JAF, Post JA (2002) C11-BODIPY(581/591), an oxidation-sensitive fluorescent lipid peroxidation probe: (micro) spectroscopic characterization and validation of methodology. Free Radic Biol Med 33:473–490
25. Reers MS, Smiley T, Mottola-Hartshorn C, Chen A, Lin M, Chen LB (1995) Mitochondrial membrane potential monitored by JC-1 dye. Methods Enzymol 260:406–417
26. Spector D, Goldman RD, Leinwald LA (1997) Cells: a laboratory manual, vol 1, Ch 15. Cold Spring Harbor Laboratory Press, Cold Spring Harbor, NY

Part IV

Biostatistics

Chapter 31

A Toolkit for Clinical Statisticians to Fix Problems Based on Biomarker Measurements Subject to Instrumental Limitations: From Repeated Measurement Techniques to a Hybrid Pooled–Unpooled Design

Albert Vexler, Ge Tao, and Xiwei Chen

Abstract

The aim of this chapter is to review and examine different methods in order to display correct and efficient statistical techniques based on complete/incomplete data subject to different sorts of measurement error (ME) problems. Instrument inaccuracies, biological variations, and/or errors in questionnaire-based self-report data can lead to significant MEs in various clinical experiments. Ignoring MEs can cause bias or inconsistency of statistical inferences. The biostatistical literature well addresses two categories of MEs: errors related to additive models and errors caused by the limit of detection (LOD). Several statistical approaches have been developed to analyze data affected by MEs, including the parametric/nonparametric likelihood methodologies, Bayesian methods, the single and multiple imputation techniques, and the repeated measurement design of experiment. We present a novel hybrid pooled–unpooled design as one of the strategies to provide correct statistical inferences when data is subject to MEs. This hybrid design and the classical techniques are compared to show the advantages and disadvantages of the considered methods.

Key words Biomarkers, Additive measurement error model, Detection limit, Measurement error, Pooling, Hybrid design, Empirical likelihood, Bayesian methodology

1 Introduction

In clinical trials involving measurements of biomarkers, the values supplied are typically estimates and hence subject to measurement errors (MEs), arising from assay or instrument inaccuracies, biological variations, and/or errors in questionnaire-based self-report data, etc. For instance, it is well known that systolic blood pressure (SBP) is measured with errors mainly due to strong daily and seasonal variations. In this case, Carroll et al. [1] suggested that approximately 1/3 of the observed variability is due to MEs. In such a circumstance, it makes sense to hypothesize an unbiased additive error model, assuming we observe the true value plus an

Donald Armstrong (ed.), *Advanced Protocols in Oxidative Stress III*, Methods in Molecular Biology, vol. 1208,
DOI 10.1007/978-1-4939-1441-8_31,

error in each measurement. Subsequently, measurements may be subject to limits of detection (LOD) where values of biospecimens below certain detection thresholds are undetectable, leading to limitations of the information one can utilize in the analysis. Ignoring the presence of ME effects in the corresponding data can result in biased estimates and invalid statistical inferences. For example, in a study of polychlorinated biphenyls (PCBs) congeners as potential indicators of endometriosis, a gynecological disease, Perkins et al. [2] pointed out that the biomarker PCB 153 is unobservable below 0.2 ng/g serum due to the sensitivity of the measurement process. The authors proved that in the case of disregarding LOD problems in the data, PCB 153 might be discarded as potentially lacking the discriminatory ability for endometriosis.

To deal with additive ME issues, several approaches have been suggested, including study design methods based on repeated measurements, as well as statistical techniques that utilize Bayesian methodology. We introduce the repeated measurement design first, where multiple measurements are assumed to be taken on the same experimental subjects at different times or under different conditions. The repeated measurement design provides the following merits: relatively small number of assumptions required on distributions of biomarkers' values, the feasibility of parameter identifiability that yields the ME effect-adjusted statistical inferences, etc. [3]. However, the repeated measurement design can lead to the following critical issues. One is that measurement processes based on bioassays can be relatively expensive, time-consuming, dangerous, or even unfeasible. To illustrate, the cost of the F2-isoprostane assay, an important biomarker for oxidative stress, was about $130 in a BioCycle study conducted to assess the reproducibility of F2-isoprostane [4]. It makes the reproducibility assessment an expensive proposition that cannot easily be repeated in practice. An additional example can be found in Faraggi et al. [5]. The authors focused on the interleukin-6 biomarker of inflammation that has been suggested to present a potential discriminatory ability for a myocardial infarction disease. However, since the cost of a single assay was $74, examination of its usefulness has been hindered. In addition to the issue of the potential high cost, the repeated measurements mostly provide information regarding ME distributions. This information can be considered as a nuisance and is not directly related to parameters of interest in general. Another problem of the repeated measurement design is that investigators may not have enough observations to achieve the desired power or efficiency in statistical inferences when the number of replicates or individual biospecimens available is restricted [6].

Due to the limitations of the repeated measurement design mentioned above, one may consider tackling additive ME problems from the Bayesian perspective as an alternative and well-developed approach. Bayesian methods (e.g., [7, 8]) allow one to efficiently

incorporate prior knowledge regarding ME distributions with information extracted from data. However, the high computational cost, along with the possible non-robustness of inferences due to model misspecification, prior selections, and distributional assumptions of data, complicates applications of Bayesian methods in several situations in practice (e.g., [9]).

Another sort of ME mechanisms can be caused by the LOD problems. Statistical estimation and inferences based on LOD-affected data are often further complicated by the inability of laboratory methods or machinery to detect biomarker levels below some detection limits (e.g., [10–12]). Ignoring the LOD problem in data results in a loss of information and may lead to significant bias in the relevant statistical analysis. As a concrete example, we consider the following case related to a receiver operating characteristic (ROC) curve. The ROC curve is a well-known statistical tool in evaluation of biomarkers' abilities to discriminate healthy and diseased populations (e.g., [13]). In the context of the ROC curve applications, Perkins et al. [14, 15] showed that ignoring the LOD effects leads to an underestimation of the areas under the ROC curves (AUC). To cope with the LOD problems, different techniques are suggested. Note that nonparametric approaches can be very non-robust since a part of the data is unobserved numerically, when data is subject to LOD effects. The Bayesian method as one of the possible approaches to deal with LOD issues may suffer from the high computational cost and the non-robustness of inferences due to model misspecification and the subjective prior selections. In this case, when LOD issues are in effect, parameter assumptions on data distributions are complicated to test. In the context of statistical techniques to solve the LOD issues, the modern statistical literature also introduces the single imputation method (e.g., [16]) and the multiple imputation method (e.g., [17]). The single imputation method suggests substituting each missing value by a single parameter. In this case, optimal or appropriate values of this parameter can be defined corresponding to aims of relevant statistical problems (e.g., [16]). Though it is simple to implement and easy to understand, the single imputation process does not reflect the uncertainty of data. Alternatively, the multiple imputation method creates multiple data sets with different imputed values that are subsequently analyzed using multiple imputation combining rules (e.g., [17]). However, this method is time intensive and requires that missing observations satisfy different assumptions related to missing mechanisms and data distributions.

As we mentioned above, the ME problems could be integrated with scenarios that assaying biomarkers can be expensive and labor intensive in practice. Sometimes even the least expensive individual assays may be infeasible to analyze in large cohorts. As a result, it is advantageous to find cost-efficient strategies for sampling.

The pooling strategy and random sampling are two different approaches commonly used by investigators to reduce overall costs of biological experiments (e.g., [10, 18–20]). The strategy of simple random sampling involves choosing and testing a random subset of available individual samples in accordance with a study budget. In this case, some individual biospecimens are ignored; however, no assumptions on data distributions should be assumed and the estimation of operating characteristics of these individual biospecimens is straightforward.

The pooling design, on the other hand, involves randomly grouping and physically mixing individual biological samples. Assays are then performed on the smaller number of pooled samples. Thus, the pooling strategy reduces the number of measurements and then the overall cost of experiments without ignoring any individual biospecimens. For example, in the BioCycle study of F2-isoprostane mentioned above, the full design would cost \$135,720, while the pooled designs with a similar efficiency of mean estimators retained would cost only \$45,240 [4]. One can note that the pooling strategy has a great potential in operating with normal or gamma distributed data since the measurements of pooled observations are proven to be the averages of the individual measurements (e.g., [18, 21, 22]). The pooling approach is more efficient than the random sampling when the mean is the only parameter of interest [5]. In the case of the LOD problems, the pooling design can be useful and efficient to reduce the number of unobserved measurements. This property of the pooling strategy can be utilized even if the cost of measurement processes is not a main concern (e.g., [18, 21]). However, applications of the pooling strategy may suffer from the following issues: (1) information may be lost regarding distributions of individual measurements since these distribution functions are hard or even impossible to reconstruct based on pooled data in some situations (e.g., [16, 23]); (2) the pooling design can be less efficient than the random sampling when the average is not close to be sufficient statistics, e.g., in the case of log-normally distributed data (e.g., [18, 21]); (3) in the case of the LOD problems, the pooling design is not recommended when LOD affects more than 50 % of the data [21]; and (4) the efficiency of the pooling design is significantly dependent on the data distribution (e.g., [21]).

As a consequence of the benefits and drawbacks that the pooling design and random sampling possess, a natural idea is to consider a cost-efficient hybrid design involving a sample of both pooled and unpooled data in a reasonable proportion. It turned out that the hybrid design can be recommended to use when data is subject to additive MEs and/or LOD problems (e.g., [6, 19]). In the presence of the additive MEs, the hybrid design allows for the estimation of parameters related to distributions of MEs without the repeated sampling required, when each measurement is informative [6].

One can show that the hybrid design helps to reduce the number of LOD-affected observations [10].

In Subheading 3, we formally address parametric and nonparametric methods based on classical approaches and the new hybrid design technique. In Subheading 4, we will provide a Monte Carlo comparison of the methods considered above. A brief review of statistical literature related to the ME issues is presented in Subheading 5. In Subheading 6, we conclude this chapter with remarks.

2 Materials

In terms of the accessibility of the statistical methods based on incomplete data, we note that the number of relevant software packages continues to expand, particularly in the R software packages (R Development Core Team [24]). As an example we can mention the link to the R package "*emplik*" that includes the R function *el.test*. This simple R function can be very useful for constructing the empirical likelihood analysis of data from clinical studies.

Statistical software to perform analysis with data subject to instrumental limitations is available upon request at avexler@buffalo.edu.

3 Methods

In this section, we present several methods for evaluating data subject to additive errors or errors caused by LOD problems.

3.1 Additive Errors

3.1.1 Repeated Measurements

In this section, we consider the parametric and nonparametric inferences based on data obtained following the repeated measurement design.

Parametric Likelihood Inference: Suppose that we repeatedly measure biospecimens observing scores $Z_{ij} = X_i + \varepsilon_{ij}$, where true values of biomarker measurements X_i, $i = 1, \ldots, t$ are independent and identically distributed (i.i.d.), and ε_{ij}, $i = 1, \ldots, t$, $j = 1, \ldots, n_i$ are i.i.d. values of MEs. Here the subscript i denotes the ith individual, and j indicates the jth repeated measure. Define the total number of measures as $N = \sum_{i=1}^{t} n_i$. In this manner, it is assumed that there is an existence of a subset of t distinct bioassays, and each of them is measured n_i times repeatedly. For simplicity and without loss of generality, we assume that X_i and ε_{ij} are independent and normally distributed, i.e., $X_i \sim N(\mu_x, \sigma_x^2)$ and $\varepsilon_{ij} \sim N(0, \sigma_m^2)$, where μ_x and σ_x^2 are the mean and variance of X_i, respectively, and 0 and σ_m^2 are the mean and variance of ε_{ij}, respectively. Accordingly, we have $Z_{ij} \sim N(\mu_x, \sigma_x^2 + \sigma_m^2)$. In this case, one can show that if

$n_i = 1$, there are no unique solutions of estimation of σ_x^2 and σ_m^2. (This case can be titled as non-identifiability since we can only estimate the sum, $\sigma_x^2 + \sigma_m^2$, but not the individual variances σ_x^2 and σ_m^2, e.g., Vexler et al. [6]). Thus, we should assume $n_i > 1$. The observations Z's in each group i are dependent because they are measured using the same bioarray. By the well-known techniques related to the maximum likelihood methodology, one can derive the maximum likelihood estimators (MLEs) of the parameters, μ_x, σ_x^2, and σ_m^2. That is, using the likelihood function

$$L_R\left(Z \mid \mu_x, \sigma_x^2, \sigma_m^2\right) = \frac{\exp\left\{-\left[\left(2\sigma_m^2\right)^{-1}\sum_i\sum_j\left(Z_{ij}-\mu_x\right)^2 - \sum_i \frac{n_i^2\sigma_x^2\left(\bar{Z}_{i\cdot}-\mu_x\right)^2}{2\sigma_m^2\left(n_i\sigma_x^2+\sigma_m^2\right)}\right]\right\}}{\left(2\pi\right)^{0.5N}\sigma_m^{2\left[0.5(N-t)\right]}\prod_i\left(n_i\sigma_x^2+\sigma_m^2\right)^{0.5}},$$

where $\bar{Z}_{i\cdot} = n_i^{-1}\sum_{j=1}^{n_i} Z_{ij}$ (see Searle et al. [25]). If n_i s are assumed to be equal to n, the MLEs of μ_x, σ_m^2, and σ_x^2 are $\hat{\mu}_x = \bar{Z}_{\cdot\cdot} = (nt)^{-1}\sum_{i=1}^{t}\sum_{j=1}^{n} Z_{ij}$, $\hat{\sigma}_m^2 = \sum_i\sum_j\left(Z_{ij}-\bar{Z}_{i\cdot}\right)^2 / \left\{t(n-1)\right\}$, and $\hat{\sigma}_x^2 = \sum_i\left(\bar{Z}_{i\cdot}-\bar{Z}_{\cdot\cdot}\right)^2 / t - \sum_i\sum_j\left(Z_{ij}-\bar{Z}_{i\cdot}\right)^2 / \left\{nt(n-1)\right\}$, respectively. For details about the properties of the MLEs, e.g., asymptotic distributions of the estimators, see Searle et al. [25] and Vexler et al. [6]. It is clear that these properties derived using the standard maximum likelihood methodology provide a simple confidence interval estimation of the parameters and can be used as basic ingredients for developing different statistical tests.

Nonparametric Likelihood Inference: In the parametric likelihood inference mentioned above, we showed that the likelihood methodology can be easily applied to develop statistical procedures based on data subject to additive errors. In this section, we will substitute parametric likelihood by its nonparametric version to create distribution-free procedures based on data subject to additive errors. To this end, we propose to utilize the maximum likelihood concept. The empirical likelihood (EL) technique has been extensively considered in both the theoretical and applied literature in the context of nonparametric approximations of the parametric likelihood approach (e.g., DiCiccio et al. [26]; Owen [27–29]; Vexler et al. [30, 31]; Vexler and Gurevich [32]; Yu et al. [33]). We begin by outlining the EL ratio method and then we will depict how to adapt the EL ratio technique based on data with repeated measures. Suppose i.i.d. random variables $\Upsilon_1, \ldots, \Upsilon_n$ with $E|\Upsilon_1|^3 < \infty$ are observable. The problem of interest, for example, is to test the hypothesis $H_0: E(\Upsilon_1) = \mu_0$ versus $H_1: E(\Upsilon_1) \neq \mu_0$, where μ_0 is fixed and known. In this case, the EL function is defined as $L_n = \prod_{i=1}^{n} p_i$, where values of p_is should be found such that p_is will

maximize L_n given the empirical constraints $\sum_{i=1}^{n} p_i = 1$, $\sum_{i=1}^{n} p_i \Upsilon_i = \mu_0$, and $0 \le p_1, \ldots \le p_n \le 1$. These constraints correspond to an empirical version of $E(\Upsilon_1) = \mu_0$. This empirical likelihood function represents a nonparametric likelihood under H_0. Using the Lagrange method, one can show that the maximum EL function under H_0 has the form of

$$L(\mu_0) = \sup\left\{\prod_{i=1}^{n} p_i : 0 \le p_1, \ldots, p_n \le 1, \sum_{i=1}^{n} p_i = 1, \sum_{i=1}^{n} p_i \Upsilon_i = \mu_0\right\} = \prod_{i=1}^{n}\left[n\left\{1 + \lambda\left(\Upsilon_i - \mu_0\right)\right\}\right]^{-1}$$

where the Lagrange multiplier λ is a root of $\sum_{i=1}^{n} (\Upsilon_i - \mu_0) / \{1 + \lambda(\Upsilon_i - \mu_0)\} = 0$.

Similarly, under the alternative hypothesis, the maximum EL function has the simple form of $L = \sup\{\prod_{i=1}^{n} p_i : 0 \le p_1, \ldots, p_n \le 1, \sum_{i=1}^{n} p_i = 1\} = \prod_{i=1}^{n} n^{-1} = n^{-n}$. As a consequence, the 2log EL ratio test statistic is $l(\mu_0) = 2[\log(L) - \log\{L(\mu_0)\}] = 2\sum_{i=1}^{n} \log\{1 + \lambda(\Upsilon_i - \mu_0)\}$. The nonparametric version of Wilk's theorem shows that the $l(\mu_0)$ follows asymptotically a χ_1^2 distribution as $n \to \infty$ (e.g., Owen [27, 29]). As mentioned above, the observations Z's in each group i are dependent. Note that Z_{ij} is independent of Z_{kl} when $i \neq k$. Therefore, one can obtain an EL function for the block sample mean $\bar{Z}_i = n_i^{-1} \sum_{j=1}^{n_i} Z_{ij}$, $i = 1, \ldots, t$, $N = \sum_{i=1}^{t} n_i$, in a similar manner to the blockwise EL method given in Kitamura [34]. Then, the random variables become $\bar{Z}_1, \bar{Z}_2, \ldots, \bar{Z}_t$, and the corresponding EL function for μ_x is defined as

$$L_R(\mu_x) = \sup\left\{\prod_{i=1}^{t} p_i : 0 \le p_1, \ldots, p_t \le 1, \sum_{i=1}^{t} p_i = 1, \sum_{i=1}^{t} p_i \bar{Z}_i = \mu_x\right\} = \prod_{i=1}^{t}\left[t\left\{1 + \lambda\left(\bar{Z}_i - \mu_x\right)\right\}\right]^{-1}$$

where λ is a root of $\sum_{i=1}^{t} \left(\bar{Z}_i - \mu_x\right) / \left\{1 + \lambda\left(\bar{Z}_i - \mu_x\right)\right\} = 0$. In this case, the 2log EL ratio test statistic is $l_R(\mu_x) = 2\sum_{i=1}^{t} \log\left\{1 + \lambda\left(\bar{Z}_i - \mu_x\right)\right\}$.

Assume $E|Z_{11}|^3 < \infty$. Then the 2log EL ratio, $l_R(\mu_x)$, is distributed as χ_1^2 when $\sum_{i=1}^{t} n_i^{-1} \to \infty$ as $t \to \infty$. The associated confidence interval estimator is then given by $CI_R = \{\mu_x : l_R(\mu_x) \le C_{1-\alpha}\}$, where $C_{1-\alpha}$ is the $100(1-\alpha)\%$ percentile of a χ_1^2 distribution (for details, see Vexler et al. [6]).

3.1.2 Bayesian Method

An alternative approach to address the additive ME problem is the Bayesian method. The Bayesian approach incorporates prior information of the distributions of the variance of the ME value, σ_m^2, with the likelihood function to correct ME bias. Assuming $X_i \sim N(\mu_x, \sigma_x^2)$ and $\varepsilon_{ij} \sim N(0, \sigma_m^2)$, then the estimators of μ_x and σ_x^2 can be obtained by

$$\left(\hat{\mu}_x, \hat{\sigma}_x^2\right) = \max_{\mu_x, \sigma_x^2} \left\{ \int \left\{ 2\pi \left(\sigma_x^2 + \sigma_m^2\right) \right\}^{-n/2} \exp\left\{ -\frac{\sum_{i=1}^{n_i} \left(X_i - \mu_x\right)^2}{2\left(\sigma_x^2 + \sigma_m^2\right)} \right\} \psi\left(\sigma_m^2\right) d\sigma_m^2 \right\},$$

where $\psi(\sigma_m^2)$ is the prior density function of σ_m^2. Possible prior distributions of σ_m^2 are, e.g., chi-square distributions, Wishart distributions, gamma distributions, inverse gamma distributions, and inverse Gaussian distributions. In this case, uniform distributions can be used as non-informative priors. It turns out that the Bayesian estimators have relatively small variances even when prior distributions are non-informative. This approach is probably similar to the empirical Bayesian method (see Carlin and Louis [35] for details), in which the parameters of priors are estimated by maximizing the marginal distributions.

3.1.3 Hybrid Pooled–Unpooled Design

Parametric Likelihood Inference: We briefly address the basic concept of the hybrid design. Let T be the number of individual biospecimens available and N be the total number of measurements that we can obtain due to the limited study budget, $N < T$. We obtain the pooling samples by randomly grouping individual samples into groups of size p. Let $Z_1^p, \ldots, Z_{n_p}^p$ present observations from pooled samples, and $Z_1, \ldots, Z_{n_{up}}$ denote the observations from unpooled samples. The ratio of pooled and unpooled samples is $\alpha/(1-\alpha)$, $\alpha \in [0,1]$. Namely, $T = \alpha Np + (1-\alpha)N$. Note that we can obtain pooled data by mixing p individual bioassays together, and we therefore divide the αNp bioassays into n_p groups, where $n_p = \alpha N$. We measure the grouped biospecimens as n_p single observations. In accordance with the pooling literature, we have $Z_i^p = p^{-1} \sum_{k=(i-1)p+1}^{ip} X_k + \varepsilon_{i1}$, $i = 1, \ldots, n_p = \alpha N$ (see, e.g., Faraggi et al. [5], Liu and Schisterman [36], Liu et al. [37], Schisterman and Vexler [38], Schisterman et al. [17], Vexler et al. [18, 20, 22, 23]). In this case, measurements of the unpooled samples based on $n_{up} = (1-\alpha)N$ independent individuals provide observations $Z_j = X_{pn_p + j} + \varepsilon_{j1}$, $j = 1, \ldots, n_{up} = (1-\alpha)N$. Since we assume that $X_i \sim N(\mu_x, \sigma_x^2)$ and $\varepsilon_{i1} \sim N(0, \sigma_m^2)$, $i = 1, \ldots, n_p$, we have $Z_i^p \sim N(\mu_x, \sigma_x^2/p + \sigma_m^2)$ and $Z_j \sim N(\mu_x, \sigma_x^2 + \sigma_m^2)$, $i = 1, \ldots, n_p$, $j = 1, \ldots, n_{up}$, and $n_p + n_{up} = N$. Thus, the likelihood function based on pooled–unpooled data takes the form of

$$L_H\left(Z \mid \mu_x, \sigma_x^2, \sigma_m^2\right) = \left(2\pi\right)^{-\frac{N}{2}} \left(\sigma_x^2 / p + \sigma_m^2\right)^{-\frac{n_p}{2}} \left(\sigma_x^2 + \sigma_m^2\right)^{-\frac{n_{up}}{2}} \exp\left\{ -\sum_{i=1}^{n_p} \frac{\left(Z_i^p - \mu_x\right)^2}{2\left(\sigma_x^2 / p + \sigma_m^2\right)} - \sum_{j=1}^{n_{up}} \frac{\left(Z_j - \mu_x\right)^2}{2\left(\sigma_x^2 + \sigma_m^2\right)} \right\}.$$

Differentiating the log-likelihood function, $l_H = \log L_H$, with respect to μ_x, σ_x^2 and σ_m^2, respectively, to solve the ML equations $\{\partial l_H/\partial \mu_x = 0,\ \partial l_H/\partial \sigma_x^2 = 0$, and $\partial l_H/\partial \sigma_m^2 = 0\}$, we obtain the MLEs of μ_x, σ_x^2, and σ_m^2 given by

$$\hat{\mu}_x = \frac{\left(\hat{\sigma}_x^2 + \hat{\sigma}_m^2\right)\sum_{i=1}^{n_p} Z_i^p + \left(\hat{\sigma}_x^2 / p + \hat{\sigma}_m^2\right)\sum_{j=1}^{n_{up}} Z_j}{n_{up}\left(\hat{\sigma}_x^2 / p + \hat{\sigma}_m^2\right) + n_p\left(\hat{\sigma}_x^2 + \hat{\sigma}_m^2\right)},$$

$$\hat{\sigma}_x^2 = \frac{p}{p-1}\left[\frac{\sum_{j=1}^{n_{up}}\left(Z_j - \hat{\mu}_x\right)^2}{n_{up}} - \frac{\sum_{j=1}^{n_p}\left(Z_i^p - \hat{\mu}_x\right)^2}{n_p}\right],$$

and

$$\hat{\sigma}_m^2 = \frac{\sum_{j=1}^{n_p}\left(Z_i^p - \hat{\mu}_x\right)^2}{n_p} - \frac{\hat{\sigma}_x^2}{p}.$$

Note that the estimator of μ_x has a structure that weighs estimations based on pooled and unpooled data in a similar manner to the Bayes posterior mean estimator based on normal–normal models (see Carlin and Louis [35]). For details related to the properties of the MLEs, see Vexler et al. [6] and Schisterman et al. [19].

Nonparametric Likelihood Inference: Utilizing the EL methodology, Vexler et al. [6] constructed the confidence interval estimators and test statistics based on pooled–unpooled data. Consider the situation described in the parametric hybrid design above. Assume we observe measurements under the null hypothesis $H_0: EZ_i^p = EZ_j = \mu_x$. In this case, the EL function for μ_x can be presented as

$$L_R(\mu_x) = \sup\left\{\prod_{i=1}^{n_p} p_i \prod_{j=1}^{n_{up}} q_j :\right.$$

$$\left. 0 \le p_1, \ldots, p_{n_p} \le 1; 0 \le q_1, \ldots, q_{n_{up}} \le 1, \sum_{i=1}^{n_p} p_i = 1, \sum_{i=t}^{n_p} p_i Z_i^p = \mu_x; \sum_{j=1}^{n_{up}} q_j = 1, \sum_{j=1}^{n_{up}} q_j Z_j = \mu_x \right\}$$

$$= \prod_{i=1}^{n_p}\left[n_p\left\{1 + \lambda_1\left(Z_i^p - \mu_x\right)\right\}\right]^{-1} \prod_{j=1}^{n_{up}}\left[n_{up}\left\{1 + \lambda_2\left(Z_j - \mu_x\right)\right\}\right]^{-1},$$

where the Lagrange multipliers λ_1 and λ_2 are roots of the equations $\sum_{i=1}^{n_p}\left(Z_i^p - \mu_x\right)/\left\{1 + \lambda_1\left(Z_i^p - \mu_x\right)\right\} = 0$ and $\sum_{j=1}^{n_{up}}\left(Z_j - \mu_x\right)/\left\{1 + \lambda_2\left(Z_j - \mu_x\right)\right\} = 0$. Then, the 2log EL ratio test statistic can be given in the form of

$$l_H(\mu_x) = 2\log\left\{1 + \lambda_1\left(Z_i^p - \mu_x\right)\right\} + 2\sum_{j=1}^{n_{up}} \log\left\{1 + \lambda_2\left(Z_j - \mu_x\right)\right\}.$$

If $E|Z_{11}|^3 < \infty$, then the 2log EL ratio, $l_H(\mu_x)$, is distributed as χ_2^2 when $n_p, n_{up} \to \infty$, under H_0 (Vexler et al. [6]). The corresponding confidence interval estimator of μ_x is then given by $CI_H = \{\mu_x : l_H(\mu_x) \le H_{1-\alpha}\}$, where $H_{1-\alpha}$ is the $100(1-\alpha)\%$ percentile of a χ_2^2.

3.2 LOD

It is mentioned in Subheading 1 that measurements of biomarkers of interest may fall below a detection threshold d in practice. For simplicity and clarity of explanation, we suppose that biomarker values are subject to an LOD and are only quantifiable above d (for situations related to multiple detection thresholds, see [11]). Thus, we assume that for the ith subject, Z_i is observed instead of the true value of biomarker measurement X_i whereby

$$Z_i = \begin{cases} X_i & ; X_i \ge d, \\ N/A & ; X_i < d. \end{cases}$$

3.2.1 Methods Based on the Maximum Likelihood Methodology

In the situation considered above, we assume true values of biomarker measurements $X \sim N(\mu_x, \sigma_x^2)$ and data is subject to the LOD. Assume k values are quantified and n-k observations are censored below d. Putting the Z_i in an ascending order with N/A values leading, we have observations of biomarker values $Z_1^*, Z_2^*, \ldots, Z_n^*$. The logarithm of the likelihood function can be written as

$$\log L\left(Z^* \mid \mu_x, \sigma_x^2\right) = C - k \log \sigma_x - \sum_{i=n-k+1}^{n} \left(Z_i^* - \mu_x\right)^2 / \left(2\sigma_x^2\right) + (n-k) \log \Phi(\eta)$$

where $\eta = (d - \mu_x)/\sigma_x$, C is a constant, $\Phi(\cdot)$ is the standard normal distribution function, and μ_x, σ_x^2 are parameters to be estimated. Let $\phi(\cdot)$ denote the standard normal density function. Differentiating the log-likelihood function with respect to μ_x and σ_x^2 yields the estimates in the form of

$$\hat{\sigma}_x = \left(d - \bar{Z}^*\right) / \left(\eta + (n/k - 1)\varphi(\eta) / \Phi(\eta)\right), \hat{\mu}_x = \bar{Z}^* + \left(\hat{\sigma}_x^2 - s_Z^2\right) / \left(d - \bar{Z}^*\right).$$

where

$$\bar{Z}^* = k^{-1} \sum_{i=n-k+1}^{n} Z_i^*, s_Z^2 = k^{-1} \sum_{i=n-k+1}^{n} \left(Z_i^* - \bar{Z}^*\right)^2.$$

These equations allow us to solve for $\hat{\sigma}_x$ numerically and, subsequently, $\hat{\mu}_x$ by substitution (e.g., [12]).

Similarly, consider the scenario where biomarker levels follow the gamma distribution with shape parameter α and scale parameter β (e.g., [39]). The log-likelihood equation is

$$\log L(Z \mid \alpha, \beta) = C - k\left[\log\Gamma(\alpha) + \log\beta\right] - (\alpha - 1)\sum_{i=n-k+1}^{n} \log(Z_i / \beta) - \beta^{-1}\sum_{i=n-k+1}^{n} Z_i + (n-k)\log G(\eta),$$

where C is a constant, $\eta = d/\beta$, and $G(\eta) = \int_0^{\eta} (\Gamma(\alpha))^{-1} x^{\alpha-1} e^{-x} dx$. The MLEs for α and β can be obtained by maximizing the log likelihood with respect to both parameters (for more details, see [15, 38]).

3.2.2 Bayesian Methods

In the LOD context, unobserved measurements of biomarkers below LOD can be treated via techniques developed for missing data problems. From the Bayesian perspective, these missing data can be considered as unknown quantities. A posterior joint distribution of missing data and parameters of interest can be computed (e.g., [35]). Let Z_{obs} and Z_{mis} denote the observed data and the missing data, respectively. Assume we are interested in the mean of biomarker measurements, μ_x, and the variance of biomarker measurements, σ_x^2. Incorporating prior information on missing data and the parameters of interest, one can show that the corresponding posterior distribution is proportional to

$$\phi\left(Z_{\text{obs}} \mid \mu_x, \sigma_x^2, Z_{\text{mis}}\right)\varphi\left(\mu_x, \sigma_x^2, Z_{\text{mis}}\right),$$

where $\varphi(\mu_x, \sigma_x^2, Z_{\text{mis}})$ is the prior joint density of parameters of interest and the missing data, and $\phi(Z_{\text{obs}}|\mu_x, \sigma_x^2, Z_{\text{mis}})$ is the density in the form of the likelihood of the observed data. Then we can estimate parameters of interest as well as missing data in the usual way using Markov chain Monte Carlo methods (e.g., [35]).

3.2.3 Single and Multiple Imputation Methods

The method of imputations is general and flexible for handling various missing data problems. Imputations are means or draws from a predictive distribution of the missing values. Thus, a method of creating a predictive distribution for the imputation based on the observed data is commonly required (e.g., [16, 17]).

We begin by outlining the single imputation method. Assume the observed continuous outcome, Υ, satisfies the following linear regression model:

$$\Upsilon_i = \gamma + \eta X_i + \varepsilon_i, i = 1, \ldots, n,$$

with the exposure variable X_i and random noise ε_i where $E(\varepsilon_i) = 0$, $\text{var}(\varepsilon_i) = \sigma_\varepsilon^2$, and $\text{cov}(X_i, \varepsilon_i) = 0$. When the LOD effect is present, we observe exposure measurements Z_i, $i = 1, \ldots, n$, instead of the unobserved true exposure values X_i, $i = 1, \ldots, n$. The formal definition of Z_i is mentioned at the beginning of Subheading 3.2. In order to estimate the linear regression coefficients above, one can use Z_i^a instead of unobserved X_i, where

$$Z_i^a = \begin{cases} X_i; & X_i \geq d, \\ a; & X_i < d. \end{cases}$$

Richardson and Ciampi [40] demonstrated that to obtain asymptotically unbiased estimates of γ and η based on Υ_i and Z_i^a, the value of a can be set up to be $E[X|X<d]$. The application of this approach to practice requires investigators assuming to know how to calculate the conditional expectation $E[X|X<d]$, since no values of X_i below d are observed. Alternatively, Schisterman et al. [16] showed that the simple solution $a=0$ can provide the asymptotically normal unbiased least-square estimators of the linear regression coefficients based on Υ_i and Z_i^a without requirements of distributional assumptions. In these cases, assuming, e.g., $\gamma=0$, the unbiased estimator $\hat{\eta}_n$ has the form of

$$\hat{\eta}_n = \sum_{i=1}^{n} \Upsilon_i Z_i^a \; / \sum_{i=1}^{n} \left(Z_i^a\right)^2.$$

For more details and more general cases, see [16, 41].

In the example above, the single imputation is applied to obtain the unbiased linear regression coefficient estimates via a replacement of the unobserved data by deriving special values for utilization. In a similar manner, the single imputation can be executed in various situations given aims of interest and/or risk functions. As an additional example, we refer to Perkins et al. [15], where the single imputation method was applied to estimate ROC curves. The authors showed that without attending to the LOD problems, the estimated ROC curves are very biased.

Note that the single imputation substitutes each missing observation only once. Due to imprecision caused by the estimated distribution of the variables, the single imputation method commonly results in an underestimation of the standard errors or too small p-values when statistical tests are based on data subject to the LOD problem [17]. This issue can be solved by creating multiple data sets to substitute the unobserved data. Each imputation is based on a random draw from estimated underlying conditional distributions. For example, in the considerations mentioned at the beginning of this section, one can use $Z_i^{\xi_i}$ instead of Z_i^a, where ξ_i is generated from the distribution function $G(u)=P(X_1<u|X_1<d)$. Subsequently, results from individual data sets are averaged using multiple imputation combining rules.

As a concrete example, we assume data $X \sim N(\mu_x, \sigma_x^2)$ and is subject to the LOD problem. We create K (typically K is from 5 to 10) new data sets $D_1, \ldots, D_K$ based on the original data X with replacing missing values by values generated from the underlying

distribution. Let θ denote the vector of parameters of interest. In this example, $\theta=\mu_x$ or $\theta=\sigma_x^2$. And then $\hat{\theta}_i$ defines a vector of estimates based on the data set D_i, $i=1,\ldots,K$. We average the results across all $\hat{\theta}_i$, $i=1,\ldots,K$, by employing the following formulas:

$$\bar{\theta}=K^{-1}\sum_{i=1}^{K}\hat{\theta}_i,\ \hat{\mathrm{var}}(\theta)=K^{-1}\sum_{i=1}^{K}\hat{\mathrm{var}}(\theta_i)+\left(1+K^{-1}\right)(K-1)^{-1}\sum_{i=1}^{K}\left(\hat{\theta}_i-\bar{\theta}\right)^2,$$

which take into account both within- and between-imputation variances [17].

3.2.4 Hybrid Pooled–Unpooled Design

In this section, we describe a novel hybrid design, which requires a consideration of assays on individual specimens and assays on pooled specimens, when the measurement process is subject to the LOD problem. Refer to the hybrid pooled–unpooled design in Subheading 3.1 for the notations of α, N, p, and T. Assume individual biomarker values are distributed as $X_i\sim N(\mu_x,\sigma_x^2)$.. Thus, we obtain that pooled measurements are distributed as $X_i^{(p)}\sim N(\mu_x,\sigma_x^2/p)$, where $X_i^{(p)}=p^{-1}\sum_{k=(i-1)p+1}^{ip}X_k$, $i=1,\ldots,n_p=\alpha N$. Due to the LOD effect, we observe

$$Z_i^{(w)}=\begin{cases}X_i^{(w)}; & X_i^{(w)}\geq d,\\ N/A; & X_i^{(w)}<d,\end{cases}$$

where $w=1,p$, $i=1,\ldots,n_w$, and $X_i^{(1)}$ are the individual specimens.

In this case, the log-likelihood function based on $Z_i^{(w)}$, $w=1,p$, say l_H, can be constructed. The maximum likelihood method can be used to estimate parameters μ_x and σ_x^2 (e.g., [12]). Toward this end, we will solve the system of the equations $\{\partial l_H/\partial\mu_x=0,\ \partial l_H/\partial\sigma_x^2=0\}$. Expressions for the solutions, the entries of the Fisher information matrix, related statistical inferences, and more general and complicated cases can be found in the supplementary materials of [10].

4 Monte Carlo Experiments

To evaluate the performance of the reviewed methods, we applied the following simulation settings: $X_i\sim N(\mu_x=1,\sigma_x^2=1)$, $i=1,\ldots,N$, which represent normally distributed exposure values; the total sample sizes $N=100,300$; normally distributed additive MEs $\varepsilon_{ij}\sim N(0,\sigma_m^2)$ with $\sigma_m^2=0.4,1$; the number of replicates $n=2,5,10$ in the repeated measures sampling method; inverse gamma distributions, inverse Gaussian distributions, uniform distributions, and chi-square distributions as the prior distribution of

MEs in the Bayesian method; the pooling group size $p = 2, 5, 10$; and the pooling proportion $\alpha = 0.5$ in the hybrid design. For each set of parameters, there were 10,000 Monte Carlo simulations. In this section, following the pooling literature [38], we assumed that the analysis of biomarkers was restricted to execute just N measurements and $T = 0.5N(p+1)$ individual biospecimens are available, when the hybrid design was compared with the repeated measurements sampling method. For example, in the repeated measurements sampling method, the setting of $N = 100$ and $n = 2$ corresponds to 100 measurements from 50 individuals each measured twice. In the hybrid design, the setting of $N = 100$ and $p = 2$ corresponds to 100 measurements with $T = 150$ individual biospecimens available. It leads to a hybrid of $(1-\alpha)N = 50$ unpooled measurements and $\alpha N = 50$ pooled measurements with a pooling group size 2.

Table 1 shows the estimated parameters based on different design methods. For the repeated measurements data using the parametric likelihood method, the results show that as the replicates increase, the standard errors of the estimates of σ_m^2 decrease, indicating that the estimations of σ_m^2 appear to be better as the number of replicates increases. Apparently, the Monte Carlo standard errors of the estimators of μ_x and σ_x^2 increase when the number of replicates increases. Table 1 also shows that the Monte Carlo standard errors of the estimates for μ_x based on pooled–unpooled data are clearly less than those of the corresponding estimates utilizing repeated measurements, when $p \geq 2$ (respectively, $n \geq 2$). One observed advantage is that the estimation for σ_x^2 based on pooled–unpooled data is very accurate when the total number of measurements is fixed at the same level. Another advantage is that the standard errors of the estimates for the mean are much smaller than those based on repeated measurements.

Table 2 shows the Monte Carlo properties of the estimators obtained via the Bayesian methods described in Subheading 3.1 in a variety of scenarios related to different choices of the prior distributions $\psi(\cdot)$ of MEs. The prior distributions were selected such that the mean of the prior distributions are very close to or very far from the true values of σ_m^2. Note that μ_x and σ_x^2 are parameters of interest while σ_m^2 is a nuisance parameter. Table 2 demonstrates that the estimates of σ_x^2 depend on prior selections. For example, when the true σ_m^2 is set to be 1, the χ_1^2 prior distribution leads to very large Monte Carlo standard errors of the estimates. On the contrary, the uniform prior distributions give the minimum standard errors of the estimates compared to other choices of prior distributions. With uniform priors, the Bayesian

Table 1
The Monte Carlo evaluations of the maximum likelihood estimates based on the repeated measurements and the hybrid design

Sample size	Replicates n; pooling size p	Parameters (μ_x, σ_x^2, σ_m^2)	Estimates			Standard errors		
			$\hat{\mu}_x$	$\hat{\sigma}_x^2$	$\hat{\sigma}_m^2$	SE($\hat{\mu}_x$)	SE($\hat{\sigma}_x^2$)	SE($\hat{\sigma}_m^2$)
Repeated measurements								
$N = 100$	$n = 2$	(1,1,0.4)	1.0021	0.9781	0.3997	0.1553	0.241	0.079
		(1,1,1.0)	1.0006	0.9688	0.9984	0.1726	0.3106	0.1994
	$n = 5$	(1,1,0.4)	0.9966	0.9462	0.399	0.2328	0.3305	0.0623
		(1,1,0.4)	1.0015	0.9362	0.9998	0.2442	0.3688	0.157
	$n = 10$	(1,1,1.0)	1.0026	0.8951	0.3999	0.3209	0.4346	0.0597
		(1,1,0.4)	1.0044	0.8917	0.9995	0.3299	0.469	0.1501
$N = 300$	$n = 2$	(1,1,0.4)	0.9987	0.9921	0.3999	0.0889	0.1405	0.0455
		(1,1,1.0)	1.0005	0.9883	0.9999	0.0995	0.1803	0.1162
	$n = 5$	(1,1,0.4)	0.9995	0.9797	0.3998	0.1356	0.195	0.0365
		(1,1,0.4)	0.999	0.9766	0.999	0.1409	0.2181	0.0906
	$n = 10$	(1,1,1.0)	0.9985	0.9682	0.3997	0.1864	0.2633	0.0344
		(1,1,0.4)	0.9985	0.966	1.0002	0.1914	0.2782	0.0861
Hybrid design ($\alpha = 0.5$)								
$N = 100$	$p = 2$	(1,1,0.4)	1.0015	1.016	0.4365	0.1048	0.6712	0.4579
		(1,1,1.0)	1.0007	1.0754	1.0098	0.1327	1.0058	0.7275
	$p = 5$	(1,1,0.4)	0.9994	1.0045	0.3889	0.0924	0.3857	0.1662
		(1,1,0.4)	1.0008	1.0053	0.988	0.124	0.5932	0.3217
	$p = 10$	(1,1,1.0)	0.9993	1.0049	0.3918	0.0871	0.3341	0.1164
		(1,1,0.4)	0.9996	1.005	0.9836	0.1197	0.5082	0.2486
$N = 300$	$p = 2$	(1,1,0.4)	0.9999	0.9974	0.4066	0.0608	0.3868	0.2652
		(1,1,1.0)	1.0002	1.0069	0.9982	0.0758	0.5788	0.4179
	$p = 5$	(1,1,0.4)	0.9995	1.0013	0.3969	0.0534	0.2197	0.0954
		(1,1,0.4)	0.9993	1.0076	0.991	0.0711	0.3386	0.1819
	$p = 10$	(1,1,1.0)	0.9995	0.9995	0.3972	0.0497	0.1935	0.0671
		(1,1,0.4)	0.9992	1.0059	0.9922	0.0688	0.2928	0.1436

method is comparable with the repeated measure designs as well as the hybrid designs. In general, the Monte Carlo standard errors of the estimates of μ_x via the Bayesian methods are slightly bigger than those of estimates obtained via the hybrid designs but still smaller than the estimates obtained via the repeated measurements designs in many scenarios.

Table 2
The Monte Carlo evaluations of the maximum likelihood estimates based on the Bayesian methods

Sample size	Prior distribution	Parameters (μ_x, σ_x^2, σ_m^2)	Estimates			Standard errors		
			$\hat{\mu}_x$	$\hat{\sigma}_x^2$	$\hat{\sigma}_m^2$	SE($\hat{\mu}_x$)	SE($\hat{\sigma}_x^2$)	SE($\hat{\sigma}_m^2$)
Bayesian method								
N = 100	IGam(2.16,0.464)	(1,1,0.4)	0.9971	1.1615	0.2341	0.1203	0.2495	0.2118
	IGam(3,2)	(1,1,1.0)	0.9986	1.3855	0.6170	0.1396	0.4679	0.3849
	IGau(0.4,0.064)	(1,1,0.4)	1.0015	1.3656	0.0358	0.1178	0.4154	0.3642
	IGau(1,1)	(1,1,1.0)	0.9994	1.6316	0.3677	0.1424	0.6789	0.6361
	Unif(0,0.2)	(1,1,0.4)	0.9993	1.2910	0.1092	0.1181	0.3517	0.2909
	Unif(0,0.5)	(1,1,1.0)	0.9981	1.7160	0.2796	0.1424	0.7517	0.7269
	Unif(0.2,0.6)	(1,1,0.4)	0.9991	1.0046	0.3946	0.1174	0.1941	0.0072
	Unif(0.8,1.2)	(1,1,1.0)	0.9983	0.9932	1.0064	0.1428	0.2801	0.0103
	Unif(0.39,0.41)	(1,1,0.4)	1.0000	0.9855	0.4140	0.1177	0.1958	0.0141
	Unif(0.99,1.01)	(1,1,1.0)	0.9969	0.9810	1.0200	0.1406	0.2816	0.0202
	Chisq(0.4)	(1,1,0.4)	0.9997	1.3164	0.0781	0.1176	0.3679	0.3221
	Chisq(1)	(1,1,1.0)	0.9970	1.8119	0.1868	0.1414	0.8528	0.8135
	Chisq(0.3)	(1,1,0.4)	0.9997	1.3164	0.0781	0.1176	0.3679	0.3290
	Chisq(0.9)	(1,1,1.0)	0.9970	1.8119	0.1868	0.1414	0.8528	0.8292
N = 300	IGam(2.16,0.464)	(1,1,0.4)	1.0000	1.2027	0.2028	0.0690	0.2308	0.1972
	IGam(3,2)	(1,1,1.0)	1.0004	1.4445	0.5595	0.0819	0.4701	0.4406
	IGau(0.4,0.064)	(1,1,0.4)	0.9996	1.3572	0.0435	0.0678	0.3767	0.3608
	IGau(1,1)	(1,1,1.0)	0.9996	1.6545	0.3417	0.0817	0.6735	0.6585
	Unif(0,0.2)	(1,1,0.4)	0.9986	1.2999	0.0999	0.0684	0.3212	0.3001
	Unif(0,0.5)	(1,1,1.0)	1.0005	1.7579	0.2420	0.0816	0.7724	0.7586
	Unif(0.2,0.6)	(1,1,0.4)	0.9989	1.0152	0.3856	0.0686	0.1134	0.0145
	Unif(0.8,1.2)	(1,1,1.0)	1.0004	1.0078	0.9933	0.0805	0.1609	0.0069
	Unif(0.3967,0.4033)	(1,1,0.4)	0.9998	1.3533	0.0474	0.0683	0.3705	0.3526
	Unif(0.9967,1.0033)	(1,1,1.0)	1.0002	1.8859	0.1168	0.0812	0.8995	0.8833
	Chisq(0.4)	(1,1,0.4)	1.0002	1.3563	0.0429	0.0684	0.3733	0.3572
	Chisq(1)	(1,1,1.0)	0.9984	1.8978	0.1063	0.0813	0.9109	0.8937
	Chisq(0.3)	(1,1,0.4)	1.0000	1.2027	0.2028	0.0690	0.2308	0.1972
	Chisq(0.9)	(1,1,1.0)	1.0004	1.4445	0.5595	0.0819	0.4701	0.4406

Note: IGam(a,b) denotes the inverse gamma distribution with shape a and scale b; IGau(a,b) denotes the inverse Gaussian distribution with mean a and dispersion b; Unif(a,b) denotes the uniform distribution with minimum a and maximum b; Chisq(a) denotes the chi-square distribution with degrees of freedom a

5 Brief Literature Review

In this section, Table 3 briefly outlines several recent publications regarding ME problems.

Table 3
Several current publications regarding the measurement error problems

References	Statement of problems	Proposed methods	Applications
[2]	To develop asymptotically unbiased estimators of areas under ROC curves of best linear combination of two bivariate normally distributed biomarkers affected by LODs	Using maximum likelihood technique to develop asymptotically unbiased estimators of the area under ROC curves of best linear combination of two bivariate normally distributed biomarkers affected by LODs	Analysis of PCB levels to classify women with and without endometriosis
[4]	To reduce the cost of performing multiple assays in longitudinal studies	Considering different pooling designs for the efficient maximum likelihood estimation of variance components and evaluated the efficiencies of different pooling design strategies using analytic and simulation study results	Evaluation of F2-isoprostane biomarker data in a BioCycle study
[11]	To create tests comparing K-populations presented by longitudinal data subject to LOD	Utilizing the maximum likelihood approach in conjunction with autoregressive modeling to compare K-populations based on longitudinal data subject to LOD	Tumor development studies in mice
[14]	To correct ROC curves for measures subject to MEs and LOD simultaneously	Utilizing replicate measures and maximum likelihood to estimate ROC curves	Analysis of vascular endothelia growth factor (VEGf) data in preeclampsia study
[15]	To estimate ROC curves of measurements subject to LOD	Using maximum likelihood techniques to develop asymptotically unbiased estimators of the area under the curve	Evaluation of PCB levels in endometriosis study
[21]	To reduce study cost and analyze data subject to LOD	Applying maximum likelihood methodology to estimate area under ROC curve of data from pooled and unpooled samples when LOD is in effect	Evaluation of cholesterol measurements in coronary heart disease study
[22]	To estimate ROC curves based on biomarkers subject to additive MEs and pooling designs	Developed an approach utilizing characteristic functions to estimate ROC curves based on data subject to additive MEs and pooling mixtures	Evaluation of *interleukin*-6 biomarker of inflammation to study myocardial infarction (MI)
[38]	To examine the effect of different sampling strategies of biospecimens for exposure assessment that cannot be detected below a detection threshold	Proposed a combined design, which applies pooled and unpooled biospecimens, in order to capture the strengths of the different sampling strategies and overcome instrument limitations	Analysis of cholesterol measurements censored below a detection threshold

(continued)

Table 3
(continued)

References	Statement of problems	Proposed methods	Applications
[41]	To compare the performance of substitution methods to that of a maximum likelihood method in linear regression study with a left-censored independent variable X due to LOD	Compared the small sample performance of these competing methods with a simulation study	Study of association between sex hormone-binding globulin and oxidative stress
[42]	To develop asymptotically consistent, efficient estimators, for the mean vector and covariance matrix of multivariate normally distributed biomarkers affected by LOD	Using maximum likelihood techniques to develop estimators, for the mean vector and covariance matrix of multivariate normally distributed biomarkers affected by LOD	Using three polychlorinated biphenyls(PCBs) to classify women with and without endometriosis
[43]	To fit a binary regression model when an important exposure is subject to pooling	Utilized a regression calibration approach and derived several methods, including plug-in methods that use a pooled measurement and other covariate information to predict the exposure level of an individual subject, and normality-based methods that make further adjustments by assuming normality of calibration error	Analysis of PCB exposure in collaborative perinatal project
[44]	To determine the presence or absence of a pool-wise exposure	Using likelihood-based methods for logistic regression analysis with binary exposure status assessed by pooling	Gene–disease association study of colorectal cancer
[45]	To estimate individual-specific probabilities of pooled data in a regression context	Derived pool-specific misclassification probabilities (sensitivity and specificity) in terms of underlying biomarker distributions and generalized the regression approach by including individual covariate information	Analysis of hepatitis B infection among Irish prisoners
[46]	To reduce the cost of epidemiological and environmental researches	Proposed and evaluated “optimal” pooling designs based on specimens ranked on the less expensive biomarker	Evaluation of interleukin-6 biomarker data in a coronary heart disease study
[47]	To develop a more flexible model than the logistic model for analysis of pooled data	Using a modified logistic regression to accommodate nonlinearity because of unequal shape parameters in gamma distributed exposure in case control studies	Study of the role of chemokine levels as indicators of miscarriage

[48]	To compare the areas under ROC curves of diagnostic biomarkers whose measurements are subject to LOD	Utilizing the likelihood ratio tests with operating characteristics that are easily obtained by classical maximum likelihood methodology	IQ study and coronary heart disease study
[49]	To correct the bias caused by random measurement error in biomarker analysis	Estimating the Youden index and associated optimal cut point for a normally distributed biomarker	Analysis of thiobarbituric acid reaction substance (TBARS) data in a cardiovascular disease study
[50]	To construct accurate estimators for homogeneous pooled data in the context of group testing for rare abnormalities	Developed new nonparametric predictors that achieve optimal rates of convergence	Analysis of National Health and Nutrition Examination Survey study data
[51]	To plan and analyze reliability studies in order to assess an exposure's measurement error	Using multistage designs that allow repeated evaluation of reliability of the measurements and stop testing if early evidence shows the measurement error is within the level of tolerance	Evaluation of the reliability of biomarkers associated with oxidative stress
[52]	To correct for heteroscedastic covariate measurement error	Considering extensions of the regression calibration and multiple imputation methods that allow for heteroscedastic measurement error	Investigation of the association between carotenoids and progesterone of BioCycle study
[53]	To correct covariate measurement error in epidemiologic studies	Using summary statistics from the calibration sample to create multiple imputations of the missing values of covariates	Bone Health and Metabolism Study
[54]	To assess the relationship between chemical exposure and disease outcome when assay is subject to LOD	Proposed a flexible class of regression models that incorporates multiple assay measurements and allows for continuous or binary outcomes	Analysis of PCB exposure data of an endometriosis study
[55]	To estimate population distributions when some data are below LOD	Utilizing the reverse Kaplan–Meier estimator to estimate population distributions	Evaluation of serum dioxin data from Dioxin Exposure Study
[56]	To assess exposures to mixtures subject to LOD	Using nonparametric Bayes shrinkage priors for model selection to investigations of complex mixtures	Evaluation of PCB exposure data in an endometriosis study

6 Concluding Remarks

In this chapter, we reviewed different methods to operate with data subject to various sorts of ME problems. When data are subject to additive errors, the methods based on the repeated measurement designs and the hybrid pooled–unpooled technique, as well as the Bayesian method, have been proposed for correcting the MEs. When the errors related to the LOD are affecting the data, the methods based on the maximum likelihood methodology, the Bayesian method, the single and multiple imputation technique, and the scheme based on the hybrid pooled–unpooled design have been proposed as possible approaches to analyze the data. This article presented a limited number of Monte Carlo results to compare the efficiency as well as to show an applicability of the considered methods. Based on the results in Subheading 4, we concluded that the novel hybrid pooled–unpooled design possesses very attractive properties of statistical procedures based on data subject to MEs. We also recommend using the Bayesian method to operate with ME-affected data. In general, one can conclude that instrumental limitations related to biostatistical studies should be taken into account to fix issues based on problematic biomarker measurements, by developing new statistical methods or modifying standard statistical methods.

References

1. Carroll RJ, Spiegelman C, Lan KK, Bailey KT, Abbott RD (1984) On errors-in-variables for binary regression models. Biometrika 71:19–26
2. Perkins NJ, Schisterman EF, Vexler A (2011) ROC curve inference for best linear combination of two biomarkers subject to limits of detection. Biom J 53:464–476
3. Fuller WA (1987) Measurement error models. Wiley, New York
4. Malinovsky Y, Albert P, Schisterman EF (2012) Pooling designs for outcomes under a Gaussian random effects model. Biometrics 68:45–52
5. Faraggi D, Reiser B, Schisterman EF (2003) ROC curve analysis for biomarkers based on pooled assessments. Stat Med 22:2515–2527
6. Vexler A, Tsai WM, Malinovsky Y (2011) Estimation and testing based on data subject to measurement errors: from parametric to nonparametric likelihood methods. Stat Med 31: 2498–2512
7. Carroll RJ, Ruppert D, Stefanski LA, Crainiceanu CM (2006) Measurement error in nonlinear models. Chapman & Hall, New York
8. Schimid CH, Rosner B (1993) A Bayesian approach to logistic regression models having measurement error following a mixture distribution. Stat Med 12:1141–1153
9. Kass RE (1993) Bayes factors in practice. J Roy Stat Soc 42:551–560
10. Schisterman EF, Vexler A, Ye A, Perkins NJ (2011) A combined efficient design for biomarker data subject to a limit of detection due to measuring instrument sensitivity. Ann Appl Stat 5(4):2651–2667
11. Vexler A, Jihnhee Y, Hutson AD (2011) Likelihood testing populations modeled by autoregressive process subject to the limit of detection in applications to longitudinal biomedical data. J Appl Stat 38(7):1333–1346
12. Gupta AK (1952) Estimation of the mean and standard deviation of a normal population from a censored sample. Biometrika 39:260–273
13. Pepe MS (2003) The statistical evaluation of medical tests for classification and prediction. Oxford, New York, NY
14. Perkins NJ, Schisterman EF, Vexler A (2009) Generalized ROC curve inference for a biomarker subject to a limit of detection and measurement error. Stat Med 28(13):1841–1860
15. Perkins NJ, Schisterman EF, Vexler A (2007) Receiver operating characteristic curve inference

from a sample with a limit of detection. Am J Epidemiol 165:325–333
16. Schisterman EF, Vexler A, Whitcomb BW, Liu A (2006) The limitations due to exposure detection limits for regression models. Am J Epidemiol 163:374–383
17. Rubin DB, Schenker N (1986) Multiple imputation for interval estimation from simple random samples with ignorable nonresponse. J Am Stat Assoc 81(394):366–374
18. Vexler A, Liu A, Schisterman EF (2006) Efficient design and analysis of biospecimens with measurements subject to detection limit. Biom J 48:780–791
19. Schisterman EF, Vexler A, Mumford SL, Perkins NJ (2010) Hybrid pooled-unpooled design for cost-efficient measurement of biomarkers. Stat Med 29:597–613
20. Vexler A, Liu S, Schisterman EF (2011) Nonparametric-likelihood inference based on cost-effectively-sampled-data. J Appl Stat 38: 769–783
21. Mumford SL, Schisterman EF, Vexler A, Liu A (2006) Pooling biospecimens and limits of detection: effects on ROC curve analysis. Biostatistics 7:585–598
22. Vexler A, Schisterman EF, Liu A (2008) Estimation of ROC curves based on stably distributed biomarkers subject to measurement error and pooling mixtures. Stat Med 27:280–296
23. Vexler A, Liu A, Schisterman EF (2010) Nonparametric deconvolution of density estimation based on observed sums. J Nonparametr Stat 22:1048–5252
24. R Development Core Team (2012) R: a language and environment for statistical computing. R foundation for statistical computing, Vienna, Austria. ISBN 3-900051-07-0 http://www.R-project.org
25. Searle SR, Casella G, McCullooch CE (1992) Variance components. Wiley, New York
26. DiCiccio T, Hall P, Romano J (1989) Comparison of parametric and empirical likelihood functions. Biometrika 76:465–476
27. Owen AB (1988) Empirical likelihood ratio confidence intervals for a single functional. Biometrika 75:237–249
28. Owen AB (1991) Empirical likelihood for linear models. Ann Stat 19:1725–1747
29. Owen AB (2001) Empirical likelihood. Chapman & Hall/CRC, New York
30. Vexler A, Liu S, Kang L, Hutson AD (2009) Modifications of the empirical likelihood interval estimation with improved coverage probabilities. Commun Stat Simulation Comput 38: 2171–2183
31. Vexler A, Yu J, Tian L, Liu S (2010) Two-sample nonparametric likelihood inference based on incomplete data with an application to a pneumonia study. Biom J 52:348–361
32. Vexler A, Gurevich G (2010) Empirical likelihood ratios applied to goodness-of-fit tests based on sample entropy. Comput Stat Data Anal 54:531–545
33. Yu J, Vexler A, Tian L (2010) Analyzing incomplete data subject to a threshold using empirical likelihood methods: an application to a pneumonia risk study in an ICU setting. Biometrics 66:123–130
34. Kitamura Y (1997) Empirical likelihood methods with weakly dependent processes. Ann Stat 25:2084–2102
35. Carlin B, Louis TA (2008) Bayes and empirical Bayes methods for data analysis. Chapman & Hall/CRC, New York
36. Liu A, Schisterman EF (2003) Comparison of diagnostic accuracy of biomarkers with pooled assessments. Biom J 45:631–644
37. Liu A, Schisterman EF, Teoh E (2004) Sample size and power calculation in comparing diagnostic accuracy of biomarkers with pooled assessments. J Appl Stat 31:49–59
38. Schisterman EF, Vexler A (2008) To pool or not to pool, from whether to when: applications of pooling to biospecimens subject to a limit of detection. Pediatr Perinat Epidemiol 22:486–496
39. Harter HL, Moore AH (1967) Asymptotic variances and covariances of maximum-likelihood estimators, from censored samples, of the parameters of Weibull and gamma populations. Ann Math Stat 38:557–570
40. Richardson DB, Ciampi A (2003) Effects of exposure measurement error when an exposure variable is constrained by a lower limit. Am J Epidemiol 157:355–363
41. Nie L, Chu H, Liu C, Cole SR, Vexler A, Schisterman EF (2010) Linear regression with an independent variable subject to a detection limit. Epidemiology 21(Suppl 4):S17–S24
42. Perkins NJ, Schisterman EF, Vexler A (2013) Multivariate normally distributed biomarkers subject to limits of detection and receiver operating characteristic curve inference. Acad Radiol 20:838–846
43. Zhang Z, Albert PS (2011) Binary regression analysis with pooled exposure measurements: a regression calibration approach. Biometrics 67:636–645
44. Lyles RH, Tang L, Lin J, Zhang Z, Mukherjee B (2012) Likelihood-based methods for regression analysis with binary exposure status assessed by pooling. Stat Med 31:2485–2497

45. Mcmahan CS, Tebbs JM, Bilder CR (2013) Regression models for group testing data with pool dilution effects. Biostatistics 14:284–298
46. Ma CX, Vexler A, Schisterman EF, Tian L (2011) Cost-efficient designs based on linearly associated biomarkers. J Appl Stat 38:2739–2750
47. Whitcomb BW, Perkins NJ, Zhang Z, Ye A, Lyles RH (2012) Assessment of skewed exposure in case-control studies with pooling. Stat Med 31:2461–2472
48. Vexler A, Liu A, Eliseeva E, Schisterman EF (2008) Maximum likelihood ratio tests for comparing the discriminatory ability of biomarkers subject to limit of detection. Biometrics 64:895–903
49. Perkins NJ, Schisterman EF (2005) The Youden index and the optimal cut-point corrected for measurement error. Biom J 47:428–441
50. Delaigle A, Hall P (2012) Nonparametric regression with homogeneous group testing data. Ann Stat 40:131–158
51. Liu A, Schisterman EF, Wu C (2006) Multistage evaluation of measurement error in a reliability study. Biometrics 62:1190–1196
52. Guo Y, Little RJ (2011) Regression analysis with covariates that have heteroscedastic measurement error. Stat Med 30:2278–2294
53. Guo Y, Little RJ, McConnell DS (2012) On using summary statistics from an external calibration sample to correct for covariate measurement error. Epidemiology 23:165–174
54. Albert PS, Harel O, Perkins N, Browne R (2010) Use of multiple assays subject to detection limits with regression modeling in assessing the relationship between exposure and outcome. Epidemiology 21(Suppl 4): S35–S43
55. Gillespie BW, Chen Q, Reichert R, Franzblau A, Hedgeman E, Lepkowski J, Adriaens P, Demond A, Luksemburg W, Garabrant DH (2010) Estimating population distributions when some data are below a limit of detection by using a reverse Kaplan-Meier estimator. Epidemiology 21:S64–S70
56. Herring AH (2010) Nonparametric Bayes shrinkage for assessing exposures to mixtures subject to limits of detection. Epidemiology 21(Suppl 4):S71–S76

INDEX

A

Donald Armstrong (ed.), *Advanced Protocols in Oxidative Stress III*, Methods in Molecular Biology, vol. 1208,
DOI 10.1007/978-1-4939-1441-8, © Springer Science+Business Media New York 2015

D

E

F

G

H

I

K

L

M

N

O

P

Q

R

S

T

U

V

W

Z